

**Department of Applied Geology**

**Petrogenesis and Tectonic Setting of Mesozoic Granitic Rocks in  
Eastern South China**

**Kongyang Zhu**

**This thesis is presented for the Degree of  
Doctor of Philosophy**

**of**

**Curtin University**

**March 2014**

## Acknowledgements

This thesis is dedicated to the memory of my grandmother, Feng-Ying Sun.

I would like to thank my supervisors Profs. Zheng-Xiang Li (Curtin University), Xi-Sheng Xu (Nanjing University) and Simon A. Wilde (Curtin University) for their guidance, inspiring ideas, time and patience. They realized the importance of the granitic rocks for constraining the tectonic evolution of eastern South China, which is the focal point of my Ph.D. studies.

I am grateful to the Chinese Scholarship Council, Curtin University and the Institute for Geoscience Research (TIGeR), for their financial supports covering my tuition fees and cost of living for the past four years. The field and laboratory work were financially supported by the Natural Science Foundation of China (41072043, 40730313), National Basic Research Program of China (2012CB416701) and Australian Research Council Discovery Project grant (DP110104799).

I thank all administrative staffs at the Department of Applied Geology, Curtin University who helped me in many ways during my time in Australia.

I thank all the research and technical staff from Curtin University (CU), the University of Western Australia (UWA), Nanjing University (NJU), the Institute of Geochemistry, Chinese Academy of Sciences (IGCAS), and China University of Geosciences, Wuhan (CUG), who helped me with experimental work. In particular, I thank Dr. Katy Evans (CU, magnetic susceptibility meter), Elaine Miller (CU, SEM and EDS), Dr. William Richard (CU, SEM), Dr. Allen Kennedy (CU, SHRIMP), Hao Gao (CU, SHRIMP), Dr. Richard Taylor (CU, SHRIMP), Dr. David T. Adams (UWA, EMPA), Dr. Janet Muhling (UWA, EMPA), Jian-Hua Geng (NJU, thin section), Guang-Hui Zhang (NJU, thin section), Bin Wu (NJU, LA-ICP-MS), Dr. Tao Yang (NJU, LA-MC-ICP-MS and ICP-MS), An-Jun Lin (NJU, LA-MC-ICP-MS), Meng-Qun Zhang (NJU, XRF), Gui-Zhen Su (NJU, XRF), Yu-Ping Lin (NJU, ICP-MS), Hai-Zhen Wei (NJU, ICP-MS), Wen-Lan Zhang (NJU, EMPA), Dr. Hong-Feng Tang (IGCAS, LA-MC-ICP-MS), Dr. Ming-Liang Wang (IGCAS, LA-MC-ICP-MS), and Prof. Yong-Sheng Liu (CUG, ICP-MS).

I thank Yun-Wen Yu from Zhejiang Geological Survey for providing age and geochemical data for the Shangyutou basalt and Dr. R. J. Sewell from the Geotechnical Engineering Office, Civil Engineering and Development Department, Hong Kong for providing geochemical data for the Deep Bay granite.

I am indebted to my colleagues in Nanjing University for their help during my field and laboratory works in China. They are: Wen-Tao Hong (NJU, field work), Lei Liu (NJU, LA-

## Acknowledgements

ICP-MS and MC-LA-ICP-MS), Yan Xia (NJU, LA-ICP-MS and MC-LA-ICP-MS), Fa-Jun Sun (NJU), and my girlfriend, Wei Zhou (China Mobile, sample management).

I thank Dr. Daniel Dunkley (CU) and Rosalind Crossley (CU) for proofreading this thesis.

I thank the following people, including fellow PhD students at Curtin University, for their helps during my four-year life in Perth: Jia-Wen Niu, Dr. Hui-Qing Huang, Qian Wang, Dr. Xuan-Ce Wang, Dr. Ying Jia Teoh, Ying-Chao Liu, Chong-Jin Pang, Wei-Hua Yao, Li-Ping Liu, Ni Tao, Dr. Yong-Jun Lv, Si-Yu Hu, Xian-Zhong Shi, Tubagus Solihuddin, Dr. Rob Madden, Fiona Mothersole, Dr. Erin Gray, Dr. Siriporn Soonpankhao, Dr. Chris Clark and Dr. Ricardo J. Jahnert.

I thank my family for their understanding and support during my years of study.

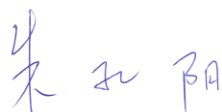
I thank the Australian people.

**Declaration**

To the best of my knowledge and belief this thesis contains no material previously published by any other person except where due acknowledge has been made. This thesis contains no material which has been accepted for the award of any other degree or diploma in any university.

Name: Kongyang Zhu

Signature:



Date: 21<sup>st</sup>/March/2014

## Abstract

South China is composed of the Yangtze and Cathaysia blocks that amalgamated along the Sibao Orogenic Belt during the Neoproterozoic. The Pingxiang-Jiangshan-Shaoxing fault zone marks the boundary between the Cathaysia Block and the Sibao Orogenic Belt. The Mesozoic geology of South China features extensive granitic magmatism, which represents important crustal reworking and growth. Previous studies showed that this was related to subduction of the paleo-Pacific plate, but detailed tectono-magmatic processes are not well constrained. The petrogenesis and tectonic setting of these granitoids can not only help to constrain regional geological evolution but also provide insights into the general understanding of granite petrogenesis and magmatic processes at continental margins. To meet these objectives, Triassic, Jurassic and Early Cretaceous granitoids in eastern South China (Zhejiang and northeastern Jiangxi provinces) were systematically sampled and analysed. In particular, the study region was chosen to straddle the boundary between the Cathaysia Block and the Sibao Orogenic Belt. For this study, the magnetic susceptibility, zircon U-Pb ages, zircon Hf isotopes, and whole-rock major and trace elements of the samples were analysed in order to constrain the source, temperature, pressure, water content and redox condition during crustal partial melting and magma differentiation and to test their variation with time.

In central Zhejiang Province, the continental crust was thickened and metasomatized by aqueous and siliceous fluids due to Triassic flat-slab subduction. As a result of thermal relaxation, the lower crust reached high enough temperatures for high-pressure, high-temperature melting, resulting in the formation of the 224 Ma Dashuang syenite (without water from the oceanic plate) and the 226–227 Ma Dashuang quartz monzonite (with water from the oceanic plate). The Jingju Complex to the southwest, which consists of 218 Ma syenogranite and 236 Ma quartz monzonite, was generated by the same processes.

In western Zhejiang Province, five stages of granitoids were produced during an Andean-type orogenic cycle: (1) granitoids were generated from thickened post-orogenic crust with variable fluid/melt contributions from the oceanic plate (230–215 Ma, the Late *Triassic*, T<sub>3</sub>); (2) low-temperature water-rich porphyritic granitoids were generated by dehydration of the foundering oceanic plate (170–150 Ma, the Middle-Late *Jurassic*, J<sub>2-3</sub>); (3) low-temperature granitoids were generated in attenuated crust caused by lithospheric extension [140–130 Ma, the first stage of the *Early Cretaceous*, K<sub>1(I)</sub>]; (4) high-temperature granitoids were the result of crustal attenuation and basaltic underplating [130–125 Ma, the second stage of the *Early Cretaceous*, K<sub>1(II)</sub>]; and finally, (5) granitoids formed by

## Abstract

differentiation of basaltic magmas that were derived from an enriched continental lithospheric mantle [115–100 Ma, the third stage of the *Early Cretaceous*, K<sub>1</sub>(III)].

In northeastern Jiangxi Province, the mid-Jurassic (175–160 Ma) and Early Cretaceous (145–120 Ma) granitic rocks are comparable to their J<sub>2-3</sub> and K<sub>1</sub>(I) counterparts in western Zhejiang Province in terms of age, petrogenesis and tectonic setting. The mid-Jurassic porphyries are wet and oxidized rocks generated by water-fluxed melting in the continental lower crust or by fractionation of hydrous mantle-derived magmas, containing fluids from the foundering subducted oceanic crust. The Early Cretaceous granites are dry and reduced rocks generated by dehydration melting in the continental lower crust, which underwent strong extension during roll-back of the paleo-Pacific plate.

In northeastern Zhejiang Province, the 225 Ma Qiuwang syenogranite was generated by dehydration melting of thickened continental crust, but the 178 Ma Xiepu syenogranite was generated by dehydration melting triggered by basaltic underplating following the break-off of the paleo-Pacific plate. Within the Ganzhou-Hangzhou rift zone (Neoproterozoic Sibao Orogenic Belt), crustal attenuation was stronger than in adjacent regions and A-type granitic magmatism was generated in the Late Jurassic, which is earlier than its counterpart in other regions of Zhejiang Province (~135 Ma). The attenuated crust in northeastern Zhejiang Province was later thickened by Early Cretaceous mantle-derived intrusions. The zircon  $\epsilon_{\text{Hf}}(t)$  values of the Early Cretaceous mafic and intermediate rocks in the Ganzhou-Hangzhou rift zone range from -4.3 to 2.1; their counterparts in the Cathaysia Block range from -4.8 to -2.6. Although the basement rocks in the Sibao Orogenic Belt feature significantly higher degrees of Neoproterozoic crustal growth, the Hf isotopic compositions of the continental lithospheric mantle is not significantly different from that of the Cathaysia Block (with Paleoproterozoic basement) during the Early Cretaceous. The less negative zircon  $\epsilon_{\text{Hf}}(t)$  values of the Early Cretaceous mafic and intermediate rocks in the Ganzhou-Hangzhou rift zone were caused by upwelling and involvement of depleted asthenospheric mantle.

Published ages, and geochemical and isotopic data for Mesozoic granitoids from eight other well-studied regions in South China are reviewed in order to place the new results in context. The characteristics of these Mesozoic granitoids indicate diachronous, tectono-magmatic processes. The age, geochemical and isotopic evolution of the Mesozoic granitoids of South China, together with other geological evidence, is consistent with a typical Andean-type orogenic cycle along the eastern margin of China in the Mesozoic.

## Table of Contents

<b>Acknowledgements .....</b>	<b>i</b>
<b>Declaration</b>	<b>iii</b>
<b>Abstract</b>	<b>iv</b>
<b>Table of Contents.....</b>	<b>vi</b>
<b>List of Figures .....</b>	<b>xiii</b>
<b>Chapter 1 Introduction.....</b>	<b>1</b>
1.1    Background .....	1
1.2    Classification of granitoid .....	2
1.2.1  Mineralogical classification .....	2
1.2.2  Geochemical classification.....	4
1.2.3  Chemical-tectonic-genetic classification.....	6
1.3    Objectives.....	9
1.4    Dissertation Structure .....	9
<b>Chapter 2 Geological Background .....</b>	<b>10</b>
2.1    Geological setting and pre-Mesozoic tectonic evolution of South China .....	10
2.2    Previous studies on Mesozoic granitoids in South China and various tectonic models .....	10
2.3    The geology of the study area .....	13
2.4    Tectonic and magmatic processes under flat-slab subduction conditions .....	15
2.4.1  Western North American flat-slab subduction.....	15
2.4.2  Andean flat-slab subduction.....	16
<b>Chapter 3 Analytical Methods .....</b>	<b>19</b>
3.1    Magnetic susceptibility.....	19
3.2    Sample preparation.....	19
3.3    Zircon cathodoluminescence imaging .....	19
3.4    LA-ICP-MS zircon U-Pb dating and trace element analyses .....	19
3.5    SHRIMP zircon U-Pb dating.....	20
3.6    LA-MC-ICP-MS zircon Hf isotopes .....	20
3.7    XRF whole-rock major elements.....	21

## Table of Contents

3.8 ICP-MS whole-rock trace elements.....	22
<b>Chapter 4 Late Triassic Quartz Monzonite and Syenite/Syenogranite Complex in Central Zhejiang Province.....</b>	<b>24</b>
4.1 Introduction .....	24
4.2 Geological setting and petrography.....	24
4.3 Results .....	25
4.3.1 Magnetic susceptibility .....	25
4.3.2 Zircon U-Pb dating, Hf isotope and trace element analyses .....	27
4.3.3 Whole-rock major and trace element data.....	30
4.4 Discussion .....	31
4.4.1 Contrasting physical and chemical conditions for the east and west bodies	31
4.4.2 Petrogenesis and tectonic model .....	34
4.5 Conclusion.....	41
<b>Chapter 5 Mesozoic Granitic Magmatism in Western Zhejiang Province.....</b>	<b>43</b>
5.1 Introduction and Geological Setting.....	43
5.2 Sampling and Petrography .....	43
5.3 Analytical Results.....	49
5.3.1 Zircon U-Pb Dating and Hf isotope .....	49
5.3.2 Whole-rock major and trace elements.....	59
5.4 Petrogenetic Interpretation .....	62
5.4.1 Late Triassic magmatism: T <sub>3</sub> .....	64
5.4.2 Middle-Late Jurassic magmatism: J <sub>2-3</sub> .....	66
5.4.3 First stage of Early Cretaceous magmatism: K <sub>1</sub> (I).....	67
5.4.4 Second stage of Early Cretaceous magmatism: K <sub>1</sub> (II) .....	68
5.4.5 Third stage of Early Cretaceous magmatism: K <sub>1</sub> (III).....	69
5.5 Discussion .....	73
5.5.1 Triassic: crustal thickening above a flat-slab .....	73
5.5.2 Middle Jurassic: foundering of the flat slab .....	75
5.5.3 Early Cretaceous: lithospheric extension .....	76

Table of Contents

5.6 Conclusions .....	78
<b>Chapter 6 Mesozoic Granitic Magmatism in Northeastern Jiangxi Province.....</b>	<b>80</b>
6.1 Introduction and Geological Setting.....	80
6.2 Sampling and Petrography .....	80
6.2.1 Lingshan syenogranite.....	80
6.2.2 Wancunxiang syenogranite .....	82
6.2.3 Damaoshan-Huaiyushan syenogranite-alkali feldspar granite .....	83
6.3 Analytical Results.....	84
6.3.1 Zircon U-Pb Dating and Hf isotopes.....	84
6.3.2 Whole-rock major and trace elements.....	87
6.4 Petrogenetic and Tectonic Interpretations .....	88
6.5 Conclusion.....	91
<b>Chapter 7 Mesozoic Magmatism in the vicinity of the Ganzhou-Hangzhou Rift Zone.</b>	<b>92</b>
7.1 Introduction .....	92
7.2 Geological setting and petrography .....	92
7.2.1 Late Triassic and Early Jurassic granitoids in the Ningbo region .....	93
7.2.2 Mesozoic granitoids and diorites in the Zhuji region.....	93
7.2.3 Porphyritic samples from the Ganzhou-Hangzhou rift zone .....	93
7.2.4 Early Cretaceous Ru'ao complex from northeastern Zhejiang Province ....	96
7.3 Results .....	96
7.3.1 Zircon age and Hf isotopes.....	96
7.3.2 Whole-rock major and trace elements.....	100
7.4 Discussion .....	102
7.4.1 Late Triassic and Early Jurassic granitoids in the Ningbo region: mountain building and collapse in northeastern Zhejiang.....	103
7.4.2 Late Jurassic granites in the Zhuji region: crustal attenuation initiation in the Ganzhou-Hangzhou rift zone .....	104
7.4.3 Late Jurassic and Cretaceous (quartz) diorite from Ganzhou-Hangzhou rift zone: crustal extension to crustal magmatic thickening .....	104

## Table of Contents

7.4.4 Comparison of Early Cretaceous magmatic rocks from the Ganzhou-Hangzhou rift zone with those from northeastern Zhejiang Province.....	105
7.5 Conclusion.....	109
<b>Chapter 8 Petrogenesis and Tectonic Implications of Mesozoic Granitoids in other regions of South China .....</b>	<b>111</b>
8.1 Southern Anhui Province .....	111
8.2 Northern Zhejiang Province .....	114
8.3 Central Hunan Province .....	115
8.4 Central Jiangxi Province.....	116
8.5 Western Fujian Province .....	119
8.6 Eastern Fujian-Guangdong Province.....	122
8.7 Nanling Range.....	124
8.8 Hong Kong .....	128
8.9 Summary and future work.....	131
<b>Chapter 9 Conclusions.....</b>	<b>136</b>
<b>Reference</b>	<b>139</b>
<b>Appendices 164</b>	
Appendix A. Table of GPS readings and magnetic susceptibilities for the granitoids and volcanic rocks in this study.....	164
Appendix B. Table of in-situ zircon U-Pb dating results.....	174
09ZJ01 (Qiuwang syenogranite, LA-ICP-MS).....	174
09ZJ02 (Xiepu syenogranite, SHRIMP) .....	175
09ZJ06 (Ru'ao diorite, LA-ICP-MS) .....	175
09ZJ07 (Ru'ao monzodiorite, LA-ICP-MS) .....	176
09ZJ09 (Dashuang quartz monzonite, LA-ICP-MS).....	177
09ZJ14 (Tongshan syenogranite, SHRIMP) .....	178
10ZJS011 (Qiuwang syenogranite, LA-ICP-MS) .....	179
10ZJS025 (Yujiashan diorite, LA-ICP-MS).....	180
10ZJS033 (Jiangzao granite, LA-ICP-MS) .....	181
10ZJS053 (Hecun dacitic-rhyolitic porphyry , LA-ICP-MS).....	182

Table of Contents

10ZJS063 (Dashuang quartz monzonite, LA-ICP-MS).....	183
10ZJS065 (Dashuang syenite, LA-ICP-MS) .....	184
10ZJS072 (Shuangcai andesitic-dacitic porphyry, LA-ICP-MS).....	184
10ZJS081 (Hongling dacitic-rhyolitic porphyry, LA-ICP-MS) .....	185
10ZJS096 (Zhujiaxiang andesitic porphyry, LA-ICP-MS) .....	186
10ZJS099 (Matou monzogranite, LA-ICP-MS) .....	187
10ZJS101 (Matou monzogranite, LA-ICP-MS) .....	188
10ZJS104 (Shanghekou syenogranite, LA-ICP-MS) .....	189
10ZJS108 (Sucun syenogranite, LA-ICP-MS).....	190
10ZJS109 (Huangkang syenogranite, LA-ICP-MS).....	191
10ZJS115 (Muchen diorite, MME, LA-ICP-MS) .....	192
10ZJS116 (Muchen quartz monzonite, LA-ICP-MS) .....	193
10ZJS121 (Wangcun syenogranite, SHRIMP).....	193
10ZJS125 (Muchen granitic porphyry, LA-ICP-MS) .....	194
10ZJS129 (Yingcun granitic porphyry, LA-ICP-MS).....	195
10ZJS131 (Muchen quartz monzonite, LA-ICP-MS) .....	196
10ZJS132 (Muchen quartz monzonite, LA-ICP-MS) .....	197
10ZJS133 (Luojia granitic porphyry, LA-ICP-MS) .....	198
10ZJS135 (Sheyang syenogranite, LA-ICP-MS) .....	199
10ZJS136 (Lingkeng syenogranite, LA-ICP-MS).....	200
10ZJS143 (Jiuhua granitic porphyry, LA-ICP-MS) .....	201
10ZJS149 (Shangsanzhi granitic porphyry, LA-ICP-MS) .....	201
10ZJS154 (Lingshan syenogranite, LA-ICP-MS) .....	202
10ZJS155 (Lingshan syenogranite, LA-ICP-MS) .....	203
10ZJS156 (Lingshan MME, LA-ICP-MS) .....	204
10ZJS170 (Wancunxiang syenogranite, LA-ICP-MS).....	205
10ZJS171 (Wancunxiang endoskarn, LA-ICP-MS) .....	206

Table of Contents

10ZJS172 (Damaoshan-Huaiyushan syenogranite-alkali feldspar granite, LA-ICP-MS) 207	
Appendix C. Table of in-situ zircon trace element results (ppm) .....	208
Appendix D. Table of in-situ zircon Hf isotope.....	209
09ZJ02 (Xiepu syenogranite) .....	209
09ZJ07 (Ru'ao monzodiorite) .....	210
09ZJ09 (Dashuang quartz monzonite).....	211
10ZJS011 (Qiuwang syenogranite) .....	211
10ZJS025 (Yujiashan diorite).....	212
10ZJS033 (Jiangzao granite) .....	213
10ZJS053 (Hecun dacitic-rhyolitic porphyry).....	214
10ZJS063 (Dashuang quartz monzonite) .....	215
10ZJS065 (Dashuang syenite).....	216
10ZJS072 (Shuangcai andesitic-dacitic porphyry).....	216
10ZJS081 (Hongling dacitic-rhyolitic porphyry).....	217
10ZJS096 (Zhujiaxiang andesitic porphyry) .....	218
10ZJS101 (Matou monzogranite).....	219
10ZJS104 (Shanghekou syenogranite) .....	220
10ZJS108 (Sucun syenogranite).....	220
10ZJS109 (Huangkang syenogranite) .....	221
10ZJS115 (Muchen diorite, MME) .....	222
10ZJS116 (Muchen quartz monzonite) .....	223
10ZJS121 (Wangcun syenogranite).....	223
10ZJS125 (Muchen granitic porphyry) .....	224
10ZJS129 (Yingcun granitic porphyry).....	225
10ZJS131 (Muchen quartz monzonite) .....	226
10ZJS132 (Muchen quartz monzonite) .....	226
10ZJS133 (Luojia granitic porphyry) .....	227

## Table of Contents

10ZJS135 (Sheyang syenogranite) .....	228
10ZJS136 (Lingkeng syenogranite).....	229
10ZJS143 (Jiuhua granitic porphyry) .....	230
10ZJS149 (Shangsanzhi granitic porphyry) .....	230
10ZJS154 (Lingshan syenogranite) .....	231
10ZJS155 (Lingshan syenogranite) .....	232
10ZJS156 (Lingshan MME) .....	233
10ZJS170 (Wancunxiang syenogranite). ....	234
10ZJS171 (Wancunxiang syenogranite, endoskarn) .....	235
10ZJS172 (Damaoshan-Huaiyushan syenogranite-alkali feldspar granite).....	235
Appendix E. Table of whole-rock chemical compositions .....	237
Appendix F. Permission to paper reproduction for Chapter 4 .....	249
Appendix G. Permission to paper reproduction for Chapter 5.....	250

**List of Figures**

Figure 1.1 Quartz-alkali feldspar-plagioclase modal classification of plutonic rocks (Streckeisen, 1974).....	3
Figure 1.2 Phase diagrams for alkali feldspars in hypersolvus (a) and subsolvus (b) granite modified from Gill (2010).....	4
Figure 1.3 $\text{FeO}_{\text{total}}/(\text{FeO}_{\text{total}}+\text{MgO})$ versus $\text{SiO}_2$ diagram showing ferroan-magnesian granitoid classification (Frost et al., 2001).....	5
Figure 1.4 $\text{K}_2\text{O}-\text{SiO}_2$ classification for granitoids (Le Maitre, 2002) .....	6
Figure 1.5 Plot of $\text{Na}_2\text{O} + \text{K}_2\text{O} - \text{CaO}$ versus $\text{SiO}_2$ showing the boundaries between alkalic, alkali-calcic, calc-alkalic, and calcic granitoids.....	7
Figure 1.6 The R1–R2 tectonic discrimination diagram for granitoids based on whole-rock major elemental composition (Batchelor and Bowden, 1985). $R1 = 4\text{Si} - 11(\text{Na} + \text{K}) - 2(\text{Fe} [\text{total as bivalent}] + \text{Ti})$ , $R2 = 6\text{Ca} + 2\text{Mg} + \text{Al}$ , all in millications. Millication of element $i = 1000 \times \text{number of } i \text{ atoms in its oxide} \times \text{oxide}_i (\text{wt.\%})/\text{molecular weight of the oxide}_i$ .....	8
Figure 1.7 Tectonic discrimination diagrams of granitoids based on whole-rock trace element composition (Pearce et al., 1984).....	9
Figure 2.1 Schematic map showing the major tectonostratigraphic terranes and sutures (Metcalfe, 2013). WB = West Burma, SWB = South West Borneo, S = Semitau, L = Lhasa, SQT = South Qiangtang, NQT = North Qiangtang, QS = Qamdo–Simao, SI = Simao, SG = Songpan Ganzi accretionary complex, QD = Qaidam, QI = Qilian, AL = Ala Shan, KT = Kurosegawa Terrane, LT = Lincang arc Terrane, CT = Chanthaburi arc Terrane, EM = East Malaya. ....	11
Figure 2.2 Tectonic framework of the South China Block modified after Li et al. (2002)....	12
Figure 2.3 Schematic diagram showing the major Neoproterozoic and Phanerozoic tectonic events in the South China Block (Li et al., 2014b). .....	12
Figure 2.4 Distribution of Mesozoic granitic rocks in the South China Block modified after Zhou et al. (2006).....	13
Figure 2.5 Simplified geological map of Zhejiang Province modified after the 1:500000 geological map of ZGS (1989).....	14
Figure 2.6 A tectonic model for the Sevier and Laramide orogenies in western North America, modified after Dumitru et al. (1991) and DeCelles (2004). .....	15
Figure 2.7 Flat-slab subduction throughout the Andes in Cenozoic times, from Ramos (2009). .....	17
Figure 2.8 Andean orogenic cycle proposed by Ramos (2009). .....	18

## List of Figures

- Figure 4.1 (A) Distribution of Mesozoic granitoids in the South China Block, modified after Zhou et al. (2006), Li et al. (2012c) and Jiang and Li (2014). Inset shows mid-Permian to mid-Cretaceous thrusts in South China fold belt, after Li and Li (2007). DS = Dashuang quartz monzonite/syenite; WS = Wengshan syenogranite; SY = Sheyang syenogranite; JJ = Jingju monzogranite; DX = Dexing; DZ = Danzhu; JN = Jingning; YF = Yangfang. (B) Geological map of the Dashuang Complex and sample numbers, after ZGS (1975). ..... 25
- Figure 4.2 Field and thin section photographs of rocks from the Dashuang complex. (A) Field photograph of syenite from the west body (sample 10ZJS065); (B) Photomicrograph of syenite from the west body, showing high modal alkali feldspar (sample 10ZJS065, cross-polarized light); (C) Field photograph of quartz monzonite from the east body, showing deformed alkali feldspar megacrysts (sample 10ZJS066); (D) Photomicrograph of quartz monzonite from the east body, showing the major ferromagnesian minerals hornblende, biotite, titanite and magnetite (sample 10ZJS066, cross-polarized light); (E) Photomicrograph of quartz monzonite from the east body, showing alkali feldspar megacrysts (sample 09ZJ09, cross-polarized light); (F) Photomicrograph of quartz monzonite from the east body, showing higher modal quartz than the west body (sample 10ZJS067, cross-polarized light). Mineral abbreviations: Afs = alkali feldspar, Mc = microcline, Bt = biotite, Ttn = titanite, Hbl = hornblende, Qz = quartz, Pl = plagioclase, Mag = magnetite. ..... 26
- Figure 4.3 Magnetic susceptibility of rocks from the Dashuang complex, with bars representing the results and numbers the whole-rock total Fe<sub>2</sub>O<sub>3</sub> contents. The boundary between the magnetite series and ilmenite series granitoids is from Ishihara et al. (2000). ..... 27
- Figure 4.4 Zircon REE spidergram, normalized to C1 chondrite (Sun and McDonough, 1989). The data are the means (Ce, Gd-Lu) or the medians (La, Pr-Eu) of the zircon analyses from each sample (Table 4). 10ZJS065 (the west body) has stronger Eu depletion; 10ZJS063 (the east body) has MREE depletion and higher Ce contents. ..... 28
- Figure 4.5 Zircon CL images, U-Pb and Hf isotope analyses for sample 10ZJS065 (A, D, G), sample 10ZJS063 (B, E, H) and sample 09ZJ09 (C, F, I). In the CL images, oscillatory zoning indicates their magmatic origin. Small circles mark the positions of LA-ICP-MS U-Pb isotope analyses and large circles mark the positions of MC-LA-ICP-MS Hf isotope analyses. In D, E and F, error ellipses and error bars are 2 standard deviation of <sup>206</sup>Pb/ <sup>238</sup>U ratios, <sup>207</sup>Pb/ <sup>235</sup>U ratios and <sup>206</sup>Pb/ <sup>238</sup>U ages, respectively. Grey ellipses and bars are excluded from weighted mean age calculations. SE = standard error. In E, F and G, the εHf(t) values (-10 to -6) of the west body are less negative than those of the

## List of Figures

east body (mostly less than -10). All three samples contain ~240 Ma zircons, likely recording a previous thermal event in the source region.....	30
Figure 4.6 Diagram of whole-rock $\text{FeO}_{\text{total}} / (\text{FeO}_{\text{total}} + \text{MgO})$ versus $\text{SiO}_2$ , after Frost et al. (2001).....	32
Figure 4.7 Whole-rock trace element spidergram. Trace element concentrations are normalized to global average upper continental crust (Rudnick and Gao, 2003). The samples from the west body are depleted in Ba, Sr, Eu, Cu, Cr, Co, V and enriched in LREE, Zr and Hf. The samples from the east body have similar trends to andesitic arc rocks in the Andes (with $\text{SiO}_2 = 57\text{--}63\%$ and $\text{Sm/Yb} = 4\text{--}8$ ). Data for the Andean rocks are from the compilation of GEOROC ( <a href="http://georoc.mpch-mainz.gwdg.de/georoc/Csv_Downloads/Convergent_Margins_comp/ANDEAN_ARC.csv">http://georoc.mpch-mainz.gwdg.de/georoc/Csv_Downloads/Convergent_Margins_comp/ANDEAN_ARC.csv</a> ). (B) Ab-Or-An ternary diagram. The trends of melt composition with water activity are from (Conrad et al., 1988). .....	33
Figure 4.8 Diagram of whole-rock Sm/Yb versus zircon saturation temperature (Hanchar and Watson, 2003) for the Mesozoic granitoids in Zhejiang Province. All age data are zircon U-Pb ages. Data sources: the Dashuang syenite and quartz monzonite (this study), the Jingju syenogranite (Li et al., 2012b), the Wengshan monzogranite (Sun et al., 2011), Cretaceous granitoids (Wong et al., 2011). The inset shows the temperature and pressure conditions for water-saturated melting and dehydration melting, after Sawyer et al. (2011). .....	35
Figure 4.9 Whole-rock geochemical data for Triassic Jingju syenogranite and quartz monzonite (Li, 2010): (A) Sr-Nd isotopic compositions; (B) Gd/Yb ratio versus zircon saturation temperature plot, the data for the 126 Ma Baijuhuajian A-type granite (Wong et al., 2009) are shown here for comparison; (C) ferroan-magnesian granitoid classification (Frost et al., 2001); (D) V/Ti versus V/Co plot; (E) Ga versus $10000 \times \text{Ga}/\text{Al}_2\text{O}_3$ plot; (F) Eu–Sr plot; (G) Trace element patterns normalized to global average upper continental crust (Rudnick and Gao, 2003). .....	39
Figure 4.10 Tectonic model for the South China continental margin during (A) the Early Triassic and (B) the Late Triassic, modified after Li and Li (2007). By the Early Triassic, crust in the Dashuang area had been thickened but did not reach high-enough temperature to produce melts. At the same time, arc-like melts may have been formed in the Dexing area in Jiangxi Province (A). In the Late Triassic, the lower crust of the Dashuang area became hot enough to cause both dehydration melting (the west body) and water-fluxed melting (the east body) (B). At this time, the subduction front propagated further inland to Hunan Province. DX = Dexing, DS = Dashuang, DZ = Danzhu, JN = Jingning, YF = Yangfang.....	40

## List of Figures

- Figure 5.1 (A) Distribution of Mesozoic granitic rocks in the South China Block, modified after Zhou et al. (2006). The oceanward-younging trend of the Jurassic and Cretaceous magmatism is from Li et al. (2013d). PJ: Pujiang basalt; DS: Dashuang quartz monzonite. (B) Major Mesozoic thrust faults in South China. The two components of the South China Block are shown in different colours (Li et al., 2010a). (C) The granitic intrusions in this study and their ages (see Table 5.1 for data sources). The Paleoproterozoic metamorphic basement and Neoproterozoic intrusions are also shown. The Jiang-Shao Fault Zone is the inferred boundary between the Yangtze and Cathaysia blocks..... 44
- Figure 5.2 Field, hand specimen and thin section photographs of the Mesozoic granitic rocks from western Zhejiang Province. All thin section photographs were taken under cross-polarized light. The temperatures shown are zircon saturation temperatures. (A, B): Sheyang syenogranite. A pink alkali feldspar megacryst (microcline) is outlined with dotted line, showing deformation in thin section. Quartz grains (Qz) also show strong deformation, with undulose extinction and recrystallization. (C, D): Wengshan syenogranite. The petrographic characteristics are similar to the Sheyang syenogranite. Pink alkali feldspar megacrysts and medium- to coarse-grained texture are common features of the Triassic granites in Zhejiang Province. (E, F) Tongcun porphyry. The phenocrysts are quartz, alkali feldspar, plagioclase (Pl), calcic clinoamphibole (Amp), biotite (Bt), titanite (Ttn) and hematite (Hem). (G, H) Shangsanzi porphyry. Quartz (Qz) and alkali feldspar (Afs) phenocrysts occur in a fine-grained groundmass and are of similar size. (I, J) Lingkeng syenogranite with a medium-grained texture. Some alkali feldspars show exsolution and quartz shows undulose extinction. (K-P) Huangkang, Tongshan and Shanghekou syenogranites, which are similar to the Lingkeng syenogranite. (Q-T) Jiuhua and Luojia granitic porphyries contain large alkali feldspar (Afs) crystals. Their porphyritic texture and lack of deformation distinguish them from the Triassic syenogranites. Large alkali feldspar phenocrysts distinguish them from the Jurassic porphyries. An alkali feldspar megacryst is outlined with dashed line in Fig. 5.2Q. (U-X) Muchen quartz monzogranite and Matou monzogranite, both of which contain titanite (Ttn), biotite (Bt), calcic clinoamphibole (Amp) and mafic enclaves (MME). ..... 48
- Figure 5.3 (continued over page) ..... 53
- Figure 5.4 (A) Zircon  $\epsilon$ Hf(t) versus zircon U-Pb ages for the Mesozoic granitic rocks in western Zhejiang Province, at 2 standard errors. The Hf isotopic compositions of the Paleoproterozoic crustal rocks of the Cathaysia Block are based on data from Yu et al. (2009) and Xia et al. (2012); the upper limit is constrained by data from Xiang et al. (2008), assuming  $^{176}\text{Lu}/^{177}\text{Hf} = 0.022$  for their amphibolite. The dashed line at 130 Ma

## List of Figures

- is the best estimate of the boundary between the K<sub>1</sub>(I) and K<sub>1</sub>(II) granitic rocks; (B) Age spectrum of detrital zircons with Mesozoic ages in the study region (Cathaysia Block) (Xu et al., 2007); (C) Zircon  $\epsilon$ Hf(t) versus zircon U-Pb ages for the same detrital zircons,  $\epsilon$ Hf(t) values were recalculated with a decay constant of  $1.867 \times 10^{-11} \text{ yr}^{-1}$  (S öderlund et al., 2004). ..... 58
- Figure 5.5 Whole-rock geochemical results for the Mesozoic samples from western Zhejiang Province. All symbols use the same as in Figure 5.5A and “+ Suichang” represents the K<sub>1</sub>(I) samples from the Lingkeng, Huangkang, Sucun, Shanghekou, Yingcun and Wangcun intrusions: (A) K<sub>2</sub>O versus SiO<sub>2</sub>; (B) molar K<sub>2</sub>O/Na<sub>2</sub>O and Al<sub>2</sub>O<sub>3</sub>/(CaO+Na<sub>2</sub>O+K<sub>2</sub>O); (C) FeO<sub>total</sub>/ (FeO<sub>total</sub> + MgO) versus SiO<sub>2</sub>, after Frost and Frost (2011); (D) Sm/Yb ratio versus age; (E) Sm/Yb ratio versus zircon saturation temperatures, based on Böhnke et al. (2013), excluding the mantle-derived K<sub>1</sub>(III) rocks and assuming M = 1.6 (Miller et al., 2003) for the altered J<sub>2-3</sub> samples. ..... 60
- Figure 5.6 Trace element patterns of the Mesozoic granitic samples from western Zhejiang Province, normalized to the global average continental upper crust (Rudnick and Gao, 2003). All data represent average composition. (A) T<sub>3</sub> granites; (B) J<sub>2-3</sub> porphyries; (C) K<sub>1</sub>(I) granitic rocks; (D) K<sub>1</sub>(II) porphyries; (E) K<sub>1</sub>(III) granites; (G) A comparison of the average of the different stages..... 62
- Figure 5.7 Magnetic susceptibility versus age plot for the Mesozoic samples from western Zhejiang Province. The boundary between the magnetite and ilmenite series granitoids is from Ishihara et al. (2000). ..... 65
- Figure 5.8 (A) Zircon  $\epsilon$ Hf(t) of seven samples from the Muchen Complex, with filled dots representing the average values. Samples MC-1 and MC-2 are from (Liu et al., 2011a). Note that there is no significant change in their initial Hf isotopic compositions. (B) REE distribution patterns for the six samples in this study, showing a general increasing trend in REE contents with SiO<sub>2</sub> and a MREE peak in the mafic enclave. (C) Whole-rock Dy/Yb versus SiO<sub>2</sub> plot for the Muchen Complex, including all the previously published data (Lu, 2007; Liu et al., 2011a; Liu et al., 2013a). A decrease in Dy/Yb with increasing SiO<sub>2</sub> indicates fractional crystallization of amphibole..... 71
- Figure 5.9 Comparisons between the K<sub>1</sub>(III) mafic (A) and intermediate (B) rocks in the study area and those from other active continental margins that likely underwent flat-slab subduction (Moll-Stalcup and Arth, 1989; Kay and Gordillo, 1994; Lipman, 2004; Lipman, 2006). The data for the average continental arc basalt and the Pujiang basaltic andesite are from Kelemen et al. (2003) and Qin (2007), respectively..... 73
- Figure 5.10 Tectonic model for southeastern China during the Mesozoic, modified after Li and Li (2007) and Li et al. (2012d). (A) Permian: normal subduction and arc magmatism (Li et al., 2006; Li et al., 2012c). (B) T<sub>3</sub>: flat-slab subduction caused the

## List of Figures

thickening of the continental crust in Zhejiang Province and dehydration melting in the lower crust. Fluids and hydrous silicate melts released from the flat slab caused mantle metasomatism and some local crustal water-fluxed melting (Zhu et al., 2013). (C) J <sub>2-3</sub> : foundering of the eclogitic flat slab caused water-fluxed melting of the oxidized and hydrous continental crust. (D) K <sub>1</sub> (I-II): extension and, possibly delamination, of the continental lithosphere generated large amounts of felsic igneous rocks from crustal dehydration melting. (E) K <sub>1</sub> (III): melting of the hydrous and enriched continental lithospheric mantle.....	77
Figure 6.1. Geological map of NE Jiangxi Province, modified after JGS (1984). All the ages are zircon U-Pb dating results (ion probe or LA-ICP-MS). Names of plutons and their data sources: Ehu syenogranite (Jiang et al., 2011b); Zhushahong, Tongchang, Fujiuwu porphyries (Wang et al., 2006; Liu et al., 2012b; Zhang et al., 2013); Yinshan porphyries (Wang et al., 2012a); Damaoshan-Huaiyushan syenogranite-alkali feldspar granite (Jiang et al., 2011b; Zhou et al., 2013 and this study); Lingshan syenogranite (Zhou et al., 2013); Wancunxiang syenogranite-alkali feldspar granite (this study); Yongping porphyries (Ding et al., 2005; Zhu et al., 2008; Li et al., 2013c) and Lengshuikeng porphyries (Su et al., 2013a; Wang et al., 2013a).....	81
Figure 6.2 Photographs of field and hand specimens from the Early Cretaceous granitic rocks in northeastern Jiangxi Province. (A) Sample 10ZJS154 is a Lingshan syenogranite with rapakivi texture; (B) an outcrop of Lingshan syenogranite showing a mafic enclave; (C) a contact between a mafic enclave and its host granite; (D) a Lingshan granite outcrop without rapakivi texture; (E) a Damaoshan-Huaiyushan syenogranite-alkali feldspar granite outcrop; (F) a contact between the Wancuanxiang syenogranite (sample 10ZJS171) and Carboniferous limestone, which were altered to endoskarn and marble, respectively. ....	82
Figure 6.3 Thin section photographs of the Early Cretaceous granitic rocks from northeastern Jiangxi Province (XL: cross-polarised light; PPL: plane-polarised light). (A) Lingshan alkali feldspar granite; (B) Lingshan syenogranite; (C and D) Lingshan syenogranite with rapakivi texture; (E and F) Lingshan syenogranite hosting the MMEs. Mineral abbreviations: Afs, alkali feldspar; Per, perthite; Pl, plagioclase; Qz, quartz; Bt, biotite; Ttn, titanite; Hbl, hornblende; Ap, apatite; Ms, muscovite; Mag, magnetite; Ep, epidote. ....	83
Figure 6.4 Zircon CL images, age and Hf isotopic results for the Early Cretaceous granitic rocks from northeastern Jiangxi Province: (A-C) Lingshan syenogranite; (D-E) Wancunxiang syenogranite-alkali feldspar granite; (F) Damaoshan-Huaiyushan syenogranite-alkali feldspar granite. On the concordia diagrams, the spots represented by dotted grey ellipses (2 SD) were excluded from the calculation of the mean age ...	86

## List of Figures

Figure 6.5 Geochemical data for Mesozoic granitoids in northeastern Jiangxi Province: (A) K <sub>2</sub> O versus SiO <sub>2</sub> (Peccerillo and Taylor, 1976); (B) εNd(t) versus age; (C) Ferroan-magnesian granitoid classification (Frost et al., 2001); (D) Gd/Yb versus age; (E) V/Co and V/Sc; (F) Eu versus Sr. In contrast to the Cretaceous granites, Eu is dominantly trivalent in Jurassic porphyries and does not follow Sr <sup>2+</sup> . The hydrothermal alteration did not change the horizontal Eu–Sr pattern. (G) The trace element patterns were normalised to the global average of the upper continental crust (Rudnick and Gao, 2003)	90
.....	
Figure 7.1 (A) Distribution of Mesozoic intrusions in Zhejiang Province. The location of the Ganzhou-Hangzhou rift zone is based on Wang et al. (2006) and Yang et al. (2012). Data sources for the 135–130 Ma intrusions from the Ganzhou-Hangzhou rift zone: 1-Tonglu complex (Zhou et al., 1999; Griffin et al., 2002; Wong et al., 2011), 2-Huajiatang granite (Wong et al., 2011), 3-Majian rhyolite/dacitic porphyry (Wong et al., 2011), 4-Hecun dacitic-rhyolitic porphyry (this study), 5-Hongling granitic porphyry (this study), 6-Shuangcai andesitic-dacitic porphyry (this study), 7-Zhujiexiang andesitic porphyry (this study), 8-Mugua dolerite (Li et al., 2011a). Data sources for the 120–100 Ma intrusions from northeastern Zhejiang Province: 1-Liangnong complex (Chen et al., 2005b; Yen, 2005; Hsieh et al., 2009; Wong et al., 2011), 2-Beizhang complex (Chen et al., 2005b; Wong et al., 2011), 3-Xiaojiang complex (Yen, 2005; Hsieh et al., 2009; Wong et al., 2011), 4-Ru’ao complex (Dong et al., 2007; this study), 5-Longhuangtang granite (Yen, 2005; Hsieh et al., 2009; Wong et al., 2011), 6-Shantouzheng quartz diorite (Zheng et al., 1990; Chen et al., 1991; Yen, 2005). (B) A simplified geological map of the Qiuwang and Xiepu granite modified after ZGS (1980); data are from Li et al. (2012d) and this study. (C) Simplified geological map of the Shaoxing–Zhuji region, modified using ZGS (1975) data from Xie et al. (2013) and this study. ....	94
Figure 7.2 Thin section photomicrographs (cross-polarised light) of Mesozoic intrusive rocks from northeastern Zhejiang Province and the Ganzhou-Hangzhou rift zone: (A) Qiuwang granite; (B) Xiepu granite; (C) Guangshan granite; (D) Jiangzao granite; (E) Yujiashan diorite; (F) Hecun dacitic-rhyolitic porphyry; (G) Zhujiexiang andesitic porphyry; (H) Ru’ao monzodiorite. Mineral abbreviations: Afs, alkali feldspar; Pl, plagioclase; Qz, quartz; Bt, biotite; Ms, muscovite; Chl, chlorite; Cpx, clinopyroxene; Ep, epidote.....	95
Figure 7.3 (continued over page) .....	98
Figure 7.4 Whole-rock geochemical data for the Qiuwang and Xiepu granites: (A) trace element patterns normalised to the average for the upper continental crust (Rudnick and	

## List of Figures

Gao, 2003); (B) plot of the Gd/Yb versus zircon saturation temperature; (C) plot of V/Co versus V/Sc.....	103
Figure 7.5 Whole-rock geochemical data for the Jiangzao and Guangshan granites: (A) trace elements normalised to the average for the upper continental crust (Rudnick and Gao, 2003); (B) plot of the Gd/Yb ratios versus zircon saturation temperatures; (C) plot of the V/Co ratio versus Ti/V.....	104
Figure 7.6 Whole-rock geochemical data for the Zhaxi and Yujiashan (quartz) diorites: (A) trace element patterns normalised to the primitive mantle (McDonough and Sun, 1995); (B) plot of SiO <sub>2</sub> -K <sub>2</sub> O (Peccerillo and Taylor, 1976); (C) plot of FeOt/(FeOt+MgO) versus SiO <sub>2</sub> (Frost et al., 2001); (D) plot of Gd/Yb versus V/Co; (E) plot of Al <sub>2</sub> O <sub>3</sub> versus SiO <sub>2</sub> .....	107
Figure 7.7 Selective whole-rock geochemical data for the Early Cretaceous intrusions and volcanic rocks of the Ganzhou-Hangzhou rift zone (135–130 Ma) and northeastern Zhejiang Province (120–100 Ma): (A) plot of FeOt/(FeOt+MgO) versus SiO <sub>2</sub> ; (B) plot of Gd/Yb versus SiO <sub>2</sub> ; (C) plot of Y versus SiO <sub>2</sub> ; (D) plot of Al <sub>2</sub> O <sub>3</sub> versus SiO <sub>2</sub> ; (E) plot of Eu/Eu* versus SiO <sub>2</sub> ; (F) plot of V/Co versus V/Ti plot. The oxygen fugacity and pressure conditions for the FeOt/(FeOt+MgO) evolution trends are from Osborn (1979, p. 156). The Eu/Eu* = 2Eu <sub>N</sub> / (Sm <sub>N</sub> × Gd <sub>N</sub> ) <sup>0.5</sup> (Rudnick and Fountain, 1995), normalised to CI carbonaceous chondrites (McDonough and Sun, 1995).....	108
Figure 7.8 Plots of FeOt/(FeOt+MgO) versus SiO <sub>2</sub> for the Early Cretaceous intrusions and volcanic rocks from the Ganzhou-Hangzhou rift zone and northeastern Zhejiang Province with symbol sizes representing the elemental content or ratios: (A) V/Ti; (B) V/Co; (C) Y; (D) Gd/Yb. Note that a low FeOt/(FeOt+MgO) ratio is generally associated with a low Y content and high Gd/Yb ratio.....	109
Figure 8.1 Map of South China showing the Mesozoic magmatic provinces discussed in Chapters 5, 6 and 7 (yellow) and this chapter (grey). .....	111
Figure 8.2 Distribution of Jurassic-Cretaceous granitic intrusions in eastern South China. 1: Jiuhua-Qingyang granitic complex (Xu et al., 2010; Su et al., 2013b); 2: Huayuangong granite (Li et al., 2012a); 3: Gunuijiang syenogranite (Xie et al., 2012a); 4: Huangshan-Taiping granitic complex (Su et al., 2013b); 5: Jingde granodiorite (Zhang et al., 2012b); 6: Fuling syenogranite (Zhou et al., 2013); 7: Xiyuan granodioritic porphyry (Li et al., 2013b); 8: Dongyuan granodioritic porphyry (Li et al., 2013b); 9: Jingtongya granodiorite; 10: Kaobeijian granodiorite; 11: Xiaoyao granodiorite (Zhou et al., 2012b; Li et al., 2013b). .....	112
Figure 8.3 Whole-rock geochemical data for the Mesozoic granitoids from southern Anhui Province. Data source as for Figure 8.2. (A) plot of K <sub>2</sub> O versus SiO <sub>2</sub> (Peccerillo and Taylor, 1976); (B) plot of molar Al <sub>2</sub> O <sub>3</sub> / (Na <sub>2</sub> O + K <sub>2</sub> O) versus molar Al <sub>2</sub> O <sub>3</sub> / (Na <sub>2</sub> O +	

## List of Figures

- K<sub>2</sub>O + CaO); (C) plot of whole-rock Gd/Yb ratio versus age, which decreased from the Late Jurassic to Early Cretaceous; (D) plot of the whole-rock Y content versus age, which increased during the Early Cretaceous; (E) plot of zircon saturation temperatures versus age, which increasing values after ~130 Ma; (F) plot of the whole-rock V/Ti ratio versus age, which significantly decreased after ~130 Ma; (G) the trace element patterns were normalised to the global average for the upper continental crust (Rudnick and Gao, 2003)..... 113
- Figure 8.4 Whole-rock geochemical data for the granitic rocks from Anji County, northern Zhejiang Province: (A) trace element patterns normalised to the global average for the upper continental crust (Rudnick and Gao, 2003); (B) plot of the Gd/Yb ratio versus age; (C) plot of the V/Co ratio versus V/Sc; (D) plot of the zircon saturation temperature versus age; (E) plot of FeOt/(FeOt + MgO) versus age (Frost et al., 2001). Data sources: Tang et al. (2012a), Tang et al. (2012b), Xie et al. (2012b), Xie et al. (2012c) and Tang et al. (2013)..... 114
- Figure 8.5 Distribution of granitoids in central Hunan Province. Data sources for labelled intrusions: Taojiang granite (Wang et al., 2012b), Weishan granite (Chen, 2006), Tangshi granite (Wang et al., 2007b), Xiangzikou granite (Wang et al., 2007b), Baimashan granite (Chen et al., 2007; Qiu et al., 2014), Xiema granite (Wang et al., 2007b), Yajiangqiao granite(Chen, 2006), Wawutang granite (Wang et al., 2007b), Guandimiao granite (Wang et al., 2007b), Wufengxian granite (Wang et al., 2007b), Xitian monzogranite (Yao et al., 2013)..... 116
- Figure 8.6 Whole-rock geochemical data for the Mesozoic granitoids from central Hunan Province. Data source as for Figure 8.5. (A)  $\varepsilon$ Nd(t) versus age; (B) Ferroan-magnesian classification (Frost et al., 2001); (C) Gd/Yb versus age; (D) V/Co versus age; (E) trace element patterns normalised to the global average for the upper continental crust (Rudnick and Gao, 2003) ..... 117
- Figure 8.7 Distribution of granitoids in central Jiangxi Province. Data sources for labelled intrusions: Mengshan granite (Zhong et al., 2011), Caijiang granite (Zhao et al., 2013a), Jintan monzogranite (Li, 2011; Zhao et al., 2013b), Daguzhai-Huangpi granite (Zhao et al., 2011b), Hukeng granite (Liu et al., 2008), Xiangshan dacitic volcanic-plutonic complex (Yang et al., 2010), Antang OIB-like basalt (Wang et al., 2008b)..... 118
- Figure 8.8 Whole-rock geochemical data for the two Jintan granite units. Data source as for Figure 8.7. (A)  $\varepsilon$ Nd(t) versus age; (B) FeOt/(FeOt+MgO) versus age; (C) Gd/Yb versus age; (D) V/Co versus age. Data sources: Li (2011) and Zhao et al. (2013b) ..... 118
- Figure 8.9 Whole-rock geochemical data for Mesozoic granitoids from central Jiangxi Province. Data source as for Figure 8.7. (A) Ferroan-magnesian classification (Frost et

## List of Figures

- al., 2001); (B) Gd/Yb versus age; (C) V/Co versus age; (D)  $\varepsilon$ Nd(t) versus age. Data source: Zhao et al. (2013b)..... 119
- Figure 8.10 Distribution of Mesozoic granitoids and volcanic rocks in Fujian Province, modified after Ma (2007) and Sun (2006). 1-Gaoxi monzogranite (Zhao et al., 2013a); 2-Dayinchang monzogranite (Wang et al., 2013b); 3-Luoguyan granite (Xiang et al., 2013); 4-Shaxi granite (Li et al., 2010b); 5-Hongshan-Fucheng granite (Zhao et al., 2004; Zhao et al., 2006; Ren et al., 2013); 6-Guikeng granite (Mao et al., 2011); 7-Zijishan syenogranite (Zhao, 2007); 8-Caixi granite (Zhao, 2007); 9-Guanyang and Zengkeng monzogranite (Sheng et al., 2013); 10-Wuping granite (Yu et al., 2005); 11-Dayang syenogranite (Yue, 2008; Zhang et al., 2012a); 12-Juzhou syenogranite (Zhang et al., 2012a); 13-Sifang and Luoboling (porphyritic) granodiorite (Zhang et al., 2012a); 14-Jintonghu quartz syenitic porphyry (Wu et al., 2013); 15-Ermiaogou dacitic porphyry (Li et al., 2013a). ..... 120
- Figure 8.11 Whole-rock geochemical data for the Mesozoic granitoids in western Fujian Province. Data source as for Figure 8.10. (A) ferroan-magnesian granitoid classification (Frost et al., 2001); (B) plot of Gd/Yb versus age; (C) plot of V/Co versus age; (D) plot of  $\varepsilon$ Nd(t) versus age; (E) trace element patterns (median of each group) normalised to the global average for the upper continental crust (Rudnick and Gao, 2003). ..... 121
- Figure 8.12 Whole-rock geochemical data for the Mesozoic intrusions and volcanic rocks in Eastern Fujian-Guangdong Province. Data source as for Figure 8.10. (A) Plot of K<sub>2</sub>O versus SiO<sub>2</sub>; (B) plot of  $\varepsilon$ Nd(t) versus SiO<sub>2</sub>. The Nd isotopic composition of the granitoids is comparable to those from the enriched lithospheric mantle in Zhejiang Province (Hsieh et al., 2009). (C) Plot of V/Co versus age; (D) plot of V/Sc versus age; (E) plot of Gd/Yb versus age; (F) Ferroan-magnesian granitoid classification (Frost et al., 2001) with circles representing the V/Sc ratio; (G) Trace element patterns for samples with SiO<sub>2</sub> >60% normalised to the average upper continental crust (Rudnick and Gao, 2003). ..... 123
- Figure 8.13 Distribution of granitoids in the Nanling Range, modified after Ma (2007). Intrusions without age or geochemical data are not shown. Data sources: Yangmingshan granite (Chen et al., 2006; Wang et al., 2007b), Qingxi monzogranite (Yu et al., 2012b), Yingqian granodiorite (Guo et al., 2010), Baoshan granodioritic porphyry (Hunan Province) (Xie, 2013), Wangxianling granite (Zheng and Guo, 2012), Hehuaping porphyritic granite (Zhang et al., 2010), Taoxikeng granite (Guo et al., 2011), Baoshan granite (Jiangxi Province) (Guo et al., 2011), Huangshaping porphyritic granite (Zhang et al., 2010), Qitianling granite (Zhu et al., 2005b; Fu et al., 2006), Jiufeng granite (Huang, 2012), Jiulongnao granite (Guo et al., 2011), Xihuashan

## List of Figures

- granite (Guo et al., 2012a), Tongshanling granite (Wei et al., 2007; Jiang et al., 2009), Jinjiling granite-alkali feldspar granite (Jiang et al., 2009), Xishan granite-dacite-rhyolite complex (Fu et al., 2004; Jiang et al., 2009; Huang et al., 2011a), Beitou granite (Chen et al., 2005a), Keshubei granite (Huang et al., 2014), Yuanlingzhai granitic porphyry (Huang et al., 2014), Dadongshan granite (Huang et al., 2008), Longyuanba granite (Tao et al., 2013), Zhaibei granite (Li et al., 2003a), Huashan complex (Gu et al., 2006; Zhang et al., 2011), Reshui monzogranite (Deng et al., 2011), Luxi-Xiaozhuang granite (Chen et al., 2012)..... 124
- Figure 8.14 Whole-rock geochemical data for the Mesozoic granitoids in the Nanling Range.  
Data source as for Figure 8.13. (A) plot of  $K_2O$  versus  $SiO_2$  (Peccerillo and Taylor, 1976); (B) the ferroan-magnesian granitoid classification (Frost et al., 2001); (C) plot of  $Gd/Yb$  versus age; (D) plot of  $V/Co$  versus age; (E) plot of Eu versus Sr, which shows the evolution trends for samples with differing  $V/Co$  ratios; (F) plot of Eu versus Sr, which shows the evolution trends for samples with different stages..... 125
- Figure 8.15 Whole-rock Nd and zircon Hf isotopic compositions for the Mesozoic granitoids in the Nanling Range. Data source as for Figure 8.13. Comparing  $J_2$  porphyries (blue) to  $J_3$  high-temperature A-type granites (yellow), the former have more negative zircon  $\varepsilon_{Hf}(t)$  but less negative  $\varepsilon_{Nd}(t)$  values. The abbreviations used in the boxplot: Q1 (lower quartile), Q2 (median), Q3 (upper quartile), IQR (interquartile)..... 126
- Figure 8.16 Whole-rock geochemical data for some Jurassic-Early Cretaceous mantle-derived plutonic-volcanic rocks. (A) Ferroan-magnesian granitoid classification (Frost et al., 2001); (B) plot of  $V/Co$  versus  $SiO_2$ ; (C) plot of V versus Ti (Shervais, 1982); (D) plot of  $Gd/Yb$  versus  $SiO_2$ . Data source: Anjishan diorite-granodiorite (Xu et al., 2002; Zeng et al., 2013a); Liangnong Complex (Chen et al., 2005b; Hsieh et al., 2009; Wong et al., 2011); Pujiang basalt-andesite (Qin, 2007); Muchen Complex (Lu, 2007; Liu et al., 2013a; this study), Huashan-Tong'an-Niumiao Complex (Zhu et al., 2005a; Gu et al., 2006; Zhang et al., 2011)..... 127
- Figure 8.17 Simplified geological map of Hong Kong (Civil Engineering and Development Department, Hong Kong, <http://www.cedd.gov.hk>). Data sources: Derbyshire and Sewell (1997), Sewell and Campbell (1997), Wong (2006) and personal communications with Dr. R.J. Sewell (Geotechnical Engineering Office, Civil Engineering and Development Department, Hong Kong)..... 129
- Figure 8.18 Whole-rock geochemical data for the Mesozoic granitoids from Hong Kong.  
Data source as for Figure 8.17. (A) whole-rock  $Gd/Yb$  ratio versus age, with decreasing trend from the Triassic to the Jurassic/Cretaceous; (B) whole-rock Y content versus age, with increasing trend from the Triassic to Jurassic/Cretaceous; (C) ferroan-magnesian granitoid classification (Frost et al., 2001); (D) whole-rock  $V/Sc$  ratio versus age, with

## List of Figures

decreasing trend from the Jurassic to Cretaceous; (E) diagram of $\varepsilon\text{Nd(t)}$ versus $^{87}\text{Sr}/^{86}\text{Sr}_i$ ; (F) trace element discrimination diagram (Pearce et al., 1984); (G) trace element patterns normalised to the global average for the upper continental crust (Rudnick and Gao, 2003).....	130
Figure 8.19 Evolution of the Mesozoic granitoids in South China. The legend shows their main sources (M: mantle, C: crust), melting/fractionation mechanism and tectonic settings.....	133
Figure 8.20 Tectono-petrogenetic cartoon for the six-stages of Mesozoic granitoids in South China.....	135

## List of Figures

### List of Tables

Table 1.1 The M-I-S-A classification of granitoids.....	8
Table 3.1 Count and delay time for zircon SHRIMP analyses .....	20
Table 5.1 Name, GPS coordinates, lithology, U-Pb isotopic age, Hf isotope, mineral assemblage, magnetic susceptibility and data source of granitoids in the study region	46
Table 6.1 Locality, lithology, age and Hf isotope of Jurassic ( <b>bold</b> ) and Cretaceous granitoids and intermediate-felsic volcanic rocks from northeastern Jiangxi Province.....	89
Table 7.1 REE patterns of Early Cretaceous dacite and rhyolite from northwestern Zhejiang (the Ganzhou-Hangzhou rift zone) and southeastern Zhejiang, data from ZGS (1989, p. 383) .....	92
Table 7.2 Locality, lithology, age and Hf isotope values for the igneous rocks from northeastern Zhejiang Province and the Ganzhou-Hangzhou rift zone.....	102
Table 8.1 Summary of properties, petrogenesis and tectonic settings of six-stage Mesozoic granitoids in South China.....	134

## Chapter 1 Introduction

### 1.1 Background

South China is characterised by widespread Mesozoic granitic rocks. They are predominantly high-K or shoshonite series with crust-like isotopic characteristics related to a mature continental crust. Therefore, the Mesozoic magmatism was an important crustal reworking event in South China.

There is a consensus that the paleo-Pacific Plate subducted under the South China Block (SCB) during the Mesozoic, and that the subduction was at least partially responsible for the granitic magmatism (Jahn et al., 1990; Zhou and Li, 2000). Nevertheless, the question remains as to when this subduction began. The answer varies from the Permian (Li and Li, 2007) to the Jurassic (Zhou et al., 2006) or the Cretaceous (Chen et al., 2008). In addition, the geometry and mechanics of the subduction zone are also a topic of debate. The key to resolving these issues is to understand the petrogenesis of the widespread Mesozoic magmatic rocks in the region, particularly that of the Jurassic–Early Cretaceous "arc-like" high-K calc-alkaline granitoids. The current petrogenesis models include formation in a continental magmatic arc (Charvet et al., 1994; Lapierre et al., 1997; Zhou et al., 2006; Li et al., 2014a), and partial melting of the continental lithosphere metasomatised by previous subduction, similar to the Oligocene calc-alkaline rocks of the North American Cordillera (Davis and Hawkesworth, 1993).

Granitic magmas are generally considered to be formed in the continental crust by partial melting and/or fractional crystallisation (Klein and Philpotts, 2013). Theoretically, infinite types of granitic rocks exist due to complex source-temperature-pressure-H<sub>2</sub>O-redox conditions and differentiation processes in the crust. Despite these observations, it has been recognised that igneous rocks produced at a given time in a specific region commonly exhibit certain similarities in terms of their mineral and geochemical characteristics (Bowen, 1928). Therefore, it is possible to build links between properties of granitoids, conditions of melting or fractionation, and sources and tectonic settings of granitoids.

It is a challenge to link the various petrological and geochemical properties of granitic rocks to the sources, processes and tectonic settings that produced them. One popular approach was first proposed by Chappell and White (1974) and emphasizes the sources of granitic rocks as a key factor that controls their characteristics. This approach originally classified granites into two types: I-type (from igneous source rocks) and S-type (from sedimentary source rocks). Such a classification is intrinsically independent of tectonic processes. This scheme has been further developed into the I-S-A-M-H classification scheme in which "A" indicates anorogenic (Loiselle and Wones, 1979), "M" represents "mantle-

derived”, and “H” denotes “hybrid” types (Castro et al., 1991). Although this classification scheme is useful, the different types may overlap. For instance, S-type granite can also be classified as A-type granite, and highly felsic I-type granites generally have an A-type affinity. Another approach is to analyse tectonic environments using trace element discrimination diagrams, such as those proposed by Pearce et al. (1984). Although many of these diagrams have gained immense popularity, as Pearce et al. (1984) pointed out in their original paper, “*the fields on the discriminant diagrams strictly reflect source regions (and crystallisation histories) rather than tectonic regimes*”. Therefore, the direct usage of such diagrams for tectonic environment analyses requires caution, especially for granitoids generated in complex tectonic settings (e.g., flat-slab subduction). Yet a third approach focuses on physico-chemical conditions, i.e., the role and sources of water, temperature and pressure in granite petrogenesis (Whitney, 1988; Miller et al., 2003; Bachmann and Bergantz, 2008). Variations of these conditions in a specific region through time reflect transitions of regional tectonic regimes. This is the main approach adopted in this study.

## 1.2 Classification of granitoid

Granite (*sensu stricto*) is defined by a restricted range of quartz-plagioclase-alkali feldspar proportions (Figure 1.1). Granitoid loosely describes silicic quartz-feldspathic plutonic rocks (Winter, 2010), which are a prevalent and major component of the continental upper crust. The main rock-forming minerals are quartz and feldspar and, therefore, granitoids have a lower density and melting point than mafic rocks. Granitic magmatism is therefore critical for the growth and differentiation of the continental crust (Hawkesworth and Kemp, 2006) and is also an important aspect for understanding tectonic processes.

### 1.2.1 Mineralogical classification

Mineralogical classification methods are the most traditional schemes and are based on optical microscopic determination of the modal composition and texture of a granitoid.

#### 1.2.1.1 QAP classification

This classification system is based on the relative modal proportions of quartz, alkali feldspar and plagioclase (recalculated to 100%, Figure 1.1). The nomenclature in this thesis is based on the QAP classification.

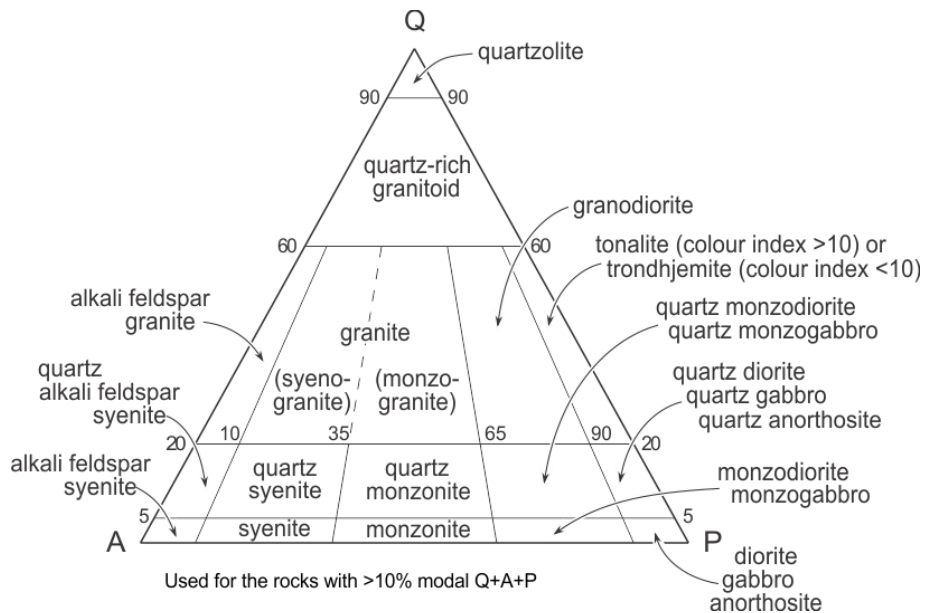


Figure 1.1 Quartz-alkali feldspar-plagioclase modal classification of plutonic rocks (Streckeisen, 1974).

### 1.2.1.2 Opaque oxide classification

This two-fold classification system is primarily based on the Fe-Ti oxides in the granitoids. Their mineral assemblages are listed below, after Ishihara (1977).

*Magnetite-series:* Magnetite (0.1-2 vol.%), ilmenite, hematite, pyrite, titanite, epidote, high  $\text{Fe}^{3+}/\text{Fe}^{2+}$  (and high Mg/Fe) biotite associated with porphyry copper-molybdenum deposits.

*Ilmenite-series:* Ilmenite (less than 0.1 vol.%), pyrrhotite, graphite, muscovite, low  $\text{Fe}^{3+}/\text{Fe}^{2+}$  (and low Mg/Fe) biotite associated with greisen-type tin-tungsten deposits.

Ishihara (1977) suggested that the magnetite-series granitoids are formed under higher oxygen fugacity conditions (with higher  $\text{Fe}^{3+}/\text{Fe}^{2+}$ ) than the ilmenite-series granitoids, and the boundary between the two series was proposed to lie in the Ni-NiO buffer. For the ilmenite-series granitoids, Ishihara (1977) stressed the importance of carbon (graphite)-bearing materials (perhaps as the host rock) in their petrogenesis; however, the magnetite-series granitoids were proposed to be generated in the lowest crust or mantle and did not interact with C-bearing rocks. Clemens and Bea (2012) maintain that the high ferric/ferrous ratios of magnetite-series granitoids are inherited from the source(s). The magnetite series and ilmenite series can be similar to I-type (igneous rock as source material) and S-type (sedimentary rock as source material), respectively. This classification method can also be applied based on the measurement of the rock magnetic susceptibilities (Ishihara et al., 2000; Ishihara, 2004).

### 1.2.1.3 Hypersolvus and subsolvus classification

This two-fold classification is used for a lime-free system and is based on the crystallisation behaviours of alkali feldspars (Tuttle and Bowen, 1958). Hypersolvus granites are characterised by the occurrence of two separate alkali feldspar components, which is associated with low water pressure. Subsolvus granites are characterised by the occurrence of single alkali feldspar or perthite, which is associated with high water pressure. Therefore, the water fugacity in the magmas will influence the texture of alkali feldspars. The hypersolvus granites will be generated under low pressure or drier crystallisation conditions.

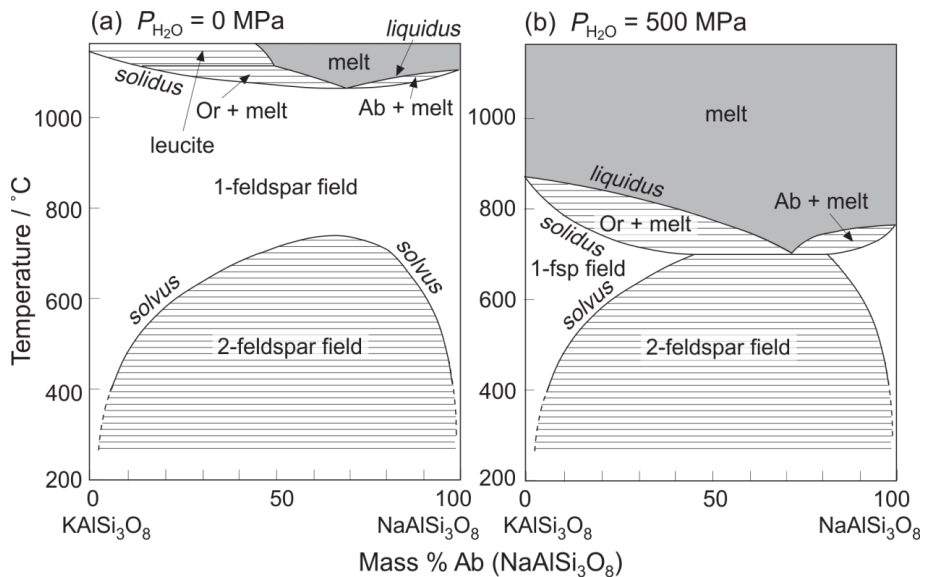


Figure 1.2 Phase diagrams for alkali feldspars in hypersolvus (a) and subsolvus (b) granite modified from Gill (2010).

### 1.2.2 Geochemical classification

Geochemical classification is based on the whole-rock major and trace element concentrations.

#### 1.2.2.1 Classification based on Shand's index (A/CNK classification)

This system (Shand, 1947) offers advantages in assessing the additional mineral phases in addition to quartz and feldspar. The A/CNK [molar  $\text{Al}_2\text{O}_3 / (\text{CaO} + \text{Na}_2\text{O} + \text{K}_2\text{O})$ ] is generally used instead of alumina-saturation if the influence of apatite can be neglected. The granitoid is peraluminous if A/CNK is  $>1$  and weakly peraluminous if  $1 < \text{A/CNK} < 1.1$ . The granitoid is peralkaline, if A/NK [molar  $\text{Al}_2\text{O}_3 / (\text{Na}_2\text{O} + \text{K}_2\text{O})$ ] is  $<1$ . The granitoids are metaluminous if A/CNK is  $<1$  and A/NK is  $>1$ .

A/CNK is equal to unity if the granitoids are simply composed of quartz and feldspar. The addition of hornblende and clinopyroxene will decrease the A/CNK to below unity, and mica, garnet, cordierite and aluminosilicate will raise the index above unity. Furthermore, if A/NK is  $<1$ , extra alkalis will enter the amphibole and pyroxene to form aegirine, riebeckite,

etc. Chappell and White (1974) attributed the strongly peraluminous character to sedimentary source rocks and the metaluminous character to igneous source rocks because weathering mobilizes calcium and sodium and increases A/CNK of source rocks .

### 1.2.2.2 Ferroan and magnesian granitoids

This two-fold geochemical classification (Frost et al., 2001; Frost and Frost, 2008; Frost and Frost, 2011) is based on the relative concentration of Fe to Mg (Figure 1.3), which is a variation of the tholeiitic/calc-alkaline classification (Tilley, 1950) for granitoid. The boundary line between ferroan and magnesian granitoids is defined as  $\text{FeO}_{\text{total}}/(\text{FeO}_{\text{total}} + \text{MgO}) = 0.446 + 0.0046 \text{ wt.\% SiO}_2$ . The significance of this classification, as Frost et al. (2001) proposed, is to constrain the redox condition of magmatism. Under oxidising conditions, fractionation of magnetite will prohibit iron enrichment, thus forming magnesian granitoids. In contrast, ferroan granitoids are formed under reducing conditions. However, based on the work of Tuttle and Bowen (1958), highly fractionated granitoids should appear as ferroan granitoids despite the redox conditions. Frost et al. (2001) showed that most Mesozoic granitoids from the North America Cordillera are magnesian, except for some high  $\text{SiO}_2$  samples. In contrast, most granitoids from intraplate environments are ferroan granitoids.

Pressure is another factor that prohibits iron enrichment by stabilising garnet and magnetite (Osborn, 1979; Pitcher, 1997). Therefore, generation of magnesian Cordilleran-type (Andean-type) granitoids is likely facilitated by both high melting/fractionation pressure and high oxygen fugacity.

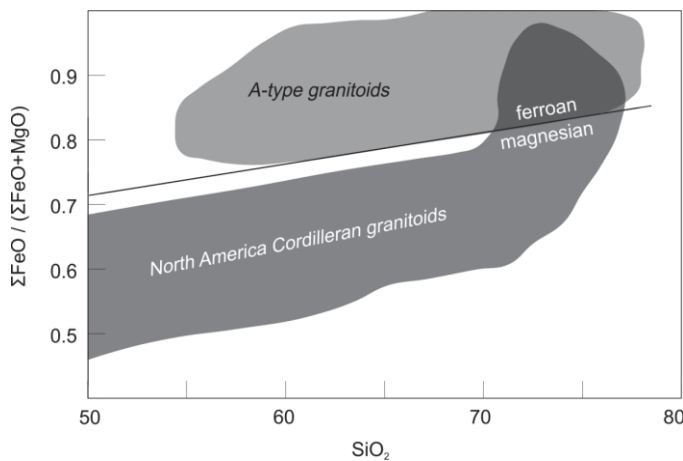


Figure 1.3  $\text{FeO}_{\text{total}}/(\text{FeO}_{\text{total}}+\text{MgO})$  versus  $\text{SiO}_2$  diagram showing ferroan-magnesian granitoid classification (Frost et al., 2001).

### 1.2.2.3 $\text{SiO}_2\text{-K}_2\text{O}$ classification

This three-fold classification scheme (Figure 1.4) was designed for volcanic rocks (Le Maitre, 2002) but can also be applied to granitoids, e.g., Roberts and Clemens (1993).

Because it is generally agreed that plutonic and volcanic rocks are simply different in texture because of formation at different depths, the same genetic model can be used for both types of rocks. For this thesis, I restrict the discussion to active continental margins only. It has been observed by Kuno (1959) that the concentration of  $K_2O$  in a lava increases with distance from the Wadati-Benioff zone and therefore from the trench. Such a relationship holds true for most arc systems (Tatsumi and Eggins, 1995). Several mechanisms have been proposed for such a phenomenon (Tatsumi and Kogiso, 2003), e.g., continental crustal thickness, source compositions, and degrees of partial melting. With respect to the reasons for different degrees of partial melting, Tatsumi and Eggins (1995) suggested that “variation in the depth of magma segregation from mantle diapirs, possibly corresponding to variable depth to the lithosphere/asthenosphere boundary, may result in differing degrees of partial melting and determine overall incompatible element concentrations in subduction zone magmas”. However, Gill (1981) suggested the degree of melting is primarily controlled by water, which has greater flux near the trench.

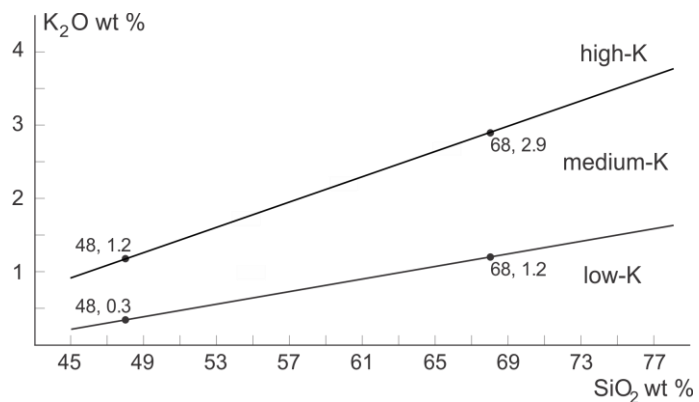


Figure 1.4  $K_2O$ - $SiO_2$  classification for granitoids (Le Maitre, 2002).

#### 1.2.2.4 Alkalic-calcic classification

The four-fold classification scheme shown in Figure 1.5 is a variation of Peacock (1931). It was given by Frost et al. (2001) based on the relationship between  $SiO_2$  and  $Na_2O + K_2O - CaO$ . This classification was proposed by Frost et al. (2001) to assess the pressure of differentiation, crustal assimilation and fluid mechanism.

#### 1.2.3 Chemical-tectonic-genetic classification

There are many attempts to link chemical and isotopic compositions to tectonic and/or genetic significance through classification (Barbarin, 1990; Barbarin, 1999). Although such chemical-tectonic-genetic classifications are often equivocal and oversimplified (Clarke, 1992, p. 14), they are useful in many cases because they are empirically made from high-quality database of granitoids from known and common tectonic settings. They are probably

not valid for granitoids from complicated, less common or controversial tectonic settings, i.e., flat-slab subduction at active continental margins.

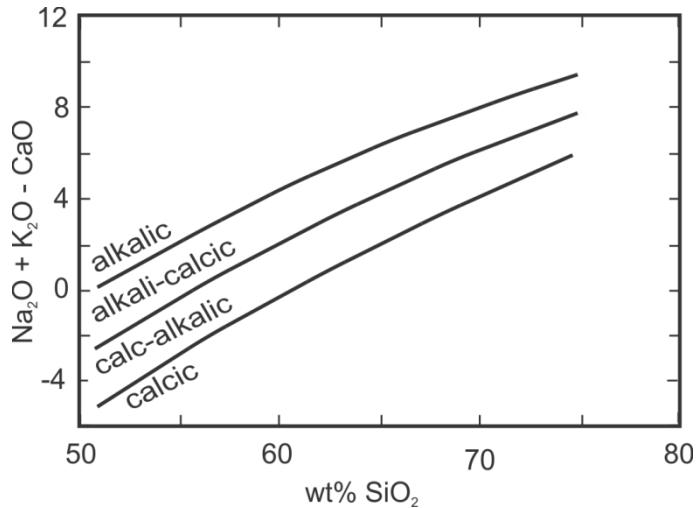


Figure 1.5 Plot of  $\text{Na}_2\text{O} + \text{K}_2\text{O} - \text{CaO}$  versus  $\text{SiO}_2$  showing the boundaries between alkalic, alkali-calcic, calc-alkalic, and calcic granitoids.

### 1.2.3.1 M-I-S-A classification

The most comprehensive chemical-genetic classification scheme for granitoid is the M-I-S-A classification. Chappell and White (1974) first introduced the concepts of I-type and S-type granite and proposed that I-type granite was derived from crustal igneous source rocks and that S-type granite was derived from crustal sedimentary source rocks. Next, the M-type (mantle-derived, White, 1979) was introduced for those granites that originated from partial melting of subducted oceanic crust. A-type granite was introduced by Loiselle and Wones (1979) to describe those granites that formed in anorogenic tectonic settings based on tectonics rather than source. An H-type (hybrid-type) was also defined that describes granitoids from multiple sources (Castro et al., 1991). The main characteristics of M-I-S-A granites are listed in Table 1.1, modified after Winter (2010, p. 385).

### 1.2.3.2 Geochemical discrimination diagrams

In this scheme, the granitoids are classified into several groups based on their major or trace element compositions that empirically discriminate between the tectonic environment(s). The two most popular schemes are those of Batchelor and Bowden (1985) and Pearce et al. (1984), as shown in Figure 1.6 and Figure 1.7, respectively. These diagrams are empirically constructed based on large data sets for which the tectonic settings are well known.

Table 1.1 The M-I-S-A classification of granitoids.

Type	M-type	I-type	S-type	A-type
$\text{SiO}_2$	46–70%	53–76%	65–74%	High–77%
$\text{K}_2\text{O}/\text{Na}_2\text{O}$	Low	Low	High	$\text{Na}_2\text{O}$ high
Ca, Sr	High	High	Low	Low
Alumina-saturation	Metaluminous	Metaluminous to weakly peraluminous	Strongly peraluminous	Variable
$\text{Fe}^{3+}/\text{Fe}^{2+}$	Low	Moderate	Low	Variable
Cr, Ni	Low	Low	High	Low
$\delta\text{O}^{18}$	<9‰	<9‰	>9‰	Variable
$^{87}\text{Sr}/^{86}\text{Sr}$	<0.705	<0.705	>0.707	Variable
Other trace elements	Low Rb, Th, U, LILE and HFSE	High LILE/HFSE, medium Rb, Th, U	Variable LILE/HFSE, high Rb, Th, U	Low LILE/HFSE, high Fe/Mg, Ga/Al, REE, Zr, F and Cl
Source	Mantle or oceanic crust	Crustal igneous rock	Crustal sedimentary rock	Variable
Typical tectonic setting	Island arc and mid-oceanic ridge	Continental arc	Continental collision zone	Rift, anorogenic stage

LILE = large-ion lithophile elements; HFSE = high field strength elements; REE = rare earth element.

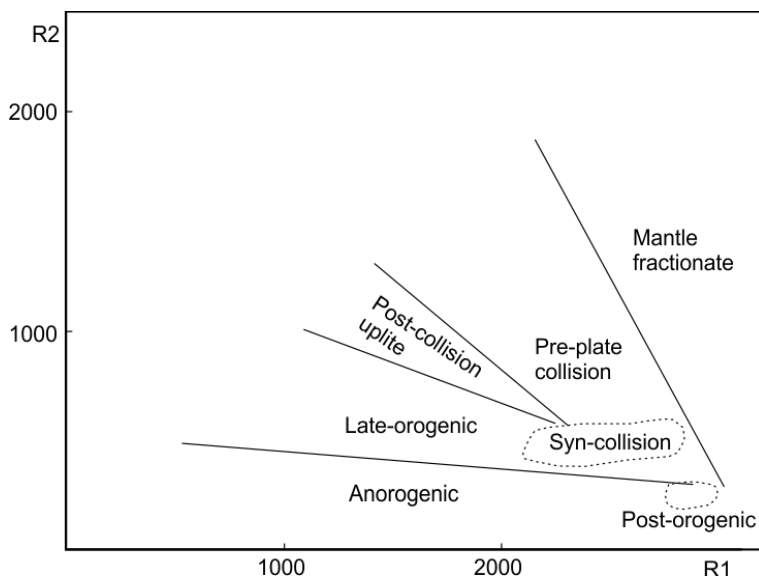


Figure 1.6 The R1–R2 tectonic discrimination diagram for granitoids based on whole-rock major elemental composition (Batchelor and Bowden, 1985).  $R1 = 4\text{Si} - 11(\text{Na} + \text{K}) - 2(\text{Fe} [\text{total as bivalent}] + \text{Ti})$ ,  $R2 = 6\text{Ca} + 2\text{Mg} + \text{Al}$ , all in millications. Millication of element  $i = 1000 \times \text{number of } i \text{ atoms in its oxide} \times \text{oxide}_i \text{ (wt.\%)} / \text{molecular weight of the oxide}_i$ .

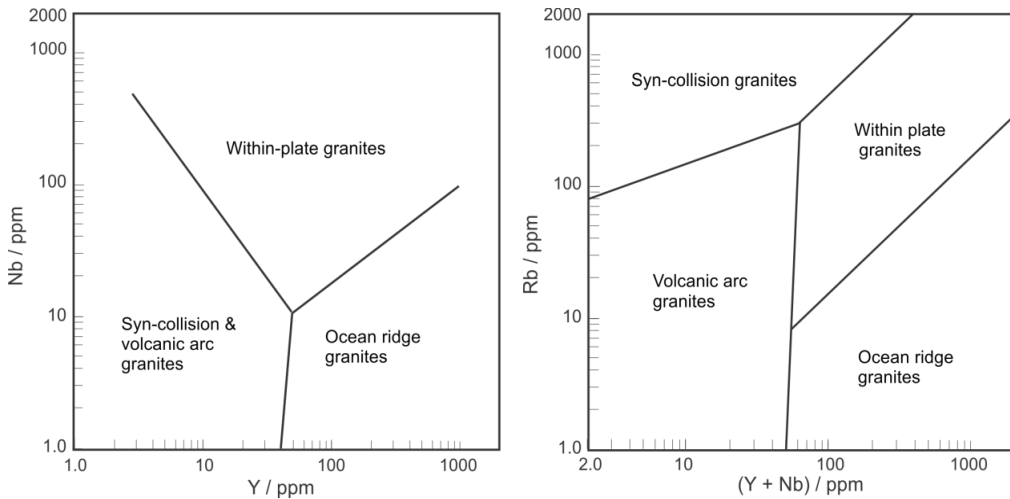


Figure 1.7 Tectonic discrimination diagrams of granitoids based on whole-rock trace element composition (Pearce et al., 1984).

### 1.3 Objectives

This study has the following objectives:

- To investigate and analyse representative Mesozoic granitoids and related mafic rocks in eastern South China (Zhejiang and northeastern Jiangxi provinces);
- To reveal their evolution in terms of age, rock texture, magnetic susceptibility and geochemical composition;
- To establish a workable tectono-petrogenetic model for South China in the Mesozoic.

### 1.4 Dissertation Structure

Chapter 1 introduces the background and objectives of the study, the structure of the dissertation and the classification schemes of granitoids. Chapter 2 reviews the geological setting and history of the South China Block, the geology of the study region and the tectonic and magmatic evolution of typical active continental margins (western North America and the Andes). Chapter 3 details the analytical procedures. Chapters 4–7 detail the characteristics of the Mesozoic granitoids in the study region (Zhejiang and northeastern Jiangxi provinces). Chapter 4 reports on the Late Triassic quartz monzonite and syenite/syenogranite complex in central Zhejiang Province, part of which has been published as Zhu et al. (2013). Chapter 5 discusses the Mesozoic granitoids in western Zhejiang Province, which has been published as Zhu et al. (2014). Chapter 6 discusses the Mesozoic granitoids in northeastern Jiangxi Province. Chapter 7 reports and compares Mesozoic granitoids in northeastern Zhejiang Province and the adjacent Ganzhou-Hangzhou rift zone. Chapter 8 discusses Mesozoic granitoids in other regions of the South China Block. Chapter 9 presents the conclusions.

## Chapter 2 Geological Background

### 2.1 Geological setting and pre-Mesozoic tectonic evolution of South China

As shown in Figure 2.1, East Asia is composed of several tectonostratigraphic terranes derived from the Indian-west Australian margin of eastern Gondwana, and South China is one of the large terranes (Metcalfe, 2013). Between these terranes, volcanic arcs and accretionary complexes were generated by convergent plate tectonic processes during the Paleozoic and Mesozoic (Metcalfe, 2013). South China was amalgamated to the North China Block by the Qinling-Dabie-Sulu Orogeny (Li and Li, 2007), collided with the Qiang-Tang Block along the Longmenshan belt (Li and Li, 2007) and was separated from the Indochina Block by the Song Ma suture zone (Metcalfe, 2013).

South China itself is composed of two blocks (Yangtze and Cathaysia, Figure 2.2), and its tectonic evolution is summarised in Figure 2.3. The Yangtze and Cathaysia blocks amalgamated along the Sibao (Jiangnan) Orogenic Belt during the Neoproterozoic (Li et al., 2009). The Precambrian basement preserved in the Cathaysia Block is represented by the Paleoproterozoic Badu Complex exposed in southwestern Zhejiang Province (Yu et al., 2009). The northwestern border of the Cathaysia Block in Zhejiang and Jiangxi provinces is the Pingxing-Jiangshan-Shaoxing fault zone (Figure 2.2). The Yangtze Block contains Archean remnants represented by the Kongling Complex (Gao et al., 2011). After its amalgamation in the Neoproterozoic, South China was influenced by a ~825 Ma mantle plume (Li et al., 2003b; Wang et al., 2007a), which resulted in the formation of the Nanhua rift and bimodal magmatism (Li et al., 2008). Another tectonic model for such magmatism is that it resulted from back-arc extension caused by oceanic subduction along the northern and western margin of the Yangtze Block (Zhao et al., 2011a). The Ordovician–Silurian Wuyi-Yunkai orogeny caused strong intracontinental shortening and anatexis, but the driving forces for this orogeny remain unclear (Li et al., 2010a).

### 2.2 Previous studies on Mesozoic granitoids in South China and various tectonic models

Gao (1936) was one of the first to recognise the existence of Late Mesozoic granitoids in South China, i.e., the Tonglu Complex and Tongshan granite in Zhejiang Province. Xu et al. (1963) divided the Mesozoic granitoids of South China into two stages (Indosinian and Yanshanian), and reported their characteristics and relationships to mineral deposits. Many more studies followed, but it was only in the past two decades that a rapid accumulation of high-quality age and geochemical data took place (Li et al., 2007). The temporal-spatial

evolution of Mesozoic granitoids was compiled and reviewed by Zhou and Li (2000), Sun (2006), Li and Li (2007), Li et al. (2013d) and Mao et al. (2013a), as shown in Figure 2.4.

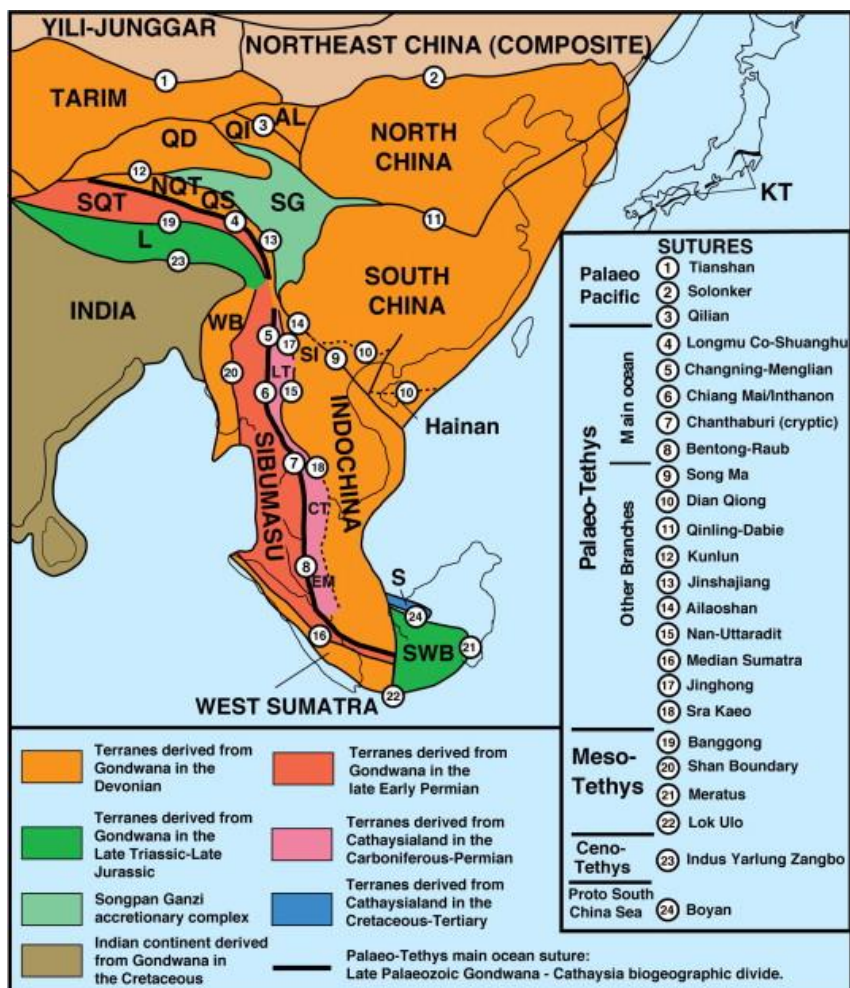


Figure 2.1 Schematic map showing the major tectonostratigraphic terranes and sutures (Metcalfe, 2013). WB = West Burma, SWB = South West Borneo, S = Sematau, L = Lhasa, SQT = South Qiangtang, NQT = North Qiangtang, QS = Qamdo-Simao, SI = Simao, SG = Songpan Ganzi accretionary complex, QD = Qaidam, QI = Qilian, AL = Ala Shan, KT = Kurosegawa Terrane, LT = Lincang arc Terrane, CT = Chanthaburi arc Terrane, EM = East Malaya.

In terms of petrogenetic models for the Mesozoic granitoids of South China, Xu et al. (1982) proposed a three-fold classification: crustal transformation (crustal origin), syntaxis-type (mixed crustal and mantle origin) and mantle-derived granites. In-situ melting of the upper crust was proposed by Chen and Grapes (2003) as the petrogenesis for some Mesozoic granitoids, which is the viewpoint of transformist school. Adakite-like granitoids (low Y and high Sr/Y ratios) are considered by some researchers to be generated in thickened lower continental crust (Xu et al., 2002; Wang et al., 2006). Mafic microgranular enclaves (MMEs) are considered as evidence for magma mixing (Chen et al., 2013a; Liu et al., 2013a). I-type granitoids are considered as arc magmatism (Zhou and Li, 2000). The A-type granites and S-type granites are considered as evidence for crustal attenuation and thickening, respectively (Wang et al., 2007b; Wong et al., 2009; Jiang et al., 2011b; Sun et al., 2011).

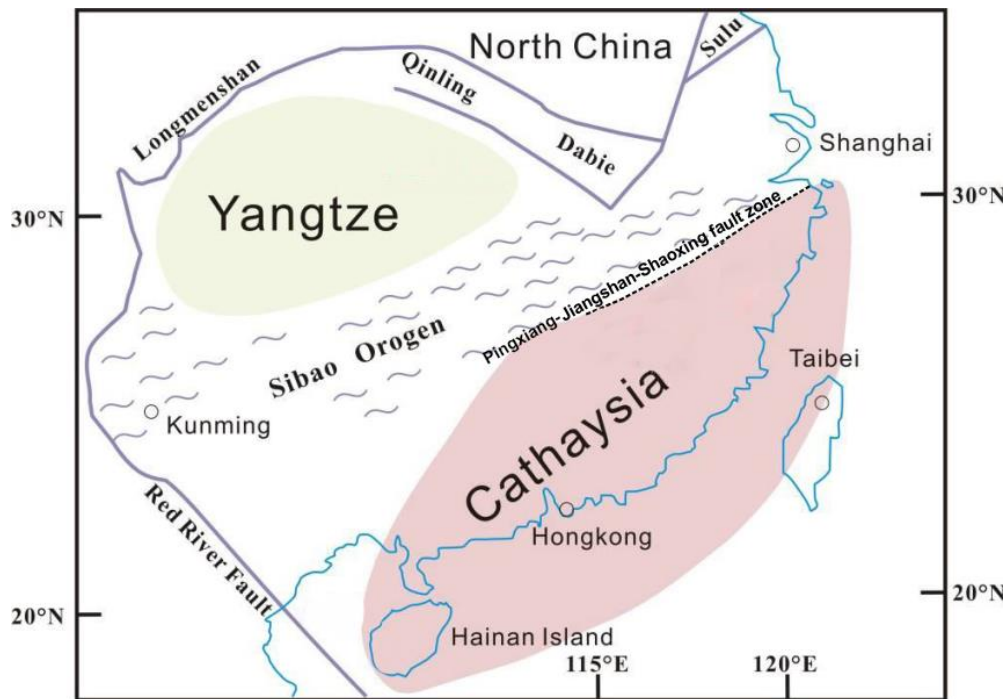


Figure 2.2 Tectonic framework of the South China Block modified after Li et al. (2002).

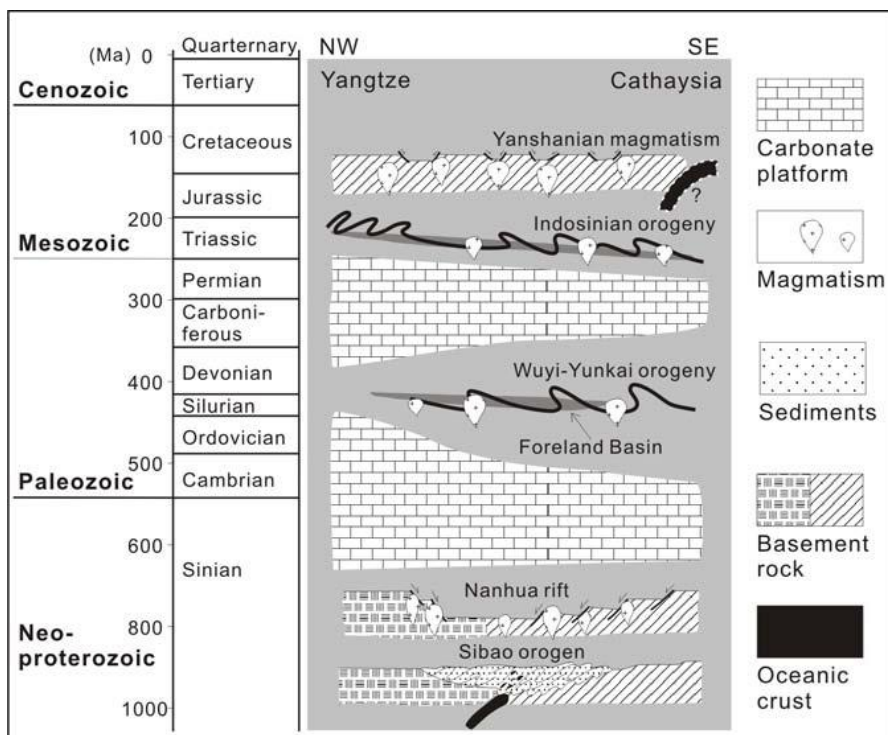


Figure 2.3 Schematic diagram showing the major Neoproterozoic and Phanerozoic tectonic events in the South China Block (Li et al., 2014b).

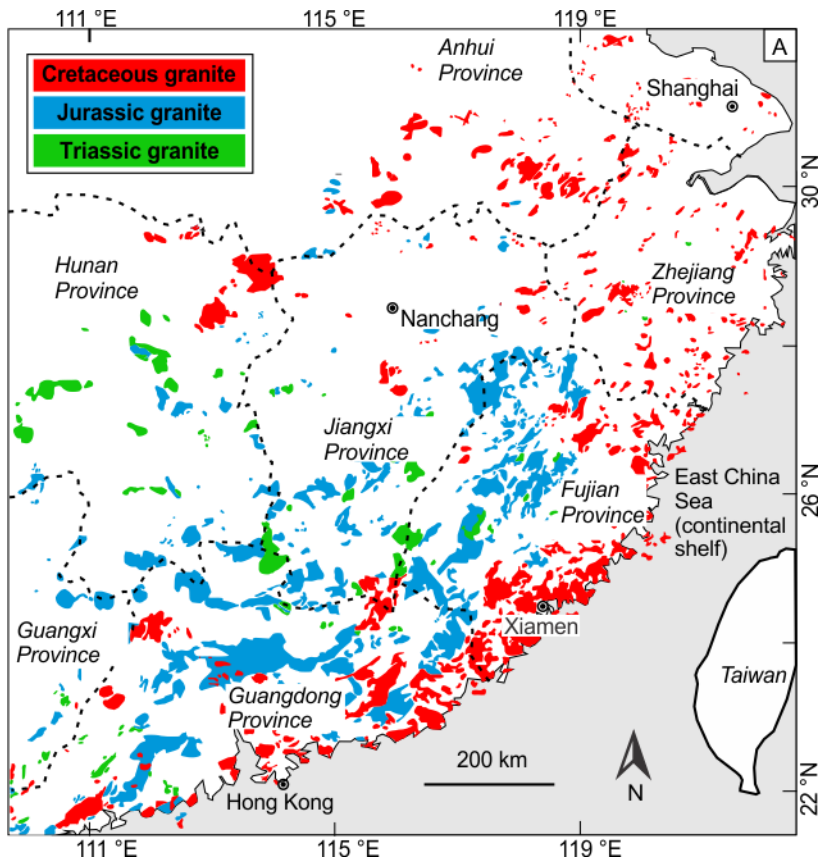


Figure 2.4 Distribution of Mesozoic granitic rocks in the South China Block modified after Zhou et al. (2006).

In terms of tectonic models, the mechanical and chemical influences from the paleo-Pacific plate were emphasised (Cui and Li, 1983; Zhou et al., 2006; Li and Li, 2007; Chen et al., 2008; Chu et al., 2012); however, there is no consensus on when subduction began and how it influenced the overriding South China Block. Some researchers emphasised the influence of the Triassic South China-Indochina collision (Zhou et al., 2006; Wang et al., 2007b). Others attributed these Mesozoic granitoids to the Paleozoic-Triassic (rather than the Neoproterozoic) amalgamation between the Yangtze and Cathaysia blocks (Hsü et al., 1988; Xiao and He, 2005). A Triassic mantle-plume model was proposed to explain the heat source for crustal melting in South China (Xu et al., 2013).

### 2.3 The geology of the study area

A simplified geological map of Zhejiang Province is shown in Figure 2.5. The Paleoproterozoic Badu Complex is distributed in the southwest of Zhejiang Province (Cathaysia Block) and is composed of biotite schist, biotite-plagioclase gneiss, amphibolite and granulite intruded by Paleoproterozoic granitoids. The Neoproterozoic Longquan Complex in the Cathaysia Block includes marble, amphibolite, biotite-plagioclase granulite, mica schist and biotite-plagioclase schist. The Chencai metamorphic complex consists of greenschist- to amphibolite-facies metavolcanic rocks, metapelites and marbles, with the

area having undergone several stages of magmatism, sedimentary deposition and metamorphism from the Paleoproterozoic to the Paleozoic (Li et al., 2010a).

To the northwest of the Jiangshan-Shaoxing fault zone (Figure 2.5), the Neoproterozoic Shuangxiwu Complex is primarily composed of mafic-intermediate lava and pyroclastic rocks. The Paleozoic strata are mostly distributed to the northwest of the Jiangshan-Shaoxing fault zone, and are composed of limestone, dolomite, mudstone and sandstone. The Triassic strata to the northwest of the Jiangshan-Shaoxing fault zone consist of limestone, dolomite and shale, and those to the southeast of the fault zone (Cathaysia Block) are composed of conglomerate, sandstone and carbonaceous shale. Jurassic strata include conglomerate, sandstone, siltstone, mudstone and carbonaceous shale. The Early Cretaceous strata are primarily composed of intermediate-felsic lavas and pyroclastic rocks; however, conglomerate, sandstone and mudstone become predominant in the Upper Cretaceous sequence. The Tertiary strata are distributed in the northeast of Zhejiang Province and include mudstone, sandstone, limestone, dolomite and basalt. The strata of northeastern Jiangxi Province are comparable to those of western Zhejiang Province (cf. Section 6.1).

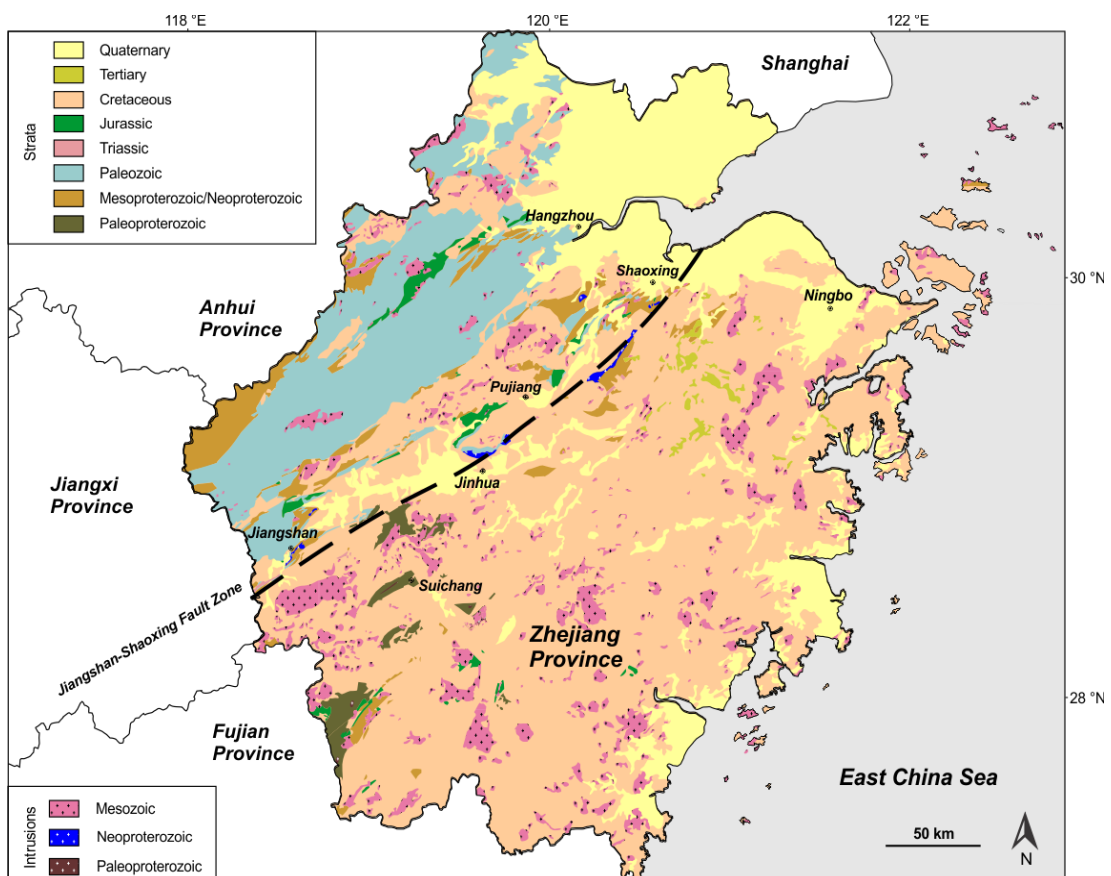


Figure 2.5 Simplified geological map of Zhejiang Province modified after the 1:500000 geological map of ZGS (1989).

## 2.4 Tectonic and magmatic processes under flat-slab subduction conditions

Because the working hypothesis for the Mesozoic tectonic mechanism in South China is flat-slab subduction of the paleo-Pacific plate, flat-slab subduction processes in western North America and the Andes are reviewed in this section.

### 2.4.1 Western North American flat-slab subduction

Late Jurassic-Tertiary deformation and magmatic events in western North America from eastern California to Colorado are generally attributed to the subduction of the Farallon Plate (Coney and Reynolds, 1977; Livaccari et al., 1981). The subduction process caused significant deformation in areas located as far as 1500 km away from the trench. The mountain-building processes have been divided into two stages: the Sevier Orogeny and the Laramide Orogeny. The two orogenies overlap to some extent both in time and location (Willis, 1999). Compared with the earlier Sevier Orogeny, the Laramide Orogeny has an eastward shift. Most deformation in the Sevier Orogeny occurs as thin-skinned thrusts in the Paleozoic and Mesozoic sedimentary rocks, but the Laramide deformation involved "basement-cored" uplifts (Dumitru et al., 1991; DeCelles, 2004). During the Sevier Orogeny, the subduction of the Farallon Plate produced normal continental arc magmas, i.e., the Sierra Nevada Batholith and Peninsular Range Batholith. However, during the Laramide Orogeny, the previous Sierran arc became extinct, and arc magmatism swept inland to Colorado and Wyoming. It has been generally accepted that variation of the subduction angle caused the different deformation styles and magmatism, i.e., the angle became notably shallower during the Laramide Orogeny (Figure 2.6).

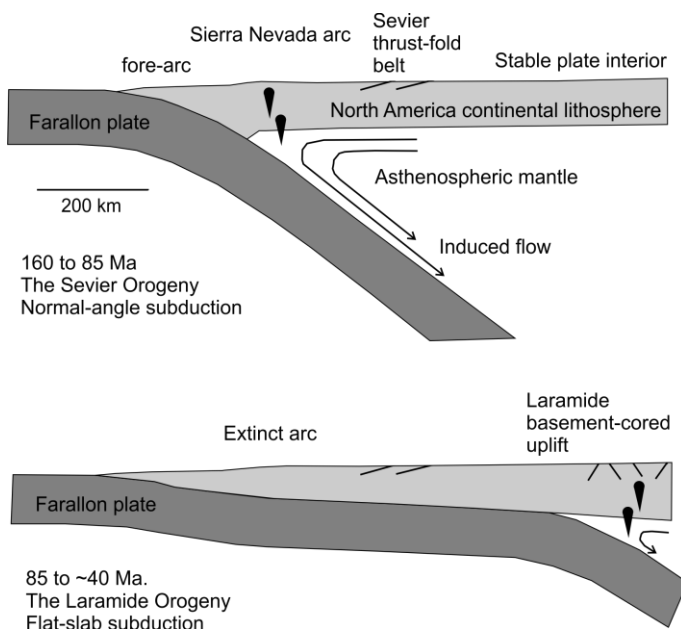


Figure 2.6 A tectonic model for the Sevier and Laramide orogenies in western North America, modified after Dumitru et al. (1991) and DeCelles (2004).

Another important consequence of flat-slab subduction is the geothermal evolution of the continental lithosphere. The crustal thickening during the Laramide Orogeny would have significantly increased the crustal geothermal gradient (Patiño-Douce et al., 1990; Spear, 1995) due to the relatively high radioactive element concentrations in the crust, but the direct interaction between the continental lithosphere and the cold oceanic plate would have exerted a refrigeration effect on the continental lithosphere (Dumitru et al., 1991). Yet a third consequence of flat-slab subduction is metasomatism of the continental lithospheric mantle and lower crust in the hinterland (Stein and Crock, 1990).

#### 2.4.2 Andean flat-slab subduction

The Andes is the largest and most well-known modern orogen developed at an active continental margin. Flat-slab subduction occurred in most segments of the Andes, with the Peruvian flat slab, and the Pampean flat slab as modern examples (Figure 2.7). For the Pampean flat-slab, the subducted Nazca plate had a normal subduction angle between 20–16 Ma. With the subduction angle continually shallowing from 15 Ma to 6 Ma, both the volcanic arc and the thin-skinned thrust front propagated eastward. A basement-cored thrust developed in the Sierra Pampeanas when the continental lithospheric mantle and the oceanic plate were coupled (Ramos et al., 2002).

Ramos (2009) reviewed the subduction processes in the Andes and proposed an Andean-type orogenic cycle for the active continental margin, which includes the initiation of normal-angle subduction and arc magmatism (Figure 2.8A); the development and propagation of the back-arc fold-thrust belt (Figure 2.8B); the shallowing of the subduction angle (because of subduction of an aseismic ridge or oceanic plateau) and the migration of the volcanic arc (Figure 2.8C); flat-slab subduction, strong crustal thickening and eclogitisation; the extinction of the volcanic arc, and metasomatism of the continental lithosphere (Figure 2.8D); the steepening of the oceanic plate and extensional collapse of the orogenic belt (Figure 2.8E); lithospheric delamination and silicic volcanism (Figure 2.8F); and thermal uplift and deformation (Figure 2.8G).

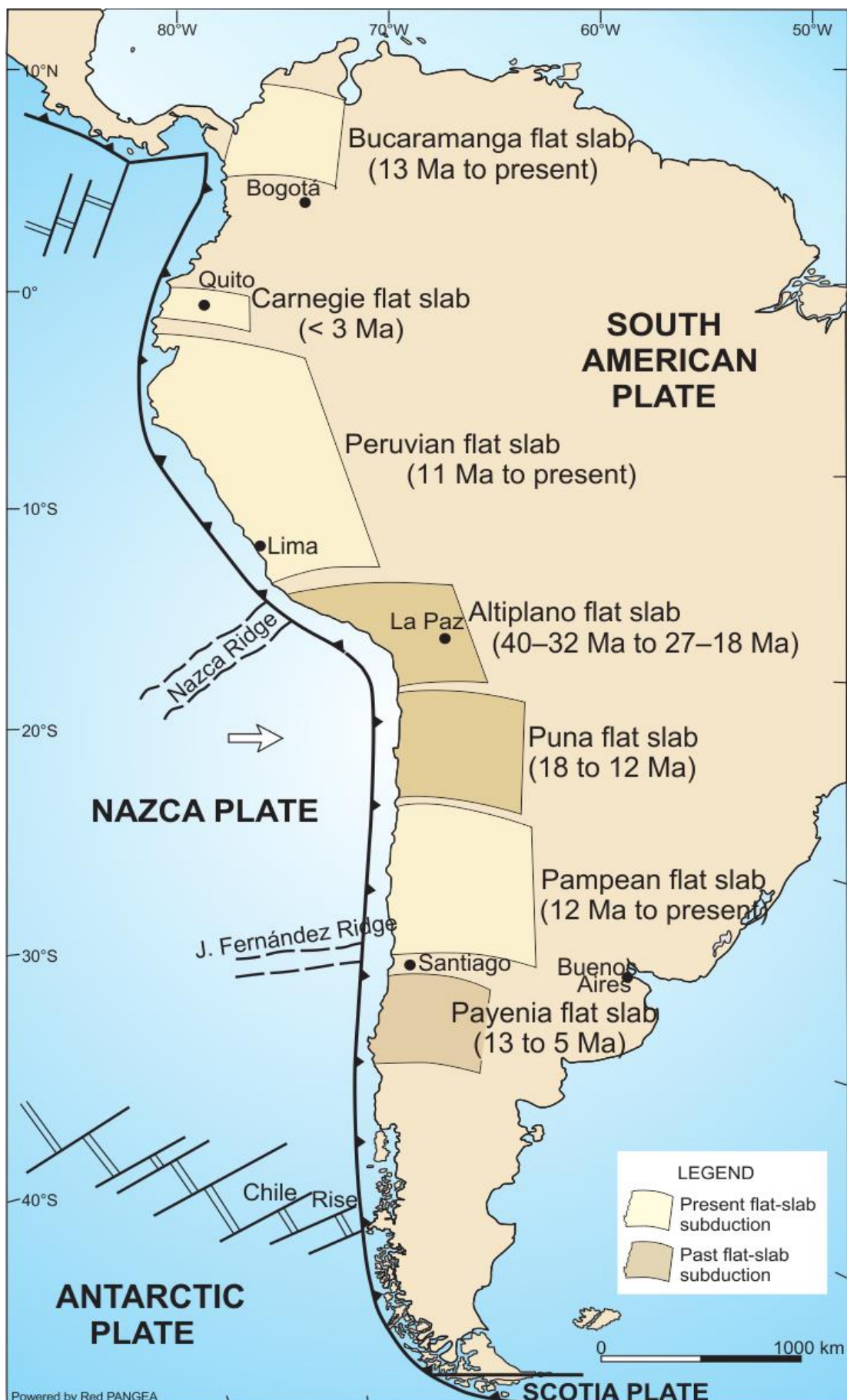


Figure 2.7 Flat-slab subduction throughout the Andes in Cenozoic times, from Ramos (2009).

## ANDEAN OROGENIC CYCLE

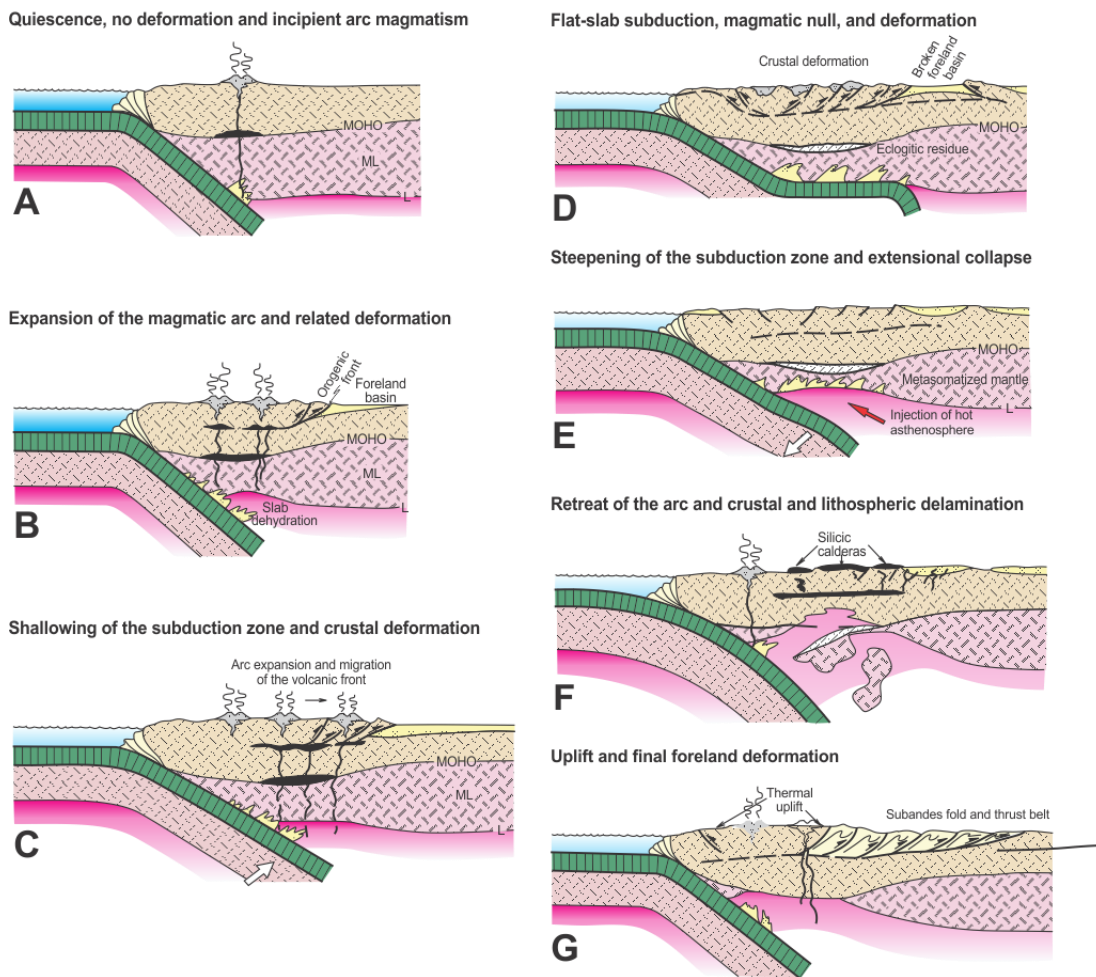


Figure 2.8 Andean orogenic cycle proposed by Ramos (2009).

## Chapter 3 Analytical Methods

### 3.1 Magnetic susceptibility

Magnetic susceptibility measurements were made in the field or undertaken on flat surfaces of the samples, with five or six measurements for each sample, using a Terraplus KT-10 magnetic susceptibility meter. The results are listed in Appendix A with GPS readings measured by a Garmin eTrex H.

### 3.2 Sample preparation

Standard thin sections (0.03 mm) were prepared. Whole-rock powders for chemical analyses were prepared by crushing the cleaned samples to 200-mesh using a ceramic ball mill. Zircons were extracted from separate portions of the original samples by heavy-liquid and magnetic techniques and then hand-picked under a binocular microscope.

### 3.3 Zircon cathodoluminescence imaging

Cathodoluminescence (CL) images were taken using a Phillips XL-30 SEM with a KE Developments CL detector at Curtin University, a Zeiss Evo 40XVP SEM at Curtin University and a JOEL JXA-8100 EPMA with a Gatan Mono CL detector at the State Key Laboratory of Mineral Deposits Research, Nanjing University. The acceleration voltages were 10–12 kV.

### 3.4 LA-ICP-MS zircon U-Pb dating and trace element analyses

The LA-ICP-MS zircon U-Pb and zircon trace element analyses were done on an Agilent 7500a ICP-MS equipped with a New Wave 213-nm laser sampler at the State Key Laboratory of Mineral Deposits Research, Nanjing University. The analyses were conducted with a beam diameter of 32 µm, a 5 Hz repetition rate and an energy of 10–20 J/cm<sup>2</sup>. It took 120 seconds to acquire the data for each analysis (40 s on the background and 80 s on the signal). The raw count rates for <sup>206</sup>Pb, <sup>207</sup>Pb, <sup>208</sup>Pb, <sup>232</sup>Th, and <sup>238</sup>U were collected for age determination. A homogeneous standard zircon, GEMOC/GJ-1 with a TIMS <sup>207</sup>Pb/<sup>206</sup>Pb age of  $608.5 \pm 0.4$  Ma (Jackson et al., 2004), was used to calibrate for mass discrimination and isotope fractionation. Mud Tank zircon with a TIMS <sup>207</sup>Pb/<sup>206</sup>Pb age of  $732 \pm 5$  Ma (Black and Gulson, 1978) was used to monitor the reproducibility and stability of the instrument. Each run included 15–18 analyses that contained 10–12 unknowns, 1–2 Mud Tank zircons, and began and ended with two GJ-1 analyses. Raw mass spectrometric data reduction was carried out using the GLITTER 4.4 program (Griffin et al., 2008). Because <sup>204</sup>Pb cannot be measured, the common lead correction was carried out using the Excel program ComPbCorr#3\_15G (Andersen, 2002). The concentration of U and Th in the zircons was

calculated using a linear relationship of the element concentrations against background-corrected signal count rates compared with that of GJ-1 standard zircon with Th = 8 ppm and U = 330 ppm (Wang et al., 2010). The results are listed in Appendix B.

Trace element analyses were separately conducted on the zircon samples using the same analytical conditions, and  $^{29}\text{Si}$  was used as the internal calibration standard, assuming a stoichiometric composition for zircon with 32.78%  $\text{SiO}_2$ . NIST 612 was used as the external standard. The Ti-in-zircon temperatures were calculated after Ferry and Watson (2007). The results are listed in Appendix C.

### 3.5 SHRIMP zircon U-Pb dating

The zircons were mounted in epoxy resin with zircon standards BR266 (Woodhead et al., 2004), M257 (Nasdala et al., 2008) and Temora 2 (Black et al., 2004). NIST 610/611 was also mounted to detect the  $^{204}\text{Pb}$  peak. The mounts were abraded and polished to reveal the zircon centres. The analyses were done on a Sensitive High Resolution Ion Microrobe (SHRIMP II) at the John de Laeter Centre for Mass Spectrometry at Curtin University. The analytical conditions were 10 kV, a 2–3 nA  $\text{O}^{2-}$  primary beam, a 30- $\mu\text{m}$  diameter spot, and mass resolution of 5200 ( $^{254}\text{UO}$ , 1% peak height). Each analysis included six scans with count and delay times as listed in Table 3.1. The standard zircon BR266 or M257 was used to calibrate the U, Th and Pb isotopic ratios and the U and Th contents. The standard zircon Temora 2 was analysed to monitor reproducibility and instrument stability. The measured  $^{204}\text{Pb}$  was used for the common Pb correction, assuming a Broken Hill Pb isotopic composition ( $^{204}\text{Pb}/^{206}\text{Pb} = 0.0625$ ,  $^{207}\text{Pb}/^{206}\text{Pb} = 0.9618$ ,  $^{208}\text{Pb}/^{206}\text{Pb} = 2.2285$ ). Data reduction was carried out using the SQUID 2.5 (Ludwig, 2009) and Isoplot 3.71 (Ludwig, 2008) programs. The results are listed in Appendix B.

Table 3.1 Count and delay time for zircon SHRIMP analyses

	$^{196}\text{Zr}_2\text{O}$	$^{204}\text{Pb}$	Background	$^{206}\text{Pb}$	$^{207}\text{Pb}$	$^{208}\text{Pb}$	$^{238}\text{U}$	$^{248}\text{ThO}$	$^{254}\text{UO}$
Count time (s)	2	10	10	20	30	10	3	3	2
Delay time (s)	8	4	2	4	2	2	3	3	3

### 3.6 LA-MC-ICP-MS zircon Hf isotopes

In-situ zircon Hf isotopes were analysed with a Thermo Scientific NEPTUNE Plus MC-ICP-MS equipped with a New Wave Research UP-193 FX laser ablation system at Nanjing University or a Nu Plasma multi-collector ICP-MS equipped with a New Wave Research 213-nm laser ablation system at the Institute of Geochemistry, Chinese Academy of Sciences (Guiyang). Helium was used as the carrier gas.

For the Thermo Scientific MC-ICP-MS, the analyses were conducted with spots with 35- $\mu\text{m}$  or 50- $\mu\text{m}$  diameter, 5–8 Hz repetition rate and an energy of approximately 10–15

J/cm<sup>2</sup>. The <sup>172</sup>Yb, <sup>173</sup>Yb, <sup>175</sup>Lu, <sup>176</sup>Hf (with <sup>176</sup>Yb and <sup>176</sup>Lu interferences), <sup>177</sup>Hf, <sup>178</sup>Hf, <sup>179</sup>Hf, and <sup>180</sup>Hf (with <sup>180</sup>W interference) measurements were collected. The isobaric interferences of <sup>176</sup>Lu and <sup>176</sup>Yb on <sup>176</sup>Hf were corrected by applying <sup>176</sup>Yb/<sup>172</sup>Yb=0.5886 and <sup>176</sup>Lu/<sup>175</sup>Lu = 0.02656 (Chu et al., 2002). The mass bias was corrected using the exponential law (Russell et al., 1978)  $R_{\text{true}} = R_{\text{measured}} (M_2/M_1)^f$ , where R is the ratio of the ion beams at masses M<sub>2</sub> and M<sub>1</sub> and f is the mass discrimination coefficient. The mass discrimination coefficient (f) of Hf was calculated from <sup>177</sup>Hf and <sup>179</sup>Hf. The mass discrimination coefficients of Yb and Lu were calculated from <sup>172</sup>Yb and <sup>173</sup>Yb, assuming Yb and Lu have similar mass discriminations. The accepted <sup>172</sup>Yb/<sup>173</sup>Yb ratio of 1.35274 and the <sup>179</sup>Hf/<sup>177</sup>Hf ratio of 0.7325 (Chu et al., 2002) were used as R<sub>true</sub> in the calculations. The standard zircons 91500 and Mud Tank were also analysed to monitor the accuracy and precision of the instruments with analytical <sup>176</sup>Hf/<sup>177</sup>Hf ratios of 0.282320 ± 14 (2 SE, n = 47) and 0.282520 ± 6 (2 SE, n = 66), respectively. These results are consistent with the solution data of Woodhead and Herdt (2005) and the MC-ICP-MS results of Griffin et al. (2006). The initial <sup>176</sup>Hf/<sup>177</sup>Hf ratios were calculated using the measured <sup>176</sup>Lu/<sup>177</sup>Hf ratios and the <sup>176</sup>Lu decay constant of  $1.867 \times 10^{-11} \text{ yr}^{-1}$  (Söderlund et al., 2004). The chondritic values of <sup>176</sup>Lu/<sup>177</sup>Hf = 0.0332 and <sup>176</sup>Hf/<sup>177</sup>Hf = 0.282772 (Blichert-Toft and Albarède, 1997) were used for ε<sub>Hf</sub> calculation.

The Nu Plasma MC-ICP-MS was optimised with a JMC-475 standard solution and a Nu Instruments DSN-100 Desolvating Nebuliser System (a sample introduction accessory). The analyses were conducted on zircons with laser spots of 60-μm diameter, a repetition rate of 10 Hz, an ablation time of 60 s, and laser energy of 0.155 mJ/pulse. The interferences of <sup>176</sup>Lu and <sup>176</sup>Yb on <sup>176</sup>Hf were corrected by applying <sup>176</sup>Yb/<sup>173</sup>Yb = 0.78696 (Thirlwall and Anczkiewicz, 2004) and <sup>176</sup>Lu/<sup>175</sup>Lu = 0.02656 (Chu et al., 2002). The mass bias was corrected using the exponential law. The mass discrimination coefficients of Yb (Lu) and Hf were calculated from <sup>173</sup>Yb/<sup>171</sup>Yb and <sup>179</sup>Hf/<sup>177</sup>Hf. The <sup>173</sup>Yb/<sup>171</sup>Yb and <sup>179</sup>Hf/<sup>177</sup>Hf ratios used in calculations are 1.12346 (Thirlwall and Anczkiewicz, 2004) and 0.7325 (Chu et al., 2002), respectively. The standard zircon 91500 was analysed once every 10 unknowns to monitor the reproducibility and stability of the instrument and yielded a weighted average of <sup>176</sup>Hf/<sup>177</sup>Hf ratio of 0.282308 ± 4 (2 SE). The two-stage depleted mantle model ages (T<sub>DM2</sub>) were calculated assuming that the granitic magmas were derived from an average continental crust with <sup>176</sup>Lu/<sup>177</sup>Hf = 0.015 (Griffin et al., 2002). The results are listed in Appendix D.

### 3.7 XRF whole-rock major elements

Major elements were analysed using XRF. Glass beads were prepared from 1 g whole-rock powders and 11 g lithium metaborate-lithium tetraborate mixtures. Major element analyses were conducted on these fused glass beads using an ARL-9800 X-ray fluorescence

spectrometer at the Centre of Modern Analysis, Nanjing University, with relative standard errors of  $\text{SiO}_2 < 1\%$ ,  $\text{Al}_2\text{O}_3 < 3\%$ ,  $\text{CaO}$ ,  $\text{K}_2\text{O}$ ,  $\text{Fe}_2\text{O}_3$ ,  $\text{TiO}_2 < 5\%$  and  $\text{MgO}$ ,  $\text{Na}_2\text{O}$ ,  $\text{P}_2\text{O}_5$ , and  $\text{MnO} < 10\%$ .

A subset of the samples were analysed using the same procedures by an ARL-9900 X-ray fluorescence spectrometer at the State Key Laboratory of Mineral Deposits Research, Nanjing University. The relative standard errors for  $\text{SiO}_2$  and  $\text{Al}_2\text{O}_3$  are less than 1% and are generally less than 5% for other elements. The results are listed in Appendix E. The geochemical plots were produced by GCDkit (Janoušek et al., 2006), Microsoft Excel 2010, SigmaPlot and OriginPro.

### 3.8 ICP-MS whole-rock trace elements

The whole-rock trace element analyses were done on the ICP-MS method at the State Key Laboratory of Geological Processes and Mineral Resources, China University of Geosciences, Wuhan, or at the State Key Laboratory of Mineral Deposits Research, Nanjing University. The uncertainties lie in the last digit of the reported data based on repeated measurements of samples and standards (BHVO-2, AGV-2, GSR-1, BCR-2 and RGM-1). The results are listed in Appendix E.

The analytical procedures used at the China University of Geosciences, Wuhan, are described as follows:

1. Approximately 50 mg of sample powder was weighed into a Teflon bomb moistened with a few drops of ultrapure water.
2. A total of 1.5 ml  $\text{HNO}_3 + 1.5$  ml HF was added. The sealed bomb was heated to 190 °C in an oven for 48 h.
3. The bomb was opened, and the solution was evaporated to dryness at 115 °C followed by addition of 1 ml  $\text{HNO}_3$  and evaporated to dryness again.
4. The resultant salt was re-dissolved by adding 3 ml of 30%  $\text{HNO}_3$  and was resealed and heated in the bomb at 190 °C for 12–24 h.
5. The final solution was diluted to 100 g with a mixture of 2%  $\text{HNO}_3$  and analysed by an Agilent 7500a ICP-MS.

The analytical procedures at Nanjing University are described as follows:

1. A total of 25 mg of sample was digested with 1 ml HF and 0.5 mL  $\text{HNO}_3$  in a screw high-pressure PTFE-stainless steel bomb at 190 °C.
2. The solution was evaporated to dryness at 120 °C followed by addition of 1 ml  $\text{HNO}_3$  and evaporation at 140 °C to the second round of dryness.

3. The resultant salt was re-dissolved by adding 5 ml of 30% (v/v) HNO<sub>3</sub> and was resealed and heated in the bomb at 140 °C for 4 h.
4. A total of 1 ml of 500 ng/ml Rh solution was added as an internal standard to correct the matrix effect and instrument drift.
5. The final solution was diluted to 50 ml by adding 18 MΩ·cm ultrapure water and analysed by ICP-MS (Element 2, Finnigan MAT).

## Chapter 4 Late Triassic Quartz Monzonite and Syenite/Syenogranite Complex in Central Zhejiang Province

### 4.1 Introduction

The continental lower crust is commonly considered “dry” (Yardley and Valley, 1997). However, underplating by hydrous basaltic-andesitic magma produced in active continental arc settings will release water from the subducting slab, and can cause water-fluxed melting in the crust (Whitney, 1988). At low-temperature conditions, the water can be directly transferred from the subducting slab to the lower crust without triggering melting in the mantle wedge (Wyllie et al., 1989). Both dehydration melting and water-fluxed melting play important roles in granite petrogenesis and crustal reworking (Sawyer et al., 2011).

One important question for the Mesozoic tectonic evolution of the South China Block is when the Paleo-Pacific plate started to subduct beneath it: was it in the Permian (Li et al., 2012c; Li et al., 2012d), the Early Jurassic (Zhou et al., 2006), the Early Cretaceous (Chen et al., 2008), or was there no subduction at all (Hsü et al., 1990)? In this chapter, petrographic, geochemical, zircon U-Pb age, Hf isotope and trace element data for the Triassic Dashuang Complex in eastern South China is used to test if there was evidence for Paleo-Pacific plate subduction at this time, and what caused the different characteristics between the Triassic and Cretaceous magmatism in the region.

### 4.2 Geological setting and petrography

The Dashuang syenite and quartz monzonite complex is located in central-northeast Zhejiang Province, South China (Figure 4.1). It intruded the Chencai metamorphic complex, resulting in contact metamorphism and metasomatism (Wang et al., 1997). The Chencai metamorphic complex consists of greenschist- to amphibolite-facies metavolcanic rocks, metapelites and marbles, with the area having undergone several stages of magmatism, sedimentation and metamorphism from the Paleoproterozoic to the Paleozoic, as described by Li et al. (2010a). Both the Dashuang Complex and the Chencai metamorphic complex are overlain by felsic volcanic rocks of the Early Cretaceous Moshishan Group (Figure 4.1B). The Dashuang Complex is composed of medium-grained syenite in the west and medium- to coarse-grained quartz monzonite in the east, separated by a fault that is followed by Expressway S26. They are referred to here as the west body and the east body, respectively (Figure 4.1B). The syenite underwent greenschist facies metamorphism. Large euhedral pink alkali feldspar crystals are well developed in the east quartz monzonitic body and this petrologic characteristic clearly distinguishes it from the west syenitic body (Figure 4.2A and Figure 4.2C). Wang et al. (1997) reported zircon U-Pb age, geochemical and Sr-Nd-Pb

isotope data for the east body, with zircon U-Pb ages of  $239.6 \pm 0.6$  Ma ( $n = 3$ ),  $\varepsilon_{\text{Nd}}(240 \text{ Ma}) = -12.4$  and  $^{87}\text{Sr}/^{86}\text{Sr}(240 \text{ Ma}) = 0.7115$ . Figure 4.2 shows field and thin section photographs of Dashuang Complex. The west body contains 1–2% quartz, 65–70% alkali feldspar (microcline), 25% plagioclase, ~5% biotite and chlorite. The accessory minerals are zircon, apatite, epidote, ilmenite (with leucoxene alteration) and magnetite. In the west body, ilmenite is primary or altered from ferromagnesian silicates and it is approximately 2–3 times more abundant than magnetite. The east body contains 10–15 % quartz, 40–45% alkali feldspar, 25–30% plagioclase, 15% hornblende + biotite and 1% titanite. The accessory minerals are zircon, apatite, magnetite and sulfides.

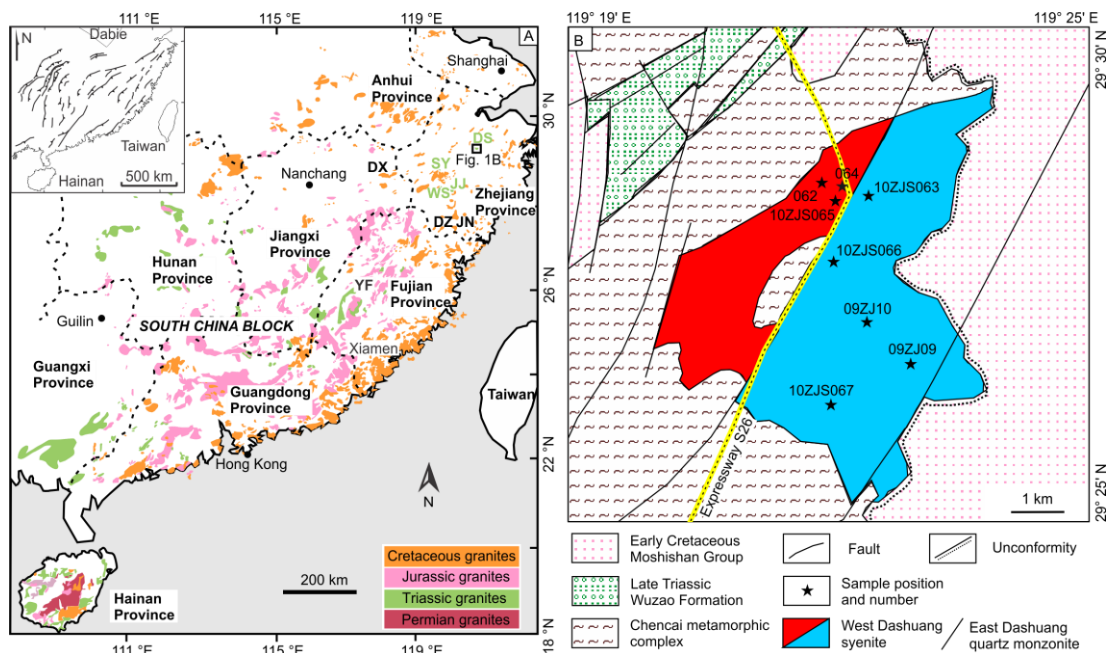


Figure 4.1 (A) Distribution of Mesozoic granitoids in the South China Block, modified after Zhou et al. (2006), Li et al. (2012c) and Jiang and Li (2014). Inset shows mid-Permian to mid-Cretaceous thrusts in South China fold belt, after Li and Li (2007). DS = Dashuang quartz monzonite/syenite; WS = Wengshan syenogranite; SY = Sheyang syenogranite; JJ = Jingjiu monzogranite; DX = Dexing; DZ = Danzhu; JN = Jingning; YF = Yangfang. (B) Geological map of the Dashuang Complex and sample numbers, after ZGS (1975).

### 4.3 Results

#### 4.3.1 Magnetic susceptibility

Magnetic susceptibility results, as well as the total Fe contents of the whole rocks, are shown in Figure 4.3. The measurements from the west body (3 locations) and the east body (5 locations) are  $0.44\text{--}1.15 \times 10^{-3}$  SI and  $2.86\text{--}14.44 \times 10^{-3}$  SI, respectively. The values from the magnetite-dominant east body are higher than those from the ilmenite-dominant west body by around an order of magnitude, indicating higher magma oxygen fugacities of the east body. In the scheme of Ishihara et al. (2000), the west body belongs to the ilmenite series of granitoids and the east body belongs to the magnetite series.

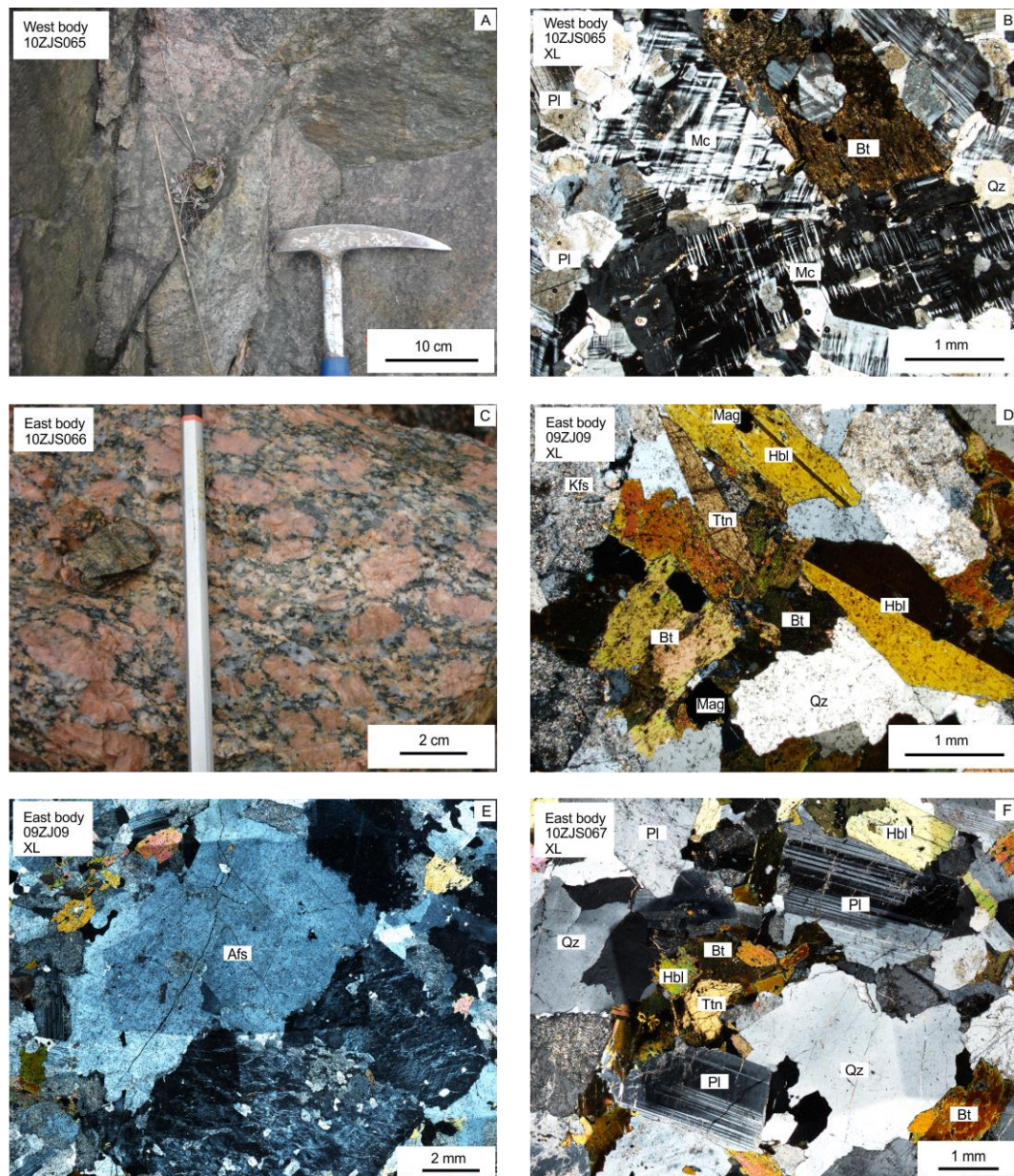


Figure 4.2 Field and thin section photographs of rocks from the Dashuang complex. (A) Field photograph of syenite from the west body (sample 10ZJS065); (B) Photomicrograph of syenite from the west body, showing high modal alkali feldspar (sample 10ZJS065, cross-polarized light); (C) Field photograph of quartz monzonite from the east body, showing deformed alkali feldspar megacrysts (sample 10ZJS066); (D) Photomicrograph of quartz monzonite from the east body, showing the major ferromagnesian minerals hornblende, biotite, titanite and magnetite (sample 10ZJS066, cross-polarized light); (E) Photomicrograph of quartz monzonite from the east body, showing alkali feldspar megacrysts (sample 09ZJ09, cross-polarized light); (F) Photomicrograph of quartz monzonite from the east body, showing higher modal quartz than the west body (sample 10ZJS067, cross-polarized light). Mineral abbreviations: Afs = alkali feldspar, Mc = microcline, Bt = biotite, Ttn = titanite, Hbl = hornblende, Qz = quartz, Pl = plagioclase, Mag = magnetite.

### 4.3.2 Zircon U-Pb dating, Hf isotope and trace element analyses

#### 4.3.2.1 Sample 10ZJS065 (the west body)

Figure 4.5 shows zircon CL images, U-Pb isotope concordia diagrams and Hf isotope histograms. Figure 4.4 shows the zircon REE spidergram.

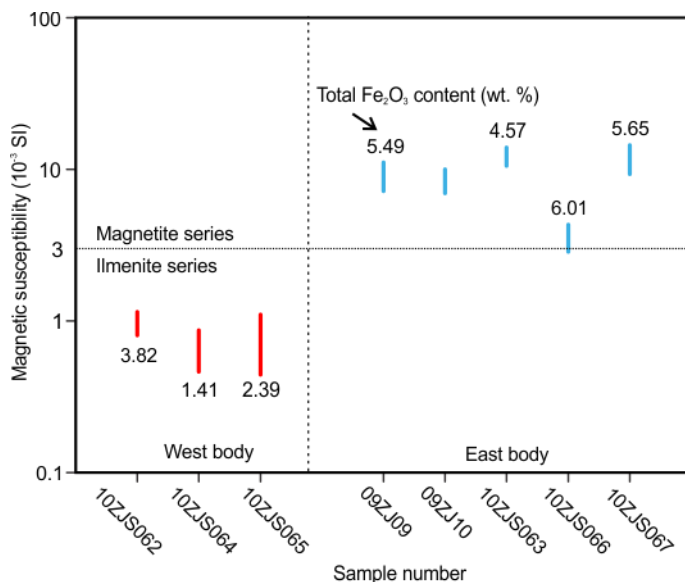


Figure 4.3 Magnetic susceptibility of rocks from the Dashuang complex, with bars representing the results and numbers the whole-rock total Fe<sub>2</sub>O<sub>3</sub> contents. The boundary between the magnetite series and ilmenite series granitoids is from Ishihara et al. (2000).

Twenty-one U-Pb isotopic analyses were carried out on 21 zircons from sample 10ZJS065. As shown in their CL images, the zircons have oscillatory zoning and no inherited cores were observed. The interior of most zircons are transparent, but with a few cracks in transmitted light. Analyzed zircons have Th contents from 93 to 2671 ppm and U contents from 56 to 1258 ppm, with Th/U = 0.94–2.97, which is consistent with their igneous origin. Spot 10ZJ065-04, 05, 06, 17, 20 are rejected due to their high degree of discordance. 10ZJ065-10 is rejected due to its large deviation from the average value. 10ZJ065-13 has a concordant  $^{206}\text{Pb}/^{238}\text{U}$  age at  $242.5 \pm 3.2$  Ma, which is consistent with the previous TIMS age for the east body ( $239.6 \pm 0.6$  Ma, Wang et al., 1997). Like other zircons, 10ZJ065-13 also has oscillatory zoning with Th/U = 0.71. The other fourteen analyses cluster on concordia and yield a weighted mean  $^{206}\text{Pb}/^{238}\text{U}$  age of  $224 \pm 3$  Ma (2 SE) with MSWD = 2.4.

Twenty-two Hf isotopic analyses were conducted on twenty-two zircons.  $\varepsilon\text{Hf}(224 \text{ Ma})$  values range from -6.5 to -10.2 with  $T_{\text{DM2}} = 1.67\text{--}1.90$  Ga. The two-stage Hf model ages are consistent with the ages of Paleoproterozoic gneiss and gneissic granitoids in eastern South China (1.86–1.89 Ga, Yu et al., 2009) and the largest population of detrital zircons in the

eastern Cathaysia Block (1.6–1.9 Ga, Xu et al., 2007). This implies that Paleoproterozoic crustal materials dominated the source region.

Zircon trace elements show a positive Ce peak and a negative Eu anomaly on the chondrite-normalized REE diagram (Figure 4.4). Dy/Yb elemental ratios = 0.30–0.59, with an average at 0.42. Like (Bea, 1996), these results (Table 4) show zircon is an important host for HREE (especially for Lu and Yb) but negligible for LREE (except for Ce). For the calculation of Ti-in-zircon temperature, the presence of quartz in the west and east body suggests  $\text{SiO}_2$  activity = 1 (Anderson et al., 2008).  $\text{TiO}_2$  activity is estimated at 0.75 for the east body, based on the presence of titanite (Matzel et al., 2007) and  $\text{TiO}_2$  activity is estimated at 0.5 for the west body, based on lower whole-rock  $\text{TiO}_2$ . Calculated Ti-in-zircon temperatures are 790–916 °C with an average of 842 °C.

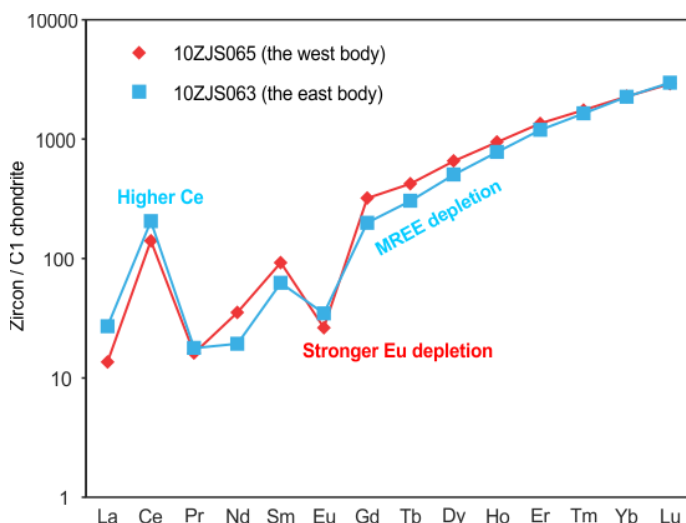


Figure 4.4 Zircon REE spidergram, normalized to C1 chondrite (Sun and McDonough, 1989). The data are the means (Ce, Gd-Lu) or the medians (La, Pr-Eu) of the zircon analyses from each sample (Table 4). 10ZJS065 (the west body) has stronger Eu depletion; 10ZJS063 (the east body) has MREE depletion and higher Ce contents.

#### 4.3.2.2 Sample 10ZJS063 (the east body)

Twenty U-Pb isotopic analyses were carried out on 20 zircons from sample 10ZJS063. Oscillatory zoning is well developed in CL images and the interior of zircons is clear in transmitted light. Th and U contents are 228–859 ppm and 100–507 ppm, respectively, with  $\text{Th}/\text{U} = 0.71\text{--}3.52$ , which is consistent with their igneous origin. Two zircons, 10ZJ063-07 and 10ZJ063-14 are highly discordant and therefore rejected from the age calculation. 10ZJS063-09 and 10ZJS063-13 have concordant  $^{206}\text{Pb}$ - $^{238}\text{U}$  ages of 237.5 Ma and 237.1 Ma. Like 10ZJS065-13 from the west body, they are consistent with the TIMS ages for the east body (Wang et al., 1997). Therefore, the difference between the LA-ICP-MS and TIMS ages are not due to analytical errors and so the two older zircons and the previous TIMS ages

coincidentally record an earlier magmatic or thermal event. The other sixteen analyses yield a weighted mean  $^{206}\text{Pb}/^{238}\text{U}$  age of  $226 \pm 2$  Ma (2 SE) with an MSWD = 1.0.

Twenty-five Hf isotopic analyses were conducted on 25 zircons. The  $\epsilon\text{Hf}(226 \text{ Ma})$  results range from -6.7 to -15.0 with  $T_{\text{DM2}} = 1.68\text{--}2.20$  Ga, which is also consistent with remelting of Paleoproterozoic source materials. However, there is a significant difference in Hf isotopic composition between the west and east bodies, indicating they were possibly derived from different source materials.

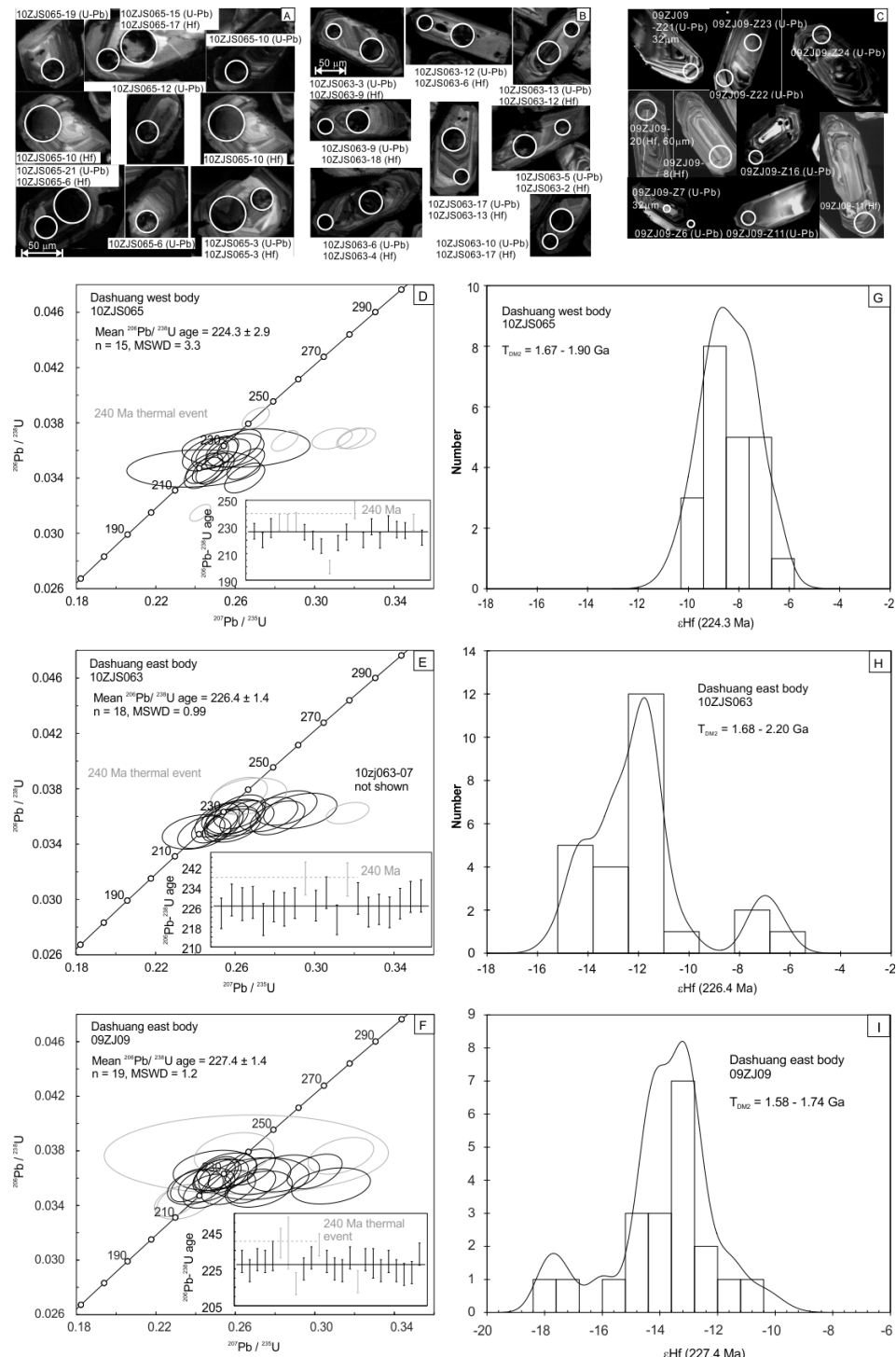


Figure 4.5 Zircon CL images, U-Pb and Hf isotope analyses for sample 10ZJS065 (A, D, G), sample 10ZJS063 (B, E, H) and sample 09ZJ09 (C, F, I). In the CL images, oscillatory zoning indicates their magmatic origin. Small circles mark the positions of LA-ICP-MS U-Pb isotope analyses and large circles mark the positions of MC-LA-ICP-MS Hf isotope analyses. In D, E and F, error ellipses and error bars are 2 standard deviation of  $^{206}\text{Pb}/^{238}\text{U}$  ratios,  $^{207}\text{Pb}/^{235}\text{U}$  ratios and  $^{206}\text{Pb}/^{238}\text{U}$  ages, respectively. Grey ellipses and bars are excluded from weighted mean age calculations. SE = standard error. In E, F and G, the  $\epsilon\text{Hf(t)}$  values ( $-10$  to  $-6$ ) of the west body are less negative than those of the east body (mostly less than  $-10$ ). All three samples contain  $\sim 240$  Ma zircons, likely recording a previous thermal event in the source region.

Compared with sample 10ZJS065, zircon trace elements show MREE depletions (average Dy/Yb elemental ratio = 0.32), a similar positive Ce peak and a less negative Eu anomaly (Figure 4.4). On average, they have higher Ce content than 10ZJS065 from the west body (125 versus 86 ppm). Ti-in-zircon temperatures are 741–994 °C, with an average of 842 °C.

#### 4.3.2.3 Sample 09ZJ09 (the east body)

Twenty-four U-Pb isotopic analyses were carried out on 24 zircons from sample 09ZJ09. Oscillatory zoning is present in zircon CL images (Figure 4.5C). Th and U contents are 43–1133 ppm and 25–705 ppm, respectively, with Th/U = 0.41–3.12, which is consistent with their igneous origin. Two zircons, 09ZJ09-z6 and 09ZJ09-z7, have concordant ages of 239 Ma. 09ZJ09-z11 has a discordant  $^{206}\text{Pb}/^{238}\text{U}$  age of 238 Ma. Like zircons from samples 10ZJS063 and 10ZJS065, they likely record a previous thermal event. Another two zircons, 09ZJ09-z8 and 09ZJ09-z16, have concordant ages of 217 Ma and 218 Ma, which were probably caused by Pb loss. Expect for the aforementioned five zircons, the remaining 19 zircons yield a weighted mean  $^{206}\text{Pb}/^{238}\text{U}$  age of  $227.4 \pm 1.4$  Ma (2 SE) with an MSWD = 1.2.

Twenty Hf isotopic analyses were conducted on 19 zircons. The  $\epsilon\text{Hf}(227 \text{ Ma})$  results range from  $-10.5$  to  $-17.9$ , with  $T_{\text{DM2}} = 1.58\text{--}1.95$  Ga, which is also consistent with remelting of Paleoproterozoic source materials. This sample, which was analyzed in the same analytical session with 10ZJS065, confirms the significant Hf isotopic difference between the west and east bodies.

#### 4.3.3 Whole-rock major and trace element data

Both the west and east body are high-K granitoids. Samples from the west body are relatively rich in quartzo-feldspathic components (K, Na, Si and Al). They have high Fe/Mg ratios and are ferroan granitoids (Figure 4.6), reflecting their low oxygen fugacities (Frost and Frost, 2008). They are all weakly peraluminous [molar  $\text{Al}_2\text{O}_3/(\text{CaO} + \text{Na}_2\text{O} + \text{K}_2\text{O}) = 1.04\text{--}1.06$ ].

Samples from the east body are relatively rich in Ca, Fe, Mg, Ti and P and are magnesian granitoids. They are metaluminous with  $A/CNK = 0.92\text{--}0.95$ , with the exception of sample 10ZJS066 (with high LOI), which likely lost Ca during alteration of plagioclase.

Overall, the trace element patterns of the east body (Figure 4.7) follow those of andesitic arc rocks of the Andes (with  $4 < Sm/Yb < 8$ , indicating a thick continental crust, Kay et al., 2010). Compared with the east body and average Andes andesitic arc rocks, the west body is depleted in Sr, Eu, Ba and transition metals (Cu, Cr, Co, V). Instead, the west body is relatively enriched in Th, LREE, Zr and Hf. LREE/HREE and MREE/HREE are also higher in the west body. Ga/Al ratios are higher in the east body (2.35–2.68, stronger A-type affinity) than the west body (1.76–2.45).

## 4.4 Discussion

### 4.4.1 Contrasting physical and chemical conditions for the east and west bodies

#### 4.4.1.1 Redox conditions

Samples from the west body belong to the ilmenite series and are ferroan granitoids, which are typically produced in reducing intraplate tectonic environments (Ishihara, 1998; Frost et al., 2001). Those from the east body, on the other hand, belong to the magnetite series and are magnesian granitoids. Such granitoids are typically related to oxidizing subduction environments, such as the North America Cordillera (Frost et al., 2001) and the Andes (Ishihara, 1998). Wones (1989) stated that “when the assemblage titanite + magnetite + quartz occurs with clinopyroxene or amphibole with intermediate or higher  $Mg/(Mg+Fe)$  ratios, relatively high oxygen fugacities are implied”. That is what we see for the east body (Figure 4.2D and Figure 4.6). Compared with the west body, the east body has much higher V contents (69.2–93.99 ppm versus 2.03–4.26 ppm), higher V/Ti ratios ( $14.0\text{--}19.0 \times 10^{-4}$  versus  $8.8\text{--}13.0 \times 10^{-4}$ ) and V/Co ratios (6.3–6.7 versus 3.4–4.6). If we assume the titanite + magnetite + quartz assemblage crystallized at 800–850 °C (zircon saturation temperatures) at an emplacement level of 3–10 km,  $f(O_2)$  should be higher than  $10^{-13.7}\text{--}10^{-12.1}$  bars (Wones, 1989). When the oxygen fugacity changes from  $10^{-12}$  bars to  $10^{-10}$  bars, the partition coefficients of V for augite and low-Ca pyroxene, which are the two most important residual minerals during crustal partial melting, are both reduced by 80% because of the increased  $V^{5+}$  proportion (Shervais, 1982). However, the partition coefficients of Ti and Co are likely not sensitive to redox conditions. Therefore, high V contents, high V/Ti and V/Co ratios in the east body indicate a higher oxygen fugacity than the west body.

MREE depletion in the zircons from the east body can be explained by their equilibrium with hornblende and especially titanite, which have large partition coefficients for MREE

(Glazner et al., 2008). The zircons from the east body have smaller negative Eu anomalies and higher Ce contents than those from the west body. Although the former does not directly imply a more oxidized environment because the whole-rock Eu/Zr ratio is higher for the east body, the latter indeed suggests a higher  $\text{Ce}^{4+}/\text{Ce}^{3+}$  ratio in the east body. Sample 10ZJS065 (west body) has higher whole-rock Ce content and Ce/Zr ratio than sample 10ZJS063 (east body). In addition, sample 10ZJS065 with a high Zr content tends to crystallize zircon at higher temperatures, whereby these zircon crystals should generally have higher Ce solubility with a given  $\text{Ce}^{4+}/\text{Ce}^{3+}$  ratio. The zircons from sample 10ZJS065 are expected to have higher Ce contents for a given  $\text{Ce}^{4+}/\text{Ce}^{3+}$  ratio, but the reverse is true. Therefore, the east body should have a higher  $\text{Ce}^{4+}/\text{Ce}^{3+}$  ratio, pointing to a more oxidized environment. To summarize, the physical, petrologic, whole-rock and zircon evidence from the east body supports an oxidized arc environment in eastern South China during the Late Triassic.

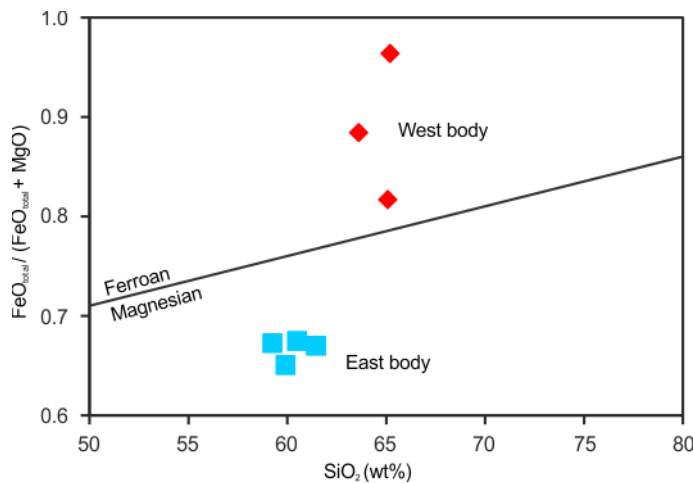


Figure 4.6 Diagram of whole-rock  $\text{FeO}_{\text{total}} / (\text{FeO}_{\text{total}} + \text{MgO})$  versus  $\text{SiO}_2$ , after Frost et al. (2001).

#### 4.4.1.2 I-type melts with varying water contents

In South China, some Triassic granitoids in Hunan Province (Wang et al., 2007b) and the Triassic cordierite-bearing Darongshan granite in Guangxi Province (Qi et al., 2007) are strongly peraluminous and have S-type affinity (Chappell and White, 1974). In contrast, the Dashuang west body has A/CNK between 1.0 and 1.1, which can be explained by the weakly peraluminous character of biotite and does not necessarily imply that sediments were involved (Chappell et al., 2012). The Dashuang east body has even lower A/CNK ratios as a result of relative high contents of hornblende and titanite. Therefore, based on their low A/CNK ratios and absence of strongly peraluminous minerals, both the west and east body have I-type affinity (Patiño-Douce and McCarthy, 1998).

Figure 4.7B shows that the east body has significantly higher normative An contents and less normative Or than the west body, which can be caused by higher water activity

(Conrad et al., 1988). In contrast to the west body and other Triassic granitoids in Zhejiang Province (e.g., Sheyang and Wengshan granitoids; for locations see Figure 4.1A), the east body is not depleted in Ca, Sr and Eu, which reflects high solubility of plagioclase (especially the An component) during partial melting processes in a water-rich environment (Conrad et al., 1988).

The east body has euhedral-subhedral titanite, hornblende and biotite as major ferromagnesian minerals (Figure 4.2D). The occurrence and stability of hornblende in the east body indicates a high water content (>4 wt. %) in the magma (Naney, 1983; Annen et al., 2006a; Behrens and Gaillard, 2006). The stability of titanite also indicates an oxidized and water-rich condition (Foley and Wheller, 1990; Xirouchakis et al., 2001). These conditions are characteristics of arc magmatism (Ballhaus, 1993) and I-type granites.

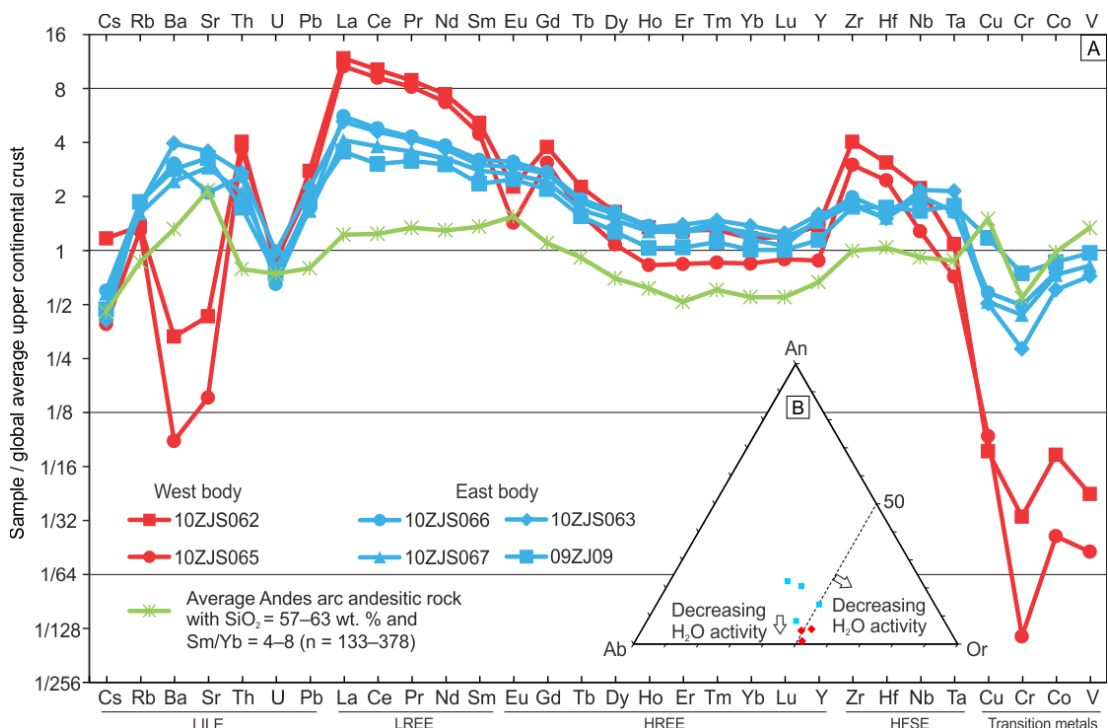


Figure 4.7 Whole-rock trace element spidergram. Trace element concentrations are normalized to global average upper continental crust (Rudnick and Gao, 2003). The samples from the west body are depleted in Ba, Sr, Eu, Cu, Cr, Co, V and enriched in LREE, Zr and Hf. The samples from the east body have similar trends to andesitic arc rocks in the Andes (with SiO<sub>2</sub> = 57–63 wt. % and Sm/Yb = 4–8). Data for the Andean rocks are from the compilation of GEOROC ([http://georoc.mpch-mainz.gwdg.de/georoc/Csv\\_Downloads/Convergent\\_Margins\\_comp/ANDEAN\\_ARC.csv](http://georoc.mpch-mainz.gwdg.de/georoc/Csv_Downloads/Convergent_Margins_comp/ANDEAN_ARC.csv)). (B) Ab-Or-An ternary diagram. The trends of melt composition with water activity are from (Conrad et al., 1988).

The content of transition metals (Cu, Cr, Co, V) in the east body is higher than that in the west body by approximately an order of magnitude. High transition metal contents in crustal melts are commonly linked to wet and oxidizing environments (Burnham and Ohmoto, 1980; Patiño Douce and Beard, 1996), such as the andesitic rocks in the Andes (Figure 4.7). This again suggests an arc-like environment for the east body.

#### 4.4.1.3 REE, Zr and Hf: melt pressure and temperature estimations

Samples from the west body are relatively enriched in Th-LREE-Gd and Zr-Hf compared to the east body. Monazite/allanite and zircon are the main host minerals for Th-LREE-Gd and Zr-Hf in potential protoliths during deep crustal melting (Bea, 1996). Solubility of monazite and zircon in silicate melt both increase with temperature (Montel, 1993; Hanchar and Watson, 2003). Allanite, if stable, also has increased solubility in silicate melt with increased temperature. Therefore, coupled Th-LREE-Gd and Zr-Hf enrichment in the west body indicates a higher melting temperature than for the east body. Zircon saturation thermometry reveals that the temperatures of the west body reached 950 °C and the east body reached 850 °C, respectively (Figure 4.8), which are consistent with their calculated Ti-in-zircon temperatures (Appendix C). Large alkali feldspar crystals are a common feature of the east body and other Triassic granitoids in Zhejiang Province (the Sheyang syenogranite and the Wengshan syenogranite, Figure 4.1A). Ostwald ripening is an ineffective process for coarsening >1 mm quartz (Cabane et al., 2001) and this effect appears not to be effective enough for growing large phenocrysts in silicate melt. According to experimental results on nucleation and growth rates of quartz-feldspathic minerals in synthetic granitic melt (Swanson, 1977), the large alkali feldspar crystals in the east body probably reflect a low nucleation rate but high growth rate of alkali feldspar at a temperature possibly as high as 850 °C.

MREE/HREE (Sm/Yb) ratios for the west body are higher than those of the east body, and both are higher than those of Cretaceous granitoids in the area (Figure 4.8), perhaps reflecting high modal residual garnet. It therefore implies that the Dashuang Complex and other Triassic granitoids in western Zhejiang Province were produced in hotter and deeper crust compared with their Cretaceous counterparts (Figure 4.8). Since the stability field of garnet shrinks with increasing water content (Patiño-Douce and Beard, 1996), slightly lower whole-rock MREE/HREE ratios (Sm/Yb) in the east body again point to higher water contents during deep crustal melting. Under both dehydration melting and water-undersaturated melting conditions, the solidus of the crustal protolith is positive (Burnham, 1997; Holtz et al., 2001). Therefore, high pressure is positively correlated with high temperature for the Triassic granitoids in the region.

#### 4.4.2 Petrogenesis and tectonic model

##### 4.4.2.1 Contrasting petrogenesis of the Dashuang west and east bodies

Both the west and east bodies of the Dashuang complex were produced from melting of an older crustal protolith in a hot and thickened crust. Based on their sources and contents of water, three major melting mechanisms for the plutons can be considered: water-saturated

melting, water-fluxed melting (where there was external water input but not enough to saturate silicate melts) and dehydration melting. The high temperatures of the Dashuang Complex ( $> \sim 850$  °C) exclude the possibility of water-saturated melting (<700 °C, Holtz et al., 2001). The west body is depleted in Ba-Sr-Eu-Fe-Mg-Ti and belongs to the ilmenite series, and is a ferroan and peraluminous granitoid. The west body also has higher zircon saturation temperatures and higher Sm/Yb ratios than the east body, possibly implying higher modal residual garnet under water-deficient conditions. These clues suggest that the west body was produced in a water-deficient environment with dehydration melting as the main mechanism. In contrast, the east body has higher contents of Ca, Fe, Mg, Ti, Ba, Sr and transition metals than the west body, belongs to the magnetite series, and is a magnesian granitoid. The east body also has high modal hornblende and titanite, important indicators of a water-rich and oxidized environment (Xirouchakis et al., 2001; Annen et al., 2006b). It has lower zircon saturation temperatures and Sm/Yb ratios relative to the west body, reflecting lower melting temperatures and higher water contents. These pieces of evidence indicate that the east body was produced by water-fluxed melting.

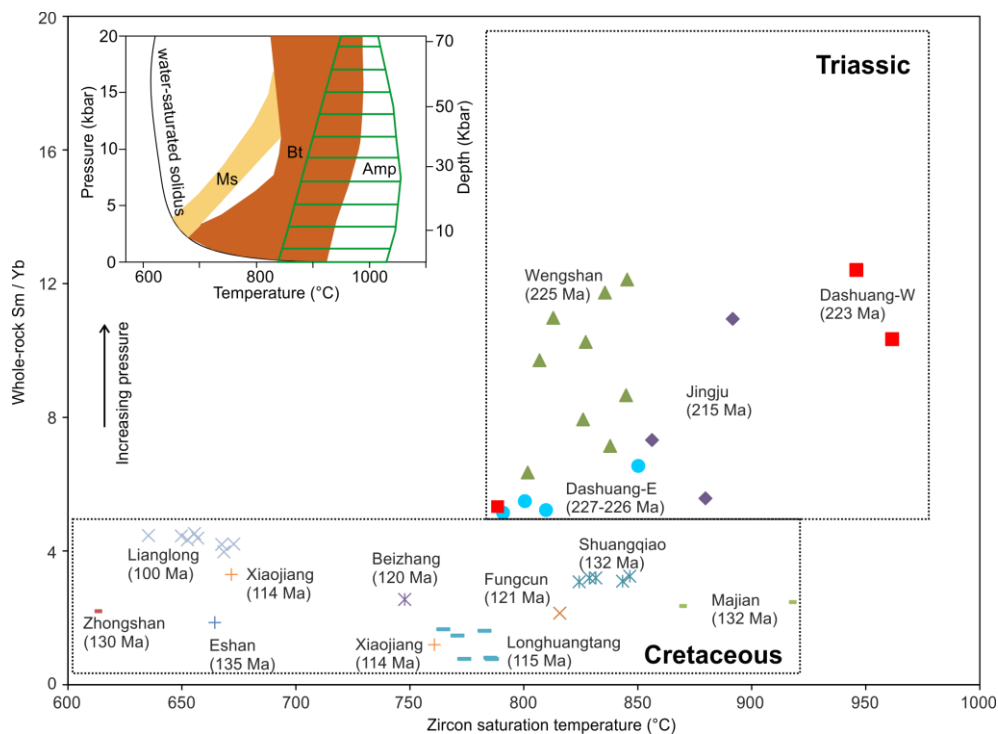


Figure 4.8 Diagram of whole-rock Sm/Yb versus zircon saturation temperature (Hanchar and Watson, 2003) for the Mesozoic granitoids in Zhejiang Province. All age data are zircon U-Pb ages. Data sources: the Dashuang syenite and quartz monzonite (this study), the Jingju syenogranite (Li et al., 2012b), the Wengshan monzogranite (Sun et al., 2011), Cretaceous granitoids (Wong et al., 2011). The inset shows the temperature and pressure conditions for water-saturated melting and dehydration melting, after Sawyer et al. (2011).

Although the Dashuang east body has a strong affinity to arc granitoids, its zircon Hf isotopic compositions are more crust-like than the west body. There are two possible explanations: (1) the lower crust is heterogeneous and the west and east body inherited their

Hf compositions from their source regions; or (2) the west and east body may have a common source because the maximum values of zircon  $\epsilon\text{Hf(t)}$  of both bodies are similar ( $-6.5$  versus  $-6.7$ , respectively), and they have similar ages, but external materials involved in the melting processes of the east body had lower  $^{176}\text{Hf}/^{177}\text{Hf}$  ratios than their common source.

#### 4.4.2.2 Middle-Late Triassic Jingju syenogranite-quartz monzonite complex

In Zhejiang Province, the Late Triassic Jingju syenogranite (218 Ma) and quartz monzonite (236 Ma) share certain characteristics with the Dachuang west and east bodies, respectively. As shown in Figure 4.9A, these materials have similarly high initial  $^{87}\text{Sr}/^{86}\text{Sr}$  ratios, low  $\epsilon\text{Nd(t)}$  values and  $T_{2\text{DM}, \text{Nd}} = 2.0\text{--}2.2$  Ga (Liew and Hofmann, 1988), pointing to Paleoproterozoic sources (Yu et al., 2009). Relative to quartz monzonite, syenogranite is depleted in Sr-Ba-Eu (Figure 4.9G) with higher zircon saturation temperatures (Figure 4.9B) and lower V/Co and V/Ti ratios (Figure 4.9D). Therefore, syenogranite is likely more deficient in water and more reduced, magnetite is therefore not stable, and the rocks have high FeOt/(FeOt+MgO) ratios (Figure 4.9C), Ga contents and Ga/Al ratios (Figure 4.9E) (Goodman, 1972) and a steeper Eu-Sr slope (a high Eu<sup>2+</sup> proportion, Figure 4.9F). Both of these bodies have significantly higher MREE/HREE ratios than the Early Cretaceous A-type granites (e.g., Wong et al., 2009) (Figure 4.9B), implying a thickened crust during the Triassic. The syenogranite has higher zircon saturation temperatures (850–900 °C, Figure 4.9B), implying that dehydration melting occurred in a hot orogenic lower crust. These geochemical features support petrogenetic and tectonic interpretations similar to those for the Dashuang Complex, i.e., crustal partial melting in an Andean-type orogeny with an increasing geothermal gradient and different water inputs from the oceanic plate.

#### 4.4.2.3 New constraints on the Mesozoic tectonic evolution of eastern South China

The most likely tectonic environment for high temperature, high pressure, high oxygen fugacity and water-rich melting is a thickened active continental margin and both water-fluxed and dehydration melting can occur under such conditions (Whitney, 1988). At an active continental margin such as the Andes, a thick felsic crust can be created above a flat oceanic slab (Fromm et al., 2004; Orozco et al., 2013), which has high radiogenic heat production. However, it would take tens of millions of years to form a steep geothermal gradient in such a thickened crust (Spear, 1995).

Li and Li (2007) reported an Early Triassic metamorphic age (240 Ma, SHRIMP zircon U-Pb method) for granitic gneisses in the Danzhu area (DZ, Figure 4.1A) in southwest Zhejiang Province, which indicated the Paleo-Pacific plate had already influenced western Zhejiang Province by the Early Triassic. Xiang et al. (2008) reported the timing of Late Permian-Middle Triassic (250–230 Ma, LA-ICP-MS zircon U-Pb method) amphibolite-

facies metamorphism in the Danzhu and Jingning areas, both in southwest Zhejiang Province (DZ and JN in Figure 4.1A). These amphibolites have high contents of hydrous minerals (biotite = 15–30% and hornblende = 25–85%), and plagioclase = 15–60%. These mineral assemblages typically occur in amphibolite-facies metabasalt. Ti-in-zircon thermometry revealed zircon recrystallization temperatures of 610–720 °C for the amphibolites (Xiang et al., 2008).

The most likely water source to produce the hydrous Dashuang east body was from a hydrated subducting oceanic slab. Under low temperature conditions, the water released from an oceanic slab will directly arrive at the lower crust rather than cause melting in the mantle and give birth to arc basalts or andesites. Such conditions can be achieved near the trench. However, for the Dashuang area in west Zhejiang Province, which is at least 500 km away from the trench, a flat oceanic slab is a more likely mechanism for transporting the water. In the Late Triassic, water could directly reach the continental lower crust when the continental lithospheric mantle had been cooled down by the flat oceanic slab. At the same time, since the temperature of the lower crust continuously increased, the peak of metamorphism would be reached at ~225-215 Ma and the basal lower crust would be the hottest location in the continental lithosphere at that time.

Li et al. (2012c) recently used U-Pb ages and Hf and O isotopes of detrital zircons from the hinterland of the South China Block to constrain the processes operative at the Permian active continental margin in eastern South China. They argued that the peak age of ~280 Ma in the detrital zircon spectrum recorded the earliest impact of the Paleo-Pacific plate on the continental margin. A significant proportion of the ~280 Ma detrital zircon population has mantle-like Hf isotopic compositions. The most feasible explanation for the Hf isotopic differences between the Early Permian detrital zircons and the Late Triassic magmatic zircons is that the former crystallized from normal arc magmas generated in the asthenospheric mantle wedge and the latter crystallized from crust-derived magmas generated in a thickened hot crust.

Liu et al. (2012b) reported two inherited Triassic zircons (09D107#14 and 09D64#18) in Jurassic granodioritic porphyries in the Dexing area (“DX” in Figure 4.1A). Zircon 09D107#14 has a U-Pb age of 241 Ma and  $\epsilon_{\text{Hf}}(t)$  of 4.1, and zircon 09D64#18 has a U-Pb age of 245.7 Ma and  $\epsilon_{\text{Hf}}(t)$  of 6.8. Dexing is further away from the coast than Dashuang and other Triassic granitic plutons in Zhejiang Province (the Jingju, Wengshan and Sheyang plutons; Figure 4.1A). However, the two inherited Triassic zircons from the Dexing area have older ages and much more positive  $\epsilon_{\text{Hf}}$  than the Late Triassic magmatic zircons in Zhejiang Province. This implies there was juvenile input (arc basalt or andesite) from the mantle to the crust in the Dexing area in the Early Triassic.

The above results, together with the new results from Dashuang, can best be explained by the flat-slab subduction model (Li and Li, 2007) with the following characteristics (Figure 4.9): (1) the two inherited Triassic zircons from the Dexing area with juvenile mantle signatures can best be explained by melt derived from a small mantle wedge in front of the advancing flat-slab (Figure 4.9A); (2) the Dashuang area was behind the subduction front in the Late Triassic, with a thickening continental crust receiving water flux from a dehydrating oceanic flat-slab (Figure 4.9A and Figure 4.9B); and (3) the Triassic lower crustal melts in Zhejiang Province (i.e., the Dashuang igneous complex) received little juvenile input from the mantle (Figure 4.9A).

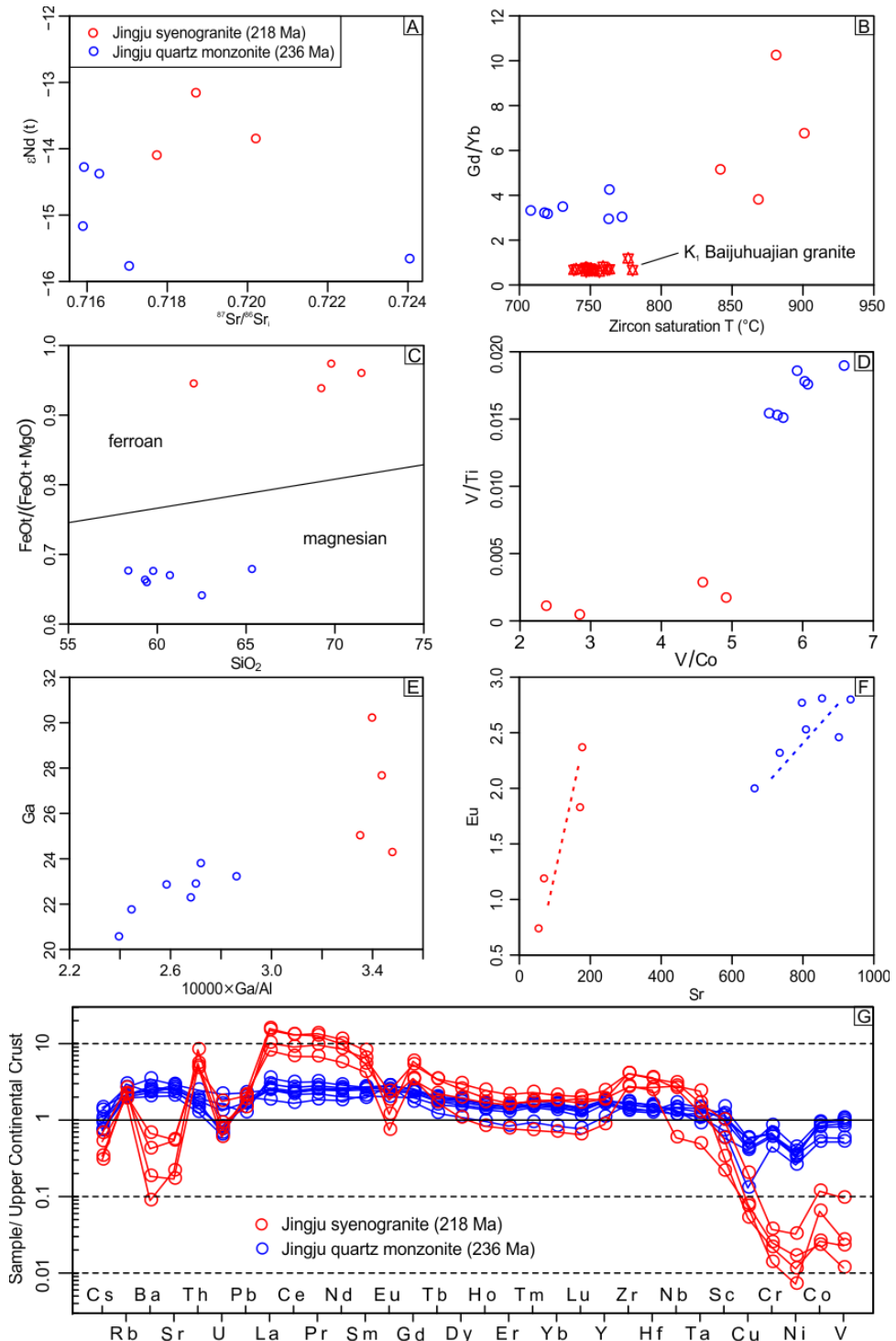


Figure 4.9 Whole-rock geochemical data for Triassic Jingju syenogranite and quartz monzonite (Li, 2010): (A) Sr-Nd isotopic compositions; (B) Gd/Yb ratio versus zircon saturation temperature plot, the data for the 126 Ma Baijihuajian A-type granite (Wong et al., 2009) are shown here for comparison; (C) ferroan-magnesian granitoid classification (Frost et al., 2001); (D) V/Ti versus V/Co plot; (E) Ga versus  $10000 \times \text{Ga}/\text{Al}_2\text{O}_3$  plot; (F) Eu-Sr plot; (G) Trace element patterns normalized to global average upper continental crust (Rudnick and Gao, 2003).

The water involved in the melting processes of the Dashuang east body was likely derived from the oceanic slab. However, its low zircon  $\epsilon_{\text{Hf}}(t)$  character and ocean-floor-sediment-like Sr-Nd isotopic composition were likely caused by previous metasomatism

(240 Ma thermal event recorded by zircon?) of hydrous silicate melt from the subducted sediments that carried upper crustal isotopic signatures. 242 Ma Yangfang syenite in western Fujian Province (Wang et al., 2005a) may represent such metasomatic melts.

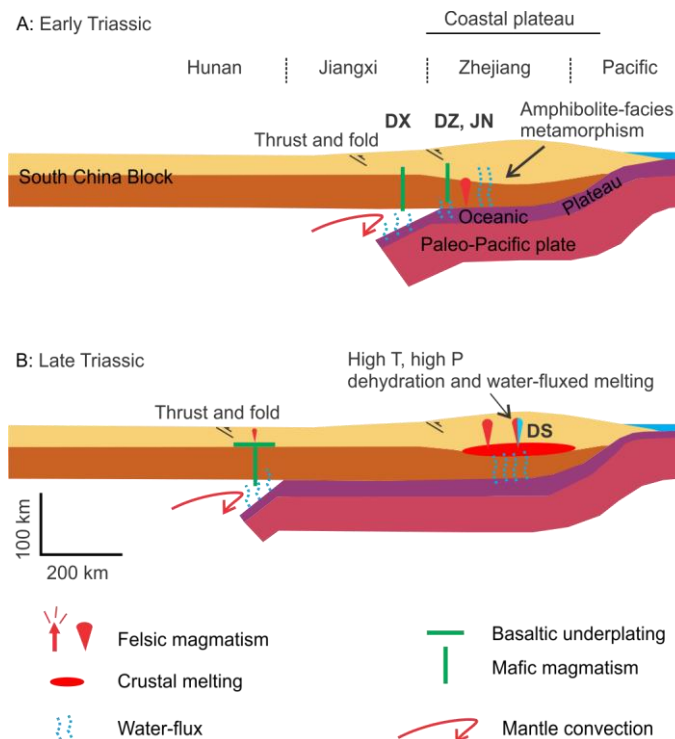


Figure 4.10 Tectonic model for the South China continental margin during (A) the Early Triassic and (B) the Late Triassic, modified after Li and Li (2007). By the Early Triassic, crust in the Dashuang area had been thickened but did not reach high-enough temperature to produce melts. At the same time, arc-like melts may have been formed in the Dexing area in Jiangxi Province (A). In the Late Triassic, the lower crust of the Dashuang area became hot enough to cause both dehydration melting (the west body) and water-fluxed melting (the east body) (B). At this time, the subduction front propagated further inland to Hunan Province. DX = Dexing, DS = Dashuang, DZ = Danzhu, JN = Jingning, YF = Yangfang.

A high melting pressure for the Dashuang Complex is also consistent with the flat-slab model of Li and Li (2007) because an active continental margin can be effectively thickened due to enhanced interaction between the subducting flat-slab and overriding continental lithosphere (Sobolev and Babeyko, 2005). Under the condition of flat-slab subduction, Zhejiang Province and part of the East China Sea Continental Shelf would have been rapidly thickened in the Late Permian to Middle Triassic (Li and Li, 2007). In the Late Triassic, the geothermal gradient in the crust would have become steep enough to cause high temperature and high pressure conditions in the lower crust. Dehydration melting and water-fluxed melting therefore resulted (Figure 4.10B).

The Dashuang Complex challenges the Triassic “continental collision” model proposed by Zhou et al. (2006) and Chen et al. (2008). These authors argued that Triassic granitoids in the interiors of the South China Block were the result of the Early Triassic collision between the South China Block and the Indosinian Block along the Songma Suture in northern

Vietnam. The position and nature of the Indosinian Block are described in Carter et al. (2001). In the model of Zhou et al. (2006), the Paleo-Pacific plate started to subduct beneath the eastern margin of the South China Block after an Early Jurassic “magmatic calm period” (205–180 Ma), with the “calm period” being a result of a tectonic regime change from Tethys-related to Pacific-related. However, such a model not only contradicts evidence of a 280–270 Ma initiation of Pacific subduction along the southeastern margin of the SCB (Li et al., 2006; Li and Li, 2007; Li et al., 2012c), it also contradicts our results from the Dashuang east body which require a hot, thickened, oxidized and water-rich crust. The location of the Dashuang Complex, at least 1500 km from the proposed Indochina-South China “collision zone” in northern Vietnam, is also against such a model. The “magmatic calm period” in the latest Triassic and earliest Jurassic, based on our model, is the result of the continuous cooling effect of flat-slab subduction.

#### 4.5 Conclusion

The Dashuang west body is a peraluminous, ferroan and ilmenite-series syenite, which is enriched in Th, LREE, Zr and Hf, but depleted in Ca, Eu, Sr, Ba and transition metals. The zircon U-Pb age of the Dashuang west body is  $224 \pm 3$  Ma and the zircon  $\epsilon\text{Hf(t)}$  values are  $-6.5$  to  $-10.2$  with  $T_{\text{DM2}} = 1.67\text{--}1.90$  Ga. It was generated from dehydration melting of Paleoproterozoic igneous protoliths in a thickened lower crust, with a high melt temperature of up to  $950$  °C.

The Dashuang east body is a metaluminous, magnesian and magnetite-series quartz monzonite, which is relatively depleted in Th, LREE, Zr and Hf, but enriched in Ca, Eu, Sr, Ba and transition metals. The zircon U-Pb age of one sample (10ZJS063) is  $226 \pm 2$  Ma and the zircon  $\epsilon\text{Hf(t)}$  values are  $-6.7$  to  $-15.0$  with  $T_{\text{DM2}} = 1.68\text{--}2.20$  Ga. Another sample (09ZJ09) from the east body has a zircon U-Pb age of  $227 \pm 1$  Ma and the zircon  $\epsilon\text{Hf(t)}$  values are  $-10.5$  to  $-17.9$ , with  $T_{\text{DM2}} = 1.58\text{--}1.95$  Ga. It was produced from water-fluxed melting of Paleoproterozoic igneous protoliths in a thickened lower crust. It is likely that external water involved in the melting process of the east body was derived from the oceanic plate and the lower crustal source was metasomatized by hydrous silicate melt from subducted sediments at  $\sim 240$  Ma. The initiation of water-fluxed melting in an oxidized, hot (up to  $850$  °C) and thickened crust is consistent with the flat-slab subduction model.

From mid-Permian to the Late Triassic, an orogeny developed along the coastal region of South China due to the initiation of an Andean-type continental margin, resulting in thickened continental crust and an increased crustal geothermal gradient. During the Early and Middle Triassic, the lower crust in west Zhejiang Province underwent amphibolite-facies metamorphism during crustal thickening and was likely metasomatized by aqueous and

siliceous fluids from the oceanic plate (Figure 4.10A). By the Late Triassic, the lower crust of the region had reached high enough temperatures for formation of high-pressure, high-temperature melts, resulting in the generation of the Dashuang syenite (without water from the oceanic plate) and quartz monzonite (with water from the oceanic plate) (Figure 4.10B).

## Chapter 5 Mesozoic Granitic Magmatism in Western Zhejiang Province

### 5.1 Introduction and Geological Setting

In this study, a series of high-K granitic and coeval/cogenetic mafic-intermediate rocks were systematically sampled and analysed from western Zhejiang Province within a region of 16000 km<sup>2</sup>, covering an age range from the Triassic to Cretaceous (Figure 5.1C). Magnetic properties, petrography, whole-rock geochemistry, zircon U-Pb ages and zircon Hf isotopes of these samples were investigated to constrain how the source-temperature-pressure-water-redox conditions in the continental lithosphere changed at different stages of the Mesozoic evolution of this area, thus enabling us to test various models that have been proposed.

The South China Block is composed of the Yangtze Block in the northwest and the Cathaysia Block in the southeast (Figure 5.1B). The Jiang-Shao Fault Zone (Figure 5.1C) is generally regarded as the boundary between the two blocks in Zhejiang Province (Zhang et al., 2005) and it separates the study area into two parts. In the southeast part of the study region, the oldest rocks of the Cathaysia Block are Paleoproterozoic granitoids and metamorphic rocks (Figure 5.1C) (Yu et al., 2009; Xia et al., 2012; Yu et al., 2012a). In the northwest part, the Phanerozoic strata are probably underlain by late Mesoproterozoic to Neoproterozoic rocks associated with the amalgamation and later rifting between the Yangtze and Cathaysia blocks (Li et al., 2002; Ye et al., 2007; Li et al., 2008; Li et al., 2009). During the Early Paleozoic (>460–420 Ma), South China underwent an intraplate orogenic event (Li et al., 2010a). From the Permian to the Cretaceous, another widespread “intracontinental” orogeny (the Indosinian Orogeny) occurred in the South China Block, accompanied with extensive deformation (Figure 5.1B) and some granitic magmatism. The Permo-Triassic folds and thrusts generally have a NE-SW trend and migrated from the coast to the continental interior (Li and Li, 2007). In the study region, the orogeny deformed Carboniferous to mid-Triassic platform carbonate strata, whereas post-orogenic Jurassic-Cretaceous volcanic and clastic strata unconformably overlie older rocks (ZGS, 1965; FGS, 1972; Charvet et al., 1994).

### 5.2 Sampling and Petrography

Representative granitic samples were collected from 16 granitic intrusions in the study region (Figure 5.1C): these are listed in Table 5.1 together with their location, mineral compositions and other information; some of them have been previously studied. The nomenclature in this study follows the IUGS QAP classification (Le Maitre, 2002). Typical photographs of the outcrops, hand specimens and thin sections are shown in Figure 5.2.

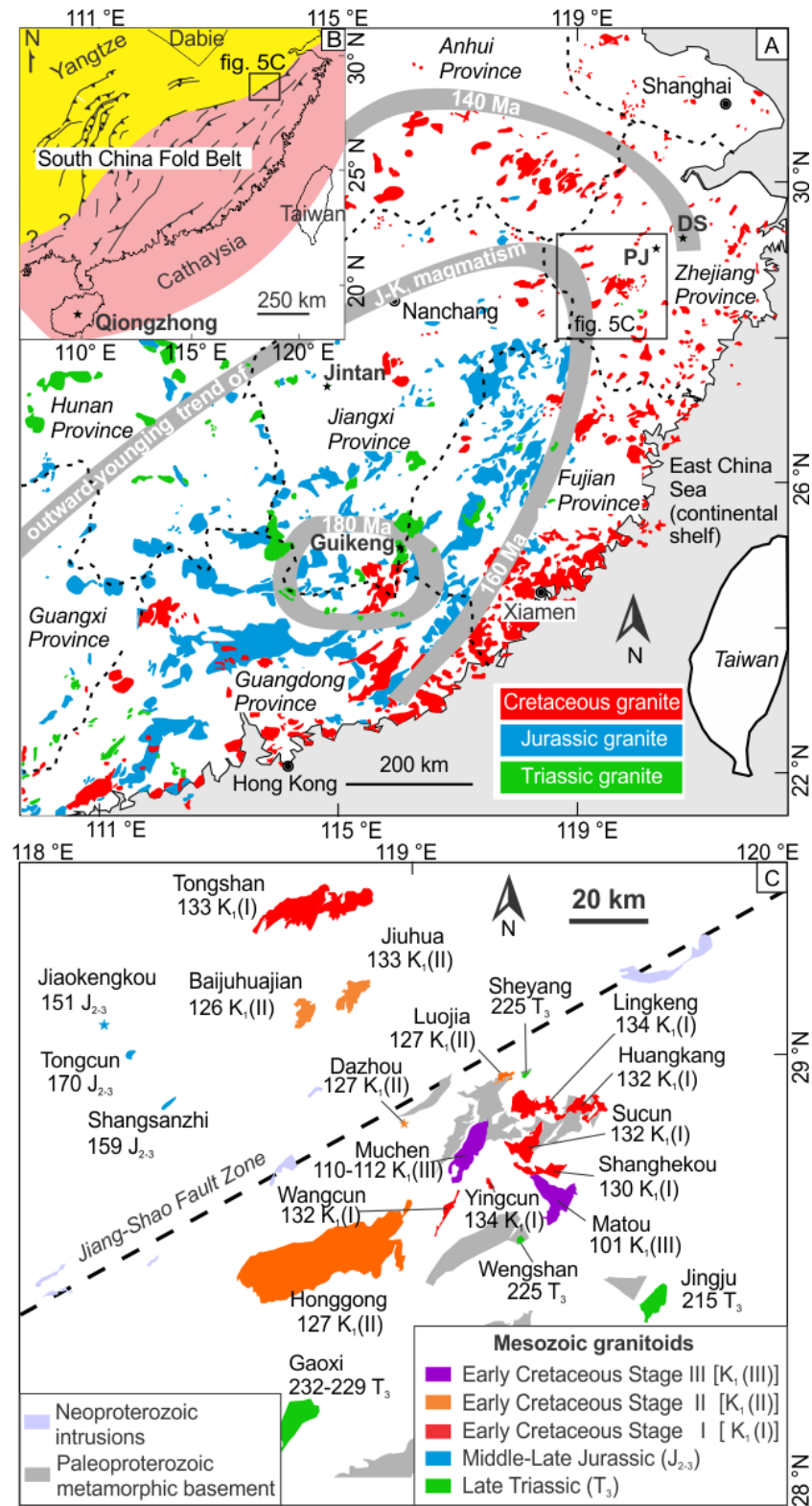


Figure 5.1 (A) Distribution of Mesozoic granitic rocks in the South China Block, modified after Zhou et al. (2006). The oceanward-younging trend of the Jurassic and Cretaceous magmatism is from Li et al. (2013d). PJ: Pujiang basalt; DS: Dashuang quartz monzonite. (B) Major Mesozoic thrust faults in South China. The two components of the South China Block are shown in different colours (Li et al., 2010a). (C) The granitic intrusions in this study and their ages (see Table 5.1 for data sources). The Paleoproterozoic metamorphic basement and Neoproterozoic intrusions are also shown. The Jiang-Shao Fault Zone is the inferred boundary between the Yangtze and Cathaysia blocks.

Triassic intrusions, as demonstrated by precise zircon U-Pb ages reported later, include the Gaoxi, Sheyang, Wengshan and Jingju syenogranites (Figure 5.1C). They intruded the Paleoproterozoic Badu Complex in western Zhejiang Province (Sheyang, Wengshan and Jingju plutons) and Early Paleozoic metamorphic rocks in northern Fujian Province (Gaoxi plutons). Early Cretaceous strata either overlie, or are in fault contact with, these Triassic intrusions (ZGS, 1966; Sun et al., 2011; Li et al., 2012b; Zhao et al., 2013a). All the Triassic granites are coarse-grained syenogranites and contain pink microcline megacrysts 1–2 cm in size (Figure 5.2A-D). The mineral composition is quartz, feldspar and biotite, with accessory zircon, titanite, apatite, magnetite and ilmenite. In addition, the Jingju syenogranite also contains amphibole. All these Triassic rocks underwent deformation, to different extents, as reflected by the undulose extinction and recrystallization of quartz (Figure 5.2B). The magmatic susceptibilities of the Triassic samples are  $0.11\text{--}3.59 \times 10^{-3}$  SI.

Early Cretaceous intrusions are the largest and most widespread granitic rocks in the study region, with the Honggong quartz syenitic porphyry and the Muchen Complex reaching tens of kilometres in length. Based on their textures and analytical results, the Early Cretaceous intrusions can be further divided into three stages.

The first stage of the Early Cretaceous granitic rocks (Figure 5.1C and Figure 5.2I-P) includes the Sucun syenogranite, Yingcun porphyry, Lingkeng syenogranite, Wangcun syenogranite, Huangkang syenogranite and Shanghekou syenogranite in the Cathaysia Block, and the Tongshan syenogranite in the Yangtze Block (Figure 5.1C). These rocks intruded the Paleoproterozoic Badu Complex and Early Cretaceous Moshishan Group in the Cathaysia Block and Paleozoic strata in the Yangtze Block. The rocks are highly evolved syenogranitic rocks with high modal alkali feldspar and quartz. The plagioclase generally has a low An mol % ( $\sim 10\%$ , ZGS, 1966). The rocks contain biotite  $\pm$  calcic clinoamphibole, and have accessory zircon, apatite, Fe-Ti oxides, muscovite and allanite. The magnetic susceptibilities are low to moderate ( $0.098\text{--}8.084 \times 10^{-3}$  SI).

The second stage of the Early Cretaceous granitic rocks (Figure 5.1C and Figure 5.2Q-T) includes the Luojia porphyry and Honggong quartz syenitic porphyry in the Cathaysia Block (intruding the Paleoproterozoic Badu Complex and Early Cretaceous Moshishan Group) and the Baijuhuajian porphyry and Jiuhua porphyry in the Yangtze Block (intruding Neoproterozoic and Early Cretaceous strata). These rocks are predominantly porphyritic with alkali feldspar megacrysts. Quartz, alkali feldspar, plagioclase (An<sub>6</sub>–15 for the Honggong quartz syenitic porphyry, JGS, 1980a) and biotite are the major minerals, but the Honggong quartz syenitic porphyry also contains amphibole and clinopyroxene. The magnetic susceptibility intensities are low to moderate ( $0.010\text{--}5.837 \times 10^{-3}$  SI).

Table 5.1 Name, GPS coordinates, lithology, U-Pb isotopic age, Hf isotope, mineral assemblage, magnetic susceptibility and data source of granitoids in the study region

Intrusion name	Location		Lithology	Age (±2SE, Ma)	$\epsilon_{\text{Hf(t)}}$ (±2SE)	Magnetic Susceptibility ( $10^{-3}$ SI)
<b>T<sub>3</sub> (The Late Triassic)</b>						
Gaoxi	28°10.8'	118°40.7'	syenogranite	229±2	-11.7±0.2	2.905-3.592
Sheyang	28°57.3'	118°18.0'	syenogranite	225±1	-6.1±0.8	0.139-0.246
Wengshan	28°34.4'	119°17.1'	syenogranite	225±1	-14.4±0.5	0.090-0.133
Jingju	28°26.0'	119°40.0'	syenogranite	215±2	No data	No data
<b>J<sub>2-3</sub> (The Middle-Late Jurassic)</b>						
Tongcun	28°59.9'	119°14.9'	granitic porphyry	170±10	No data	0.030-0.640
Shangsanzhī	28°53.1'	118°21.0'	granitic porphyry	159±1	-1.4±0.9	0.052-0.136
Jiaokengkou	29°03.8'	118°10.5'	granitic porphyry	151±2	No data	No data
<b>K<sub>1(I)-K<sub>1(II)</sub></sub></b> (the first and second stages of the Early Cretaceous)						
Yingcun	28°42.1'	119°12.3'	granitic porphyry	134±1	-7.8±0.7	4.854-6.451
Lingkeng	28°54.3'	119°17.8'	syenogranite	134±1	-7.5±0.6	1.756-2.257
Jiuhua	29°08.9'	118°51.6'	granitic porphyry	133±1	-4.8±0.5	0.130-5.837
Tongshan	29°21.0'	118°42.0'	syenogranite	133±1	-3.9±0.4	0.432-2.364
Sucun	28°46.8'	119°18.4'	syenogranite	132±1	-8.7±0.8	0.446-4.063
Wangcun	28°38.9'	119°05.7'	syenogranite	132±2	-7.6±0.6	0.472-8.084
Huangkang	28°53.0'	119°26.7'	syenogranite	132±1	-7.1±0.5	0.098-0.235
Shanghekou	28°44.0'	119°22.2'	syenogranite	130±1	-10.5±1.3	0.136-2.107
Luojia	28°57.3'	119°13.9'	porphyry	127±2	-2.8±0.8	0.010-0.141
Dachayuan	28°50.6'	118°58.7'	rhyolite	127±2	-5.1±0.2	No data
Honggong	28°33.0'	118°47.0'	quartz syenite	127±2	-5.9±0.5	No data
Baijuhuajian	29°06.6'	118°38.9'	granitic porphyry	126±3	1.5±0.6	No data
<b>K<sub>1(III)</sub> (the third stage of the Early Cretaceous)</b>						
Muchen	28°47.9'	119°10.1'	(quartz) monzonite, granitic porphyry	110~112	-1.7~1.3	6.69-38.164
Matou	28°39.8'	119°23.8'	monzogranite	101±1	-5.7±1.9	12.50-24.84

Table 5.1 (continued)

Intrusion name	Mineral assemblage with estimated mode	Data source
T <sub>3</sub>		
Gaoxi	Afs (50%), Pl (20%), Qz (20–25%), Bt (5%), Mag, Ttn	this study; Zhao et al. (2013a)
Sheyang	Afs (60%), Pl (15%), Qz (20%), Bt, Mt	this study
Wengshan	Afs (60%), Pl (15%), Qz (20%), Bt, Ilm	this study; Sun et al. (2011)
Jingju	Afs (45–65%), Pl (10–15%), Qz (10–35%), Bt, Amp	Li et al. (2012b)
J2-3		
Tongcun	Afs, Pl, Qz, Bt, Ttn, Amp, Hem	this study; Chen (2011); Zeng et al. (2013b)
Shangsanzhi	Afs, Pl, Qz, Amp, Mag	this study; Chen (2011)
Jiaokengkou	Afs, Pl, Qz, Bt, Amp	Li et al. (2013b)
K <sub>1</sub> (I)-K <sub>1</sub> (II)		
Yingcun	Afs, Pl, Qz, Bt, Amp, Mag	this study
Lingkeng	Afs (60%), Pl (10%), Qz (30%), Bt, Mag	this study
Jiuhua	Afs, Pl, Qz, Bt, Mag, Ilm	this study; Wong et al. (2011)
Tongshan	Afs (50%), Pl (15%), Qz (30%), Mag	this study; Jiang et al. (2011b)
Sucun	Afs (50%), Pl (10%), Qz (35%), Bt, Mag, Ilm	this study
Wangcun	Afs (50%), Pl (15%), Qz (30%), Bt, Mag, Ilm	this study
Huangkang	Afs (50%), Pl (10%), Qz (35%), Mag, Ilm	this study
Shanghekou	Afs (50%), Pl (10%), Qz (35%), Mag	this study
Luojia	Afs, Pl, Qz	this study
Dachayuan	Afs, Qz and Bt as phenocrysts	Yang et al. (2013b)
Honggong	Afs (55–67%), Pl (8–22%), Qz (6–20%), Bt, Amp, Cpx	Lu et al. (2006); He and Xu (2012)
Baijuhuajian	Afs, Pl, Qz, Bt	Wong et al. (2009)
K <sub>1</sub> (III)		
Muchen	Afs, Pl, Qz, Bt, Amp, Cpx, Ttn, Mag	this study; Lu (2007);
Matou	Afs (40%), Pl (35%), Qz (20%), Bt, Amp, Ttn, Mag	this study

Mineral abbreviations: Afs, alkali feldspar; Pl, plagioclase; Qz, quartz; Bt, biotite; Ttn, titanite; Amp, amphibole; Cpx, clinopyroxene; Mag, magnetite; Ilm, ilmenite; Hem, hematite.

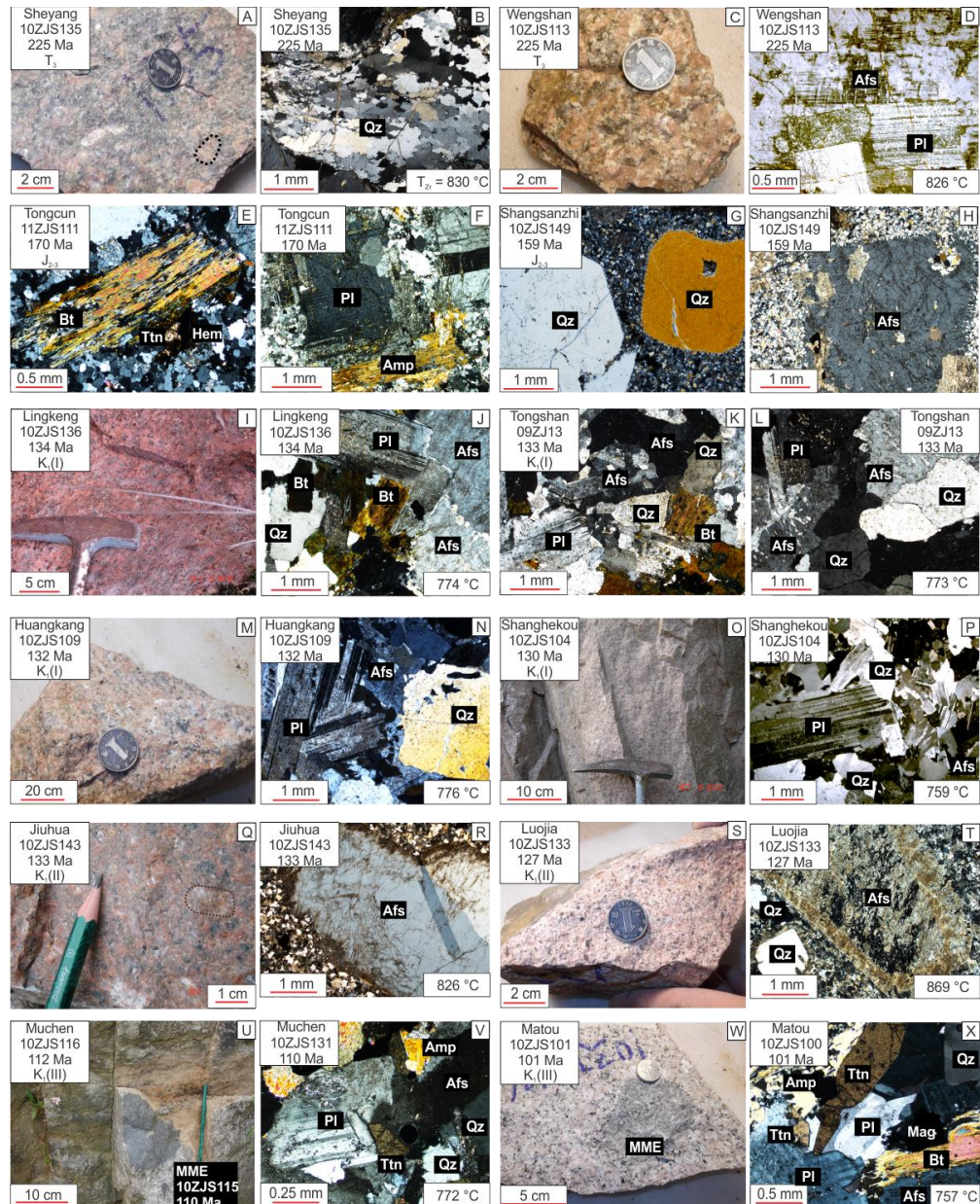


Figure 5.2 Field, hand specimen and thin section photographs of the Mesozoic granitic rocks from western Zhejiang Province. All thin section photographs were taken under cross-polarized light. The temperatures shown are zircon saturation temperatures. (A, B): Sheyang syenogranite. A pink alkali feldspar megacryst (microcline) is outlined with dotted line, showing deformation in thin section. Quartz grains (Qz) also show strong deformation, with undulose extinction and recrystallization. (C, D): Wengshan syenogranite. The petrographic characteristics are similar to the Sheyang syenogranite. Pink alkali feldspar megacrysts and medium- to coarse-grained texture are common features of the Triassic granites in Zhejiang Province. (E, F) Tongcun porphyry. The phenocrysts are quartz, alkali feldspar, plagioclase (Pl), calcic clinoamphibole (Amp), biotite (Bt), titanite (Ttn) and hematite (Hem). (G, H) Shangsanzi porphyry. Quartz (Qz) and alkali feldspar (Afs) phenocrysts occur in a fine-grained groundmass and are of similar size. (I, J) Lingkeng syenogranite with a medium-grained texture. Some alkali feldspars show exsolution and quartz shows undulose extinction. (K-P) Huangkang, Tongshan and Shanghekou syenogranites, which are similar to the Lingkeng syenogranite. (Q-T) Jiuhua and Luojia granitic porphyries contain large alkali feldspar (Afs) crystals. Their porphyritic texture and lack of deformation distinguish them from the Jurassic porphyries. Large alkali feldspar phenocrysts distinguish them from the Jurasssic syenogranites. An alkali feldspar megacryst is outlined with dashed line in Fig. 5.2Q. (U-X) Muchen quartz monzogranite and Matou monzogranite, both of which contain titanite (Ttn), biotite (Bt), calcic clinoamphibole (Amp) and mafic enclaves (MME).

The third stage of the Early Cretaceous granitic rocks is present only in the Cathaysia Block and includes the Muchen Complex and the Matou monzogranite (Figure 5.1C and Figure 5.2U-X), which intrude the Paleoproterozoic Badu Complex and the Early Cretaceous Moshishan Group. They are distinct from the other Mesozoic granites in terms of their significantly higher magnetic susceptibilities ( $6.690\text{--}38.164 \times 10^{-3}$  SI for the Muchen Complex and  $15.034\text{--}22.004 \times 10^{-3}$  SI for the Matou monzogranite) and the occurrence of mafic microgranular enclaves (MME, Figure 5.2U and W). Mafic minerals include biotite, calcic clinoamphibole, titanite and magnetite. Accessory minerals include titanite, zircon and apatite. The Muchen Complex is highly variable, ranging from monzonite and quartz monzonite to porphyritic syenogranite, whereas the Matou pluton is a relatively homogeneous monzogranite. Plagioclase in these two intrusions has a much higher An mol% (14–42%, ZGS, 1966) than in the stage 1 and 2 granitic rocks. The MMEs in both intrusions are dioritic, and their size varies from sub-centimeter to approximately 30 cm in diameter. A MME sample (10ZJS115) was collected from the Muchen Complex for further study.

### 5.3 Analytical Results

#### 5.3.1 Zircon U-Pb Dating and Hf isotope

The results for individual samples, including representative CL images, are presented in Figure 5.3. All the U-Pb-Hf results, together with some previously published data, are summarized in Figure 5.4A. Most zircon grains have high Th/U ratios and show well-developed oscillatory zoning in CL images, indicating their magmatic origin. Some zircons from the most siliceous granites, for example, the Shanghekou syenogranite (10ZJS104), have extremely high U and Th contents (up to 1–2 wt.%), which is probably related to low solubility of U in highly polymerized granitic melt (Farges et al., 1992), and the high whole-rock U/Zr ratios in these rocks. For instance, the whole-rock U/Zr ratio of the Shanghekou syenogranite (10ZJS104) is 0.066; however, the ratios are only 0.018–0.020 for the Muchen monzogranite. The weighted mean  $^{206}\text{Pb}/^{238}\text{U}$  age of the dominant zircon population of each sample is interpreted to be the crystallization age of that sample. Except for inherited zircons, the values of  $\epsilon\text{Hf}(t)$  were calculated using weighted mean ages from the zircon U-Pb isotopic analyses for each sample. Uncertainties are quoted at 2 SE (or 95% confidence interval) for the weighted mean ages and  $\epsilon\text{Hf}(t)$ .

##### 5.3.1.1 Matou monzogranite

Zircon U-Pb isotopic analyses were carried out on two samples from the Matou monzogranite (10ZJS099 and 10ZJS101). Twenty-one analyses were conducted on twenty-one zircons (Figure 5.3A) and Th contents are 75–1194 ppm and U contents are 66–741 ppm,

with  $\text{Th}/\text{U} = 0.15\text{--}2.07$ . Seventeen analyses are clustered on concordia and record a  $^{206}\text{Pb}/^{238}\text{U}$  weighted mean age of  $101 \pm 1$  Ma ( $\text{MSWD} = 0.57$ ). Spot 10ZJS099-14 is discordant and was therefore rejected from the calculation. Three inherited zircons are present. Spot 10ZJS099-9, with a  $^{207}\text{Pb}/^{206}\text{Pb}$  age of  $1741 \pm 23$  Ma, implies the involvement of Paleoproterozoic basement materials. Spots 10ZJS099-6 and 10ZJS099-13, with  $^{206}\text{Pb}/^{238}\text{U}$  ages of  $130 \pm 2$  Ma and  $217 \pm 3$  Ma, respectively, are also xenocrysts.

Twenty U-Pb analyses were conducted on twenty zircons from sample 10ZJS101 (Figure 5.3B). Th contents are 149–804 ppm and U contents are 69–370 ppm, with  $\text{Th}/\text{U} = 1.14\text{--}2.82$ . Fifteen analyses yield a weighted mean  $^{206}\text{Pb}/^{238}\text{U}$  age of  $101 \pm 1$  Ma ( $\text{MSWD} = 0.78$ ). Spots 10ZJS101-12, 16, 17 are discordant and were rejected from the age calculation. Spots 10ZJS101-3 and 10ZJS101-10 have ages of  $205 \pm 3$  Ma and  $206 \pm 3$  Ma, respectively, indicating incorporation of Triassic grains. Nineteen Hf isotopic analyses were obtained (Figure 5.3B). The two Triassic inherited zircons have  $\epsilon\text{Hf(t)}$  values of  $-4.0$  and  $-3.0$ . For the zircons with a crystallization age of  $101 \pm 1$  Ma, there are two strongly negative values ( $-15.8$  and  $-10.6$ ), whereas the remaining 15 zircons range between  $-1.8$  and  $-6.2$ .

### 5.3.1.2 Shanghekou syenogranite

Twenty-one U-Pb analyses were conducted on twenty-one zircons from the Shanghekou syenogranite (10ZJS104, Figure 5.3C). Th and U contents in most zircons show a range to high values (137–13904 ppm and 93–26112 ppm, respectively), with  $\text{Th}/\text{U} = 0.39\text{--}2.03$ . Spots 10ZJS104-4a, 11a and 21a were rejected from the age calculation because of discordance. Spots 10ZJS104-7a and 18a, with concordant  $^{206}\text{Pb}/^{238}\text{U}$  ages of  $148 \pm 2$  Ma and  $151 \pm 2$  Ma, respectively, are interpreted as inherited zircons. The remaining sixteen analyses cluster on concordia and yield a weighted mean  $^{206}\text{Pb}/^{238}\text{U}$  age of  $130 \pm 1$  Ma ( $\text{MSWD} = 1.05$ ). Seventeen Hf isotopic analyses were conducted on grains with concordant U-Pb ages. Fifteen analyses from the young population have  $\epsilon\text{Hf(t)}$  values ranging between  $-7.5$  and  $-18.7$ . The two inherited zircons have  $\epsilon\text{Hf(t)}$  values of  $-10.0$  and  $-9.8$ .

### 5.3.1.3 Sucun syenogranite

Twenty-three U-Pb analyses were conducted on 23 zircons from the Sucun syenogranite (10ZJS108, Figure 5.3D). The zircons have Th contents of 58–3096 ppm and U contents of 41–4768 ppm, with  $\text{Th}/\text{U} = 0.65\text{--}2.27$ . Spots 10ZJS108-04 and 10ZJS108-06 have  $^{206}\text{Pb}/^{238}\text{U}$  ages of 158 Ma and 228 Ma and are inherited grains. Spots 10ZJS108-03, 08, 09 are discordant and were rejected from the age calculation. The other 18 analyses cluster on concordia and yield a weighted mean  $^{206}\text{Pb}/^{238}\text{U}$  age of  $132 \pm 1$  Ma ( $\text{MSWD} = 0.51$ ). Eleven Hf isotopic analyses were obtained from these grains and  $\epsilon\text{Hf(t)}$  values range from  $-6.1$  to  $-10.4$ .

### 5.3.1.4 Huangkang syenogranite

Thirty U-Pb analyses were conducted on twenty-nine zircons from the Huangkang syenogranite (10ZJS109, Figure 5.3E). Th and U contents are 51–5085 ppm and 44–4963 ppm, respectively, with Th/U = 0.72–1.51. There are two main age groups of zircon. The older group ( $n = 10$ ) have discordant  $^{206}\text{Pb}/^{238}\text{U}$  ages of 223–196 Ma, and are inherited grains, whereas the younger concordant group ( $n = 19$ ) has a weighted mean  $^{206}\text{Pb}/^{238}\text{U}$  age of  $132 \pm 1$  Ma (MSWD = 0.83). Spot 10ZJS109-19 records a  $^{206}\text{Pb}/^{238}\text{U}$  age of  $166 \pm 2$  Ma. Fifteen Hf isotopic analyses were obtained, with three zircons from the older group having  $\epsilon\text{Hf(t)}$  values of -6.7, -6.4 and -3.6 and twelve zircons from the younger group having  $\epsilon\text{Hf(t)}$  values ranging between -8.8 and -6.1.

### 5.3.1.5 Muchen Complex

Zircons from five samples of the Muchen Complex were analysed by LA-ICP-MS and MC-ICP-MS, including one enclave sample. In contrast to the other samples, zircon ages and  $\epsilon\text{Hf(t)}$  values within individual samples show less of a spread. Our results are consistent with the zircon age and Hf isotopic results of Liu et al. (2011a) for an MME and a quartz monzonite sample.

Twenty U-Pb isotopic analyses were conducted on eighteen zircons from sample 10ZJS115, a mafic enclave (Figure 5.3F). Th and U contents are 178–1627 ppm and 146–653 ppm, respectively, with Th/U = 1.02–2.54. All analyses plot on concordia. The weighted mean  $^{206}\text{Pb}/^{238}\text{U}$  age is  $111 \pm 1$  Ma (MSWD = 0.77). Twenty Hf isotopic analyses were conducted on sixteen zircons with U-Pb analyses (four zircons have two analyses) and  $\epsilon\text{Hf(t)}$  values range from -2.3 to 2.4.

Twenty U-Pb analyses were conducted on twenty zircons from sample 10ZJS116, a quartz monzonite (Figure 5.3G). Th and U contents are 164–906 ppm and 107–589 ppm, respectively, with Th/U = 1.28–2.22. All analyses plot on concordia. The weighted mean  $^{206}\text{Pb}/^{238}\text{U}$  age of the 20 zircons is  $112 \pm 1$  Ma (MSWD = 1.4). Eighteen Hf isotopic analyses were obtained and  $\epsilon\text{Hf(t)}$  values range from -2.3 to 0.4.

Seventeen U-Pb analyses were conducted on fifteen zircons from sample 10ZJS125, a porphyritic syenogranite (Figure 5.3H), which is the most siliceous rock ( $\text{SiO}_2 = 72.18\%$ ) sampled from the Muchen Complex. Th and U contents are 95–478 ppm and 66–566 ppm, respectively, with Th/U = 0.43–2.00. All analyses plot on concordia. The weighted mean  $^{206}\text{Pb}/^{238}\text{U}$  age is  $110 \pm 1$  Ma (MSWD = 0.66). Thirteen Hf isotopic analyses were conducted and  $\epsilon\text{Hf(t)}$  values range from -2.6 to 0.2.

Twenty-four U-Pb analyses were conducted on twenty-four zircons from sample 10ZJS131, a quartz monzonite (Figure 5.3I). Th and U contents are 151–4031 ppm and 108–1065 ppm, respectively, with Th/U = 1.02–3.78. Most analyses plot on or near concordia, although Spot 10ZJS131-11 was rejected due to its strong discordance. One zircon (10ZJS131-6) has an older  $^{206}\text{Pb}/^{238}\text{U}$  age of  $131 \pm 2$  Ma. The other 22 analyses yield a weighted mean  $^{206}\text{Pb}/^{238}\text{U}$  age of  $110 \pm 1$  Ma (MSWD = 0.76). Fifteen Hf isotopic analyses were obtained.  $\varepsilon\text{Hf(t)}$  values range from –0.9 to 3.0. The age of spot 10ZJS131-11 was assumed to be 110 Ma for the calculation.

Sixteen U-Pb analyses were conducted on fifteen zircons from sample 10ZJS132, a quartz monzonite (Figure 5.3J). Th and U contents are 70–522 ppm and 90–413 ppm, respectively, with Th/U = 0.70–1.63. Excluding one discordant analysis that has a younger age (Spot 10ZJS132-13), the weighted mean  $^{206}\text{Pb}/^{238}\text{U}$  age of the remaining fifteen analyses is  $112 \pm 1$  Ma (MSWD = 0.67). Ten Hf isotopic analyses were conducted and  $\varepsilon\text{Hf(t)}$  values range from –1.0 to 3.8.

### 5.3.1.6 Wangcun syenogranite

Sample 10ZJS121 was analyzed using SHRIMP II. Twenty U-Pb analyses were obtained from 20 zircons (Figure 5.3K) and Hf isotopic analyses were conducted on fifteen of them. Th and U contents are 105–938 ppm and 113–872 ppm, respectively, with Th/U = 0.51–1.77. Spot 10ZJS121-17 has a high content of common Pb (11%) and a strongly discordant age (not shown in the concordia diagram), and hence was rejected. Spot 10ZJS121-10 has a concordant  $^{206}\text{Pb}/^{238}\text{U}$  age of  $151 \pm 2$  Ma, indicating it is an inherited zircon. Spot 10ZJS121-8 was rejected because it has a younger  $^{206}\text{Pb}/^{238}\text{U}$  age (124 Ma) than the main group, which was possibly caused by lead loss as indicated by cracks in the zircon. The remaining seventeen analyses cluster on concordia and yield a weighted mean  $^{206}\text{Pb}/^{238}\text{U}$  age of  $132 \pm 2$  Ma (MSWD = 3.7).  $\varepsilon\text{Hf(t)}$  values range from –4.9 to –9.0 ( $n = 15$ ).

### 5.3.1.7 Yingcun porphyry

Twenty U-Pb and fourteen Hf analyses were conducted on 20 zircons from the Yingcun porphyry (10ZJS129, Figure 5.3L). Th and U contents are 172–1046 ppm and 119–902 ppm, respectively, with Th/U = 1.08–1.96. All analyses fall on or near concordia and record a weighted mean  $^{206}\text{Pb}/^{238}\text{U}$  age of  $134 \pm 1$  Ma (MSWD = 0.35).  $\varepsilon\text{Hf(t)}$  values range from –5.3 to –9.3 ( $n = 14$ ).

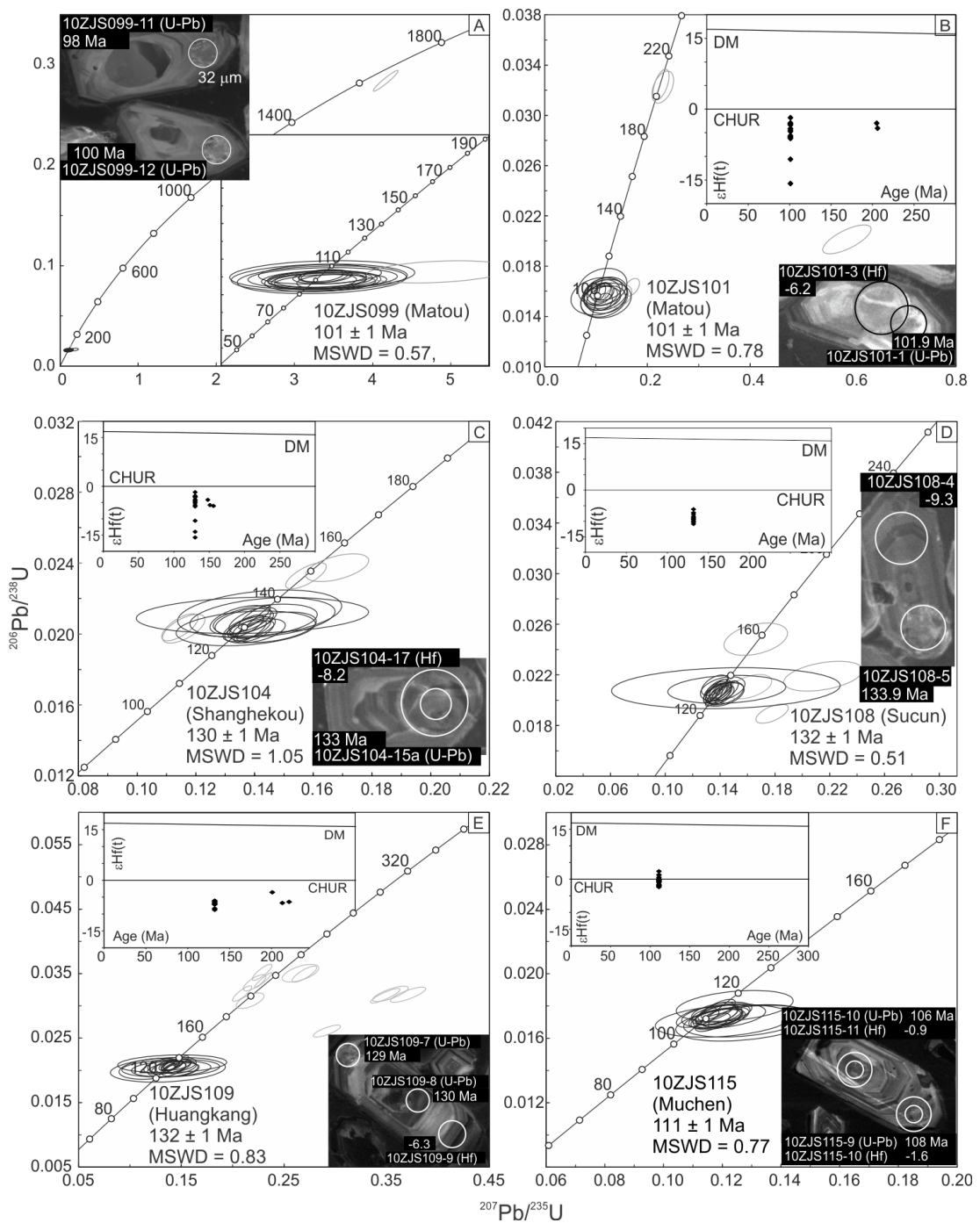


Figure 5.3 (continued over page)

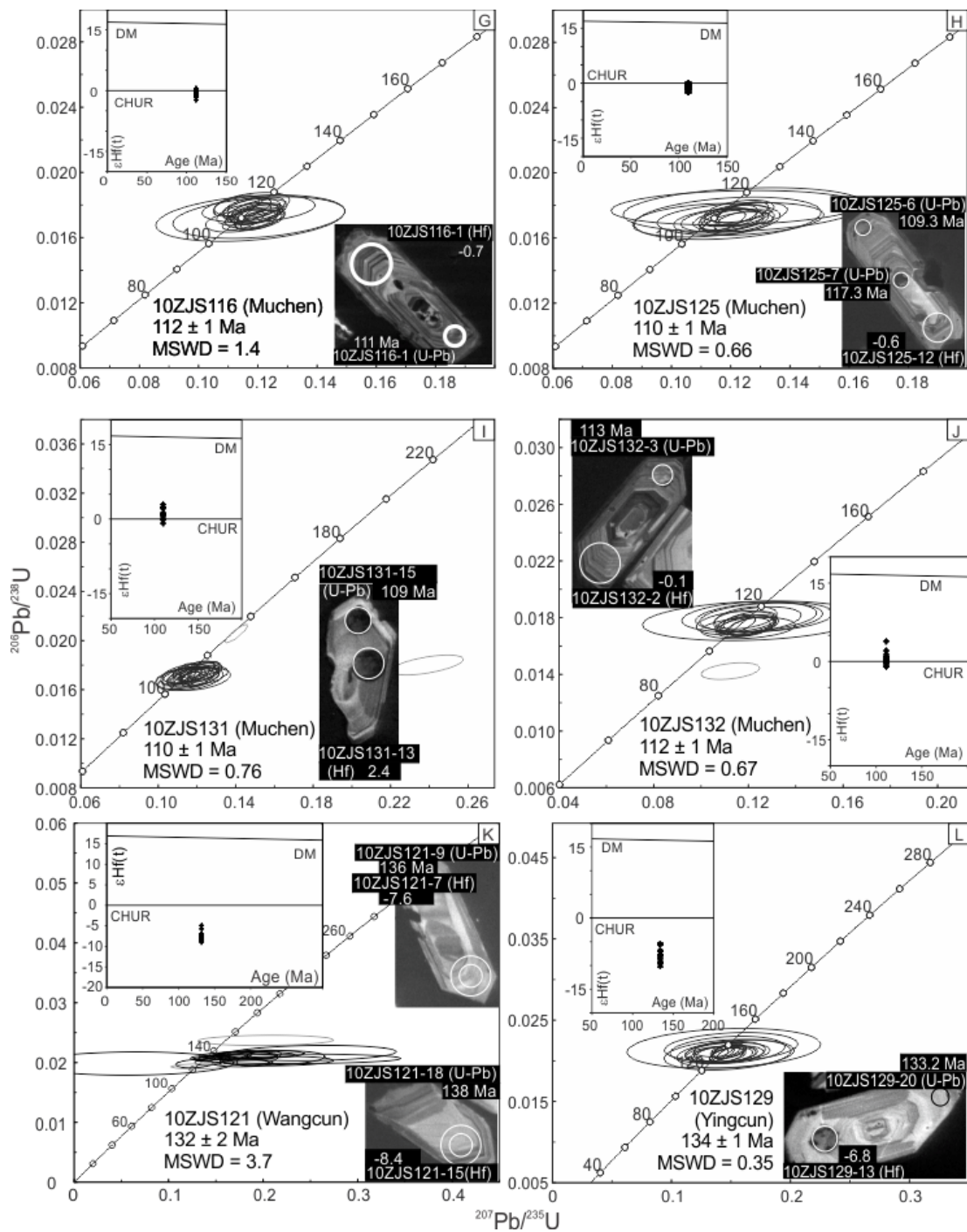


Figure 5.3 (continued)

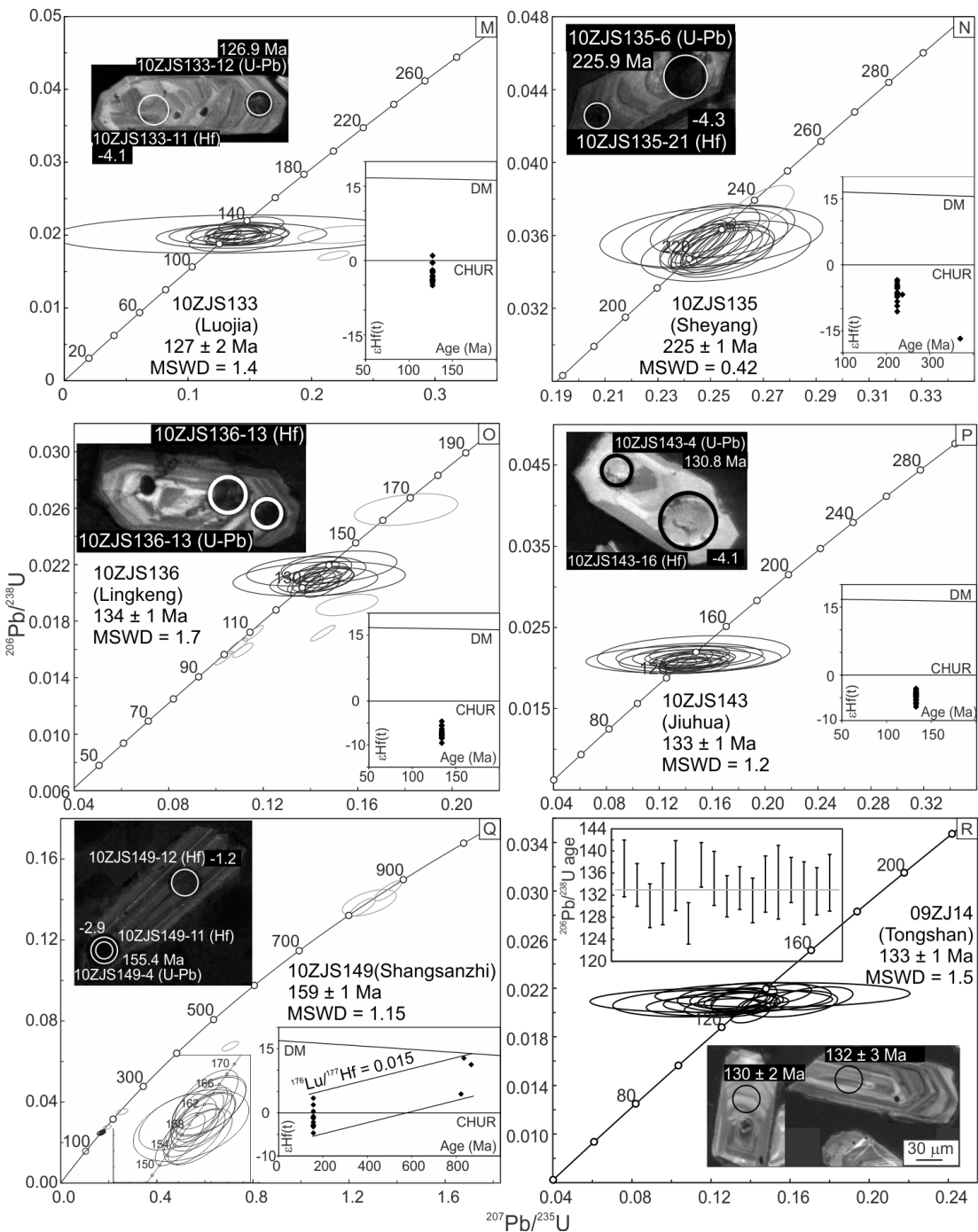


Figure 5.3 Zircon CL images, zircon LA-ICP-MS/SIRMP U-Pb results and zircon MC-LA-ICP-MS Hf isotopic results (where available) for eighteen Mesozoic granitic samples from western Zhejiang Province. In CL images, the oscillatory zoning of zircons shows their magmatic origin. Small circles (30  $\mu\text{m}$  for SHRIMP and 32  $\mu\text{m}$  for LA-ICP-MS) indicate the analytical location for U-Pb isotopic analyses, with 2 SE. Larger circles (35, 50 or 60  $\mu\text{m}$ ) in the CL images show the analytical positions of Hf isotopes, with  $\epsilon\text{Hf(t)}$  values at 2 SE. On the concordia diagrams, the spots represented by grey error ellipses (2 SD) were excluded from the calculation of the mean age. (A-B): Matou monzogranite; (C) Shanghekou syenogranite; (D) Sucun syenogranite; (E) Huangkang syenogranite; (F) MME within Muchen quartz monzonite (10ZJS116); (G) Muchen quartz monzonite; (H) Wangcun syenogranite (SHRIMP); (I) Muchen porphyry; (J) Yingcun porphyry; (K) Muchen quartz monzonite; (L) Muchen quartz monzonite; (M) Luojia porphyry; (N) Sheyang syenogranite; (O) Lingkeng syenogranite; (P) Jiuhua porphyry; (Q) Shangsanzhi porphyry; (R) Tongshan syenogranite (SHRIMP).

### 5.3.1.8 Luojia porphyry

Twenty analyses were conducted on nineteen zircons from the Luojia porphyry (10ZJS133, Figure 5.3M). Th contents are 39–1124 ppm and U contents are 24–682 ppm, with Th/U = 0.82–3.76. Except for spots 10ZJS133-13 and 10ZJS133-20 that are strongly discordant, the remaining eighteen analyses yield a weighted mean  $^{206}\text{Pb}/^{238}\text{U}$  age of  $127 \pm 2$  Ma (MSWD = 1.4). Thirteen Hf isotopic analyses were obtained and  $\epsilon\text{Hf(t)}$  values range from –4.2 to 1.0.

### 5.3.1.9 Sheyang syenogranite

Twenty-two U-Pb and twenty-one Hf analyses were carried out on 22 zircons from the Sheyang syenogranite (10ZJS135, Figure 5.3N). The zircons have Th contents of 72–1089 ppm and U contents of 35–920 ppm, with Th/U = 0.75–2.95. Spot 10ZJS135-19 with a discordant  $^{206}\text{Pb}/^{238}\text{U}$  age of  $370 \pm 5$  Ma is an inherited grain. The  $^{206}\text{Pb}/^{238}\text{U}$  age of spot 10ZJS135-21 is  $237 \pm 3$ : it is also interpreted as an inherited grain. The remaining 20 analyses cluster on concordia and yield a weighted mean  $^{206}\text{Pb}/^{238}\text{U}$  age of  $225 \pm 1$  Ma with MSWD = 0.42. The  $\epsilon\text{Hf(t)}$  values of the two inherited zircons (370 Ma and 237 Ma) are –16.8 and –6.8, respectively; the  $\epsilon\text{Hf(t)}$  values of the remaining zircons range from –3.4 to –10.6.

### 5.3.1.10 Lingkeng syenogranite

Twenty-four U-Pb analyses were conducted on twenty-three zircons from the Lingkeng syenogranite (10ZJS136, Figure 5.3O) and Hf analyses were conducted on eleven of them. Th and U contents are 133–10225 ppm and 79–8512 ppm, respectively. Spots 10ZJS136-04, 05, 06, 09, and 17, with  $^{206}\text{Pb}/^{238}\text{U}$  ages of ca. 100 Ma, are probably the result of Pb loss due to their high contents of U and Th and they are assumed to have the crystallization age of the

Lingkeng syenogranite in the  $\epsilon\text{Hf(t)}$  calculations. Spot 10ZJS136-20 has a discordant  $^{206}\text{Pb}/^{238}\text{U}$  age of  $122 \pm 2$  Ma. There is also a zircon with a concordant  $^{206}\text{Pb}/^{238}\text{U}$  age of 165 Ma, representing an inherited Jurassic zircon. The remaining seventeen analyses cluster on concordia and record a weighted mean  $^{206}\text{Pb}/^{238}\text{U}$  age of  $134 \pm 1$  Ma (MSWD = 1.7).  $\epsilon\text{Hf(t)}$  values range from –4.6 to –9.5.

### 5.3.1.11 Jiuhua porphyry

Twenty U-Pb analyses and seventeen Hf analyses were conducted on 20 zircons from the Jiuhua porphyry (10ZJS143, Figure 5.3P). Th and U contents are 47–366 ppm and 32–176 ppm, respectively, with Th/U ratios of 1.14–2.27. All spots are concordant and the weighted mean  $^{206}\text{Pb}/^{238}\text{U}$  age is  $133 \pm 1$  Ma (MSWD = 1.2).  $\epsilon\text{Hf(t)}$  values range from –3.0

to  $-7.0$ . The weighted average of  $\epsilon\text{Hf(t)}$ ,  $-4.8 \pm 0.5$ , is consistent with the analytical result ( $-4.76 \pm 0.49$ ) of Wong et al. (2011) on the same porphyry.

### 5.3.1.12 Shangsanzi porphyry

Twenty-one U-Pb analyses were conducted on 18 zircons from the Shangsanzi porphyry (10ZJS149, Figure 5.3Q). Apart from spot 10ZJS149-20, the analyzed zircons have Th contents of 134 to 649 ppm and U contents of 128 to 1180 ppm. In contrast, zircon 10ZJS149-20 has a very high U content (9925 ppm), a low Th/U ratio of 0.03 and a concordant  $^{206}\text{Pb}/^{238}\text{U}$  age of 106 Ma, which is possibly related to Cretaceous hydrothermal processes. Spots 10ZJS149-02, 10ZJS149-03 and 10ZJS149-07 have concordant  $^{206}\text{Pb}/^{238}\text{U}$  ages of  $823 \pm 10$  Ma,  $836 \pm 15$  Ma and  $869 \pm 11$  Ma, respectively. Spots 10ZJS149-5, 10ZJS149-16 and 10ZJS149-18 have  $^{206}\text{Pb}/^{238}\text{U}$  ages of  $223 \pm 4$  Ma,  $422 \pm 6$  Ma and  $175 \pm 3$  Ma, respectively; all grains are interpreted as xenocrysts. The remaining fourteen analyses cluster on concordia and yield a weighted mean  $^{206}\text{Pb}/^{238}\text{U}$  age of  $159 \pm 1$  Ma (MSWD = 1.15), which is consistent with the result ( $155.6 \pm 2.5$  Ma) of Chen (2011) on the same porphyry using the zircon LA-ICP-MS method. Nineteen Hf isotopic analyses were conducted on fifteen zircons. The  $\epsilon\text{Hf(t)}$  values for the three Neoproterozoic zircons are 4.4, 11.3 and 12.8. The  $\epsilon\text{Hf(t)}$  values of the Jurassic zircons range from  $-4.6$  to  $3.5$ .

### 5.3.1.13 Tongshan syenogranite

Eighteen U-Pb isotopic analyses were conducted on 18 zircons from the Tongshan syenogranite (09ZJ14, Figure 5.3R) using the SHRIMP method. Th and U contents are 43–319 ppm and 86–602 ppm, respectively, with Th/U = 0.30–0.81. One inherited zircon has a  $^{206}\text{Pb}/^{238}\text{U}$  age of  $327 \pm 9$  Ma. The remaining 17 zircons yield a weighted mean  $^{206}\text{Pb}/^{238}\text{U}$  age of  $133 \pm 1$  Ma (MSWD = 1.5). This result is consistent with the zircon SHRIMP ages ( $130 \pm 3$  Ma and  $129 \pm 2$  Ma) of Jiang et al. (2011a) on the same pluton.

The ages of the five magmatic groups and the gaps between them are generally consistent with the age spectrum of the Mesozoic detrital zircons from a modern river (the Oujiang River) to the southeast of the study region (Figure 5.4B, Xu et al., 2007). The evolution trends of Hf isotopes are also similar, showing a rise in  $\epsilon\text{Hf(t)}$  during the Early Cretaceous (Figure 5.4C).

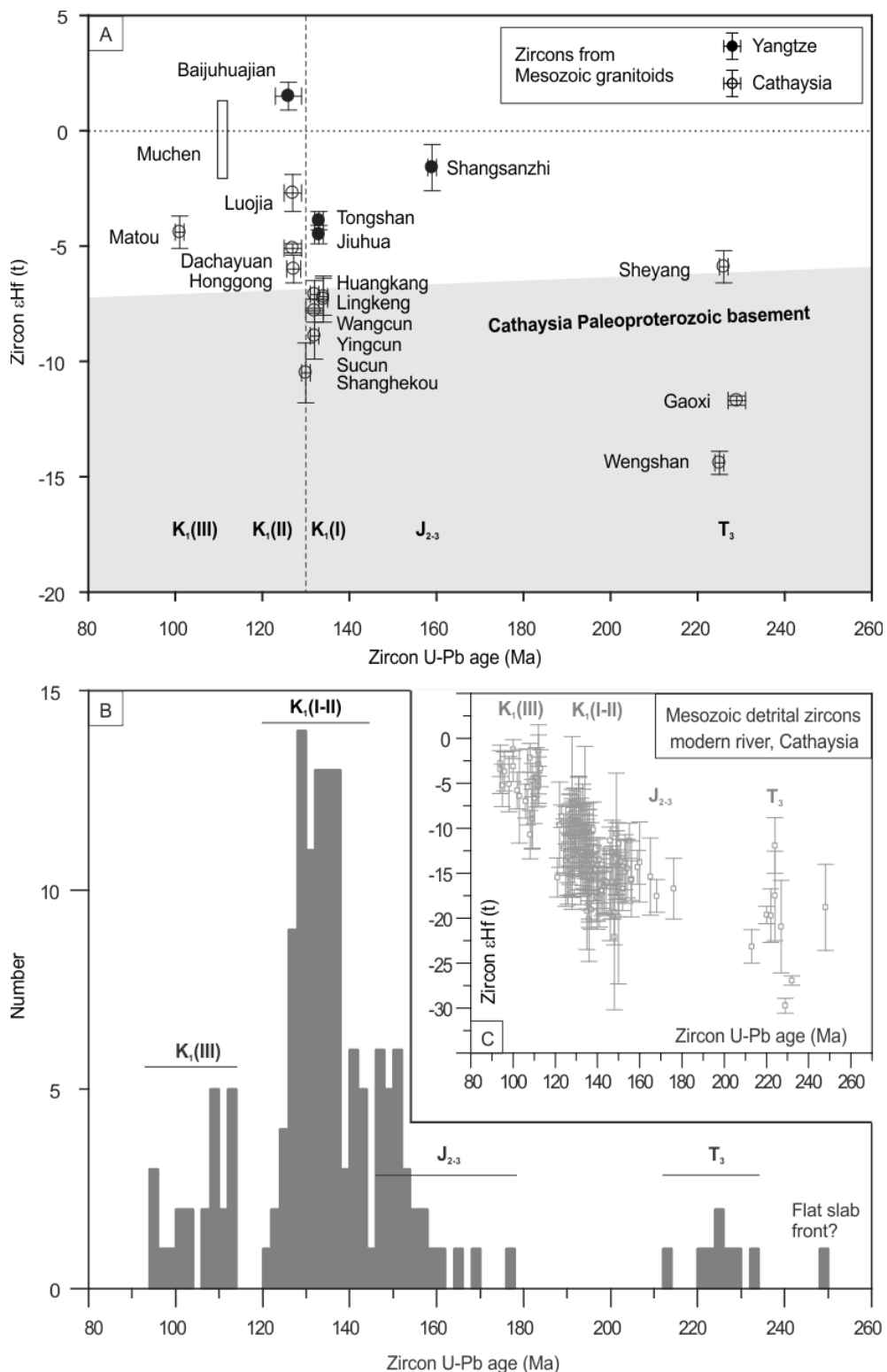


Figure 5.4 (A) Zircon  $\epsilon\text{Hf}(t)$  versus zircon U-Pb ages for the Mesozoic granitic rocks in western Zhejiang Province, at 2 standard errors. The Hf isotopic compositions of the Paleoproterozoic crustal rocks of the Cathaysia Block are based on data from Yu et al. (2009) and Xia et al. (2012); the upper limit is constrained by data from Xiang et al. (2008), assuming  $^{176}\text{Lu}/^{177}\text{Hf} = 0.022$  for their amphibolite. The dashed line at 130 Ma is the best estimate of the boundary between the K<sub>1</sub>(I) and K<sub>1</sub>(II) granitic rocks; (B) Age spectrum of detrital zircons with Mesozoic ages in the study region (Cathaysia Block) (Xu et al., 2007); (C) Zircon  $\epsilon\text{Hf}(t)$  versus zircon U-Pb ages for the same detrital zircons,  $\epsilon\text{Hf}(t)$  values were recalculated with a decay constant of  $1.867 \times 10^{-11} \text{ yr}^{-1}$  (S öderlund et al., 2004).

### 5.3.2 Whole-rock major and trace elements

#### 5.3.2.1 Major elements

The most notable feature of the major element data is that each magmatic stage has distinct chemical compositions (Figure 5.5), although the samples in this study are all high-K series granitoids (Figure 5.5A). Based on their age and whole-rock geochemistry, five distinct groups of granitic rocks are identified. They are denoted by T<sub>3</sub> (the Late Triassic, 230–215 Ma), J<sub>2-3</sub> (the Middle-Late Jurassic, 170–150 Ma), K<sub>1</sub>(I) (the first stage in the Early Cretaceous, 140–130 Ma), K<sub>1</sub> (II) (the second stage in the Early Cretaceous, 130–125 Ma) and K<sub>1</sub>(III) (the third stage in the Early Cretaceous, 115–100 Ma).

The T<sub>3</sub> samples have moderate SiO<sub>2</sub> contents (66–71%) and the highest K<sub>2</sub>O contents amongst all the Mesozoic samples (Figure 5.5A). Apart from the Jingju syenogranite, they tend to have molar Al<sub>2</sub>O<sub>3</sub>/(CaO + Na<sub>2</sub>O + K<sub>2</sub>O) >1.05 and molar K<sub>2</sub>O/ Na<sub>2</sub>O ratios >1 (Figure 5.5B). A lower A/CNK ratio for the Jingju syenogranite is associated with the occurrence of amphibole. The Suichang and Wengshan syenogranites have moderate FeO<sub>total</sub>/(MgO+FeO<sub>total</sub>) ratios (~0.8). The Jingju syenogranite has much higher Fe/Mg ratios and also higher K<sub>2</sub>O contents. The T<sub>3</sub> samples mainly plot in the field of ferroan granitic rocks in Figure 5.5C.

Similar to the T<sub>3</sub> samples, the J<sub>2-3</sub> samples have moderate SiO<sub>2</sub> contents (65–73%); however, their K<sub>2</sub>O contents and FeO<sub>total</sub>/(FeO<sub>total</sub> + MgO) ratios are lower. Apart from one analysis from the Tongcun porphyry, all the Jurassic samples plot in the field of magnesian granitic rocks (Figure 5.5C).

The K<sub>1</sub> (I) samples mostly have high SiO<sub>2</sub> contents (>73%, Figure 5.5A). The molar Al<sub>2</sub>O<sub>3</sub>/(CaO + Na<sub>2</sub>O + K<sub>2</sub>O) ratios are around unity with most results ranging from 1 to 1.05, which is consistent with their mineral assemblage being mostly quartz and feldspar. Molar K<sub>2</sub>O/Na<sub>2</sub>O ratios are generally less than unity and K<sub>2</sub>O contents in most samples are less than 5%. They are ferroan granites with FeO<sub>total</sub>/(FeO<sub>total</sub> + MgO) ratios >0.8, which are the highest among all the five groups.

The K<sub>1</sub> (II) samples have moderate to high SiO<sub>2</sub> contents (64–78%). The majority of samples have K<sub>2</sub>O >5% but highly fractionated samples from the Baijuhuajian pluton have relatively low K<sub>2</sub>O contents (4–5%). Their molar Al<sub>2</sub>O<sub>3</sub> /(CaO + Na<sub>2</sub>O + K<sub>2</sub>O) and K<sub>2</sub>O/Na<sub>2</sub>O ratios are scattered. They are ferroan granites with FeO<sub>total</sub>/ (FeO<sub>total</sub> + MgO) ratios >0.8.

The K<sub>1</sub> (III) samples have variable SiO<sub>2</sub> contents (57–72%). The molar Al<sub>2</sub>O<sub>3</sub> / (CaO + Na<sub>2</sub>O + K<sub>2</sub>O) ratios are between 0.85 and 1.05, but generally less than 1. The molar K<sub>2</sub>O/

$\text{Na}_2\text{O}$  ratios are lower than unity.  $\text{K}_2\text{O}$  contents (4–6%) are comparable to  $\text{J}_{2-3}$  and  $\text{K}_1$  (I) samples, but lower than  $\text{T}_3$  and  $\text{K}_1$  (II) samples. On the  $\text{FeO}_{\text{total}}/(\text{FeO}_{\text{total}} + \text{MgO})$  versus  $\text{SiO}_2$  diagram, they straddle the boundary between ferroan and magnesian rocks (Figure 5.5C).

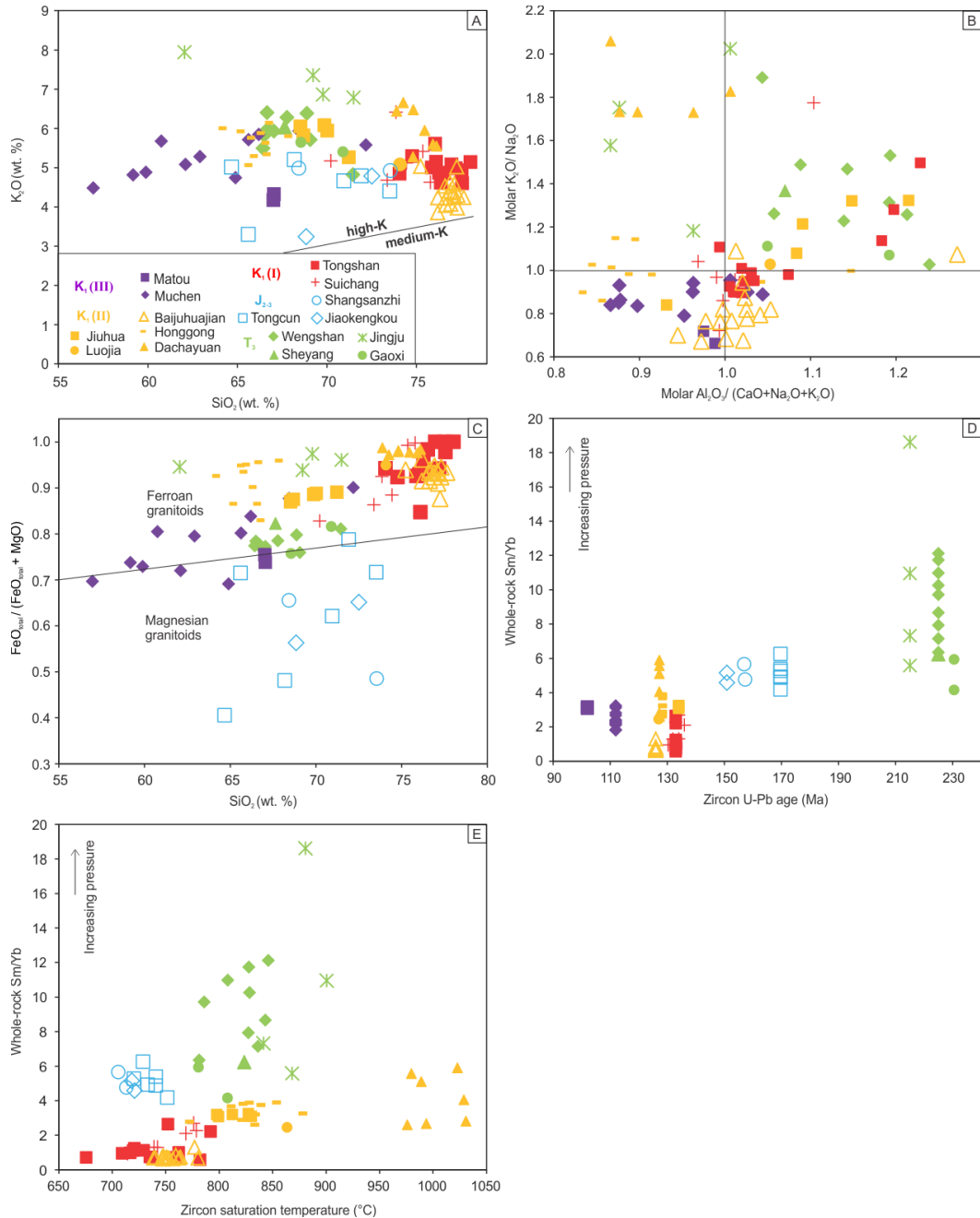


Figure 5.5 Whole-rock geochemical results for the Mesozoic samples from western Zhejiang Province. All symbols use the same as in Figure 5.5A and “+ Suichang” represents the  $\text{K}_1$ (I) samples from the Lingkeng, Huangkang, Sucun, Shanghekou, Yingcun and Wangcun intrusions: (A)  $\text{K}_2\text{O}$  versus  $\text{SiO}_2$ ; (B) molar  $\text{K}_2\text{O}/\text{Na}_2\text{O}$  and  $\text{Al}_2\text{O}_3/(\text{CaO}+\text{Na}_2\text{O}+\text{K}_2\text{O})$ ; (C)  $\text{FeO}_{\text{total}}/(\text{FeO}_{\text{total}} + \text{MgO})$  versus  $\text{SiO}_2$ , after Frost and Frost (2011); (D) Sm/Yb ratio versus age; (E) Sm/Yb ratio versus zircon saturation temperatures, based on Boehrke et al. (2013), excluding the mantle-derived  $\text{K}_1$ (III) rocks and assuming  $M = 1.6$  (Miller et al., 2003) for the altered  $\text{J}_{2-3}$  samples.

### 5.3.2.2 Trace elements

The whole-rock trace element analytical results are listed in table 2. Like major element results, each age group has a distinctive trace element pattern (Figure 5.6). The results are normalized to the global average upper continental crust (UCC, Rudnick and Gao, 2003), in groups of large ion lithophile elements, rare earth elements, high field strength elements and transition metal elements. The most significant differences in trace element compositions among the five groups are in REE, Ba, Sr, Eu, HFSE elements (Nb, Ta, Zr, Hf) and V/Co. All five groups have lower transition metal contents than the global average of continental upper crust. In addition, there are Ni and Cr depletions relative to other transition metal elements. Such a “W” shape pattern in the normalized diagrams has been explained by high binding energies of Ni and Cr in the ferromagnesian minerals (Allègre and Michard, 1974). From the Triassic to Early Cretaceous, there is a general decreasing trend in the Sm/Yb ratio (Figure 5.5D).

For the T<sub>3</sub> samples (Figure 5.6A), Ba, Sr, Eu, U and Pb are depleted, but LREE, Th, Hf and Zr are relatively enriched. LREE/HREE ratios are the highest among all 5 groups, with Sm/Yb = 5–12. Their Ga/Al ratios are 2.8–3.5. Cr and Ni are depleted relative to other transition metal elements, with (V/Co)<sub>UCC</sub> = ~1.

The J<sub>2-3</sub> samples (Figure 5.6B) are also enriched in LREE relative to HREE, with Sm/Yb = 4–7. They have the lowest REE contents among all the five groups. Both the Tongcun and Shangsanzi samples show positive Eu anomalies. One sample from the Shangsanzi porphyry has Ga/Al = 2.6. There is enrichment in V, with (V/Co)<sub>UCC</sub> >1. These trace element results are consistent with those reported by Chen (2011) for the Shangsanzi porphyry.

The K<sub>1</sub> (I) samples (Figure 5.6C) are strongly depleted in Ba, Sr, Eu, Zr, Hf and transition metals, but have high contents of Rb, Th, U, Pb, Nb and Ta. They are also enriched in HREE relative to LREE and MREE, with Sm/Yb <3. The samples from the Tongshan syenogranite and the Shanghekou porphyry show notable depletions in LREE. (V/Co)<sub>UCC</sub> values are ~1. They have Ga/Al ratios of 2.4–6.4.

The K<sub>1</sub> (II) samples (Figure 5.6D) have flat REE patterns, with Sm/Yb = 2–4 and they are depleted in Ba, Sr and Eu. Their Ga/Al ratios are 2.1–4.3. Relative to the K<sub>1</sub> (I) samples, they have higher Zr and Hf but lower Nb and Ta contents, which reflect different geochemical behavior of the high field strength elements. (V/Co)<sub>UCC</sub> values are less than 1.

The K<sub>1</sub> (III) samples (Figure 5.6E) show flat trace element patterns, similar to those of the J<sub>2-3</sub> samples. The contents of most trace elements are comparable to those of the global average upper continental crust and their Sm/Yb ratios are between 2 and 4. Their Ga/Al

ratios are the lowest amongst the five groups (2.1–2.7). These samples also have the highest contents of transition metal elements among the five groups. Like the  $J_{2-3}$  samples, the  $K_1$  (III) samples are enriched in V, with  $(V/Co)_{UCC} > 1$ .

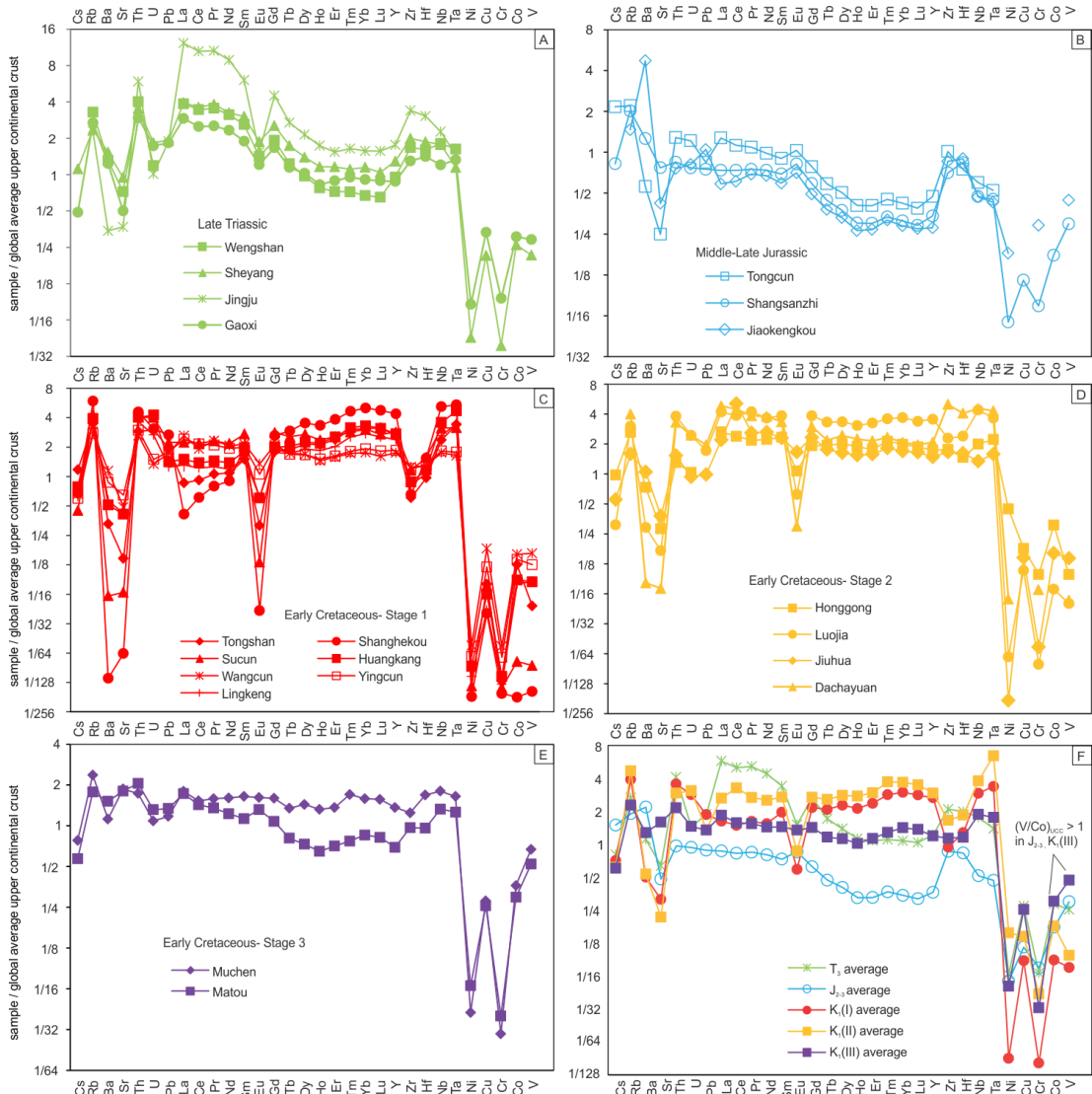


Figure 5.6 Trace element patterns of the Mesozoic granitic samples from western Zhejiang Province, normalized to the global average continental upper crust (Rudnick and Gao, 2003). All data represent average composition. (A)  $T_3$  granites; (B)  $J_{2-3}$  porphyries; (C)  $K_1$ (I) granitic rocks; (D)  $K_1$ (II) porphyries; (E)  $K_1$ (III) granites; (F) A comparison of the average of the different stages.

#### 5.4 Petrogenetic Interpretation

The five geochemically distinct groups of granitic rocks (Figures 5.5 and 5.6) in western Zhejiang Province can be distinguished based on their ages, which range from the Triassic to the Early Cretaceous (Figure 5.4A). The different isotopic and elemental compositions of the five groups reflect different source-temperature-pressure-water-redox conditions in the continental lithosphere. In the following discussion, the sources are constrained by zircon Hf isotopes. Figures 5.4 and 5.6 show that the granitoids in the northwest of the study region have zircon  $\epsilon\text{Hf}(t) > -5$ , which is significantly higher than those from the southeast part of

the study region – the Cathaysia Block (as low as –30). The data support the interpretation that the basement rocks of the two regions are mainly of Neoproterozoic (Li et al., 2009) and Paleoproterozoic (Yu et al., 2009) age, respectively.

Water content in granitic magmas will affect the stability of certain mafic minerals, such as amphibole and titanite (Richards, 2011) and the solubility of plagioclase (especially the An component) (Conrad et al., 1988), therefore controlling the trace element patterns (Bachmann and Bergantz, 2008).

The initial magma temperatures of the samples are estimated by zircon saturation geothermometry (Watson, 1979; Bohnke et al., 2013). The J<sub>2,3</sub> samples have low Zr contents but still have inherited zircons (an average of 1/4 of the total analyzed grains for the three porphyries) (Li et al., 2013b; Zeng et al., 2013b). Their magmas were therefore likely to be wet and cold (Miller et al., 2003). The zircon saturation thermometry may thus overestimate the initial magma temperatures of these rocks.

In contrast, inherited zircons are rarely found in the T<sub>3</sub>, K<sub>1</sub>(I) and K<sub>1</sub>(II) samples. The T<sub>3</sub> and K<sub>1</sub>(II) rocks have high Zr contents: 200–780 ppm and 270–1140 ppm, respectively. Such high values imply that zircons in the source regions probably approached complete dissolution and the zircon saturation temperatures either approximate or slightly underestimate the initial temperatures of crustal melts (see Figure 4 of Miller et al., 2003). The K<sub>1</sub>(I) rocks have low Zr contents (80–280 ppm) and low-temperature geochemical characteristics (low MgO, Ba, Sr, Eu and transition metal contents; Figure 5.6C), and therefore the K<sub>1</sub>(I) magmas should have initially been saturated in zircon. The zircon saturation temperatures for the K<sub>1</sub>(I) magmas are therefore reasonable estimations of initial magma temperatures. The K<sub>1</sub>(III) magmas, especially the basic (MME) and intermediate ones, were most likely zircon-undersaturated mantle-derived magmas, and the zircon saturation temperatures would therefore significantly underestimate the initial magma temperatures.

The MREE/HREE ratio is regarded as a relatively reliable index of melting/fractionation pressures for magmas, as it is mainly controlled by the proportion of residual garnet (Qian and Hermann, 2013). Although garnet can be stable as a peritectic product in melts from sedimentary sources at relatively low pressures, high contents of peritectic garnet and high magma Sm/Yb ratios still imply high pressures (Vielzeuf and Holloway, 1988). An extensive data set from the Andes shows that the maximum value of the MREE/HREE ratio is a good indicator of crustal thickness (Mamani et al., 2010). Few Mesozoic S-type granitoids in South China have high Sm/Yb ratios (Qi et al., 2007; Wang et al., 2007b; Huang et al., 2011b). In the study region, all the Triassic samples have high

Sm/Yb ratios, whereas all the K<sub>1</sub>(I) samples that share similar zircon  $\epsilon\text{Hf(t)}$  values (Figure 5.4A) have much lower Sm/Yb ratios (Figure 5.5D). Such variations cannot be accounted for by differences in the magma sources. The Sm/Yb ratio is therefore used to qualitatively constrain the melting pressures for the T<sub>3</sub>, J<sub>2-3</sub> and K<sub>1</sub>(I-II) samples, and the fractionation pressures for K<sub>1</sub>(III) samples (see further discussion below on partial melting/fractional crystallization).

The ratio of a pair of transition metal elements (V and Co) is used for redox condition estimation. The partition coefficient of V in major ferromagnesian minerals significantly decreases with oxygen fugacity (Shervais, 1982). In contrast, with  $E^{\circ}(\text{Co}^{3+}, \text{Co}^{2+}) = +1.92$  V, cobalt is expected to be divalent in most geological environments (Goldschmidt, 1958; Wedepohl, 1973) and is a compatible element in high-temperature ferromagnesian silicate minerals. High/low V contents relative to other transition metals qualitatively reflect high/low magma oxygen fugacities (Shervais, 1982; Lee et al., 2005), which are also consistent with zircon Ce anomalies (Li et al., 2011b; Qiu et al., 2013; Zhang et al., 2013; Zhu et al., 2013) and petrographic evidence (crystallization of fayalite) (Osborn, 1979; Fu et al., 2004; Huang et al., 2011a).

#### 5.4.1 Late Triassic magmatism: T<sub>3</sub>

The high Sm/Yb ratios of the Late Triassic granites (4–19; Figure 5.5D), based on the estimation of Kay and Mpodozis (2001), probably reflect high melting pressures and a crustal thickness of approximately 45–50 km. The granites of this stage are mainly strongly peraluminous (Figure 5.5B), which is a common characteristic of dehydration melts (Patiño-Douce and Beard, 1995). They are depleted in Sr and Eu (Figure 5.6A), reflecting the low solubility of plagioclase under water-deficient conditions (Conrad et al., 1988). The high temperatures estimated for the Late Triassic granites using zircon saturation thermometry (800–900 °C, Figure 5.5E) are consistent with dehydration melting rather than water-fluxed melting. The T<sub>3</sub> rocks are ferroan granites, which are generally produced in intraplate environments (Frost and Frost, 2008). For the 215 Ma Jingju syenogranite, the occurrence of amphibole and associated low A/CNK ratios implies a higher melting temperature (~850–900 °C) than the earlier ~225 Ma granites (~800–850 °C), suggesting that dehydration melting was triggered by amphibole breakdown (Whitney, 1988; Beard and Lorgren, 1991). The magnetic susceptibilities of the T<sub>3</sub> granites are relatively low (Figure 5.7), suggesting that the granites were generated in relatively reducing conditions. Their negative zircon  $\epsilon\text{Hf(t)}$  values indicate that mantle materials were not significantly involved in the melting processes and the source is likely to be the Paleoproterozoic basement (Yu et al., 2009).

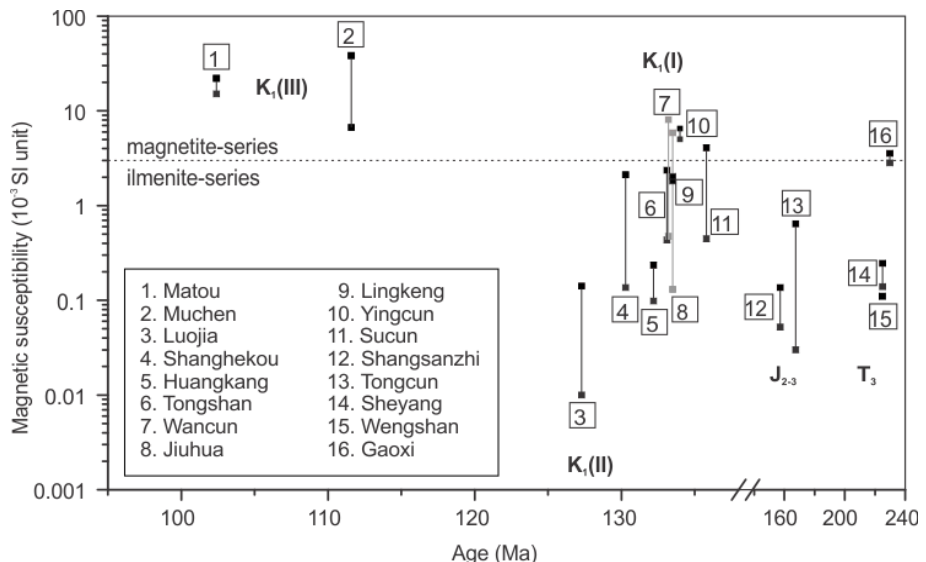


Figure 5.7 Magnetic susceptibility versus age plot for the Mesozoic samples from western Zhejiang Province. The boundary between the magnetite and ilmenite series granitoids is from Ishihara et al. (2000).

The Wengshan and Jingju syenogranites were classified as aluminous A-type granites by Sun et al. (2011) and Li et al. (2012b), based on their high whole-rock Ga/Al ratios (Whalen et al., 1987). Those two studies further argued that the T<sub>3</sub> granites were generated in a transtensional tectonic setting. However, such high Ga/Al ratios could reflect other factors rather than a lower pressure. High melting pressures under dehydration conditions result in high modal garnet (Patiño Douce and Beard, 1995) and it has been shown that Ga is notably depleted in garnet relative to plagioclase and other rock-forming minerals (DeVore, 1955; O'Hara, 1961). As a result, the melt tends to become richer in Ga. Another factor is the relatively stable An-rich plagioclase in the source under dry melting conditions. Ga and Al both form complexes with oxygen and they are network-formers for silicate minerals (Ringwood, 1955). Since the Ga ion has a larger radius than Al,  $\text{GaO}_4^{5-}$  tends to accumulate in the melt relative to  $\text{AlO}_4^{5-}$  (Goldschmidt, 1958). The phenomenon can also be understood by the lower melting point of  $\text{NaGaSi}_3\text{O}_8$  (1015 °C, Goldsmith, 1950) than plagioclase. Goodman (1972) noticed that later-formed Ab-rich plagioclase has higher Ga contents than earlier-formed An-rich plagioclase, which implies that Ga tends to be scavenged by low melting point Al-bearing minerals such as Ab-rich plagioclase and alkali feldspar. Therefore, under water-deficient conditions with low An solubility and a low degree of partial melting, alkali feldspar granites and syenogranites tend to have high Ga/Al ratios. The same explanation can be applied to the K<sub>1</sub> (I-II) A-type granitic rocks and I would argue that the Ga/Al ratios are not relevant to the crustal melting pressure, at least in the study area. Overall, the T<sub>3</sub> granites were generated by high temperature and high pressure dehydration melting in a reduced lower crust.

### 5.4.2 Middle-Late Jurassic magmatism: J<sub>2-3</sub>

The zircon Hf isotope results alone cannot distinguish whether the J<sub>2-3</sub> porphyries were derived from a metasomatic mantle or from Neoproterozoic crustal rocks (see discussions on K<sub>1</sub>(III) samples and Figure 5.3Q). However, the porphyries have low zircon saturation temperatures (Figure 5.5E) and many inherited Neoproterozoic zircons (Li et al., 2013b; Zeng et al., 2013b), and therefore more likely represent crust-derived granitic melts saturated in zirconium (Miller et al., 2003). This is consistent with the low Ti-in-zircon temperatures of the Tongcun porphyries (< 781 °C, Qiu et al., 2013).

No mafic enclaves and coeval mafic rocks have been found associated with the J<sub>2-3</sub> intrusions, and there is no evidence for any direct involvement of mantle-derived magmas in the genesis of the J<sub>2-3</sub> granitic porphyries. The fact that the J<sub>2-3</sub> granitic porphyries are Mo-bearing also implies they were most likely generated from a crust that had a much higher content of Mo than the mantle (Palme and O'Neill, 2003). The Sm/Yb ratios of the Jurassic porphyries are lower than for the Triassic granites, but still higher than the Cretaceous ones (Figure 5.5E), suggesting that these granitic porphyries were also generated in thickened crust. A high water flux would be required to generate such low-temperature melts from the Neoproterozoic materials in a thickened lower crust.

The properties of the J<sub>2-3</sub> granitic porphyries suggest that the melting processes involved high contents of water and high oxygen fugacities. For example, these porphyries are not depleted in Eu and are magnesian rocks which are typical products of wet arc environments (Frost and Frost, 2011). Also, their low Zr contents were likely caused by water-fluxed melting processes. Their trace element patterns resemble those of felsic rocks produced in a cold-wet-oxidized environment (Bachmann and Bergantz, 2008). These rocks have porphyritic textures, which were possibly controlled by high water contents and earlier water saturation because “crystallization under vapor-saturated conditions will cause a shorter temperature range and finer grain size” (Whitney, 1988). As Qiu et al. (2013) reported for the Tongcun porphyry, there are no Eu anomalies in the zircon REE patterns, which indicate a high Eu<sup>3+</sup>/Eu<sup>2+</sup> ratio in the magma and therefore a highly oxidized environment during zircon crystallization. Log(fO<sub>2</sub>) is FMQ +2.7 based on the zircon Ce anomaly, which is much higher than that of the K<sub>1</sub>(I) samples, for example, the Shanghekou porphyry with FMQ -1.1 (Qiu et al., 2013). A high V/Co ratio is observed in the Shansanzhi porphyry which was likely generated from water-fluxed melting. However, in the T<sub>3</sub> granites formed by dehydration melting, this signature is less obvious or absent. Such a high V/Co ratio reflects a relatively oxidized condition which lowered the partition coefficients of V in mafic minerals. To summarize, the results indicate that the J<sub>2-3</sub> granites were generated at low temperatures and high pressures through water-fluxed melting in an oxidized lower crust.

### 5.4.3 First stage of Early Cretaceous magmatism: K<sub>1</sub>(I)

These granitic rocks are highly felsic syenogranites that are depleted in anorthite and ferromagnesian components. Strong depletions in Ba, Sr and Eu, and the impoverishment in transition metal elements, imply low temperatures and/or depletion in volatile components. They belong to the ferroan granitic rocks, which are typically generated in intraplate environments. The decreased V/Co ratios and significantly increased REE contents relative to the J<sub>2-3</sub> porphyries also imply a reduced and water-deficient melting environment (Bachmann and Bergantz, 2008). The A-type affinities (high whole-rock Ga/Al ratios) of the K<sub>1</sub>(I) granitic rocks were likely caused by low-degree dehydration melting at relatively low temperatures (700–800 °C, Figure 5.5E). The low LREE/HREE ratios of the K<sub>1</sub>(I) granitic rocks can be interpreted as a result of low-pressure partial melting. Low Sm/Yb ratios (Figure 5.5E) are generally linked to a thin crust (Kay and Mpodozis, 2001; Mamani et al., 2010), where garnet is unstable and does not fractionate rare earth elements. Since feldspars are important hosts for LREE during partial melting (Villaseca et al., 2007), the depletion of feldspar components (Table 5.1) in low-pressure melts (Tuttle and Bowen, 1958; Gualda and Ghiorso, 2013) will also cause relative LREE depletion.

Samples from the Tongshan syenogranite and the Shanghekou porphyry are notably depleted in LREE. Miller and Mittlefehldt (1982) attributed such a phenomenon to the fractionation of LREE-rich minerals: notably monazite or allanite. Since both minerals contain considerable amounts of Th, their fractionation will not only deplete LREE but also Th. We did not find such results within individual intrusions or between intrusions. We note that low LREE content is associated with low Ba, Sr, Eu, Zr and transition metals (Figure 5.6C). All these elements are generally depleted in low-temperature granitic melts. Because the beryllium-feldspar component tends to be stable as a solid phase at low temperature (Rankama and Sahama, 1950), the substitution of K<sup>+</sup> (Na<sup>+</sup>)-Si<sup>4+</sup> by LREE<sup>3+</sup>-Be<sup>2+</sup> will cause LREE depletion. Therefore, we interpret the low LREE property of some K<sub>1</sub>(I) granitic rocks as being mainly caused by low magma temperatures.

It has been shown that dehydration melting is responsible for producing both the T<sub>3</sub> and K<sub>1</sub>(I) granitic rocks, but at different temperatures and pressures. Comparing the T<sub>3</sub> and K<sub>1</sub>(I) samples from the Cathaysia Block, their zircon  $\epsilon\text{Hf(t)}$  values are comparable and therefore suggest that both were sourced from the Paleoproterozoic basement (Figure 5.4). It can be inferred that different melting temperatures of the T<sub>3</sub> syenogranites and K<sub>1</sub>(I) syenogranites were largely controlled by different melting depths (and thus pressures; Figure 5.5E).

Overall, the results indicate that the K<sub>1</sub>(I) granitic rocks were produced from low temperature and low pressure dehydration melting in a reduced lower crust.

#### 5.4.4 Second stage of Early Cretaceous magmatism: K<sub>1</sub>(II)

Although overlapping to some extent, the K<sub>1</sub>(II) porphyries mainly formed after 130 Ma, whereas all the K<sub>1</sub>(I) granitic rocks formed before 130 Ma. However, more significant are their differences in petrology, geochemistry and isotopic compositions. Except for the highly fractionated Baijuhuajian pluton, the K<sub>1</sub> (II) porphyries have lower SiO<sub>2</sub> and higher K<sub>2</sub>O contents than the K<sub>1</sub>(I) samples. Moreover, their Sm/Yb ratios and Zr contents reveal their higher melting pressures and temperatures (>800 °C). Coeval rhyolites in this region (Yang et al., 2013a) also have high Zr contents and indicate high temperature. Like the T<sub>3</sub> granites, the K<sub>1</sub> (II) porphyries contain alkali feldspar megacrysts (Figure 5.2). In contrast, most K<sub>1</sub>(I) samples show medium-grained textures.

Relative to the K<sub>1</sub>(I) samples, Sr and Eu are less depleted in the K<sub>1</sub>(II) samples (Figure 5.6D), suggesting increased solubility of the An component with temperature. Higher ferromagnesian contents and Mg/Fe ratios also reveal their higher melting temperatures. These geochemical characteristics support the view that the K<sub>1</sub>(II) rocks were produced through dehydration melting, but at higher temperature than the K<sub>1</sub>(I) rocks. The K<sub>1</sub>(II) samples have higher Zr/Nb ratios than the K<sub>1</sub>(I) samples. Although tetravalent Zr and Hf and pentavalent Nb and Ta are all high field strength elements, their geochemical behaviours are different during crustal melting. During low-temperature crustal partial melting, zircon behaves as a refractory mineral; the Nb- and Ta-bearing minerals, in contrast, are low melting point components in the melt. The increased Zr/Nb ratios of the K<sub>1</sub>(II) samples compared to the K<sub>1</sub>(I) samples can be simply explained by a higher degree of partial melting at higher temperatures. Comparing the T<sub>3</sub> and K<sub>1</sub> (II) samples with similar SiO<sub>2</sub> contents, we find they have similar major and trace element characteristics, except that the K<sub>1</sub> (II) samples have lower Sm/Yb ratios. The T<sub>3</sub> and K<sub>1</sub> (II) granitic rocks were likely generated at similar high temperatures but at different depths.

Another significant change that occurred during the formation of the K<sub>1</sub>(I) and K<sub>1</sub>(II) rocks is the increase of initial <sup>176</sup>Hf/<sup>177</sup>Hf ratios (Figure 5.4A). The ages and Hf isotopes of the detrital zircons from the Cathaysia Block reveal a similar trend (Figure 5.4C). I attribute this to the involvement of mantle-derived materials in the source of the K<sub>1</sub>(II) magmas.

Under high temperature conditions, enhanced zircon solubilities in the granitic melt result in high HREE contents due to high HREE contents in zircon. Relative to the K<sub>1</sub>(I) rocks, the increased melting pressures of the K<sub>1</sub>(II) porphyries (but not high enough to stabilize garnet) increase feldspar components in the granitic melt and therefore LREE contents. Therefore, the K<sub>1</sub>(II) porphyries have high REE contents and flat REE patterns. Such REE characteristics (with negative anomalies in Eu) support that these rocks were hot,

dry, reduced magmas (Bachmann and Bergantz, 2008). Low V/Co ratios also indicate that the sources were relatively reduced.

In summary, the K<sub>1</sub>(II) rocks were produced from high-temperature dehydration melting in a reduced lower crust. The sources of the K<sub>1</sub>(II) rocks were possibly more refractory and had more depleted Hf isotopic compositions than those of the K<sub>1</sub>(I) rocks, suggesting mantle input during the K<sub>1</sub>(I-II) stage.

#### 5.4.5 Third stage of Early Cretaceous magmatism: K<sub>1</sub>(III)

Geochemically, the K<sub>1</sub>(III) samples bear similarities to the J<sub>2-3</sub> samples in terms of major and trace element composition. Like the J<sub>2-3</sub> samples, they have low SiO<sub>2</sub> contents, high Fe-Mg-Ti contents and low FeO<sub>total</sub>/ (FeO<sub>total</sub> + MgO) ratios. The K<sub>1</sub>(III) and J<sub>2-3</sub> samples also have subparallel trace element patterns (Figure 5.6). Compared with the earlier water-deficient K<sub>1</sub>(II) rocks (for example, the Honggong quartz syenitic porphyry and the Jiuhua porphyry, Figure 5.6D and E), the felsic samples of the K<sub>1</sub>(III) rocks (such as the Matou monzogranite) are not depleted in Sr and Eu, implying an increase in magma water content from K<sub>1</sub>(II) to K<sub>1</sub>(III), whereby the liquidus and solidus of plagioclase decreased (Bowen, 1913; Yoder et al., 1957; Moore and Carmichael, 1998). The stability of amphibole in these metaluminous K<sub>1</sub>(III) granites also reflects high water contents (Naney, 1983; Annen et al., 2006a; Behrens and Gaillard, 2006). Like the J<sub>2-3</sub> granitic porphyries, the low REE contents of the K<sub>1</sub>(III) granites likely reflect the stability of titanite and amphibole during partial melting and/or fractional crystallization in a wet and oxidized environment (Bachmann and Bergantz, 2008). Nonetheless, there is likely a source variation between the J<sub>2-3</sub> and K<sub>1</sub>(III) rocks because the Muchen Complex shows the rare occurrence of inherited zircons (Liu et al., 2013a and this study). Therefore, most samples from the Muchen Complex were initially high-temperature, mantle-derived magmas that were undersaturated in zirconium. Also, abundant magmatic mafic enclaves are evidence for extensive involvement of mafic magmas in their genesis.

The magnetic susceptibilities of the K<sub>1</sub>(III) samples are higher than samples from the other four stages (Figure 5.7). That is the case even for the highly felsic K<sub>1</sub>(III) granites, consistent with their relatively high magnetite contents and high V/Co ratios. Therefore, the K<sub>1</sub>(III) granites were produced in an oxidized environment, under which the following reaction is shifted to the right-hand side (Wones, 1989): hedenbergite + ilmenite + oxygen  $\leftrightarrow$  titanite + magnetite + quartz. These pieces of evidence reveal that the K<sub>1</sub>(III) granites, like the J<sub>2-3</sub> porphyries, were generated in a wet and oxidized environment with water-fluxed melting as the major mechanism. The K<sub>1</sub>(III) granites have lower Ga/Al ratios (2.1–2.7) than the other groups. Since these rocks have high An contents, the Ga/Al ratios decrease because

anorthite has a much higher Al content and lower Ga content than sodic plagioclase (Goodman, 1972).

In this study, the Hf isotopic analyses on zircons from samples with different SiO<sub>2</sub> contents from the Muchen Complex give relatively uniform results (Figure 5.8A). Liu et al. (2011a) reported similar data and argued that magma differentiation was a result of mixing between crust-derived and depleted mantle-derived magmas, whereby the Hf isotopes were well mixed. Although the property of isotopic homogenization across chemical diversity is theoretically one of the fundamentals of isotope geochemistry (Allègre, 2008), the heterogeneity of zircon Hf isotopic compositions at a hand specimen scale (Wong et al., 2011) reflects considerable kinetic difficulties. Therefore, the homogeneity of zircon Hf isotopic compositions in the Muchen Complex (with a scale of tens of kilometers) was unlikely caused by crust-level mixing. Most Early Cretaceous basalts in Zhejiang Province have enriched Sr-Nd isotopic compositions (Qin, 2007; Cui et al., 2011) and the zircon Hf isotopic compositions of the MMEs and intermediate rocks in the Muchen Complex were likely inherited from their enriched mantle sources.

For the felsic rocks in the Muchen Complex, Liu et al. (2011a) noted that the zircon  $\epsilon_{\text{Hf}}(t)$  values of a quartz monzonite sample were more positive than those of the MME sample. This implies that the source of the Muchen Complex was heterogeneous and the source rock of the quartz monzonite had even more depleted Hf isotopic compositions. Noting that all the other Mesozoic granitoid samples from the Cathaysia Block have negative zircon  $\epsilon_{\text{Hf}}(t)$  values (Figure 5.4), it is unlikely that the quartz monzonite sample with positive zircon  $\epsilon_{\text{Hf}}(t)$  values (Liu et al., 2011a) was sourced from the older lower crustal materials. The felsic samples in this study (Samples 10ZJS125 and 10ZJS132) also show more depleted Hf isotopic compositions than the older granitoids. Therefore, the felsic rocks in the Muchen Complex, like the MME and intermediate rocks, were also sourced from oxidized and enriched mantle materials rather than the continental lower crust.

The cogenetic characteristic of the Muchen Complex is further supported by its continuous range in magnetic susceptibility and linear major element trends on Harker diagrams (Lu, 2007). Initial  $^{87}\text{Sr}/^{86}\text{Sr}$  of the adjacent 105 Ma Shangyutou basalt, the MMEs in the Muchen Complex and Muchen quartz monzonite are 0.7059, 0.7062 to 0.7065 and 0.7058 to 0.7070, respectively;  $\epsilon_{\text{Nd}}(t)$  values are -0.95, -2.6 to -0.6 and -3.2 to -2.4, respectively (Liu et al., 2013a). The Sr-Nd isotopic data also support a single mantle source (with some crustal contamination) for the K<sub>1</sub>(III) basalts, MMEs and granitic rocks.

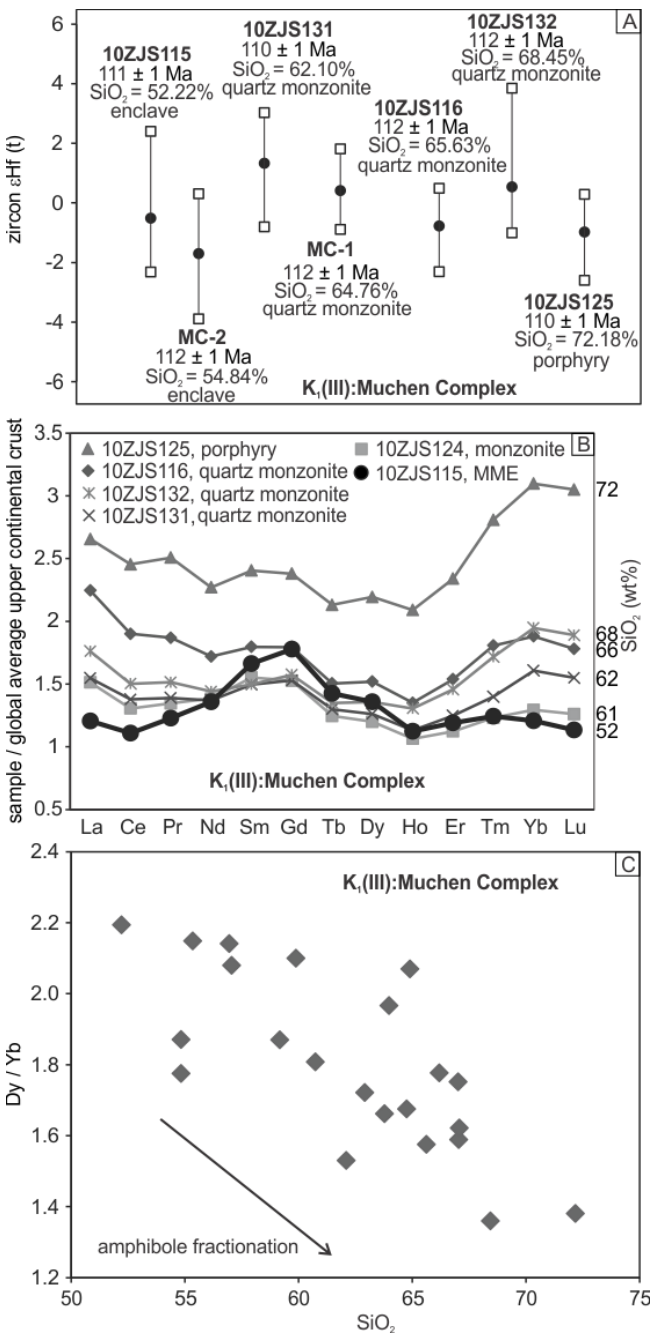


Figure 5.8 (A) Zircon  $\epsilon\text{Hf}(t)$  of seven samples from the Muchen Complex, with filled dots representing the average values. Samples MC-1 and MC-2 are from (Liu et al., 2011a). Note that there is no significant change in their initial Hf isotopic compositions. (B) REE distribution patterns for the six samples in this study, showing a general increasing trend in REE contents with  $\text{SiO}_2$  and a MREE peak in the mafic enclave. (C) Whole-rock Dy/Yb versus  $\text{SiO}_2$  plot for the Muchen Complex, including all the previously published data (Lu, 2007; Liu et al., 2011a; Liu et al., 2013a). A decrease in Dy/Yb with increasing  $\text{SiO}_2$  indicates fractional crystallization of amphibole.

Figure 5.8B shows that the REE patterns of the intermediate and felsic samples are subparallel but the MME sample has a significant peak of MREE compared with the other samples. If the MME is regarded as closer to the primary magma composition for the Muchen Complex, this phenomenon and the decrease in the Dy/Yb ratio with increase in

$\text{SiO}_2$  (Figure 5.8C) should reflect the fractionation of amphibole, which sequestered MREE (Davidson et al., 2007; Richards, 2011).

As to the similarities in Sr-Nd-Hf isotopic compositions of contemporaneous mafic, intermediate and felsic rocks, an alternative explanation to fractionation crystallization model is that the felsic rocks were generated by partial melting of underplated mafic rocks (Chen et al., 2014). However, such a remelting mechanism has difficulties in explaining the continuous variation in magma chemical compositions and magnetic susceptibilities. Furthermore, the loss of volatile substances in the underplating mafic rocks makes remelting a less feasible mechanism than fractionation crystallization to produce felsic magma (Eskola, 1932). Numerical modeling results have shown that “cool, wet magmas tend to generate large proportions of residual melt, whereas hot dry basalts tend to be very effective at remelting fertile crust but generate relatively little residual melt” (Annen and Sparks, 2002; Annen et al., 2006a). The hornblende-bearing (Lu, 2007)  $K_1(\text{III})$  mafic rocks (MME) with arc-like geochemical compositions (Figure 5.9A) imply that the magmas were water-rich at relatively low temperatures (Richards, 2011). Such a magma would therefore have a high potential to produce a large amount of intermediate arc-like melts (Figure 5.9B). In contrast, the generation of  $K_1(\text{I-II})$  highly felsic and plagioclase-poor granitoids from crustal dehydration melting is most likely driven by the heat from underplating of dry and hot basalts.

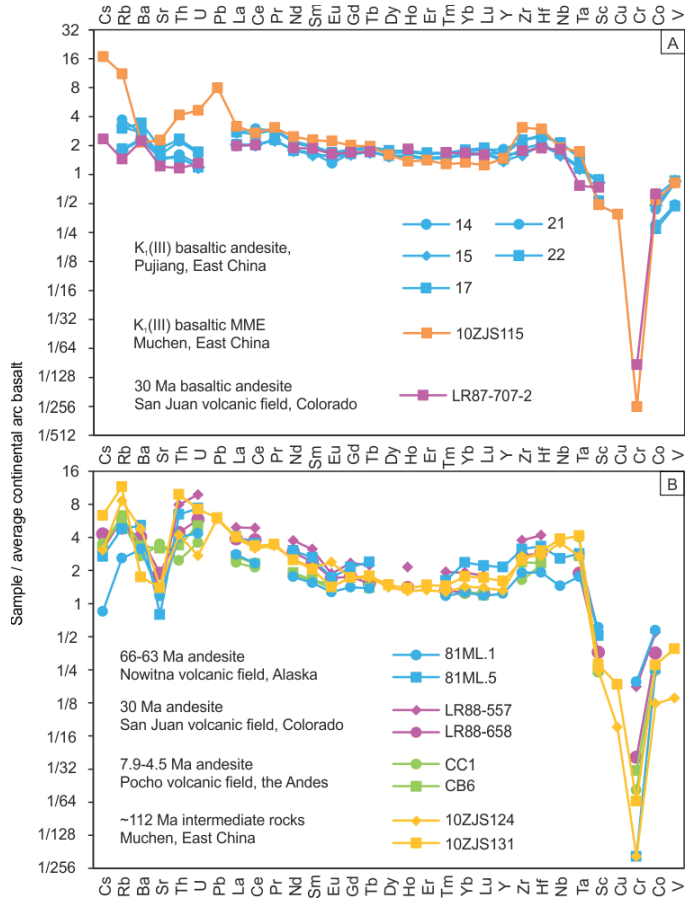


Figure 5.9 Comparisons between the K<sub>I</sub>(III) mafic (A) and intermediate (B) rocks in the study area and those from other active continental margins that likely underwent flat-slab subduction (Moll-Stalcup and Arth, 1989; Kay and Gordillo, 1994; Lipman, 2004; Lipman, 2006). The data for the average continental arc basalt and the Pujiang basaltic andesite are from Kelemen et al. (2003) and Qin (2007), respectively.

## 5.5 Discussion

The petrogenetic results from the region can best be explained by the model of flat-slab subduction and foundering (Li and Li, 2007) in South China during the Mesozoic, as outlined below.

### **5.5.1 Triassic: crustal thickening above a flat-slab**

Mesozoic magmatic rocks in southeastern South China are generally regarded as the products of paleo-Pacific plate subduction (Jahn et al., 1990; Zhou and Li, 2000), although there is no consensus on when subduction started. The high-K characteristics (Figure 5.5A) and predominantly negative zircon  $\delta\text{Hf(t)}$  values (Figure 5.4A) of the Mesozoic granitoids are associated with a mature continental crust in the region, and do not support the existence of a deep sea between the Yangtze and Cathaysia blocks during the Late Permian-Early Triassic (Xiao and He, 2005). The extensive Triassic folds, thrusts and local metamorphism in the region (Li and Li, 2007) imply a mountain-building crustal thickening event in western

Zhejiang Province during that time, which generated the Late Triassic granites with high melting temperatures and high Sm/Yb ratios. The occurrence of wet and oxidized 226 Ma quartz monzonite implies that the orogeny was most likely caused by oceanic plate subduction (Zhu et al., 2013). However, the region was about 600 km from the continental margin, which is much further inland than an orogenic-magmatic belt associated with a normal continental arc (for example, the NE Honshu arc and the Sunda arc). However, it is consistent with a flat-slab or shallow-angle subduction, similar to the Peruvian and Pampean flat-slab subduction in the Andes (Ramos and Folguera, 2009). The U–Pb ages and Hf and O isotopes of detrital zircons from the hinterland of South China support the view that Permian magmatism was caused by a normal arc along the continental margin (Figure 5.10A) (Li et al., 2012c).

There are some fundamental differences between the flat-slab subduction (Li and Li, 2007) and shallow-angle subduction (Zhou and Li, 2000) models. One significant difference is that for flat-slab subduction, the oceanic lithosphere is coupled with the overlying continental lithosphere, dramatically reducing the conductive heat from the asthenospheric mantle and exerting a strong cooling effect on the basal continental lithosphere (Dumitru et al., 1991). Another consequence of flat-slab subduction is thickening of the overriding continental plate (Figure 5.10B) because of its strong coupling with the propagating flat-slab (Fromm et al., 2004; Orozco et al., 2013). Regional metamorphism and crustal partial melting may therefore result.

The flat-slab subduction model can explain the petrogenesis of the Triassic granites found in the region. At the front of the flat-slab, the fluid released from the slab could have triggered melting in the continental lithospheric mantle when it had not cooled down (Figure 5.10B). The 254 Ma Tieshan and 242 Ma Yangfang syenites (Wang et al., 2005a) were possibly generated by this process. The high V/Co ratios (9.4–23.0 for the Tieshan syenite and 5.5–16.1 for the Yangfang syenite) reflect strongly oxidized environments related to the subduction process. The detrital zircon spectrum also records an Early Triassic thermal event (Figure 5.4C). Therefore, the front of the flat-slab likely reached the study region by the Early Triassic.

Since the overriding continental crust was thickened during flat-slab subduction, its geothermal gradient increased and Triassic regional medium- to high-grade (up to granulite facies) metamorphism occurred (Li and Li, 2007; Yu et al., 2009; Xia et al., 2012). The recrystallized rims of the zircons from some metamorphic rocks recorded almost the same age as the  $T_3$  granites of this study, implying that both the  $T_3$  metamorphism and granites were generated in the thickened crust, although fluids or melts from the flat-slab may have caused local metasomatism and water-fluxed melting in the lower crust (Zhu et al., 2013).

Triassic high-grade metamorphism and crustal melting occurred dominantly to the southeast of the Jiang-Shao Fault (Figure 5.1C). To the northwest of the fault, the 280(?)–200 Ma Indosinian orogenic event is shown mainly as a thin-skinned fold-and-thrust belt (Wang et al., 2005b; Xiao and He, 2005; Li and Li, 2007). The fact that only the coastal belt of the Cathaysia Block (in Zhejiang and possibly Fujian provinces) recorded widespread high-grade metamorphism and partial melting supports the view that thick-skinned deformation was caused by flat-slab subduction rather than by the amalgamation of the Yangtze and Cathaysia blocks (Xiao and He, 2005).

Another tectonic model for the Triassic of South China is the collision between the South China and Indochina blocks (Zhou et al., 2006). However, an oxidized continental lithosphere can be explained by flat-slab subduction, but not a continental collision over a thousand kilometers away. Some Triassic granitic rocks near the coast of South China (Figure 5.1A) have high V/Co ratios, such as the 226 Ma Dashuang quartz monzonite in eastern Zhejiang Province (6.3–6.7) (Zhu et al., 2013), the 226 Ma Jintan biotite granite in central Jiangxi Province (6.4–10.5) (Li, 2011; Zhao et al., 2013b), the 234 Ma and 220 Ma Guikeng granite in southern Fujian Province (6.0–20.8) (Mao et al., 2011), the Triassic Dayinchang granite in northern Fujian Province (8.3–20.3) (Wang et al., 2013b) and the 237 Ma Qiongzhong granite in Hainan Province (5.7–23.1) (Ge, 2003). In contrast, thirteen Triassic granitic intrusions from Hunan Province have low and uniform V/Co ratios (5.0–6.4) (Wang et al., 2007b). It thus appears that the Triassic granitic rocks near the coast were more oxidized than those in the hinterland, which again can best be explained by the subduction of an oxidized oceanic plate.

### 5.5.2 Middle Jurassic: foundering of the flat slab

Since the continental lithosphere was continuously cooled down by the flat slab after the Triassic crustal melting and high-grade metamorphism, the decreasing geothermal gradient is no longer favorable to magmatism, resulting in a magmatic hiatus in the Early Jurassic. Further crustal melting did not occur until the next water-fluxing and/or heating event. During the Jurassic, eclogitization of the oceanic plateau started to cause the flat slab to break up and founder (Figure 5.10C) (Li and Li, 2007). Heat and water caused melting of the overriding continental lithosphere, with heat being provided by upwelling asthenosphere through the slab window, and the water being from the hydrous metasomatic continental lithospheric mantle and/or the foundering oceanic slab. The 170–150 Ma porphyries in western Zhejiang Province were mainly derived from melting of Neoproterozoic crustal rocks. In eastern Zhejiang Province, the Nd and Hf isotopes of the earlier 180 Ma Xiepu granite (Li et al., 2012d) and the 177 Ma Maonong dacitic tuff (Liu et al., 2012a) show that they were sourced from the Paleoproterozoic basement of the Cathaysia Block as were the

Late Triassic granitoids (also see Figure 5.4C for detrital zircon records), and they were probably triggered by basaltic underplating following slab break-off (Ferrari, 2004; Li et al., 2012d; Meng et al., 2012).

### 5.5.3 Early Cretaceous: lithospheric extension

Since the Early Cretaceous, the tectonics of the South China Block has been characterized by strong extension (Li, 2000; Zhou et al., 2006). In western Zhejiang Province, the extension of the lithosphere is evident from the development of the “Ganzhou-Hangzhou Rift” during this period, which approximately followed the Jiang-Shao Fault Zone (Gilder et al., 1991). The location of the “Ganzhou-Hangzhou Rift” is shown in Goodell et al. (1991). The K<sub>1</sub>(I) rocks in this study had lower melting pressures than their T<sub>3</sub> and J<sub>2-3</sub> counterparts, consistent with stronger extension during K<sub>1</sub> time. Increased geothermal gradients in the extensional continental lithosphere, and possibly basaltic underplating, were responsible for the extensive crustal melting during K<sub>1</sub>(I-II), with no significant addition of external water. This indicates that foundering of the flat-slab was completed by the Early Cretaceous (Figure 5.10D). The extensional tectonics, such as the Ganzhou-Hangzhou Rift and many other graben in the region, were probably promoted by two coupled mechanisms: cessation of horizontal compression due to steep subduction of the paleo-Pacific plate, and gravitation collapse following the foundering of the eclogized oceanic flat-slab (Figures 5.10C and 5.9D), similar to the early Basin and Range Province in North America (Howell, 1995; Humphreys, 2009) and the Jurassic Nanling Range in China (Li and Li, 2007). Thermal uplifting exhumed the Precambrian metamorphic rocks and Late Triassic intrusions in the region, upon which the Early Cretaceous strata were deposited.

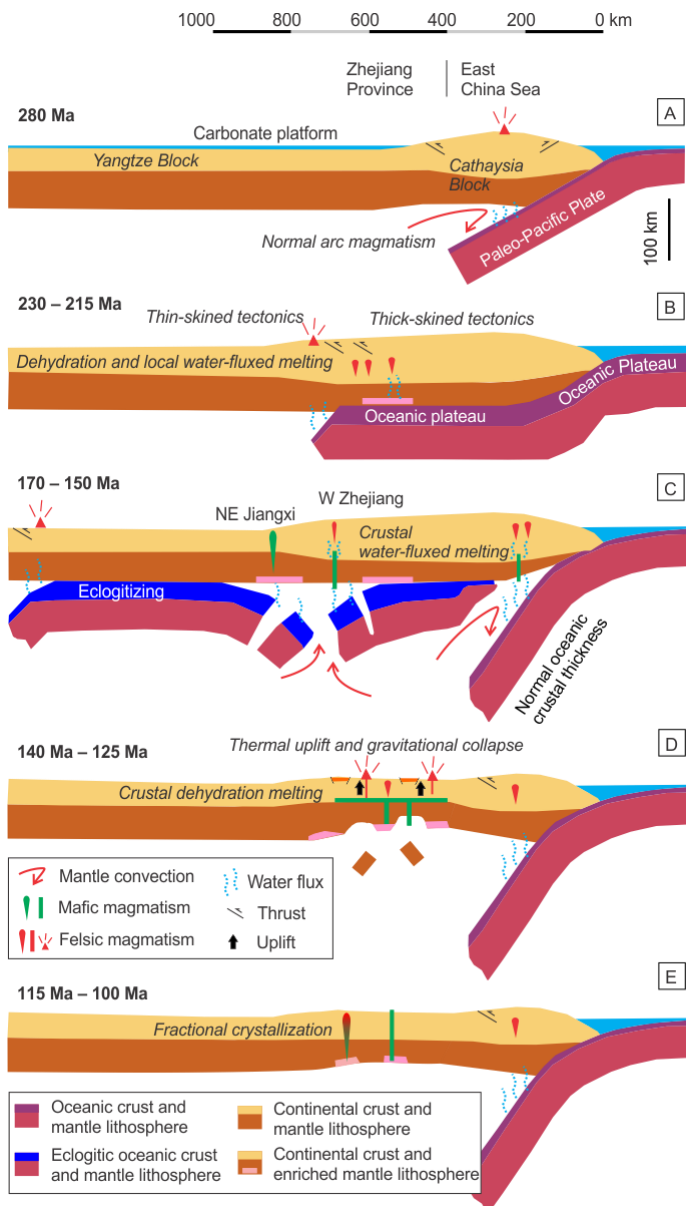


Figure 5.10 Tectonic model for southeastern China during the Mesozoic, modified after Li and Li (2007) and Li et al. (2012d). (A) Permian: normal subduction and arc magmatism (Li et al., 2006; Li et al., 2012c). (B) T<sub>3</sub>: flat-slab subduction caused the thickening of the continental crust in Zhejiang Province and dehydration melting in the lower crust. Fluids and hydrous silicate melts released from the flat slab caused mantle metasomatism and some local crustal water-fluxed melting (Zhu et al., 2013). (C) J<sub>2-3</sub>: foundering of the eclogitic flat slab caused water-fluxed melting of the oxidized and hydrous continental crust. (D) K<sub>1(I-II)</sub>: extension and, possibly delamination, of the continental lithosphere generated large amounts of felsic igneous rocks from crustal dehydration melting. (E) K<sub>1(III)</sub>: melting of the hydrous and enriched continental lithospheric mantle.

The K<sub>1(III)</sub> basaltic and andesitic rocks (including the MME samples) in western Zhejiang Province, such as those from the Muchen Complex and the Pujiang basaltic andesite (Qin, 2007), share similar trace element patterns with those from other active continental margins, such as the Nowitna (Moll-Stalcup and Arth, 1989), San Juan (Lipman et al., 1978; Lipman, 1987) and Pocho (Kay and Gordillo, 1994) volcanic fields in the North and East Pacific (**Error! Reference source not found.**). There are two general models for

such high-K, arc-like magmas far away from the trench. One is low-angle subduction (Lipman et al., 1978); the other is melting of an enriched continental lithospheric mantle during lithospheric extension (Davis and Hawkesworth, 1993; Humphreys et al., 2003). The Early Cretaceous tectonics in South China was dominated by extension with no evidence for shallow-angle subduction. Furthermore, Hf is generally immobile during subduction-dehydration processes. The zircon  $\varepsilon\text{Hf(t)}$  values of most K<sub>1</sub>(III) basaltic and andesitic rocks are approximately zero or weakly negative, indicating they were unlikely sourced from the asthenospheric mantle wedge. Therefore, the second model is more realistic. Triassic–Early Jurassic flat-slab subduction likely resulted in the metasomatism of the continental lithospheric mantle, which melted and produced arc-like magmas during K<sub>1</sub>(III) (Figure 5.10E), with some of these mafic magmas trapped in the cogenetic granitic magmas as enclaves. Compared to J<sub>2-3</sub>, the continental lithosphere was much hotter during K<sub>1</sub>(III), which facilitated the fractional crystallization of mantle-derived magmas in the crust. There is an age gap between the K<sub>1</sub>(II) and K<sub>1</sub>(III) granitoids in the region, which is also shown in the detrital zircon record (Figure 5.4). Such a gap probably reflects the transition in magma source from the crust to the metasomatic lithospheric mantle. The latter did not undergo partial melting until appropriate pressure-temperature conditions were reached.

## 5.6 Conclusions

Based on a new petrogenetic analysis, the Mesozoic granitic rocks of western Zhejiang Province have been divided into a five-stage evolutionary sequence, representing a typical Andean-type orogenic cycle (Ramos and Folguera, 2009). The results show that the properties of granitoids are mainly determined by their sources and temperature-pressure-water-redox conditions during melting and fractionation processes. Late Triassic (T<sub>3</sub>) granites in western Zhejiang Province were produced from high temperature and high pressure dehydration melting in the lower crust (Figure 5.10B). The high pressure and high temperature were the result of crustal thickening caused by flat-slab subduction of the paleo-Pacific Plate, which cooled and metasomatised the continental lithosphere at the same time. The Middle and Late Jurassic (J<sub>2-3</sub>) porphyries were generated from low temperature and high pressure water-fluxed melting of the oxidized lower crust (Figure 5.10C). The low temperature was caused by Triassic thermal insulation of the flat-slab prior to its foundering. Since the Early Cretaceous (Figure 5.10D-E), the continental lithosphere in South China has undergone strong extension as a result of roll-back of the paleo-Pacific Plate. The first stage of granitic rocks in the Early Cretaceous [K<sub>1</sub>(I)] was the result of low-temperature and low-pressure dehydration melting in attenuated crust. The low temperatures were determined by the low pressures due to lithospheric thinning. The second stage granitic rocks in the Early Cretaceous [K<sub>1</sub>(II)] were produced by similar processes to the K<sub>1</sub>(I) granitic rocks, but from

more refractory crustal materials. Mantle materials were possibly involved before or during the melting process. The third stage of granitic magmatism in the Early Cretaceous [K<sub>1</sub>(III)] formed by fractionation of hydrous and oxidized basaltic magmas, which were generated from the subcontinental lithospheric mantle.

## Chapter 6 Mesozoic Granitic Magmatism in Northeastern Jiangxi Province

### 6.1 Introduction and Geological Setting

In northeastern Jiangxi Province, the Cathaysia Block is separated from the Neoproterozoic Sibao Orogenic Belt by the Guangfeng-Pingxiang Fault Zone, which is the southwestern extension of the Jiangshan-Shaoxing Fault Zone in Zhejiang Province (Figure 6.1). The oldest strata exposed in the Sibao Orogenic Belt are the Neoproterozoic Shuangqiaoshan Group, which mainly consists of meta-tuffaceous sandstone, siltstone, micaceous schist and phyllite (JGS, 1984) and were most likely deposited within a back-arc basin during the amalgamation of the Yangtze and Cathaysia blocks (Wang et al., 2008a; Charvet, 2013). The oldest rocks exposed in the Cathaysia Block are the Neoproterozoic Shenshan Group, which consists of phyllite with intermediate to mafic lava and volcanic breccia at the base (JGS, 1984). The Paleoproterozoic basement is not exposed, but based on isotopic evidence (Ding et al., 2005; Zhu et al., 2008; Li et al., 2013c), it is likely to be similar to the Badu Complex in western Zhejiang Province.

As shown in Figure 6.1, no Triassic magmatic rocks have been found in northeastern Jiangxi Province. Jurassic granitoids are small-scale porphyries containing mineralisation such as the Cu-Mo deposits at Dexing (Hou et al., 2013) and Yongping (Li et al., 2013c) and the Cu-Au-Pb-Zn-Ag deposits at Yinshan (Liu et al., 2013b). Early Cretaceous granitoids have the greatest volume; however, compared to Zhejiang Province, the contemporaneous volcanism was of limited extent.

### 6.2 Sampling and Petrography

#### 6.2.1 Lingshan syenogranite

Five samples, including an MME (mafic microgranular enclave) sample, were collected from the northern part of the Lingshan syenogranite, which intruded Neoproterozoic and Paleozoic lithologies (JGS, 1980b; JGS, 1980c). The outcrop shape is almost circular with a diameter of ~16 km. Samples 10ZJS151, 155 and 156 are from an early intrusive unit and samples 10ZJS153 and 154 are from a later intrusive unit (JGS, 1980b; JGS, 1980c). The early unit is MME-bearing, and both units have rapakivi textures. The magnetic susceptibilities of the samples are  $2.3\text{--}6.6 \times 10^{-3}$  SI, except for 10ZJS151 ( $0.085 \times 10^{-3}$  SI).

Sample 10ZJS151 ( $28^{\circ} 40.921'\text{N}$ ,  $117^{\circ} 48.750'\text{E}$ ) is a fine- to medium-grained grey quartz syenite primarily composed of perthite and quartz, with 1-2% biotite. Samples 10ZJS155 and 10ZJS156 (MME) were from the same outcrop ( $28^{\circ} 39.806'\text{N}$ ,  $117^{\circ} 45.202'\text{E}$ , Figure 6.2C). The MME sizes are up to 20 centimetres. The boundaries between the MMEs

and their host granites are diffuse. Sample 10ZJS155 is a coarse-grained pink-grey syenogranite with rapakivi texture and sericitised plagioclase. The mafic minerals include hornblende (replaced by biotite), biotite, titanite and magnetite. The dioritic MME (sample 10ZJS156) was contaminated by granitic magma as reflected by the presence of quartz and alkali feldspar megacrysts (Figure 6.2C). This sample is composed of plagioclase, hornblende, biotite, quartz, alkali feldspar, titanite, magnetite and acicular apatite. Samples 10ZJS153 ( $28^{\circ}40.189'N$ ,  $117^{\circ}47.026'E$ ) and 10ZJS154 ( $28^{\circ}40.144'N$ ,  $117^{\circ}47.015'E$ ) are pink porphyritic syenogranites with coarse-grained rapakivi alkali feldspar set in a fine-grained groundmass. The mineral assemblages are mainly feldspar and quartz with minor hornblende (partly replaced by biotite), biotite and magnetite.

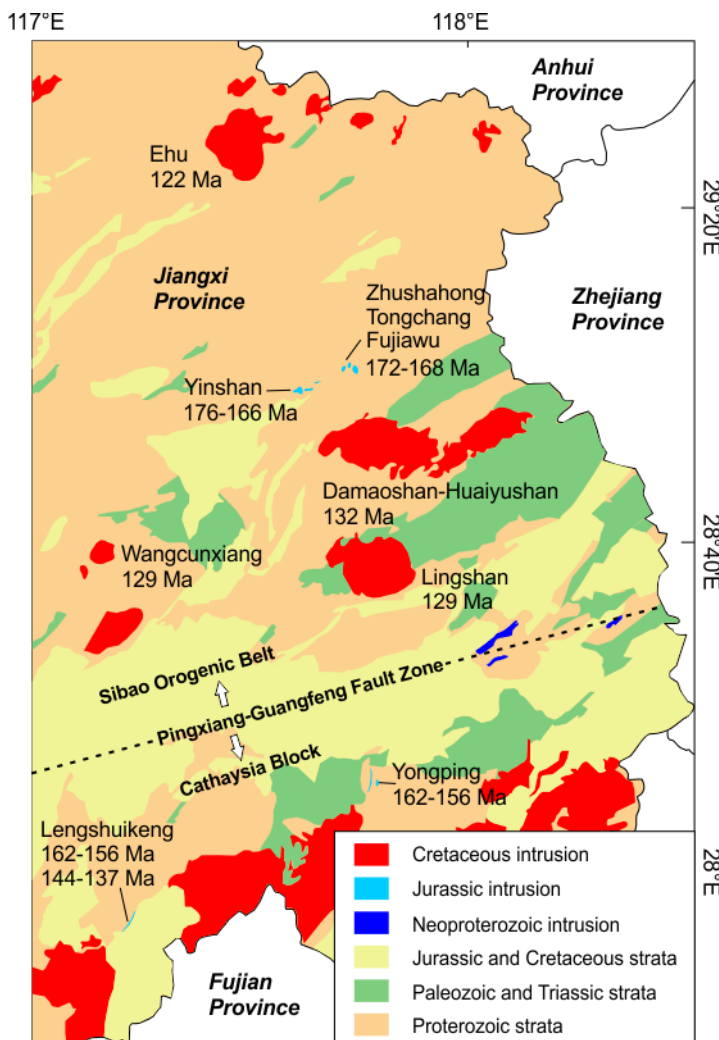


Figure 6.1. Geological map of NE Jiangxi Province, modified after JGS (1984). All the ages are zircon U-Pb dating results (ion probe or LA-ICP-MS). Names of plutons and their data sources: Ehu syenogranite (Jiang et al., 2011b); Zhushahong, Tongchang, Fujiawu porphyries (Wang et al., 2006; Liu et al., 2012b; Zhang et al., 2013); Yinshan porphyries (Wang et al., 2012a); Damaoshan-Huaiyushan syenogranite-alkali feldspar granite (Jiang et al., 2011b; Zhou et al., 2013 and this study); Lingshan syenogranite (Zhou et al., 2013); Wancunxiang syenogranite-alkali feldspar granite (this study); Yongping porphyries (Ding et al., 2005; Zhu et al., 2008; Li et al., 2013c) and Lengshuikeng porphyries (Su et al., 2013a; Wang et al., 2013a).

### 6.2.2 Wancunxiang syenogranite

Samples 10ZJS170 ( $28^{\circ} 42.206'N$ ,  $117^{\circ} 26.327'E$ ) and 10ZJS171 ( $28^{\circ} 43.625'N$ ,  $117^{\circ} 26.728'E$ ) are from the Wancunxiang porphyritic syenogranite with medium-grained feldspar in a fine-grained groundmass. This syenogranite intruded the Proterozoic Shuangqiaoshan Group and Carboniferous limestone. The latter underwent contact metamorphism and formed marble. Sample 10ZJS171 (Figure 6.2F) is from metasomatic zone adjacent to the marble. The magnetic susceptibilities of samples 10ZJS170 and 10ZJS171 are  $0.131 \times 10^{-3}$  SI and  $0.420 \times 10^{-3}$  SI, respectively.

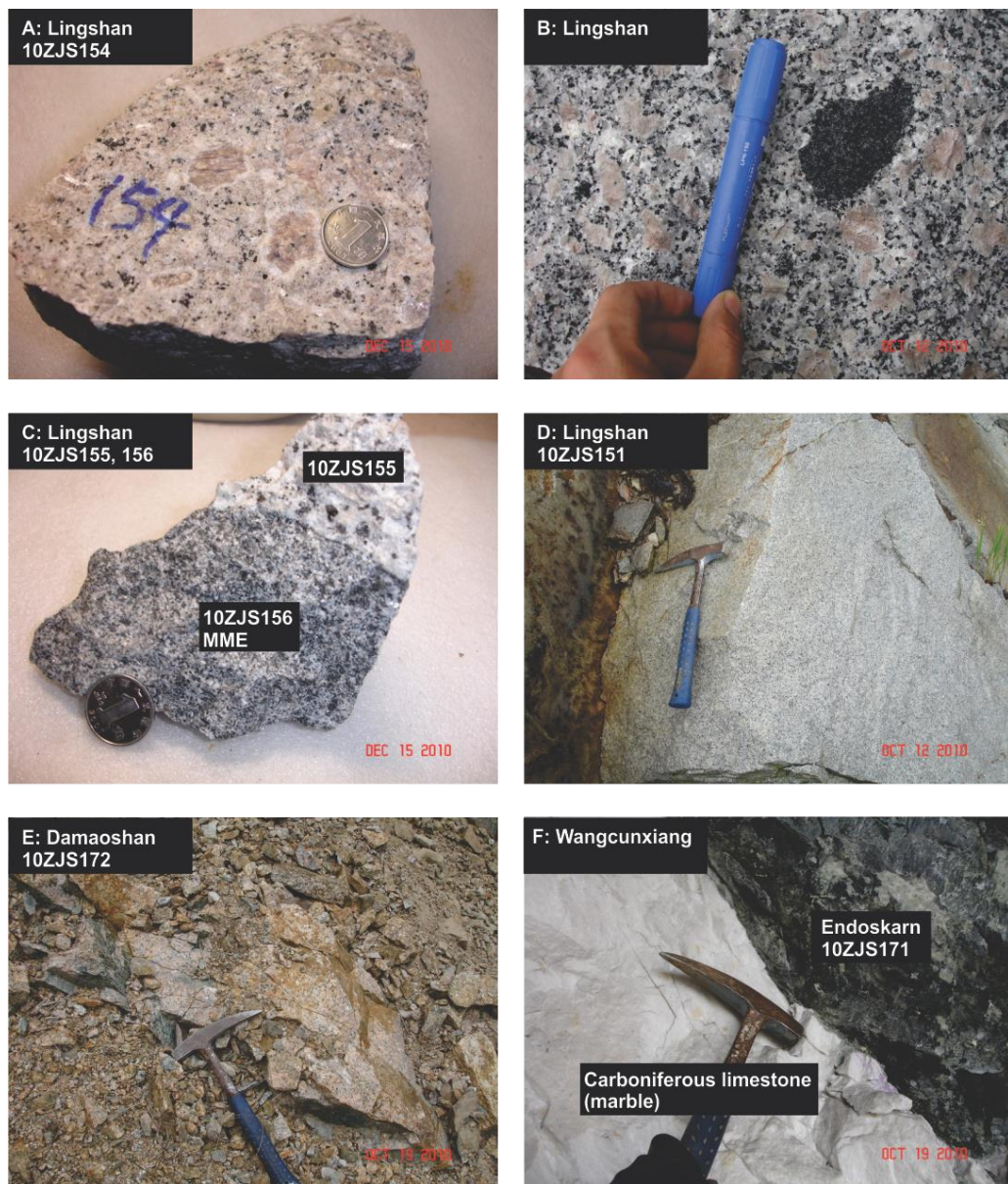


Figure 6.2 Photographs of field and hand specimens from the Early Cretaceous granitic rocks in northeastern Jiangxi Province. (A) Sample 10ZJS154 is a Lingshan syenogranite with rapakivi texture; (B) an outcrop of Lingshan syenogranite showing a mafic enclave; (C) a contact between a mafic enclave and its host granite; (D) a Lingshan granite outcrop without rapakivi texture; (E) a Damaoshan-Huayiushan syenogranite-alkali feldspar granite outcrop; (F) a contact between the Wancuanxiang syenogranite (sample 10ZJS171) and Carboniferous limestone, which were altered to endoskarn and marble, respectively.

### 6.2.3 Damaoshan-Huaiyushan syenogranite-alkali feldspar granite

Seven samples were collected from the Damaoshan-Huaiyushan syenogranite-alkali feldspar granite. Samples 10ZJS162, 10ZJS163 and 10ZJS165 are from the eastern portion of the intrusion (Huaiyushan) and samples 10ZJS172, 10ZJS173, 10ZJS175 and 10ZJS177 are from the western portion (Damaoshan). All of these samples are pink to grey, medium- or coarse-grained and primarily composed of quartz, alkali feldspar and plagioclase ( $An_{11-13}$ ) with minor biotite, muscovite and opaque minerals. The magnetic susceptibilities of these samples are  $0.065\text{--}0.964 \times 10^{-3}$  SI.

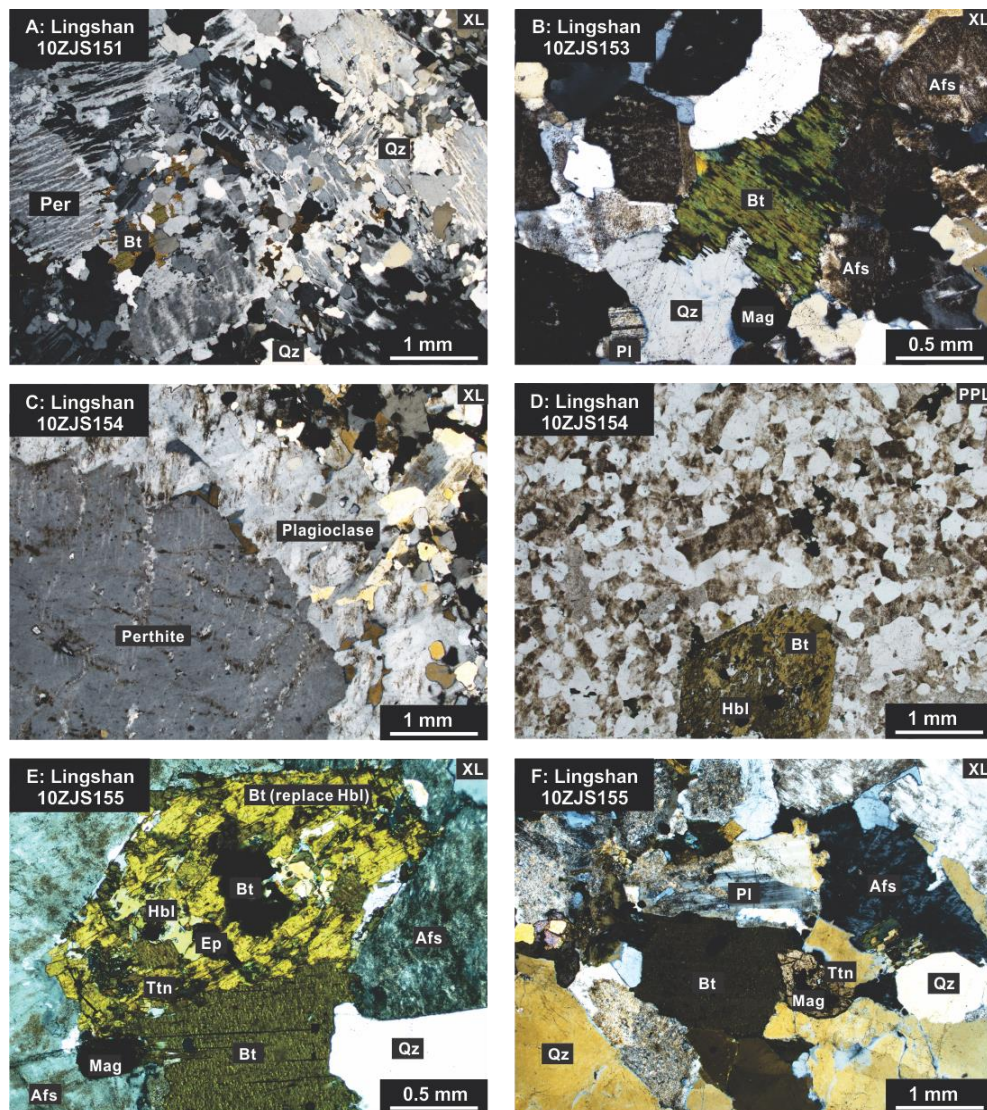


Figure 6.3 Thin section photographs of the Early Cretaceous granitic rocks from northeastern Jiangxi Province (XL: cross-polarised light; PPL: plane-polarised light). (A) Lingshan alkali feldspar granite; (B) Lingshan syenogranite; (C and D) Lingshan syenogranite with rapakivi texture; (E and F) Lingshan syenogranite hosting the MMEs. Mineral abbreviations: Afs, alkali feldspar; Per, perthite; Pl, plagioclase; Qz, quartz; Bt, biotite; Ttn, titanite; Hbl, hornblende; Ap, apatite; Ms, muscovite; Mag, magnetite; Ep, epidote.

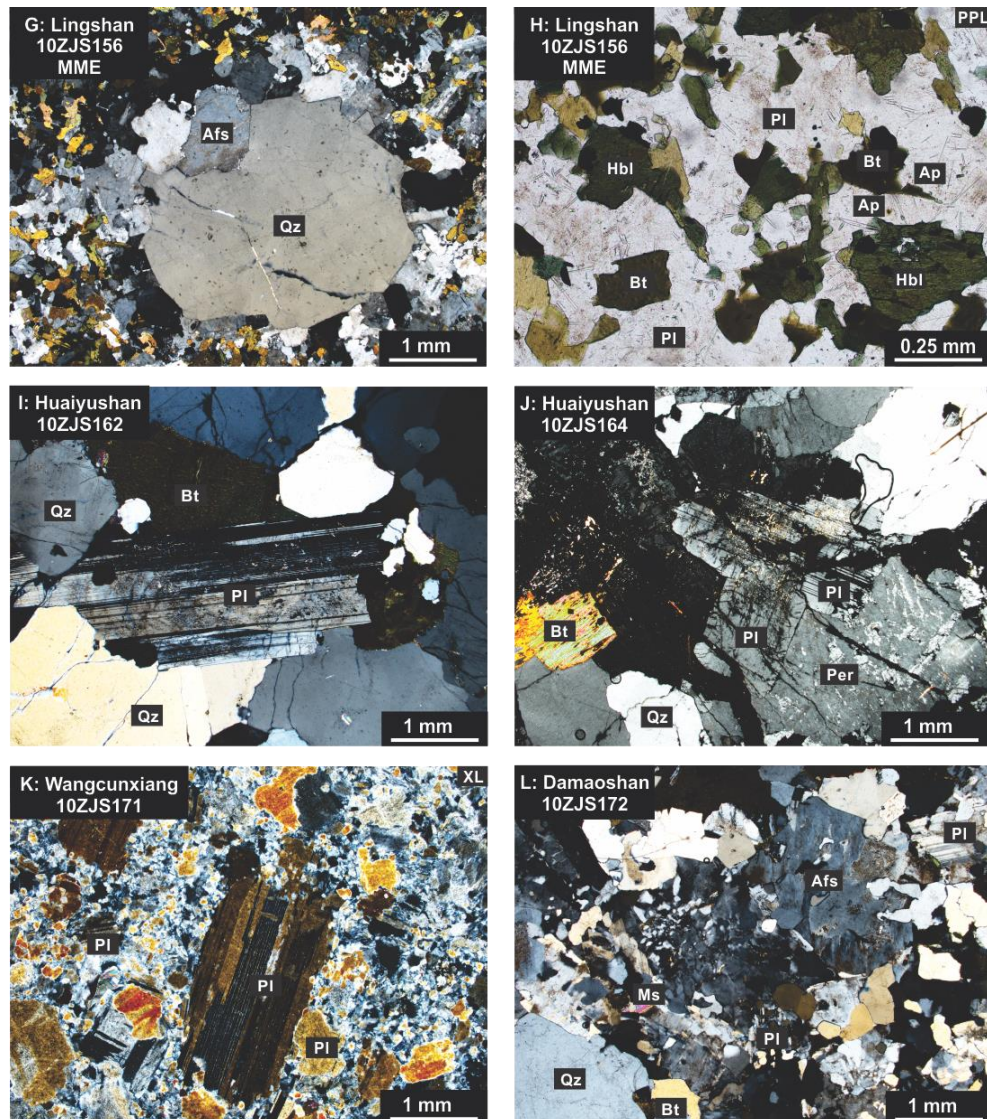


Figure 6.3 (continued) (G and H) MME sample from the Lingshan syenogranite; (I and J) Huaiyushan syenogranite-alkali feldspar granite; (K) Wancunxiang syenogranite; (L) Damaoshan syenogranite-alkali feldspar granite.

### 6.3 Analytical Results

#### 6.3.1 Zircon U-Pb Dating and Hf isotopes

##### 6.3.1.1 10ZJS154 (Lingshan syenogranite).

LA-ICP-MS U-Pb dating was performed using 22 zircon grains from Sample 10ZJS154 (Figure 6.4A). The majority of these were cracked and some had inclusions visible in transmitted light. The zircon were mainly 120–300 µm long and 70–110 µm wide with elongation ratios from 1.4–3.8. The zircons have magmatic oscillatory zoning visible in CL images. The analysed zircons had Th contents from 636–10644 ppm and U contents from 666–5188 ppm with Th/U = 0.44–2.05. Spots 10ZJS154-06, -09, -10 and -15 yielded either

discordant or significant younger outliers (probably caused by lead loss) and were rejected from the mean age calculations. The remaining 18 data points yielded a weighted mean  $^{206}\text{Pb}/^{238}\text{U}$  age of  $131 \pm 1$  Ma with  $\text{MSWD} = 0.91$  and their  $\epsilon\text{Hf(t)}$  values ranged from  $-5.5$  to  $-1.2$ .

### 6.3.1.2 10ZJS155 (Lingshan syenogranite)

Twenty zircons from sample 10ZJS155 (Figure 6.4B) were dated. Their morphology and texture are similar to those of sample 10ZJS154 under transmitted light but with more inclusions. The oscillatory zoning was well developed. These analysed zircons had Th contents from 566–1738 ppm and U contents from 737–1830 ppm with  $\text{Th/U} = 0.55\text{--}1.74$ . The spot 10ZJS155-20 was strongly discordant and rejected from the mean  $^{206}\text{Pb}/^{238}\text{U}$  age calculations, which yielded  $129 \pm 1$  Ma with an  $\text{MSWD} = 1.4$ . Nineteen Hf isotopic analyses were done on 18 dated and 1 undated grain (which was assumed to be 129 Ma), with  $\epsilon\text{Hf(t)}$  values ranging from  $-3.6$  to  $1.1$ .

### 6.3.1.3 10ZJS156 (Lingshan MME)

Twenty-six zircons from sample 10ZJS156 (Figure 6.4C), the MME hosted by sample 10ZJS155, were dated. These zircons had large size ranges (lengths = 130–420  $\mu\text{m}$ , widths = 60–130  $\mu\text{m}$ , elongations = 2.2–4.4). Approximately half of the zircons had clear interiors with few inclusions, the others were turbid and cracked. Most zircons ( $\text{Th} = 162\text{--}1367$  ppm,  $\text{U} = 245\text{--}2048$  ppm and  $\text{Th/U} = 0.12\text{--}1.07$ ) had oscillatory zonings; however, those with high Th and U contents appeared dark (Spot 22) in CL images and were rejected from the mean age calculations. Spots 10ZJS156-6 (high discordancy), -13, -22 and -26 (outside 2 SEs) were also rejected. The weighted mean  $^{206}\text{Pb}/^{238}\text{U}$  age is  $133 \pm 1$  Ma with  $\text{MSWD} = 1.3$ . Twenty Hf isotopic analyses were done on 20 dated grains, with  $\epsilon\text{Hf(t)}$  values ranging from  $-2.5$  to  $3.3$ .

### 6.3.1.4 10ZJS170 (Wancunxiang granite)

Twenty-four zircons from sample 10ZJS170 were dated. These zircons were mostly transparent with few inclusions. In the CL images (Figure 6.4D), the zircon zonings were mainly oscillatory with some complexes. The Th and U contents were 70–2084 ppm and 53–1709 ppm with  $\text{Th/U} = 0.18\text{--}1.77$ . One inherited zircon had a  $^{206}\text{Pb}/^{238}\text{U}$  age of  $870 \pm 12$  Ma (1 SD). Some zircons yielded obviously discordant results, whereas the other 17 zircons yielded a weighted mean  $^{206}\text{Pb}/^{238}\text{U}$  age of  $131 \pm 1$  Ma. A total of 18 Hf isotopic analyses were done on the grains with concordant ages and the Neoproterozoic zircon. The inherited Neoproterozoic zircon had a  $\epsilon\text{Hf}(870 \text{ Ma})$  value of  $-15.0$ . For the other analyses, the  $\epsilon\text{Hf}(131 \text{ Ma})$  values ranged between  $-1.9$  and  $1.9$ .

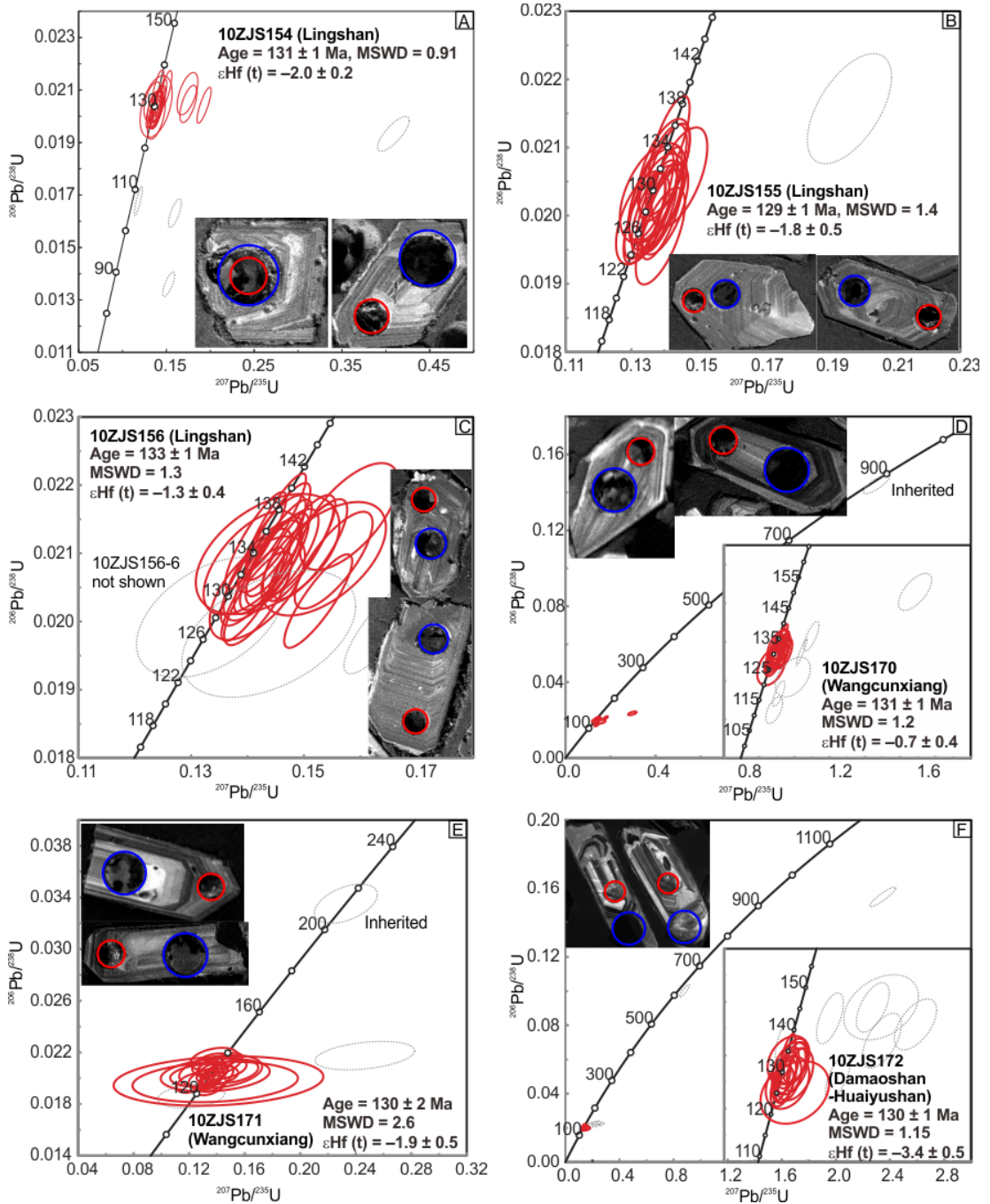


Figure 6.4 Zircon CL images, age and Hf isotopic results for the Early Cretaceous granitic rocks from northeastern Jiangxi Province: (A-C) Lingshan syenogranite; (D-E) Wancunxiang syenogranite-alkali feldspar granite; (F) Damaoshan-Huaiyushan syenogranite-alkali feldspar granite. On the concordia diagrams, the spots represented by dotted grey ellipses (2 SD) were excluded from the calculation of the mean age.

### 6.3.1.5 10ZJS171 (Wancunxiang endoskarn)

Twenty-two zircons from sample 10ZJS171 (Figure 6.4E) were dated. The grain sizes ranged from 150–300 µm in length and 80–120 µm in width. Under transmitted light, this sample is similar to sample 10ZJS170, transparent with a few inclusions. A few zircons had turbid interiors. The CL images show zircon grains have zonings. The Th and U contents of the analysed zircons were 60–1102 ppm and 58–1162 ppm with Th/U = 0.56–1.56. The

$^{206}\text{Pb}/^{238}\text{U}$  age of the inherited zircon (10ZJS171-17) was  $212 \pm 4$  Ma (1 SD). Spot 10ZJS171-11 was strongly discordant, and Spot 10ZJS171-3 was an significant younger outlier (probably caused by lead loss). These points were rejected from the weighted mean  $^{206}\text{Pb}/^{238}\text{U}$  age calculations, which yielded  $130 \pm 2$  Ma with an MSWD = 2.6. Eighteen Hf isotopic analyses were done on the dated zircons with concordant ages. The  $\epsilon\text{Hf}(212 \text{ Ma})$  of the inherited zircon was  $-3.7 \pm 0.8$ . The remaining zircons had  $\epsilon\text{Hf(t)}$  values between  $-5.5$  and  $-0.6$ .

### 6.3.1.6 10ZJS172 (Damaoshan-Huaiyushan granite)

Twenty-four zircons from sample 10ZJS172 (Figure 6.4F) were dated. The grains were 100–250 mm long and 70–110 mm wide. The CL images show a well-developed oscillatory zoning with some grains apparently containing inherited cores. The Th and U contents were 127–1651 ppm and 106–1172 with Th/U = 0.60–1.94. Spots 10ZJS172-15 and -16 contained inherited cores, with  $^{207}\text{Pb}/^{206}\text{Pb}$  ages of  $735 \pm 29$  Ma and  $1794 \pm 25$  Ma (1 SD), respectively. Spots 10ZJS172-1, -3, -7, -12, -21, -22 were rejected due to their strong discordancy. Spot 10ZJS172-6 was an older outlier and probably an inherited zircon grain. The remaining 15 analyses yielded a weighted mean  $^{206}\text{Pb}/^{238}\text{U}$  age of  $130 \pm 1$  Ma with MSWD = 1.15 and these grains had  $\epsilon\text{Hf(t)}$  between  $-5.1$  and  $-1.6$ .

### 6.3.2 Whole-rock major and trace elements

A total of 14 major and trace elements were analysed in the granitic and MME samples: five Lingshan syenogranite, two Wancunxiang granitic porphyry and seven Damaoshan-Huaiyushan syenogranite-alkali feldspar granite samples. Samples from these intrusions had similar geochemical characteristics.

The granitic samples from the three intrusions all have high-K contents with  $\text{SiO}_2 = 70\text{--}76\%$ ,  $\text{K}_2\text{O} = \sim 5\%$ ,  $\text{K}_2\text{O}/\text{Na}_2\text{O} = \sim 1.5$  and A/CNK ratios = 0.9–1.1. All these samples are highly fractionated with low  $\text{MgO}$  (0–0.66%), low  $\text{TiO}_2$  (< 0.5%), high Nb (23–93 ppm) and high Ga/Al ratios ( $2.7\text{--}4.3 \times 10^{-4}$ ). The total REE contents were 273–595 ppm with  $\text{La/Yb} = 2\text{--}19$  and  $\text{Sm/Yb} < 2.5$ . The Eu anomalies were negative with  $\delta\text{Eu} < 0.6$ .

The MME sample from the Lingshan granite was K-rich ( $\text{K}_2\text{O} = 5.83\%$ ) and belonged to the tholeiite series. Its trace element composition was similar to the host granites; however, the sample had a reduced Eu anomaly, lower Th and U content and higher Sr content.

The Wancunxiang porphyry endoskarn (Sample 10ZJS171) had a similar trace element pattern to the unaltered sample, but it was enriched in  $\text{MgO}$ ,  $\text{CaO}$  and  $\text{Na}_2\text{O}$ , and depleted in  $\text{SiO}_2$  and  $\text{K}_2\text{O}$ . The endoskarn also had a high loss-on-ignition (LOI = 4.28%) relative to other unaltered samples (LOI < 0.8%).

## 6.4 Petrogenetic and Tectonic Interpretations

The Jurassic porphyries have relatively high Sr and low Y contents (adakitic signatures). These low Y contents and high Gd/Yb ratios (Figure 6.5D) were likely caused by residual garnet in partial melting of thick crust. In the Cathaysia Block, the Yongping and Lengshuikeng Jurassic porphyries had comparable or lower Gd/Yb ratios relative to those for the Late Triassic in Jingju and Wengshan syenogranites (Sun et al., 2011; Li et al., 2012b). These Late Triassic granites were generated from the dehydration melting of thickened crust but depleted in Sr and Eu, as discussed in Chapter 5 (Figure 5.6A). Therefore, the high Sr contents of Jurassic porphyries were most likely caused by the high plagioclase solubilities of water-rich magmas (Conrad et al., 1988) rather than plagioclase-garnet transitions. Under water-rich (often oxidised) conditions, amphibole and titanite stabilise and sequester rare earth elements (Bachmann and Bergantz, 2008; Richards, 2011). The adakitic signatures of Jurassic porphyries from the northeastern Jiangxi Province were caused by two independent factors: high water content and high fractionation/melting pressure in a thick crust.

The  $J_{2-3}$  porphyries have low FeOt/(FeOt+MgO) ratios (Figure 6.5C), which reflects the garnet and magnetite stability at high pressure. Some of these high ratios may be caused by hydrothermal alteration. These porphyries were also more oxidised as indicated by their high V/Co and V/Sc ratios (Figure 6.5E). The  $J_{2-3}$  porphyries had a horizontal Eu–Sr slope (Figure 6.5F), which indicates Eu is dominantly trivalent and does not fractionate with the divalent Sr.

In contrast, the  $K_1$  granites were primarily ferroan granitoids with low V/Co, V/Sc, Gd/Yb ratios and steep Eu–Sr slopes (Figure 6.5), which indicates they were generated under low pressures and reduced conditions. The low modal plagioclase and strong Sr-Ba-Eu depletion (Figure 6.5G) are consistent with a low water content during partial melting (Conrad et al., 1988). Lingshan syenogranite MMEs may represent cogenetic magmas with the host syenogranites or newly underplated  $K_1$  mafic rocks.

In general, the  $J_{2-3}$  and  $K_1$  rocks in northeastern Jiangxi Province are comparable to their  $J_{2-3}$  and  $K_1(I)$  counterparts in western Zhejiang Province based on trace element patterns (Figure 6.5G and Figure 5.6F). The Yongping and Lengshuikeng (Cathaysia Block) Jurassic porphyries are products of the  $J_{2-3}$  magmatism that occurred in both the Sibao Orogenic Belt and the Cathaysia Block.

Table 6.1 Locality, lithology, age and Hf isotope of Jurassic (bold) and Cretaceous granitoids and intermediate-felsic volcanic rocks from northeastern Jiangxi Province.

Locality	Sample	Lithology	Age	2SE	$\epsilon\text{Hf(t)}$	2SE	Data source
<b>Neoproterozoic Sibao Orogenic Belt</b>							
Ehu	Ehu-1	granite	122	3	-5.8	1.0	Jiang et al. (2011b)
	10LS-1-1	alkali-feldspar granite	131	2	0.5	0.3	Zhou et al. (2013)
	10LS-3-1	syenogranite	132	1	-2.0	0.3	
Lingshan	10ZJS154	syenogranite	131	1	-2.0	0.2	
	10ZJS155	syenogranite	129	1	-1.8	0.5	this study
	10ZJS156	MME	133	1	-1.3	0.4	
Wancunxiang	10ZJS170	syenogranite	131	1	-0.7	0.4	
	10ZJS171	syenogranite (endoskarn)	130	2	-1.9	0.5	this study
Damaoshan-Huaiyushan	10ZJS172	syenogranite-alkali feldspar granite	130	1	-3.4	0.5	
	<b>YS250</b>	<b>andesitic porphyry</b>	<b>166</b>	<b>1</b>	<b>2.5</b>	<b>0.2</b>	
	<b>YS03</b>	<b>dacitic porphyry</b>	<b>170</b>	<b>1</b>	<b>3.7</b>	<b>0.3</b>	
Yinshan	<b>YS416</b>	<b>quartz porphyry</b>	<b>172</b>	<b>1</b>	<b>2.2</b>	<b>0.2</b>	Wang et al. (2012a)
	<b>YS249</b>	<b>rhyolite</b>	<b>176</b>	<b>1</b>	<b>3.0</b>	<b>0.2</b>	
	<b>YS13</b>	<b>quartz porphyry</b>	<b>176</b>	<b>1</b>	<b>2.2</b>	<b>0.2</b>	
	<b>09D64</b>	<b>granodioritic porphyry</b>	<b>171</b>	<b>1</b>	<b>4.7</b>	<b>0.2</b>	
	<b>09D107</b>	<b>granodioritic porphyry</b>	<b>172</b>	<b>1</b>	<b>5.4</b>	<b>0.8</b>	
Dexing	<b>09D52</b>	<b>granodioritic porphyry</b>	<b>173</b>	<b>1</b>	<b>4.6</b>	<b>0.2</b>	Liu et al. (2012b)
	<b>09D122</b>	<b>granodioritic porphyry</b>	<b>173</b>	<b>1</b>	<b>4.5</b>	<b>0.2</b>	
	<b>09D45</b>	<b>granodioritic porphyry</b>	<b>174</b>	<b>1</b>	<b>4.3</b>	<b>0.2</b>	
<b>Cathaysia Block</b>							
	MD06	rhyolitic ignimbrite	137	1	-6.9	0.3	
	SH10-15	tuffite	140	1	-1.3	0.3	
	LSK-30	rhyolite	140	1	-10.0	0.3	
	LSK-96	rhyolite porphyry	140	1	-8.0	0.3	
Lengshuikeng	LSK-07	alkali-feldspar granite porphyry	140	1	-7.0	0.3	
	LSK-107	andesite	142	1	-8.7	0.6	Su et al. (2013a)
	SH10-27	tuff	144	1	-2.3	0.5	
	LSK-24	quartz syenite porphyry	144	1	-8.0	0.3	
	<b>ZK12208-12</b>	<b>granitic porphyry</b>	<b>157</b>	<b>1</b>	<b>-8.8</b>	<b>0.4</b>	
	<b>LSK-08</b>	<b>granitic porphyry</b>	<b>158</b>	<b>1</b>	<b>-9.3</b>	<b>0.5</b>	
	<b>Q862</b>	<b>granitic porphyry</b>	<b>160</b>	<b>2</b>	<b>-6.1</b>	<b>1.4</b>	Ding et al. (2005); Zhu et al. (2008)
	<b>Q889-1</b>	<b>granitic porphyry</b>	<b>160</b>	<b>2</b>	<b>-10.4</b>	<b>0.2</b>	
Yongping	<b>YP06-16</b>	<b>granitic porphyry</b>	<b>158</b>	<b>3</b>	<b>-9.3</b>	<b>0.7</b>	
	<b>YP06-17</b>	<b>granitic porphyry</b>	<b>156</b>	<b>3</b>	<b>-11.2</b>	<b>1.1</b>	Li et al. (2013c)
	<b>YP06-18</b>	<b>granitic porphyry</b>	<b>162</b>	<b>3</b>	<b>-14.4</b>	<b>0.9</b>	

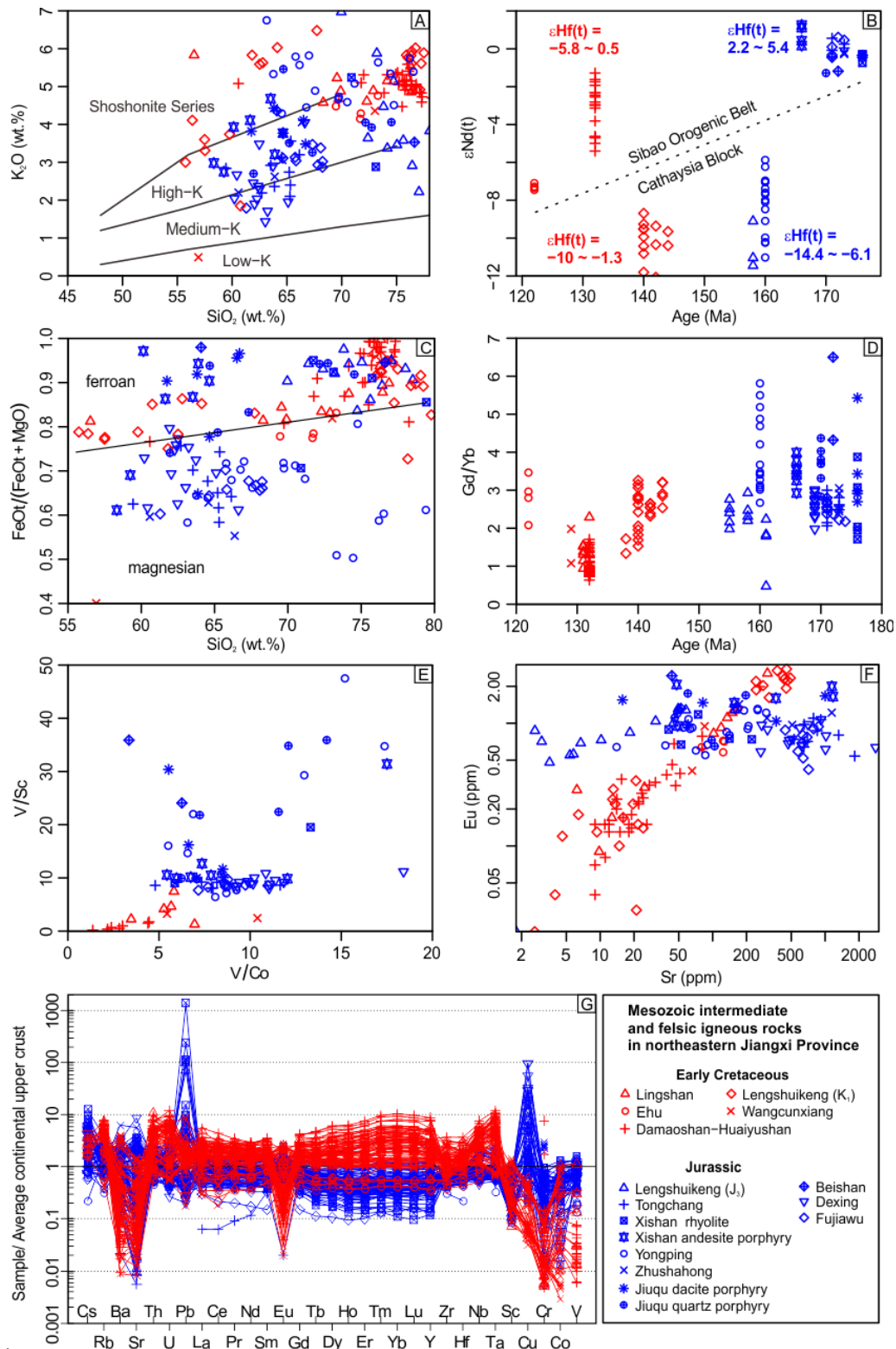


Figure 6.5 Geochemical data for Mesozoic granitoids in northeastern Jiangxi Province: (A)  $K_2O$  versus  $SiO_2$  (Peccerillo and Taylor, 1976); (B)  $\epsilon_{Nd(t)}$  versus age; (C) Ferroan-magnesian granitoid classification (Frost et al., 2001); (D)  $Gd/Yb$  versus age; (E)  $V/Co$  and  $V/Sc$ ; (F)  $Eu$  versus  $Sr$ . In contrast to the Cretaceous granites,  $Eu$  is dominantly trivalent in Jurassic porphyries and does not follow  $Sr^{2+}$ . The hydrothermal alteration did not change the horizontal  $Eu$ - $Sr$  pattern. (G) The trace element patterns were normalised to the global average of the upper continental crust (Rudnick and Gao, 2003)

The different basement compositions between the Cathaysia Block and Sibao Orogenic Belt are reflected by differing Hf-Nd isotopes in the Jurassic and Cretaceous intermediate and felsic rocks (Table 6.1 and Figure 6.5B). The arc and adakitic signatures of these Jurassic porphyries are variously interpreted as (1) products of a continental arc above a shallow-angle subduction zone (Zhou and Li, 2000), (2) slab melting (Zhang et al., 2013) or (3) Neoproterozoic arc rock melting (Liu et al., 2012b). However, (1) the flat-subduction and associated orogeny started in the Triassic; (2) the rocks should have strongly depleted Sr-Nd-Hf isotopic features if slab melting is the cause; (3) the petrogeochemical transition from J<sub>2-3</sub> to K<sub>1</sub> is sharp, and it is unlikely that only J<sub>2-3</sub> granitic rocks were derived from the Neoproterozoic arc rocks whereas K<sub>1</sub> counterparts were derived from other source rocks.

The J<sub>2-3</sub> rocks in the Cathaysia Block have lower zircon  $\varepsilon\text{Hf(t)}$  but higher  $\varepsilon\text{Nd(t)}$  values than the K<sub>1</sub> rocks; however, the  $\varepsilon\text{Nd(t)}$  and zircon  $\varepsilon\text{Hf(t)}$  values for samples from the Sibao Orogenic Belt are positively correlated (Figure 6.5B). This can be interpreted using the following model: Middle-Late Jurassic crustal melting in the Cathaysia basement was triggered by external fluids (carrying negligible Hf) depleted of Nd isotopes. Such a fluid originated from the contemporaneous underplating of mantle-derived hydrous magmas triggered by slab foundering and dehydration (Figure 5.10C). In contrast, in the Sibao Orogenic Belt these mantle-derived magmas emplaced the upper continental crust.

Since the Early Cretaceous granitic magmatism of the northeastern Jiangxi Province have similar geochemical compositions to their counterpart of the western Zhejiang Province, they likely reflect a lithospheric extension following the Triassic compressional orogeny (Howell, 1995, p. 9).

## 6.5 Conclusion

The Mid-Late Jurassic and Early Cretaceous granitic rocks in northeastern Jiangxi Province are comparable to their J<sub>2-3</sub> and K<sub>1</sub> counterparts in western Zhejiang Province in terms of age, petrogenesis and tectonic setting. The Mid-Late Jurassic porphyries in northeastern Jiangxi Province were wet and oxidized, generated by water-fluxed melting processes in the continental lower crust or by fractionation of hydrous mantle-derived magmas, containing fluids was from the foundering and dehydration of subducted oceanic crust. In contrast, the Early Cretaceous granites were dry and reduced, generated by dehydration melting processes in the continental lower crust, which underwent strong extension during the roll-back of paleo-Pacific plate.

## Chapter 7 Mesozoic Magmatism in the vicinity of the Ganzhou-Hangzhou Rift Zone

### 7.1 Introduction

The study region has undergone crustal attenuation since the Late Jurassic–Early Cretaceous (Wong et al., 2009; Jia et al., 2013). In northeastern Zhejiang Province, however, the tectonic processes are not as well known. It is particularly difficult to trace the Triassic history of the area, since no Triassic granitoids have been reported. Previous investigations found that dacite and rhyolite from southeastern Zhejiang Province have weaker Eu negative anomalies and higher Sm/Yb ratios than their counterparts from northwestern Zhejiang Province (Table 7.1), which has been related to variable of garnet stability during fractionation or to crustal melting processes (Osborn, 1979; Pitcher, 1997). The Ganzhou-Hangzhou rift formed in northwestern Zhejiang Province during the Early Cretaceous (Goodell et al., 1991). The variation in the amount of fractionation or crustal melting pressure that produced the different magmas described above was most likely controlled by differences in crustal thickness. This chapter reports new data for the Mesozoic granitoids from northeastern Zhejiang Province and the Ganzhou-Hangzhou rift zone (Figure 7.1). When combined with previously published data, more detailed constraints can be placed on the Mesozoic tectono-magmatic processes in the region.

Table 7.1 REE patterns of Early Cretaceous dacite and rhyolite from northwestern Zhejiang (the Ganzhou-Hangzhou rift zone) and southeastern Zhejiang, data from ZGS (1989, p. 383)

Region	Rock type	$\Sigma$ REE contents (ppm)	$\delta$ Eu	La/Sm	Sm/Yb
Northwestern Zhejiang Province	dacite	293	0.28	5.71	1.91
Southeastern Zhejiang Province		216	0.59	7.71	2.35
Northwestern Zhejiang Province	rhyolite	270	0.58	5.51	2.13
Southeastern Zhejiang Province		244	0.85	7.75	2.90

### 7.2 Geological setting and petrography

The Ganzhou-Hangzhou rift zone is regarded as a failed rift that developed during the Early Cretaceous (Goodell et al., 1991) and generally follows the suture zone of the Yangtze and Cathaysia blocks (Sibao Orogenic Belt) in Zhejiang Province (Figure 7.1A). The Early Cretaceous magmatic rocks predominantly consist of highly fractionated syenogranites and alkali feldspar granites with relatively depleted Nd-Hf isotopic signatures (Shen et al., 2000; Jiang et al., 2011b). The samples in this study were collected from several Cretaceous intermediate and felsic intrusions in the region, including Tongshan, Jiuhua, Zhujiaxiang, Shuangcai, Hongling, Hecun and Yujiashan (Figure 7.1A).

Mostly, Early Cretaceous volcanic rocks cover the basement in northeastern Zhejiang Province, which is generally considered to consist of Paleoproterozoic rocks, similar to the exposed Babu Complex in southwestern Zhejiang Province (Yu et al., 2009; Xia et al., 2012). The Cretaceous magmatic rocks are intermediate and felsic volcanic rocks and related intrusions, with minor contemporaneous basalts and gabbros (ZGS, 1989). In this study, diorite, monzodiorite and monzonite were sampled from the Ru'ao intrusion (Figure 7.1A).

### 7.2.1 Late Triassic and Early Jurassic granitoids in the Ningbo region

The Qiuwang and Xiepu syenogranite intrusions are located in northeast Zhejiang Province, near the coast (Figure 7.1B), in fault contact with Late Triassic–Early Jurassic strata. The Early Cretaceous volcaniclastic units are in fault contact with or are unconformably overlying Xiepu syenogranite (ZGS, 1980). Qiuwang syenogranite is coarse-grained and mainly comprises feldspar, quartz and muscovite (Figure 7.2A). Xiepu syenogranite is medium-grained and mainly comprises quartz, feldspar and biotite (Figure 7.2B). Plagioclase in Xiepu syenogranite has a myrmekitic texture. Li et al. (2012d) reported an age (180 Ma) and geochemical data for the Xiepu syenogranite. The low  $\epsilon_{\text{Nd}}(t)$  value of the Xiepu syenogranite indicates that the source was likely the Paleoproterozoic basement of the region (Li et al., 2012d). Three samples were collected from each intrusion (Figure 7.1B).

### 7.2.2 Mesozoic granitoids and diorites in the Zhuji region

The Guangshan and Jiangzao intrusions (Figure 7.1C), which intruded the Neoproterozoic Shuangxiwu Group and Paleozoic strata, are inequigranular medium- to coarse-grained syenogranite. These intrusions contain mainly quartz, perthite, plagioclase and partly chloritised biotite (Figures 7.2C and 7.2D). Some plagioclase grains have oscillatory zoning. The samples from the Zhaxi intrusion are quartz diorites, primarily consisting of plagioclase, quartz, clinopyroxene, hornblende and titanite. The interior of this intrusion was reported to be granodiorite (Xie et al., 2013).

The Yujiashan diorite (Figure 7.1C), which intrudes the Neoproterozoic and Early Cretaceous strata, comprises ~85–90% plagioclase ( $\text{An}_{30-40}$ ), ~10% clinopyroxene (partly replaced with amphibolite and biotite) and ~1% quartz (Figure 7.2E). Accessory minerals include zircon, apatite, epidote and opaque minerals.

### 7.2.3 Porphyritic samples from the Ganzhou-Hangzhou rift zone

Figure 7.1A shows the localities of the porphyritic samples from the Ganzhou-Hangzhou rift zone.

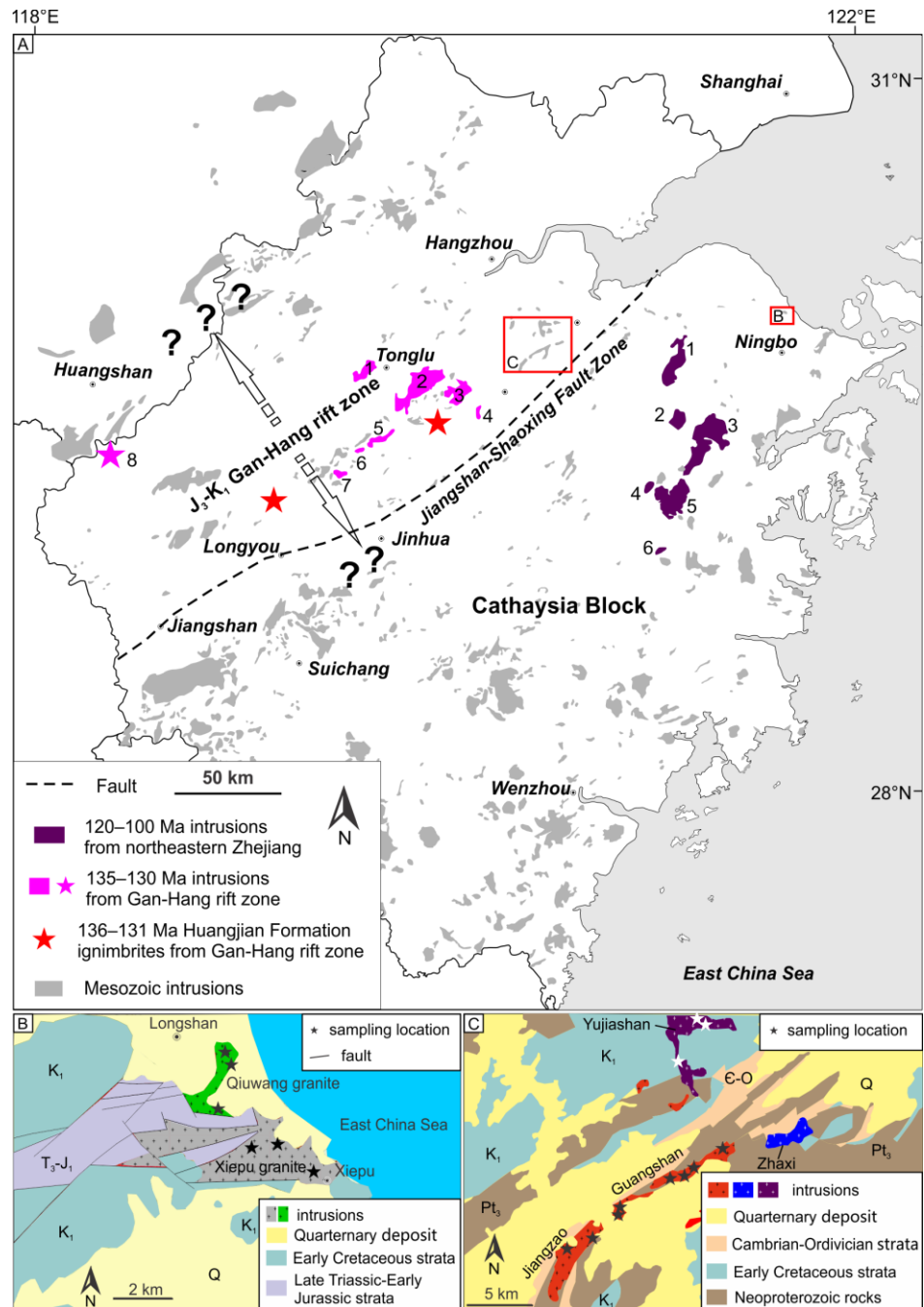


Figure 7.1 (A) Distribution of Mesozoic intrusions in Zhejiang Province. The location of the Ganzhou-Hangzhou rift zone is based on Wang et al. (2006) and Yang et al. (2012). Data sources for the 135–130 Ma intrusions from the Ganzhou-Hangzhou rift zone: 1-Tonglu complex (Zhou et al., 1999; Griffin et al., 2002; Wong et al., 2011), 2-Huajiatang granite (Wong et al., 2011), 3-Majian rhyolite/dacitic porphyry (Wong et al., 2011), 4-Hecun dacitic-rhyolitic porphyry (this study), 5-Hongling granitic porphyry (this study), 6-Shuangcai andesitic-dacitic porphyry (this study), 7-Zhujiaxiang andesitic porphyry (this study), 8-Mugua dolerite (Li et al., 2011a). Data sources for the 120–100 Ma intrusions from northeastern Zhejiang Province: 1-Liangnong complex (Chen et al., 2005b; Yen, 2005; Hsieh et al., 2009; Wong et al., 2011), 2-Beizhang complex (Chen et al., 2005b; Wong et al., 2011), 3-Xiaojiang complex (Yen, 2005; Hsieh et al., 2009; Wong et al., 2011), 4-Ru’ao complex (Dong et al., 2007; this study), 5-Longhuangtang granite (Yen, 2005; Hsieh et al., 2009; Wong et al., 2011), 6-Shantouzheng quartz diorite (Zheng et al., 1990; Chen et al., 1991; Yen, 2005). (B) A simplified geological map of the Qiuwang and Xiepu granite modified after ZGS (1980); data are from Li et al. (2012d) and this study. (C) Simplified geological map of the Shaoxing-Zhuji region, modified using ZGS (1975) data from Xie et al. (2013) and this study.

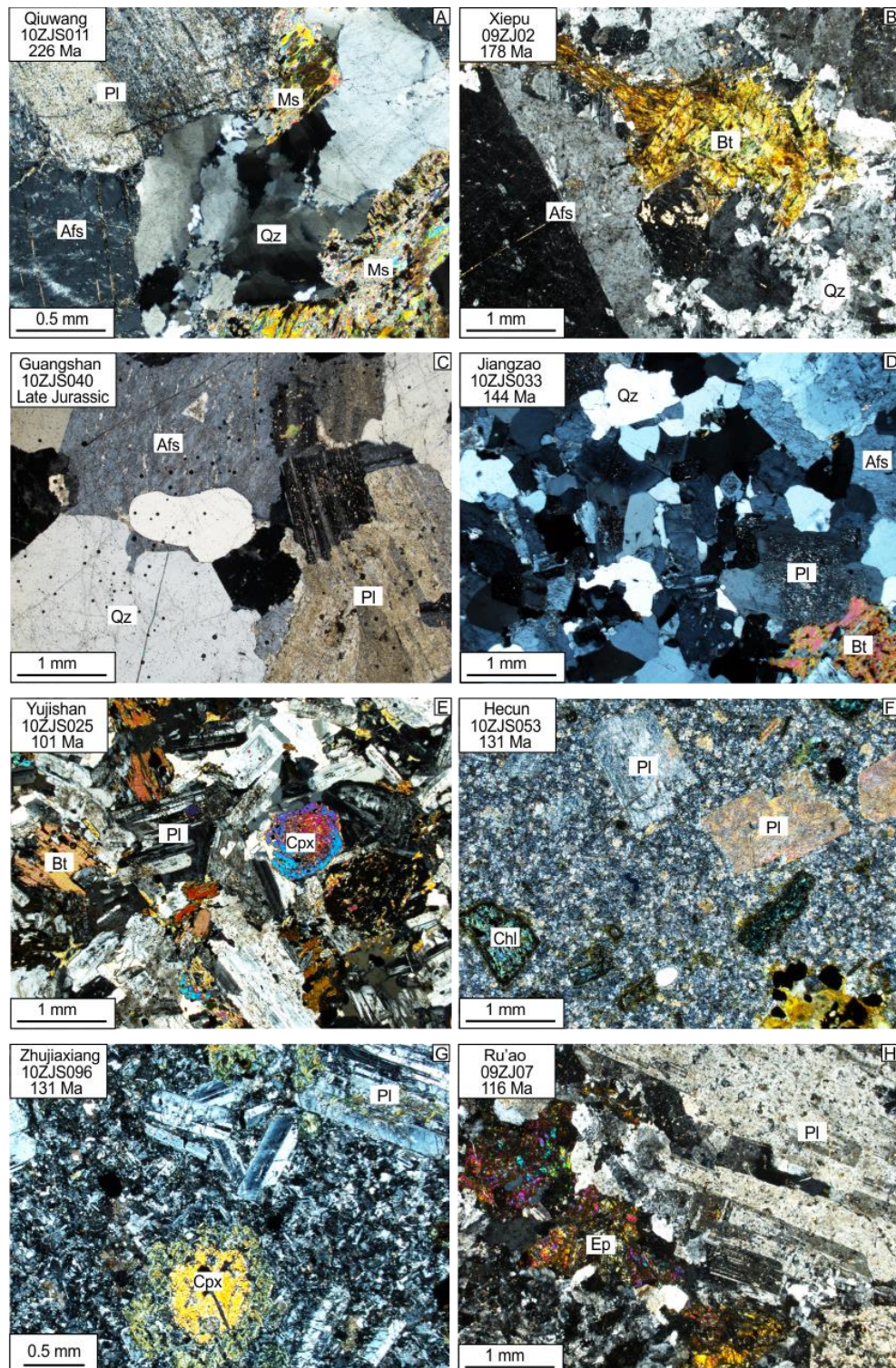


Figure 7.2 Thin section photomicrographs (cross-polarised light) of Mesozoic intrusive rocks from northeastern Zhejiang Province and the Ganzhou-Hangzhou rift zone: (A) Qiuwang granite; (B) Xiepu granite; (C) Guangshan granite; (D) Jiangzao granite; (E) Yujiashan diorite; (F) Hecun dacitic-rhyolitic porphyry; (G) Zhujiashang andesitic porphyry; (H) Ru'ao monzodiorite. Mineral abbreviations: Afs, alkali feldspar; Pl, plagioclase; Qz, quartz; Bt, biotite; Ms, muscovite; Chl, chlorite; Cpx, clinopyroxene; Ep, epidote.

The Hongling intrusion comprises dacitic-rhyolitic porphyries. The phenocrysts are quartz, plagioclase, alkali feldspar, muscovite, chlorite (most likely altered from biotite) and

opaque minerals. The matrix mainly consists of fine-grained feldspar and quartz. The country rocks are the Middle-Late Jurassic Yujiashan and Early Cretaceous Laocun/Huangjian Formations.

The Hecun intrusion consists of dacitic-rhyolitic porphyries (Figure 7.2F). The phenocrysts are quartz, feldspar and minor biotite/amphibole. The matrix mainly consists of fine-grained feldspar and quartz. The country rock is from the Early Cretaceous Huangjian Formation.

The Zhujiaxiang intrusion consists of andesitic porphyries with plagioclase and clinopyroxene phenocrysts (Figure 7.2G). The matrix mainly consists of fine-grained plagioclase. The country rocks are from the Early Cretaceous Laocun Formation.

The Shuangcai intrusion consists of andesitic-dacitic porphyries. The phenocrysts are plagioclase, chlorite (most likely altered from amphibole) and opaque minerals. The matrix mainly consists of fine-grained to cryptocrystalline feldspar and quartz. The country rocks are from the Early Cretaceous Laocun Formation.

#### 7.2.4 Early Cretaceous Ru'ao complex from northeastern Zhejiang Province

The Ru'ao complex (Figure 7.1A) in northeastern Zhejiang Province contains mafic, intermediate and felsic rocks. Diorite, monzodiorite and monzonite have fine-grained or porphyritic textures, with ferromagnesian minerals altered to chlorite and epidote (Figure 7.2H). Most rocks contain minor mounts of quartz and opaque minerals. As reported by Dong et al. (2007), dolerite from the Ru'ao complex is primarily plagioclase, clinopyroxene and hornblende; syenogranite from the Ru'ao complex contains perthite, quartz and plagioclase, with minor biotite and magnetite.

### 7.3 Results

#### 7.3.1 Zircon age and Hf isotopes

Most zircon grains have oscillatory magmatic zoning. Weighted mean  $^{206}\text{Pb}/^{238}\text{U}$  ages of the dominant zircon populations are interpreted as the crystallisation ages of each sample. Zircon U-Pb concordia diagrams with the representative CL images, their U-Pb ages, Th/U ratios and  $\epsilon\text{Hf(t)}$  values are shown in Figure 7.3 and are summarised in Table 7.2 along with previously published data.

##### 7.3.1.1 Qiuwang syenogranite

Twenty-five U-Pb analyses were undertaken on twenty-five zircons from sample 10ZJS011 (Figure 7.3A). The Th contents range from 178–1875 ppm and the U contents

from 404–2348 ppm, with Th/U = 0.27–1.25. All analyses are concordant and yield a weighted mean  $^{206}\text{Pb}/^{238}\text{U}$  age of  $225 \pm 2$  Ma (MSWD = 2.5). Twenty-three Hf isotopic analyses were carried out on twenty-one grains from the dated zircons. The  $\epsilon\text{Hf(t)}$  values range from −15.7 to −9.9.

Twenty-nine analyses were undertaken on twenty-nine zircons from sample 09ZJ01 (Figure 7.3B). The Th content ranges from 228–4954 ppm and the U content from 281–6537 ppm, with Th/U = 0.37–1.48. Twenty-four concordant analyses yield a  $^{206}\text{Pb}/^{238}\text{U}$  weighted mean age of  $226 \pm 1$  Ma (MSWD = 1.04), which is consistent with the mean age of sample 10ZJS011. Spots 09ZJ01-03, -04, -25, -28, -31 and -35 have  $^{206}\text{Pb}/^{238}\text{U}$  ages ranging from 155 Ma to 188 Ma, which probably reflects Pb loss during Jurassic magmatism (sample 09ZJ01 was taken close to the Jurassic Xiepu granite).

### 7.3.1.2 Xiepu syenogranite

Ten U-Pb (SHRIMP) and Hf isotopic analyses were undertaken on 10 zircons from the Xiepu granite (sample 09ZJ02, Figure 7.3C). The Th and U contents ranged from 230–2047 ppm and 93–1832 ppm, respectively, with Th/U = 0.13–1.16. These analyses are concordant and yield a  $^{206}\text{Pb}/^{238}\text{U}$  weighted mean age of  $178 \pm 1$  Ma (MSWD = 1.2), which is consistent with the zircon SHRIMP and LA-ICP-MS dating results of Li et al. (2012d) for the same pluton. The  $\epsilon\text{Hf(t)}$  values range between −17.6 and −13.4.

### 7.3.1.3 Jiangzao syenogranite

Eighteen U-Pb analyses were carried out on eighteen zircons from the Jiangzao granite (sample 10ZJS033, Figure 5.3D). The Th and U contents ranged from 32–4202 ppm and 40–4962 ppm, respectively, with Th/U = 0.25–2.73. Fourteen analyses were clustered on a concordia and record a  $^{206}\text{Pb}/^{238}\text{U}$  weighted mean age of  $144 \pm 2$  Ma (MSWD = 2.4). The  $\epsilon\text{Hf(t)}$  values of these grains range from −4.2 to 0.1. Discordant analyses 10ZJS033-4, -5, -12 and -17 have  $^{206}\text{Pb}/^{238}\text{U}$  ages between 108 Ma and 125 Ma, which indicates they were influenced by younger thermal events.

### 7.3.1.4 Shuangcail andesitic porphyry

Sixteen U-Pb and fifteen Hf isotopic analyses were undertaken on sixteen zircons from the Shuangcail andesitic porphyry (sample 10ZJ072, Figure 7.3E). The Th and U contents ranged from 25–790 ppm and 38–1709 ppm, respectively, with Th/U = 0.46–1.77. These analyses are all concordant, yielding a  $^{206}\text{Pb}/^{238}\text{U}$  weighted mean age of  $132 \pm 1$  Ma (MSWD = 0.81). The  $\epsilon\text{Hf(t)}$  values range between −5.3 and 0.

### 7.3.1.5 Hongling rhyolitic porphyry

Twenty U-Pb and Hf isotopic analyses were undertaken on twenty zircons from the Hongling rhyolitic porphyry (sample 10ZJS081, Figure 7.3F). The Th and U contents ranged from 80–526 ppm and 91–491 ppm, respectively, with Th/U = 0.81–1.48. These analyses were all concordant, yielding a  $^{206}\text{Pb}/^{238}\text{U}$  weighted mean age of  $131 \pm 1$  Ma (MSWD = 1.02). The  $\epsilon\text{Hf(t)}$  values range between –4.8 and 1.1.

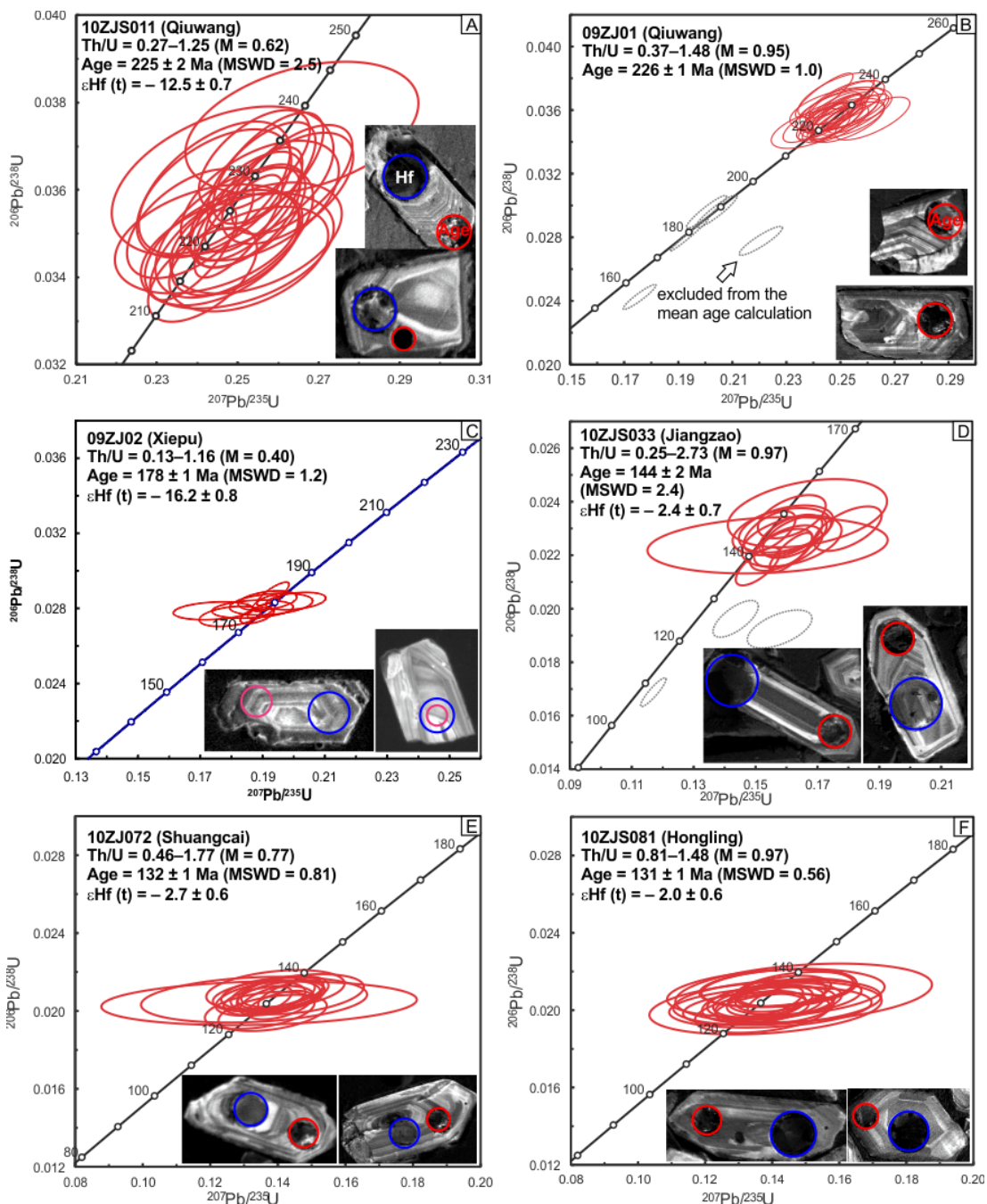


Figure 7.3 (continued over page)

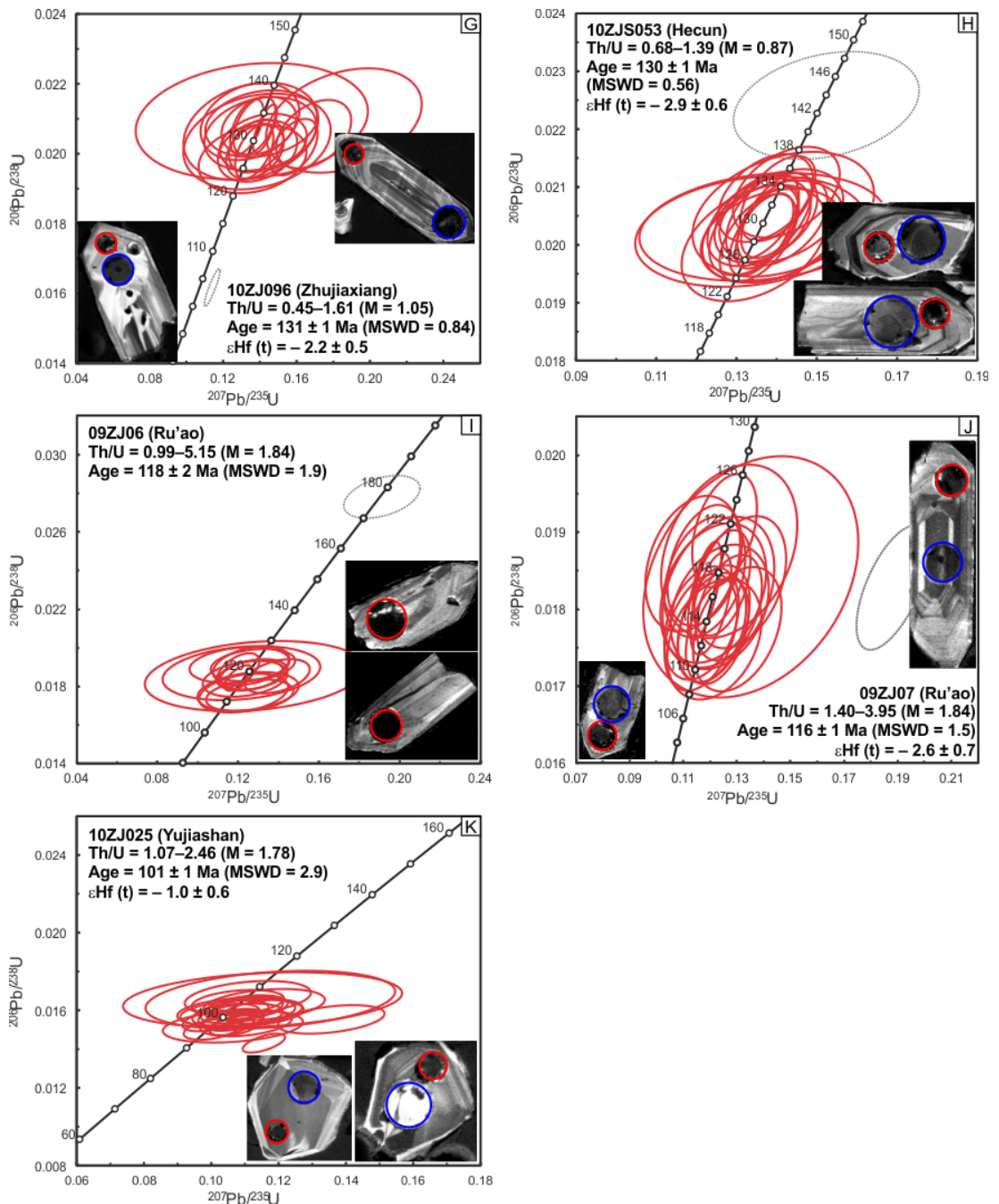


Figure 7.3 Zircon CL images, zircon age and Hf isotopic results for the Mesozoic intermediate/felsic intrusions from northeastern Zhejiang Province and the Ganzhou-Hangzhou rift zone. On the concordia diagrams, the analyses represented by dotted grey ellipses (2 SD) were excluded from the calculation of the mean age. Median of Th/U ratios is notated as M. (A, B) Qiuwang granite; (C) Xiepu granite; (D) Jiangzao granite; (E) Shuangcail andesitic-dacitic porphyry; (F) Hongling dacitic-rhyolitic porphyry; (G) Zhujiaxiang andesitic porphyry; (H) Hecun dacitic-rhyolitic porphyry; (I) Ru'ao diorite; (J) Ru'ao monzodiorite; (K) Yujiashan diorite.

### 7.3.1.6 Zhujiaxiang andesitic porphyry

Twenty U-Pb analyses were undertaken on twenty zircons from the Zhujiaxiang andesitic porphyry (sample 10ZJS096, Figure 7.3G). The Th and U contents ranged from 53–1037 ppm and 42–2328 ppm, respectively, with  $\text{Th/U} = 0.45\text{--}1.61$ . Nineteen concordant

analyses yield a  $^{206}\text{Pb}/^{238}\text{U}$  weighted mean age of  $131 \pm 1$  Ma (MSWD = 0.84). Eighteen of these zircons had  $\epsilon\text{Hf(t)}$  values between  $-3.8$  and  $0.1$ . Analysis 10ZJS096-3 is discordant and has a  $^{206}\text{Pb}/^{238}\text{U}$  age of  $103 \pm 1$  Ma, which indicates it was influenced by a younger thermal event.

### 7.3.1.7 Hecun dacitic porphyry

Twenty analyses were carried out on twenty zircons from sample 10ZJS053 (Figure 7.3H). Th and U contents ranged from 55–589 ppm and 72–643 ppm, respectively, with Th/U = 0.68–1.39. Spot 10ZJS053-7 has a concordant  $^{206}\text{Pb}/^{238}\text{U}$  age of  $143 \pm 2$  Ma, which indicates it is an inherited zircon. The remaining nineteen concordant analyses define a  $^{206}\text{Pb}/^{238}\text{U}$  weighted mean age of  $130 \pm 1$  Ma (MSWD = 0.56). The  $\epsilon\text{Hf(t)}$  values of these nineteen zircons range from  $-6.5$  to  $-0.8$ .

### 7.3.1.8 Ru'ao diorite and monzodiorite

Fifteen U-Pb analyses were undertaken on fifteen zircons from the Ru'ao diorite (sample 09ZJ06, Figure 7.3I). The Th and U contents ranged from 101–2290 ppm and 70–444 ppm, respectively, with Th/U = 0.99–5.15. Fourteen concordant analyses yield a  $^{206}\text{Pb}/^{238}\text{U}$  weighted mean age of  $118 \pm 2$  Ma (MSWD = 1.9).

Twenty-two U-Pb and twenty Hf isotopic analyses were undertaken on twenty-two zircons from the Ru'ao monzodiorite (sample 09ZJ07, Figure 7.3J). The Th and U contents ranged from 126–1571 ppm and 87–449 ppm, respectively, with Th/U = 1.40–3.95. With the exception of analysis 09zj07-6, all other analyses are concordant. The concordant analyses have a  $^{206}\text{Pb}/^{238}\text{U}$  weighted mean age of  $116 \pm 1$  Ma (MSWD = 1.5), which is consistent with sample 09ZJ06. The  $\epsilon\text{Hf(t)}$  values range from  $-5.4$  to  $-0.2$  (with an outlier at 4.8).

### 7.3.1.9 Yujiashan diorite

Twenty-two U-Pb analyses were undertaken on twenty-two zircons from the Yujiashan diorite (sample 10ZJS025, Figure 7.3K). The Th and U contents ranged from 165–1554 ppm and 108–826 ppm, respectively, with Th/U = 1.07–2.46. With the exception of analyses 10ZJS025-17 and -20, all other analyses are concordant. The twenty concordant analyses yield a  $^{206}\text{Pb}/^{238}\text{U}$  weighted mean age of  $101 \pm 1$  Ma (MSWD = 2.9) and  $\epsilon\text{Hf(t)}$  values between  $-3.3$  and  $2.1$ .

## 7.3.2 Whole-rock major and trace elements

The Qiuwang granite samples have moderate to high  $\text{SiO}_2$  contents (66–74%) with  $\text{MgO} = 0.39\text{--}0.78\%$  and  $\text{P}_2\text{O}_5 = 0.05\text{--}0.27\%$ . The  $\text{FeOt}/(\text{FeOt}+\text{MgO})$  ratios range from 0.82–

0.87. These granites are strongly peraluminous with an A/CNK = 1.18–1.48, K<sub>2</sub>O = 4.71–6.05%, K<sub>2</sub>O/Na<sub>2</sub>O = 1.5–7.1. They have high Y contents (57–72 ppm) and Gd/Yb ratios (2.8–4.8). The V/Co ratios are low (3.3–3.8). The Ga/Al ratios are 3.7–4.6 × 10<sup>-4</sup>. The zircon saturation temperatures range from 850–895 °C, which are calculated by the formula given by Boehnke et al. (2013).

The analytical results for the 178 Ma Xiepu granite were similar to the data reported by Li et al. (2012d) for the same intrusion. These samples are highly fractionated with a high SiO<sub>2</sub> content (71–75%) and low MgO (0.03–0.28%) and P<sub>2</sub>O<sub>5</sub> contents (0.03–0.06%). The FeOt/(FeOt+MgO) ratios are 0.89–0.98. The samples have an A/CNK ratio of 1.0 with K<sub>2</sub>O = 4.78–5.90% and K<sub>2</sub>O/Na<sub>2</sub>O = 1.2–2.1. They have high Y contents (38–42 ppm), low Gd/Yb ratios (1.02–1.07) and low V/Co ratios (2.9–3.5). The Ga/Al ratios are 2.4–2.6 × 10<sup>-4</sup>. The zircon saturation temperatures are very consistent and record values of 665–666 °C.

The 147 Ma Guangshan and 144 Ma Jiangzao granites have similar compositions, which are consistent with those previously reported for the Guangshan granite (Xie et al., 2013). They have high SiO<sub>2</sub> contents (70–75%), with MgO = 0.14–0.61% and P<sub>2</sub>O<sub>5</sub> = 0.02–0.08%. Their FeOt/(FeOt+MgO) ratios range from 0.77 to 0.90. These granites are weakly peraluminous with an A/CNK = 1.0–1.1, K<sub>2</sub>O = 4.01–4.83% and K<sub>2</sub>O/Na<sub>2</sub>O = 1.08–1.48. They have high Y contents (32–68 ppm), low Gd/Yb ratios (0.91–1.49) and moderate V/Co ratios (5.4–8.8). The Ga/Al ratios are 2.2–2.7 × 10<sup>-4</sup>. The zircon saturation temperatures range from 681 to 724 °C.

The samples of the 132–130 Ma porphyries from Ganzhou-Hangzhou Belt, including Shuangcai, Hongling, Zhujiexiang and Hecun, have SiO<sub>2</sub> contents ranging from 59–70%, with MgO = 0.54–2.07% and P<sub>2</sub>O<sub>5</sub> = 0.02–0.25. The FeOt/(FeOt+MgO) ratios are 0.71–0.84. These porphyries are metaluminous to weakly peraluminous with an A/CNK = 0.95–1.10, K<sub>2</sub>O = 2.97–5.34% and K<sub>2</sub>O/Na<sub>2</sub>O = 0.56–6.09. They have moderate Y contents (29–36 ppm) and Gd/Yb ratios (1.85–1.99), with moderate to high V/Co ratios (5.7–9.3). The Ga/Al ratios are 2.2–2.5 × 10<sup>-4</sup>.

The 118–116 Ma samples from the Ru'ao Complex have intermediate compositions with SiO<sub>2</sub> = 55–66%, MgO = 1.16–2.86 % and P<sub>2</sub>O<sub>5</sub> = 0.20–0.51. The FeOt/(FeOt+MgO) ratios range from 0.73 to 0.75. They are metaluminous to weakly peraluminous with an A/CNK = 0.85–1.06, K<sub>2</sub>O = 3.96–4.54% and K<sub>2</sub>O/Na<sub>2</sub>O = 0.82–1.08. These materials have moderate Y contents (20–30 ppm) and Gd/Yb ratios (2.00–2.29) with high V/Co ratios (9.2–9.8). The Ga/Al ratios are 1.9–2.3 × 10<sup>-4</sup>.

The 101 Ma Yujiashan diorites have intermediate compositions with  $\text{SiO}_2 = 58\text{--}59\%$ ,  $\text{MgO} = 3.11\text{--}3.83\%$  and  $\text{P}_2\text{O}_5 = 0.23\text{--}0.24$ . The  $\text{FeOt}/(\text{FeOt}+\text{MgO})$  ratios range from 0.57 to 0.63. They are metaluminous with  $\text{A/CNK} = 0.85\text{--}0.86$ ,  $\text{K}_2\text{O} = 2.07\text{--}2.33\%$  and  $\text{K}_2\text{O}/\text{Na}_2\text{O} = 0.47\text{--}1.60$ . These rocks have low Y contents (14–16 ppm), high  $\text{Gd}/\text{Yb}$  ratios (2.89–3.17) and moderate  $\text{V}/\text{Co}$  ratios (6.5–6.7). The  $\text{Ga}/\text{Al}$  ratios are  $2.3\text{--}2.4 \times 10^{-4}$ .

Table 7.2 Locality, lithology, age and Hf isotope values for the igneous rocks from northeastern Zhejiang Province and the Ganzhou-Hangzhou rift zone.

Locality	Sample	Lithology	Age	2SE	$\varepsilon\text{Hf(t)}$	2SE	Data source
<b>Northeastern Zhejiang (Cathaysia Block)</b>							
Qiuwang	09ZJ01	syenogranite	226	1			this study
Qiuwang	10ZJ011	syenogranite	225	2	-12.5	0.7	this study
Xiepu	04JZ-31	syenogranite	180	2			Li et al. (2012d)
Xiepu	09ZJ02	syenogranite	178	2	-16.2	0.8	this study
Xiepu	D1245	syenogranite	177	1			Li et al. (2012d)
Beizhang	06ZBZ01	granite	120	3	-4.8	1.4	Wong et al. (2011)
Ru'ao	09ZJ06	diorite	118	2			this study
Ru'ao	09ZJ07	monzodiorite	116	1	-2.6	0.7	this study
Longhuangtang	09ZLHT02	granite	115	4	-4.6	0.6	Wong et al. (2011)
Xiaojiang	06ZXJ01	quartz diorite	114	1	-3.0	1.0	Wong et al. (2011)
Santouzheng	87ZI411	quartz diorite	108	1			Chen et al. (1991)
Liangnong	07ZLL01	quartz diorite	100	2	-4.3	0.3	Wong et al. (2011)
<b>Ganzhou-Hangzhou rift zone (Neoproterozoic Sibao Orogenic Belt)</b>							
Guangshan	LZC-4A	synogranite	162	1	-1.9	0.7	Jia et al. (2013)
Guangshan	LZC-5A	synogranite	156	1	-2.4	0.5	Jia et al. (2013)
Zhaxi	JS001	quartz diorite	150	3			Gu et al. (2011)
Guangshan	JS002	synogranite	147	2			Gu et al. (2011)
Jiangzao	10ZJS033	synogranite	144	2	-2.4	0.7	this study
Tonglu	06ZHC01	granodiorite	135	1	-4.3	0.9	Wong et al. (2011)
Mugua	842-13	dolerite	135	2			Li et al. (2011a)
Shuangcai	10ZJS072	andesitic-dacitic porphyry	132	1	-2.7	0.6	this study
Majian	06ZMJ05	rhyolite	132	2	2.1	0.8	Wong et al. (2011)
Hongling	10ZJS81	dacitic-rhyolitic porphyry	131	1	-2.0	0.6	this study
Zhujiashiang	10ZJS096	andesitic porphyry	131	1	-2.2	0.5	this study
Hecun	10ZJS053	dacitic-rhyolitic porphyry	130	1	-2.9	0.6	this study
Tonglu	06ZZS01	granite	130	2	-2.5	1.1	Wong et al. (2011)
Majian	06ZMJ02	granite	130	1	1.7	0.9	Wong et al. (2011)
Tonglu	06ZFC01	granite	121	2	1.0	0.7	Wong et al. (2011)
Yujiashan	10ZJS025	diorite	101	1	-1.0	0.6	this study

## 7.4 Discussion

Three stages of intrusion (Late Triassic, Early Jurassic and Early Cretaceous) are recorded from northeastern Zhejiang Province, with  $\varepsilon\text{Hf(t)}$  values significantly higher in the third stage. These data are consistent with zircons from Mesozoic volcanic rocks (Liu et al., 2012a). Intermediate and felsic samples from the third stage have similar Hf isotopic compositions.

In the Gang-Hang rift zone, Mesozoic magmatism spans the Late Jurassic and Early Cretaceous, and Hf isotopic compositions do not vary significantly with age or composition. No Triassic or Early-Mid Jurassic magmatism has been found in this region.

#### 7.4.1 Late Triassic and Early Jurassic granitoids in the Ningbo region: mountain building and collapse in northeastern Zhejiang

The strongly negative zircon  $\epsilon\text{Hf(t)}$  values for the T<sub>3</sub> Qiuwang and J<sub>1</sub> Xiepu granites imply they both originated from the Paleoproterozoic basement rocks of the Cathaysia Block. These two plutons have Sr-Ba-Eu depletions (Figure 7.4A), which implies they were both generated by dehydration melting processes. However, the Late Triassic Qiuwang granite was likely generated at a deeper crustal level with higher magma temperatures (Figure 7.4B) than the Early Jurassic Xiepu granite. The low V/Co and V/Sc ratios reflect reduced magmas (Figure 7.4C), with no input of oxidising agents from oceanic crust. Therefore, the Mesozoic tectonic evolution in this region was most likely similar to that of western Zhejiang Province: mountain building during the Triassic and collapse since the Jurassic, as discussed in Chapter 5.

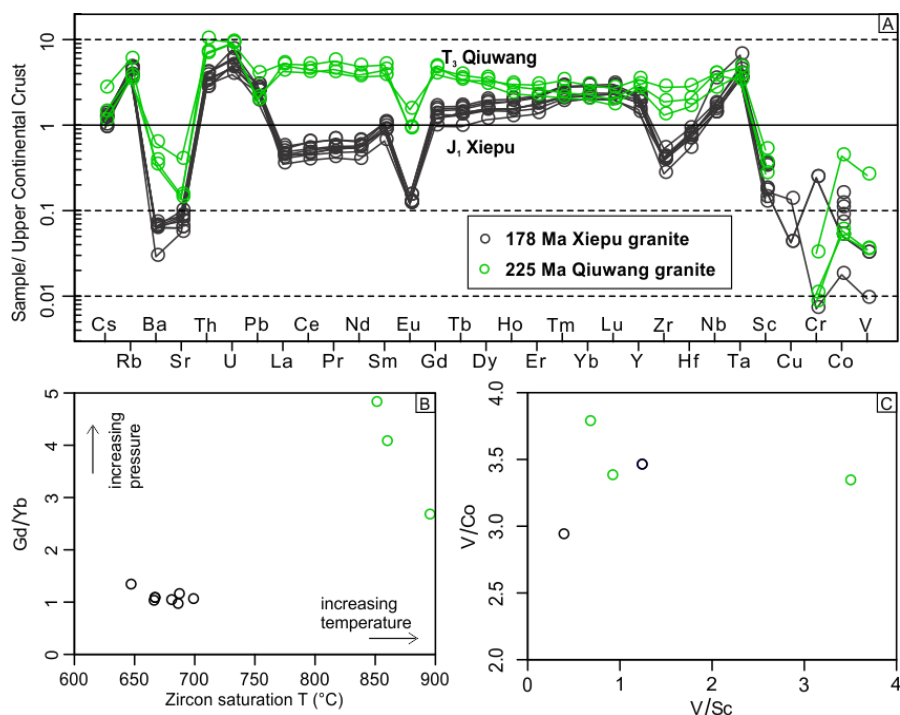


Figure 7.4 Whole-rock geochemical data for the Qiuwang and Xiepu granites: (A) trace element patterns normalised to the average for the upper continental crust (Rudnick and Gao, 2003); (B) plot of the Gd/Yb versus zircon saturation temperature; (C) plot of V/Co versus V/Sc.

### 7.4.2 Late Jurassic granites in the Zhuji region: crustal attenuation initiation in the Ganzhou-Hangzhou rift zone

The Late Jurassic Guangshan and Jiangzao intrusions have similar compositions (Figure 7.5A). They have low Gd/Yb ratios (low melting/fractionation pressures) and zircon saturation temperatures (Figure 7.5B). Their V/Co (2–9) and V/Sc (0–4) ratios are low-moderate (Figure 7.5C), which reflects a reduced or weakly oxidised magma. Overall, these rocks are comparable to the K<sub>I</sub>(I) granites in western Zhejiang Province, which implies that crustal attenuation began earlier (since the Late Jurassic) in the Ganzhou-Hangzhou rift zone than western Zhejiang Province.

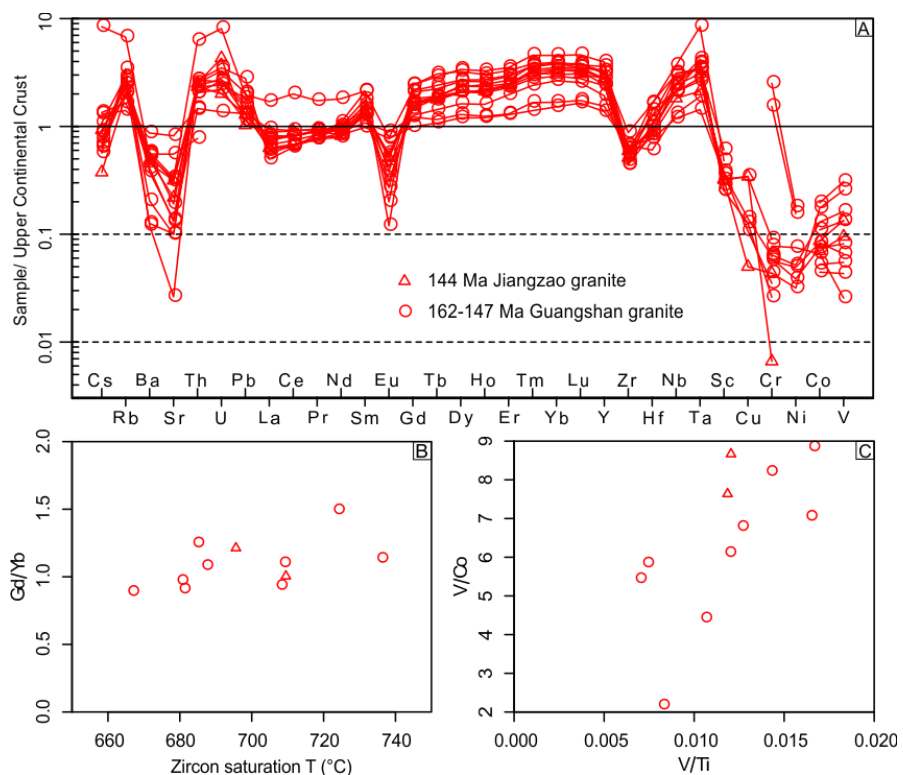


Figure 7.5 Whole-rock geochemical data for the Jiangzao and Guangshan granites: (A) trace elements normalised to the average for the upper continental crust (Rudnick and Gao, 2003); (B) plot of the Gd/Yb ratios versus zircon saturation temperatures; (C) plot of the V/Co ratio versus Ti/V.

### 7.4.3 Late Jurassic and Cretaceous (quartz) diorite from Ganzhou-Hangzhou rift zone: crustal extension to crustal magmatic thickening

The Zhaxi quartz diorite and Yujiashan diorite intrusions from the Ganzhou-Hangzhou rift zone have different ages but similar Hf isotopic features, most likely derived from a lithospheric mantle source modified by subducted oceanic crust (relatively depleted in HFSE, Figure 7.6A). However, the Zhaxi quartz diorite has low Sr (Figure 7.6A) and K<sub>2</sub>O contents (Figure 7.6B), high FeOt/(FeOt+MgO) ratios (Figure 7.6C), low Gd/Yb ratios (Figure 7.6D)

and low  $\text{Al}_2\text{O}_3$  contents (Figure 7.6E and cf. Figure 7.7D). The V/Co ratios of the two intrusions were similar and ranged from 6.5 to 8.5 (Figure 7.6D).

Regional lithospheric extension began by the Late Jurassic, as indicated by A-type magmatism at Guangshan and Jiangzao (Section 7.4.2). The 150 Ma Zhaxi quartz diorite was most likely related attenuation of the crust, which reduced the  $\text{K}_2\text{O}$  content (Coulon and Thorpe, 1981) and increased plagioclase stability (Osborn, 1979). Iron enrichment was facilitated by garnet (Pitcher, 1997, p. 38) and magnetite (Osborn, 1979, p. 157-158) breakdown under low-pressure conditions. In contrast, the 101 Ma Yujiashan diorite was generated in a thick continental crust.

The Cretaceous rocks from the coastal region of Zhejiang Province likely records similar processes. The region has undergone extensive mantle-derived magmatism during Early Cretaceous (120–100 Ma, Table 7.2), which caused the growth and thickening of the continental crust. The Early Cretaceous felsic rocks are dominated by alkali feldspar granite, granite (*sensu stricto*) and granodiorite (Hsieh et al., 2009). However, the Late Cretaceous felsic rocks are dominated by quartz syenite and syenite, including the 98 Ma Wanghaigang quartz syenite (Qiu et al., 2011), 88 Ma Xiaoxiong syenite (He and Xu, 2012) and 86 Ma Daheshan syenite (He and Xu, 2012). Such a transition reflects crustal thickening, which promotes generation of more quartz-deficient felsic rocks at higher crustal pressures (Tuttle and Bowen, 1958; Gualda and Ghiorso, 2013). This crustal thickening and the disconformities above the Early Cretaceous Moshishan Group (ZGS, 1989; Gu, 2005) are consistent with a crustal deformation event caused by extensive intrusions following Early Cretaceous lithospheric extension (Howell, 1995, p. 18; Eaton, 2008; Ramos, 2009, p. 55) rather than a compressional orogeny (South China-Okhotomorsk Block collision, Yang, 2013).

#### 7.4.4 Comparison of Early Cretaceous magmatic rocks from the Ganzhou-Hangzhou rift zone with those from northeastern Zhejiang Province

The 135–100 Ma magmatic rocks from the Ganzhou-Hangzhou rift zone and the 120–100 Ma magmatic rocks from northeastern Zhejiang Province do not exhibit significant differences in their Sr-Nd-Hf isotopic compositions between the basic, intermediate and acid rocks (Zhou et al., 1999; Dong et al., 2007; Hsieh et al., 2009). This is consistent with a common mantle source. The basement rocks in the Ganzhou-Hangzhou rift zone likely have similar isotopic signatures to the metasomatised mantle during the Early Cretaceous and therefore these two sources cannot be distinguished (Liu et al., 2012b; Zhou et al., 2012a). However, zircon  $\epsilon\text{Hf(t)}$  values of Early Cretaceous granites in northeastern Zhejiang Province differ significantly from their Triassic and Jurassic counterparts (Table 7.2);

therefore, the Paleoproterozoic basement rocks of the Cathaysia Block can be distinguished from the metasomatised mantle. Compared to their counterparts in northeastern Zhejiang Province, certain rocks in the Ganzhou-Hangzhou rift zone exhibit depleted zircon Hf isotopic compositions (Wong et al., 2011, p. 253). This can be attributed to the involvement of depleted asthenosphere during continental lithospheric extension (Gilder et al., 1996). Liu et al. (2014) reported the age and Hf isotopic compositions of volcanic rocks from the Early Cretaceous Laocun Formation in the Ganzhou-Hangzhou rift zone. These rocks had more negative zircon  $\epsilon\text{Hf(t)}$  values (approximately  $-10$ ) than adjacent contemporaneous intrusions (Figure 7.1A and Table 7.2); instead, they are similar to the K<sub>1</sub>(I) granites from the Longyong-Suichang region and are most likely derived from the Paleoproterozoic basement of the Cathaysia Block (Figure 5.4A). This finding supports the view that the Ganzhou-Hangzhou rift zone, with a thinner crust due to isostasy, was topographically lower than the Longyong-Suichang region.

Among the 135–100 Ma magmatic rocks from the Ganzhou-Hangzhou rift zone and the 120–100 Ma magmatic rocks from northeastern Zhejiang Province, the intermediate and felsic rocks may be generated by partial melting of previously underplated mafic-intermediate material. However, the available age data indicate that local mafic, intermediate and felsic rocks were coeval. In addition, to produce intermediate-felsic magmas, re-melting requires higher temperatures due to the loss of volatiles due to the magma solidification (Eskola, 1932). Therefore, fractional crystallisation is likely the most important mechanism to produce the aforementioned intermediate and felsic rocks.

A thin continental crust for the Ganzhou-Hangzhou rift zone is also indicated by the overall high FeOt/(FeOt+MgO) ratios (Figure 7.7A), low Gd/Yb ratios (Figure 7.7B), high Y contents (Figure 7.7C), low Al<sub>2</sub>O<sub>3</sub> contents (Figure 7.7D) and low Eu/Eu\* ratios (Figure 7.7E) (early plagioclase crystallisation under low pressure conditions and/or with a low water content) for the intermediate rocks (no residual garnet). Overall, the rocks from northeastern Zhejiang Province are more oxidised than those from the Ganzhou-Hangzhou rift zone, as indicated by higher V/Co and V/Ti ratios (Figure 7.7F). It is probably resulted from strong continental lithospheric metasomatism during the Triassic flat-slab subduction (close to the trench). However, the low FeOt/(FeOt+MgO) ratios were not determined by redox conditions but high fractionation pressures, as indicated by low Y contents and high Gd/Yb ratios (Figure 7.8) (Gill, 1981; Mamani et al., 2010). Iron enrichment during magma evolution is still a controversial topic with two factors often being discussed: pressure and redox conditions (Osborn, 1959; Osborn, 1979; Grove and Kinzler, 1986; Lee et al., 2010; Chiaradia, 2014). Mesozoic granitoids from South China empirically show that only high

redox conditions ( $V/Co > \sim 5$ ) allow high pressure (high  $Gd/Yb$  ratios) to effectively inhibit iron enrichment. The best examples include the Dashuang complex (Figure 4.6), Jingju complex (Figure 4.9), Zhaxi and Yujishan diorite and  $J_{1-2}$  A-type granitoids from the Nanling Range (Figure 8.14).

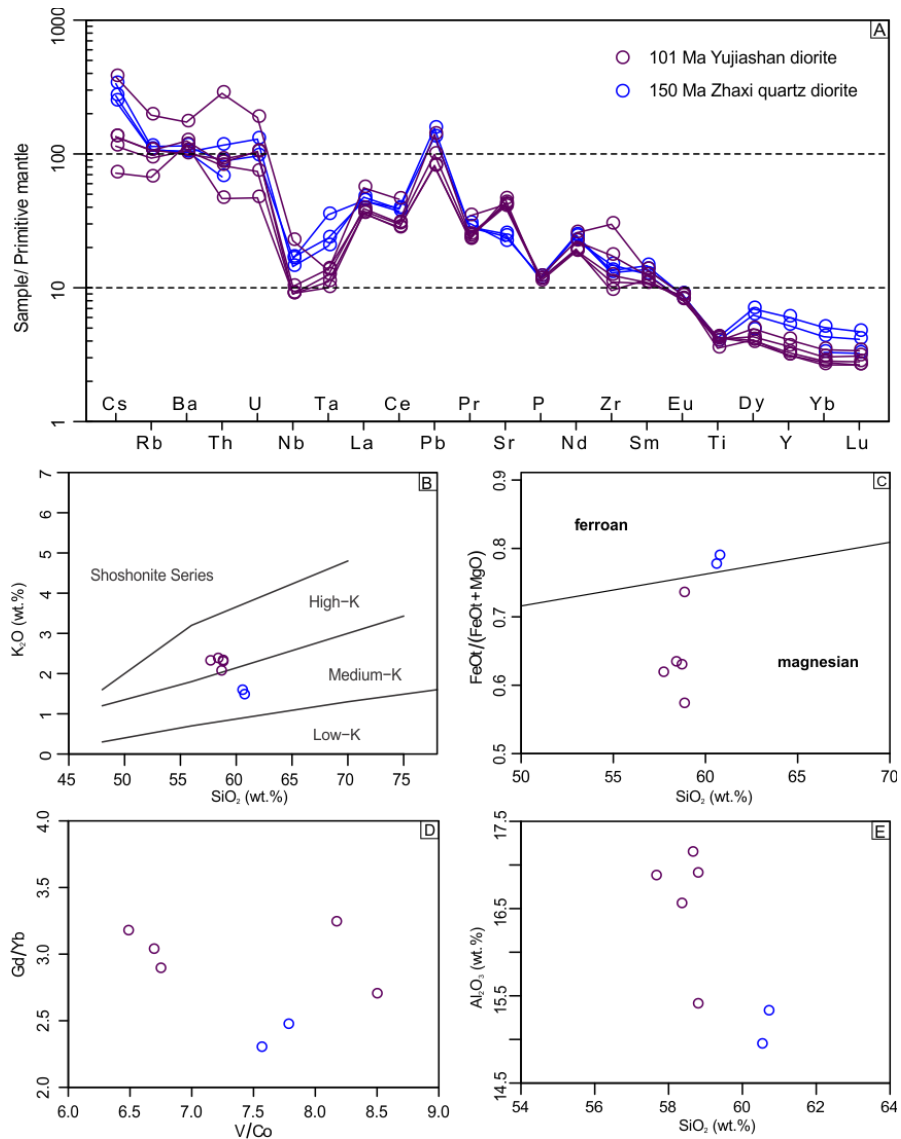


Figure 7.6 Whole-rock geochemical data for the Zhaxi and Yujishan (quartz) diorites: (A) trace element patterns normalised to the primitive mantle (McDonough and Sun, 1995); (B) plot of  $SiO_2$ - $K_2O$  (Peccerillo and Taylor, 1976); (C) plot of  $FeOt/(FeOt+MgO)$  versus  $SiO_2$  (Frost et al., 2001); (D) plot of  $Gd/Yb$  versus  $V/Co$ ; (E) plot of  $Al_2O_3$  versus  $SiO_2$ .

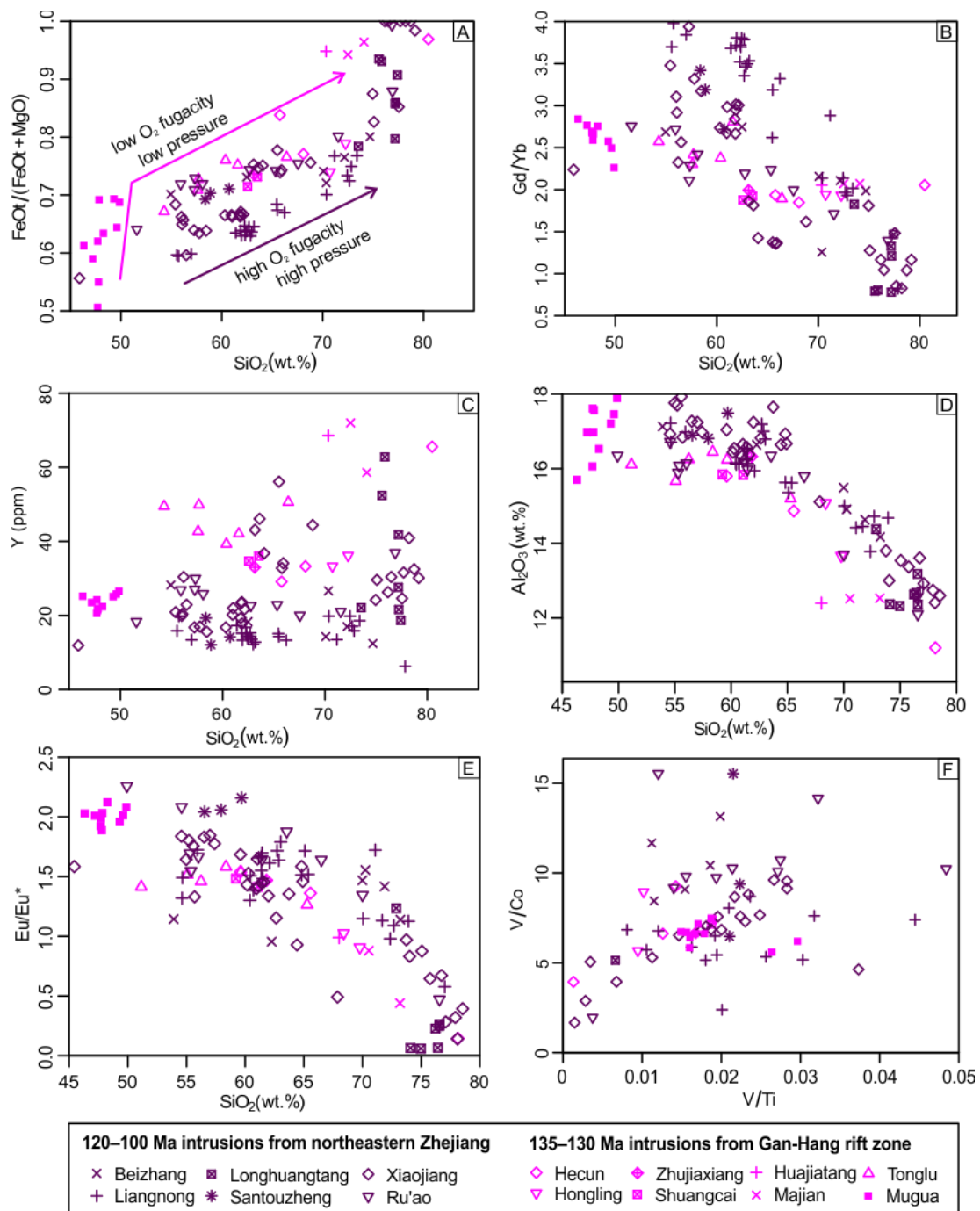


Figure 7.7 Selective whole-rock geochemical data for the Early Cretaceous intrusions and volcanic rocks of the Ganzhou-Hangzhou rift zone (135–130 Ma) and northeastern Zhejiang Province (120–100 Ma): (A) plot of  $\text{FeOt}/(\text{FeOt}+\text{MgO})$  versus  $\text{SiO}_2$ ; (B) plot of  $\text{Gd/Yb}$  versus  $\text{SiO}_2$ ; (C) plot of  $\text{Y}$  versus  $\text{SiO}_2$ ; (D) plot of  $\text{Al}_2\text{O}_3$  versus  $\text{SiO}_2$ ; (E) plot of  $\text{Eu/Eu}^*$  versus  $\text{SiO}_2$ ; (F) plot of  $\text{V/Co}$  versus  $\text{V/Ti}$  plot. The oxygen fugacity and pressure conditions for the  $\text{FeOt}/(\text{FeOt}+\text{MgO})$  evolution trends are from Osborn (1979, p. 156). The  $\text{Eu/Eu}^* = 2\text{Eu}_N / (\text{Sm}_N \times \text{Gd}_N)^{0.5}$  (Rudnick and Fountain, 1995), normalised to CI carbonaceous chondrites (McDonough and Sun, 1995).

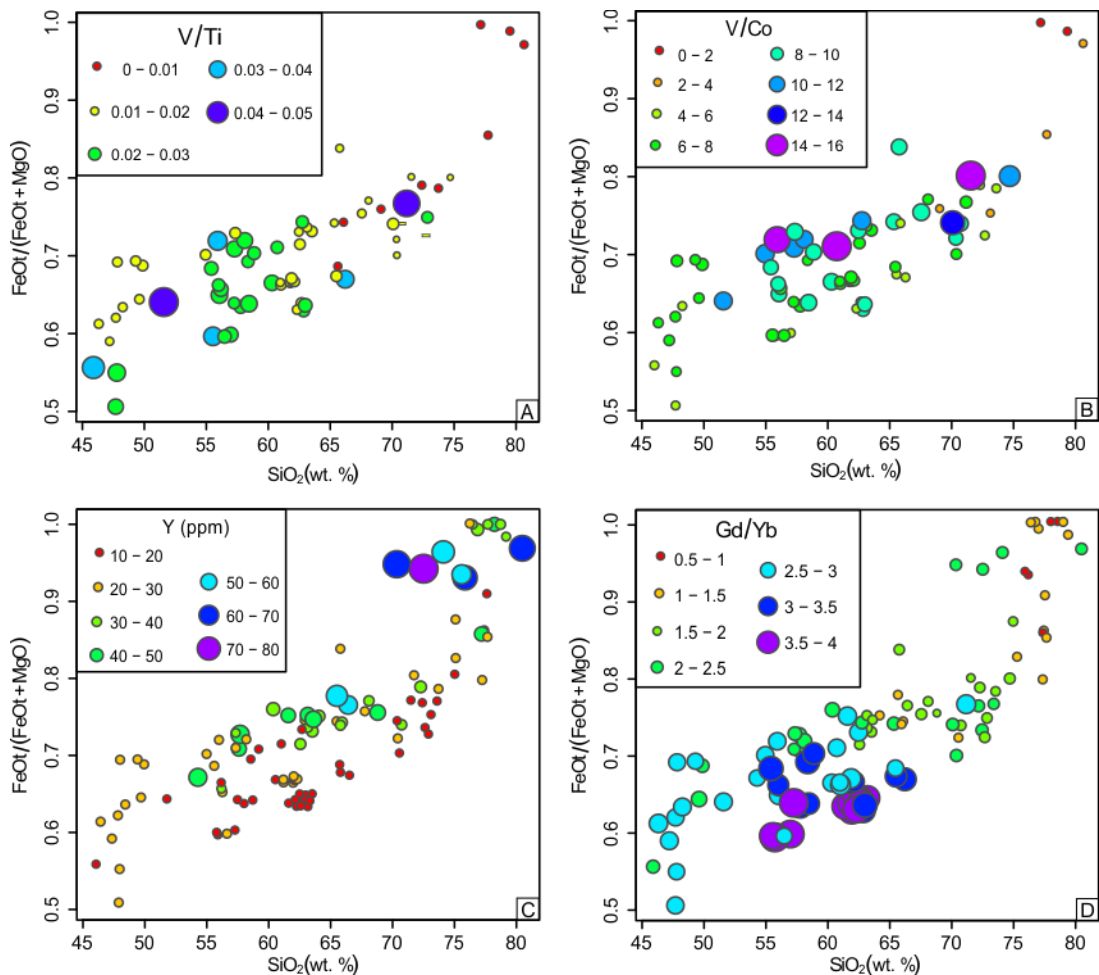


Figure 7.8 Plots of  $\text{FeOt}/(\text{FeOt}+\text{MgO})$  versus  $\text{SiO}_2$  for the Early Cretaceous intrusions and volcanic rocks from the Ganzhou-Hangzhou rift zone and northeastern Zhejiang Province with symbol sizes representing the elemental content or ratios: (A) V/Ti; (B) V/Co; (C) Y; (D) Gd/Yb. Note that a low  $\text{FeOt}/(\text{FeOt}+\text{MgO})$  ratio is generally associated with a low Y content and high Gd/Yb ratio.

## 7.5 Conclusion

The Mesozoic tectonic processes in northeastern Zhejiang Province were similar to those in western Zhejiang Province: mountain building during the Triassic and orogenic collapse since the Early-Mid Jurassic. Multiple stages of magmatism were associated with tectonism. Late Triassic Qiuwang granite is similar to most Triassic granitoids in Zhejiang Province, and was generated by dehydration melting of thickened continental crust. The Early Jurassic Xiepu granite in this region was most likely generated by crustal dehydration melting triggered by basaltic underplating following the break-off of the paleo-Pacific plate (see Section 5.5.2).

In the Ganzhou-Hangzhou rift zone, the crustal attenuation and A-type granitic magmatism began by the Late Jurassic, which is earlier than for the other regions in Zhejiang Province (~135 Ma). A relatively thin continental crust and asthenospheric upwelling along

the Ganzhou-Hangzhou rift zone caused the elemental and isotopic compositions of the Early Cretaceous magmatic rocks to differ from their counterparts outside the rift zone: higher Y contents, lower Gd/Yb ratios, higher FeOt/(FeOt+MgO) ratios and more depleted Hf isotopic compositions.

The attenuated crust in the Ganzhou-Hangzhou rift zone and northeastern Zhejiang Province was thickened by intrusions of Early Cretaceous mantle-derived rocks.

## Chapter 8 Petrogenesis and Tectonic Implications of Mesozoic Granitoids in other regions of South China

Using the granitoid evolutionary trend as determined for Zhejiang and northeastern Jiangxi Province as a general working hypothesis, this chapter reviews the published age, elemental and isotopic data for Mesozoic granitoids from eight other well-studied regions in South China (Figure 8.1), to test the wider applicability of the results to the rest of the SCB. The influence of the heterogeneity of crustal source rocks (Chappell and White, 1974), can also be assessed by additional data.

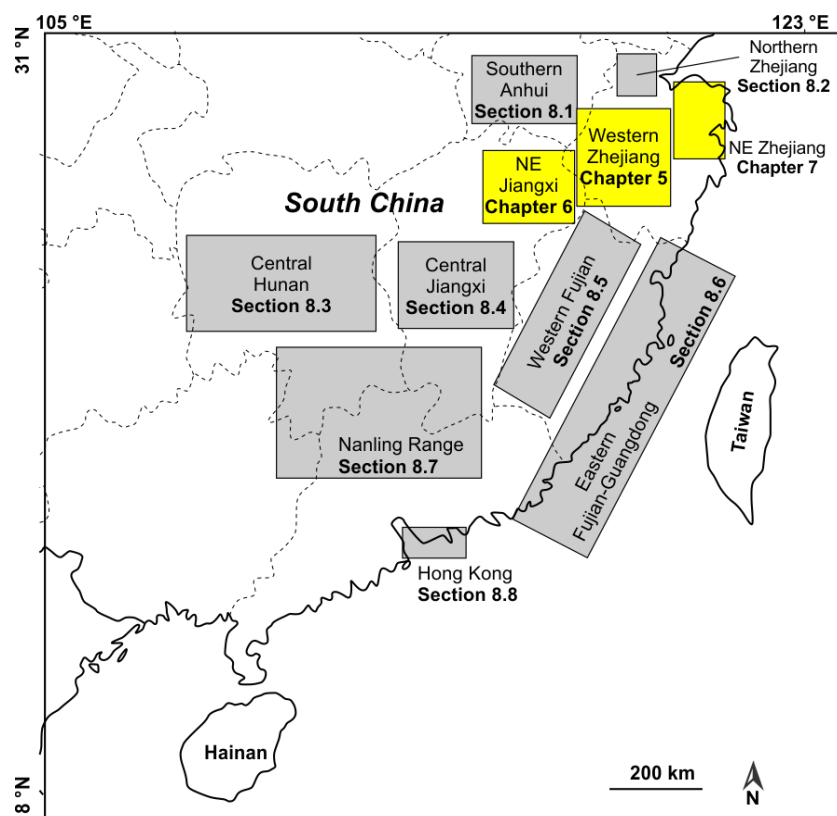


Figure 8.1 Map of South China showing the Mesozoic magmatic provinces discussed in Chapters 5, 6 and 7 (yellow) and this chapter (grey).

### 8.1 Southern Anhui Province

The crystalline basement of southern Anhui Province mainly consists of Mesoproterozoic rocks as indicated by the zircon Hf model ages (Wu et al., 2012) of the Late Jurassic and Early Cretaceous granitoids (Figure 8.2) that mainly intrude the Paleozoic rocks (AGS, 1987). The Mesozoic granitoids in southern Anhui Province are high-K or shoshonite series rocks (Figure 8.3A) with A/CNK ratios between 0.7 and 1.3. From the Late Jurassic to the Early Cretaceous, these granitoids show increasing FeOt/(FeOt+MgO) ratios (Figure 8.3B), decreasing Gd/Yb ratios (Figure 8.3C), increasing Y contents (Figure 8.3D), increasing zircon saturation temperatures (with a jump after ~130 Ma) (Figure 8.3E),

decreasing V/Ti ratios (Figure 8.3F), and decreasing Sr-Ba-Eu depletion and decreasing REE-Nb-Ta contents (Figure 8.3G). Triassic magmatism has not been discovered in this region.

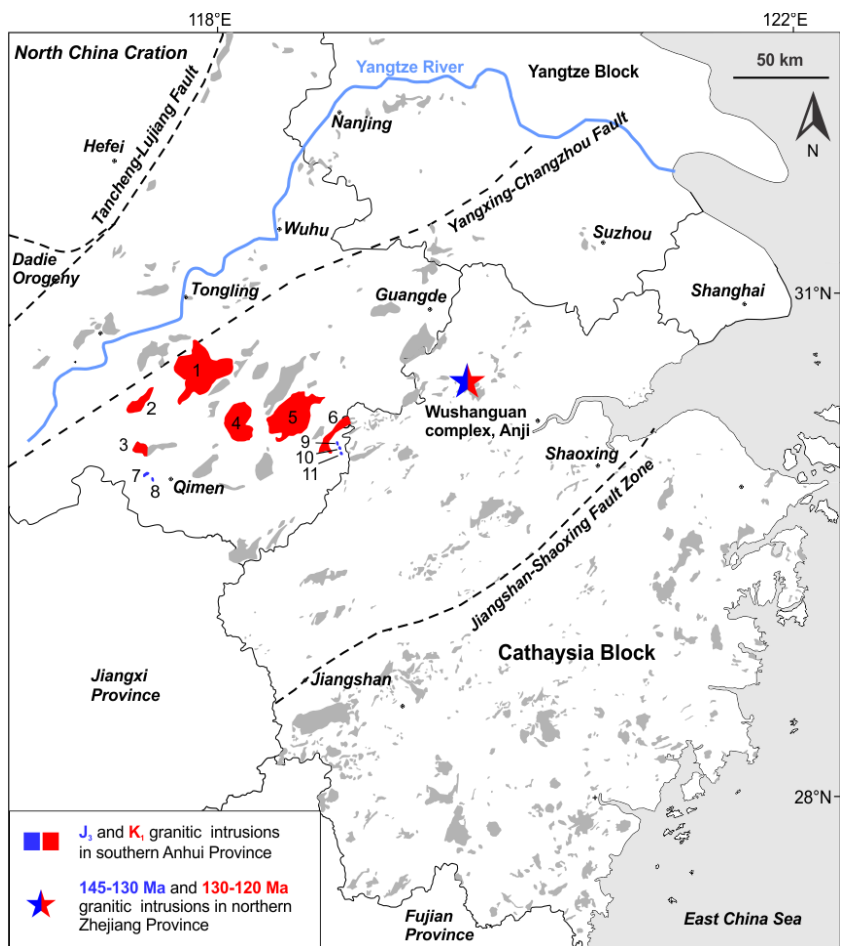


Figure 8.2 Distribution of Jurassic-Cretaceous granitic intrusions in eastern South China.  
 1: Jiuhua-Qingyang granitic complex (Xu et al., 2010; Su et al., 2013b); 2: Huayuangong granite (Li et al., 2012a); 3: Guniujiang syenogranite (Xie et al., 2012a); 4: Huangshan-Taiping granitic complex (Su et al., 2013b); 5: Jingde granodiorite (Zhang et al., 2012b); 6: Fuling syenogranite (Zhou et al., 2013); 7: Xiyuan granodioritic porphyry (Li et al., 2013b); 8: Dongyuan granodioritic porphyry (Li et al., 2013b); 9: Jingtongya granodiorite; 10: Kaobeijian granodiorite; 11: Xiaoyao granodiorite (Zhou et al., 2012b; Li et al., 2013b).

The petrography and geochemistry of these Late Jurassic and Early Cretaceous granitoids are comparable to the  $J_{2-3}$  and  $K_1(I-II)$  granitoids in western Zhejiang Province, which indicates similar tectono-magmatic processes, as explained in Chapter 5. The Late Jurassic granitoids were most likely generated from a water-fluxed melt within a relatively thick continental crust during the foundering of the paleo-Pacific plate. The Early Cretaceous granitoids were generated by low-pressure crustal dehydration melting due to continental lithospheric extension, which probably involved heat from basaltic underplating.

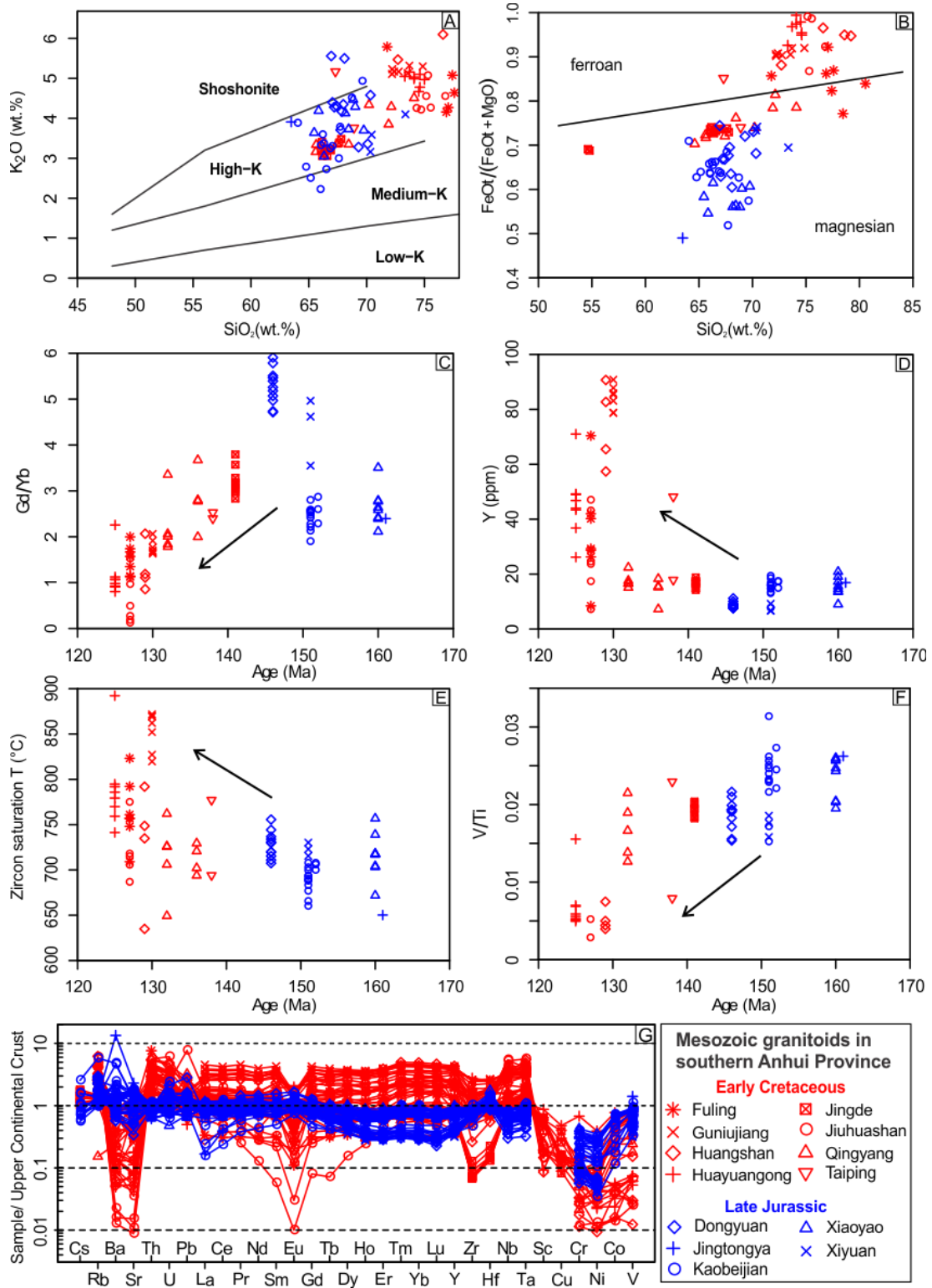


Figure 8.3 Whole-rock geochemical data for the Mesozoic granitoids from southern Anhui Province. Data source as for Figure 8.2. (A) plot of  $K_2O$  versus  $SiO_2$  (Peccerillo and Taylor, 1976); (B) plot of molar  $Al_2O_3 / (Na_2O + K_2O)$  versus molar  $Al_2O_3 / (Na_2O + K_2O + CaO)$ ; (C) plot of whole-rock Gd/Yb ratio versus age, which decreased from the Late Jurassic to Early Cretaceous; (D) plot of the whole-rock Y content versus age, which increased during the Early Cretaceous; (E) plot of zircon saturation temperatures versus age, which increasing values after ~130 Ma; (F) plot of the whole-rock V/Ti ratio versus age, which significantly decreased after ~130 Ma; (G) the trace element patterns were normalised to the global average for the upper continental crust (Rudnick and Gao, 2003).

## 8.2 Northern Zhejiang Province

The Early Cretaceous granitic rocks in Northern Zhejiang Province (Figure 8.2) have related Pb-Zn polymetallic deposits. Similar to southern Anhui Province, zircon Hf isotopic compositions [ $\varepsilon\text{Hf}(t) = -7$  to 0] (Wu et al., 2012) of the Early Cretaceous granitoids and felsic volcanic rocks in this region indicate a Mesoproterozoic crystalline basement was the source that melted.

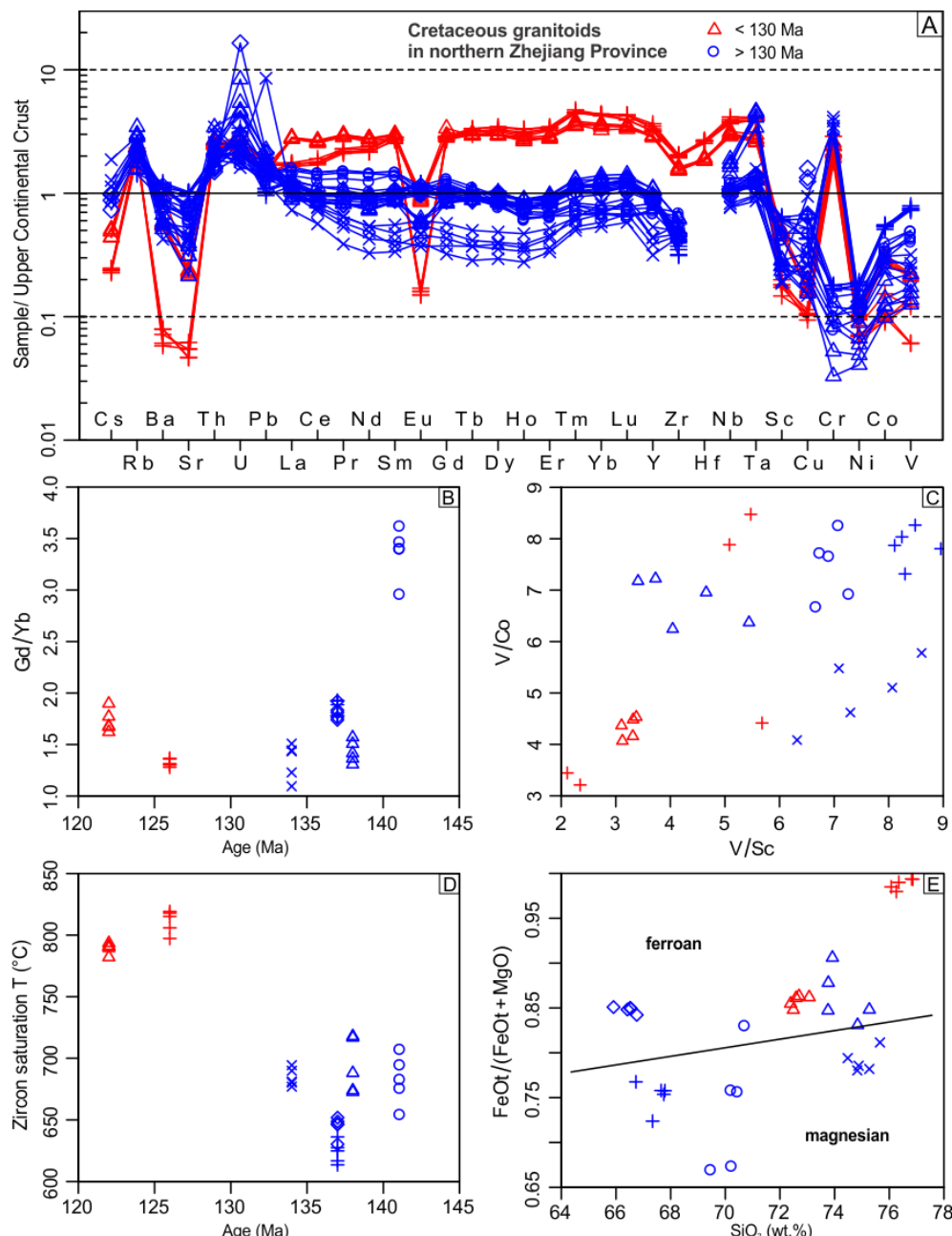


Figure 8.4 Whole-rock geochemical data for the granitic rocks from Anji County, northern Zhejiang Province: (A) trace element patterns normalised to the global average for the upper continental crust (Rudnick and Gao, 2003); (B) plot of the Gd/Yb ratio versus age; (C) plot of the V/Co ratio versus V/Sc; (D) plot of the zircon saturation temperature versus age; (E) plot of FeOt/(FeOt + MgO) versus age (Frost et al., 2001). Data sources: Tang et al. (2012a), Tang et al. (2012b), Xie et al. (2012b), Xie et al. (2012c) and Tang et al. (2013).

The evolution of these granitoids is similar to the J<sub>2-3</sub> to K<sub>1</sub>(I-II) transition in western Zhejiang Province. They show:

- (1) An increasing REE content with time and have more significant negative Ba-Sr-Eu anomalies (Figure 8.4A);
- (2) A dramatic decrease in the MREE/HREE ratio (Gd/Yb) at ~ 140 Ma (Figure 8.4B);
- (3) An overall decreasing trend for the V/Co and V/Sc ratios (Figure 8.4C);
- (4) An increase in the zircon saturation temperature after 130 Ma (Figure 8.4D);
- (5) A general increase in the FeOt/(FeOt+MgO) ratio (Figure 8.4E).

Early Cretaceous tectono-magmatic processes are therefore similar to those in western Zhejiang Province: crustal attenuation with the lower crust becoming more water deficient and reduced with time.

### 8.3 Central Hunan Province

Two major crustal deformation events during the Mesozoic affected Central Hunan Province: the Late Triassic Anyuan (Indosinian) and the Late Jurassic Yanglukou-Ningzhen (Yanshanian) events (HGS, 1988). The former strongly folded the Devonian-Triassic shallow marine carbonate deposits; the latter event primarily caused regional uplift and normal faulting during the Mid-Late Jurassic. Both tectonic events have accompanying granitic magmatism. Several tectonic models have been proposed, including flat-slab subduction (Li and Li, 2007), Indosinian-South China collision (Zhou et al., 2006; Wang et al., 2007b) and mantle plume activity (Xu et al., 2013).

The Triassic and Early Jurassic granitoids in Central Hunan Province have negative  $\epsilon_{\text{Nd}}(t)$  (Figure 8.6A), magnesian compositions (Figure 8.6B) and relatively high Gd/Yb (Figure 8.6C), which indicates they formed in thick continental crust. The J<sub>3</sub> Xitian granites (Figure 8.6E) are geochemically similar to the K<sub>1</sub>(I) granites from western Zhejiang Province (135–130 Ma, Figure 5.6C). These granites indicate a diachronous crustal extension of the South China Block during the Jurassic and Early Cretaceous.

A thick continental crust is consistent with an orogenic setting, which contradicts the mantle plume model (Xu et al., 2013). The Indosinian-South China collision model (Zhou et al., 2006; Wang et al., 2007b) is consistent with the orogenic setting but cannot explain the orientation (predominantly NE- or N-trending) of the Triassic fold axes in this region, and flat-slab subduction is still the most feasible model.

The Triassic Xitian granite near the Hunan-Jiangxi Province boundary (Figure 8.5) is the only Triassic granite in central Hunan Province with high V/Co (Figure 8.6D). In contrast, other Triassic samples have uniformly low V/Co. It is implied that the flat-slab

subduction front reached the present Hunan-Jiangxi boundary by 221 Ma. Central Hunan Province underwent crustal thickening during the Triassic but no significant continental lithospheric metasomatism. The locality of the Xitian granite most likely marked the western border of a region significantly metasomatised by flat-slab subduction.

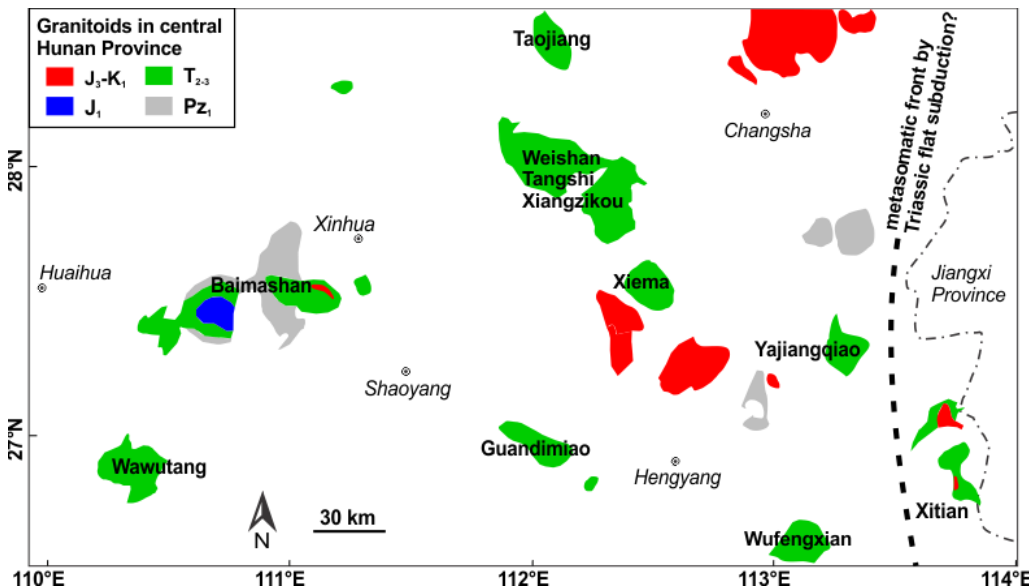


Figure 8.5 Distribution of granitoids in central Hunan Province. Data sources for labelled intrusions: Taojiang granite (Wang et al., 2012b), Weishan granite (Chen, 2006), Tangshi granite (Wang et al., 2007b), Xiangzikou granite (Wang et al., 2007b), Baimashan granite (Chen et al., 2007; Qiu et al., 2014), Xiema granite (Wang et al., 2007b), Yajiangqiao granite (Chen, 2006), Wawutang granite (Wang et al., 2007b), Guandimiao granite (Wang et al., 2007b), Wufengxian granite (Wang et al., 2007b), Xitian monzogranite (Yao et al., 2013).

#### 8.4 Central Jiangxi Province

The Pingxiang-Guangfeng Fault Zone is the western extension of the Jiangshan-Shaoxing Fault Zone in Zhejiang Province, and divides Jiangxi Province into the Cathaysia Block and Sibao Orogenic Belt (Figure 8.7). Similar to southern Anhui Province, the late Mesoproterozoic to Neoproterozoic Sibao Orogenic Belt is to north of the fault zone. The Cathaysia Block with Paleoproterozoic crystalline basement is to the south (Yu et al., 2007; Yu et al., 2009; Yu et al., 2012a). The different basement compositions are reflected in different Hf isotopic compositions for the Mesozoic granitoids. For instance, the Triassic Mengshan granite in the Sibao Orogenic Belt has zircon  $\epsilon_{\text{Hf}}(t)$  values between 1 and 5 (Zhong et al., 2011), whereas the Triassic Jintan granite in the Cathaysia Block has zircon  $\epsilon_{\text{Hf}}(t)$  values between -8 and -5 (Li, 2011).

Like the Triassic Dashuang and Jingju complexes in Zhejiang Province (Chapter 4), the Jintan granitic complex in central Jiangxi Province also consists of two different intrusions: a 239 Ma two-mica granite and a 226 Ma biotite granite (Figure 8.8). These intrusions have similar Nd-Hf isotopic compositions; however, the 226 Ma granite has higher Gd/Yb, higher

V/Co and lower FeOt/(FeOt+MgO) ratios, which indicates an increasing melting pressure and oxygen fugacity with time. Such a change most likely reflected the Andean-type orogeny caused by flat-slab subduction.

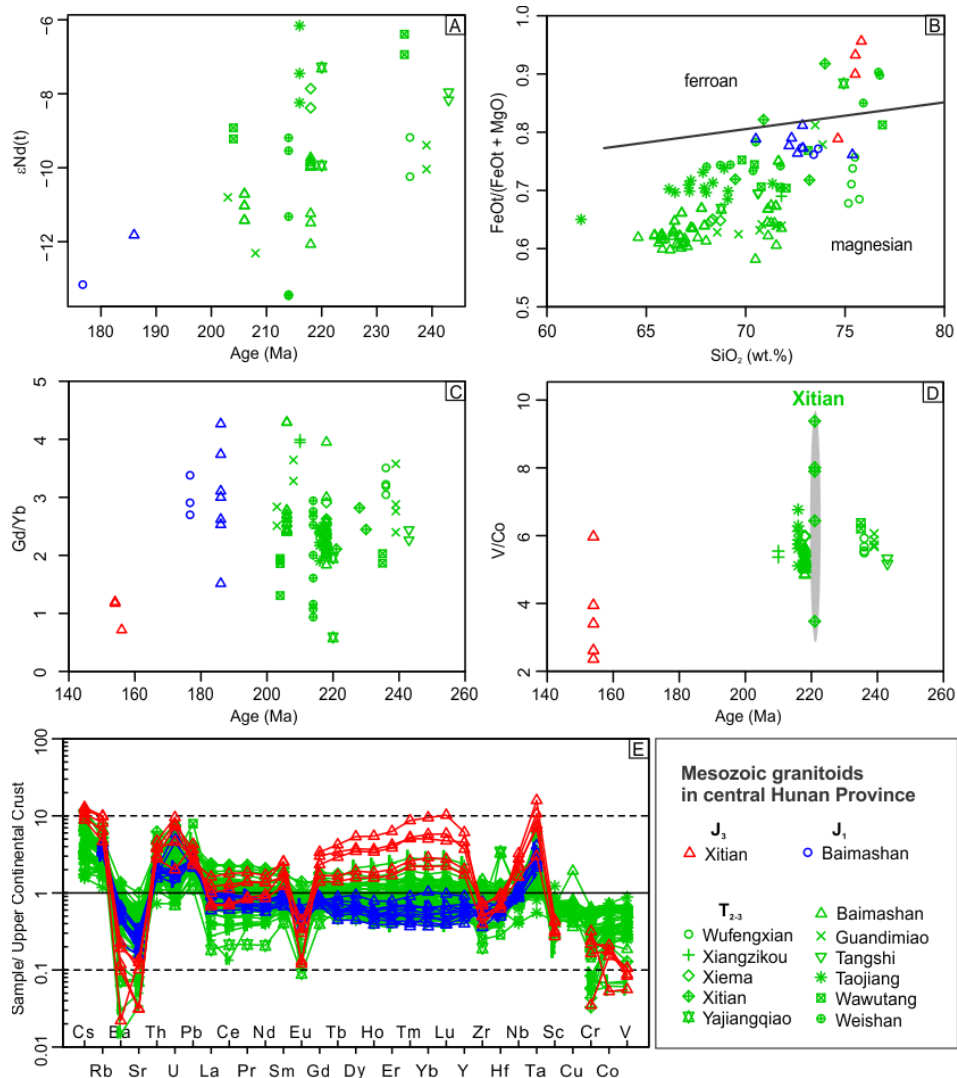


Figure 8.6 Whole-rock geochemical data for the Mesozoic granitoids from central Hunan Province. Data source as for Figure 8.5. (A)  $\varepsilon\text{Nd(t)}$  versus age; (B) Ferroan-magnesian classification (Frost et al., 2001); (C) Gd/Yb versus age; (D) V/Co versus age; (E) trace element patterns normalised to the global average for the upper continental crust (Rudnick and Gao, 2003).

There is also a 168 Ma OIB-like basalt at Antang Town (Figure 8.7).

The  $J_3$  Daguzhai-Huangpi intrusion is a magnesian granitoid with a low REE-Nb-Ta content and no Eu depletion (Figure 8.9), comparable to the wet and oxidised  $J_{2-3}$  porphyries in western Zhejiang Province. This intrusion was generated in a thick continental crust with water from the dehydrating oceanic plate.

The  $J_3$  Hukeng granite is similar to the  $K_1(I)$  granites in western Zhejiang in terms of its low Zr and LREE content and strong Ba-Sr-Eu depletion. The  $K_1$  Xiangshan dacitic

volcanic-plutonic complex resembles the K<sub>1</sub>(II) granites in western Zhejiang Province, with higher zircon saturation temperatures,  $\epsilon_{\text{Nd}}(t)$  values and REE contents (Figure 8.9). The Hukeng granite and Xiangshan complex have high FeOt/(FeOt+MgO) and low Gd/Yb ratios and were most likely produced during continental lithospheric extension.

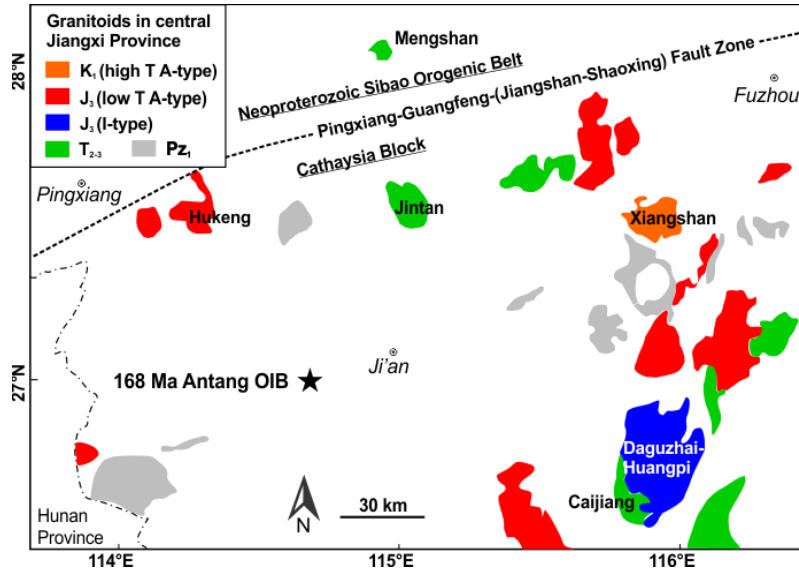


Figure 8.7 Distribution of granitoids in central Jiangxi Province. Data sources for labelled intrusions: Mengshan granite (Zhong et al., 2011), Caijiang granite (Zhao et al., 2013a), Jitan monzogranite (Li, 2011; Zhao et al., 2013b), Daguzhai-Huangpi granite (Zhao et al., 2011b), Hukeng granite (Liu et al., 2008), Xiangshan dacitic volcanic-plutonic complex (Yang et al., 2010), Antang OIB-like basalt (Wang et al., 2008b).

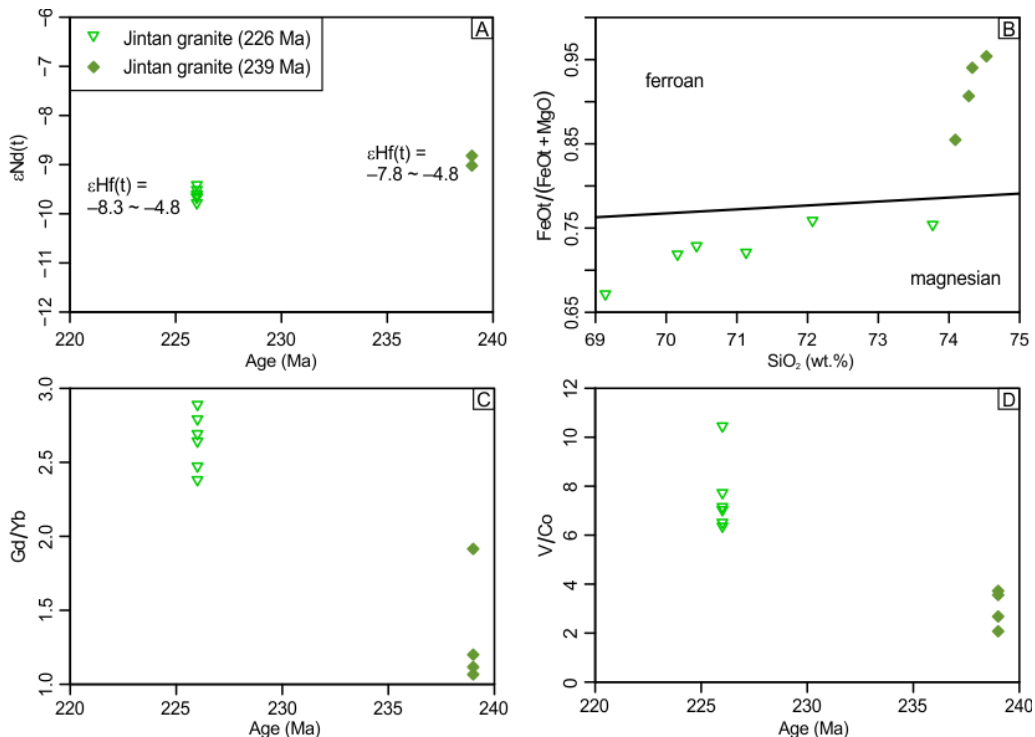


Figure 8.8 Whole-rock geochemical data for the two Jitan granite units. Data source as for Figure 8.7. (A)  $\epsilon_{\text{Nd}}(t)$  versus age; (B) FeOt/(FeOt+MgO) versus age; (C) Gd/Yb versus age; (D) V/Co versus age. Data sources: Li (2011) and Zhao et al. (2013b).

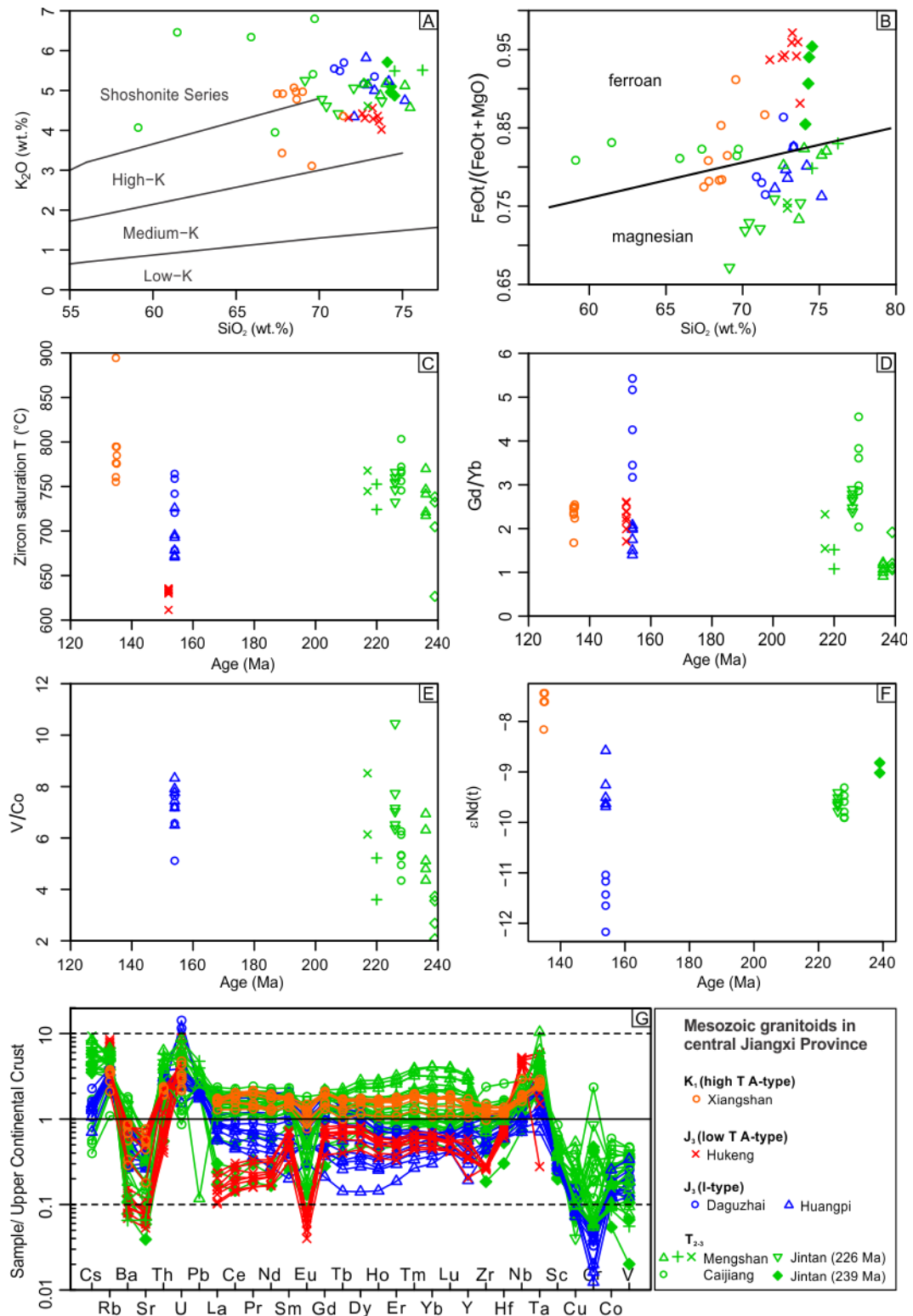


Figure 8.9 Whole-rock geochemical data for Mesozoic granitoids from central Jiangxi Province. Data source as for Figure 8.7. (A) Ferroan-magnesian classification (Frost et al., 2001); (B) Gd/Yb versus age; (C) V/Co versus age; (D)  $\varepsilon_{\text{Nd}}(t)$  versus age. Data source: Zhao et al. (2013b).

## 8.5 Western Fujian Province

Fujian Province lies within the Cathaysia Block, and its oldest known crystalline rocks are Paleoproterozoic metavolcano-sedimentary rocks (Mayuan Group) and granitoids (Li et

al., 2011c). During the Phanerozoic, the region underwent two major tectonic events: the Ordovician-Silurian Wuyi-Yunkai (Caledonian) and Triassic (Indosinian) orogenies. These events created northeast-trending folds and angular unconformities beneath the Late Devonian and Late Triassic strata, respectively (FGS, 1985, p. 494 and 500). Caledonian and Indosinian granitoids are exposed to the west of the Zhenghe-Dapu Fault (Sun, 2006). This region is considered to be an uplifted Proterozoic terrane (Pirajno and Bagas, 2002). East of this fault is a series of northeast-trending graben containing voluminous Jurassic-Cretaceous (Yanshanian) felsic volcanic rocks (FGS, 1985, p. 506, 556 and 557) and granitoids (Guo et al., 2012b; Li et al., 2014c).

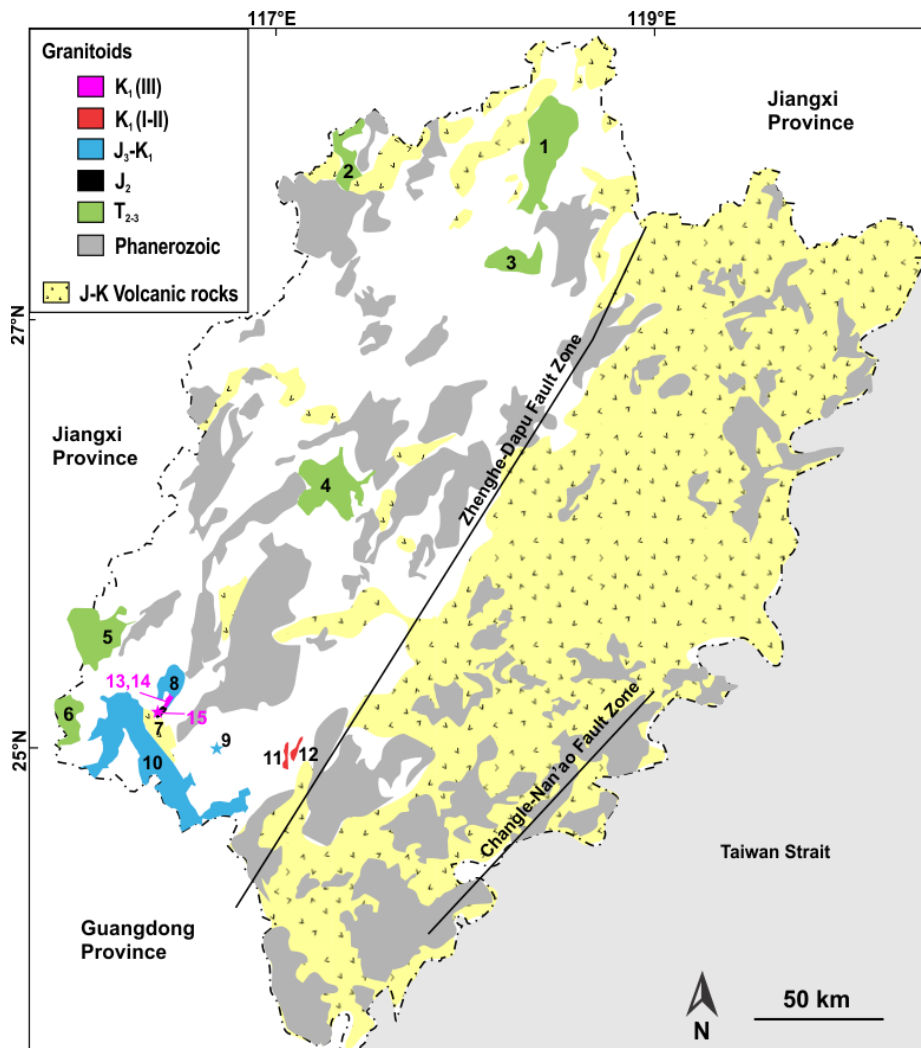


Figure 8.10 Distribution of Mesozoic granitoids and volcanic rocks in Fujian Province, modified after Ma (2007) and Sun (2006). 1-Gaoxi monzogranite (Zhao et al., 2013a); 2-Dayinchang monzogranite (Wang et al., 2013b); 3-Luoguyan granite (Xiang et al., 2013); 4-Shaxi granite (Li et al., 2010b); 5-Hongshan-Fucheng granite (Zhao et al., 2004; Zhao et al., 2006; Ren et al., 2013); 6-Guikeng granite (Mao et al., 2011); 7-Zijishan syenogranite (Zhao, 2007); 8-Caixi granite (Zhao, 2007); 9-Guanyang and Zengkeng monzogranite (Sheng et al., 2013); 10-Wuping granite (Yu et al., 2005); 11-Dayang syenogranite (Yue, 2008; Zhang et al., 2012a); 12-Juzhou syenogranite (Zhang et al., 2012a); 13-Sifang and Luoboling (porphyritic) granodiorite (Zhang et al., 2012b); 14-Luoguyan granite (Xiang et al., 2013); 15-Zijishan syenogranite (Zhao, 2007).

al., 2012a); 14-Jintonghu quartz syenitic porphyry (Wu et al., 2013); 15-Ermiaogou dacitic porphyry (Li et al., 2013a).

The Mesozoic granitoids in western Fujian Province can be divided into five stages (Figure 8.10). Their evolution is comparable to that of Zhejiang Province and likely reflects common tectonic processes.

Samples from  $T_{2-3}$  rocks have the lowest  $\epsilon\text{Nd}(t)$  values with wide ranges of Gd/Yb and V/Co (Figure 8.11), which reflects the various melting pressures and redox conditions caused by flat-slab subduction. The less fractionated samples (e.g., Gaoxi monzogranite and Guikeng granite) are generally magnesian (Figure 8.11A), which indicates a relatively thick crust.

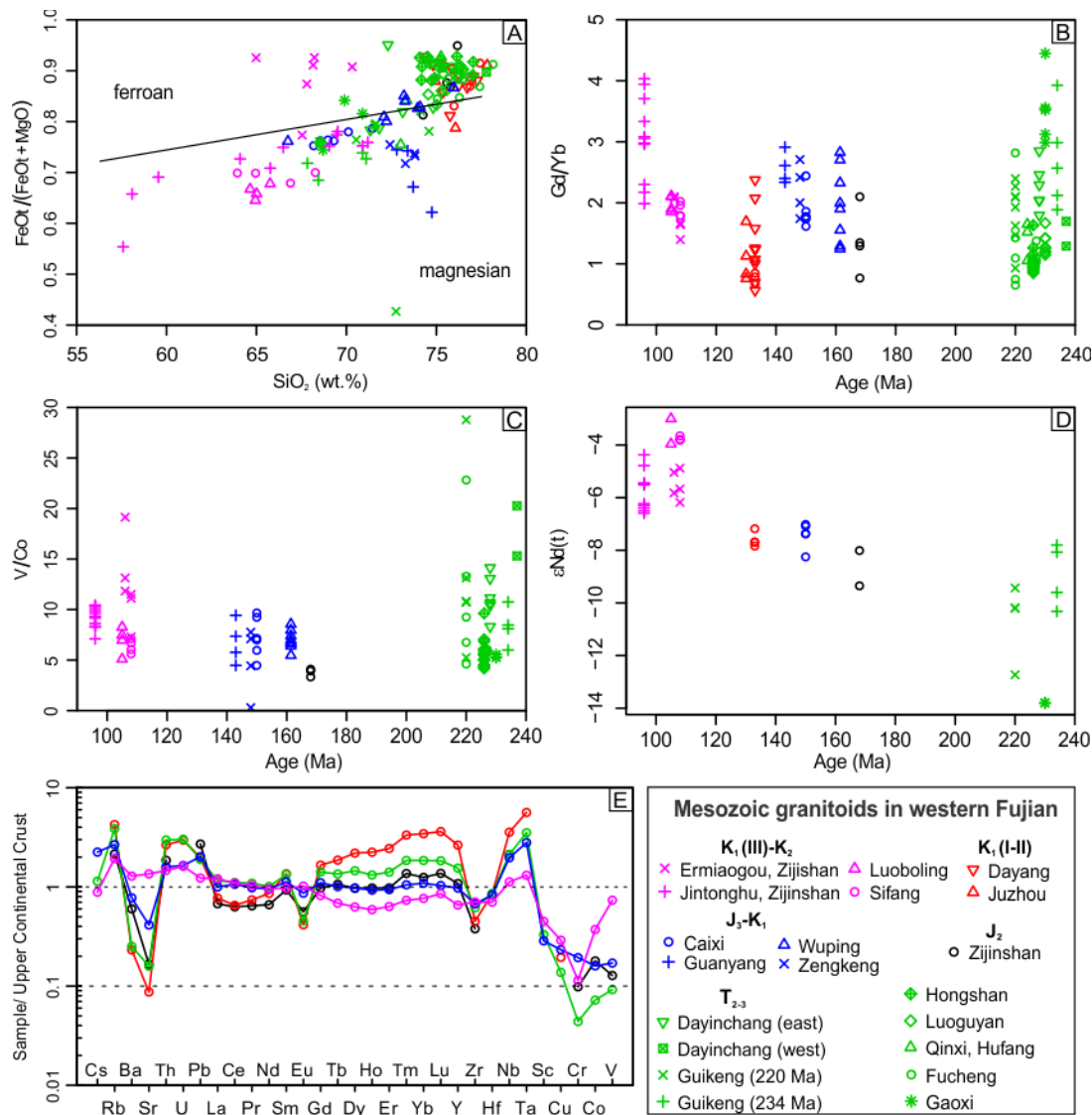


Figure 8.11 Whole-rock geochemical data for the Mesozoic granitoids in western Fujian Province. Data source as for Figure 8.10. (A) ferroan-magnesian granitoid classification (Frost et al., 2001); (B) plot of Gd/Yb versus age; (C) plot of V/Co versus age; (D) plot of  $\epsilon\text{Nd}(t)$  versus age; (E) trace element patterns (median of each group) normalised to the global average for the upper continental crust (Rudnick and Gao, 2003).

The oldest anorogenic granitoid (Zijinshan syenogranite, 168 Ma) has the lowest V/Co ratios (Figure 8.11C). As with their counterparts in the Nanling Range (Section 8.3) and Zhejiang Province (Section 7.4), a reduced environment was most likely related to underplating of reduced basalts following slab break-off.

The ensuing J<sub>3</sub>-K<sub>1</sub> granites show less Ba-Sr-Eu depletion (Figure 8.11E) and an increased V/Co, which likely indicates a fluid or melt input from the foundering slab.

The K<sub>1</sub>(I-II) high-silica granites in western Fujian Province are similar to their K<sub>1</sub>(I) counterparts in Zhejiang Province, which reflects strong crustal attenuation (Gualda and Ghiorso, 2013).

The K<sub>1</sub>(III)-K<sub>2</sub> granitoids have significantly less negative  $\varepsilon$ Nd(t) values than earlier rocks derived from the Paleoproterozoic basement (Figure 8.11D). They were geochemically similar to the K<sub>1</sub>(III) granitoids from Zhejiang Province and were likely generated from an enriched continental lithospheric mantle. The 108–106 Ma Ermiaogou dacitic porphyry has high FeOt/(FeOt+MgO), high V/Co and low Gd/Yb ratios (Figure 8.11), which indicates oxidized and low pressure conditions that may also produce ferroan granitoids, including island arc tholeiitic series rocks. In contrast, the 95 Ma Jintonghu magnesian quartz syenitic porphyry with high Gd/Yb ratios (Figure 8.11B) was most likely generated in continental crust thickened by intrusions (cf. Section 7.4.3).

## 8.6 Eastern Fujian-Guangdong Province

The present distance between eastern Fujian-Guangdong Province and the paleo-Pacific trench in central Taiwan is approximately 300–400 km. Jurassic-Cretaceous granitoids are abundant in this region (Figure 8.10). Older rocks were covered by the extensive Jurassic-Cretaceous volcano-sedimentary rocks.

The age and geochemical data for the Jurassic–Cretaceous volcanic and plutonic rocks in this region were reported and reviewed by Liu et al. (2011b), Guo et al. (2012b) and Li et al. (2014c). Relative to their counterparts in other regions of Southern China, the most notable geochemical feature is their relatively low K<sub>2</sub>O content (Figure 8.12A), which is consistent with their proximity to the trench (Tatsumi and Kogiso, 2003). The enriched lithospheric mantle and/or newly underplated basaltic rocks are major sources because their Nd isotope compositions (Figure 8.12B) are significantly less negative than for the granitoids from the Paleoproterozoic basement of the Cathaysia Block (Figure 8.11D). These rocks have higher V/Co and V/Sc ratios than their counterparts further west in Hunan Province, which indicate a higher oxygen fugacity (Figure 8.12C and D). The Late Cretaceous rocks have slightly lower Gd/Yb ratios than their Jurassic and Early Cretaceous counterparts on

average (Figure 8.12E). High oxygen fugacity (high V/Sc ratio) is the major factor inhibiting iron enrichment (Figure 8.12F). The Late Cretaceous granitoids were significantly depleted in Sr and Eu (Figure 8.12G), which indicates low plagioclase solubility under water-deficient conditions and/or increased plagioclase stability at low pressures.

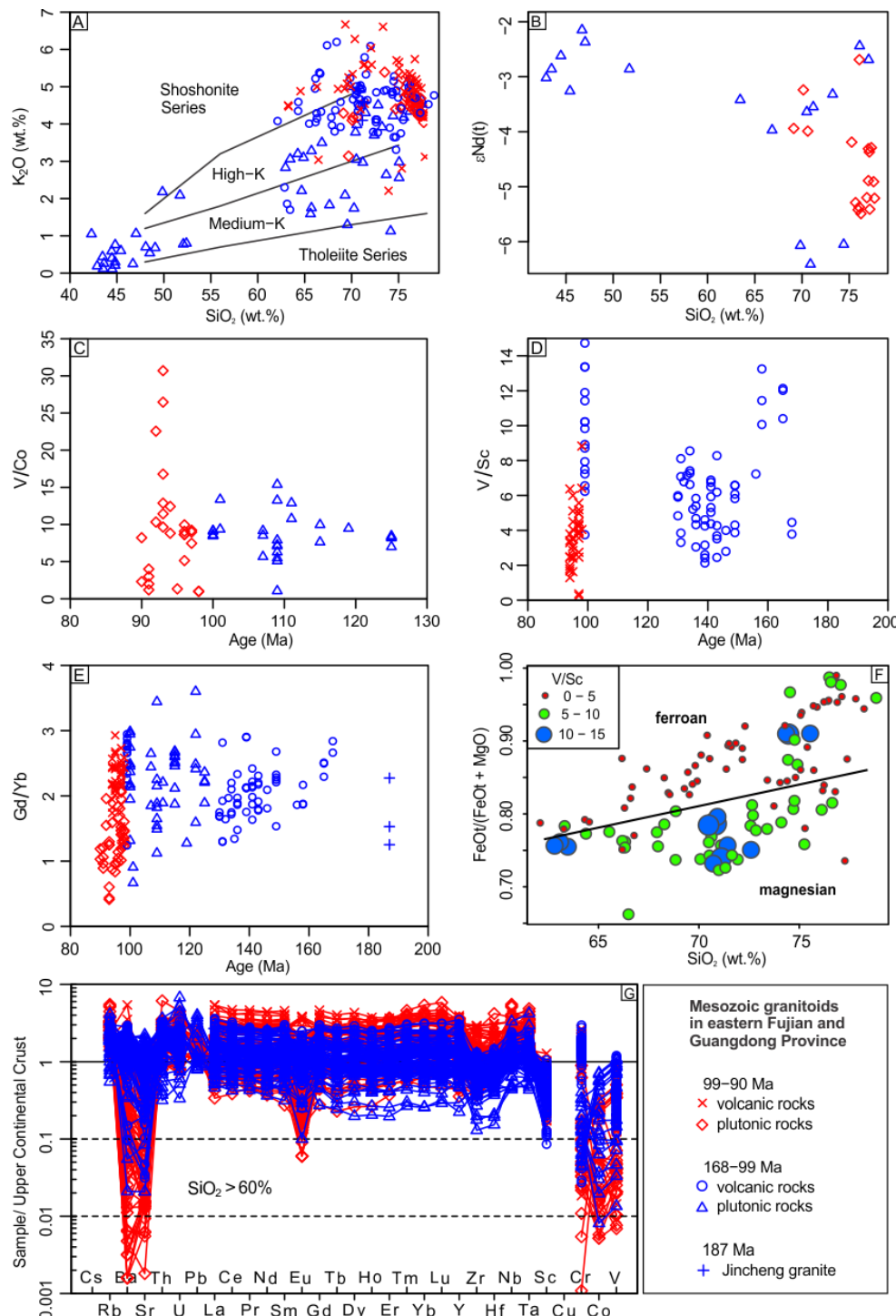


Figure 8.12 Whole-rock geochemical data for the Mesozoic intrusions and volcanic rocks in Eastern Fujian-Guangdong Province. Data source as for Figure 8.10. (A) Plot of  $K_2O$  versus  $SiO_2$ ; (B) plot of  $\epsilon_{Nd}(t)$  versus  $SiO_2$ . The Nd isotopic composition of the granitoids is comparable to those from the enriched lithospheric mantle in Zhejiang Province (Hsieh et al.,

2009). (C) Plot of V/Co versus age; (D) plot of V/Sc versus age; (E) plot of Gd/Yb versus age; (F) Ferroan-magnesian granitoid classification (Frost et al., 2001) with circles representing the V/Sc ratio; (G) Trace element patterns for samples with  $\text{SiO}_2 > 60\%$  normalised to the average upper continental crust (Rudnick and Gao, 2003).

The evolution of geochemical features with time indicates the Jurassic-Early Cretaceous granitoids were most likely formed above a subducting or foundering oceanic plate; however, the Late Cretaceous granitoids were most likely generated in a back-arc extensional setting.

## 8.7 Nanling Range

Nanling Range is a mountainous region in southern Hunan Province, southern Jiangxi Province and northern Guangdong Province (Zhou et al., 2006; Chen et al., 2013b). The region is characterised by world-class tungsten-tin mineralisation related to the granitoids (Figure 8.13) (Chen et al., 2013b). Evidence for a Triassic orogeny (the Indosinian Orogeny) in the Nanling Range is the angular unconformities beneath the Late Triassic strata (JGS, 1984, p. 667; GGS, 1988, p. 739; HGS, 1988, p. 530) and predominantly northeast- and north-trending folds in the Devonian-Middle Triassic strata (JGS, 1984, p. 684; GGS, 1988, p. 748; HGS, 1988, p. 542). The major tectonic events in the Nanling Range from the Jurassic to Cretaceous are the uplift and development of sag basins and graben (JGS, 1984, p. 668; GGS, 1988, p. 825; HGS, 1988, p. 531-532).

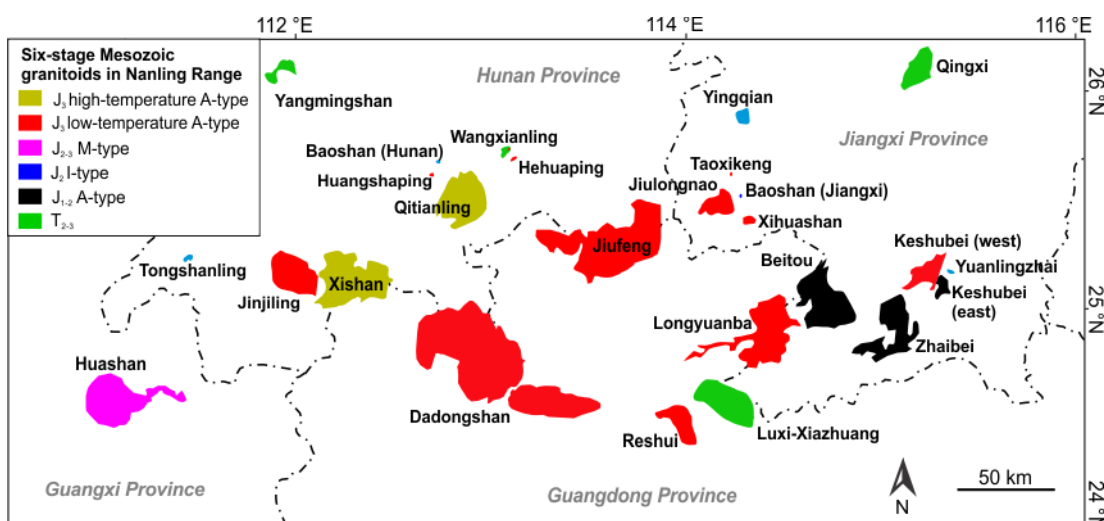


Figure 8.13 Distribution of granitoids in the Nanling Range, modified after Ma (2007). Intrusions without age or geochemical data are not shown. Data sources: Yangmingshan granite (Chen et al., 2006; Wang et al., 2007b), Qingxi monzogranite (Yu et al., 2012b), Yingqian granodiorite (Guo et al., 2010), Baoshan granodioritic porphyry (Hunan Province) (Xie, 2013), Wangxianling granite (Zheng and Guo, 2012), Hehuaping porphyritic granite (Zhang et al., 2010), Taoxikeng granite (Guo et al., 2011), Baoshan granite (Jiangxi Province) (Guo et al., 2011), Huangshaping porphyritic granite (Zhang et al., 2010), Qitianling granite (Zhu et al., 2005b; Fu et al., 2006), Jiufeng granite (Huang, 2012), Jiulongnao granite (Guo et al., 2011), Xihuashan granite (Guo et al., 2012a), Tongshanling granite (Wei et al., 2007; Jiang et al., 2009), Jinjiling granite-alkali feldspar granite (Jiang et al., 2009), Xishan granite-dacite-rhyolite complex (Fu et al., 2004; Jiang et al., 2009; Huang et al., 2011a), Beitou granite (Chen et al., 2005a), Keshubei granite (Huang et al., 2014), Yuanlingzhai granitic porphyry (Huang et al., 2014), Dadongshan granite (Huang et al., 2008), Longyuamba granite (Tao et

al., 2013), Zhaibei granite (Li et al., 2003a), Huashan complex (Gu et al., 2006; Zhang et al., 2011), Reshui monzogranite (Deng et al., 2011), Luxi-Xiazhuang granite (Chen et al., 2012).

The Mesozoic granitoids primarily belong to the high-K or shoshonite series (Figure 8.14A) with A/CNK values ranging from 0.8 to 1.4. The majority of the Triassic and Middle Jurassic granitoids are magnesian (Figure 8.14B), which is a result of relatively high pressure and oxygen fugacity environment (Osborn, 1979; Chiaradia, 2014). In contrast, the Middle-Late Jurassic and Cretaceous granitoids are mostly ferroan (Figure 8.14B), which indicates a low pressure or a low oxygen fugacity environment. The V/Co ratios of the Triassic samples primarily range from 4 to 7, which is relatively low and uniform as in Central Hunan (Wang et al., 2007b). In contrast, the V/Co ratios for the Jurassic samples vary widely, which reflects variable redox conditions.

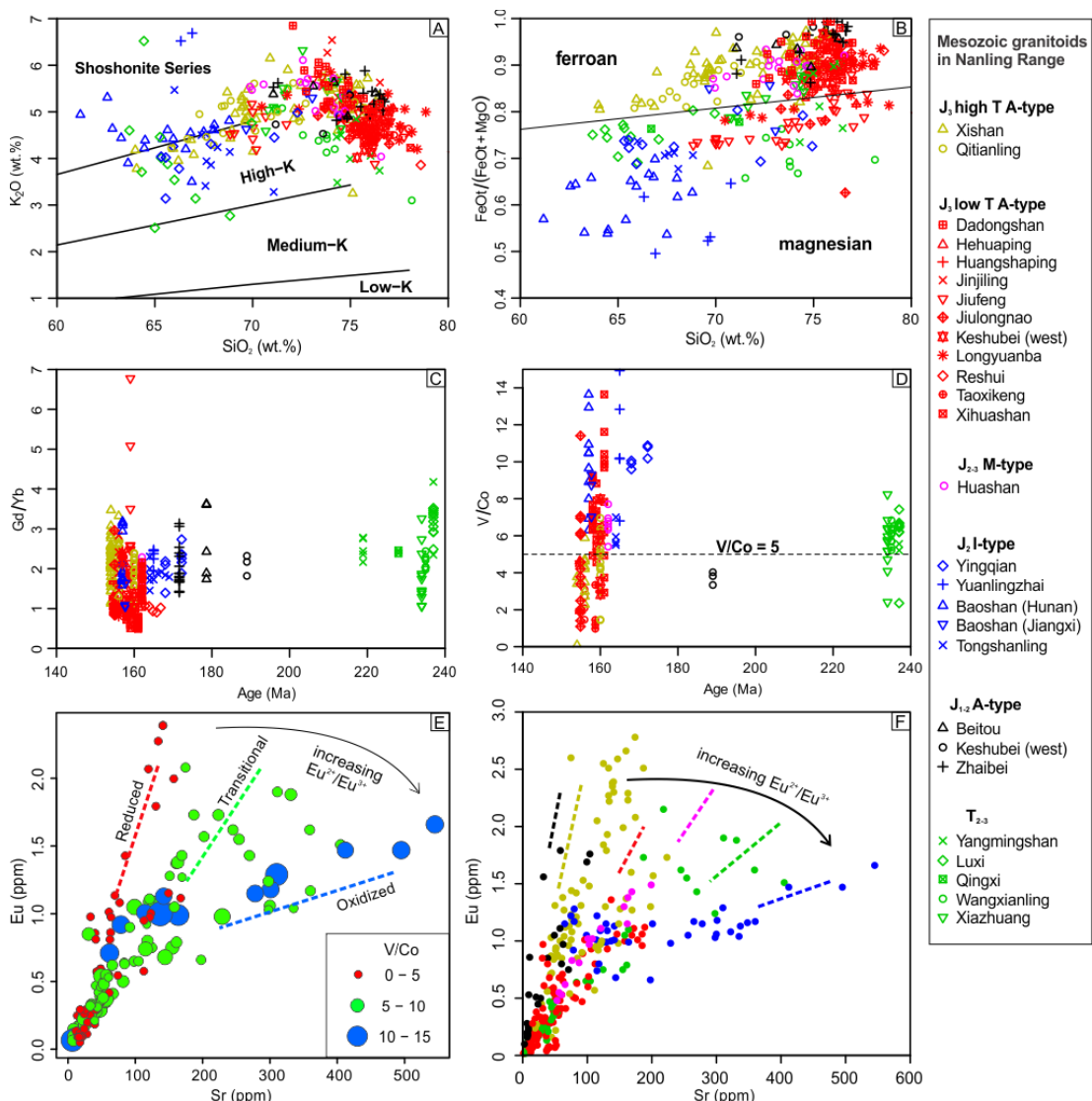


Figure 8.14 Whole-rock geochemical data for the Mesozoic granitoids in the Nanling Range. Data source as for Figure 8.13. (A) plot of  $K_2O$  versus  $SiO_2$  (Peccerillo and Taylor, 1976); (B) the ferroan-magnesian granitoid classification (Frost et al., 2001); (C) plot of  $Gd/Yb$  versus age; (D) plot of  $V/Co$  versus age; (E) plot of Eu versus Sr, which shows the evolution trends for

samples with differing V/Co ratios; (F) plot of Eu versus Sr, which shows the evolution trends for samples with different stages.

$T_{2-3}$  magnesian granitoids with high Gd/Yb ratios were generated in a thick post-orogenic crust by thermal relaxation (Figure 8.14C). Their different zircon Hf isotopic compositions (Figure 8.15) may be controlled by the age of their crustal sources: the Paleoproterozoic basement of the Cathaysia block or the rocks from the Sibao Orogenic Belt.

The low V/Co and Sr/Eu ratios of  $J_{1-2}$  ferroan A-type granitoids (Figure 8.14) are characteristic of reduced magmas (as discussed in Section 5.4), that can be produced by low degree of crustal melting caused by basaltic underplating and possible addition of mafic magmas from the same source (Ferrari, 2004; Ye et al., 2013).

$J_{2-3}$  I-type porphyries resemble the Jurassic porphyries from western Zhejiang and northeastern Jiangxi Province with high V/Co ratios and a related Cu-Mo mineralisation (Mao et al., 2013b; Xie, 2013; Huang et al., 2014), which indicates a high magma oxygen fugacity (Robb, 2005, p. 106). The magmatism of this stage was triggered by water from the foundered oceanic plate. The decoupled Nd-Hf isotopes in these wet, oxidised Jurassic porphyries (Figure 8.15) most likely reflects the involvement of subduction fluids carrying Nd but not Hf (Pearce and Peate, 1995; Hoffmann et al., 2011).

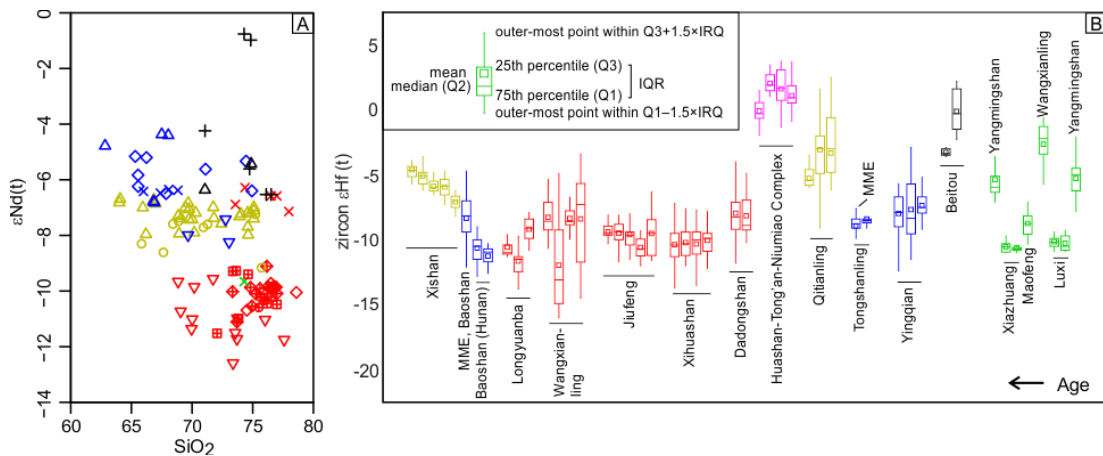


Figure 8.15 Whole-rock Nd and zircon Hf isotopic compositions for the Mesozoic granitoids in the Nanling Range. Data source as for Figure 8.13. Comparing  $J_2$  porphyries (blue) to  $J_3$  high-temperature A-type granites (yellow), the former have more negative zircon  $\epsilon\text{Hf}(t)$  but less negative  $\epsilon\text{Nd}(t)$  values. The abbreviations used in the boxplot: Q1 (lower quartile), Q2 (median), Q3 (upper quartile), IQR (interquartile).

The most extensive magmatism in the Nanling Range was the production of  $J_3$  high-silica granite-rhyolite, which is similar to its  $K_1(I)$  counterpart in western Zhejiang Province. These rocks have strongly negative  $\epsilon\text{Nd}(t)$  and zircon  $\epsilon\text{Hf}(t)$  values and represent low-temperature, low-pressure crustal melts during strong crustal attenuation.

Some  $J_3$  samples, such as the Xishan granite, are high-temperature and strongly reduced fayalite-bearing granitoids (Osborn, 1979; Fu et al., 2004; Huang et al., 2011a). The reduced property is indicated by their low V/Co ratios (Figure 8.14D) and rapid decrease in Eu with Sr (Figure 8.14E and F). These rocks have more depleted Nd-Hf isotopic compositions than the  $J_3$  high-silica granite-rhyolite. They are similar to the  $K_1(II)$  granites from western Zhejiang Province, which indicates crustal melting was probably triggered by underplating of reduced basaltic magmas during lithospheric extension.

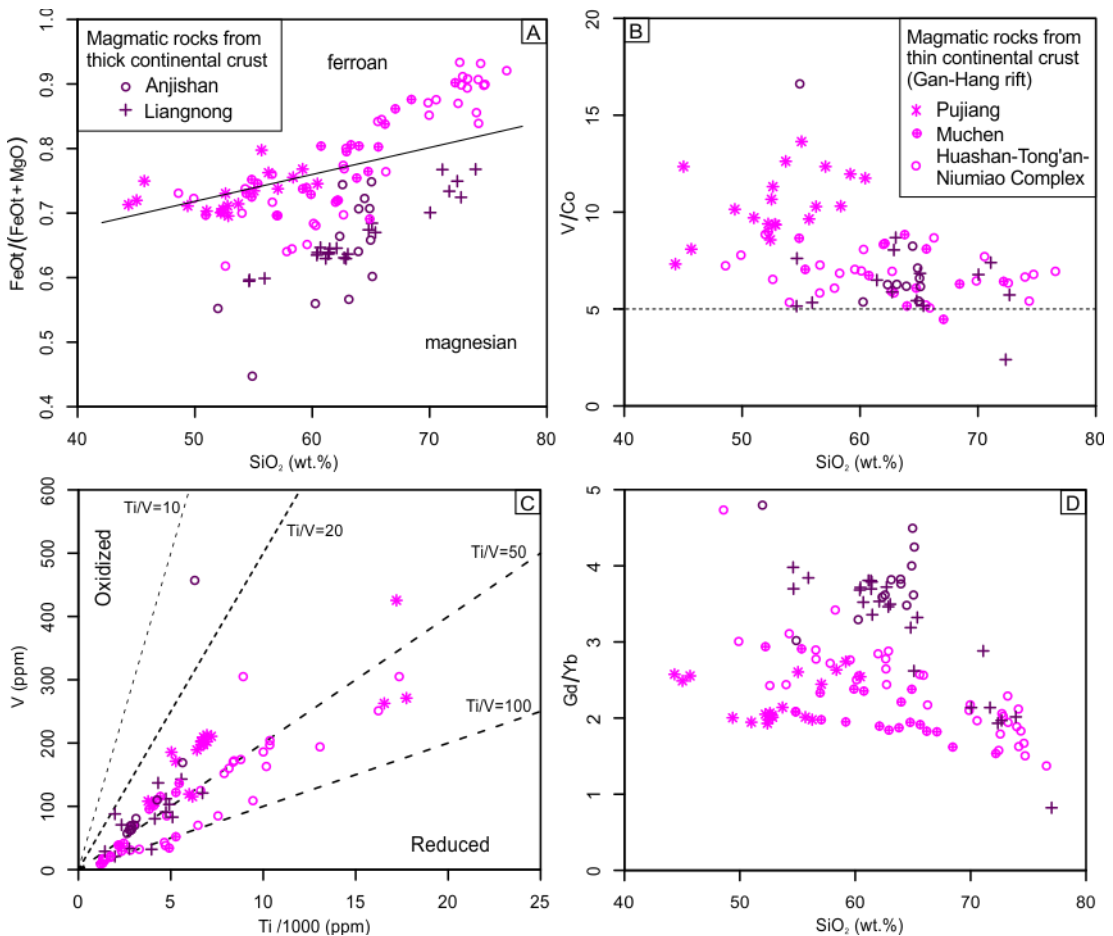


Figure 8.16 Whole-rock geochemical data for some Jurassic-Early Cretaceous mantle-derived plutonic-volcanic rocks. (A) Ferroan-magnesian granitoid classification (Frost et al., 2001); (B) plot of V/Co versus  $\text{SiO}_2$ ; (C) plot of V versus Ti (Shervais, 1982); (D) plot of Gd/Yb versus  $\text{SiO}_2$ . Data source: Anjishan diorite-granodiorite (Xu et al., 2002; Zeng et al., 2013a); Liangnong Complex (Chen et al., 2005b; Hsieh et al., 2009; Wong et al., 2011); Pujiang basalt-andesite (Qin, 2007); Muchen Complex (Lu, 2007; Liu et al., 2013a; this study), Huashan-Tong'an-Niumiao Complex (Zhu et al., 2005a; Gu et al., 2006; Zhang et al., 2011).

The Huashan-Tong'an-Niumiao Complex contains different lithologic units including diorite, quartz monzonite and granite similar to the ~112 Ma M-type Muchen Complex from western Zhejiang Province in terms of their petrology and isotopes. These units have similar ages (~163 Ma) and Sr-Nd-Hf isotopic compositions (Zhu et al., 2005a; Zhu et al., 2006; Zhao et al., 2010; Shu et al., 2013). The increase in whole-rock  $\delta\text{O}^{18}$  (~1‰) from the

intermediate to felsic rocks can be explained by crystal fractionation (Zhu et al., 1989; Hoefs, 2009). Therefore, the different lithologic units in the Huashan-Tong'an-Niumiao Complex, similar to the K<sub>1</sub>(III) Muchen Complex in western Zhejiang Province, were most likely cogenetic rocks derived from similar mafic magmas represented by MME with some crustal contamination. These mafic magmas were derived from a mantle source contaminated with (subducted) crustal material.

The Huashan-Tong'an-Niumiao Complex is located in the Shi-Hang zone. The Ganzhou-Hangzhou rift zone discussed in Chapter 7 is part of this failed Mesozoic rift (Goodell et al., 1991). Rocks of the complex have relatively depleted Nd isotopic compositions (Gilder et al., 1991) that may involve the upwelling asthenosphere. Within the Shi-Hang zone, the Huashan-Tong'an-Niumiao Complex and some Early Cretaceous magmatic rocks from Zhejiang Province (Pujiang basalt-andesite and Muchen Complex) have high FeOt/(FeOt+MgO) ratios. In contrast, some Early Cretaceous intrusions outside the Shi-Hang zone, such as the Liangnong and Anjishan Complexes, have low FeOt/(FeOt+MgO) ratios. Apparently, low FeOt/(FeOt+MgO) ratios are not determined by the high oxygen fugacity (high V/Co and V/Ti ratios) but by the high fractionation pressure (high Gd/Yb ratio) (Figure 8.16). However, as discussed in Section 7.4.4, a redox threshold ( $V/Co > 5$ ) must be reached for this high pressure to inhibit iron enrichment (Figure 8.16B). Below this redox threshold ( $V/Co < 5$ ), ferroan (mostly A-type) granitoids are still generated under high-pressure conditions (compare J<sub>1-2</sub> A-type, J<sub>2</sub> I-type and J<sub>3</sub> high-temperature A-type granitoids in Figure 8.14).

## 8.8 Hong Kong

As shown in Figure 8.17, the oldest lithostratigraphic unit exposed in Hong Kong is the Devonian Bluff Head Formation (conglomerate and sandstone) deposited in a fluvial and deltaic environment (Sewell et al., 2009). Carboniferous and Permian strata were deposited in shallow and deep continental seas, respectively. The Triassic tectonic event in Hong Kong caused granitic magmatism, strong deformation in older rocks and a depositional hiatus. There are shallow marine/fluvial plain deposits from the Early Jurassic and extensive volcanism and plutonism from the Mid-Late Jurassic. Graben developed during the Cretaceous, with fluvial and alluvial deposits formed under a hot and dry climate.

The Mesozoic intermediate and felsic rocks in Hong Kong have decreasing whole-rock Sm/Yb (Figure 8.18A) and increasing Y contents (Figure 8.18B) with age, which indicates thick Triassic and attenuated Jurassic and Cretaceous crust, as discussed in Chapter 5. The Triassic granitoids are magnesian (Figure 8.18C), which also indicates a thick crust. The lower V/Sc of the 145–140 Ma granitoids indicates lower oxygen fugacities relative to their

Jurassic counterparts (Figure 8.18D). There is a trend to more positive in  $\varepsilon\text{Nd(t)}$  during  $\text{J}_3\text{--K}_1$  (Figure 8.18E), which most likely reflects the involvement of mantle-derived magmas. The  $\text{J}_3\text{--K}_1$  granitoids have strong Ba, Sr and Eu depletions (Figure 8.18G), which imply a water-deficient environment. On the trace element discrimination diagram, both Triassic and  $>160$  Ma granitoids plot in the volcanic arc/syn-collision field; however, the younger suite plot in the within-plate field (Figure 8.18F). According to Wong (2006), the Late Cretaceous (100–87 Ma) mafic-intermediate rocks in Hong Kong belong to the high-K series rocks and they were derived from an subduction-related metasomatized mantle. They resemble the  $\text{K}_1(\text{III})$  mantle-derived rocks from western Zhejiang Province. Based on the aforementioned geochemical data and geological evidence, the Mesozoic tectono-magmatic processes in Hong Kong can be interpreted as an Andean-type orogenic cycle similar to other regions in South China.

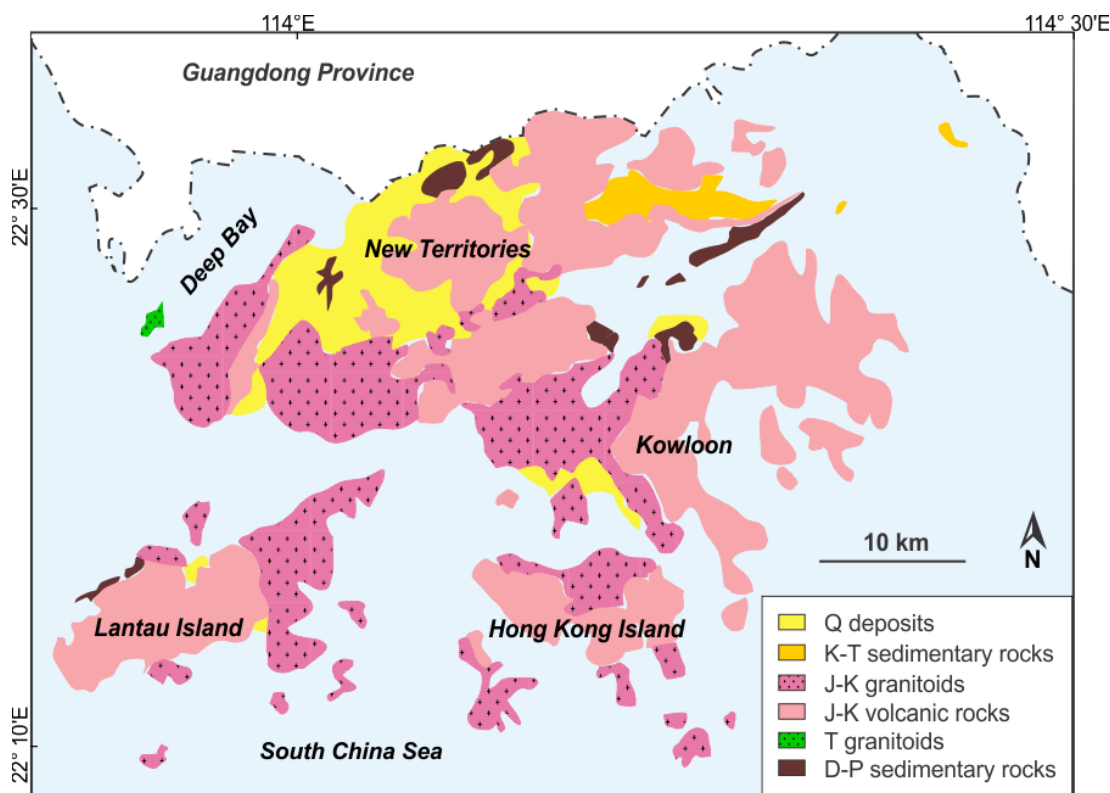


Figure 8.17 Simplified geological map of Hong Kong (Civil Engineering and Development Department, Hong Kong, <http://www.cedd.gov.hk>). Data sources: Darbyshire and Sewell (1997), Sewell and Campbell (1997), Wong (2006) and personal communications with Dr. R.J. Sewell (Geotechnical Engineering Office, Civil Engineering and Development Department, Hong Kong).

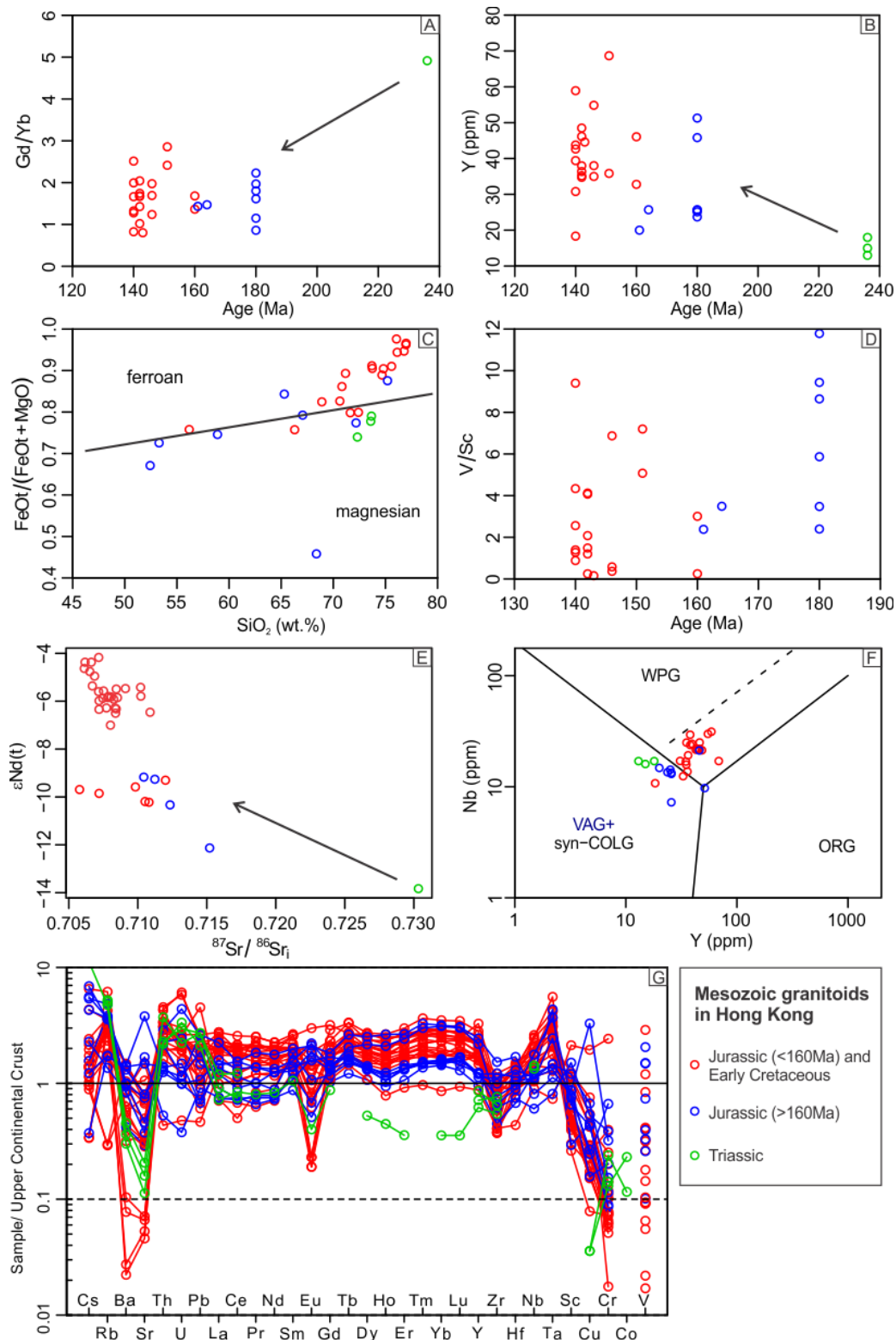


Figure 8.18 Whole-rock geochemical data for the Mesozoic granitoids from Hong Kong. Data source as for Figure 8.17. (A) whole-rock Gd/Yb ratio versus age, with decreasing trend from the Triassic to the Jurassic/Cretaceous; (B) whole-rock Y content versus age, with increasing trend from the Triassic to Jurassic/Cretaceous; (C) ferroan-magnesian granitoid classification (Frost et al., 2001); (D) whole-rock V/Sc ratio versus age, with decreasing trend from the Jurassic to Cretaceous; (E) diagram of  $\epsilon_{\text{Nd}}(t)$  versus  $^{87}\text{Sr}/^{86}\text{Sr}_i$ ; (F) trace element discrimination diagram (Pearce et al., 1984); (G) trace element patterns normalised to the global average for the upper continental crust (Rudnick and Gao, 2003).

## 8.9 Summary and future work

The Mesozoic granitoids discussed in this chapter have similar evolution trends to their counterparts in Zhejiang and northeastern Jiangxi Province (Chapters 5, 6 and 7). They provide support to the tectono-magmatic model presented in Sections 5.4 and 5.5. The characteristics of the Mesozoic granitoids from the southeastern margin and interior of the South China Block indicate common but diachronous tectonic processes, which are also consistent with the tectono-magmatic processes in a typical Andean-type orogenic cycle (Figure 2.8D–G). The normal-angle subduction processes before the flat-slab subduction, like their counterparts in the Andes (Figures 2.8A–C), was probably recorded by detrital zircons from South China (Li et al., 2012c).

The crustal source rocks across the South China Block are heterogeneous, as reflected by isotopic compositions of the Mesozoic granitoids. Regular evolution of the properties of these granitoids supports that tectonic setting rather than source plays a primary role in controlling the characteristics of granitoids (Pearce et al., 1984).

Generally, six-stage Mesozoic granitoids with different ages, textures and geochemical characteristics can be identified in South China. The properties, petrogenesis and tectonic settings of these granitoids are summarised in Figure 8.19 and Table 8.1. The tectono-magmatic cartoon is shown in Figure 8.20.

The first stage (Middle–Late Triassic) of granitoids in South China is composed of syn-/post-orogenic granitoids (Figure 8.20A). The main rock types are syenogranite, monzogranite, quartz monzonite and syenite. They have high melting temperatures, high melting pressures, variable water contents and redox conditions. Oxidized and reduced melting conditions resulted in ferroan and magnesian granitoids, respectively. The typical petrographic characteristic is alkali feldspar megacrysts set in a medium-grained matrix. Orogeny was driven by flat-slab subduction of the paleo-Pacific Plate. Thermal relaxation caused dehydration melting and water-fluxed melting, depending on the availability of fluids from the oceanic plate. The fluids and melts from the oceanic plate metasomatised the overriding lower continental crust and continental lithospheric mantle; however, such effects are only significant in regions adjacent to the continental margin (Zhejiang, Fujian and Jiangxi Provinces).

The second stage (Early–Middle Jurassic) of granitoids in South China is made up of post-orogenic ferroan granitoids (Figure 8.20B). The main rock types are syenogranite, quartz syenite and syenite. These granitoids were formed at high temperature with low water contents and low oxygen fugacities. They were formed during contemporaneous

underplating of reduced intraplate basalts following the break-off of the paleo-Pacific Plate. The continental crust had not started to attenuate at this stage.

The third stage (Middle Jurassic–Early Cretaceous) of granitoids in South China is composed of post-orogenic magnesian granitoids (Figure 8.20C). Most of them are granodioritic porphyries that were generated from water-fluxed melting or fractionated from hydrous basaltic magmas in a still thick, lower continental crust. They have high oxygen fugacities, high water contents and were formed at low temperatures. The water was derived from hydrous metasomatic continental lithospheric mantle and/or the foundering oceanic slab.

The fourth stage (Late Jurassic–Cretaceous) of granitoids in South China consists of anorogenic ferroan granitoids (Figure 8.20D). They are alkali feldspar granite or syenogranite with high silica contents that were generated under low-temperatures as a result of low-pressure dehydration melting processes, with variable redox conditions. They were generated in attenuated continental crust caused by the roll-back of the paleo-Pacific Plate.

The fifth stage (Late Jurassic–Cretaceous) of granitoids in South China consist of anorogenic ferroan granitoids (Figure 8.20E). The main rock types are porphyritic quartz syenite and syenogranite. They have a petrogenesis and tectonic setting similar to the fourth stage, but record higher magma temperatures, lower oxygen fugacities and more depleted Nd-Hf isotopic compositions. It is implied that underplated reduced intraplate basalts were involved in the crustal melting process.

The sixth stage (Late Jurassic–Cretaceous) of granitoids in South China was generated by fractional crystallization of mantle-derived magmas from the enriched continental lithospheric mantle in an anorogenic setting (Figure 8.20F). The main rock types are (quartz) diorite, (quartz) monzonite, granodiorite, monzogranite, (quartz) syenite. They are MME-bearing and oxidized granitoids. For the oxidized granitoids, high/low fractionation pressures, generally associated with a thick/thin continental crust, resulted in magnesian/ferroan characteristics. Intrusion of these granitoids caused growth and thickening of the continental crust.

This thesis focuses on the Mesozoic granitic rocks of eastern South China. However, similar-aged granitic rocks in Hainan, western Guangdong and eastern Guangxi provinces require additional work to understand their petrogenesis and tectonic settings, and possible links to events discussed in this study..

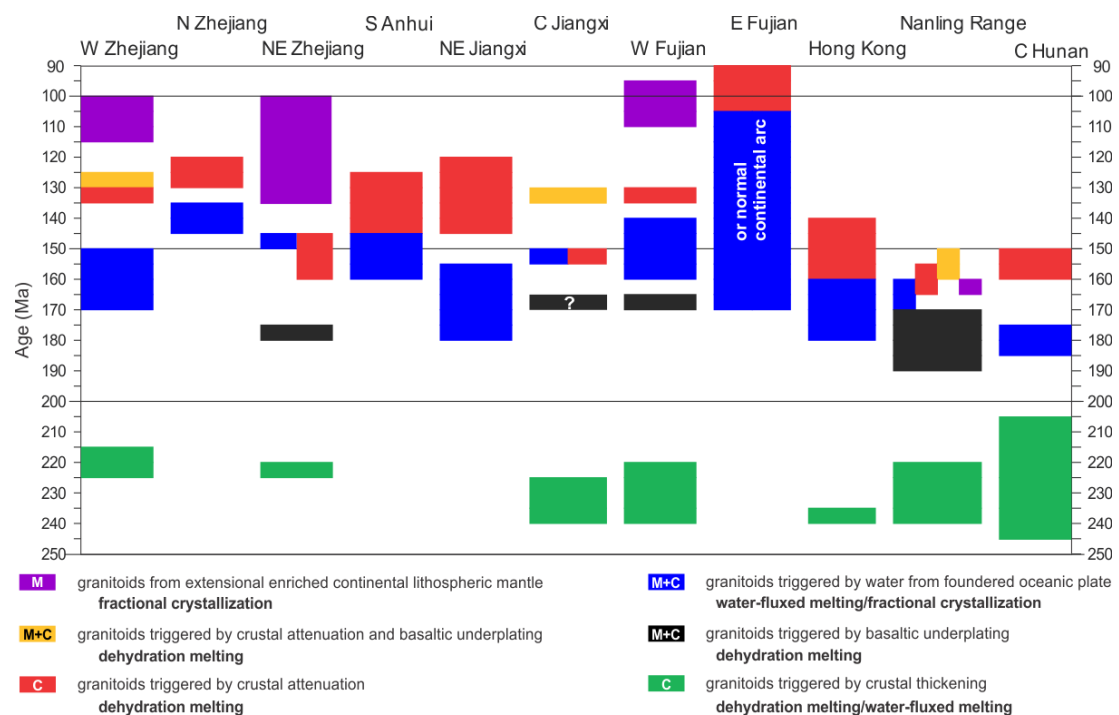


Figure 8.19 Evolution of the Mesozoic granitoids in South China. The legend shows their main sources (M: mantle, C: crust), melting/fractionation mechanism and tectonic settings.

Table 8.1 Summary of properties, petrogenesis and tectonic settings of six-stage Mesozoic granitoids in South China

Stage	I	II	III	IV	V	VI
Colour of symbols <sup>#</sup>						
Age	T <sub>2-3</sub>	J <sub>1-2</sub>	J <sub>2-3</sub>	J <sub>3-K<sub>1</sub></sub>	J <sub>3-K<sub>1</sub></sub>	J <sub>3-K<sub>2</sub></sub>
Outcrop area	Moderate	Small	Small	Large	Moderate	Moderate
Notable Petrographic Characteristics <sup>*</sup>	Alkali feldspar megacryst in medium-grained matrix		Porphyry with strong alteration	Coarse-grained, quartz-rich, equigranular	Alkali feldspar megacryst in aphanitic matrix	MME-rich
Magnetic Susceptibility* ( $\times 10^{-3}$ SI)	10 <sup>-1</sup> ~10	10 <sup>-1</sup> ~1	10 <sup>-2</sup> ~10 <sup>-1</sup>	10 <sup>-1</sup> ~10	10 <sup>-2</sup> ~10 <sup>-1</sup>	10~10 <sup>2</sup>
S-I-M-A Classification	S, I, A	A	M, I	A	A	M
Ferroan/Magnesian Classification	Ferroan/Magnesian	Ferroan	Magnesian	Ferroan	Ferroan	Ferroan/Magnesian
Typical Lithology	Syenogranite, monzogranite, quartz monzonite, syenite	Syenogranite, quartz syenite, syenite	Granodioritic porphyry	Alkali feldspar granite/syenogranite	Quartz syenite, syenogranite	(Quartz) diorite, (quartz) monzonite, granodiorite, monzogranite, (quartz) syenite
Source	Crust	Mantle + Crust	Mantle + Crust	Crust	Crust + Mantle	Mantle
Melting/Fractionation mechanism	Dehydration melting/Water-fluxed melting	Dehydration melting/Fractional crystallisation	Water-fluxed melting	Dehydration melting	Dehydration melting	Fractional crystallisation
Redox Conditions	Reduced/Oxidised	Reduced	Oxidised	Oxidised→Reduced	Reduced	Oxidised
Melting/Fractionation Pressure	High (Post-orogenic)	High (Post-orogenic)	High (Post-orogenic)	Low (anorogenic extension)	Low (anorogenic extension)	Low→ High (anorogenic extension→ magmatic thickening)
Temperature	High (800–900 °C)	High (800–900 °C)	Low (700–800 °C)	Low (700–800 °C)	High (800–900 °C)	High (800–900 °C)
Tectonic Setting	Post-orogenic thermal relaxation	Basaltic underplating following the break-off of the flat slab	Oceanic plate dehydration	Continental extension caused by the roll-back of the oceanic plate	Continental extension + basaltic underplating	Continental extension

<sup>#</sup>as used in Chapters 5–8. \*based on Zhejiang and northeastern Jiangxi Province.

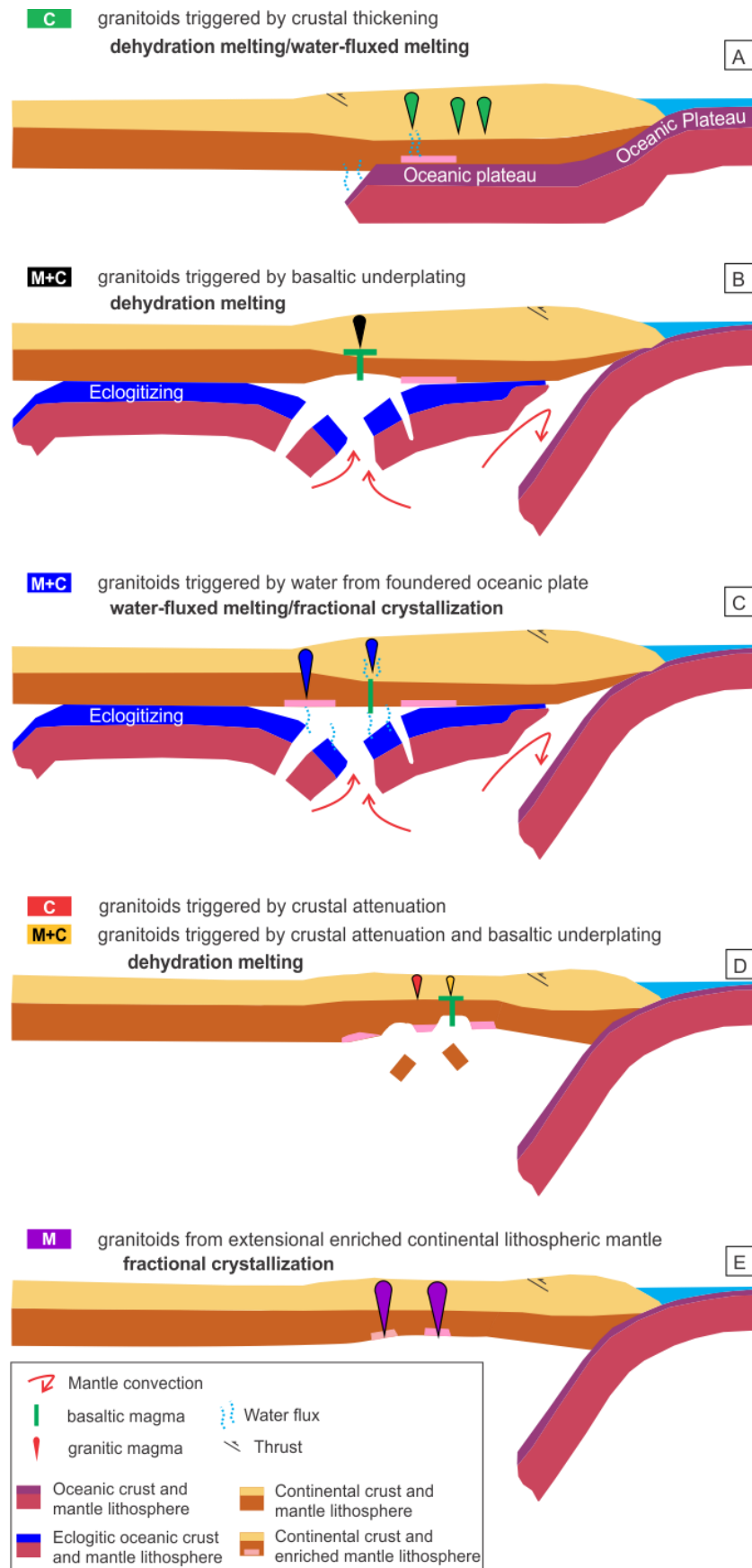


Figure 8.20 Tectono-petrogenetic cartoon for the six-stages of Mesozoic granitoids in South China.

## Chapter 9 Conclusions

Six stages of Mesozoic granitoids with different ages, textures and geochemical characteristics, can be identified in South China. The results of this study show that the properties of these granitoids are mainly determined by their source and temperature-pressure-water-redox conditions during melting and fractionation processes.

In central Zhejiang Province, the continental crust was thickened and metasomatized by aqueous and siliceous fluids due to Triassic flat-slab subduction. As a result of thermal relaxation, the lower crust reached high enough temperatures for high-pressure, high-temperature melting, resulting in the formation of the 226–227 Ma Dashuang quartz monzonite (with water from the oceanic plate) and the 224 Ma Dashuang syenite (without water from the oceanic plate). The syenite belongs to the ferroan, peraluminous, ilmenite-series granitoids with a low water content, low oxygen fugacity and high magma temperature; the quartz monzonite belongs to the magnesian, metaluminous, magnetite-series granitoids with high water content, high oxygen fugacity and relatively low magma temperature. The Jingju Complex to the southwest, which consists of 236 Ma quartz monzonite and 218 Ma syenogranite. They have similar characteristics to the Dashuang quartz monzonite and syenite, respectively.

In western Zhejiang Province, several stages of granitoids were produced during an Andean-type orogenic cycle. Late Triassic ( $T_3$ , 230–215 Ma) granitoids were generated from post-orogenic crust thickened by flat-slab subduction of the paleo-Pacific Plate, with variable fluid/melt contributions from the oceanic plate. They were generated by dehydration melting caused by thermal relaxation of the orogeny and have high melting temperatures and pressures. Mid- to Late-Jurassic ( $J_{2-3}$ , 170–150 Ma) granitoids are granodioritic porphyries that were generated from water-fluxed melting or were fractionated from hydrous basaltic magmas in a thick, lower continental crust. They have high oxygen fugacities, high water contents and were formed at low temperatures. The water was derived from hydrous metasomatic continental lithospheric mantle and/or the foundering oceanic slab. The first stage of granitic rocks in the Early Cretaceous [ $K_1(I)$ , 140–130 Ma] are ferroan alkali feldspar granite or syenogranite with high silica contents, which were generated by low-temperature, low-pressure dehydration melting under variable redox conditions. They were generated in attenuated continental crust caused by roll-back of the paleo-Pacific Plate. The second stage of granitic rocks in the Early Cretaceous [ $K_1(II)$ , 130–125 Ma] are ferroan porphyritic quartz syenite and syenogranite. They have a petrogenesis and tectonic setting similar to the  $K_1(I)$  granitoids, but record higher magma temperatures, lower oxygen fugacities and more depleted Nd-Hf isotopic compositions. It is interpreted that underplated

reduced intraplate basalts were involved in the crustal melting process. The third stage of granitic rocks in the Early Cretaceous [K<sub>1</sub>(III), 115–100 Ma] were generated by fractional crystallization of mantle-derived magmas from the enriched continental lithospheric mantle in an anorogenic setting. They are MME-bearing and oxidized granitoids, with notably high magnetic susceptibilities.

In northeastern Zhejiang Province, the 225 Ma Qiuwang syenogranite was generated by dehydration melting of thickened continental crust (the Paleoproterozoic rocks of the Cathaysia Block). The 178 Ma Xiepu syenogranite was generated by dehydration melting of the Paleoproterozoic rocks, triggered by basaltic underplating following the break-off of the paleo-Pacific plate. The Xiepu syenogranite represents a stage of Mesozoic granitoid not found in western Zhejiang Province (between the T<sub>3</sub> and J<sub>2-3</sub> granitoids). Within the Ganzhou-Hangzhou rift zone (Neoproterozoic Sibao Orogenic Belt), crustal attenuation was stronger than in adjacent regions and A-type granitic magmatism (the Guangshan and Jiangzao granites) resulted in the Late Jurassic, which is earlier than the K<sub>1</sub>(I) granitoids in other regions of Zhejiang Province (~135 Ma). A relatively thin continental crust, accompanied by asthenospheric upwelling along the Ganzhou-Hangzhou rift zone caused the magmatic rocks to have higher Y contents, lower Gd/Yb ratios, higher FeOt/(FeOt+MgO) ratios and more depleted Hf isotopic compositions than their counterparts from adjacent regions. The attenuated crust in the Ganzhou-Hangzhou rift zone and adjacent regions was thickened by intrusions of Early Cretaceous mantle-derived magmas and the ensuing granitoids became more quartz-deficient. The zircon  $\epsilon_{\text{Hf}}(t)$  values of the Early Cretaceous mafic and intermediate rocks in the Ganzhou-Hangzhou rift zone range from -4.3 to 2.1; in contrast, similar rocks in the Cathaysia Block have  $\epsilon_{\text{Hf}}(t)$  values ranging from -4.8 to -2.6. Although the basement rocks in the Sibao Orogenic Belt feature significantly higher degree of Neoproterozoic crustal growth, the Hf isotopic compositions of its continental lithospheric mantle is not significantly different from that of the Cathaysia Block (with Paleoproterozoic basement) during the Early Cretaceous. The less negative zircon  $\epsilon_{\text{Hf}}(t)$  values of the Early Cretaceous mafic and intermediate rocks in the Ganzhou-Hangzhou rift zone were the result of involvement of depleted asthenospheric mantle.

In northeastern Jiangxi Province, the Mid-Jurassic (175–160 Ma) and Early Cretaceous (145–120 Ma) granitic rocks are comparable to their J<sub>2-3</sub> and K<sub>1</sub>(I) counterparts in western Zhejiang Province in terms of age, petrogenesis and tectonic setting. The Mid-Jurassic porphyries are wet and oxidized rocks generated by water-fluxed melting in the continental lower crust or by fractionation of hydrous mantle-derived magmas, containing fluids from the foundering subducted oceanic crust. The Early Cretaceous granites are dry and reduced

rocks generated by dehydration melting in the continental lower crust, which underwent strong extension during roll-back of the paleo-Pacific plate.

Published ages, and geochemical and isotopic data for Mesozoic granitoids from eight other well-studied regions in South China are reviewed in order to place the new results in context. The characteristics of these Mesozoic granitoids indicate common, but diachronous, tectono-magmatic processes. The age, geochemical and isotopic evolution of the Mesozoic granitoids of South China, together with other geological evidence, is consistent with a typical Andean-type orogenic cycle along the eastern margin of China in the Mesozoic.

## Reference

- AGS, 1987. Regional geology of Anhui Province Geological memoirs, 5. Geological Publishing House, Beijing, 721 pp.
- Allègre, C.J., Michard, G., 1974. Introduction to geochemistry. D. Reidel Publishing Company, Dordrecht, Boston, 142 pp.
- Allègre, C.J., 2008. Isotope Geology. Cambridge University Press, 512 pp.
- Andersen, T., 2002. Correction of common lead in U-Pb analyses that do not report  $^{204}\text{Pb}$ . Chemical Geology 192, 59-79.
- Anderson, J.L., Barth, A.P., Wooden, J.L., Mazdab, F., 2008. Thermometers and thermobarometers in granitic systems, Reviews in Mineralogy and Geochemistry, pp. 121-142.
- Annen, C., Sparks, R.S.J., 2002. Effects of repetitive emplacement of basaltic intrusions on thermal evolution and melt generation in the crust. Earth and Planetary Science Letters 203, 937-955.
- Annen, C., Blundy, J.D., Sparks, R.S.J., 2006a. The sources of granitic melt in Deep Hot Zones. Transactions of the Royal Society of Edinburgh: Earth Sciences 97, 297-309.
- Annen, C., Blundy, J.D., Sparks, R.S.J., 2006b. The genesis of intermediate and silicic magmas in deep crustal hot zones. Journal of Petrology 47, 505-539.
- Bachmann, O., Bergantz, G.W., 2008. Rhyolites and their source mushes across tectonic settings. Journal of Petrology 49, 2277-2285.
- Ballhaus, C., 1993. Redox states of lithospheric and asthenospheric upper mantle. Contributions to Mineralogy and Petrology 114, 331-348.
- Barbarin, B., 1990. Granitoids: Main petrogenetic classifications in relation to origin and tectonic setting. Geological Journal 25, 227-238.
- Barbarin, B., 1999. A review of the relationships between granitoid types, their origins and their geodynamic environments. Lithos 46, 605-626.
- Batchelor, R.A., Bowden, P., 1985. Petrogenetic interpretation of granitoid rock series using multicationic parameters. Chemical Geology 48, 43-55.
- Bea, F., 1996. Residence of REE, Y, Th and U in granites and crustal protoliths; Implications for the chemistry of crustal melts. Journal of Petrology 37, 521-552.
- Beard, J.S., Lorgren, G.E., 1991. Dehydration Melting and Water-Saturated Melting of Basaltic and Andesitic Greenstones and Amphibolites at 1, 3, and 6.9 kb. Journal of Petrology 32, 365-401.
- Behrens, H., Gaillard, F., 2006. Geochemical aspects of melts: Volatiles and redox behavior. Elements 2, 275-280.
- Black, L.P., Gulson, B.L., 1978. The age of the Mud Tank carbonatite, Strangways Range, Northern Territory. BMR Journal of Australian Geology and Geophysics 3, 227-232.
- Black, L.P., Kamo, S.L., Allen, C.M., Davis, D.W., Aleinikoff, J.N., Valley, J.W., Mundil, R., Campbell, I.H., Korsch, R.J., Williams, I.S., Foudoulis, C., 2004. Improved  $^{206}\text{Pb}/^{238}\text{U}$  microprobe geochronology by the monitoring of a trace-element-related matrix effect; SHRIMP, ID-TIMS, ELA-ICP-MS and oxygen isotope documentation for a series of zircon standards. Chemical Geology 205, 115-140.

- Blichert-Toft, J., Albarède, F., 1997. The Lu-Hf isotope geochemistry of chondrites and the evolution of the mantle-crust system. *Earth and Planetary Science Letters* 148, 243-258.
- Boehnke, P., Watson, E.B., Trail, D., Harrison, T.M., Schmitt, A.K., 2013. Zircon saturation revisited. *Chemical Geology* 351, 324-334.
- Bowen, N.L., 1913. The melting phenomena of the plagioclase feldspars. *American Journal of Science* 35, 577-599.
- Bowen, N.L., 1928. *The Evolution of the Igneous Rocks*. Princeton University Press, Princeton.
- Burnham, C.W., Ohmoto, H., 1980. Late-stage processes of felsic magmatism. *Mining Geology Special Issue* 8, 1-11.
- Burnham, C.W., 1997. Magmas and hydrothermal fluids. In: Barnes H.L. (Editor), *Geochemistry of hydrothermal ore deposits*. John Wiley & Sons, New York, pp. 63-125.
- Cabane, H., Laporte, D., Provost, A., 2001. Experimental investigation of the kinetics of Ostwald ripening of quartz in silicic melts. *Contributions to Mineralogy and Petrology* 142, 361-373.
- Carter, A., Roques, D., Bristow, C., Kinny, P., 2001. Understanding Mesozoic accretion in Southeast Asia: Significance of Triassic thermotectonism (Indosinian orogeny) in Vietnam. *Geology* 29, 211-214.
- Castro, A., Moreno-Ventas, I., de la Rosa, J.D., 1991. H-type (hybrid) granitoids: a proposed revision of the granite-type classification and nomenclature. *Earth-Science Reviews* 31, 237-253.
- Chappell, B.W., White, A.J.R., 1974. Two contrasting granite types. *Pacific Geology* 8, 173-174.
- Chappell, B.W., Bryant, C.J., Wyborn, D., 2012. Peraluminous I-type granites. *Lithos* 153, 142-153.
- Charvet, J., Lapierre, H., Yu, Y.-W., 1994. Geodynamic significance of the Mesozoic volcanism of southeastern China. *Journal of Southeast Asian Earth Sciences* 9, 387-396.
- Charvet, J., 2013. The Neoproterozoic-Early Paleozoic tectonic evolution of the South China Block: An overview. *Journal of Asian Earth Sciences* 74, 198-209.
- Chen, C.-H., Lee, C., Shinjo, R., 2008. Was there Jurassic paleo-Pacific subduction in South China?: Constraints from  $^{40}\text{Ar}$ - $^{39}\text{Ar}$  dating, elemental and Sr-Nd-Pb isotopic geochemistry of the Mesozoic basalts. *Lithos* 106, 83-92.
- Chen, G.-N., Grapes, R., 2003. An In-Situ Melting Model of Granite Formation: Geological Evidence from Southeast China. *International Geology Review* 45, 611-622.
- Chen, J.-F., Zhou, T.-X., Yin, C.-S., 1991.  $^{40}\text{Ar}$ - $^{39}\text{Ar}$  dating of several Mesozoic plutons in southeastern Zhejiang Province. *Acta Petrologica Sinica*, 37-44.
- Chen, J.-Y., Yang, J.-H., Zhang, J.-H., Sun, J.-F., Wilde, S.A., 2013a. Petrogenesis of the Cretaceous Zhangzhou batholith in southeastern China: Zircon U-Pb age and Sr-Nd-Hf-O isotopic evidence. *Lithos* 162-163, 140-156.
- Chen, J.-Y., Yang, J.-H., Zhang, J.-H., Sun, J.-F., 2014. Geochemical transition shown by Cretaceous granitoids in southeastern China: Implications for continental crustal reworking and growth. *Lithos* 196-197, 115-130.
- Chen, J., Wang, R.-C., Zhu, J.-C., Lu, J.-J., Ma, D.-S., 2013b. Multiple-aged granitoids and related tungsten-tin mineralization in the Nanling Range, South China. *Science China Earth Sciences*, 1-11.

- Chen, P.-R., Zhou, X.-M., Zhang, W.-L., Li, H.-M., Fan, C.-F., Sun, T., Chen, W.-F., Zhang, M., 2005a. Petrogenesis and significance of early Yanshanian syenite-granite complex in eastern Nanling Range. *Science in China Series D-Earth Sciences* 48, 912-924.
- Chen, R., Xing, G.-F., Yang, Z.-L., Shen, J.-L., Zhou, Y.-Z., 2005b. Study on Beizhang and Lianglong granite and their dark enclaves. *Geological Journal of China Universities* 11, 264-275.
- Chen, S.-Q., 2011. Discussion on the Yangshan Epoch rock characteristics and ore-forming background in Zhejiang Kaihua region. thesis Thesis, China University of Geosciences, Beijing, 53 pp.
- Chen, W.-F., 2006. Genesis of granite and intraplate orogenesis during Indosinian in South China, Nanjing University, Nanjing, 96 pp.
- Chen, W.-F., Chen, P.-R., Zhou, X.-M., Huang, H.-Y., Ding, X., Sun, T., 2006. Single-zircon LA-ICP-MS U-Pb dating of the Yangmingshan granitic pluton in Hunan, South China and its petrogenetic study. *Acta Geologica Sinica* 80, 1065-1077.
- Chen, W.-F., Chen, P.-R., Huang, H.-Y., Ding, X., Sun, T., 2007. Chronological and geochemical studies of granite and enclave in Baimashan pluton, Hunan, South China. *Science in China Series D: Earth Sciences* 50, 1606-1627.
- Chen, Y.-W., Bi, X.-W., Hu, R.-Z., Dong, S.-H., 2012. Element geochemistry, mineralogy, geochronology and zircon Hf isotope of the Luxi and Xiazhuang granites in Guangdong province, China: Implications for U mineralization. *Lithos* 150, 119-134.
- Chiaradia, M., 2014. Copper enrichment in arc magmas controlled by overriding plate thickness. *Nature Geoscience* 7, 43-46.
- Chu, N.-C., Taylor, R.N., Chavagnac, V., Nesbitt, R.W., Boella, R.M., Milton, J.A., German, C.R., Bayon, G., Burton, K., 2002. Hf isotope ratio analysis using multi-collector inductively coupled plasma mass spectrometry: an evaluation of isobaric interference corrections. *Journal of Analytical Atomic Spectrometry* 17, 1567-1574.
- Chu, Y., Lin, W., Faure, M., Wang, Q.-C., Ji, W.-B., 2012. Phanerozoic tectonothermal events of the Xuefengshan Belt, central South China: Implications from U-Pb age and Lu-Hf determinations of granites. *Lithos* 150, 243-255.
- Clarke, D.B., 1992. Granitoid rocks. Chapman & Hall.
- Clemens, J.D., Bea, F., 2012. Landmark papers: granite petrogenesis. *Mineralogical Society of Great Britain and Ireland*, 343 pp.
- Coney, P.J., Reynolds, S.J., 1977. Cordilleran Benioff zones. *Nature* 270, 403-406.
- Conrad, W.K., Nicholls, I.A., Wall, V.J., 1988. Water-saturated and -undersaturated melting of metaluminous and peraluminous crustal compositions at 10 kb: evidence for the origin of silicic magmas in the Taupo Volcanic Zone, New Zealand, and other occurrences. *Journal of Petrology* 29, 765-803.
- Coulon, C., Thorpe, R.S., 1981. Role of continental crust in petrogenesis of orogenic volcanic associations. *Tectonophysics* 77, 79-93.

- Cui, S.-Q., Li, J.-R., 1983. On the Indosinian orogeny along the Chinese Western Pacific belt. *Acta Geologica Sinica* 67, 51-61.
- Cui, Y.-R., Xie, Z., Wang, B., Chen, J.-F., Yu, Y.-W., He, J.-F., 2011. Geochemical Characteristics of the Late Mesozoic Basalts in Southeastern Zhejiang Province and Constraints on Magma Source Materials. *Geological Journal of China Universities* 17, 492-512.
- Darbyshire, D.P.F., Sewell, R.J., 1997. Nd and Sr isotope geochemistry of plutonic rocks from Hong Kong: implications for granite petrogenesis, regional structure and crustal evolution. *Chemical Geology* 143, 81-93.
- Davidson, J., Turner, S., Handley, H., Macpherson, C., Dosseto, A., 2007. Amphibole "sponge" in arc crust? *Geology* 35, 787-790.
- Davis, J., Hawkesworth, C., 1993. The petrogenesis of 30–20 Ma basic and intermediate volcanics from the Mogollon-Datil Volcanic Field, New Mexico, USA. *Contributions to Mineralogy and Petrology* 115, 165-183.
- DeCelles, P.G., 2004. Late Jurassic to Eocene evolution of the Cordilleran thrust belt and foreland basin system, western U.S.A. *American Journal of Science* 304, 105-168.
- Deng, P., Ling, H.-F., Shen, W.-Z., Sun, L.-Q., Zhu, B., Huang, G.-L., Tan, Z.-Z., 2011. SHRIMP zircon U-Pb dating and geochemical characteristics of Reshui granitic batholith, northern Guangdong. *Acta Geologica Sinica* 85, 1274-1283.
- DeVore, G.W., 1955. Crystal Growth and the Distribution of Elements. *The Journal of Geology* 63, 471-494.
- Ding, X., Jiang, S.-Y., Ni, P., Gu, L.-X., Jiang, Y.-H., 2005. Zircon SIMS U-Pb geochronology of host granitoids in Wushan and Yongping copper deposits, Jiangxi Province. *Geological Journal of China Universities* 11, 383-389.
- Dong, C.-W., Xu, X.-S., Yan, Q., Lin, X.-B., Zhu, G.-Q., 2007. A new case of Late Mesozoic crust-mantle interaction in eastern Zhejiang: geochronology and geochemistry of the Ru'ao diabase-granite composite intrusions. *Acta Petrologica Sinica* 23, 1303-1312.
- Dumitru, T.A., Gans, P.B., Foster, D.A., Miller, E.L., 1991. Refrigeration of the western Cordilleran lithosphere during Laramide shallow-angle subduction. *Geology* 19, 1145-1148.
- Eaton, G.P., 2008. Epeirogeny in the Southern Rocky Mountains region: Evidence and origin. *Geosphere* 4, 764-784.
- Eskola, P., 1932. On the origin of granitic magmas. *Zeitschrift für Kristallographie, Mineralogie und Petrographie* 42, 455-481.
- Farges, F., Ponader, C.W., Calas, G., Brown Jr, G.E., 1992. Structural environments of incompatible elements in silicate glass/melt systems: II. UIV, UV, and UVI. *Geochimica et Cosmochimica Acta* 56, 4205-4220.
- Ferrari, L., 2004. Slab detachment control on mafic volcanic pulse and mantle heterogeneity in central Mexico. *Geology* 32, 77-80.
- Ferry, J., Watson, E., 2007. New thermodynamic models and revised calibrations for the Ti-in-zircon and Zr-in-rutile thermometers. *Contributions to Mineralogy and Petrology* 154, 429-437.

- FGS, 1972. Regional Geology of Guangfeng area. Bureau of Geology and Mineral Resources of Fujian Province, Fuzhou, 289 pp.
- FGS, 1985. Regional geology of Fujian Province Geological Publishing House, Beijing, 671 pp.
- Foley, S.F., Wheller, G.E., 1990. Parallels in the origin of the geochemical signatures of island arc volcanics and continental potassic igneous rocks: The role of residual titanates. *Chemical Geology* 85, 1-18.
- Fromm, R., Zandt, G., Beck, S.L., 2004. Crustal thickness beneath the Andes and Sierras Pampeanas at 30°S inferred from Pn apparent phase velocities. *Geophysical Research Letter* 31, L06625.
- Frost, B.R., Barnes, C.G., Collins, W.J., Arculus, R.J., Ellis, D.J., Frost, C.D., 2001. A Geochemical Classification for Granitic Rocks. *Journal of Petrology* 42, 2033-2048.
- Frost, B.R., Frost, C.D., 2008. A Geochemical Classification for Feldspathic Igneous Rocks. *Journal of Petrology* 49, 1955-1969.
- Frost, C.D., Frost, B.R., 2011. On Ferroan (A-type) Granitoids: their Compositional Variability and Modes of Origin. *Journal of Petrology* 52, 39-53.
- Fu, J.-M., Ma, C.-Q., Xie, C.-F., Zhang, Y.-M., Peng, S.-B., 2004. Geochemistry and tectonic setting of Xishan aluminous A-type granitic volcanic-intrusive complex, southern Hunan. *Journal of Earth Sciences and Environment* 26, 15-23.
- Fu, J.-M., Xie, C.-F., Peng, S.-B., Yang, X.-Y., Mei, Y.-P., 2006. Geochemistry and crust-mantle magmatic mixing of the Qitianling granites and their dark microgranular enclaves in Hunan Province. *Acta Geoscientifica Sinica* 27, 557-569.
- Gao, P., 1936. Late Mesozoic granitoids in southeastern China and their relation to geological structure. *Geological Review* 1, 407-416.
- Gao, S., Yang, J., Zhou, L., Li, M., Hu, Z.-C., Guo, J.-L., Yuan, H.-L., Gong, H.-J., Xiao, G.-Q., Wei, J.-Q., 2011. Age and growth of the Archean Kongling terrain, South China, with emphasis on 3.3 ga granitoid gneisses. *American Journal of Science* 311, 153-182.
- Ge, X.-Y., 2003. Mesozoic magmatism in Hainan Island (SE China) and its tectonic significance: geochronology, geochemistry and Sr-Nd isotope evidences, The Chinese Academy of Sciences, Guangzhou, 87 pp.
- GGS, 1988. Regional Geology of Guangdong province Geological Publishing House, Beijing, 941 pp.
- Gilder, S., Gill, J., Coe, R., Zhao, X., Liu, Z., Wang, G., Yuan, K., Liu, W., Kuang, G., Wu, H., 1996. Isotopic and paleomagnetic constraints on the Mesozoic tectonic evolution of south China. *Journal of Geophysical Research* 101, 16137-16154.
- Gilder, S.A., Keller, G.R., Luo, M., Goodell, P.C., 1991. Eastern Asia and the Western Pacific timing and spatial distribution of rifting in China. *Tectonophysics* 197, 225-243.
- Gill, J.B., 1981. Orogenic andesites and plate tectonics, 16. Springer Verlag.
- Gill, R., 2010. Igneous rocks and processes. Blackwell Publishing.
- Glazner, A.F., Coleman, D.S., Bartley, J.M., 2008. The tenuous connection between high-silica rhyolites and granodiorite plutons. *Geology* 36, 183-186.
- Goldschmidt, V.M., 1958. Geochemistry. Oxford University Press, London, 730 pp.

- Goldsmith, J.R., 1950. Gallium and Germanium Substitutions in Synthetic Feldspars. *The Journal of Geology* 58, 518-536.
- Goodell, P.C., Gilder, S., Fang, X., 1991. A preliminary description of the Gan-Hang failed rift, southeastern China. *Tectonophysics* 197, 245-255.
- Goodman, R.J., 1972. The distribution of Ga and Rb in coexisting groundmass and phenocryst phases of some basic volcanic rocks. *Geochimica et Cosmochimica Acta* 36, 303-317.
- Griffin, W., Powell, W., Pearson, N., O'Reilly, S., 2008. GLITTER: data reduction software for laser ablation ICP-MS. In: Sylvester P. (Editor), *Laser Ablation-ICP-MS in the Earth Sciences*. Mineralogical Association of Canada, pp. 204-207.
- Griffin, W.L., Wang, X., Jackson, S.E., Pearson, N.J., O'Reilly, S.Y., Xu, X.-S., Zhou, X.-M., 2002. Zircon chemistry and magma mixing, SE China: In-situ analysis of Hf isotopes, Tonglu and Pingtan igneous complexes. *Lithos* 61, 237-269.
- Griffin, W.L., Pearson, N.J., Belousova, E.A., Saeed, A., 2006. Comment: Hf-isotope heterogeneity in zircon 91500. *Chemical Geology* 233, 358-363.
- Grove, T.L., Kinzler, R.J., 1986. Petrogenesis of Andesites. *Annual Review of Earth and Planetary Sciences* 14, 417-454.
- Gu, C.-Y., Hua, R.-M., Qi, H.-W., 2006. Geochemistry and petrogenesis of the Yanshanian Huashan-Guposhan granites in Guangxi. *Acta Petrologica et Mineralogica* 25, 97-109.
- Gu, M.-G., Feng, L.-X., Hu, Y.-H., Yu, S.-Q., Wu, M., 2011. U-Pb dating of zircons from Guangshan and Zhaxi plutons in Shaoxing area, Zhejiang Province: constraint on the ore-forming epoch of the Lizhu iron ore deposit. *Geological Bulletin of China* 30, 1212-1219.
- Gu, Z.-W., 2005. On the Mincheian Movement. *Journal of Stratigraphy* 29, 1-6.
- Gualda, G.A.R., Ghiorso, M.S., 2013. Low-Pressure Origin of High-Silica Rhyolites and Granites. *The Journal of Geology* 121, 537-545.
- Guo, C.-L., Mao, J.-W., Chen, Y.-C., 2010. SHRIMP zircon U-Pb dating, geochemistry, Sr-Nd-Hf isotopic analysis of the Yingqian intrusion in Jiangxi Province, South China and its geological significance. *Acta Petrologica Sinica* 26, 919-937.
- Guo, C.-L., Chen, Y.-C., Li, C.-B., Chen, Z.-H., Lou, F.-S., 2011. Zircon SHRIMP U-Pb Dating, Geochemistry, Sr-Nd Isotopic Analysis of the Late Jurassic Granitoids in Jiulongnao W-Sn-Pb-Zn Ore-Concentrated Areas in Jiangxi Province and Its Geological Significance. *Acta Geologica Sinica* 85, 1188-1205.
- Guo, C.-L., Chen, Y.-C., Zeng, Z.-L., Lou, F.-S., 2012a. Petrogenesis of the Xihuashan granites in southeastern China: Constraints from geochemistry and in-situ analyses of zircon UPbHfO isotopes. *Lithos* 148, 209-227.
- Guo, F., Fan, W.-M., Li, C.-W., Zhao, L., Li, H.-X., Yang, J.-H., 2012b. Multi-stage crust-mantle interaction in SE China: Temporal, thermal and compositional constraints from the Mesozoic felsic volcanic rocks in eastern Guangdong-Fujian provinces. *Lithos* 150, 62-84.
- Hanchar, J.M., Watson, E.B., 2003. Zircon Saturation Thermometry. *Reviews in Mineralogy and Geochemistry* 53, 89-112.
- Hawkesworth, C.J., Kemp, A.I.S., 2006. Evolution of the continental crust. *Nature* 443, 811-817.

- He, Z.-Y., Xu, X.-S., 2012. Petrogenesis of the Late Yanshanian mantle-derived intrusions in southeastern China: Response to the geodynamics of paleo-Pacific plate subduction. *Chemical Geology* 328, 208-221.
- HGS, 1988. Regional geology of Hunan Province Geological Publishing House, Beijing, 721 pp.
- Hoefs, J., 2009. Stable isotope geochemistry. Springer.
- Hoffmann, J.E., Münker, C., Polat, A., Rosing, M.T., Schulz, T., 2011. The origin of decoupled Hf–Nd isotope compositions in Eoarchean rocks from southern West Greenland. *Geochimica et Cosmochimica Acta* 75, 6610-6628.
- Holtz, F., Johannes, W., Tamic, N., Behrens, H., 2001. Maximum and minimum water contents of granitic melts generated in the crust: a reevaluation and implications. *Lithos* 56, 1-14.
- Hou, Z., Pan, X., Li, Q., Yang, Z., Song, Y., 2013. The giant Dexing porphyry Cu–Mo–Au deposit in east China: product of melting of juvenile lower crust in an intracontinental setting. *Mineralium Deposita*, 1-27.
- Howell, D.G., 1995. Principles of Terrane Analysis. Topics in the Earth Sciences, 8. Chapman & Hall, 245 pp.
- Hsu, K.J., Shu, S., Ji-Liang, L., Hai-Hong, C., Hai-Po, P., Sengor, A.M.C., 1988. Mesozoic overthrust tectonics in south China. *Geology* 16, 418-421.
- Hsu, K.J., Li, J.-L., Chen, H.-H., Wang, Q.-C., Sun, S., Sengör, A.M.C., 1990. Tectonics of South China: Key to understanding West Pacific geology. *Tectonophysics* 183, 9-39.
- Hsieh, P.-S., Chen, C.-H., Yen, C.-M., Lee, C.-Y., 2009. Origin of mafic microgranular enclaves (MMEs) and their host rocks of the Cretaceous Xiaojiang-Liangnong granitic complexes in the Southeast Coast Magmatic Belt, S China. *Terrestrial, Atmospheric and Oceanic Sciences* 20, 480-500.
- Huang, F., Wang, D.-H., Santosh, M., Wang, C.-H., Zeng, Z.-L., Liu, S.-B., Wang, L.-Q., Zhang, Y.-Z., 2014. Genesis of the Yuanlingzhai porphyry molybdenum deposit, Jiangxi province, South China: Constraints from petrochemistry and geochronology. *Journal of Asian Earth Sciences* 79, Part B, 759-776.
- Huang, H.-Q., Li, X.-H., Li, W.-X., Liu, Y., 2008. Age and origin of the Dadongshan granite from the Nanling Range: SHRIMP U-Pb zircon age, geochemistry and Sr-Nd-Hf isotopes. *Geological Journal of China Universities* 14, 317-333.
- Huang, H.-Q., Li, X.-H., Li, W.-X., Li, Z.-X., 2011a. Formation of high  $\delta^{18}\text{O}$  fayalite-bearing A-type granite by high-temperature melting of granulitic metasedimentary rocks, southern China. *Geology* 36, 903-906.
- Huang, H.-Q., Li, X.-H., Li, W.-X., Li, Z.-X., 2011b. Formation of high  $\delta^{18}\text{O}$  fayalite-bearing A-type granite by high-temperature melting of granulitic metasedimentary rocks, southern China. *Geology*.
- Huang, H.-Q., 2012. Sources and conditions for the formation of Jurassic post-orogenic high-K granites in the Western Guangdong Province, SE China, Curtin University, Perth, 226 pp.

- Humphreys, E., Hessler, E., Dueker, K., Farmer, G.L., Erslev, E., Atwater, T., 2003. How Laramide-age hydration of North American lithosphere by the Farallon slab controlled subsequent activity in the western United States. *International Geology Review* 45, 575-595.
- Humphreys, E., 2009. Relation of flat subduction to magmatism and deformation in the Western United States. In: Kay S.M., Ramos V.A., Dickinson W.R. (Editors), *Geological Society of America Memoir*, pp. 85-98.
- Ishihara, S., 1977. The magnetite-series and ilmenite-series granitic rocks. *Mining Geology* 27, 293-305.
- Ishihara, S., 1998. Granitoid Series and Mineralization in the Circum-Pacific Phanerozoic Granitic Belts. *Resource Geology* 48, 219-224.
- Ishihara, S., Hashimoto, M., Machida, M., 2000. Magnetite/Ilmenite-series Classification and Magnetic Susceptibility of the Mesozoic-Cenozoic Batholiths in Peru. *Resource Geology* 50, 123-129.
- Ishihara, S., 2004. The redox state of granitoids relative to tectonic setting and earth history: The magnetite-ilmenite series 30 years later. *Earth and Environmental Science Transactions of the Royal Society of Edinburgh* 95, 23-33.
- Jackson, S.E., Pearson, N.J., Griffin, W.L., Belousova, E.A., 2004. The application of laser ablation-inductively coupled plasma-mass spectrometry to in situ U-Pb zircon geochronology. *Chemical Geology* 211, 47-69.
- Jahn, B.-M., Zhou, X.-H., Li, J.-L., 1990. Formation and tectonic evolution of Southeastern China and Taiwan: Isotopic and geochemical constraints. *Tectonophysics* 183, 145-160.
- Janoušek, V., Farrow, C.M., Erban, V., 2006. Interpretation of Whole-rock Geochemical Data in Igneous Geochemistry: Introducing Geochemical Data Toolkit (GCDkit). *Journal of Petrology* 47, 1255-1259.
- JGS, 1980a. Regional Geology of Guangfeng area. Bureau of Geology and Mineral Resources of Fujian Province, Fuzhou, 289 pp.
- JGS, 1980b. Geological Map of Leping, Jiangxi Province. China Geological Map Press, Beijing.
- JGS, 1980c. Geological Map of Shangrao, Jiangxi Province. China Geological Map Press, Beijing.
- JGS, 1984. Regional Geology of Jiangxi province Geological memoirs. Geological Publishing House, Beijing, 921 pp.
- Jia, D.-L., Yang, G.-S., Ye, T.-Z., Pang, Z.-S., Li, Y.-S., He, P.-F., Yao, L., Liu, P., 2013. Zircon U-Pb dating, Hf isotopic compositions and petrochemistry of the Guangshan granitic complex in Shaoxing area of Zhejiang Province and its geological significance. *Acta Petrologica Sinica* 29, 4087-4103.
- Jiang, N., Guo, J., Zhai, M., 2011a. Nature and origin of the Wenquan granite: Implications for the provenance of Proterozoic A-type granites in the North China craton. *Journal of Asian Earth Sciences* 42, 76-82.
- Jiang, X.-Y., Li, X.-H., 2014. In situ zircon U-Pb and Hf-O isotopic results for ca. 73<sup>Ma</sup> granite in Hainan Island: Implications for the termination of an Andean-type active continental margin in southeast China. *Journal of Asian Earth Sciences* 82, 32-46.

- Jiang, Y.-H., Jiang, S.-Y., Dai, B.-Z., Liao, S.-Y., Zhao, K.-D., Ling, H.-F., 2009. Middle to late Jurassic felsic and mafic magmatism in southern Hunan province, southeast China: Implications for a continental arc to rifting. *Lithos* 107, 185-204.
- Jiang, Y.-H., Zhao, P., Zhou, Q., Liao, S.-Y., Jin, G.-D., 2011b. Petrogenesis and tectonic implications of Early Cretaceous S- and A-type granites in the northwest of the Gan-Hang rift, SE China. *Lithos* 121, 55-73.
- Kay, S., Gordillo, C., 1994. Pocho volcanic rocks and the melting of depleted continental lithosphere above a shallowly dipping subduction zone in the central Andes. *Contributions to Mineralogy and Petrology* 117, 25-44.
- Kay, S.M., Mpodozis, C., 2001. Central Andean ore deposits linked to evolving shallow subduction systems and thickening crust. *GSA Today* 11, 4-9.
- Kay, S.M., Coira, B.L., Caffe, P.J., Chen, C.-H., 2010. Regional chemical diversity, crustal and mantle sources and evolution of central Andean Puna plateau ignimbrites. *Journal of Volcanology and Geothermal Research* 198, 81-111.
- Kelemen, P.B., Hanghøj, K., Greene, A.R., 2003. One View of the Geochemistry of Subduction-Related Magmatic Arcs, with an Emphasis on Primitive Andesite and Lower Crust. In: Heinrich D.H., Karl K.T. (Editors), *Treatise on geochemistry*. Pergamon, Oxford, pp. 1-70.
- Klein, C., Philpotts, A.R., 2013. Earth materials: introduction to mineralogy and petrology. Cambridge University Press.
- Kuno, H., 1959. Origin of cenozoic petrographic provinces of Japan and surrounding areas. *Bulletin Volcanologique* 20, 37-76.
- Lapierre, H., Jahn, B.-M., Charvet, J., Yu, Y.-W., 1997. Mesozoic felsic arc magmatism and continental olivine tholeiites in Zhejiang Province and their relationship with the tectonic activity in southeastern China. *Tectonophysics* 274, 321-338.
- Le Maitre, R.W., 2002. Igneous rocks: a classification and glossary of terms: recommendations of the International Union of Geological Sciences, Subcommission on the Systematics of Igneous Rocks. Cambridge University Press, 236 pp.
- Lee, C.-T.A., Leeman, W.P., Canil, D., Li, Z.-X.A., 2005. Similar V/Sc Systematics in MORB and Arc Basalts: Implications for the Oxygen Fugacities of their Mantle Source Regions. *Journal of Petrology* 46, 2313-2336.
- Lee, C.-T.A., Luffi, P., Le Roux, V., Dasgupta, R., Albarede, F., Leeman, W.P., 2010. The redox state of arc mantle using Zn/Fe systematics. *Nature* 468, 681-685.
- Li, B., Zhao, K.-D., Yang, S.-Y., Dai, B.-Z., 2013a. Petrogenesis of the porphyritic dacite from Ermiaogou Cu-Au deposit in Zijinshan ore field and its metallogenetic implications. *Acta Petroiogica Sinica* 29, 4167-4185.
- Li, F.-L., Zhou, H.-W., Tang, Z.-C., Li, Y.-L., Wang, F.-X., Xu, Y.-C., Tan, H.-F., Luo, W., Guan, C.-G., 2011a. U-Pb ages, geochemistry and tectonic implications of mafic dyke swarms in Mugua, Chun'an county, Zhejiang Province. *Geochimica* 40, 22-34.
- Li, H., Zhang, H., Ling, M.-X., Wang, F.-Y., Ding, X., Zhou, J.-B., Yang, X.-Y., Tu, X.-L., Sun, W.-D., 2011b. Geochemical and zircon U-Pb study of the Huangmeijian A-type granite:

- implications for geological evolution of the Lower Yangtze River belt. International Geology Review 53, 499 - 525.
- Li, H., Ling, M.-X., Li, C.-Y., Zhang, H., Ding, X., Yang, X.-Y., Fan, W.-M., Li, Y.-L., Sun, W.-D., 2012a. A-type granite belts of two chemical subgroups in central eastern China: Indication of ridge subduction. Lithos 150, 26-36.
- Li, J.-R., 2011. Geochronology, geochemistry and petrogenesis of the Jintan granites from the Xiajiang uranium ore district, Jiangxi. M.Phil. Thesis, Nanjing University, 49 pp.
- Li, L.-M., Sun, M., Wang, Y., Xing, G., Zhao, G., Cai, K., Zhang, Y., 2011c. Geochronological and Geochemical study of Palaeoproterozoic gneissic granites and clinopyroxenite xenoliths from NW Fujian, SE China: Implications for the crustal evolution of the Cathaysia Block. Journal of Asian Earth Sciences 41, 204-212.
- Li, P.-J., Yu, X.-Q., Li, H.-Y., Qiu, J.-T., Zhou, X., 2013b. Jurassic–Cretaceous tectonic evolution of Southeast China: geochronological and geochemical constraints of Yanshanian granitoids. International Geology Review, 1-18.
- Li, W.-Y., 2010. Petrogenesis of granitoids related to Mo-Cu deposits in Jingju Area, southwestern Zhejiang Province: evidence from petrology and geochronology, China University of Geosciences, Wuhan, 83 pp.
- Li, W.-Y., Ma, C.-Q., Liu, Y.-Y., Robinson, P., 2012b. Discovery of the Indosinian aluminum A-type granite in Zhejiang Province and its geological significance. Science China Earth Sciences 55, 13-25.
- Li, X.-F., Watanabe, Y., Yi, X.-K., 2013c. Ages and Sources of Ore-Related Porphyries at Yongping Cu–Mo Deposit in Jiangxi Province, Southeast China. Resource Geology 63, 288-312.
- Li, X.-H., 2000. Cretaceous magmatism and lithospheric extension in Southeast China. Journal of Asian Earth Sciences 18, 293-305.
- Li, X.-H., Chen, Z., Liu, D., Li, W.-X., 2003a. Jurassic Gabbro-Granite-Syenite Suites from Southern Jiangxi Province, SE China: Age, Origin, and Tectonic Significance. International Geology Review 45, 898 - 921.
- Li, X.-H., Li, Z.-X., Ge, W.-C., Zhou, H.-W., Li, W.-X., Liu, Y., Wingate, M.T.D., 2003b. Neoproterozoic granitoids in South China: crustal melting above a mantle plume at ca. 825 Ma? Precambrian Research 122, 45-83.
- Li, X.-H., Li, Z.-X., Li, W.-X., Wang, Y.-J., 2006. Initiation of the Indosinian Orogeny in South China: Evidence for a Permian Magmatic Arc on Hainan Island. The Journal of Geology 114, 341-353.
- Li, X.-H., Li, W.-X., Li, Z.-X., 2007. On the genetic classification and tectonic implications of the Early Yanshanian granitoids in the Nanling Range, South China. Chinese Science Bulletin 52, 1873-1885.
- Li, X.-H., Li, W.-X., Li, Z.-X., Liu, Y., 2008. 850–790 Ma bimodal volcanic and intrusive rocks in northern Zhejiang, South China: A major episode of continental rift magmatism during the breakup of Rodinia. Lithos 102, 341-357.

- Li, X.-H., Li, W.-X., Li, Z.-X., Lo, C.-H., Wang, J., Ye, M.-F., Yang, Y.-H., 2009. Amalgamation between the Yangtze and Cathaysia Blocks in South China: Constraints from SHRIMP U-Pb zircon ages, geochemistry and Nd-Hf isotopes of the Shuangxiwu volcanic rocks. *Precambrian Research* 174, 117-128.
- Li, X.-H., Li, Z.-X., He, B., Li, W.-X., Li, Q.-L., Gao, Y.-Y., Wang, X.-C., 2012c. The Early Permian active continental margin and crustal growth of the Cathaysia Block: In situ U-Pb, Lu-Hf and O isotope analyses of detrital zircons. *Chemical Geology* 328, 195-207.
- Li, X.-H., Li, Z.-X., Li, W.-X., Wang, X.-C., Gao, Y., 2013d. Revisiting the “C-type adakites” of the Lower Yangtze River Belt, central eastern China: In-situ zircon Hf-O isotope and geochemical constraints. *Chemical Geology* 345, 1-15.
- Li, Y.H.M., Zhou, M.-F., Lai, K.W., Chan, L.S., Chen, W.T., 2014a. Geochemical and geochronological constraints on Late Jurassic volcanic rocks at Tuen Mun, Hong Kong, with implications for the Palaeo-Pacific subduction. *International Geology Review*, 1-22.
- Li, Z.-X., Li, X.-H., Zhou, H.-W., Kinny, P.D., 2002. Grenvillian continental collision in south China: New SHRIMP U-Pb zircon results and implications for the configuration of Rodinia. *Geology* 30, 163-166.
- Li, Z.-X., Li, X.-H., 2007. Formation of the 1300-km-wide intracontinental orogen and postorogenic magmatic province in Mesozoic South China: A flat-slab subduction model. *Geology* 35, 179-182.
- Li, Z.-X., Li, X.-H., Wartho, J.-A., Clark, C., Li, W.-H., Zhang, C.-L., Bao, C.-M., 2010a. Magmatic and metamorphic events during the early Paleozoic Wuyi-Yunkai orogeny, southeastern South China: New age constraints and pressure-temperature conditions. *Geological Society of America Bulletin*, B30021.1.
- Li, Z.-X., Li, X.-H., Chung, S.-L., Lo, C.-H., Xu, X.-S., Li, W.-X., 2012d. Magmatic switch-on and switch-off along the South China continental margin since the Permian: Transition from an Andean-type to a Western Pacific-type plate boundary. *Tectonophysics* 532–535, 271-290.
- Li, Z.-X., Chen, H.-L., Li, X.-H., Zhang, F.-Q., 2014b. Tectonics of the South China Block: Interpreting the Rock Record. Chinese Science Press (in press), Beijing.
- Li, Z., Qiu, J.-S., Zhou, J.-C., 2010b. Geochronology, geochemistry, and Nd-Hf isotopes of early Palaeozoic-early Mesozoic I-type granites from the Hufang composite pluton, Fujian, South China: crust-mantle interactions and tectonic implications. *International Geology Review* 99999, 1-18.
- Li, Z., Qiu, J.-S., Yang, X.-M., 2014c. A review of the geochronology and geochemistry of Late Yanshanian (Cretaceous) plutons along the Fujian coastal area of southeastern China: Implications for magma evolution related to slab break-off and rollback in the Cretaceous. *Earth-Science Reviews* 128, 232-248.
- Liew, T.C., Hofmann, A.W., 1988. Precambrian crustal components, plutonic associations, plate environment of the Hercynian Fold Belt of central Europe: Indications from a Nd and Sr isotopic study. *Contributions to Mineralogy and Petrology* 98, 129-138.

- Lipman, P.W., Doe, B.R., Hedge, C.E., Steven, T.A., 1978. Petrologic evolution of the San Juan volcanic field, southwestern Colorado: Pb and Sr isotope evidence. Geological Society of America Bulletin 89, 59-82.
- Lipman, P.W., 1987. Rare-earth-element compositions of Cenozoic volcanic rocks in the southern Rocky Mountains and adjacent areas. USGS Bulletin 1668.
- Lipman, P.W., 2004. Chemical Analyses Of Tertiary Volcanic Rocks, Central San Juan Caldera Complex, Southwestern Colorado. USGS Open-File Report 2004-1194.
- Lipman, P.W., 2006. Geologic Map of the Central San Juan Caldera Cluster, Southwestern Colorado. USGS Geologic Investigations Series I-2799.
- Liu, J., Mao, J.-W., Ye, H.-S., Xie, G.-Q., Yang, G.-Q., Zhang, W., 2008. Zircon LA-ICPMS U-Pb dating of Hukeng granite in Wugongshan area, Jiangxi Province and its geochemical characteristics. *Acta Petroiogica Sinica* 24, 1813-1822.
- Liu, L., Qiu, J.-S., Li, Z., 2011a. Zircon U-Pb age and Hf isotopic compositions of quartz monzonite and enclosed mafic enclaves in Muchen pluton, Zhejiang Province: tracing magma mixing in their petrogenesis. *Geological Review (in Chinese with English abstract)* 57, 327-336.
- Liu, L., Xu, X.-S., Zou, H.-B., 2012a. Episodic eruptions of the Late Mesozoic volcanic sequences in southeastern Zhejiang, SE China: Petrogenesis and implications for the geodynamics of paleo-Pacific subduction. *Lithos* 154, 166-180.
- Liu, L., Qiu, J.-S., Li, Z., 2013a. Origin of mafic microgranular enclaves (MMEs) and their host quartz monzonites from the Muchen pluton in Zhejiang Province, Southeast China: Implications for magma mixing and crust–mantle interaction. *Lithos* 160–161, 145-163.
- Liu, L., Xu, X.-S., Xia, Y., 2014. Cretaceous Pacific plate movement beneath SE China: Evidence from episodic volcanism and related intrusions. *Tectonophysics* 614, 170-184.
- Liu, Q., Yu, J.-H., Su, B., Wang, Q., Tang, H.-F., Xu, H., Cui, X., 2011b. Discovery of the 187 Ma granite in Jincheng area, Fujian Province: constraint on Early Jurassic tectonic evolution of southeastern China. *Acta Petrologica Sinica* 27, 3575-3589.
- Liu, X., Fan, H.-R., Santosh, M., Hu, F.-F., Yang, K.-F., Li, Q.-L., Yang, Y.-H., Liu, Y., 2012b. Remelting of Neoproterozoic relict volcanic arcs in the Middle Jurassic: Implication for the formation of the Dexing porphyry copper deposit, Southeastern China. *Lithos* 150, 85-100.
- Liu, X., Fan, H.-R., Santosh, M., Hu, F.-F., Yang, K.-F., Wen, B.-J., Yang, Y.-H., Liu, Y., 2013b. Origin of the Yinshan epithermal-porphyry Cu–Au–Pb–Zn–Ag deposit, southeastern China: insights from geochemistry, Sr–Nd and zircon U–Pb–Hf–O isotopes. *International Geology Review*, 1-30.
- Livaccari, R.F., Burke, K., Sengor, A.M.C., 1981. Was the Laramide orogeny related to subduction of an oceanic plateau? *Nature* 289, 276-278.
- Loiselle, M.C., Wones, D.R., 1979. Characteristics and origin of anorogenic granites, Geological Society of America Abstracts with Programs, pp. 468.
- Lu, C.-Z., Wang, Q.-H., Dong, C.-W., Dong, X.-F., 2006. Geochemical characteristics of the Honggong aluminous A-type granite pluton in Zhejiang Province and its tectonic setting. *Geological Journal of China Universities* 12, 500-506.

- Lu, C.-Z., 2007. Geochemical characteristics and tectonic implications of Muchen quartz monzonite pluton in Zhejiang Province. *Geochimica* (in Chinese with English abstract) 36, 457-466.
- Ludwig, K.R., 2008. Isoplot 3.7: A geochronological toolkit for Microsoft Excel. Berkeley Geochronology Center Special Publication 4, 77 pp.
- Ludwig, K.R., 2009. SQUID 2: A User's Manual. Berkeley Geochronology Center Special Publication 5, 110 pp.
- Ma, L.-F., 2007. Geological Atlas of China. Geological Publishing House, Beijing, 348 pp.
- Mamani, M., Wörner, G., Sempere, T., 2010. Geochemical variations in igneous rocks of the Central Andean orocline (13°S to 18°S): Tracing crustal thickening and magma generation through time and space. *Geological Society of America Bulletin* 122, 162-182.
- Mao, J.-R., Takahashi, Y., Kee, W.-S., Li, Z.-L., Ye, H.-M., Zhao, X.-L., Liu, K., Zhou, J., 2011. Characteristics and geodynamic evolution of Indosinian magmatism in South China: A case study of the Guikeng pluton. *Lithos* 127, 535-551.
- Mao, J.-R., Xing, G.-F., Ye, H.-M., Zhao, X.-L., Yu, M.-G., Liu, K., Chen, R., Li, Z.-L., Li, J.-Y., Xu, W.-G., Takahashi, Y., Kee, W.-S., 2013a. Mesozoic-Cenozoic magmatism and mineralization in southeastern China and adjacent regions. Science Press, Beijing, 526 pp.
- Mao, J.-W., Cheng, Y.-B., Chen, M.-H., Pirajno, F., 2013b. Major types and time-space distribution of Mesozoic ore deposits in South China and their geodynamic settings. *Mineralium Deposita* 48, 267-294.
- Matzel, J., Miller, J., Mundil, R., Wooden, J., Mazdab, F., Burgess, S., Paterson, S., Memeti, V., 2007. Growth of the Tuolumne Batholith: zircon crystallization temperature, age and trace element data, AGU Fall Meeting Abstracts, pp. 08.
- McDonough, W.F., Sun, S.s., 1995. The composition of the Earth. *Chemical Geology* 120, 223-253.
- Meng, L.-F., Li, Z.-X., Chen, H.-L., Li, X.-H., Wang, X.-C., 2012. Geochronological and geochemical results from Mesozoic basalts in southern South China Block support the flat-slab subduction model. *Lithos* 132–133, 127-140.
- Metcalfe, I., 2013. Gondwana dispersion and Asian accretion: Tectonic and palaeogeographic evolution of eastern Tethys. *Journal of Asian Earth Sciences* 66, 1-33.
- Miller, C.F., Mittlefehldt, D.W., 1982. Depletion of light rare-earth elements in felsic magmas. *Geology* 10, 129-133.
- Miller, C.F., McDowell, S.M., Mapes, R.W., 2003. Hot and cold granites? Implications of zircon saturation temperatures and preservation of inheritance. *Geology* 31, 529-532.
- Moll-Stalcup, E., Arth, J.G., 1989. The Nature of the Crust in the Yukon-Koyukuk Province as Inferred From the Chemical and Isotopic Composition of Five Late Cretaceous to Early Tertiary Volcanic Fields in Western Alaska. *Journal of Geophysical Research* 94, 15989-16020.
- Montel, J.-M., 1993. A model for monazite/melt equilibrium and application to the generation of granitic magmas. *Chemical Geology* 110, 127-146.
- Moore, G., Carmichael, I.S.E., 1998. The hydrous phase equilibria (to 3 kbar) of an andesite and basaltic andesite from western Mexico: constraints on water content and conditions of phenocryst growth. *Contributions to Mineralogy and Petrology* 130, 304-319.

- Naney, M.T., 1983. Phase equilibria of rock-forming ferromagnesian silicates in granitic systems. *American Journal of Science* 283, 993-1033.
- Nasdala, L., Hofmeister, W., Norberg, N., Martinson, J.M., Corfu, F., Dörr, W., Kamo, S.L., Kennedy, A.K., Kronz, A., Reiners, P.W., Frei, D., Kosler, J., Wan, Y., Götz, J., Häger, T., Kröner, A., Valley, J.W., 2008. Zircon M257 - a Homogeneous Natural Reference Material for the Ion Microprobe U-Pb Analysis of Zircon. *Geostandards and Geoanalytical Research* 32, 247-265.
- O'Hara, M.J., 1961. Zoned Ultrabasic and Basic Gneiss Masses in the Early Lewisian Metamorphic Complex at Scourie, Sutherland. *Journal of Petrology* 2, 248-276.
- Orozco, L.A., Favetto, A., Pomposiello, C., Rossello, E., Booker, J., 2013. Crustal deformation of the Andean foreland at 31°30'S (Argentina) constrained by magnetotelluric survey. *Tectonophysics* 582, 126-139.
- Osborn, E.F., 1959. Role of oxygen pressure in the crystallization and differentiation of basaltic magma. *American Journal of Science* 257, 609-647.
- Osborn, E.F., 1979. The reaction principle. In: Yoder H.S. (Editor), *The evolution of the igneous rocks*. Princeton University Press, Princeton, pp. 288.
- Palme, H., O'Neill, H.S.C., 2003. Cosmochemical Estimates of Mantle Composition. In: Heinrich D.H., Karl K.T. (Editors), *Treatise on geochemistry*. Pergamon, Oxford, pp. 1-38.
- Patiño Douce, A.E., Humphreys, E.D., Dana Johnston, A., 1990. Anatexis and metamorphism in tectonically thickened continental crust exemplified by the Sevier hinterland, western North America. *Earth and Planetary Science Letters* 97, 290-315.
- Patiño Douce, A.E., Beard, J.S., 1995. Dehydration-melting of Biotite Gneiss and Quartz Amphibolite from 3 to 15 kbar. *Journal of Petrology* 36, 707-738.
- Patiño Douce, A.E., Beard, J.S., 1996. Effects of P, f(O<sub>2</sub>) and Mg/Fe Ratio on Dehydration Melting of Model Metagreywackes. *Journal of Petrology* 37, 999-1024.
- Patiño Douce, A.E., McCarthy, T.C., 1998. Melting of crustal rocks during continental collision and subduction. In: Bradley R.H., Liou J.G. (Editors), *When Continents Collide: Geodynamics and Geochemistry of Ultrahigh-Pressure Rocks*. Dordrecht: Kluwer Academic, pp. 27-55.
- Peacock, M.A., 1931. Classification of Igneous Rock Series. *The Journal of Geology* 39, 54-67.
- Pearce, J.A., Harris, N.B.W., Tindle, A.G., 1984. Trace Element Discrimination Diagrams for the Tectonic Interpretation of Granitic Rocks. *Journal of Petrology* 25, 956-983.
- Pearce, J.A., Peate, D.W., 1995. Tectonic Implications of the Composition of Volcanic Arc Magmas. *Annual Review of Earth and Planetary Sciences* 23, 251-285.
- Peccerillo, A., Taylor, S., 1976. Geochemistry of Eocene calc-alkaline volcanic rocks from the Kastamonu area, northern Turkey. *Contributions to Mineralogy and Petrology* 58, 63-81.
- Prajno, F., Bagas, L., 2002. Gold and silver metallogeny of the South China Fold Belt: a consequence of multiple mineralizing events? *Ore Geology Reviews* 20, 109-126.
- Pitcher, W.S., 1997. The nature and origin of granite. Chapman & Hall, 387 pp.
- Qi, C.-S., Deng, X.-G., Li, X.-H., Li, W.-X., Yang, Y.-H., Xie, L.-W., 2007. Origin of the Darongshan-Shiwanashan S-type granitoid belt from southeastern Guangxi: geochemical and Sr-Nd-Hf isotopic constraints. *Acta Petrologica Sinica* 23, 403-412.

- Qian, Q., Hermann, J., 2013. Partial melting of lower crust at 10–15 kbar: constraints on adakite and TTG formation. *Contributions to Mineralogy and Petrology* 165, 1195-1224.
- Qin, S.-C., 2007. Geochronology and geochemistry of Cretaceous mafic volcanic rocks from Zhejiang and Fujian Provinces, SE China: petrogenesis and geodynamic implication for lithospheric extension, The Chinese Academy of Sciences, Guangzhou, 113 pp.
- Qiu, J.-S., Liu, L., Li, Z., 2011. Zircon U-Pb geochronology and Sr-Nd-Hf isotopic geochemistry of quartz syenite from Wanghaigang pluton in Huangyan County, Zhejiang Province and their implications for petrogenesis. *Acta Petrologica Sinica* 27, 1557-1572.
- Qiu, J.-T., Yu, X.-Q., Santosh, M., Zhang, D.-H., Chen, S.-Q., Li, P.-J., 2013. Geochronology and magmatic oxygen fugacity of the Tongcun molybdenum deposit, northwest Zhejiang, SE China. *Mineralium Deposita*, 1-12.
- Qiu, L., Yan, D.-P., Zhou, M.-F., Arndt, N., Tang, S.-L., Qi, L., 2014. Geochronology and geochemistry of the Late Triassic Longtan pluton in South China: termination of the crustal melting and Indosinian orogenesis. *International Journal of Earth Sciences*, 1-18.
- Ramos, V.A., Cristallini, E.O., Pérez, D.J., 2002. The Pampean flat-slab of the Central Andes. *Journal of South American Earth Sciences* 15, 59-78.
- Ramos, V.A., 2009. Anatomy and global context of the Andes: main geologic features and the Andean orogenic cycle. *Geological Society of America Memoir* 204, 31-65.
- Ramos, V.A., Folguera, A., 2009. Andean flat-slab subduction through time. *Geological Society Special Publications* 327, 31-54.
- Rankama, K., Sahama, T.G., 1950. *Geochemistry*. The University of Chicago Press, 912 pp.
- Ren, H.-T., Wu, J.-Q., Ye, X.-F., Ling, H.-F., Chen, P.-R., 2013. Zircon U-Pb age and geochemical characteristics of peraluminous fine-grained granite in western part of the Fucheng pluton, Jiangxi Province. *Geological Journal of China Universities* 19, 327-345.
- Richards, J.P., 2011. High Sr/Y arc magmas and porphyry Cu ± Mo ± Au deposits: just add water. *Economic Geology* 106, 1075-1081.
- Ringwood, A.E., 1955. The principles governing trace-element behaviour during magmatic crystallization: Part II. The role of complex formation. *Geochimica et Cosmochimica Acta* 7, 242-254.
- Robb, L., 2005. *Introduction to ore-forming processes*. Blackwell Publishing, Malden, MA.
- Roberts, M.P., Clemens, J.D., 1993. Origin of high-potassium, calc-alkaline, I-type granitoids. *Geology* 21, 825-828.
- Rudnick, R., Fountain, D., 1995. Nature and composition of the continental crust: a lower crustal perspective. *Rev. Geophysys* 33, 267–309.
- Rudnick, R.L., Gao, S., 2003. Composition of the Continental Crust. In: Heinrich D.H., Karl K.T. (Editors), *Treatise on geochemistry*. Pergamon, Oxford, pp. 1-64.
- Russell, W.A., Papanastassiou, D.A., Tombrello, T.A., 1978. Ca isotope fractionation on the Earth and other solar system materials. *Geochimica et Cosmochimica Acta* 42, 1075-1090.

- Söderlund, U., Patchett, P.J., Vervoort, J.D., Isachsen, C.E., 2004. The  $^{176}\text{Lu}$  decay constant determined by Lu–Hf and U–Pb isotope systematics of Precambrian mafic intrusions. *Earth and Planetary Science Letters* 219, 311-324.
- Sawyer, E.W., Cesare, B., Brown, M., 2011. When the Continental Crust Melts. *Elements* 7, 229-234.
- Sewell, R.J., Campbell, S.D.G., 1997. Geochemistry of coeval Mesozoic plutonic and volcanic suites in Hong Kong. *Journal of the Geological Society* 154, 1053-1066.
- Sewell, R.J., Tang, L.K.D., Shaw, R., 2009. Hong Kong Geology—A 400-million year journey. The Government of the Hong Kong Special Administrative Region, 158 pp.
- Shand, S.J., 1947. Eruptive Rocks. Their Genesis, Composition, Classification, and Their Relation to Ore-Deposits. J. Wiley & Sons, New York.
- Shen, W.-Z., Ling, H.-F., Li, W.-X., Wang, D.-Z., 2000. Crust evolution in Southeast China: evidence from Nd model ages of granitoids. *Science in China Series D: Earth Sciences* 43, 36-49.
- Sheng, M.-T., Zhou, Y., Zhang, X.-D., Wu, B., 2013. LA-MC-ICP-MS zircon U-Pb dating, geochemical features of the two granites in Hugang area, southwestern Fujian and their geological significances. *Geological Review* 59, 369-381.
- Shervais, J.W., 1982. Ti-V plots and the petrogenesis of modern and ophiolitic lavas. *Earth and Planetary Science Letters* 59, 101-118.
- Shu, X.-J., Wang, X.-L., Sun, T., Chen, W.-F., Shen, W.-Z., 2013. Crustal formation in the Nanling Range, South China Block: Hf isotope evidence of zircons from Phanerozoic granitoids. *Journal of Asian Earth Sciences* 74, 210-224.
- Sobolev, S.V., Babeyko, A.Y., 2005. What drives orogeny in the Andes? *Geology* 33, 617-620.
- Spear, F.S., 1995. Metamorphic phase equilibria and pressure-temperature-time paths. *Mineralogical Society of America Washington, Washington, D.C.*, 799 pp.
- Stein, H.J., Crock, J.G., 1990. Late Cretaceous-Tertiary magmatism in the Colorado mineral belt: Rare earth element and samarium-neodymium isotopic studies. In: Anderson J.L. (Editor), *Geological Society of America Memoir*, pp. 195-223.
- Streckeisen, A., 1974. Classification and nomenclature of plutonic rocks recommendations of the IUGS subcommission on the systematics of Igneous Rocks. *Geologische Rundschau* 63, 773-786.
- Su, H.-M., Mao, J.-W., Santosh, M., Xie, G.-Q., 2013a. Petrogenesis and tectonic significance of Late Jurassic - Early Cretaceous volcanic - intrusive complex in the Tianhuashan basin, South China. *Ore Geology Reviews* 56, 566–583.
- Su, Y.-P., Zheng, J.-P., Griffin, W.L., Zhao, J.-H., O'Reilly, S.Y., Tang, H.-Y., Ping, X.-Q., Xiong, Q., 2013b. Petrogenesis and geochronology of Cretaceous adakitic, I- and A-type granitoids in the NE Yangtze block: Constraints on the eastern subsurface boundary between the North and South China blocks. *Lithos* 175–176, 333-350.
- Sun, S.-s., McDonough, W.F., 1989. Chemical and isotopic systematics of oceanic basalts: implications for mantle composition and processes. *Geological Society, London, Special Publications* 42, 313-345.

- Sun, T., 2006. A new map showing the distribution of granites in South China and its explanatory notes. *Geological Bulletin of China* 25, 332-337.
- Sun, Y., Ma, C.-Q., Liu, Y.-Y., She, Z.-B., 2011. Geochronological and geochemical constraints on the petrogenesis of late Triassic aluminous A-type granites in southeast China. *Journal of Asian Earth Sciences* 42, 1117-1131.
- Swanson, S.E., 1977. Relation of nucleation and crystal-growth rate to the development of granitic textures. *American Mineralogist* 62, 966-978.
- Tang, Y.-W., Xie, Y.-L., Li, Y.-X., Qiu, L.-M., Liu, B.-S., Li, Y., Zhang, X.-X., Jiang, Y.-C., Han, Y.-D., 2012a. Petrogeochemical and petrographic characteristics and genesis of Wushanguan complex body in Anji ore district, Zhejiang Province. *Mineral Deposits* 31, 903-916.
- Tang, Y.-W., Xie, Y.-L., Li, Y.-X., Qiu, L.-M., Liu, B.-S., Li, Y., Zhang, X.-X., Jiang, Y.-C., Han, Y.-D., Zhou, J.-J., 2012b. Geochemical characteristics and zircon LA-ICP-MS U-Pb ages of quartz-monzonite porphyry in Anji polymetallic ore district of Zhejiang and their geological implications. *Geoscience* 26, 647-655.
- Tang, Y.-W., Xie, Y.-L., Li, Y.-X., Qiu, L.-M., Zhang, X.-X., Han, Y.-D., Jiang, Y.-C., 2013. LA-ICP-MS ages, geochemical characteristics of the zircons from Wushanguan complex body in Anji mining area, northwestern Zhejiang and their geological significances. *Geological Review* 59, 702-715.
- Tao, J.-H., Li, W.-X., Li, X.-H., Cen, T., 2013. Petrogenesis of early Yanshanian highly evolved granites in the Longyuanba area, southern Jiangxi Province: Evidence from zircon U-Pb dating, Hf-O isotope and whole-rock geochemistry. *Science China Earth Sciences* 56, 922-939.
- Tatsumi, Y., Eggins, S., 1995. Subduction Zone Magmatism.
- Tatsumi, Y., Kogiso, T., 2003. The subduction factory: its role in the evolution of the Earth's crust and mantle. *Geological Society, London, Special Publications* 219, 55-80.
- Thirlwall, M.F., Anczkiewicz, R., 2004. Multidynamic isotope ratio analysis using MC-ICP-MS and the causes of secular drift in Hf, Nd and Pb isotope ratios. *International Journal of Mass Spectrometry* 235, 59-81.
- Tilley, C.E., 1950. Some aspects of magmatic evolution. *Quarterly Journal of the Geological Society* 106, 37-61.
- Tuttle, O.F., Bowen, N.L., 1958. Origin of granite in the light of experimental studies in the system NaAlSi<sub>3</sub>O<sub>8</sub>-KAiSi<sub>3</sub>O<sub>8</sub>-SiO<sub>2</sub>-H<sub>2</sub>O. *The Geological Society of America, New York*, 153 pp.
- Vielzeuf, D., Holloway, J.R., 1988. Experimental determination of the fluid-absent melting relations in the pelitic system. *Contributions to Mineralogy and Petrology* 98, 257-276.
- Villaseca, C., Orejana, D., Paterson, B.A., 2007. Zr-LREE rich minerals in residual peraluminous granulites, another factor in the origin of low Zr-LREE granitic melts? *Lithos* 96, 375-386.
- Wang, C.-M., Zhang, D., Wu, G.-G., Xu, Y.-G., Carranza, E., Zhang, Y.-Y., Li, H.-K., Geng, J.-Z., 2013a. Zircon U-Pb geochronology and geochemistry of rhyolitic tuff, granite porphyry and syenogranite in the Lengshuikeng ore district, SE China: Implications for a continental arc to intra-arc rift setting. *Journal of Earth System Science* 122, 809-830.

- Wang, G.-G., Ni, P., Zhao, K.-D., Wang, X.-L., Liu, J.-Q., Jiang, S.-Y., Chen, H., 2012a. Petrogenesis of the Middle Jurassic Yinshan volcanic-intrusive complex, SE China: Implications for tectonic evolution and Cu-Au mineralization. *Lithos* 150, 135-154.
- Wang, K.-X., Chen, P.-R., Chen, W.-F., Ling, H.-F., Zhao, K.-D., Yu, Z.-Q., 2012b. Magma mingling and chemical diffusion in the Taojiang granitoids in the Hunan Province, China: evidences from petrography, geochronology and geochemistry. *Mineralogy and Petrology*, 1-22.
- Wang, K.-X., Sun, T., Chen, P.-R., Ling, H.-F., Xiang, T.-F., 2013b. The geochronological and geochemical constraints on the petrogenesis of the Early Mesozoic A-type granite and diabase in northwestern Fujian province. *Lithos*.
- Wang, Q., Li, J.-W., Jian, P., Zhao, Z.-H., Xiong, X.-L., Bao, Z.-W., Xu, J.-F., Li, C.-F., Ma, J.-L., 2005a. Alkaline syenites in eastern Cathaysia (South China): link to Permian-Triassic transtension. *Earth and Planetary Science Letters* 230, 339-354.
- Wang, Q., Xu, J.-F., Jian, P., Bao, Z.-W., Zhao, Z.-H., Li, C.-F., Xiong, X.-L., Ma, J.-L., 2006. Petrogenesis of adakitic porphyries in an extensional tectonic setting, Dexing, South China: implications for the genesis of porphyry copper mineralization. *Journal of Petrology* 47, 119-144.
- Wang, X.-C., Li, X.-H., Li, W.-X., Li, Z.-X., 2007a. Ca. 825 Ma komatiitic basalts in South China: First evidence for >1500 °C mantle melts by a Rodinian mantle plume. *Geology* 35, 1103.
- Wang, X.-L., Zhao, G.-C., Zhou, J.-C., Liu, Y.-S., Hu, J., 2008a. Geochronology and Hf isotopes of zircon from volcanic rocks of the Shuangqiaoshan Group, South China: Implications for the Neoproterozoic tectonic evolution of the eastern Jiangnan orogen. *Gondwana Research* 14, 355-367.
- Wang, X.-L., Jiang, S.-Y., Dai, B.-Z., 2010. Melting of enriched Archean subcontinental lithospheric mantle: Evidence from the ca. 1760 Ma volcanic rocks of the Xiong'er Group, southern margin of the North China Craton. *Precambrian Research* 182, 204-216.
- Wang, Y.-J., Zhang, Y.-H., Fan, W.-M., Peng, T.-P., 2005b. Structural signatures and  $^{40}\text{Ar}/^{39}\text{Ar}$  geochronology of the Indosinian Xuefengshan tectonic belt, South China Block. *Journal of Structural Geology* 27, 985-998.
- Wang, Y.-J., Fan, W.-M., Sun, M., Liang, X.-Q., Zhang, Y.-H., Peng, T.-P., 2007b. Geochronological, geochemical and geothermal constraints on petrogenesis of the Indosinian peraluminous granites in the South China Block: A case study in the Hunan Province. *Lithos* 96, 475-502.
- Wang, Y.-J., Fan, W.-M., Cawood, P.A., Li, S.-Z., 2008b. Sr-Nd-Pb isotopic constraints on multiple mantle domains for Mesozoic mafic rocks beneath the South China Block hinterland. *Lithos* 106, 297-308.
- Wang, Y.-X., Zhao, Z.-H., Bao, Z.-W., Li, X.-H., 1997. Geochemistry of granitoids from Zhejiang province and crustal evolution- I. Phanerozoic granitoids. *Geochemica* 26, 1-15.
- Watson, E.B., 1979. Zircon saturation in felsic liquids: Experimental results and applications to trace element geochemistry. *Contributions to Mineralogy and Petrology* 70, 407-419.
- Wedepohl, K.H., 1973. *Handbook of geochemistry*. Springer-Verlag.

- Wei, D.-F., Bao, Z.-Y., Fu, J.-M., 2007. Geochemical characteristics and zircon SHRIMP U-Pb dating of the Tongshanling granite in Hunan Province, South China. *Geotectonica et Metallogenica* 31, 482-489.
- Whalen, J.B., Currie, K.L., Chappell, B.W., 1987. A-type granites: geochemical characteristics, discrimination and petrogenesis. *Contributions to Mineralogy and Petrology* 95, 407-419.
- White, A., 1979. Sources of granite magmas, Geological Society of America, Abstracts with Programs, pp. 539.
- Whitney, J.A., 1988. The origin of granite: The role and source of water in the evolution of granitic magmas. *Geological Society of America Bulletin* 100, 1886-1897.
- Willis, G.C., 1999. The Utah thrust system-an overview.
- Winter, J.D.N., 2010. Principles of igneous and metamorphic petrology. Prentice Hall.
- Wones, D.R., 1989. Significance of the assemblage titanite+magnetite+quartz in granitic rocks. *American Mineralogist* 74, 744-749.
- Wong, J., Sun, M., Xing, G.-F., Li, X.-H., Zhao, G.-C., Wong, K., Yuan, C., Xia, X.-P., Li, L.-M., Wu, F.-Y., 2009. Geochemical and zircon U-Pb and Hf isotopic study of the Baijuhuajian metaluminous A-type granite: Extension at 125-100 Ma and its tectonic significance for South China. *Lithos* 112, 289-305.
- Wong, J., Sun, M., Xing, G.-F., Li, X.-H., Zhao, G.-C., Wong, K., Wu, F.-Y., 2011. Zircon U-Pb and Hf isotopic study of Mesozoic felsic rocks from eastern Zhejiang, South China: Geochemical contrast between the Yangtze and Cathaysia blocks. *Gondwana Research* 19, 244-259.
- Wong, P.-W., 2006. Mesozoic magmatic activity in Hong Kong, The University of Hong Kong, Hong Kong, 199 pp.
- Woodhead, J., Hergt, J., Shelley, M., Eggins, S., Kemp, R., 2004. Zircon Hf-isotope analysis with an excimer laser, depth profiling, ablation of complex geometries, and concomitant age estimation. *Chemical Geology* 209, 121-135.
- Woodhead, J., Hergt, J., 2005. A preliminary appraisal of seven natural zircon reference materials for in situ Hf isotope determination. *Geostandards and Geoanalytical Research* 29, 183-195.
- Wu, F.-Y., Ji, W.-Q., Sun, D.-H., Yang, Y.-H., Li, X.-H., 2012. Zircon U-Pb geochronology and Hf isotopic compositions of the Mesozoic granites in southern Anhui Province, China. *Lithos* 150, 6-25.
- Wu, L.-Y., Hu, R.-Z., Qi, Y.-Q., Zhu, J.-J., 2013. Zircon LA-ICP-MS U-Pb ages and geochemical characteristics of quartz syenite porphyry from Jintonghu deposit in Zijinshan ore field, Fujian Province, South China. *Acta Petrologica Sinica* 29, 4151-4166.
- Wyllie, P.J., Carroll, M.R., Johnston, A.D., Rutter, M.J., Sekine, T., Van der Laan, S.R., 1989. Interactions among magmas and rocks in subduction zone regions; experimental studies from slab to mantle to crust. *European Journal of Mineralogy* 1, 165-179.
- Xia, Y., Xu, X.-S., Zhu, K.-Y., 2012. Paleoproterozoic S- and A-type granites in southwestern Zhejiang: Magmatism, metamorphism and implications for the crustal evolution of the Cathaysia basement. *Precambrian Research* 216–219, 177-207.

- Xiang, H., Zhang, L., Zhou, H.-W., Zhong, Z.-Q., Zeng, W., Liu, R., Jin, S., 2008. U-Pb zircon geochronology and Hf isotope study of metamorphosed basic-ultrabasic rocks from metamorphic basement in southwestern Zhejiang: The response of the Cathaysia Block to Indosinian orogenic event. *Science in China Series D: Earth Sciences* 51, 788-800.
- Xiang, T.-F., Sun, T., Chen, P.-R., Wang, K.-X., 2013. Discovery of an Indosinian granite: Luoguyan pluton in northwestern Fujian Province, South China, and its petrogenesis and tectonic significance. *Geological Journal of China Universities* 19, 274-292.
- Xiao, W.-J., He, H.-Q., 2005. Early Mesozoic thrust tectonics of the northwest Zhejiang region (Southeast China). *Geological Society of America Bulletin* 117, 945-961.
- Xie, H.-S., Zhang, J.-F., Gong, R.-J., Xu, X.-M., 2013. Geochemistry and tectonic significance of Late Mesozoic intrusive rock in Xiaoshan-Zhuji region, Northwest Zhejiang. *Contributions to Geology and Mineral Resources Research* 28, 424-433.
- Xie, J.-C., Chen, S., Rong, W., Li, Q.-Z., Yang, X.-Y., Sun, W.-D., 2012a. Geochronology, geochemistry and tectonic significance of Guniujiang A-type granite in Anhui Province. *Acta Petrologica Sinica* 28, 4007-4020.
- Xie, Y.-C., 2013. Genesis of the granodiorite porphyry and sources of metallogenetic materials in the Baoshan Pb-Zn polymetallic deposit, southern Hunan Province Nanjing University, Nanjing, 104 pp.
- Xie, Y.-L., Tang, Y.-W., Li, Y.-X., Li, Y., Liu, B.-S., Qiu, L.-M., Zhang, X.-X., Jiang, Y.-C., 2012b. Magmatic intrusive series and their implication for the ore prospecting in Anji exploration area, Zhejiang Province. *Acta Petrologica Sinica* 28, 3334-3346.
- Xie, Y.-L., Tang, Y.-W., Li, Y.-X., Qiu, L.-M., Liu, B.-S., Li, Y., Zhang, X.-X., Han, Y.-D., Jiang, Y.-C., 2012c. Petrochemistry, chronology and ore-forming geological significance of fine-crystalline granite in Anji polymetallic deposit of Zhejiang Province. *Mineral Deposits* 31, 891-902.
- Xirouchakis, D., Lindsley, D.H., Frost, B.R., 2001. Assemblages with titanite ( $\text{CaTiOSiO}_4$ ), Ca-Mg-Fe olivine and pyroxenes, Fe-Mg-Ti oxides, and quartz: Part II. Application. *American Mineralogist* 86, 254-264.
- Xu, H.-J., Ma, C.-Q., Zhao, J.-H., Zhang, J.-F., 2013. Petrogenesis of Dashenshan I-type granodiorite: implications for Triassic crust-mantle interaction, South China. *International Geology Review*, 1-19.
- Xu, J.-F., Shinjo, R., Defant, M.J., Wang, Q., Rapp, R.P., 2002. Origin of Mesozoic adakitic intrusive rocks in the Ningzhen area of east China: Partial melting of delaminated lower continental crust? *Geology* 30, 1111-1114.
- Xu, K.-Q., Sun, N., Wang, D.-Z., Hu, S.-X., 1963. Investigation on the polycyclic granite intrusions of southern China, with special notice on their ages of intusions, distribution, characteristics, and their genetic relations to mineral deposits. *Acta Geologica Sinica* 43, 141-155.
- Xu, K.-Q., Sun, N., Wang, D.-Z., Hu, S.-X., Liu, Y.-J., Ji, S.-Y., 1982. On the origin and metallogeny of the granites in South China. In: Xu K.-Q., Tu G.-C. (Editors), *Geology of granites and their metallogenetic relations*. Science Press, Beijing, pp. 1-20.

- Xu, X.-S., O'Reilly, S.Y., Griffin, W.L., Wang, X.-L., Pearson, N.J., He, Z.-Y., 2007. The crust of Cathaysia: Age, assembly and reworking of two terranes. *Precambrian Research* 158, 51-78.
- Xu, X.-S., Suzukl, K., Liu, L., Wang, D.-Z., 2010. Petrogenesis and tectonic implications of Late Mesozoic granites in the NE Yangtze Block, China: further insights from the Jiuhuashan-Qingyang complex. *Geological Magazine* 147, 219-232.
- Yang, S.-Y., Jiang, S.-Y., Jiang, Y.-H., Zhao, K.-D., Fan, H.-H., 2010. Zircon U-Pb geochronology, Hf isotopic composition and geological implications of the rhyodacite and rhyodacitic porphyry in the Xiangshan uranium ore field, Jiangxi Province, China. *Science in China Series D: Earth Sciences* 40, 953-969.
- Yang, S.-Y., Jiang, S.-Y., Zhao, K.-D., Jiang, Y.-H., Ling, H.-F., Luo, L., 2012. Geochronology, geochemistry and tectonic significance of two Early Cretaceous A-type granites in the Gan-Hang Belt, Southeast China. *Lithos* 150, 155-170.
- Yang, S.-Y., Jiang, S.-Y., Zhao, K.-D., Jiang, Y.-H., 2013a. Petrogenesis and tectonic significance of Early Cretaceous high-Zr rhyolite in the Dazhou uranium district, Gan-Hang Belt, Southeast China. *Journal of Asian Earth Sciences* 74, 303-315.
- Yang, S.-Y., Jiang, S.-Y., Zhao, K.-D., Jiang, Y.-H., 2013b. Petrogenesis and tectonic significance of Early Cretaceous high-Zr rhyolite in the Dazhou uranium district, Gan-Hang Belt, Southeast China. *Journal of Asian Earth Sciences*.
- Yang, Y.-T., 2013. An unrecognized major collision of the Okhotomorsk Block with East Asia during the Late Cretaceous, constraints on the plate reorganization of the Northwest Pacific. *Earth-Science Reviews* 126, 96-115.
- Yao, Y., Chen, J., Lu, J.-J., Zhang, R.-Q., 2013. Geochronology, Hf isotopic compositions and geochemical characteristics of Xitian A-type granite and its geological significance. *Mineral Deposits* 32, 467-488.
- Yardley, B.W.D., Valley, J.W., 1997. The petrologic case for a dry lower crust. *J. Geophys. Res.* 102, 12173-12185.
- Ye, H.-M., Mao, J.-R., Zhao, X.-L., Liu, K., Chen, D.-D., 2013. Revisiting Early-Middle Jurassic igneous activity in the Nanling Mountains, South China: Geochemistry and implications for regional geodynamics. *Journal of Asian Earth Sciences* 72, 108-117.
- Ye, M.-F., Li, X.-H., Li, W.-X., Liu, Y., Li, Z.-X., 2007. SHRIMP zircon U-Pb geochronological and whole-rock geochemical evidence for an early Neoproterozoic Sibaoan magmatic arc along the southeastern margin of the Yangtze Block. *Gondwana Research* 12, 144-156.
- Yen, C.-M., 2005. Mineral chemistry and geochemistry of the Xiaojiang-Liangnong Complexes and their enclaves in Zhejiang, National Taiwan University, Taipei, 138 pp.
- Yoder, H.S., Stewart, D.B., Smith, J.R., 1957. Ternary feldspars. In: Washington C.I.o. (Editor), Year book, Washington, D.C., pp. 206-214.
- Yu, J.-H., Zhou, X.-M., Zhao, L., Jiang, S.-y., Wang, L.-J., Ling, H.-F., 2005. Mantle-crust interaction generating the Wuping granites: evidenced from Sr-Nd-Hf-U-Pb isotopes. *Acta Petroiogica Sinica* 21, 651-664.

- Yu, J.-H., O'Reilly, S.Y., Wang, L.-J., Griffin, W.L., Jiang, S.-Y., Wang, R.-C., Xu, X.-S., 2007. Finding of ancient materials in Cathaysia and implication for the formation of Precambrian crust. *Chinese Science Bulletin* 52, 13-22.
- Yu, J.-H., Wang, L.-J., O'Reilly, S.Y., Griffin, W.L., Zhang, M., Li, C.-Z., Shu, L.-S., 2009. A Paleoproterozoic orogeny recorded in a long-lived cratonic remnant (Wuyishan terrane), eastern Cathaysia Block, China. *Precambrian Research* 174, 347-363.
- Yu, J.-H., O'Reilly, S.Y., Zhou, M.-F., Griffin, W.L., Wang, L., 2012a. U-Pb geochronology and Hf-Nd isotopic geochemistry of the Badu Complex, Southeastern China: Implications for the Precambrian crustal evolution and paleogeography of the Cathaysia Block. *Precambrian Research* 222–223, 424-449.
- Yu, Y., Chen, Z.-Y., Chen, Z.-H., Hou, K.-J., Zhao, Z., XU, J.-X., Zhang, J.-J., Zeng, H.-L., 2012b. Zircon U-Pb dating and mineralization prospective of the Triassic Qingxi Pluton in southern Jiangxi Province. *Geotectonica et Metallogenica* 36, 413-421.
- Yue, F., 2008. The relationship between lithology characteristics and mineralization of Xuetangkeng molybdenum mineral deposit in Longyan City, Fujian Province, Central South University, Changsha, 58 pp.
- Zeng, J.-N., Li, J.-W., Chen, J.-H., Lu, J.-P., 2013a. SHRIMP zircon U-Pb dating of Anjishan intrusive rocks in Ningzhen District, Jiangsu, and its geological significance. *Earth Science-Journal of China University of Geosciences* 38, 57-67.
- Zeng, Q.-D., Wang, Y.-B., Zhang, S., Liu, J.-M., Qin, K.-Z., Yang, J.-H., Sun, W.-D., Qu, W.-J., 2013b. U-Pb and Re-Os Geochronology of the Tongcun Molybdenum Deposit and Zhilingtou Gold-Silver Deposit in Zhejiang Province, Southeast China, and Its Geological Implications. *Resource Geology* 63, 99-109.
- ZGS, 1965. Regional Geology of Jiande area, Zhejiang Province. Bureau of Geology and Mineral Resources of Zhejiang Province, Meicheng, 162 pp.
- ZGS, 1966. Regional Geology of Jinhua area, Zhejiang Province. Bureau of Geology and Mineral Resources of Zhejiang Province, Meicheng, 117 pp.
- ZGS, 1975. Regional Geology of Zhuji area, Zhejiang Province. Bureau of Geology and Mineral Resources of Zhejiang Province, Meicheng, 722 pp.
- ZGS, 1980. Regional Geology of Ningbo, Yuyao, Shengsi, Dinghai, Shenjiamen area, Zhejiang Province. Bureau of Geology and Mineral Resources of Zhejiang Province, Meicheng, 475 pp.
- ZGS, 1989. Regional geology of Zhejiang Province Geological memoirs, 11. Geological Publishing House, Beijing, 688 pp.
- Zhang, C.-S., Su, H.-M., Miao, Y., Hu, Z.-G., 2012a. Zircon U-Pb age and Nd-Sr-Pb isotopic characteristics of Dayang-Juzhou granite in Longyan, Fujian Province and its geological significance. *Acta Petroiogica Sinica* 28, 225-242.
- Zhang, H., Ling, M.-X., Liu, Y.-L., Tu, X.-L., Wang, F.-Y., Li, C.-Y., Liang, H.-Y., Yang, X.-Y., Arndt, N.T., Sun, W.-D., 2013. High Oxygen Fugacity and Slab Melting Linked to Cu Mineralization: Evidence from Dexing Porphyry Copper Deposits, Southeastern China. *The Journal of Geology* 121, 289-305.

- Zhang, J.-J., Wang, G.-J., Yang, X.-Y., Sun, W.-D., Dai, S.-Q., 2012b. The petrogenesis of the Jingde granodiorite and its MMEs: constraints from geochemistry, zircon U-Pb dating and Hf isotopic compositions. *Acta Petrologica Sinica* 28, 4047-4063.
- Zhang, R.-Q., Lu, J.-J., Zhu, J.-C., Yao, Y., Gao, J.-F., Chen, W.-F., Zhao, Z.-J., 2010. Zircon U-Pb geochronology and Hf isotopic compositions of Hehuaping granite porphyry, southern hunan province, and its geological significance. *Geological Journal of China Universities* 16, 436-447.
- Zhang, X.-F., Liu, X.-D., Liu, J.-Z., 2011. Geochemical characteristics of the Huashan granites in Guangxi Province and their uranium-bearing potential. *Geology and Exploration* 47, 1050-1058.
- Zhang, Z.-J., Badal, J., Li, Y.-K., Chen, Y., Yang, L.-Q., Teng, J.-W., 2005. Crust–upper mantle seismic velocity structure across Southeastern China. *Tectonophysics* 395, 137-157.
- Zhao, J.-H., Zhou, M.-F., Yan, D.-P., Zheng, J.-P., Li, J.-W., 2011a. Reappraisal of the ages of Neoproterozoic strata in South China: No connection with the Grenvillian orogeny. *Geology* 39, 299-302.
- Zhao, K.-D., Jiang, S.-Y., Zhu, J.-C., Li, L., Dai, B.-Z., Jiang, Y.-H., Ling, H.-F., 2010. Hf isotopic composition of zircons from the Huashan-Guposhan intrusive complex and their mafic enclaves in northeastern Guangxi: Implication for petrogenesis. *Chinese Science Bulletin* 55, 509-519.
- Zhao, K.-D., Jiang, S.-Y., Dong, C.-Y., Chen, W.-F., Chen, P.-R., Ling, H.-F., Zhang, J., Wang, K.-X., 2011b. Uranium-bearing and barren granites from the Taoshan Complex, Jiangxi Province, South China: Geochemical and petrogenetic discrimination and exploration significance. *Journal of Geochemical Exploration* 110, 126-135.
- Zhao, K.-D., Jiang, S.-Y., Chen, W.-F., Chen, P.-R., Ling, H.-F., 2013a. Zircon U–Pb chronology and elemental and Sr–Nd–Hf isotope geochemistry of two Triassic A-type granites in South China: Implication for petrogenesis and Indosinian transtensional tectonism. *Lithos* 160–161, 292-306.
- Zhao, K.-D., Li, J.-R., Ling, H.-F., Chen, P.-R., Chen, W.-F., Sun, T., 2013b. Geochronology, geochemistry and petrogenesis of two-stage Indosinian granites from the Xiajiang uranium ore deposit, Jiangxi Province: implication for Indosinian tectonics and genesis of uranium-bearing granites in South China. *Acta Petroiogica Sinica* 29, 4349-4361.
- Zhao, L., Yu, J.-H., Xie, L., 2004. Geochemistry and origin of the Hongshan topaz-bearing leucogranites in southwestern Fujian Province. *Geochimica* 33, 372-386.
- Zhao, L., Yu, J.-H., Wang, L.-J., Xie, L., Sun, T., Qiu, J.-S., 2006. Formation time of Hongshan topaz-bearing granite and its metallogenetic potential prognosis. *Mineral Deposits* 25, 672-682.
- Zhao, X.-L., 2007. The geochronology, petrography and geochemical characteristics of Mesozoic granitoids from Shanghang area in SW Fujian and their implicationa, Chinese Academy of Geological Sciences, Beijing, 57 pp.
- Zheng, J.-H., Guo, C.-L., 2012. Geochronology, geochemistry and zircon Hf isotopes of the Wangxianling granitic intrusion in South Hunan Province and its geological significance. *Acta Petroiogica Sinica* 28, 75-90.

- Zheng, J.-L., Ruan, H.-H., Xie, J.-Y., Ge, Y.-M., Xu, Z.-L., 1990. Research on petrogenesis of Shantouzheng volcano-intrusive complex. *Bulletin of the Nanjing Institute of Geology and Mineral Resources, Chinese Academy of Geological Sciences* 11, 58-70.
- Zhong, Y.-F., Ma, C.-Q., Yu, Z.-B., Xu, H.-J., 2011. U-Pb-Hf isotope of zircons, geochemistry and genesis of Mengshan granitoids in northwestern Jiangxi Province. *Earth Science-Journal of China University of Geosciences* 36, 703-720.
- Zhou, J.-C., Wang, D.-Z., Wang, X., Chen, X.-M., 1999. An understanding of the origin of the Tonglu Early Cretaceous volcanic-intrusive rocks. *Acta Petrologica Sinica* 15, 263-271.
- Zhou, J., Jiang, Y.-H., Xing, G., Zeng, Y., Ge, W., 2013. Geochronology and petrogenesis of Cretaceous A-type granites from the NE Jiangnan Orogen, SE China. *International Geology Review*, 1-25.
- Zhou, Q., Jiang, Y.-H., Zhang, H.-H., Liao, S.-Y., Jin, G.-D., Zhao, P., Jia, R.-Y., Liu, Z., 2012a. Mantle origin of the Dexing porphyry copper deposit, SE China. *International Geology Review* 55, 337-349.
- Zhou, X.-M., Li, W.-X., 2000. Origin of Late Mesozoic igneous rocks in Southeastern China: implications for lithosphere subduction and underplating of mafic magmas. *Tectonophysics* 326, 269-287.
- Zhou, X.-M., Sun, T., Shen, W.-Z., Shu, L.-S., Niu, Y.-L., 2006. Petrogenesis of Mesozoic granitoids and volcanic rocks in South China: A response to tectonic evolution. *Episodes* 29, 26-33.
- Zhou, X., Yu, X.-Q., Yang, H.-M., Wang, D.-E., Du, Y.-D., Ke, H.-B., 2012b. Petrogenesis and geochronology of the high Ba-Sr Kaobeijian granodiorite porphyry, Jixi County, South Anhui Province. *Acta Petrologica Sinica* 28, 3403-3417.
- Zhu, B., Jiang, S.-Y., Ding, X., Jiang, Y.-H., Ni, P., Gu, L., 2008. Hydrothermal alteration and petrogenesis of granites in the Yongping copper deposit, Jiangxi Province: Constraints from mineral chemistry, element geochemistry, and Sr-Nd-Hf isotopes. *Acta Petrologica Sinica* 24, 1900-1916.
- Zhu, J.-C., Li, X.-D., Shen, W.-Z., Wang, Y.-X., Yang, J.-D., 1989. Sr, Nd and O isotope studies on the genesis of the Huashan granite complex. *Acta Geologica Sinica*.
- Zhu, J.-C., Xie, C.-F., Zhang, P.-H., Yang, C., Gu, C.-Y., 2005a. Niumiao and Tong'an intrusive bodies of NE Guangxi: petrology, zircon SHRIMP U-Pb geochronology and geochemistry. *Acta Petrologica Sinica* 21, 665-676.
- Zhu, J.-C., Zhang, H., Xie, C.-F., Zhang, P.-H., Yang, C., 2005b. Zircon SHRIMP U-Pb geochronology, petrology and geochemistry of the Zhujianshui granite, Qitianling pluton, Southern Hunan Province. *Geological Journal of China Universities* 11, 335-342.
- Zhu, J.-C., Zhang, P.-H., Xie, C.-F., Zhang, H., Yang, C., 2006. The Huashan-Guposhan A-type granitoid belt in the western part of the Nanling Mountains: petrology, geochemistry and genetic interpretations. *Acta Geologica Sinica* 80, 529-542.
- Zhu, K.-Y., Li, Z.-X., Xu, X.-S., Wilde, S.A., 2013. Late Triassic melting of a thickened crust in southeastern China: Evidence for flat-slab subduction of the Paleo-Pacific plate. *Journal of Asian Earth Sciences* 74, 265-279.

Every reasonable effort has been made to acknowledge the owners of copyright material. I would be pleased to hear from any copyright owner who has been omitted or incorrectly acknowledged.

## Appendices

### Appendix A. Table of GPS readings and magnetic susceptibilities for the granitoids and volcanic rocks in this study

Sample No.	GPS		Measurement ( $\times 10^{-3}$ SI)					
	Latitude	Longitude	1	2	3	4	5	6
Triassic								
Qiuwang syenogranite								
09ZJ01	30°3'35.00"N	121°34'8.00"E	0.072	0.060	0.113	0.097	0.070	
10ZJS010	30°4'16.36"N	121°34'23.23"E	0.237	0.207	0.176	0.240	0.194	
10ZJS011	30°4'28.63"N	121°34'16.21"E	0.099	0.152	0.096	0.068	0.109	
11ZJS009	30°4'28.42"N	121°34'20.75"E	0.187	0.175	0.167	0.135	0.139	0.177
11ZJS010	30°4'28.42"N	121°34'20.75"E	0.156	0.179	0.159	0.107	0.155	0.191
11ZJS011	30°4'28.42"N	121°34'20.75"E	0.076	0.076	0.085	0.089	0.073	0.104
11ZJS012	30°4'28.42"N	121°34'20.75"E	0.032	0.053	0.072	0.066	0.034	0.057
Dashuang quartz monzonite (east body)								
09ZJ09	29°26'33.16"N	120°23'6.65"E	7.184	10.54	8.428	11.09	9.217	
09ZJ10	29°26'54.19"N	120°22'32.60"E	10.02	7.594	9.583	6.957	9.206	
10ZJS063	29°28'12.90"N	120°22'40.37"E	13.19	13.43	10.54	13.64	13.93	
10ZJS066	29°27'24.16"N	120°22'8.29"E	3.525	2.859	4.316	3.380	3.461	
10ZJS067	29°26'13.78"N	120°22'9.66"E	9.436	9.303	14.44	12.3	10.56	
Dashuang syenite (west body)								
10ZJS062	29°28'21.94"N	120°22'6.78"E	1.145	0.836	0.803	0.862	0.829	
10ZJS064	29°28'16.50"N	120°22'19.13"E	0.513	0.833	0.869	0.463	0.535	
10ZJS065	29°28'12.90"N	120°22'13.12"E	0.591	0.996	0.442	0.540	1.104	
Sheyang syenogranite								
10ZJS135	28°57'5.47"N	119°18'2.30"E	0.791	0.772	0.733	0.632	0.746	

Appendices

11ZJS065	28 °57'6.08"N	119 °18'1.37"E	0.195	0.161	0.141	0.182	0.160	0.140
11ZJS066	28 °57'6.08"N	119 °18'1.37"E	0.251	0.288	0.219	0.228	0.218	0.272
11ZJS067	28 °57'6.41"N	119 °18'0.58"E	0.267	0.208	0.179	0.230	0.210	0.227
11ZJS068	28 °57'6.41"N	119 °18'0.58"E	0.135	0.131	0.128	0.176	0.142	0.120
11ZJS069	28 °57'6.41"N	119 °18'0.58"E	0.271	0.235	0.200	0.179	0.192	0.218
Wengshan syenogranite								
10ZJS113	28 °34'22.73"N	119 °17'5.57"E	0.126	0.090	0.091	0.113	0.133	
Gaoxi syenogranite								
11ZJS157	28 °10'50.20"N	118 °40'41.77"E	3.192	2.984	3.731	3.145	3.547	3.074
11ZJS158	28 °10'50.20"N	118 °40'41.77"E	3.887	2.750	2.507	3.983	3.370	2.717
11ZJS159	28 °10'50.20"N	118 °40'41.77"E	3.609	2.358	2.671	3.356	2.989	2.449
11ZJS160	28 °10'50.20"N	118 °40'41.77"E	3.885	2.845	2.639	2.934	3.641	2.973
11ZJS163	28 °10'41.66"N	118 °41'5.24"E	0.087	0.024	0.089	0.065	0.057	0.058
11ZJS164	28 °10'41.66"N	118 °41'5.24"E	0.064	0.065	0.06	0.062	0.057	0.064
11ZJS165	28 °10'41.66"N	118 °41'5.24"E	0.076	0.129	0.101	0.071	0.081	0.103
11ZJS166	28 °10'41.66"N	118 °41'5.24"E	0.071	0.081	0.075	0.066	0.079	0.059
11ZJS175	28 °10'9.70"N	118 °41'33.32"E	0.066	0.068	0.059	0.057	0.06	0.056
11ZJS176	28 °10'9.70"N	118 °41'33.32"E	0.092	0.095	0.105	0.067	0.064	0.062
11ZJS177	28 °10'9.70"N	118 °41'33.32"E	0.059	0.054	0.060	0.068	0.052	0.055
Jurassic								
Xiepu syenogranite								
09ZJ02	30 °2'57.00"N	121 °35'19.00"E	1.715	1.118	1.432	1.025	1.254	
10ZJS001	30 °2'29.90"N	121 °35'57.91"E	0.085	0.093	0.073	0.063	0.060	
10ZJS012	30 °2'50.21"N	121 °34'48.07"E	0.169	0.150	0.167	0.144	0.172	
Jiangzao syenogranite								
10ZJS033	29 °50'5.75"N	120 °18'47.30"E	6.465	6.988	5.098	4.848	4.949	
10ZJS034	29 °50'32.10"N	120 °19'57.76"E	5.307	4.704	3.809	4.504	5.398	

---

Guangshan syenogranite							
10ZJS035	29°51'22.93"N	120°21'9.72"E	6.758	8.169	6.608	6.253	6.318
10ZJS036	29°51'38.12"N	120°21'13.86"E	7.100	6.095	5.764	6.494	6.081
10ZJS038	29°52'58.51"N	120°23'59.93"E	0.068	0.139	0.067	0.064	0.139
10ZJS039	29°53'12.98"N	120°24'32.08"E	0.071	0.066	0.074	0.027	0.125
10ZJS044	29°54'19.76"N	120°26'0.31"E	3.420	4.110	2.967	2.848	2.869
Shangsanzi granitic porphyry							
10ZJS149	28°52'56.50"N	118°20'54.96"E	0.216	0.105	0.151	0.094	0.116
11ZJS124	28°52'56.60"N	118°20'36.67"E	0.070	0.058	0.069	0.065	0.073
11ZJS125	28°52'56.60"N	118°20'36.67"E	0.091	0.077	0.088	0.169	0.109
11ZJS126	28°52'56.60"N	118°20'36.67"E	0.093	0.111	0.103	0.081	0.094
11ZJS127	28°52'56.60"N	118°20'36.67"E	0.064	0.057	0.072	0.079	0.064
11ZJS128	28°52'56.60"N	118°20'36.67"E	0.078	0.021	0.053	0.062	0.068
11ZJS129	28°52'56.60"N	118°20'36.67"E	0.100	0.087	0.131	0.113	0.128
11ZJS130	28°52'56.60"N	118°20'36.67"E	0.060	0.055	0.063	0.066	0.054
Tongcun granitic porphyry							
11ZJS104	28°59'53.59"N	118°14'45.82"E	1.290	0.291	0.552	0.464	0.682
11ZJS105	28°59'53.59"N	118°14'45.82"E	0.066	0.073	0.058	0.056	0.031
11ZJS106	28°59'53.59"N	118°14'45.82"E	0.075	0.058	0.027	0.059	0.052
11ZJS107	28°59'53.59"N	118°14'45.82"E	0.018	0.059	0.070	0.073	0.058
11ZJS108	28°59'53.59"N	118°14'45.82"E	0.073	0.058	0.072	0.066	0.071
11ZJS109	28°59'53.59"N	118°14'45.82"E	0.068	0.066	0.363	0.119	0.060
11ZJS110	28°59'53.59"N	118°14'45.82"E	0.028	0.067	0.027	0.02	0.019
11ZJS111	28°59'53.59"N	118°14'45.82"E	0.059	0.095	0.095	0.052	0.087
11ZJS112	28°58'54.23"N	118°13'8.08"E	0.091	0.075	0.066	0.059	0.091
11ZJS113	28°58'54.23"N	118°13'8.08"E	0.065	0.067	0.058	0.072	0.081
11ZJS114	28°58'54.23"N	118°13'8.08"E	0.070	0.069	0.071	0.071	0.064
11ZJS115	28°58'54.23"N	118°13'8.08"E	0.067	0.065	0.069	0.067	0.064

## Appendices

11ZJS116	28°58'54.23"N	118°13'8.08"E	0.070	0.075	0.055	0.064	0.076	0.069
11ZJS117	28°58'54.23"N	118°13'8.08"E	0.087	0.094	0.060	0.073	0.060	0.055
<b>Early Cretaceous</b>								
Yujiashan diorite								
10ZJS025	29°59'41.32"N	120°25'23.27"E	19.51	18.29	20.92	21.26	18.26	
10ZJS026	29°59'57.16"N	120°25'22.87"E	24.63	24.12	26.73	27.25	26.34	
10ZJS030	29°58'1.78"N	120°24'5.76"E	27.43	20.24	26.27	27.40	19.29	
11ZJS034	29°57'21.53"N	120°25'15.28"E	17.78	12.99	16.24	17.93	14.19	16.65
11ZJS035	29°57'21.53"N	120°25'15.28"E	11.94	6.942	6.801	11.20	11.80	7.784
11ZJS036	29°57'21.53"N	120°25'15.28"E	3.434	3.098	2.075	2.916	5.503	3.738
11ZJS037	29°57'21.53"N	120°25'15.28"E	37.33	39.26	24.02	38.69	41.23	37.49
Lishiwan diorite-gabbro								
10ZJS031	29°57'3.13"N	120°22'16.64"E	0.559	0.367	0.463	0.456	0.449	
10ZJS032	29°56'59.24"N	120°22'9.77"E	24.90	25.57	21.84	22.62	23.86	
Cao'er granite								
10ZJS014	29°58'56.68"N	120°51'8.42"E	0.177	0.213	0.331	0.184	0.232	
Rhyolite, Huangjian Group								
10ZJS023	29°54'56.92"N	120°46'2.32"E						
Rhyolite, Zhiji Group								
10ZJS024	29°55'7.18"N	120°46'44.40"E						
Ru'ao complex								
09ZJ05	29°18'40.00"N	120°56'25.00"E	14.72	14.43	14.05	12.77	13.37	
09ZJ06	29°18'44.90"N	120°56'20.90"E	36.00	37.31	29.51	36.17	34.62	
09ZJ07	29°18'44.64"N	120°56'21.31"E	8.789	7.689	7.267	5.514	7.389	
09ZJ08	29°18'45.30"N	120°56'9.76"E	66.53	65.40	58.98	61.13	69.86	

Appendices

---

Hecun dacitic-rhyolitic porphyry

10ZJS053	29 °37'31.58"N	120 °5'58.52"E	3.361	3.223	3.727	3.997	3.227
10ZJS054	29 °38'4.81"N	120 °6'0.79"E	7.637	9.043	7.560	8.579	7.272

Hongling dacitic-rhyolitic porphyry

10ZJS074	29 °30'20.52"N	119 °35'34.48"E	0.713	0.649	0.700	0.602	0.652
10ZJS075	29 °29'58.31"N	119 °35'53.23"E	0.279	0.347	0.306	0.318	0.289
10ZJS076	29 °29'43.37"N	119 °36'17.75"E	0.328	0.417	0.314	0.434	0.344
10ZJS077	29 °31'13.73"N	119 °36'41.36"E	0.388	0.405	0.346	0.414	0.412
10ZJS078	29 °31'23.56"N	119 °38'8.30"E	0.452	0.429	0.449	0.390	0.570
10ZJS079	29 °31'7.54"N	119 °38'52.40"E	0.307	0.293	0.294	0.341	0.244
10ZJS080	29 °31'24.49"N	119 °39'50.40"E	1.846	1.787	1.926	1.727	1.845
10ZJS081	29 °31'40.69"N	119 °40'21.90"E	0.247	0.278	0.244	0.186	0.261
10ZJS082	29 °32'10.54"N	119 °41'24.86"E	0.437	0.321	0.295	0.406	0.319
10ZJS083	29 °33'10.66"N	119 °42'1.84"E	2.319	2.373	2.306	2.401	2.193

Zhujiaxiang andesitic porphyry

10ZJS095	29 °22'37.78"N	119 °25'50.38"E	6.430	8.457	7.993	6.659	8.145
10ZJS097	29 °23'1.18"N	119 °26'22.99"E	11.72	10.75	11.93	12.16	13.12
10ZJS098	29 °23'6.79"N	119 °26'22.34"E	17.07	16.74	17.24	17.05	17.93

Tongshan syenogranite

09ZJ13	29 °21'27.60"N	118 °42'18.60"E	2.532	2.246	2.085	2.360	2.598
09ZJ14	29 °20'21.90"N	118 °42'9.90"E	0.374	0.505	0.551	0.303	0.428
09ZJ15	29 °20'0.19"N	118 °40'16.90"E	1.579	1.229	1.254	1.597	1.976

Jiuhua-Baijuhuajian syenogranite

10ZJS142	29 °8'7.22"N	118 °51'17.03"E	2.234	2.024	2.592	2.232	2.015
10ZJS143	29 °8'56.65"N	118 °51'43.52"E	5.764	5.479	8.416	4.947	4.581
10ZJS144	29 °9'54.94"N	118 °50'35.05"E	0.128	0.152	0.109	0.122	0.138
10ZJS145	29 °9'32.18"N	118 °48'14.76"E	0.155	0.163	0.168	0.169	0.123

Appendices

---

10ZJS146	29 °8'0.38"N	118 °45'7.88"E	0.196	0.267	0.266	0.206	0.228	
10ZJS147	29 °7'44.83"N	118 °45'18.97"E	0.723	0.543	0.719	0.535	0.563	
10ZJS148	29 °5'30.70"N	118 °43'59.12"E	7.158	6.626	5.832	5.393	5.566	
<b>Muchen complex</b>								
10ZJS115	28 °49'10.81"N	119 °11'24.43"E	27.66	31.95	32.01	29.19	30.82	
10ZJS116	28 °49'10.81"N	119 °11'24.43"E	20.34	19.78	18.53	20.71	18.41	
10ZJS123	28 °43'6.31"N	119 °6'46.37"E	12.79	7.715	10.67	12.49	9.714	
10ZJS124	28 °43'49.01"N	119 °5'52.30"E	39.03	37.55	34.91	40.17	39.16	
10ZJS125	28 °42'39.74"N	119 °7'35.65"E	6.782	6.614	6.420	7.213	6.424	
10ZJS131	28 °47'32.39"N	119 °10'6.13"E	29.66	20.87	19.48	23.05	28.72	
10ZJS132	28 °46'36.37"N	119 °9'10.26"E	32.00	34.38	51.78	33.01	35.74	
11ZJS048	28 °50'17.95"N	119 °10'52.10"E	16.30	13.11	18.92	16.42	21.81	18.74
11ZJS049	28 °50'0.67"N	119 °10'34.90"E	20.22	20.15	23.09	24.39	20.49	26.11
11ZJS050	28 °50'0.67"N	119 °10'34.90"E	25.52	28.34	22.75	21.22	25.98	24.66
11ZJS051	28 °50'0.67"N	119 °10'34.90"E	23.82	22.07	23.97	25.62	24.78	23.32
11ZJS052	28 °50'0.67"N	119 °10'34.90"E	24.44	25.30	27.09	23.52	22.46	22.09
11ZJS053	28 °50'0.67"N	119 °10'34.90"E	29.11	24.07	27.05	27.79	22.54	21.79
11ZJS054	28 °50'0.67"N	119 °10'34.90"E	23.66	20.27	20.03	18.03	16.65	16.97
11ZJS055	28 °49'31.84"N	119 °10'24.02"E	16.03	17.78	30.60	21.70	17.15	16.77
11ZJS056	28 °49'31.84"N	119 °10'24.02"E	20.30	17.76	17.44	18.07	22.04	21.33
11ZJS057	28 °48'12.10"N	119 °9'59.15"E	25.09	26.92	21.36	19.97	22.38	23.83
11ZJS058	28 °48'12.10"N	119 °9'59.15"E	25.07	26.18	24.03	22.24	22.90	19.54
11ZJS059	28 °49'1.74"N	119 °11'4.06"E	32.49	21.73	20.65	35.72	34.80	33.85
11ZJS060	28 °49'30.40"N	119 °11'32.96"E	18.46	18.23	17.18	21.26	18.06	22.19
11ZJS061	28 °49'29.21"N	119 °11'36.53"E	15.17	17.40	18.49	15.60	16.05	17.55
11ZJS062	28 °49'8.22"N	119 °10'46.42"E	22.66	19.36	23.07	21.90	18.88	17.96
11ZJS063	28 °50'18.42"N	119 °10'51.20"E	14.77	11.02	13.33	22.33	24.91	14.28
11ZJS072	28 °48'17.06"N	119 °11'10.50"E	21.33	22.82	28.81	22.17	23.70	22.42
11ZJS073	28 °48'17.06"N	119 °11'10.50"E	19.44	18.21	21.54	20.86	19.61	21.28
11ZJS074	28 °47'59.06"N	119 °11'9.96"E	17.85	13.69	16.95	14.93	14.83	15.72

Appendices

---

11ZJS075	28 °47'40.78"N	119 °10'49.33"E	18.06	17.46	15.16	19.32	17.94	16.24
11ZJS076	28 °47'33.40"N	119 °10'6.10"E	22.84	25.53	30.14	28.06	28.04	26.26
11ZJS077	28 °47'22.70"N	119 °9'43.45"E	29.49	27.15	29.73	28.31	23.87	30.08
11ZJS078	28 °47'22.70"N	119 °9'43.45"E	20.56	26.57	29.30	32.85	29.49	22.44
11ZJS079	28 °46'52.21"N	119 °9'34.13"E	22.06	20.06	18.06	20.89	16.86	14.87
11ZJS080	28 °47'7.12"N	119 °9'11.38"E	22.78	26.95	28.19	23.71	24.53	22.23
11ZJS082	28 °47'18.78"N	119 °8'54.46"E	0.410	0.346	0.453	0.432	0.405	0.455
11ZJS083	28 °47'18.78"N	119 °8'54.46"E	21.44	25.45	24.81	29.02	23.04	26.15
11ZJS084	28 °47'18.78"N	119 °8'54.46"E	14.89	19.86	13.49	24.06	25.15	21.91
11ZJS085	28 °46'50.70"N	119 °9'14.33"E	47.34	53.15	38.83	42.67	52.15	45.53
11ZJS086	28 °46'50.70"N	119 °9'14.33"E	12.82	11.94	15.85	16.05	13.03	16.06
11ZJS087	28 °46'50.70"N	119 °9'14.33"E	19.09	14.70	17.59	14.73	9.629	13.07
11ZJS088	28 °46'50.70"N	119 °9'14.33"E	82.51	77.54	78.75	75.12	85.28	58.56
11ZJS089	28 °46'50.70"N	119 °9'14.33"E	18.46	13.48	17.37	24.88	17.50	11.36
11ZJS090	28 °46'50.70"N	119 °9'14.33"E	62.38	65.00	54.06	60.72	43.70	49.98
11ZJS092	28 °46'50.70"N	119 °9'14.33"E	24.14	20.32	26.87	24.46	22.07	22.34
11ZJS093	28 °46'50.70"N	119 °9'14.33"E	11.04	10.91	10.57	12.11	10.98	11.31
11ZJS094	28 °46'50.70"N	119 °9'14.33"E	51.29	61.27	31.96	31.34	31.92	25.19
11ZJS095	28 °46'50.70"N	119 °9'14.33"E	18.36	23.30	21.32	23.02	15.63	14.84
11ZJS096	28 °46'36.70"N	119 °9'11.63"E	11.10	10.48	11.29	14.56	10.70	10.22
11ZJS097	28 °46'36.70"N	119 °9'11.63"E	27.41	14.48	18.09	20.31	21.37	18.22
11ZJS098	28 °46'23.74"N	119 °9'2.92"E	16.18	16.11	15.42	14.87	15.19	19.85
11ZJS099	28 °46'24.46"N	119 °8'40.56"E	14.87	13.55	14.18	15.61	12.04	12.14
11ZJS100	28 °45'6.77"N	119 °8'35.16"E	22.13	23.56	28.45	24.50	24.42	21.70
11ZJS101	28 °45'10.15"N	119 °8'28.25"E	20.44	18.97	25.64	21.14	24.91	25.08
11ZJS102	28 °45'12.02"N	119 °8'15.43"E	24.13	20.58	26.10	20.88	27.20	16.47
11ZJS103	28 °45'11.92"N	119 °8'7.33"E	32.13	26.46	26.57	27.56	27.83	28.63
Wangcun syenogranite								
10ZJS119	28 °35'31.96"N	119 °3'46.08"E	7.975	7.054	7.550	8.989	8.851	
10ZJS121	28 °37'53.94"N	119 °5'19.72"E	3.459	3.188	3.778	3.938	3.896	

Appendices

---

10ZJS122	28 °40'16.32"N	119 °6'43.56"E	0.311	0.522	0.977	0.111	0.439
<b>Matou monzogranite</b>							
10ZJS099	28 °39'46.08"N	119 °23'44.34"E	18.29	24.71	17.83	24.84	24.35
10ZJS100	28 °40'47.57"N	119 °21'50.80"E	20.80	17.34	15.23	15.54	15.68
10ZJS101	28 °42'53.57"N	119 °20'5.86"E	12.50	16.14	16.57	16.52	13.44
<b>Shanghekou syenogranite</b>							
10ZJS102	28 °44'15.07"N	119 °21'56.05"E	0.136	0.155	0.131	0.129	0.129
10ZJS103	28 °44'15.07"N	119 °21'56.05"E					
10ZJS104	28 °43'53.11"N	119 °21'49.25"E	1.877	2.451	2.345	1.944	1.917
<b>Huangkang syenogranite</b>							
10ZJS109	28 °52'39.50"N	119 °25'2.28"E	0.238	0.177	0.209	0.162	0.390
10ZJS110	28 °53'5.57"N	119 °25'7.68"E	0.172	0.097	0.070	0.087	0.066
<b>Lingkeng syenogranite</b>							
10ZJS136	28 °54'19.26"N	119 °17'49.60"E	2.217	1.830	1.756	2.081	2.257
<b>Luojia granitic porphyry</b>							
10ZJS133	28 °57'8.28"N	119 °13'37.63"E	0.140	0.157	0.137	0.138	0.133
10ZJS134	28 °56'50.39"N	119 °15'24.62"E	0.105	0.092	0.080	0.076	0.080
11ZJS070	28 °57'12.38"N	119 °13'38.64"E	0.011	0.025	0.017	0.015	0.016
11ZJS071	28 °57'6.48"N	119 °13'40.80"E	0.009	0.008	0.012	0.016	0.008
<b>Sucun syenogranite</b>							
10ZJS107	28 °46'38.06"N	119 °17'17.88"E	0.386	0.284	0.408	0.631	0.520
10ZJS108	28 °46'46.45"N	119 °18'56.20"E	4.157	3.693	4.344	3.509	4.610
<b>Beijie granite</b>							
10ZJS105	28 °45'31.82"N	119 °13'15.02"E	4.931	4.541	3.735	3.736	3.958

Appendices

---

10ZJS106	28 °46'19.06"N	119 °13'0.80"E	5.776	5.135	5.251	5.562	5.854	
10ZJS111	28 °45'2.70"N	119 °13'49.80"E	5.344	6.433	6.250	5.026	6.387	
<b>Yingcun granitic porphyry</b>								
10ZJS129	28 °42'46.55"N	119 °12'4.00"E	6.451	4.854	6.200	4.964	5.635	
<b>Gaoxi syenogranite</b>								
11ZJS169	28 °10'23.56"N	118 °41'21.01"E	10.84	12.80	12.25	10.77	10.81	12.04
11ZJS170	28 °10'23.56"N	118 °41'21.01"E	9.081	2.950	5.529	2.822	1.704	3.661
11ZJS171	28 °10'23.56"N	118 °41'21.01"E	8.075	10.93	4.571	6.829	6.329	9.006
11ZJS172	28 °10'23.56"N	118 °41'21.01"E	8.715	7.399	8.803	7.047	6.444	7.546
11ZJS173	28 °10'23.56"N	118 °41'21.01"E	3.663	3.865	3.449	4.818	7.836	3.260
11ZJS174	28 °10'23.56"N	118 °41'21.01"E	4.929	5.435	5.272	3.627	4.901	4.289
11ZJS192	28 °9'37.12"N	118 °43'32.81"E	5.221	5.352	4.415	5.007	5.769	4.916
11ZJS193	28 °9'37.12"N	118 °43'32.81"E	4.622	4.471	5.428	4.270	4.243	4.075
11ZJS194	28 °9'37.12"N	118 °43'32.81"E	11.46	10.41	9.227	5.552	5.169	4.797
11ZJS195	28 °9'37.12"N	118 °43'32.81"E	10.56	11.82	8.007	6.107	5.812	8.183
11ZJS196	28 °9'37.12"N	118 °43'32.81"E	11.32	7.345	12.05	7.587	9.464	7.138
11ZJS197	28 °9'37.12"N	118 °43'32.81"E	10.07	12.69	5.140	5.149	6.148	7.129
11ZJS198	28 °9'37.12"N	118 °43'32.81"E	10.15	9.525	11.70	9.278	10.54	10.08
11ZJS199	28 °9'37.12"N	118 °43'32.81"E	11.14	8.707	7.018	6.876	7.216	8.193
11ZJS200	28 °9'37.12"N	118 °43'32.81"E	9.027	8.073	8.730	7.398	7.937	8.738
11ZJS201	28 °9'37.12"N	118 °43'32.81"E	5.887	5.121	7.057	7.532	8.450	5.316
11ZJS202	28 °9'37.12"N	118 °43'32.81"E	7.926	7.863	7.618	7.118	6.557	6.453
11ZJS203	28 °9'37.12"N	118 °43'32.81"E	5.363	7.837	7.087	6.221	6.331	5.577
11ZJS204	28 °9'37.12"N	118 °43'32.81"E	7.232	8.539	7.492	8.190	9.796	7.383
<b>Damaoshan-Huaiyushan syenogranite-alkali feldspar granite</b>								
10ZJS162	28 °48'6.30"N	117 °54'56.23"E	0.343	0.453	0.863	0.280	0.353	
10ZJS163	28 °51'4.46"N	117 °57'58.18"E	0.267	0.086	0.145	0.133	0.079	
10ZJS164	28 °52'57.50"N	118 °3'39.20"E	0.243	0.181	0.204	0.264	0.126	

Appendices

---

10ZJS165	28 °54'14.26"N	118 °6'40.54"E	0.751	0.721	0.775	0.843	0.746
10ZJS172	28 °52'38.60"N	117 °39'13.57"E	0.593	0.935	0.871	0.424	0.557
10ZJS173	28 °50'14.82"N	117 °42'41.08"E	0.073	0.054	0.055	0.077	0.064
10ZJS174	28 °51'50.36"N	117 °48'30.92"E	0.145	0.131	0.181	0.138	0.141
10ZJS175	28 °51'35.42"N	117 °49'18.23"E	0.485	0.976	1.265	0.729	1.363
10ZJS176	28 °51'5.08"N	117 °45'59.58"E	0.040	0.057	0.030	0.026	0.029
10ZJS177	28 °50'58.34"N	117 °45'53.53"E	0.076	0.058	0.060	0.031	0.068

Lingshan syenogranite-alkali feldspar granite

10ZJS151	28 °40'55.24"N	117 °48'45.00"E	0.096	0.076	0.059	0.070	0.126	
10ZJS152	28 °39'47.09"N	117 °47'6.32"E	0.896	0.558	0.938	0.699	0.656	
10ZJS153	28 °40'11.32"N	117 °47'1.57"E	2.854	3.827	3.782	3.422	2.145	
10ZJS154	28 °40'8.65"N	117 °47'0.89"E	2.052	2.429	2.597	2.042	2.366	
10ZJS155	28 °39'48.35"N	117 °45'12.13"E	7.688	6.552	6.254	6.490	6.248	
10ZJS156	28 °39'48.35"N	117 °45'12.13"E	7.069	4.528	5.304	6.976	6.500	
11ZJS237	28 °35'7.51"N	117 °44'6.94"E	7.472	8.082	6.307	6.903	7.230	7.020
11ZJS238	28 °35'7.51"N	117 °44'6.94"E	5.619	6.729	5.883	6.345	5.519	5.835
11ZJS239	28 °35'7.51"N	117 °44'6.94"E	7.028	6.398	5.981	7.299	7.346	6.228
11ZJS240	28 °35'7.51"N	117 °44'6.94"E	6.622	6.559	7.101	5.628	6.799	8.041
11ZJS241	28 °35'7.51"N	117 °44'6.94"E	8.291	8.052	8.144	7.360	6.483	8.244
11ZJS242	28 °35'7.51"N	117 °44'6.94"E	8.042	6.138	5.902	7.283	6.117	6.262
11ZJS243	28 °35'7.51"N	117 °44'6.94"E	7.631	7.636	7.744	4.679	6.244	5.596
11ZJS244	28 °35'7.51"N	117 °44'6.94"E	6.500	7.766	7.129	6.191	8.012	6.423
11ZJS245	28 °35'7.51"N	117 °44'6.94"E	8.240	8.680	6.597	8.528	5.438	8.273

Wancunxiang syenogranite

10ZJS170	28 °42'12.35"N	117 °26'19.61"E	0.130	0.118	0.136	0.130	0.140
10ZJS171	28 °43'37.49"N	117 °26'43.66"E	0.371	0.545	0.389	0.426	0.369

---

## Appendix B. Table of in-situ zircon U-Pb dating results

### 09ZJ01 (Qiuwang syenogranite, LA-ICP-MS)

Spot No.	Th (ppm)	U (ppm)	Th/U	Corrected isotope ratios						Isotope ages (Ma)			
				$^{207}\text{Pb}/^{206}\text{Pb}$	1 SD	$^{207}\text{Pb}/^{235}\text{U}$	1 SD	$^{206}\text{Pb}/^{238}\text{U}$	1 SD	$^{207}\text{Pb}/^{235}\text{U}$	1 SD	$^{206}\text{Pb}/^{238}\text{U}$	1 SD
09zj01-01	775	824	0.94	0.05357	0.00104	0.262	0.006	0.03547	0.00055	236	5	225	3
09zj01-02	1051	1056	0.99	0.05028	0.00081	0.248	0.005	0.03576	0.00051	225	4	227	3
09zj01-03	2802	3420	0.82	0.04911	0.00058	0.200	0.003	0.02960	0.00042	186	3	188	3
09zj01-04	2764	4512	0.61	0.05006	0.00055	0.194	0.003	0.02813	0.00041	180	2	179	3
09zj01-05	762	650	1.17	0.05044	0.00127	0.251	0.007	0.03608	0.00055	227	5	229	3
09zj01-06	850	836	1.02	0.05154	0.00079	0.253	0.004	0.03567	0.00051	229	4	226	3
09zj01-07	1072	722	1.48	0.04797	0.00072	0.244	0.004	0.03693	0.00057	222	4	234	4
09zj01-08	927	770	1.21	0.05099	0.00079	0.249	0.004	0.03534	0.00050	225	4	224	3
09zj01-15	411	481	0.85	0.04954	0.00088	0.240	0.005	0.03522	0.00051	219	4	223	3
09zj01-16	567	430	1.32	0.05031	0.00156	0.250	0.008	0.03607	0.00056	227	6	228	3
09zj01-17	882	931	0.95	0.05026	0.00107	0.252	0.006	0.03648	0.00056	228	5	231	3
09zj01-18	623	747	0.83	0.04978	0.00096	0.250	0.005	0.03647	0.00056	227	4	231	3
09zj01-19	351	346	1.02	0.05028	0.00123	0.249	0.006	0.03594	0.00055	226	5	228	3
09zj01-20	228	281	0.81	0.04888	0.00107	0.248	0.006	0.03693	0.00058	225	5	234	4
09zj01-21	564	568	0.99	0.04989	0.00078	0.247	0.004	0.03588	0.00051	224	4	227	3
09zj01-22	701	711	0.99	0.05059	0.00074	0.250	0.004	0.03590	0.00050	227	3	227	3
09zj01-23	1398	1493	0.94	0.05128	0.00130	0.251	0.006	0.03547	0.00052	227	5	225	3
09zj01-24	1384	1480	0.94	0.05120	0.00073	0.248	0.004	0.03520	0.00048	225	3	223	3
09zj01-25	3102	4057	0.76	0.05000	0.00063	0.204	0.003	0.02963	0.00042	189	3	188	3
09zj01-27	591	473	1.25	0.05202	0.00085	0.257	0.005	0.03578	0.00050	232	4	227	3
09zj01-28	410	310	1.32	0.05206	0.00106	0.253	0.005	0.03525	0.00052	229	4	223	3
09zj01-29	722	792	0.91	0.05018	0.00071	0.244	0.004	0.03527	0.00048	222	3	224	3
09zj01-30	463	1254	0.37	0.05027	0.00071	0.248	0.004	0.03582	0.00049	225	3	227	3
09zj01-31	3026	4444	0.68	0.05759	0.00074	0.221	0.003	0.02778	0.00037	202	3	177	2

Appendices

09zj01-32	1127	1091	1.03	0.05047	0.00068	0.249	0.004	0.03578	0.00048	226	3	227	3
09zj01-33	752	623	1.21	0.04976	0.00122	0.239	0.006	0.03484	0.00051	218	5	221	3
09zj01-34	805	844	0.95	0.05020	0.00082	0.244	0.004	0.03532	0.00048	222	4	224	3
09zj01-35	4954	6537	0.76	0.05254	0.00062	0.176	0.002	0.02425	0.00032	164	2	155	2
09zj01-36	754	754	1.00	0.05120	0.00099	0.248	0.005	0.03515	0.00049	225	4	223	3

**09ZJ02 (Xiepu syenogranite, SHRIMP)**

Spot Name	U (ppm)	Th (ppm)	Th/U	204-corr %com206		4corr 207* /206*	4corr 207* /235	% err	4corr 206* /238	% err	ρ	204corr $^{207}\text{Pb}$ /235U	1 SD	204corr $^{206}\text{Pb}$ /238U	1 SD
				Age (Ma)		Age (Ma)									
09ZJ02-02	230	93	0.40	0.47	0.0563	4.4	0.210	4.7	0.0271	1.6	0.3	194	8	172	3
09ZJ02-03	2047	826	0.40	0.11	0.0487	1.0	0.193	1.8	0.0288	1.4	0.8	179	3	183	3
09ZJ02-06	699	505	0.72	0.81	0.0472	3.4	0.180	3.6	0.0276	1.3	0.4	174	7	175	2
09ZJ02-09	508	197	0.39	0.81	0.0485	4.5	0.187	4.6	0.0280	1.1	0.2	179	8	178	2
09ZJ02-12	1188	456	0.38	0.21	0.0494	1.6	0.188	1.9	0.0276	1.0	0.5	178	5	176	2
09ZJ02-17	1583	1832	1.16	0.28	0.0489	3.0	0.192	3.2	0.0284	1.2	0.4	163	7	181	2
09ZJ02-18	1973	727	0.37	0.16	0.0490	1.1	0.191	1.5	0.0283	1.0	0.7	177	2	180	2
09ZJ02-19	1283	495	0.39	1.33	0.0495	4.4	0.193	4.6	0.0282	1.4	0.3	186	5	179	2
09ZJ02-42	555	262	0.47	7.26	0.0576	14.5	0.222	14.6	0.0279	1.4	0.1	176	2	177	2
09ZJ02-43	1953	260	0.13	0.20	0.0494	1.2	0.190	1.5	0.0279	1.0	0.7	168	6	177	2

**09ZJ06 (Ru'ao diorite, LA-ICP-MS)**

Spot No.	Th (ppm)	U (ppm)	Th/U	Corrected isotope ratios				Isotope ages (Ma)			
				$^{207}\text{Pb}/^{206}\text{Pb}$	1 SD	$^{207}\text{Pb}/^{235}\text{U}$	1 SD	$^{206}\text{Pb}/^{238}\text{U}$	1 SD	$^{207}\text{Pb}/^{235}\text{U}$	1 SD
09zj06-01	101	75	1.34	0.04832	0.00325	0.127	0.009	0.01911	0.00034	122	8

Appendices

09zj06-02	404	407	0.99	0.05454	0.00266	0.139	0.007	0.01853	0.00036	132	6	118	2
09zj06-03	243	117	2.08	0.04924	0.00262	0.126	0.007	0.01857	0.00032	121	6	119	2
09zj06-04	164	103	1.60	0.05107	0.00426	0.125	0.010	0.01774	0.00041	120	9	113	3
09zj06-05	180	110	1.65	0.04720	0.00631	0.122	0.016	0.01869	0.00057	117	14	119	4
09zj06-06	183	73	2.50	0.05018	0.00886	0.128	0.022	0.01854	0.00074	122	20	118	5
09zj06-07	2290	444	5.15	0.04637	0.00166	0.120	0.004	0.01884	0.00036	115	4	120	2
09zj06-08	113	70	1.61	0.05198	0.00370	0.126	0.009	0.01754	0.00034	120	8	112	2
09zj06-09	1353	347	3.90	0.04731	0.00107	0.120	0.003	0.01844	0.00027	115	3	118	2
09zj06-10	228	112	2.03	0.04582	0.00388	0.121	0.010	0.01911	0.00038	116	9	122	2
09zj06-11	211	175	1.20	0.04986	0.00201	0.191	0.008	0.02781	0.00045	178	7	177	3
09zj06-12	174	106	1.65	0.04866	0.00343	0.123	0.009	0.01840	0.00038	118	8	118	2
09zj06-13	235	127	1.84	0.04971	0.00266	0.128	0.007	0.01863	0.00032	122	6	119	2
09zj06-14	1660	360	4.61	0.04806	0.00301	0.126	0.008	0.01908	0.00041	121	7	122	3
09zj06-15	225	115	1.95	0.05040	0.00379	0.123	0.009	0.01766	0.00041	118	8	113	3

**09ZJ07 (Ru'ao monzodiorite, LA-ICP-MS)**

Spot No.	Th (ppm)	U (ppm)	Th/U	Corrected isotope ratios						Isotope ages (Ma)			
				$^{207}\text{Pb}/^{206}\text{Pb}$	1 SD	$^{207}\text{Pb}/^{235}\text{U}$	1 SD	$^{206}\text{Pb}/^{238}\text{U}$	1 SD	$^{207}\text{Pb}/^{235}\text{U}$	1 SD	$^{206}\text{Pb}/^{238}\text{U}$	1 SD
09zj07-01	135	87	1.56	0.05332	0.00665	0.135	0.016	0.01842	0.00064	129	15	118	4
09zj07-02	581	227	2.56	0.05322	0.00280	0.130	0.007	0.01774	0.00033	124	6	113	2
09zj07-03	126	90	1.40	0.04974	0.00304	0.124	0.007	0.01803	0.00033	118	7	115	2
09zj07-04	162	108	1.51	0.05009	0.00299	0.122	0.007	0.01761	0.00032	117	7	113	2
09zj07-05	256	134	1.91	0.04903	0.00345	0.123	0.009	0.01822	0.00040	118	8	116	3
09zj07-06	1571	398	3.95	0.07468	0.00218	0.188	0.006	0.01828	0.00033	175	5	117	2
09zj07-07	246	123	2.00	0.04651	0.00245	0.118	0.006	0.01842	0.00032	113	6	118	2
09zj07-08	314	177	1.77	0.04919	0.00411	0.127	0.010	0.01875	0.00046	122	9	120	3
09zj07-09	315	138	2.28	0.04946	0.00223	0.121	0.005	0.01781	0.00031	116	5	114	2
09zj07-10	214	144	1.49	0.05026	0.00195	0.123	0.005	0.01771	0.00028	118	4	113	2

Appendices

09zj07-11	347	156	2.22	0.04918	0.00171	0.124	0.004	0.01834	0.00028	119	4	117	2
09zj07-12	414	166	2.50	0.04780	0.00228	0.117	0.006	0.01770	0.00031	112	5	113	2
09zj07-13	187	122	1.54	0.04610	0.00222	0.118	0.006	0.01857	0.00032	113	5	119	2
09zj07-14	205	129	1.59	0.04784	0.00187	0.125	0.005	0.01902	0.00030	120	4	122	2
09zj07-15	1142	449	2.54	0.04692	0.00095	0.118	0.003	0.01824	0.00026	113	2	117	2
09zj07-16	306	157	1.95	0.05118	0.00201	0.127	0.005	0.01802	0.00028	122	5	115	2
09zj07-17	211	126	1.68	0.04758	0.00231	0.117	0.006	0.01782	0.00030	112	5	114	2
09zj07-18	180	118	1.52	0.04432	0.00285	0.114	0.007	0.01859	0.00036	109	7	119	2
09zj07-19	180	117	1.54	0.04828	0.00327	0.121	0.008	0.01821	0.00037	116	7	116	2
09zj07-20	449	209	2.15	0.04928	0.00216	0.121	0.005	0.01776	0.00029	116	5	114	2
09zj07-21	748	298	2.51	0.04832	0.00120	0.120	0.003	0.01807	0.00027	115	3	116	2
09zj07-22	245	153	1.61	0.05188	0.00282	0.131	0.007	0.01835	0.00035	125	6	117	2

**09ZJ09 (Dashuang quartz monzonite, LA-ICP-MS)**

Spot No.	Th (ppm)	U (ppm)	Th/U	Corrected isotope ratios						Isotope ages (Ma)			
				$^{207}\text{Pb}/^{206}\text{Pb}$	1 SD	$^{207}\text{Pb}/^{235}\text{U}$	1 SD	$^{206}\text{Pb}/^{238}\text{U}$	1 SD	$^{207}\text{Pb}/^{235}\text{U}$	1 SD	$^{206}\text{Pb}/^{238}\text{U}$	1 SD
09zj09-z1	477	340	1.40	0.05098	0.00097	0.254	0.005	0.03614	0.00051	230	4	229	3
09zj09-z2	438	244	1.79	0.05267	0.00110	0.256	0.006	0.03532	0.00051	232	5	224	3
09zj09-z3	488	286	1.71	0.05669	0.00147	0.284	0.007	0.03635	0.00055	254	6	230	3
09zj09-z4	1071	498	2.15	0.05028	0.00093	0.251	0.005	0.03620	0.00050	227	4	229	3
09zj09-z5	323	145	2.23	0.04954	0.00174	0.250	0.009	0.03657	0.00060	226	7	232	4
09zj09-z6	314	232	1.35	0.04980	0.00158	0.259	0.008	0.03779	0.00063	234	7	239	4
09zj09-z7	43	25	1.75	0.05102	0.00578	0.266	0.029	0.03774	0.00118	239	23	239	7
09zj09-z8	680	411	1.65	0.04945	0.00123	0.234	0.006	0.03427	0.00052	213	5	217	3
09zj09-z9	743	492	1.51	0.05016	0.00117	0.246	0.006	0.03550	0.00051	223	5	225	3
09zj09-z10	162	395	0.41	0.05073	0.00120	0.256	0.006	0.03655	0.00053	231	5	231	3
09zj09-z11	707	503	1.41	0.06034	0.00126	0.313	0.007	0.03764	0.00055	277	5	238	3
09zj09-z12	602	199	3.03	0.05447	0.00135	0.271	0.007	0.03613	0.00055	244	5	229	3

Appendices

09zj09-z13	953	657	1.45	0.04853	0.00076	0.237	0.004	0.03547	0.00049	216	3	225	3
09zj09-z14	500	216	2.32	0.06308	0.00167	0.308	0.008	0.03543	0.00054	273	6	224	3
09zj09-z15	1002	542	1.85	0.05963	0.00106	0.300	0.006	0.03649	0.00052	266	4	231	3
09zj09-z16	710	477	1.49	0.04877	0.00084	0.231	0.004	0.03435	0.00048	211	4	218	3
09zj09-z17	996	541	1.84	0.05003	0.00084	0.251	0.005	0.03633	0.00051	227	4	230	3
09zj09-z18	258	83	3.12	0.05480	0.00213	0.272	0.010	0.03597	0.00063	244	8	228	4
09zj09-z19	536	345	1.55	0.04924	0.00116	0.240	0.006	0.03534	0.00052	218	5	224	3
09zj09-z20	1133	705	1.61	0.05001	0.00081	0.249	0.004	0.03616	0.00050	226	4	229	3
09zj09-z21	850	519	1.64	0.05490	0.00095	0.268	0.005	0.03542	0.00051	241	4	224	3
09zj09-z22	554	420	1.32	0.05089	0.00097	0.246	0.005	0.03505	0.00051	223	4	222	3
09zj09-z23	181	167	1.09	0.05600	0.00141	0.272	0.007	0.03520	0.00054	244	6	223	3
09zj09-z24	546	419	1.31	0.05267	0.00097	0.267	0.005	0.03681	0.00054	240	4	233	3

**09ZJ14 (Tongshan syenogranite, SHRIMP)**

Spot Name	U (ppm)	Th (ppm)	Th/U	204-corr		4corr		4corr		%	4corr		%	204corr	204corr
				%com206	207*/ 206*	%err	207*/ 235	err	206*/ 238	err	ρ	<sup>207</sup> Pb/ <sup>235</sup> U	1 SD	<sup>206</sup> Pb/ <sup>238</sup> U	1 SD
09ZJ14-01	89	62	0.69	1.84	0.0528	16.8	0.156	16.9	0.0214	1.9	0.1	147	23	137	3
09ZJ14-02	434	319	0.74	0.59	0.0458	5.7	0.133	5.9	0.0210	1.5	0.2	126	7	134	2
09ZJ14-04	282	148	0.52	1.01	0.0457	6.8	0.128	7.0	0.0204	1.5	0.2	123	8	130	2
09ZJ14-03	184	150	0.81	-0.20	0.0559	5.9	0.160	6.2	0.0207	2.1	0.3	150	9	132	3
09ZJ14-05	120	58	0.48	1.22	0.0485	11.0	0.142	11.2	0.0212	2.4	0.2	135	14	135	3
09ZJ14-07	309	92	0.30	0	0.0510	2.4	0.140	2.8	0.0199	1.5	0.5	133	4	127	2
09ZJ14-08	332	201	0.61	-0.33	0.0526	3.5	0.156	3.8	0.0216	1.5	0.4	147	5	137	2
09ZJ14-09	184	114	0.62	-0.36	0.0589	4.4	0.172	4.7	0.0212	1.8	0.4	161	7	135	2

Appendices

09ZJ14-10	602	272	0.45	0.20	0.0503	2.5	0.143	2.9	0.0207	1.4	0.5	136	4	132	2
09ZJ14-11	375	178	0.47	0.49	0.0474	5.8	0.137	6.0	0.0209	1.5	0.2	130	7	133	2
09ZJ14-12	265	119	0.45	1.73	0.0410	10.1	0.116	10.2	0.0205	1.6	0.2	112	11	131	2
09ZJ14-13	86	43	0.50	2.16	0.0415	20.8	0.120	20.9	0.0210	1.9	0.1	115	23	134	3
09ZJ14-14	434	160	0.37	0.62	0.0471	4.2	0.137	4.9	0.0211	2.5	0.5	130	6	134	3
09ZJ14-15	116	79	0.69	0.57	0.0576	4.1	0.414	5.0	0.0521	2.8	0.6	352	15	327	9
09ZJ14-16	290	126	0.44	0.95	0.0445	6.2	0.130	6.4	0.0211	1.5	0.2	124	7	135	2
09ZJ14-17	157	71	0.46	1.88	0.0394	15.2	0.112	15.4	0.0207	2.2	0.1	108	16	132	3
09ZJ14-18	175	100	0.57	1.47	0.0445	10.0	0.128	10.2	0.0208	1.6	0.2	122	12	133	2
09ZJ14-19	385	124	0.32	0.53	0.0463	3.9	0.134	4.4	0.0210	1.9	0.4	128	5	134	3

**10ZJS011 (Qiuwang syenogranite, LA-ICP-MS)**

Spot No.	Th (ppm)	U (ppm)	Th/U	Corrected isotope ratios				Isotope ages (Ma)			
				$^{207}\text{Pb}/^{206}\text{Pb}$	1 SD	$^{207}\text{Pb}/^{235}\text{U}$	1 SD	$^{206}\text{Pb}/^{238}\text{U}$	1 SD	$^{207}\text{Pb}/^{235}\text{U}$	1 SD
10zj011-01a	851	1856	0.46	0.05161	0.00162	0.249	0.008	0.03503	0.00061	226	6
10zj011-02a	1630	1882	0.87	0.05323	0.00172	0.253	0.008	0.03442	0.00049	229	7
10zj011-03a	210	703	0.30	0.05139	0.00114	0.241	0.005	0.03406	0.00044	220	4
10zj011-04a	756	1215	0.62	0.05013	0.00085	0.239	0.004	0.03458	0.00045	218	4
10zj011-05a	441	722	0.61	0.05149	0.00161	0.246	0.008	0.03468	0.00054	224	6
10zj011-06a	295	609	0.48	0.05148	0.00232	0.266	0.012	0.03742	0.00062	239	9
10zj011-07a	178	404	0.44	0.05212	0.00135	0.250	0.007	0.03476	0.00048	226	5
10zj011-08a	476	929	0.51	0.05117	0.00103	0.258	0.006	0.03650	0.00052	233	4
10zj011-09a	753	2348	0.32	0.05020	0.00109	0.254	0.006	0.03668	0.00047	230	5
10zj011-10a	1875	2202	0.85	0.05158	0.00082	0.250	0.004	0.03517	0.00048	227	4
10zj011-11a	1259	1183	1.06	0.05289	0.00182	0.255	0.009	0.03490	0.00052	230	7
10zj011-12a	548	554	0.99	0.05234	0.00207	0.250	0.010	0.03461	0.00054	227	8

Appendices

10zj011-13a	346	1304	0.27	0.05174	0.00105	0.252	0.005	0.03537	0.00047	229	4	224	3
10zj011-14a	379	535	0.71	0.05036	0.00194	0.242	0.009	0.03488	0.00051	220	8	221	3
10zj011-15a	398	807	0.49	0.05106	0.00103	0.256	0.005	0.03633	0.00050	231	4	230	3
10zj011-16a	906	1091	0.83	0.05170	0.00115	0.252	0.006	0.03541	0.00048	229	5	224	3
10zj011-17a	856	1938	0.44	0.05271	0.00117	0.263	0.006	0.03624	0.00051	237	5	230	3
10zj011-18a	885	1362	0.65	0.05147	0.00092	0.254	0.005	0.03578	0.00049	230	4	227	3
10zj011-19a	284	429	0.66	0.04935	0.00227	0.246	0.011	0.03620	0.00070	224	9	229	4
10zj011-20a	724	764	0.95	0.05279	0.00129	0.262	0.007	0.03604	0.00052	237	5	228	3
10zj011-21a	304	486	0.63	0.05180	0.00158	0.255	0.008	0.03576	0.00056	231	6	227	3
10zj011-22a	347	559	0.62	0.04904	0.00127	0.238	0.006	0.03523	0.00051	217	5	223	3
10zj011-23a	464	887	0.52	0.05129	0.00109	0.252	0.006	0.03563	0.00051	228	5	226	3
10zj011-24a	353	873	0.40	0.04914	0.00151	0.244	0.008	0.03605	0.00062	222	6	228	4
10zj011-25a	1093	874	1.25	0.04929	0.00154	0.244	0.008	0.03592	0.00060	222	6	228	4

**10ZJS025 (Yujiashan diorite, LA-ICP-MS)**

Spot No.	Th (ppm)	U (ppm)	Th/U	Corrected isotope ratios				Isotope ages (Ma)			
				$^{207}\text{Pb}/^{206}\text{Pb}$	1 SD	$^{207}\text{Pb}/^{235}\text{U}$	1 SD	$^{206}\text{Pb}/^{238}\text{U}$	1 SD	$^{207}\text{Pb}/^{235}\text{U}$	1 SD
10zj025-01	590	263	2.24	0.04998	0.00185	0.111	0.004	0.01612	0.00024	107	4
10zj025-02	555	300	1.85	0.05241	0.00221	0.115	0.005	0.01593	0.00025	111	4
10zj025-03	454	205	2.22	0.04960	0.00222	0.111	0.005	0.01616	0.00025	107	5
10zj025-04	356	192	1.86	0.04894	0.00331	0.107	0.007	0.01592	0.00030	104	7
10zj025-05	561	262	2.14	0.05219	0.00267	0.110	0.006	0.01532	0.00027	106	5
10zj025-06	188	108	1.74	0.05054	0.00759	0.115	0.017	0.01654	0.00058	111	15
10zj025-07	496	260	1.91	0.04984	0.00173	0.107	0.004	0.01551	0.00023	103	3
10zj025-08	293	164	1.78	0.04992	0.00346	0.109	0.007	0.01585	0.00029	105	7
10zj025-09	248	214	1.16	0.04767	0.00247	0.108	0.006	0.01641	0.00026	104	5
10zj025-10	611	342	1.78	0.05108	0.00148	0.107	0.003	0.01522	0.00022	103	3
10zj025-11	460	227	2.03	0.04798	0.00186	0.104	0.004	0.01577	0.00023	101	4

Appendices

10zj025-12	759	332	2.28	0.04663	0.00149	0.099	0.003	0.01546	0.00022	96	3	99	1
10zj025-13	455	259	1.76	0.04839	0.00165	0.100	0.003	0.01502	0.00022	97	3	96	1
10zj025-14	271	176	1.54	0.05152	0.00686	0.118	0.015	0.01654	0.00061	113	14	106	4
10zj025-15	398	228	1.75	0.04870	0.00188	0.107	0.004	0.01592	0.00024	103	4	102	2
10zj025-16	274	257	1.07	0.04835	0.00342	0.111	0.008	0.01663	0.00036	107	7	106	2
10zj025-17	1554	826	1.88	0.05859	0.00125	0.116	0.003	0.01431	0.00020	111	2	92	1
10zj025-18	165	117	1.41	0.05087	0.00415	0.106	0.009	0.01517	0.00034	103	8	97	2
10zj025-19	273	178	1.53	0.05149	0.00335	0.116	0.007	0.01629	0.00033	111	7	104	2
10zj025-20	661	483	1.37	0.06335	0.00310	0.136	0.006	0.01553	0.00030	129	6	99	2
10zj025-21	960	390	2.46	0.05057	0.00124	0.106	0.003	0.01522	0.00021	102	2	97	1
10zj025-22	306	172	1.78	0.05018	0.00239	0.109	0.005	0.01571	0.00026	105	5	101	2

**10ZJS033 (Jiangzao granite, LA-ICP-MS)**

Spot No.	Th (ppm)	U (ppm)	Th/U	Corrected isotope ratios				Isotope ages (Ma)			
				$^{207}\text{Pb}/^{206}\text{Pb}$	1 SD	$^{207}\text{Pb}/^{235}\text{U}$	1 SD	$^{206}\text{Pb}/^{238}\text{U}$	1 SD	$^{207}\text{Pb}/^{235}\text{U}$	1 SD
10zj033-01	240	231	1.04	0.05202	0.00131	0.163	0.004	0.02268	0.00032	153	4
10zj033-02	203	277	0.73	0.05174	0.00133	0.158	0.004	0.02220	0.00032	149	4
10zj033-03	32	40	0.81	0.04989	0.00517	0.154	0.016	0.02237	0.00043	145	14
10zj033-04	1906	1502	1.27	0.05306	0.00105	0.144	0.003	0.01962	0.00028	136	3
10zj033-05	404	409	0.99	0.05947	0.00160	0.158	0.004	0.01924	0.00029	149	4
10zj033-06	351	318	1.11	0.05671	0.00139	0.180	0.004	0.02299	0.00034	168	4
10zj033-07	204	222	0.92	0.05004	0.00136	0.162	0.004	0.02344	0.00033	152	4
10zj033-08	161	164	0.98	0.05045	0.00197	0.160	0.006	0.02298	0.00036	151	5
10zj033-09	356	322	1.11	0.05131	0.00333	0.167	0.011	0.02357	0.00052	157	9
10zj033-10	1227	449	2.73	0.05066	0.00091	0.151	0.003	0.02158	0.00029	143	3
10zj033-11	214	321	0.67	0.04900	0.00102	0.155	0.003	0.02288	0.00031	146	3
10zj033-12	2405	4962	0.48	0.05025	0.00060	0.117	0.002	0.01688	0.00022	112	2
10zj033-13	176	185	0.95	0.05215	0.00143	0.161	0.005	0.02233	0.00032	151	4

Appendices

10zj033-14	310	256	1.21	0.05151	0.00129	0.161	0.004	0.02273	0.00032	152	4	145	2
10zj033-15	107	122	0.87	0.05023	0.00207	0.158	0.007	0.02288	0.00036	149	6	146	2
10zj033-16	354	1412	0.25	0.05295	0.00083	0.161	0.003	0.02210	0.00030	152	2	141	2
10zj033-17	4202	1978	2.12	0.07663	0.00090	0.193	0.003	0.01831	0.00024	180	2	117	2
10zj033-18	333	524	0.64	0.05204	0.00216	0.162	0.007	0.02253	0.00039	152	6	144	2

**10ZJS053 (Hecun dacitic-rhyolitic porphyry , LA-ICP-MS)**

Spot No.	Th (ppm)	U (ppm)	Th/U	Corrected isotope ratios						Isotope ages (Ma)			
				$^{207}\text{Pb}/^{206}\text{Pb}$	1 SD	$^{207}\text{Pb}/^{235}\text{U}$	1 SD	$^{206}\text{Pb}/^{238}\text{U}$	1 SD	$^{207}\text{Pb}/^{235}\text{U}$	1 SD	$^{206}\text{Pb}/^{238}\text{U}$	1 SD
10zj053-01	589	643	0.92	0.04814	0.00163	0.134	0.005	0.02026	0.00032	128	4	129	2
10zj053-02	220	322	0.68	0.04833	0.00127	0.136	0.004	0.02048	0.00030	130	3	131	2
10zj053-03	295	337	0.88	0.04950	0.00122	0.140	0.004	0.02051	0.00030	133	3	131	2
10zj053-04	305	331	0.92	0.04894	0.00129	0.140	0.004	0.02080	0.00030	133	3	133	2
10zj053-05	142	102	1.39	0.04785	0.00423	0.133	0.012	0.02023	0.00039	127	10	129	2
10zj053-06	55	72	0.77	0.04876	0.00451	0.137	0.013	0.02031	0.00038	130	11	130	2
10zj053-07	143	112	1.28	0.04932	0.00308	0.152	0.009	0.02241	0.00038	144	8	143	2
10zj053-08	581	563	1.03	0.05029	0.00163	0.141	0.005	0.02040	0.00031	134	4	130	2
10zj053-09	353	488	0.72	0.04917	0.00110	0.138	0.003	0.02030	0.00029	131	3	130	2
10zj053-10	223	194	1.15	0.04823	0.00186	0.136	0.005	0.02039	0.00031	129	5	130	2
10zj053-11	212	251	0.85	0.04782	0.00167	0.137	0.005	0.02081	0.00031	131	4	133	2
10zj053-12	278	223	1.25	0.04997	0.00333	0.142	0.009	0.02053	0.00044	135	8	131	3
10zj053-13	378	457	0.83	0.04894	0.00112	0.136	0.003	0.02018	0.00029	130	3	129	2
10zj053-14	433	444	0.97	0.04873	0.00274	0.134	0.007	0.02003	0.00041	128	7	128	3
10zj053-15	271	277	0.98	0.04986	0.00262	0.139	0.007	0.02023	0.00036	132	6	129	2
10zj053-16	106	132	0.81	0.04990	0.00260	0.139	0.007	0.02016	0.00033	132	6	129	2
10zj053-17	150	202	0.74	0.04939	0.00187	0.142	0.005	0.02091	0.00032	135	5	133	2
10zj053-18	181	212	0.85	0.04862	0.00185	0.137	0.005	0.02048	0.00032	131	5	131	2
10zj053-19	324	440	0.74	0.04877	0.00139	0.135	0.004	0.02012	0.00031	129	3	128	2

## Appendices

10zj053-20	133	169	0.78	0.04992	0.00223	0.141	0.006	0.02050	0.00033	134	6	131	2
------------	-----	-----	------	---------	---------	-------	-------	---------	---------	-----	---	-----	---

**10ZJS063 (Dashuang quartz monzonite, LA-ICP-MS)**

Spot No.	Th (ppm)	U (ppm)	Th/U	Corrected isotope ratios						Isotope ages (Ma)			
				$^{207}\text{Pb}/^{206}\text{Pb}$	1 SD	$^{207}\text{Pb}/^{235}\text{U}$	1 SD	$^{206}\text{Pb}/^{238}\text{U}$	1 SD	$^{207}\text{Pb}/^{235}\text{U}$	1 SD	$^{206}\text{Pb}/^{238}\text{U}$	1 SD
10zj063-01	843	336	2.51	0.05134	0.00088	0.250	0.005	0.03528	0.00049	226	4	224	3
10zj063-02	274	215	1.27	0.05553	0.00115	0.277	0.006	0.03614	0.00051	248	5	229	3
10zj063-03	403	129	3.13	0.05285	0.00147	0.261	0.007	0.03588	0.00053	236	6	227	3
10zj063-04	464	197	2.35	0.05245	0.00117	0.260	0.006	0.03599	0.00051	235	5	228	3
10zj063-05	471	134	3.52	0.05005	0.00144	0.241	0.007	0.03488	0.00051	219	6	221	3
10zj063-06	574	389	1.48	0.05095	0.00084	0.251	0.005	0.03573	0.00050	227	4	226	3
10zj063-07	327	100	3.28	0.07747	0.00206	0.380	0.010	0.03553	0.00054	327	8	225	3
10zj063-08	859	507	1.69	0.05311	0.00079	0.263	0.004	0.03594	0.00049	237	4	228	3
10zj063-09	452	210	2.15	0.05063	0.00107	0.262	0.006	0.03753	0.00053	236	5	238	3
10zj063-10	642	409	1.57	0.05180	0.00083	0.256	0.005	0.03578	0.00050	231	4	227	3
10zj063-11	377	174	2.16	0.05663	0.00118	0.286	0.006	0.03661	0.00051	255	5	232	3
10zj063-12	838	255	3.29	0.05056	0.00094	0.243	0.005	0.03486	0.00048	221	4	221	3
10zj063-13	356	111	3.20	0.05167	0.00148	0.267	0.008	0.03746	0.00054	240	6	237	3
10zj063-14	465	153	3.04	0.06337	0.00136	0.317	0.007	0.03624	0.00051	279	6	230	3
10zj063-15	334	470	0.71	0.05209	0.00075	0.254	0.004	0.03536	0.00048	230	3	224	3
10zj063-16	381	231	1.65	0.05282	0.00101	0.259	0.005	0.03554	0.00049	234	4	225	3
10zj063-17	240	188	1.28	0.05312	0.00112	0.259	0.006	0.03534	0.00049	234	5	224	3
10zj063-18	324	230	1.40	0.05686	0.00106	0.281	0.006	0.03590	0.00050	252	5	227	3
10zj063-19	383	236	1.62	0.05235	0.00099	0.262	0.005	0.03634	0.00050	237	4	230	3
10zj063-20	228	129	1.77	0.05835	0.00146	0.293	0.008	0.03640	0.00052	261	6	231	3

Appendices

**10ZJS065 (Dashuang syenite, LA-ICP-MS)**

Spot No.	Th (ppm)	U (ppm)	Th/U	Corrected isotope ratios						Isotope ages (Ma)			
				$^{207}\text{Pb}/^{206}\text{Pb}$	1 SD	$^{207}\text{Pb}/^{235}\text{U}$	1 SD	$^{206}\text{Pb}/^{238}\text{U}$	1 SD	$^{207}\text{Pb}/^{235}\text{U}$	1 SD	$^{206}\text{Pb}/^{238}\text{U}$	1 SD
10zj065-01	516	335	1.54	0.05059	0.00090	0.250	0.005	0.03579	0.00047	226	4	227	3
10zj065-02	851	721	1.18	0.05107	0.00070	0.244	0.004	0.03471	0.00045	222	3	220	3
10zj065-03	97	61	1.59	0.05322	0.00265	0.265	0.013	0.03618	0.00057	239	11	229	4
10zj065-04	291	195	1.49	0.06075	0.00126	0.309	0.007	0.03686	0.00050	273	5	233	3
10zj065-05	321	244	1.32	0.06319	0.00115	0.321	0.006	0.03687	0.00049	283	5	233	3
10zj065-06	93	56	1.66	0.07744	0.00305	0.394	0.015	0.03689	0.00058	337	11	234	4
10zj065-07	611	368	1.66	0.05211	0.00088	0.256	0.005	0.03568	0.00047	232	4	226	3
10zj065-08	95	59	1.61	0.04994	0.00287	0.239	0.014	0.03470	0.00055	218	11	220	3
10zj065-09	1225	673	1.82	0.05647	0.00078	0.265	0.004	0.03401	0.00044	239	3	216	3
10zj065-10	2671	1258	2.12	0.05582	0.00069	0.242	0.003	0.03149	0.00040	220	3	200	3
10zj065-11	1577	530	2.97	0.05154	0.00076	0.244	0.004	0.03438	0.00046	222	3	218	3
10zj065-12	785	322	2.44	0.04978	0.00089	0.245	0.005	0.03570	0.00048	223	4	226	3
10zj065-13	679	482	1.41	0.05115	0.00076	0.270	0.005	0.03833	0.00051	243	4	243	3
10zj065-14	1091	755	1.44	0.05169	0.00068	0.248	0.004	0.03475	0.00046	225	3	220	3
10zj065-15	738	424	1.74	0.05231	0.00081	0.262	0.005	0.03634	0.00048	236	4	230	3
10zj065-16	1016	655	1.55	0.05225	0.00072	0.250	0.004	0.03468	0.00046	227	3	220	3
10zj065-17	984	587	1.68	0.05632	0.00077	0.285	0.004	0.03670	0.00049	255	4	232	3
10zj065-18	187	199	0.94	0.05236	0.00115	0.260	0.006	0.03601	0.00050	235	5	228	3
10zj065-19	815	438	1.86	0.05075	0.00080	0.251	0.004	0.03587	0.00048	227	4	227	3
10zj065-20	929	546	1.70	0.06264	0.00085	0.319	0.005	0.03689	0.00049	281	4	234	3
10zj065-21	1215	1035	1.17	0.05495	0.00068	0.265	0.004	0.03502	0.00046	239	3	222	3

**10ZJS072 (Shuangcail andesitic-dacitic porphyry, LA-ICP-MS)**

Spot No.	Th (ppm)	U (ppm)	Th/U	Corrected isotope ratios	Isotope ages (Ma)
----------	----------	---------	------	--------------------------	-------------------

Appendices

				$^{207}\text{Pb}/^{206}\text{Pb}$	1 SD	$^{207}\text{Pb}/^{235}\text{U}$	1 SD	$^{206}\text{Pb}/^{238}\text{U}$	1 SD	$^{207}\text{Pb}/^{235}\text{U}$	1 SD	$^{206}\text{Pb}/^{238}\text{U}$	1 SD
10zj072-01	195	280	0.70	0.04823	0.00106	0.136	0.003	0.02052	0.00029	130	3	131	2
10zj072-02	26	51	0.51	0.04772	0.00227	0.137	0.006	0.02077	0.00033	130	6	133	2
10zj072-03	79	68	1.17	0.04686	0.00489	0.133	0.014	0.02058	0.00048	127	12	131	3
10zj072-04	102	139	0.73	0.04849	0.00190	0.137	0.005	0.02053	0.00031	131	5	131	2
10zj072-05	204	182	1.12	0.04886	0.00170	0.141	0.005	0.02098	0.00032	134	4	134	2
10zj072-06	504	299	1.69	0.05022	0.00134	0.144	0.004	0.02078	0.00033	137	4	133	2
10zj072-07	438	248	1.77	0.05025	0.00136	0.141	0.004	0.02030	0.00030	134	3	130	2
10zj072-08	25	38	0.65	0.04782	0.00683	0.134	0.019	0.02040	0.00046	128	17	130	3
10zj072-09	328	219	1.50	0.04744	0.00190	0.135	0.005	0.02062	0.00035	129	5	132	2
10zj072-10	206	155	1.33	0.04758	0.00196	0.137	0.006	0.02090	0.00033	131	5	133	2
10zj072-11	162	200	0.81	0.04902	0.00192	0.142	0.006	0.02094	0.00035	134	5	134	2
10zj072-12	103	144	0.71	0.04930	0.00184	0.141	0.005	0.02073	0.00033	134	5	132	2
10zj072-13	165	240	0.69	0.04796	0.00294	0.139	0.008	0.02107	0.00042	132	7	134	3
10zj072-14	790	1709	0.46	0.04874	0.00249	0.135	0.007	0.02003	0.00039	128	6	128	2
10zj072-15	568	1026	0.55	0.05044	0.00244	0.138	0.007	0.01990	0.00038	132	6	127	2
10zj072-16	302	373	0.81	0.05066	0.00287	0.146	0.008	0.02086	0.00042	138	7	133	3

**10ZJS081 (Hongling dacitic-rhyolitic porphyry, LA-ICP-MS)**

Spot No.	Th (ppm)	U (ppm)	Th/U	Corrected isotope ratios				Isotope ages (Ma)			
				$^{207}\text{Pb}/^{206}\text{Pb}$	1 SD	$^{207}\text{Pb}/^{235}\text{U}$	1 SD	$^{206}\text{Pb}/^{238}\text{U}$	1 SD	$^{207}\text{Pb}/^{235}\text{U}$	1 SD
10zj081-01	211	222	0.95	0.04936	0.00186	0.139	0.005	0.02047	0.00032	132	5
10zj081-02	152	149	1.02	0.04844	0.00325	0.141	0.009	0.02115	0.00039	134	8
10zj081-03	89	94	0.95	0.04871	0.00328	0.142	0.009	0.02115	0.00040	135	8
10zj081-04	190	187	1.02	0.04896	0.00274	0.137	0.007	0.02034	0.00040	131	7
10zj081-05	95	97	0.98	0.05090	0.00262	0.141	0.007	0.02006	0.00033	134	6
10zj081-06	80	92	0.86	0.05021	0.00450	0.139	0.012	0.02015	0.00043	133	11
10zj081-07	331	224	1.48	0.05063	0.00256	0.147	0.007	0.02108	0.00037	139	6

Appendices

10zj081-08	125	139	0.90	0.04983	0.00195	0.143	0.006	0.02075	0.00034	135	5	132	2
10zj081-09	88	91	0.97	0.04955	0.00203	0.143	0.006	0.02097	0.00033	136	5	134	2
10zj081-10	185	206	0.90	0.04898	0.00470	0.141	0.013	0.02088	0.00051	134	12	133	3
10zj081-11	144	127	1.13	0.04995	0.00267	0.141	0.007	0.02041	0.00034	134	7	130	2
10zj081-12	526	491	1.07	0.04992	0.00116	0.141	0.003	0.02048	0.00029	134	3	131	2
10zj081-13	112	124	0.91	0.04777	0.00279	0.132	0.008	0.02007	0.00034	126	7	128	2
10zj081-14	163	168	0.97	0.04888	0.00198	0.136	0.006	0.02024	0.00031	130	5	129	2
10zj081-15	124	128	0.97	0.04967	0.00521	0.138	0.014	0.02012	0.00056	131	13	128	4
10zj081-16	97	121	0.81	0.05028	0.00459	0.141	0.013	0.02041	0.00048	134	11	130	3
10zj081-17	186	127	1.47	0.05189	0.00558	0.149	0.016	0.02089	0.00062	141	14	133	4
10zj081-18	259	237	1.09	0.05011	0.00309	0.137	0.008	0.01986	0.00042	130	7	127	3
10zj081-19	172	188	0.91	0.04985	0.00295	0.141	0.008	0.02046	0.00039	134	7	131	2
10zj081-20	143	154	0.93	0.05143	0.00289	0.147	0.008	0.02070	0.00038	139	7	132	2

**10ZJS096 (Zhujiaxiang andesitic porphyry, LA-ICP-MS)**

Spot No.	Th (ppm)	U (ppm)	Th/U	Corrected isotope ratios				Isotope ages (Ma)			
				$^{207}\text{Pb}/^{206}\text{Pb}$	1 SD	$^{207}\text{Pb}/^{235}\text{U}$	1 SD	$^{206}\text{Pb}/^{238}\text{U}$	1 SD	$^{207}\text{Pb}/^{235}\text{U}$	1 SD
10zj096-01	131	126	1.04	0.04668	0.00387	0.135	0.011	0.02092	0.00045	128	10
10zj096-02	159	146	1.09	0.04949	0.00217	0.138	0.006	0.02022	0.00031	131	5
10zj096-03	1037	2328	0.45	0.05116	0.00066	0.114	0.002	0.01617	0.00022	110	2
10zj096-04	356	701	0.51	0.04999	0.00085	0.143	0.003	0.02072	0.00028	136	2
10zj096-05	104	105	0.99	0.05012	0.00321	0.139	0.009	0.02008	0.00036	132	8
10zj096-06	595	371	1.61	0.04950	0.00152	0.137	0.004	0.02007	0.00032	130	4
10zj096-07	258	424	0.61	0.04643	0.00126	0.133	0.004	0.02077	0.00032	127	3
10zj096-08	1019	2044	0.50	0.05702	0.00195	0.158	0.005	0.02019	0.00033	149	5
10zj096-09	122	81	1.51	0.04936	0.00593	0.138	0.016	0.02035	0.00056	132	15
10zj096-10	83	79	1.05	0.04971	0.00443	0.136	0.012	0.01985	0.00040	130	11
10zj096-11	71	68	1.05	0.04948	0.00444	0.140	0.012	0.02057	0.00043	133	11

Appendices

10zj096-12	114	100	1.14	0.04867	0.00291	0.140	0.008	0.02080	0.00034	133	7	133	2
10zj096-13	369	475	0.78	0.04781	0.00162	0.137	0.005	0.02080	0.00034	130	4	133	2
10zj096-14	108	131	0.82	0.04751	0.00536	0.135	0.015	0.02064	0.00057	129	13	132	4
10zj096-15	53	42	1.25	0.04699	0.00905	0.136	0.026	0.02093	0.00068	129	23	134	4
10zj096-16	73	67	1.09	0.04896	0.00437	0.141	0.012	0.02086	0.00039	134	11	133	2
10zj096-17	200	152	1.32	0.04964	0.00232	0.137	0.006	0.02007	0.00032	131	6	128	2
10zj096-18	122	84	1.44	0.05068	0.00347	0.142	0.010	0.02031	0.00034	135	9	130	2
10zj096-19	155	159	0.97	0.05975	0.00299	0.169	0.008	0.02056	0.00040	159	7	131	3
10zj096-20	80	74	1.07	0.06433	0.00616	0.186	0.017	0.02095	0.00061	173	15	134	4

**10ZJS099 (Matou monzogranite, LA-ICP-MS)**

Spot No.	Th (ppm)	U (ppm)	Th/U	Corrected isotope ratios				Isotope ages (Ma)			
				$^{207}\text{Pb}/^{206}\text{Pb}$	1 SD	$^{207}\text{Pb}/^{235}\text{U}$	1 SD	$^{206}\text{Pb}/^{238}\text{U}$	1 SD	$^{207}\text{Pb}/^{235}\text{U}$	1 SD
10zj099-01	167	102	1.63	0.04984	0.01090	0.108	0.023	0.01570	0.00060	104	21
10zj099-02	337	174	1.93	0.04831	0.00273	0.107	0.006	0.01610	0.00030	104	6
10zj099-03	133	83	1.61	0.04838	0.01118	0.106	0.024	0.01590	0.00060	102	22
10zj099-04	112	66	1.69	0.04833	0.01152	0.108	0.025	0.01620	0.00070	104	23
10zj099-05	195	113	1.72	0.04911	0.00745	0.106	0.016	0.01570	0.00040	102	15
10zj099-06	1194	741	1.61	0.04995	0.00120	0.141	0.004	0.02040	0.00030	134	3
10zj099-07	159	80	1.99	0.04939	0.00612	0.106	0.013	0.01550	0.00040	102	12
10zj099-08	252	122	2.07	0.05070	0.00760	0.108	0.016	0.01550	0.00050	104	15
10zj099-09	85	76	1.11	0.10652	0.00136	4.171	0.065	0.28410	0.00420	1668	13
10zj099-10	259	148	1.75	0.04743	0.00761	0.106	0.017	0.01630	0.00050	103	16
10zj099-11	200	115	1.73	0.05187	0.00662	0.110	0.014	0.01540	0.00040	106	13
10zj099-12	150	92	1.62	0.05195	0.00766	0.111	0.016	0.01560	0.00040	107	15
10zj099-13	75	497	0.15	0.05061	0.00112	0.239	0.006	0.03420	0.00050	217	5
10zj099-14	168	96	1.74	0.08140	0.00893	0.186	0.020	0.01660	0.00050	173	17
10zj099-15	128	71	1.81	0.04950	0.00947	0.108	0.021	0.01590	0.00050	104	19

Appendices

10zj099-16	158	87	1.81	0.04910	0.00672	0.106	0.014	0.01570	0.00040	103	13	101	2
10zj099-17	231	124	1.87	0.04948	0.00290	0.110	0.006	0.01610	0.00030	106	6	103	2
10zj099-18	204	107	1.90	0.05137	0.00462	0.113	0.010	0.01590	0.00030	109	9	102	2
10zj099-19	202	116	1.74	0.04962	0.00335	0.110	0.007	0.01610	0.00030	106	7	103	2
10zj099-20	258	143	1.80	0.05197	0.00389	0.111	0.008	0.01550	0.00030	107	8	99	2
10zj099-21	175	85	2.05	0.04952	0.00587	0.107	0.013	0.01570	0.00030	103	12	100	2

**10ZJS101 (Matou monzogranite, LA-ICP-MS)**

Spot No.	Th (ppm)	U (ppm)	Th/U	Corrected isotope ratios				Isotope ages (Ma)			
				$^{207}\text{Pb}/^{206}\text{Pb}$	1 SD	$^{207}\text{Pb}/^{235}\text{U}$	1 SD	$^{206}\text{Pb}/^{238}\text{U}$	1 SD	$^{207}\text{Pb}/^{235}\text{U}$	1 SD
10zj101-01	149	69	2.16	0.04918	0.01047	0.106	0.022	0.01560	0.00060	102	20
10zj101-02	315	136	2.32	0.05403	0.00820	0.118	0.018	0.01580	0.00050	113	16
10zj101-03	163	143	1.14	0.05173	0.00190	0.230	0.009	0.03230	0.00050	210	7
10zj101-04	196	83	2.38	0.05078	0.00615	0.110	0.013	0.01570	0.00030	106	12
10zj101-05	250	141	1.77	0.05456	0.00899	0.116	0.019	0.01540	0.00060	112	17
10zj101-06	462	164	2.82	0.05126	0.00421	0.112	0.009	0.01590	0.00030	108	8
10zj101-07	760	271	2.81	0.04909	0.00202	0.108	0.004	0.01600	0.00030	104	4
10zj101-08	188	107	1.76	0.05273	0.00683	0.113	0.015	0.01550	0.00040	109	13
10zj101-09	332	189	1.76	0.05477	0.00342	0.115	0.007	0.01520	0.00030	110	7
10zj101-10	520	324	1.60	0.05066	0.00136	0.227	0.006	0.03250	0.00050	207	5
10zj101-11	182	89	2.05	0.05262	0.00628	0.117	0.014	0.01620	0.00040	113	13
10zj101-12	804	370	2.18	0.07532	0.00282	0.169	0.006	0.01630	0.00030	159	5
10zj101-13	225	111	2.02	0.05670	0.00748	0.120	0.016	0.01530	0.00050	115	14
10zj101-14	461	233	1.98	0.05138	0.00287	0.113	0.006	0.01600	0.00030	109	6
10zj101-15	309	156	1.97	0.04908	0.00466	0.107	0.010	0.01580	0.00030	103	9
10zj101-16	369	180	2.05	0.06659	0.00515	0.143	0.011	0.01560	0.00040	136	10
10zj101-17	753	354	2.13	0.21186	0.00764	0.588	0.019	0.02010	0.00050	470	12
10zj101-18	315	155	2.03	0.05012	0.00875	0.113	0.019	0.01630	0.00060	109	18

Appendices

10zj101-19	224	123	1.81	0.05683	0.00968	0.120	0.020	0.01530	0.00060	115	18	98	4
10zj101-20	207	139	1.49	0.05153	0.00692	0.112	0.015	0.01570	0.00050	107	13	100	3

**10ZJS104 (Shanghekou syenogranite, LA-ICP-MS)**

Spot No.	Th (ppm)	U (ppm)	Th/U	Corrected isotope ratios				Isotope ages (Ma)			
				$^{207}\text{Pb}/^{206}\text{Pb}$	1 SD	$^{207}\text{Pb}/^{235}\text{U}$	1 SD	$^{206}\text{Pb}/^{238}\text{U}$	1 SD	$^{207}\text{Pb}/^{235}\text{U}$	1 SD
10ZJ104-01a	3502	9043	0.39	0.05048	0.00093	0.140	0.003	0.02020	0.00020	133	2
10ZJ104-02a	3394	6478	0.52	0.04848	0.00072	0.140	0.002	0.02100	0.00030	133	2
10ZJ104-03a	11462	14882	0.77	0.05049	0.00158	0.140	0.004	0.02020	0.00030	133	4
10ZJ104-04a	9908	16663	0.59	0.04195	0.00107	0.116	0.003	0.02030	0.00030	111	3
10ZJ104-05a	4736	6941	0.68	0.04983	0.00077	0.138	0.002	0.02020	0.00030	132	2
10ZJ104-06a	3375	5769	0.58	0.04873	0.00116	0.139	0.003	0.02080	0.00030	133	3
10ZJ104-07a	1568	1834	0.85	0.04908	0.00084	0.158	0.003	0.02330	0.00030	149	2
10ZJ104-08a	732	614	1.19	0.05014	0.00260	0.144	0.007	0.02080	0.00040	136	6
10ZJ104-09a	307	299	1.03	0.04880	0.00404	0.142	0.011	0.02120	0.00050	135	10
10ZJ104-10a	724	802	0.90	0.04782	0.00143	0.136	0.004	0.02070	0.00030	130	4
10ZJ104-11a	13904	26112	0.53	0.04089	0.00088	0.115	0.003	0.02040	0.00030	110	2
10ZJ104-12a	340	168	2.03	0.04888	0.00352	0.137	0.010	0.02030	0.00040	130	9
10ZJ104-13a	5523	10192	0.54	0.04716	0.00149	0.135	0.004	0.02080	0.00030	129	4
10ZJ104-14a	8614	17568	0.49	0.04985	0.00106	0.140	0.003	0.02040	0.00030	133	3
10ZJ104-15a	858	646	1.33	0.04949	0.00361	0.143	0.010	0.02090	0.00050	135	9
10ZJ104-16a	5410	11202	0.48	0.05203	0.00224	0.146	0.006	0.02040	0.00040	138	5
10ZJ104-17a	137	93	1.48	0.04797	0.00562	0.139	0.016	0.02110	0.00040	132	14
10ZJ104-18a	1786	3891	0.46	0.05140	0.00136	0.168	0.004	0.02370	0.00030	158	4
10ZJ104-19a	9068	12302	0.74	0.04906	0.00117	0.137	0.003	0.02030	0.00030	131	3
10ZJ104-20a	2217	3938	0.56	0.04867	0.00081	0.137	0.002	0.02050	0.00030	131	2
10ZJ104-21a	1046	1468	0.71	0.11266	0.00355	0.381	0.012	0.02450	0.00040	328	9

## Appendices

**10ZJS108 (Sucun syenogranite, LA-ICP-MS)**

Spot No.	Th (ppm)	U (ppm)	Th/U	Corrected isotope ratios						Isotope ages (Ma)			
				$^{207}\text{Pb}/^{206}\text{Pb}$	1 SD	$^{207}\text{Pb}/^{235}\text{U}$	1 SD	$^{206}\text{Pb}/^{238}\text{U}$	1 SD	$^{207}\text{Pb}/^{235}\text{U}$	1 SD	$^{206}\text{Pb}/^{238}\text{U}$	1 SD
10ZJ108-01	1025	671	1.53	0.04910	0.00135	0.139	0.004	0.02060	0.00030	132	4	131	2
10ZJ108-02	374	379	0.99	0.04994	0.00133	0.141	0.004	0.02040	0.00030	134	3	130	2
10ZJ108-03	544	431	1.26	0.07130	0.00403	0.215	0.012	0.02190	0.00050	198	10	140	3
10ZJ108-04	1506	663	2.27	0.04851	0.00283	0.166	0.009	0.02480	0.00050	156	8	158	3
10ZJ108-05	1208	875	1.38	0.04957	0.00094	0.142	0.003	0.02070	0.00030	135	3	132	2
10ZJ108-06	1520	1787	0.85	0.05112	0.00076	0.254	0.004	0.03600	0.00050	230	4	228	3
10ZJ108-07	800	749	1.07	0.05058	0.00202	0.143	0.006	0.02050	0.00040	136	5	131	2
10ZJ108-08	383	430	0.89	0.05567	0.00229	0.162	0.007	0.02110	0.00040	152	6	134	2
10ZJ108-09	865	567	1.52	0.06816	0.00182	0.178	0.005	0.01890	0.00030	166	4	121	2
10ZJ108-10	613	523	1.17	0.04748	0.00088	0.135	0.003	0.02060	0.00030	128	2	131	2
10ZJ108-11	474	452	1.05	0.04828	0.00104	0.137	0.003	0.02060	0.00030	131	3	132	2
10ZJ108-12	1366	730	1.87	0.04857	0.00081	0.136	0.003	0.02020	0.00030	129	2	129	2
10ZJ108-13	3096	4768	0.65	0.05076	0.00110	0.145	0.003	0.02080	0.00030	138	3	132	2
10ZJ108-15	63	50	1.26	0.05036	0.00615	0.145	0.018	0.02090	0.00050	137	16	133	3
10ZJ108-16	639	604	1.06	0.04803	0.00124	0.137	0.004	0.02070	0.00030	130	3	132	2
10ZJ108-17	1355	720	1.88	0.04656	0.00131	0.136	0.004	0.02120	0.00030	130	4	135	2
10ZJ108-18	545	406	1.34	0.04926	0.00103	0.140	0.003	0.02070	0.00030	134	3	132	2
10ZJ108-19	341	336	1.02	0.04922	0.00234	0.142	0.007	0.02090	0.00040	135	6	133	2
10ZJ108-20	394	443	0.89	0.04991	0.00101	0.140	0.003	0.02040	0.00030	133	3	130	2
10ZJ108-21	983	630	1.56	0.04825	0.00126	0.139	0.004	0.02090	0.00030	132	3	133	2
10ZJ108-22	58	41	1.41	0.04990	0.01188	0.144	0.034	0.02100	0.00070	137	30	134	4
10ZJ108-23	1067	595	1.79	0.04808	0.00084	0.139	0.003	0.02090	0.00030	132	2	133	2
10ZJ108-24	1404	767	1.83	0.05059	0.00219	0.143	0.006	0.02050	0.00040	135	5	131	2

## Appendices

**10ZJS109 (Huangkang syenogranite, LA-ICP-MS)**

Spot No.	Th (ppm)	U (ppm)	Th/U	Corrected isotope ratios						Isotope ages (Ma)			
				$^{207}\text{Pb}/^{206}\text{Pb}$	1 SD	$^{207}\text{Pb}/^{235}\text{U}$	1 SD	$^{206}\text{Pb}/^{238}\text{U}$	1 SD	$^{207}\text{Pb}/^{235}\text{U}$	1 SD	$^{206}\text{Pb}/^{238}\text{U}$	1 SD
10ZJ109-01	51	44	1.18	0.05019	0.00573	0.140	0.016	0.02020	0.00050	133	14	129	3
10ZJ109-02	929	885	1.05	0.04965	0.00258	0.142	0.007	0.02070	0.00040	135	6	132	3
10ZJ109-03	247	309	0.80	0.04948	0.00130	0.142	0.004	0.02080	0.00030	135	3	133	2
10ZJ109-04	142	123	1.15	0.04743	0.00300	0.134	0.008	0.02050	0.00040	128	8	131	3
10ZJ109-05	917	1057	0.87	0.04754	0.00073	0.209	0.004	0.03190	0.00050	193	3	203	3
10ZJ109-06	560	432	1.30	0.05371	0.00280	0.149	0.008	0.02010	0.00040	141	7	128	3
10ZJ109-07	125	174	0.72	0.05092	0.00370	0.142	0.010	0.02020	0.00050	134	9	129	3
10ZJ109-08	326	324	1.00	0.04734	0.00166	0.133	0.005	0.02030	0.00040	127	4	130	2
10ZJ109-09	340	385	0.88	0.04888	0.00144	0.141	0.004	0.02090	0.00040	134	4	133	2
10ZJ109-10	158	187	0.84	0.04365	0.00488	0.122	0.013	0.02020	0.00070	117	12	129	4
10ZJ109-11	1125	1013	1.11	0.04776	0.00088	0.221	0.004	0.03360	0.00050	203	4	213	3
10ZJ109-12	474	525	0.90	0.05109	0.00126	0.217	0.006	0.03080	0.00050	199	5	196	3
10ZJ109-13	5085	3984	1.28	0.08006	0.00116	0.349	0.006	0.03160	0.00050	304	4	200	3
10ZJ109-14	3638	4963	0.73	0.08472	0.00147	0.371	0.007	0.03170	0.00050	320	5	201	3
10ZJ109-15	1977	1539	1.28	0.08048	0.00151	0.354	0.007	0.03190	0.00050	307	5	202	3
10ZJ109-16	1128	921	1.22	0.05055	0.00097	0.150	0.003	0.02150	0.00030	142	3	137	2
10ZJ109-17	1465	1358	1.08	0.04709	0.00071	0.229	0.004	0.03520	0.00050	209	3	223	3
10ZJ109-18	1537	1772	0.87	0.05501	0.00149	0.266	0.007	0.03510	0.00060	240	6	222	4
10ZJ109-19	1126	1062	1.06	0.08110	0.00139	0.292	0.005	0.02610	0.00040	260	4	166	2
10ZJ109-20	778	910	0.86	0.05299	0.00227	0.149	0.006	0.02040	0.00040	141	6	130	2
10ZJ109-21	123	123	1.00	0.04868	0.00755	0.141	0.022	0.02100	0.00060	134	19	134	4
10ZJ109-22	80	81	0.99	0.04985	0.00703	0.140	0.019	0.02030	0.00060	133	17	130	4
10ZJ109-23	1058	774	1.37	0.04936	0.00090	0.139	0.003	0.02040	0.00030	132	2	130	2
10ZJ109-24	1472	975	1.51	0.04910	0.00347	0.141	0.010	0.02080	0.00050	134	9	133	3
10ZJ109-25	590	539	1.09	0.04832	0.00139	0.138	0.004	0.02080	0.00030	132	4	132	2
10ZJ109-26	169	174	0.97	0.04945	0.00844	0.137	0.023	0.02010	0.00080	130	20	128	5
10ZJ109-27	1750	2017	0.87	0.04903	0.00060	0.230	0.003	0.03400	0.00050	210	3	216	3

Appendices

10ZJ109-28	1248	900	1.39	0.04881	0.00117	0.139	0.003	0.02070	0.00030	132	3	132	2
10ZJ109-29	973	789	1.23	0.05057	0.00197	0.146	0.006	0.02090	0.00040	138	5	134	2
10ZJ109-30	1565	1298	1.21	0.05604	0.00091	0.270	0.005	0.03490	0.00050	243	4	221	3

**10ZJS115 (Muchen diorite, MME, LA-ICP-MS)**

Spot No.	Th (ppm)	U (ppm)	Th/U	Corrected isotope ratios				Isotope ages (Ma)			
				$^{207}\text{Pb}/^{206}\text{Pb}$	1 SD	$^{207}\text{Pb}/^{235}\text{U}$	1 SD	$^{206}\text{Pb}/^{238}\text{U}$	1 SD	$^{207}\text{Pb}/^{235}\text{U}$	1 SD
10zj115-01	657	358	1.83	0.05479	0.00432	0.128	0.010	0.01690	0.00050	122	9
10zj115-02	178	174	1.02	0.04936	0.00171	0.120	0.004	0.01760	0.00030	115	4
10zj115-03	333	226	1.48	0.05003	0.00336	0.124	0.008	0.01800	0.00040	119	7
10zj115-04	675	339	1.99	0.04681	0.00121	0.112	0.003	0.01730	0.00030	107	3
10zj115-05	1614	653	2.47	0.05095	0.00093	0.121	0.002	0.01720	0.00020	116	2
10zj115-06	492	310	1.59	0.05026	0.00115	0.120	0.003	0.01730	0.00020	115	3
10zj115-07	207	152	1.36	0.05023	0.00247	0.120	0.006	0.01740	0.00030	116	5
10zj115-08	1627	639	2.54	0.04835	0.00090	0.119	0.002	0.01780	0.00030	114	2
10zj115-09	359	231	1.55	0.04978	0.00145	0.119	0.003	0.01730	0.00030	114	3
10zj115-10	311	146	2.13	0.05117	0.00414	0.120	0.009	0.01710	0.00040	115	9
10zj115-11	399	232	1.72	0.05007	0.00158	0.119	0.004	0.01720	0.00030	114	3
10zj115-12	388	208	1.86	0.04994	0.00155	0.120	0.004	0.01750	0.00030	115	3
10zj115-13	756	478	1.58	0.04841	0.00097	0.118	0.003	0.01770	0.00020	113	2
10zj115-14	469	265	1.77	0.04953	0.00152	0.118	0.004	0.01720	0.00030	113	3
10zj115-15	437	241	1.82	0.04908	0.00144	0.118	0.004	0.01750	0.00030	113	3
10zj115-16	462	281	1.64	0.05433	0.00379	0.128	0.009	0.01710	0.00040	122	8
10zj115-17	776	375	2.07	0.04913	0.00120	0.118	0.003	0.01740	0.00030	113	3
10zj115-18	348	229	1.52	0.05069	0.00136	0.121	0.003	0.01730	0.00030	116	3
10zj115-19	1066	468	2.28	0.04983	0.00098	0.117	0.002	0.01700	0.00020	112	2
10zj115-20	450	326	1.38	0.04912	0.00119	0.118	0.003	0.01740	0.00030	113	3

Appendices

**10ZJS116 (Muchen quartz monzonite, LA-ICP-MS)**

Spot No.	Th (ppm)	U (ppm)	Th/U	Corrected isotope ratios				Isotope ages (Ma)			
				$^{207}\text{Pb}/^{206}\text{Pb}$	1 SD	$^{207}\text{Pb}/^{235}\text{U}$	1 SD	$^{206}\text{Pb}/^{238}\text{U}$	1 SD	$^{207}\text{Pb}/^{235}\text{U}$	1 SD
10zj116-01	444	277	1.60	0.04847	0.00179	0.117	0.004	0.01740	0.00030	112	4
10zj116-02	538	325	1.66	0.04853	0.00161	0.119	0.004	0.01790	0.00030	115	4
10zj116-03	340	231	1.47	0.04963	0.00138	0.119	0.003	0.01740	0.00030	114	3
10zj116-04	383	274	1.40	0.04835	0.00125	0.117	0.003	0.01750	0.00030	112	3
10zj116-05	236	184	1.28	0.04747	0.00211	0.118	0.005	0.01800	0.00030	113	5
10zj116-06	375	258	1.45	0.04730	0.00130	0.116	0.003	0.01790	0.00030	112	3
10zj116-07	164	107	1.53	0.04911	0.00322	0.120	0.008	0.01780	0.00030	115	7
10zj116-08	310	224	1.38	0.04957	0.00569	0.118	0.013	0.01720	0.00060	113	12
10zj116-09	642	304	2.11	0.05113	0.00133	0.120	0.003	0.01710	0.00030	115	3
10zj116-10	826	589	1.40	0.05108	0.00102	0.120	0.003	0.01710	0.00020	116	2
10zj116-11	334	232	1.44	0.05068	0.00515	0.120	0.012	0.01720	0.00050	115	11
10zj116-12	906	409	2.22	0.04889	0.00119	0.115	0.003	0.01710	0.00030	111	3
10zj116-13	379	259	1.47	0.05000	0.00138	0.120	0.003	0.01740	0.00030	115	3
10zj116-14	321	199	1.61	0.04967	0.00151	0.120	0.004	0.01750	0.00030	115	3
10zj116-15	341	231	1.48	0.05117	0.00144	0.121	0.003	0.01710	0.00030	116	3
10zj116-16	228	162	1.41	0.05015	0.00172	0.119	0.004	0.01720	0.00030	114	4
10zj116-17	367	220	1.67	0.04552	0.00123	0.113	0.003	0.01800	0.00030	108	3
10zj116-18	752	395	1.90	0.04943	0.00157	0.121	0.004	0.01770	0.00030	116	3
10zj116-19	335	220	1.52	0.04869	0.00212	0.114	0.005	0.01710	0.00030	110	4
10zj116-20	440	255	1.73	0.04816	0.00164	0.118	0.004	0.01770	0.00030	113	4

**10ZJS121 (Wangcun syenogranite, SHRIMP)**

Spot Name	U (ppm)	Th (ppm)	Th/U	204-corr %com206	4corr 207*	%err	4corr 207*	% err	4corr 206*	% err	$\rho$	204corr $^{207}\text{Pb}$	1 SD	204corr $^{206}\text{Pb}$	1 SD
-----------	------------	-------------	------	---------------------	---------------	------	---------------	----------	---------------	----------	--------	------------------------------	------	------------------------------	------

Appendices

	10ZJS121-1	/206*					/235			/238			/235U		/238U	
		348	247	0.71	-0.24	0.0578	4.4	0.169	4.5	0.0212	1.2	0.3	159	7	135	2
	10ZJS121-2	872	446	0.51	0	0.0516	4.2	0.144	4.4	0.0202	1.3	0.3	136	6	129	2
	10ZJS121-3	596	346	0.58	0.44	0.0466	6.2	0.127	6.4	0.0198	1.4	0.2	122	7	126	2
	10ZJS121-4	636	624	0.98	-0.28	0.0503	6.0	0.144	6.0	0.0208	0.7	0.1	137	8	133	1
	10ZJS121-5	154	123	0.80	0	0.0684	4.2	0.195	4.9	0.0207	2.6	0.5	181	8	132	3
	10ZJS121-6	134	105	0.79	-1.86	0.0769	11.2	0.215	11.3	0.0203	1.6	0.1	198	20	129	2
	10ZJS121-7	301	331	1.10	-1.42	0.0613	8.5	0.177	8.6	0.0210	1.1	0.1	165	13	134	1
	10ZJS121-8	518	418	0.81	0.83	0.0492	8.8	0.131	8.8	0.0194	0.9	0.1	125	10	124	1
	10ZJS121-9	399	389	0.97	-1.90	0.0649	9.2	0.190	9.3	0.0213	1.0	0.1	177	15	136	1
	10ZJS121-10	241	207	0.86	3.32	0.0620	14.4	0.203	14.4	0.0237	1.5	0.1	187	25	151	2
	10ZJS121-11	540	938	1.74	0	0.0493	2.6	0.140	2.7	0.0206	0.7	0.3	133	3	131	1
	10ZJS121-12	254	266	1.05	-1.59	0.0596	9.7	0.174	9.8	0.0212	1.2	0.1	163	15	135	2
	10ZJS121-13	181	156	0.87	-2.22	0.0731	10.7	0.209	11.0	0.0208	2.4	0.2	193	19	132	3
	10ZJS121-14	528	937	1.77	-0.84	0.0559	5.8	0.162	5.8	0.0210	0.8	0.1	152	8	134	1
	10ZJS121-15	145	156	1.08	2.17	0.0828	19.0	0.236	19.1	0.0206	1.6	0.1	215	37	132	2
	10ZJS121-16	206	224	1.09	-0.48	0.0656	6.9	0.180	7.0	0.0199	1.1	0.2	168	11	127	1
	10ZJS121-17	310	424	1.37	11.05	0.3120	7.9	1.302	8.8	0.0303	3.9	0.4	847	51	192	7
	10ZJS121-18	139	125	0.90	-4.26	0.0845	14.2	0.252	14.4	0.0216	2.4	0.2	228	29	138	3
	10ZJS121-19	278	290	1.04	-1.96	0.0667	9.6	0.197	9.7	0.0214	1.2	0.1	182	16	137	2
	10ZJS121-20	113	127	1.12	4.20	0.0222	72.8	0.061	73.0	0.0198	4.0	0.1	60	42	127	5

**10ZJS125 (Muchen granitic porphyry, LA-ICP-MS)**

Spot No.	Th (ppm)	U (ppm)	Th/U	Corrected isotope ratios				Isotope ages (Ma)			
				$^{207}\text{Pb}/^{206}\text{Pb}$	1 SD	$^{207}\text{Pb}/^{235}\text{U}$	1 SD	$^{206}\text{Pb}/^{238}\text{U}$	1 SD	$^{207}\text{Pb}/^{235}\text{U}$	1 SD
10ZJ125-01	267	195	1.37	0.04746	0.00440	0.112	0.010	0.01710	0.00040	108	9
10ZJ125-02	396	198	2.00	0.05089	0.00219	0.120	0.005	0.01710	0.00030	115	5

Appendices

10ZJ125-03	300	231	1.30	0.05052	0.00194	0.123	0.005	0.01760	0.00030	118	4	113	2
10ZJ125-04	403	269	1.50	0.05267	0.00209	0.127	0.005	0.01750	0.00030	121	5	112	2
10ZJ125-05	418	326	1.28	0.05027	0.00165	0.119	0.004	0.01720	0.00030	114	4	110	2
10ZJ125-06	301	242	1.25	0.05101	0.00188	0.122	0.005	0.01740	0.00030	117	4	111	2
10ZJ125-07	184	171	1.08	0.05206	0.00492	0.123	0.011	0.01720	0.00040	118	10	110	3
10ZJ125-08	263	278	0.95	0.04991	0.00159	0.120	0.004	0.01740	0.00030	115	4	111	2
10ZJ125-09	484	339	1.43	0.05011	0.00557	0.119	0.013	0.01720	0.00050	114	12	110	3
10ZJ125-10	547	365	1.50	0.05129	0.00139	0.124	0.004	0.01760	0.00030	119	3	112	2
10ZJ125-11	95	66	1.43	0.04941	0.00702	0.122	0.017	0.01790	0.00040	117	16	114	3
10ZJ125-12	366	433	0.85	0.04994	0.00124	0.117	0.003	0.01710	0.00030	113	3	109	2
10ZJ125-13	292	263	1.11	0.04933	0.00265	0.116	0.006	0.01710	0.00030	111	6	109	2
10ZJ125-14	173	163	1.06	0.05088	0.00692	0.124	0.017	0.01770	0.00060	119	15	113	3
10ZJ125-15	748	566	1.32	0.05298	0.00173	0.125	0.004	0.01710	0.00030	119	4	109	2
10ZJ125-16	191	434	0.44	0.04962	0.00239	0.117	0.006	0.01710	0.00030	112	5	109	2
10ZJ125-17	375	289	1.30	0.05251	0.00205	0.122	0.005	0.01690	0.00030	117	4	108	2

**10ZJS129 (Yingcun granitic porphyry, LA-ICP-MS)**

Spot No.	Th (ppm)	U (ppm)	Th/U	Corrected isotope ratios				Isotope ages (Ma)			
				$^{207}\text{Pb}/^{206}\text{Pb}$	1 SD	$^{207}\text{Pb}/^{235}\text{U}$	1 SD	$^{206}\text{Pb}/^{238}\text{U}$	1 SD	$^{207}\text{Pb}/^{235}\text{U}$	1 SD
10ZJ129-01	315	235	1.34	0.05319	0.00265	0.152	0.008	0.02080	0.00040	144	7
10ZJ129-02	523	296	1.77	0.05053	0.00183	0.147	0.005	0.02110	0.00040	139	5
10ZJ129-03	261	167	1.56	0.05009	0.00483	0.145	0.014	0.02100	0.00060	138	12
10ZJ129-04	182	130	1.41	0.04784	0.00303	0.141	0.009	0.02140	0.00040	134	8
10ZJ129-05	219	139	1.57	0.04998	0.00683	0.147	0.020	0.02130	0.00070	139	17
10ZJ129-06	208	136	1.54	0.04868	0.00329	0.139	0.009	0.02080	0.00040	133	8
10ZJ129-07	368	240	1.54	0.04848	0.01136	0.144	0.033	0.02160	0.00100	137	29
10ZJ129-08	175	127	1.38	0.05152	0.00418	0.148	0.012	0.02090	0.00040	140	11
10ZJ129-09	247	223	1.11	0.05064	0.00206	0.148	0.006	0.02120	0.00040	140	5

Appendices

10ZJ129-10	266	186	1.43	0.05074	0.00506	0.147	0.015	0.02100	0.00050	139	13	134	3
10ZJ129-11	620	526	1.18	0.04902	0.00104	0.140	0.003	0.02070	0.00030	133	3	132	2
10ZJ129-12	505	469	1.08	0.04905	0.00110	0.144	0.003	0.02130	0.00030	137	3	136	2
10ZJ129-13	598	384	1.56	0.05017	0.00152	0.146	0.005	0.02110	0.00030	138	4	135	2
10ZJ129-14	268	183	1.46	0.05085	0.00368	0.146	0.011	0.02090	0.00040	139	9	133	3
10ZJ129-15	1046	903	1.16	0.05054	0.00095	0.146	0.003	0.02090	0.00030	138	3	133	2
10ZJ129-16	315	243	1.30	0.05016	0.00778	0.150	0.023	0.02170	0.00070	142	20	138	5
10ZJ129-17	571	404	1.41	0.05125	0.00203	0.146	0.006	0.02070	0.00040	139	5	132	2
10ZJ129-18	395	202	1.96	0.05142	0.00779	0.147	0.022	0.02080	0.00080	139	19	133	5
10ZJ129-19	204	147	1.39	0.05358	0.00714	0.154	0.020	0.02090	0.00070	145	18	133	4
10ZJ129-20	172	119	1.44	0.04893	0.00406	0.140	0.012	0.02080	0.00040	133	10	132	3

**10ZJS131 (Muchen quartz monzonite, LA-ICP-MS)**

Spot No.	Th (ppm)	U (ppm)	Th/U	Corrected isotope ratios						Isotope ages (Ma)			
				$^{207}\text{Pb}/^{206}\text{Pb}$	1 SD	$^{207}\text{Pb}/^{235}\text{U}$	1 SD	$^{206}\text{Pb}/^{238}\text{U}$	1 SD	$^{207}\text{Pb}/^{235}\text{U}$	1 SD	$^{206}\text{Pb}/^{238}\text{U}$	1 SD
10ZJS131-01	151	108	1.40	0.04980	0.00215	0.116	0.005	0.01700	0.00030	112	5	109	2
10ZJS131-02	217	145	1.50	0.04967	0.00121	0.115	0.003	0.01680	0.00030	111	3	108	2
10ZJS131-03	290	208	1.39	0.04854	0.00117	0.115	0.003	0.01710	0.00030	110	3	110	2
10ZJS131-04	719	554	1.30	0.04676	0.00092	0.113	0.002	0.01760	0.00020	109	2	112	2
10ZJS131-05	377	249	1.52	0.04675	0.00128	0.110	0.003	0.01700	0.00030	106	3	109	2
10ZJS131-06	4031	1065	3.78	0.04953	0.00067	0.140	0.002	0.02060	0.00030	133	2	131	2
10ZJS131-07	158	119	1.32	0.04985	0.00316	0.116	0.007	0.01690	0.00040	112	6	108	2
10ZJS131-08	298	229	1.30	0.04825	0.00148	0.114	0.004	0.01720	0.00030	110	3	110	2
10ZJS131-09	278	212	1.31	0.04989	0.00154	0.120	0.004	0.01750	0.00030	115	3	112	2
10ZJS131-10	187	131	1.43	0.04910	0.00154	0.116	0.004	0.01710	0.00030	111	3	109	2
10ZJS131-11	293	253	1.16	0.09622	0.00315	0.239	0.008	0.01800	0.00030	218	6	115	2
10ZJS131-12	389	213	1.83	0.05264	0.00108	0.123	0.003	0.01690	0.00030	117	2	108	2
10ZJS131-13	1896	723	2.62	0.04846	0.00077	0.116	0.002	0.01730	0.00020	111	2	111	2

Appendices

10ZJS131-14	324	188	1.73	0.05218	0.00289	0.121	0.007	0.01690	0.00040	116	6	108	2
10ZJS131-15	314	205	1.53	0.04681	0.00156	0.110	0.004	0.01710	0.00030	106	3	109	2
10ZJS131-16	323	231	1.40	0.04916	0.00293	0.115	0.007	0.01700	0.00040	111	6	109	2
10ZJS131-17	212	114	1.86	0.04985	0.00215	0.120	0.005	0.01750	0.00030	115	5	112	2
10ZJS131-18	157	120	1.31	0.04934	0.00151	0.120	0.004	0.01760	0.00030	115	3	113	2
10ZJS131-19	154	151	1.02	0.05181	0.00174	0.121	0.004	0.01700	0.00030	116	4	109	2
10ZJS131-20	262	165	1.59	0.05166	0.00132	0.123	0.003	0.01730	0.00030	118	3	111	2
10ZJS131-21	431	238	1.81	0.05231	0.00217	0.124	0.005	0.01720	0.00030	118	5	110	2
10ZJS131-22	297	254	1.17	0.05100	0.00130	0.124	0.003	0.01760	0.00030	118	3	112	2
10ZJS131-23	241	206	1.17	0.05101	0.00183	0.122	0.004	0.01740	0.00030	117	4	111	2
10ZJS131-24	278	180	1.55	0.04795	0.00211	0.114	0.005	0.01730	0.00030	110	4	111	2

**10ZJS132 (Muchen quartz monzonite, LA-ICP-MS)**

Spot No.	Th (ppm)	U (ppm)	Th/U	Corrected isotope ratios						Isotope ages (Ma)			
				$^{207}\text{Pb}/^{206}\text{Pb}$	1 SD	$^{207}\text{Pb}/^{235}\text{U}$	1 SD	$^{206}\text{Pb}/^{238}\text{U}$	1 SD	$^{207}\text{Pb}/^{235}\text{U}$	1 SD	$^{206}\text{Pb}/^{238}\text{U}$	1 SD
10ZJS132-01	182	170	1.07	0.04930	0.00214	0.119	0.005	0.01750	0.00030	114	5	112	2
10ZJS132-02	192	124	1.54	0.05032	0.00343	0.120	0.008	0.01730	0.00030	115	7	110	2
10ZJS132-03	245	217	1.13	0.04934	0.00185	0.121	0.005	0.01780	0.00030	116	4	113	2
10ZJS132-04	522	369	1.41	0.04749	0.00131	0.115	0.003	0.01750	0.00030	110	3	112	2
10ZJS132-05	359	292	1.23	0.05065	0.00173	0.121	0.004	0.01740	0.00030	116	4	111	2
10ZJS132-06	193	171	1.13	0.04833	0.00473	0.120	0.012	0.01810	0.00040	115	11	115	3
10ZJS132-07	320	264	1.21	0.05049	0.00434	0.125	0.011	0.01800	0.00040	120	10	115	3
10ZJS132-08	315	267	1.18	0.04733	0.00287	0.115	0.007	0.01760	0.00030	111	6	113	2
10ZJS132-09	430	296	1.45	0.04998	0.00206	0.120	0.005	0.01750	0.00030	116	5	112	2
10ZJS132-10	70	90	0.78	0.04975	0.00789	0.122	0.019	0.01780	0.00060	117	17	114	4
10ZJS132-11	343	233	1.47	0.04937	0.00193	0.118	0.005	0.01730	0.00030	113	4	111	2
10ZJS132-12	387	238	1.63	0.05019	0.00312	0.124	0.008	0.01790	0.00040	118	7	114	2
10ZJS132-13	144	205	0.70	0.05731	0.00256	0.112	0.005	0.01420	0.00020	108	5	91	2

Appendices

10ZJS132-14	144	146	0.98	0.05095	0.00484	0.127	0.012	0.01810	0.00040	121	11	115	3
10ZJS132-15	483	413	1.17	0.04795	0.00217	0.119	0.005	0.01800	0.00030	114	5	115	2
10ZJS132-16	441	393	1.12	0.05057	0.00159	0.121	0.004	0.01740	0.00030	116	4	111	2

**10ZJS133 (Luojia granitic porphyry, LA-ICP-MS)**

Spot No.	Th (ppm)	U (ppm)	Th/U	Corrected isotope ratios				Isotope ages (Ma)			
				$^{207}\text{Pb}/^{206}\text{Pb}$	1 SD	$^{207}\text{Pb}/^{235}\text{U}$	1 SD	$^{206}\text{Pb}/^{238}\text{U}$	1 SD	$^{207}\text{Pb}/^{235}\text{U}$	1 SD
10ZJ133-01	332	334	1.00	0.04830	0.00128	0.132	0.004	0.01980	0.00030	126	3
10ZJ133-02	141	125	1.13	0.04920	0.00351	0.138	0.010	0.02030	0.00040	131	9
10ZJ133-03	187	200	0.93	0.05356	0.00342	0.145	0.009	0.01960	0.00040	138	8
10ZJ133-04	92	69	1.32	0.04823	0.00727	0.133	0.020	0.02010	0.00060	127	18
10ZJ133-05	90	51	1.78	0.05222	0.01040	0.143	0.028	0.01990	0.00070	136	25
10ZJ133-06	1125	683	1.65	0.05587	0.00193	0.150	0.005	0.01950	0.00030	142	5
10ZJ133-07	120	98	1.23	0.05022	0.00375	0.141	0.010	0.02040	0.00040	134	9
10ZJ133-08	284	345	0.82	0.05009	0.00326	0.138	0.009	0.01990	0.00040	131	8
10ZJ133-09	213	175	1.22	0.05275	0.00603	0.139	0.016	0.01910	0.00060	132	14
10ZJ133-10	100	92	1.08	0.05106	0.00628	0.140	0.017	0.01990	0.00060	133	15
10ZJ133-11	107	126	0.85	0.05000	0.00569	0.140	0.016	0.02040	0.00060	133	14
10ZJ133-12	194	181	1.07	0.05131	0.00351	0.145	0.010	0.02050	0.00040	137	9
10ZJ133-13	948	252	3.77	0.09195	0.00207	0.218	0.005	0.01720	0.00030	200	4
10ZJ133-14	90	77	1.18	0.04893	0.00243	0.130	0.007	0.01930	0.00030	124	6
10ZJ133-15	521	605	0.86	0.04928	0.00099	0.136	0.003	0.02000	0.00030	130	3
10ZJ133-16	39	25	1.59	0.04820	0.02131	0.134	0.059	0.02010	0.00110	128	53
10ZJ133-17	184	171	1.08	0.05003	0.00279	0.139	0.008	0.02020	0.00040	132	7
10ZJ133-18	137	121	1.13	0.05052	0.00365	0.137	0.010	0.01960	0.00040	130	9
10ZJ133-19	269	285	0.94	0.05146	0.00375	0.151	0.011	0.02130	0.00050	143	10
10ZJ133-20	196	132	1.48	0.08201	0.00581	0.227	0.016	0.02010	0.00050	208	13

## Appendices

**10ZJS135 (Sheyang syenogranite, LA-ICP-MS)**

Spot No.	Th (ppm)	U (ppm)	Th/U	Corrected isotope ratios						Isotope ages (Ma)			
				$^{207}\text{Pb}/^{206}\text{Pb}$	1 SD	$^{207}\text{Pb}/^{235}\text{U}$	1 SD	$^{206}\text{Pb}/^{238}\text{U}$	1 SD	$^{207}\text{Pb}/^{235}\text{U}$	1 SD	$^{206}\text{Pb}/^{238}\text{U}$	1 SD
10ZJ135-01	523	378	1.38	0.05166	0.00127	0.250	0.006	0.03520	0.00050	227	5	223	3
10ZJ135-02	720	707	1.02	0.05091	0.00072	0.249	0.004	0.03550	0.00050	226	3	225	3
10ZJ135-03	600	258	2.32	0.05235	0.00127	0.254	0.006	0.03520	0.00050	230	5	223	3
10ZJ135-04	217	96	2.25	0.05150	0.00173	0.252	0.008	0.03540	0.00050	228	7	225	3
10ZJ135-05	664	490	1.36	0.04999	0.00078	0.244	0.004	0.03550	0.00050	222	3	225	3
10ZJ135-06	644	458	1.41	0.05048	0.00077	0.249	0.004	0.03580	0.00050	226	3	227	3
10ZJ135-07	497	171	2.90	0.05163	0.00200	0.258	0.010	0.03620	0.00060	233	8	229	4
10ZJ135-08	898	585	1.54	0.05056	0.00079	0.247	0.004	0.03550	0.00050	224	3	225	3
10ZJ135-09	1089	555	1.96	0.05099	0.00079	0.249	0.004	0.03540	0.00050	226	3	224	3
10ZJ135-10	941	920	1.02	0.05133	0.00068	0.251	0.004	0.03550	0.00050	228	3	225	3
10ZJ135-11	983	612	1.61	0.05183	0.00088	0.253	0.005	0.03540	0.00050	229	4	224	3
10ZJ135-12	669	372	1.80	0.04999	0.00080	0.246	0.004	0.03570	0.00050	223	4	226	3
10ZJ135-13	108	98	1.10	0.05017	0.00266	0.248	0.013	0.03580	0.00070	225	10	227	4
10ZJ135-14	195	105	1.87	0.05281	0.00278	0.256	0.013	0.03520	0.00070	231	11	223	4
10ZJ135-15	302	109	2.78	0.05272	0.00165	0.254	0.008	0.03500	0.00050	230	6	222	3
10ZJ135-16	168	99	1.69	0.05201	0.00184	0.253	0.009	0.03520	0.00060	229	7	223	3
10ZJ135-17	73	35	2.07	0.05052	0.00353	0.250	0.017	0.03590	0.00070	227	14	228	4
10ZJ135-18	311	106	2.93	0.04947	0.00169	0.248	0.008	0.03640	0.00060	225	7	230	4
10ZJ135-19	252	338	0.75	0.08067	0.00135	0.658	0.012	0.05910	0.00080	513	7	370	5
10ZJ135-20	368	125	2.95	0.05149	0.00132	0.256	0.007	0.03600	0.00050	231	5	228	3
10ZJ135-21	510	232	2.20	0.05195	0.00098	0.268	0.005	0.03750	0.00050	241	4	237	3
10ZJ135-22	639	548	1.17	0.05199	0.00073	0.255	0.004	0.03550	0.00050	230	3	225	3

## Appendices

**10ZJS136 (Lingkeng syenogranite, LA-ICP-MS)**

Spot No.	Th (ppm)	U (ppm)	Th/U	Corrected isotope ratios						Isotope ages (Ma)			
				$^{207}\text{Pb}/^{206}\text{Pb}$	1 SD	$^{207}\text{Pb}/^{235}\text{U}$	1 SD	$^{206}\text{Pb}/^{238}\text{U}$	1 SD	$^{207}\text{Pb}/^{235}\text{U}$	1 SD	$^{206}\text{Pb}/^{238}\text{U}$	1 SD
10ZJ136-01	168	171	0.98	0.05055	0.00254	0.180	0.009	0.02590	0.00050	169	8	165	3
10ZJ136-02	933	803	1.16	0.04829	0.00072	0.143	0.002	0.02150	0.00030	136	2	137	2
10ZJ136-03	2188	1647	1.33	0.05152	0.00105	0.145	0.003	0.02040	0.00030	137	3	130	2
10ZJ136-04	3217	2902	1.11	0.06142	0.00077	0.145	0.002	0.01720	0.00020	138	2	110	1
10ZJ136-05	10225	8512	1.20	0.04867	0.00061	0.103	0.002	0.01540	0.00020	100	1	99	1
10ZJ136-06	2845	4121	0.69	0.05070	0.00071	0.111	0.002	0.01590	0.00020	107	2	102	1
10ZJ136-07	399	258	1.55	0.05091	0.00161	0.147	0.005	0.02090	0.00030	139	4	134	2
10ZJ136-08	485	327	1.48	0.04899	0.00164	0.144	0.005	0.02140	0.00030	137	4	136	2
10ZJ136-09	3348	2942	1.14	0.04903	0.00062	0.116	0.002	0.01710	0.00020	111	2	110	1
10ZJ136-10	885	565	1.57	0.04808	0.00095	0.137	0.003	0.02070	0.00030	131	3	132	2
10ZJ136-11	3502	3653	0.96	0.04902	0.00095	0.139	0.003	0.02050	0.00030	132	3	131	2
10ZJ136-12	458	294	1.56	0.04933	0.00234	0.142	0.007	0.02090	0.00040	135	6	134	2
10ZJ136-13	466	301	1.55	0.05018	0.00128	0.144	0.004	0.02080	0.00030	137	3	133	2
10ZJ136-14	213	109	1.94	0.04656	0.00353	0.138	0.010	0.02150	0.00040	132	9	137	3
10ZJ136-15	1822	753	2.42	0.05034	0.00087	0.144	0.003	0.02070	0.00030	137	2	132	2
10ZJ136-16	570	432	1.32	0.04869	0.00099	0.144	0.003	0.02150	0.00030	137	3	137	2
10ZJ136-17	2079	2944	0.71	0.04879	0.00068	0.109	0.002	0.01620	0.00020	105	2	104	1
10ZJ136-18	301	176	1.70	0.05050	0.00340	0.152	0.010	0.02190	0.00050	144	9	139	3
10ZJ136-19	245	323	0.76	0.04962	0.00143	0.142	0.004	0.02080	0.00030	135	4	133	2
10ZJ136-20	329	308	1.07	0.05888	0.00205	0.155	0.005	0.01920	0.00030	147	5	122	2
10ZJ136-21	218	168	1.30	0.04778	0.00203	0.143	0.006	0.02170	0.00040	136	5	138	2
10ZJ136-22	133	79	1.69	0.04966	0.00523	0.144	0.015	0.02100	0.00050	136	13	134	3
10ZJ136-23	1100	340	3.24	0.05085	0.00332	0.146	0.009	0.02080	0.00040	138	8	133	3
10ZJ136-24	519	223	2.32	0.05042	0.00150	0.147	0.004	0.02110	0.00030	139	4	135	2

Appendices

**10ZJS143 (Jiuhua granitic porphyry, LA-ICP-MS)**

Spot No.	Th (ppm)	U (ppm)	Th/U	Corrected isotope ratios				Isotope ages (Ma)			
				$^{207}\text{Pb}/^{206}\text{Pb}$	1 SD	$^{207}\text{Pb}/^{235}\text{U}$	1 SD	$^{206}\text{Pb}/^{238}\text{U}$	1 SD	$^{207}\text{Pb}/^{235}\text{U}$	1 SD
10ZJ143-01	59	36	1.63	0.05021	0.00790	0.145	0.023	0.02090	0.00060	137	20
10ZJ143-02	95	67	1.41	0.04763	0.00418	0.143	0.012	0.02170	0.00040	136	11
10ZJ143-03	64	45	1.42	0.04897	0.00624	0.144	0.018	0.02140	0.00050	137	16
10ZJ143-04	98	71	1.37	0.05212	0.00397	0.146	0.011	0.02030	0.00040	138	10
10ZJ143-05	78	58	1.35	0.04712	0.00416	0.139	0.012	0.02130	0.00040	132	11
10ZJ143-06	161	116	1.38	0.04830	0.00229	0.140	0.007	0.02100	0.00030	133	6
10ZJ143-07	312	176	1.77	0.04964	0.00195	0.147	0.006	0.02140	0.00030	139	5
10ZJ143-08	161	141	1.14	0.04771	0.00195	0.135	0.006	0.02050	0.00030	128	5
10ZJ143-09	197	140	1.41	0.04963	0.00268	0.141	0.008	0.02060	0.00040	134	7
10ZJ143-10	170	107	1.60	0.05020	0.00247	0.141	0.007	0.02040	0.00030	134	6
10ZJ143-11	79	52	1.52	0.04997	0.00457	0.144	0.013	0.02100	0.00040	137	12
10ZJ143-12	104	56	1.87	0.05045	0.00427	0.147	0.012	0.02120	0.00040	140	11
10ZJ143-13	47	32	1.47	0.04763	0.01048	0.138	0.030	0.02110	0.00070	132	27
10ZJ143-14	135	70	1.93	0.04988	0.00407	0.143	0.012	0.02080	0.00040	136	10
10ZJ143-15	82	56	1.48	0.04891	0.01018	0.146	0.030	0.02170	0.00100	138	26
10ZJ143-16	124	84	1.49	0.05185	0.00319	0.146	0.009	0.02050	0.00030	139	8
10ZJ143-17	209	145	1.45	0.05172	0.00216	0.145	0.006	0.02040	0.00030	138	5
10ZJ143-18	65	46	1.39	0.04831	0.00777	0.143	0.023	0.02150	0.00060	136	20
10ZJ143-19	123	78	1.58	0.05006	0.00329	0.144	0.009	0.02090	0.00040	137	8
10ZJ143-20	366	161	2.27	0.05073	0.00373	0.147	0.011	0.02110	0.00050	140	9

**10ZJS149 (Shangsanzhi granitic porphyry, LA-ICP-MS)**

Spot No.	Th (ppm)	U (ppm)	Th/U	Corrected isotope ratios				Isotope ages (Ma)			
				$^{207}\text{Pb}/^{206}\text{Pb}$	1 SD	$^{207}\text{Pb}/^{235}\text{U}$	1 SD	$^{206}\text{Pb}/^{238}\text{U}$	1 SD	$^{207}\text{Pb}/^{235}\text{U}$	1 SD

Appendices

10ZJ149-01	191	770	0.25	0.04989	0.00093	0.173	0.003	0.02510	0.00040	162	3	160	2
10ZJ149-02	347	183	1.90	0.06690	0.00103	1.257	0.021	0.13620	0.00180	826	10	823	10
10ZJ149-03	134	128	1.05	0.06730	0.00241	1.284	0.046	0.13840	0.00270	839	20	836	15
10ZJ149-04	207	630	0.33	0.05011	0.00113	0.173	0.004	0.02500	0.00040	162	4	159	2
10ZJ149-05	430	1100	0.39	0.05269	0.00199	0.256	0.010	0.03520	0.00060	231	8	223	4
10ZJ149-06	148	693	0.21	0.05017	0.00114	0.172	0.004	0.02490	0.00040	161	4	159	2
10ZJ149-07	272	261	1.04	0.06846	0.00102	1.363	0.023	0.14440	0.00200	873	10	869	11
10ZJ149-08	324	883	0.37	0.05061	0.00098	0.171	0.004	0.02440	0.00040	160	3	156	2
10ZJ149-09	202	731	0.28	0.04918	0.00106	0.174	0.004	0.02560	0.00040	163	3	163	2
10ZJ149-10	559	1180	0.47	0.04928	0.00084	0.166	0.003	0.02440	0.00030	156	3	155	2
10ZJ149-11	331	763	0.43	0.04978	0.00131	0.174	0.005	0.02540	0.00040	163	4	162	2
10ZJ149-12	649	1086	0.60	0.04962	0.00086	0.171	0.003	0.02500	0.00040	160	3	159	2
10ZJ149-13	402	358	1.12	0.04798	0.00138	0.165	0.005	0.02490	0.00040	155	4	159	2
10ZJ149-14	398	797	0.50	0.04942	0.00218	0.169	0.007	0.02480	0.00050	158	6	158	3
10ZJ149-15	246	716	0.34	0.04932	0.00095	0.171	0.004	0.02520	0.00040	161	3	161	2
10ZJ149-16	242	386	0.63	0.07572	0.00141	0.706	0.014	0.06760	0.00100	542	8	422	6
10ZJ149-17	154	672	0.23	0.05076	0.00123	0.171	0.004	0.02440	0.00040	160	4	156	2
10ZJ149-18	162	416	0.39	0.05097	0.00183	0.193	0.007	0.02750	0.00040	179	6	175	3
10ZJ149-19	173	673	0.26	0.04980	0.00129	0.174	0.005	0.02540	0.00040	163	4	162	2
10ZJ149-20	251	9925	0.03	0.04935	0.00099	0.113	0.002	0.01660	0.00030	109	2	106	2
10ZJ149-21	305	808	0.38	0.04971	0.00098	0.169	0.004	0.02460	0.00030	159	3	157	2

**10ZJS154 (Lingshan syenogranite, LA-ICP-MS)**

Spot No.	Th (ppm)	U (ppm)	Th/U	Corrected isotope ratios				Isotope ages (Ma)			
				$^{207}\text{Pb}/^{206}\text{Pb}$	1 SD	$^{207}\text{Pb}/^{235}\text{U}$	1 SD	$^{206}\text{Pb}/^{238}\text{U}$	1 SD	$^{207}\text{Pb}/^{235}\text{U}$	1 SD
10zj154-01	994	885	1.12	0.05045	0.00083	0.144	0.003	0.02070	0.00029	137	2
10zj154-02	1670	2252	0.74	0.06204	0.00137	0.175	0.004	0.02047	0.00029	164	3
10zj154-03	951	1225	0.78	0.06049	0.00165	0.174	0.005	0.02086	0.00033	163	4

Appendices

10zj154-04	1281	1078	1.19	0.04921	0.00074	0.139	0.002	0.02042	0.00028	132	2	130	2
10zj154-05	1067	1270	0.84	0.04889	0.00275	0.138	0.007	0.02037	0.00048	132	7	130	3
10zj154-06	6159	4379	1.41	0.08143	0.00142	0.153	0.003	0.01360	0.00019	144	2	87	1
10zj154-07	964	1074	0.90	0.05157	0.00086	0.150	0.003	0.02103	0.00029	142	2	134	2
10zj154-08	1078	1334	0.81	0.05026	0.00096	0.142	0.003	0.02047	0.00029	135	3	131	2
10zj154-09	4236	5188	0.82	0.05104	0.00069	0.118	0.002	0.01677	0.00023	113	2	107	1
10zj154-10	10644	5182	2.05	0.15333	0.00257	0.409	0.007	0.01933	0.00027	348	5	123	2
10zj154-11	636	666	0.95	0.04741	0.00142	0.134	0.004	0.02057	0.00030	128	4	131	2
10zj154-12	666	739	0.90	0.04999	0.00096	0.140	0.003	0.02025	0.00029	133	3	129	2
10zj154-13	715	718	1.00	0.04840	0.00086	0.140	0.003	0.02105	0.00029	134	2	134	2
10zj154-14	989	1223	0.81	0.04916	0.00096	0.138	0.003	0.02033	0.00029	131	3	130	2
10zj154-15	852	1915	0.44	0.07105	0.00126	0.160	0.003	0.01631	0.00022	151	3	104	1
10zj154-16	906	1226	0.74	0.04908	0.00130	0.137	0.004	0.02027	0.00030	131	3	129	2
10zj154-17	922	939	0.98	0.04982	0.00084	0.141	0.003	0.02048	0.00028	134	2	131	2
10zj154-18	962	1110	0.87	0.04933	0.00102	0.138	0.003	0.02025	0.00028	131	3	129	2
10zj154-19	1669	1612	1.03	0.05036	0.00149	0.138	0.004	0.01996	0.00034	132	4	127	2
10zj154-20	1406	1295	1.09	0.06851	0.00103	0.193	0.003	0.02042	0.00028	179	3	130	2
10zj154-21	1244	1250	0.99	0.04970	0.00106	0.139	0.003	0.02025	0.00030	132	3	129	2
10zj154-22	945	946	1.00	0.04767	0.00082	0.133	0.002	0.02023	0.00028	127	2	129	2

**10ZJS155 (Lingshan syenogranite, LA-ICP-MS)**

Spot No.	Th (ppm)	U (ppm)	Th/U	Corrected isotope ratios						Isotope ages (Ma)			
				$^{207}\text{Pb}/^{206}\text{Pb}$	1 SD	$^{207}\text{Pb}/^{235}\text{U}$	1 SD	$^{206}\text{Pb}/^{238}\text{U}$	1 SD	$^{207}\text{Pb}/^{235}\text{U}$	1 SD	$^{206}\text{Pb}/^{238}\text{U}$	1 SD
10zj155-01	819	1036	0.79	0.04871	0.00079	0.141	0.003	0.02107	0.00028	134	2	134	2
10zj155-02	630	737	0.85	0.05063	0.00098	0.140	0.003	0.02009	0.00027	133	3	128	2
10zj155-03	871	1006	0.87	0.04871	0.00088	0.134	0.003	0.01996	0.00027	128	2	127	2
10zj155-04	884	1034	0.86	0.04946	0.00090	0.141	0.003	0.02069	0.00027	134	2	132	2
10zj155-05	958	1028	0.93	0.05023	0.00083	0.139	0.003	0.02013	0.00027	133	2	128	2

Appendices

10zj155-06	926	1114	0.83	0.04909	0.00097	0.140	0.003	0.02063	0.00029	133	3	132	2
10zj155-07	1190	1260	0.94	0.04861	0.00086	0.134	0.003	0.02000	0.00026	128	2	128	2
10zj155-08	605	776	0.78	0.04952	0.00096	0.137	0.003	0.02007	0.00027	130	3	128	2
10zj155-09	868	1152	0.75	0.04849	0.00118	0.133	0.003	0.01997	0.00028	127	3	127	2
10zj155-10	912	1105	0.83	0.04873	0.00147	0.137	0.004	0.02033	0.00030	130	4	130	2
10zj155-11	1738	999	1.74	0.05113	0.00107	0.139	0.003	0.01970	0.00029	132	3	126	2
10zj155-12	888	1031	0.86	0.04955	0.00083	0.138	0.003	0.02015	0.00027	131	2	129	2
10zj155-13	958	1198	0.80	0.04973	0.00080	0.139	0.002	0.02032	0.00028	132	2	130	2
10zj155-14	1039	1225	0.85	0.04851	0.00095	0.136	0.003	0.02033	0.00028	129	3	130	2
10zj155-15	772	934	0.83	0.05103	0.00118	0.145	0.003	0.02056	0.00030	137	3	131	2
10zj155-16	1074	1104	0.97	0.04898	0.00110	0.140	0.003	0.02071	0.00029	133	3	132	2
10zj155-17	1135	1419	0.80	0.05049	0.00086	0.139	0.003	0.02002	0.00027	132	2	128	2
10zj155-18	1336	1830	0.73	0.04944	0.00120	0.138	0.003	0.02020	0.00029	131	3	129	2
10zj155-19	1013	1299	0.78	0.04883	0.00105	0.137	0.003	0.02030	0.00028	130	3	130	2
10zj155-20	566	1024	0.55	0.06600	0.00175	0.196	0.005	0.02157	0.00033	182	4	138	2

**10ZJS156 (Lingshan MME, LA-ICP-MS)**

Spot No.	Th (ppm)	U (ppm)	Th/U	Corrected isotope ratios				Isotope ages (Ma)			
				$^{207}\text{Pb}/^{206}\text{Pb}$	1 SD	$^{207}\text{Pb}/^{235}\text{U}$	1 SD	$^{206}\text{Pb}/^{238}\text{U}$	1 SD	$^{207}\text{Pb}/^{235}\text{U}$	1 SD
10ZJS156-1	1127	1408	0.80	0.05060	0.00078	0.142	0.002	0.02034	0.00028	135	2
10ZJS156-2	244	2048	0.12	0.05451	0.00075	0.153	0.002	0.02030	0.00028	144	2
10ZJS156-3	1044	1405	0.74	0.05010	0.00070	0.146	0.002	0.02108	0.00029	138	2
10ZJS156-4	1367	1654	0.83	0.05011	0.00069	0.141	0.002	0.02040	0.00028	134	2
10ZJS156-5	930	1172	0.79	0.04990	0.00092	0.143	0.003	0.02075	0.00030	136	3
10ZJS156-6	448	1399	0.32	0.41937	0.00506	1.267	0.018	0.02191	0.00031	831	8
10ZJS156-7	297	397	0.75	0.04970	0.00080	0.141	0.003	0.02065	0.00029	134	2
10ZJS156-8	222	245	0.91	0.04895	0.00117	0.141	0.003	0.02086	0.00031	134	3
10ZJS156-9	1174	1432	0.82	0.04904	0.00061	0.145	0.002	0.02146	0.00029	138	2

Appendices

10ZJS156-10	1177	1379	0.85	0.04844	0.00064	0.141	0.002	0.02119	0.00029	134	2	135	2	
10ZJS156-11	1074	1446	0.74	0.04953	0.00074	0.144	0.002	0.02114	0.00029	137	2	135	2	
10ZJS156-12	999	1238	0.81	0.05323	0.00114	0.158	0.004	0.02154	0.00032	149	3	137	2	
10ZJS156-13	162	479	0.34	0.04824	0.00197	0.133	0.005	0.02006	0.00036	127	5	128	2	
10ZJS156-14	1274	1761	0.72	0.05391	0.00089	0.155	0.003	0.02090	0.00029	147	2	133	2	
10ZJS156-15	602	883	0.68	0.05124	0.00080	0.149	0.003	0.02112	0.00030	141	2	135	2	
10ZJS156-16	1081	1009	1.07	0.04961	0.00182	0.144	0.005	0.02099	0.00036	136	5	134	2	
10ZJS156-17	1155	1417	0.81	0.04950	0.00068	0.145	0.002	0.02132	0.00029	138	2	136	2	
10ZJS156-18	346	328	1.05	0.05019	0.00118	0.142	0.003	0.02049	0.00031	135	3	131	2	
10ZJS156-19	1264	1431	0.88	0.05160	0.00069	0.149	0.002	0.02101	0.00029	141	2	134	2	
10ZJS156-20	579	872	0.66	0.05062	0.00082	0.146	0.003	0.02094	0.00029	139	2	134	2	
10ZJS156-21	923	1086	0.85	0.05325	0.00156	0.154	0.005	0.02092	0.00034	145	4	133	2	
10ZJS156-22	6537	3443	1.90	0.05969	0.00089	0.164	0.003	0.01992	0.00028	154	2	127	2	
10ZJS156-23	1218	1402	0.87	0.05006	0.00076	0.144	0.002	0.02082	0.00029	136	2	133	2	
10ZJS156-24	483	647	0.75	0.05205	0.00083	0.151	0.003	0.02106	0.00030	143	2	134	2	
10ZJS156-25	1140	1367	0.83	0.05030	0.00076	0.145	0.002	0.02088	0.00029	137	2	133	2	
10ZJS156-26	414	701	0.59	0.05264	0.00237	0.144	0.006	0.01982	0.00038	136	6	127	2	

**10ZJS170 (Wancunxiang syenogranite, LA-ICP-MS)**

Spot No.	Th (ppm)	U (ppm)	Th/U	Corrected isotope ratios				Isotope ages (Ma)			
				$^{207}\text{Pb}/^{206}\text{Pb}$	1 SD	$^{207}\text{Pb}/^{235}\text{U}$	1 SD	$^{206}\text{Pb}/^{238}\text{U}$	1 SD	$^{207}\text{Pb}/^{235}\text{U}$	1 SD
10ZJS170-1	299	538	0.56	0.05015	0.00071	0.146	0.002	0.02119	0.00030	139	2
10ZJS170-2	173	184	0.94	0.04911	0.00115	0.139	0.003	0.02050	0.00031	132	3
10ZJS170-3	2084	1709	1.22	0.05952	0.00068	0.168	0.002	0.02048	0.00028	158	2
10ZJS170-4	311	466	0.67	0.05307	0.00076	0.149	0.003	0.02040	0.00029	141	2
10ZJS170-5	103	98	1.05	0.05110	0.00133	0.143	0.004	0.02033	0.00031	136	3
10ZJS170-6	79	53	1.50	0.06938	0.00106	1.382	0.024	0.14443	0.00207	881	10
10ZJS170-7	118	129	0.91	0.04916	0.00139	0.136	0.004	0.02002	0.00032	129	3

Appendices

10ZJS170-8	166	199	0.83	0.04912	0.00126	0.138	0.004	0.02044	0.00032	132	3	130	2
10ZJS170-9	70	57	1.24	0.04919	0.00244	0.134	0.006	0.01972	0.00039	128	6	126	2
10ZJS170-10	267	315	0.85	0.05689	0.00160	0.137	0.004	0.01748	0.00028	131	3	112	2
10ZJS170-11	586	787	0.75	0.05296	0.00120	0.149	0.004	0.02041	0.00031	141	3	130	2
10ZJS170-12	308	355	0.87	0.05141	0.00079	0.148	0.003	0.02082	0.00030	140	2	133	2
10ZJS170-13	162	226	0.72	0.05019	0.00124	0.142	0.004	0.02057	0.00032	135	3	131	2
10ZJS170-14	176	236	0.75	0.04963	0.00093	0.141	0.003	0.02065	0.00030	134	3	132	2
10ZJS170-15	118	67	1.77	0.09132	0.00236	0.297	0.008	0.02359	0.00039	264	6	150	2
10ZJS170-16	564	617	0.91	0.04810	0.00065	0.133	0.002	0.02012	0.00028	127	2	128	2
10ZJS170-17	252	256	0.99	0.04879	0.00116	0.135	0.003	0.02011	0.00030	129	3	128	2
10ZJS170-18	101	58	1.73	0.05980	0.00319	0.158	0.008	0.01919	0.00042	149	7	123	3
10ZJS170-19	302	1672	0.18	0.05626	0.00103	0.142	0.003	0.01834	0.00027	135	3	117	2
10ZJS170-20	335	494	0.68	0.05062	0.00081	0.142	0.003	0.02028	0.00029	134	2	130	2
10ZJS170-21	75	94	0.80	0.04985	0.00190	0.142	0.005	0.02071	0.00036	135	5	132	2
10ZJS170-22	233	220	1.06	0.04959	0.00101	0.141	0.003	0.02057	0.00030	134	3	131	2
10ZJS170-23	406	470	0.86	0.04990	0.00126	0.144	0.004	0.02090	0.00032	136	3	133	2
10ZJS170-24	162	181	0.89	0.06109	0.00108	0.179	0.003	0.02130	0.00031	168	3	136	2

**10ZJS171 (Wancunxiang endoskarn, LA-ICP-MS)**

Spot No.	Th (ppm)	U (ppm)	Th/U	Corrected isotope ratios				Isotope ages (Ma)			
				$^{207}\text{Pb}/^{206}\text{Pb}$	1 SD	$^{207}\text{Pb}/^{235}\text{U}$	1 SD	$^{206}\text{Pb}/^{238}\text{U}$	1 SD	$^{207}\text{Pb}/^{235}\text{U}$	1 SD
10zj171-01	267	344	0.78	0.04857	0.00160	0.137	0.005	0.02041	0.00032	130	4
10zj171-02	239	349	0.68	0.05048	0.00143	0.147	0.004	0.02119	0.00032	140	4
10zj171-03	89	159	0.56	0.04735	0.00386	0.121	0.010	0.01860	0.00037	116	9
10zj171-04	141	118	1.19	0.04693	0.00359	0.131	0.010	0.02022	0.00036	125	9
10zj171-05	183	205	0.89	0.05328	0.00276	0.151	0.008	0.02052	0.00036	143	7
10zj171-06	133	112	1.19	0.04970	0.00582	0.139	0.016	0.02025	0.00052	132	14
10zj171-07	327	209	1.56	0.04665	0.00236	0.138	0.007	0.02147	0.00036	131	6

Appendices

10zj171-08	585	697	0.84	0.05059	0.00165	0.136	0.005	0.01944	0.00031	129	4	124	2
10zj171-09	87	73	1.19	0.05107	0.00907	0.139	0.024	0.01971	0.00064	132	22	126	4
10zj171-10	186	191	0.98	0.05013	0.00253	0.143	0.007	0.02075	0.00034	136	6	132	2
10zj171-11	83	102	0.81	0.08222	0.00497	0.247	0.015	0.02175	0.00045	224	12	139	3
10zj171-12	299	442	0.68	0.04754	0.00163	0.131	0.005	0.01995	0.00031	125	4	127	2
10zj171-13	695	848	0.82	0.04966	0.00121	0.136	0.004	0.01991	0.00033	130	3	127	2
10zj171-14	1102	891	1.24	0.05041	0.00190	0.139	0.005	0.02001	0.00043	133	5	128	3
10zj171-15	286	382	0.75	0.04938	0.00136	0.138	0.004	0.02023	0.00032	131	4	129	2
10zj171-16	197	212	0.93	0.04701	0.00198	0.136	0.006	0.02106	0.00035	130	5	134	2
10zj171-17	210	253	0.83	0.05039	0.00201	0.233	0.009	0.03352	0.00062	213	8	213	4
10zj171-18	220	296	0.74	0.05046	0.00442	0.143	0.012	0.02052	0.00052	136	11	131	3
10zj171-19	279	332	0.84	0.04515	0.00167	0.122	0.005	0.01963	0.00031	117	4	125	2
10zj171-20	60	58	1.04	0.05176	0.01146	0.141	0.031	0.01978	0.00078	134	27	126	5
10zj171-21	282	422	0.67	0.04710	0.00124	0.135	0.004	0.02087	0.00032	129	3	133	2
10zj171-22	964	1162	0.83	0.04837	0.00082	0.132	0.003	0.01987	0.00030	126	2	127	2

**10ZJS172 (Damaoshan-Huaiyushan syenogranite-alkali feldspar granite, LA-ICP-MS)**

Spot No.	Th (ppm)	U (ppm)	Th/U	Corrected isotope ratios				Isotope ages (Ma)				
				$^{207}\text{Pb}/^{206}\text{Pb}$	1 SD	$^{207}\text{Pb}/^{235}\text{U}$	1 SD	$^{206}\text{Pb}/^{238}\text{U}$	1 SD	$^{207}\text{Pb}/^{235}\text{U}$	1 SD	
10zj172-01	127	106	1.20	0.07396	0.00481	0.233	0.015	0.02280	0.00050	212	12	
10zj172-02	231	229	1.01	0.05309	0.00270	0.148	0.007	0.02029	0.00040	140	7	
10zj172-03	1651	1172	1.41	0.05924	0.00170	0.183	0.005	0.02239	0.00039	171	5	
10zj172-04	536	277	1.94	0.05219	0.00159	0.149	0.005	0.02071	0.00032	141	4	
10zj172-05	432	471	0.92	0.05063	0.00145	0.140	0.004	0.02005	0.00033	133	4	
10zj172-06	539	659	0.82	0.04701	0.00129	0.139	0.004	0.02149	0.00035	132	4	
10zj172-07	719	677	1.06	0.07874	0.00265	0.233	0.008	0.02155	0.00042	213	6	
10zj172-08	1108	903	1.23	0.04898	0.00102	0.141	0.003	0.02097	0.00034	134	3	
10zj172-09	383	338	1.13	0.05028	0.00135	0.141	0.004	0.02037	0.00032	134	4	
											130	2

Appendices

10zj172-10	485	351	1.38	0.05034	0.00138	0.143	0.004	0.02054	0.00032	135	4	131	2
10zj172-11	358	306	1.17	0.04980	0.00164	0.136	0.005	0.01984	0.00031	130	4	127	2
10zj172-12	541	607	0.89	0.06839	0.00172	0.191	0.005	0.02020	0.00034	177	4	129	2
10zj172-13	200	152	1.32	0.05492	0.00510	0.149	0.014	0.01961	0.00048	141	12	125	3
10zj172-14	228	148	1.54	0.05141	0.00317	0.142	0.009	0.01997	0.00040	134	8	127	3
10zj172-15	377	278	1.36	0.06380	0.00088	0.881	0.015	0.10011	0.00148	641	8	615	9
10zj172-16	223	372	0.60	0.10970	0.00153	2.345	0.039	0.15506	0.00233	1226	12	929	13
10zj172-17	489	481	1.02	0.04930	0.00114	0.136	0.003	0.02006	0.00031	130	3	128	2
10zj172-18	402	256	1.57	0.05095	0.00257	0.144	0.007	0.02051	0.00040	137	6	131	3
10zj172-19	284	258	1.10	0.05071	0.00213	0.141	0.006	0.02010	0.00036	134	5	128	2
10zj172-20	246	241	1.02	0.05138	0.00201	0.147	0.006	0.02077	0.00035	139	5	133	2
10zj172-21	264	258	1.02	0.07142	0.00202	0.224	0.007	0.02280	0.00038	206	5	145	2
10zj172-22	702	442	1.59	0.08704	0.00274	0.266	0.008	0.02216	0.00039	239	7	141	2
10zj172-23	1129	998	1.13	0.05320	0.00128	0.150	0.004	0.02045	0.00033	142	3	131	2
10zj172-24	174	146	1.19	0.04964	0.00289	0.142	0.008	0.02082	0.00037	135	7	133	2

**Appendix C. Table of in-situ zircon trace element results (ppm)**

	Ti	Zrn T (°C)	Sr	Y	La	Ce	Pr	Nd	Sm	Eu	Gd	Tb	Dy	Ho	Er	Tm	Yb	Lu
<b>10ZJS065 (Dashuang syenite, LA-ICP-MS)</b>																		
10zjs065-01t	9	798	0.28	2214	2.48	63	1.35	18.3	16.1	0.51	74	21.7	243	81	339	68	572	105
10zjs065-02t	42	994	0.13	782	0.06	14	0.3	4.8	7.4	3.31	28	7	77	25	112	23	203	41
10zjs065-03t	6	763	0.63	1429	9.89	59	4.55	27.2	15.3	0.57	49	13.2	149	50	212	43	381	72
10zjs065-04t	*n.d.	–	0.28	1648	1.32	26	0.7	5.4	7.8	0.08	43	14	170	59	260	53	463	87
10zjs065-05t	17	877	0.36	2620	33.81	116	8.88	53.7	35.2	1.67	120	29.3	307	95	381	75	637	119
10zjs065-06t	8	785	0.19	1135	n.d.	44	0.24	4.2	8.2	0.7	38	10.5	117	38	162	33	292	55
10zjs065-07t	19	890	0.2	1198	0.05	37	0.5	7.6	10.6	1.69	42	11.1	120	40	175	35	311	62
10zjs065-08t	15	864	0.25	996	24.22	73	7.41	38.5	14.2	1.38	42	10	107	34	142	28	253	52
10zjs065-09t	5	741	1.62	1648	108.28	394	64.53	384	129.5	10.64	165	26.6	214	59	227	42	360	67

Appendices

10zjs065-10t	15	864	0.13	1157	3.22	34	1.71	14.7	14.1	1.99	56	14.4	161	53	223	46	403	78
#Average or median	15	842	0.26	1483	3.22	86	1.53	16.5	14.1	1.53	66	15.79	166	53	223	45	387	74
Whole rock	2277		48	18	329.9	579	58.1	181.5	21.01	1.43	12.3	1.12	4.2	0.69	1.94	0.26	1.69	0.28
**Zircon/rock	0.00%		0.00%	9.35%	0.00%	0.02%	0.00%	0.01%	0.08%	0.12%	0.62%	1.64%	4.59%	9.04%	13%	20%	27%	31%
<b>10ZJS063 (Dashuang quartz monzonite, LA-ICP-MS)</b>																		
10zjs063-01t	12	796	17.78	1224	54.78	153	12.09	45.5	9.5	1.37	26	7.9	100	37	185	42	420	87
10zjs063-02t	18	832	0.27	1459	0.8	38	0.62	9	12.6	3.49	46	12.8	142	48	210	43	394	77
10zjs063-03t	14	811	29.19	2893	97.36	285	26.2	116.3	38	5.38	107	28	294	96	409	82	715	134
10zjs063-04t	28	886	17.95	785	105.07	208	16.23	55.6	9.6	1.99	21	5.9	69	24	114	25	233	45
10zjs063-05t	36	916	0.88	853	0.09	46	0.22	4	6.1	2.01	24	6.7	75	26	121	27	252	51
10zjs063-06t	22	860	0.46	1459	0.06	96	0.53	7.5	10.5	3.83	44	12.4	143	50	220	47	418	82
10zjs063-07t	12	790	2.24	829	6.4	51	1.69	7.4	4.2	0.80	19	5.8	71	26	124	27	260	50
Average or median	20	842	2.24	1224	6.4	125	1.69	9	9.6	2.01	41	11.36	128	44	197	42	385	75
Whole rock	4674		1144	33	162	289	29.8	99.1	14.13	2.93	10.7	1.29	6.2	1.12	3.2	0.44	2.75	0.39
Zircon/rock	0.00%		0.00%	4.27%	0.00%	0.05%	0.01%	0.01%	0.08%	0.08%	0.44%	1.02%	2.40%	4.60%	7%	11%	16%	23%

\*n.d. = not detected. #Average for Ti, Y, Ce, Gd-Lu; median for Sr, La, Pr-Eu. \*\*Assuming zircon is the only residence of Zr.

#### Appendix D. Table of in-situ zircon Hf isotope

##### 09ZJ02 (Xiepu syenogranite)

Spot No.	Age*	$^{176}\text{Hf}/^{177}\text{Hf}$	1 SD	$^{176}\text{Lu}/^{177}\text{Hf}$	1 SD	$^{176}\text{Yb}/^{177}\text{Hf}$	1 SD	$I_{\text{Hf}}$	$\varepsilon_{\text{Hf(t)}}$	1 SD	$T_{\text{DM}}^*$	1 SD	$T_{\text{DM2}}^*$	1 SD
09ZJ02-01	178	0.282195	0.000014	0.001550	0.000046	0.069966	0.000700	0.282190	-16.7	0.5	1512	20	2264	31
09ZJ02-02	178	0.282208	0.000012	0.002866	0.000010	0.138282	0.001100	0.282198	-16.4	0.4	1548	18	2245	26
09ZJ02-03	178	0.282205	0.000017	0.001819	0.000013	0.087540	0.001300	0.282199	-16.4	0.6	1509	24	2244	37
09ZJ02-04	178	0.282262	0.000010	0.000845	0.000007	0.036789	0.000620	0.282259	-14.2	0.4	1391	14	2111	22
09ZJ02-05	178	0.282200	0.000010	0.001148	0.000024	0.051640	0.001200	0.282196	-16.5	0.3	1489	13	2250	21
09ZJ02-06	178	0.282287	0.000018	0.001314	0.000095	0.059672	0.005000	0.282283	-13.4	0.6	1373	26	2060	40
09ZJ02-07	178	0.282175	0.000017	0.003391	0.000057	0.159969	0.003400	0.282164	-17.6	0.6	1620	25	2321	37

Appendices

09ZJ02-08	178	0.282192	0.000013	0.003303	0.000130	0.137601	0.001300	0.282181	-17.0	0.5	1591	20	2283	29
09ZJ02-09	178	0.282206	0.000010	0.003095	0.000032	0.146943	0.002300	0.282196	-16.5	0.4	1561	15	2251	22
09ZJ02-10	178	0.282188	0.000014	0.001061	0.000005	0.049998	0.000400	0.282184	-16.9	0.5	1502	20	2275	31

\*Units of age and model age are Ma.

**09ZJ07 (Ru'ao monzodiorite)**

Spot No.	Age	$^{176}\text{Hf}/^{177}\text{Hf}$	1 SD	$^{176}\text{Lu}/^{177}\text{Hf}$	1 SD	$^{176}\text{Yb}/^{177}\text{Hf}$	$I_{\text{Hf}}$	$\varepsilon_{\text{Hf}(t)}$	1 SD	$T_{\text{DM}}$	1 SD	$T_{\text{DM}2}$	1 SD
09ZJ07-01	116	0.282676	0.000022	0.001211	0.000054	0.033807	0.282673	-0.9	0.8	821	31	1233	49
09ZJ07-02	116	0.282551	0.000021	0.001351	0.000026	0.038479	0.282548	-5.4	0.7	1002	30	1512	47
09ZJ07-03	116	0.282849	0.000042	0.006110	0.000099	0.198242	0.282836	4.8	1.5	662	69	868	95
09ZJ07-04	116	0.282700	0.000035	0.001935	0.000084	0.056464	0.282696	-0.2	1.2	803	51	1182	78
09ZJ07-05	116	0.282616	0.000020	0.000815	0.000013	0.022619	0.282614	-3.0	0.7	897	28	1365	45
09ZJ07-06	116	0.282663	0.000028	0.002458	0.000035	0.071867	0.282658	-1.5	1.0	869	41	1268	63
09ZJ07-07	116	0.282603	0.000023	0.001115	0.000008	0.031712	0.282601	-3.5	0.8	922	33	1395	51
09ZJ07-08	116	0.282659	0.000026	0.000882	0.000027	0.024676	0.282657	-1.5	0.9	838	37	1269	58
09ZJ07-09	116	0.282591	0.000026	0.001571	0.000024	0.044969	0.282588	-4.0	0.9	951	37	1424	58
09ZJ07-10	116	0.282617	0.000022	0.001167	0.000011	0.032673	0.282614	-3.0	0.8	904	31	1364	49
09ZJ07-11	116	0.282626	0.000020	0.000940	0.000003	0.026139	0.282624	-2.7	0.7	886	28	1343	45
09ZJ07-12	116	0.282613	0.000023	0.001652	0.000050	0.047310	0.282609	-3.2	0.8	921	33	1376	51
09ZJ07-13	116	0.282659	0.000024	0.001505	0.000021	0.042158	0.282656	-1.6	0.8	852	34	1272	54
09ZJ07-14	116	0.282618	0.000021	0.001099	0.000010	0.031600	0.282616	-3.0	0.7	901	30	1362	47
09ZJ07-15	116	0.282613	0.000020	0.001267	0.000010	0.036685	0.282610	-3.2	0.7	912	28	1374	45
09ZJ07-16	116	0.282675	0.000023	0.003839	0.000051	0.114492	0.282667	-1.2	0.8	885	35	1248	51
09ZJ07-17	116	0.282664	0.000019	0.001270	0.000023	0.035347	0.282661	-1.4	0.7	840	27	1260	43
09ZJ07-18	116	0.282596	0.000018	0.001579	0.000008	0.044643	0.282593	-3.8	0.6	944	26	1413	40
09ZJ07-19	116	0.282632	0.000024	0.002662	0.000051	0.076192	0.282626	-2.6	0.8	919	35	1338	54
09ZJ07-20	116	0.282632	0.000023	0.000974	0.000030	0.026315	0.282630	-2.5	0.8	878	32	1330	51

Appendices

---

**09ZJ09 (Dashuang quartz monzonite)**

Spot No.	Age	$^{176}\text{Hf}/^{177}\text{Hf}$	1 SD	$^{176}\text{Lu}/^{177}\text{Hf}$	1 SD	$^{176}\text{Yb}/^{177}\text{Hf}$	1 SD	$I_{\text{Hf}}$	$\varepsilon_{\text{Hf(t)}}$	1 SD	$T_{\text{DM}}$	1 SD	$T_{\text{DM2}}$	1 SD
09ZJ09-01	227	0.282226	0.000015	0.000705	0.000010	0.030212	0.000360	0.282223	-14.4	0.5	1437	21	1774	33
09ZJ09-02	227	0.282234	0.000012	0.000776	0.000011	0.033577	0.000180	0.282231	-14.2	0.4	1429	17	1760	26
09ZJ09-03	227	0.282182	0.000014	0.000683	0.000006	0.028839	0.000240	0.282179	-16.0	0.5	1497	19	1851	31
09ZJ09-04	227	0.282217	0.000013	0.000583	0.000011	0.024864	0.000310	0.282215	-14.7	0.5	1445	18	1789	29
09ZJ09-05	227	0.282266	0.000014	0.000841	0.000048	0.032820	0.000720	0.282262	-13.1	0.5	1387	20	1704	31
09ZJ09-06	227	0.282307	0.000013	0.000554	0.000013	0.024865	0.001400	0.282305	-11.6	0.5	1320	18	1630	29
09ZJ09-07	227	0.282262	0.000014	0.000675	0.000006	0.030464	0.000590	0.282259	-13.2	0.5	1386	19	1710	31
09ZJ09-08	227	0.282258	0.000016	0.000673	0.000020	0.030820	0.000720	0.282255	-13.3	0.6	1392	22	1717	35
09ZJ09-09	227	0.282270	0.000015	0.000520	0.000002	0.022382	0.000390	0.282268	-12.9	0.5	1370	21	1695	33
09ZJ09-10	227	0.282236	0.000011	0.000535	0.000011	0.022517	0.000310	0.282234	-14.1	0.4	1417	15	1755	24
09ZJ09-11	227	0.282336	0.000020	0.000613	0.000001	0.029652	0.000170	0.282333	-10.5	0.7	1282	28	1579	44
09ZJ09-12	227	0.282144	0.000014	0.000777	0.000007	0.035032	0.000400	0.282141	-17.4	0.5	1553	19	1919	31
09ZJ09-13	227	0.282128	0.000013	0.000925	0.000014	0.039998	0.000290	0.282124	-17.9	0.5	1582	18	1948	28
09ZJ09-14	227	0.282232	0.000014	0.000413	0.000013	0.017036	0.000760	0.282230	-14.2	0.5	1418	19	1761	31
09ZJ09-15	227	0.282280	0.000016	0.000711	0.000057	0.026321	0.000680	0.282277	-12.5	0.6	1363	22	1678	35
09ZJ09-16	227	0.282227	0.000012	0.000825	0.000028	0.036760	0.001400	0.282224	-14.4	0.4	1440	17	1773	26
09ZJ09-17	227	0.282250	0.000012	0.000511	0.000002	0.021882	0.000150	0.282248	-13.6	0.4	1397	17	1730	26
09ZJ09-18	227	0.282264	0.000011	0.000598	0.000002	0.024389	0.000210	0.282261	-13.1	0.4	1381	15	1706	24
09ZJ09-19	227	0.282254	0.000014	0.000672	0.000026	0.027725	0.000820	0.282251	-13.4	0.5	1397	19	1724	31
09ZJ09-20	227	0.282275	0.000015	0.000563	0.000008	0.026647	0.000550	0.282273	-12.7	0.5	1364	21	1686	33

**10ZJS011 (Qiuwang syenogranite)**

Spot No.	Age	$^{176}\text{Hf}/^{177}\text{Hf}$	1 SD	$^{176}\text{Lu}/^{177}\text{Hf}$	1 SD	$^{176}\text{Yb}/^{177}\text{Hf}$	1 SD	$I_{\text{Hf}}$	$\varepsilon_{\text{Hf(t)}}$	1 SD	$T_{\text{DM}}$	1 SD	$T_{\text{DM2}}$	1 SD
10ZJS011-01	225	0.282204	0.000022	0.000675	0.000020	0.039048	0.001400	0.282201	-15.3	0.8	1465	30	2210	48
10ZJS011-02	225	0.282199	0.000022	0.001730	0.000240	0.080153	0.008100	0.282192	-15.6	0.8	1514	33	2231	48

Appendices

10ZJS011-03	225	0.282345	0.000016	0.000689	0.000013	0.038605	0.001200	0.282342	-10.3	0.6	1270	22	1900	35
10ZJS011-04	225	0.282332	0.000016	0.000684	0.000012	0.038241	0.000320	0.282329	-10.7	0.6	1288	22	1928	35
10ZJS011-05	225	0.282282	0.000014	0.000677	0.000025	0.039272	0.000970	0.282279	-12.5	0.5	1357	19	2038	31
10ZJS011-06	225	0.282242	0.000017	0.001144	0.000031	0.070937	0.002100	0.282237	-14.0	0.6	1430	24	2131	37
10ZJS011-07	225	0.282278	0.000013	0.001086	0.000072	0.057335	0.001300	0.282273	-12.7	0.5	1377	18	2051	29
10ZJS011-08	225	0.282247	0.000014	0.000897	0.000004	0.059437	0.000610	0.282243	-13.8	0.5	1414	19	2118	31
10ZJS011-09	225	0.282302	0.000019	0.001267	0.000110	0.063387	0.002400	0.282297	-11.9	0.7	1350	27	2000	42
10ZJS011-10	225	0.282232	0.000019	0.001750	0.000130	0.099384	0.004300	0.282225	-14.4	0.7	1467	28	2158	42
10ZJS011-11	225	0.282356	0.000017	0.000577	0.000002	0.035296	0.000180	0.282354	-9.9	0.6	1251	24	1874	38
10ZJS011-12	225	0.282310	0.000016	0.000937	0.000013	0.065400	0.000460	0.282306	-11.5	0.6	1327	22	1979	35
10ZJS011-13	225	0.282325	0.000022	0.000731	0.000011	0.047156	0.000530	0.282322	-11.0	0.8	1299	31	1944	49
10ZJS011-14	225	0.282285	0.000018	0.000778	0.000012	0.049832	0.001600	0.282282	-12.4	0.6	1357	25	2033	40
10ZJS011-15	225	0.282254	0.000023	0.000711	0.000024	0.041079	0.000740	0.282251	-13.5	0.8	1397	32	2100	51
10ZJS011-16	225	0.282247	0.000015	0.000765	0.000004	0.047758	0.000600	0.282244	-13.7	0.5	1409	21	2116	33
10ZJS011-17	225	0.282322	0.000017	0.000781	0.000023	0.051169	0.001600	0.282319	-11.1	0.6	1305	24	1951	38
10ZJS011-18	225	0.282331	0.000013	0.001223	0.000089	0.058313	0.001900	0.282326	-10.8	0.5	1308	19	1935	29
10ZJS011-19	225	0.282292	0.000016	0.000784	0.000025	0.048131	0.000870	0.282289	-12.2	0.6	1347	22	2017	35
10ZJS011-20	225	0.282258	0.000017	0.001175	0.000012	0.070248	0.000770	0.282253	-13.4	0.6	1409	24	2096	37
10ZJS011-21	225	0.282216	0.000016	0.001002	0.000024	0.057583	0.001100	0.282212	-14.9	0.6	1461	22	2187	35

**10ZJS025 (Yujiashan diorite)**

Spot No.	Age	$^{176}\text{Hf}/^{177}\text{Hf}$	1 SD	$^{176}\text{Lu}/^{177}\text{Hf}$	1 SD	$^{176}\text{Yb}/^{177}\text{Hf}$	1 SD	$I_{\text{Hf}}$	$\epsilon_{\text{Hf}(t)}$	1 SD	$T_{\text{DM}}$	1 SD	$T_{\text{DM2}}$	1 SD
10ZJS025-01	101	0.282687	0.000012	0.001685	0.000045	0.080395	0.001100	0.282684	-0.9	0.4	815	17	1217	27
10ZJS025-02	101	0.282699	0.000014	0.000803	0.000023	0.036257	0.001400	0.282697	-0.4	0.5	779	20	1187	31
10ZJS025-03	101	0.282709	0.000015	0.001147	0.000076	0.046602	0.001900	0.282707	-0.1	0.5	772	21	1166	34
10ZJS025-04	101	0.282708	0.000016	0.000800	0.000016	0.037806	0.001300	0.282706	-0.1	0.6	767	22	1166	36
10ZJS025-05	101	0.282709	0.000017	0.000625	0.000011	0.028792	0.000650	0.282708	-0.1	0.6	762	24	1163	38
10ZJS025-06	101	0.282664	0.000016	0.000945	0.000013	0.043437	0.001200	0.282662	-1.7	0.6	832	23	1266	36

Appendices

10ZJS025-07	101	0.282708	0.000018	0.000895	0.000057	0.042555	0.003200	0.282706	-0.1	0.6	769	25	1167	40
10ZJS025-08	101	0.282654	0.000015	0.000812	0.000008	0.035606	0.000450	0.282652	-2.0	0.5	843	21	1287	34
10ZJS025-09	101	0.282654	0.000015	0.000907	0.000016	0.043292	0.001200	0.282652	-2.0	0.5	845	21	1288	34
10ZJS025-10	101	0.282680	0.000014	0.001363	0.000036	0.063381	0.002100	0.282677	-1.1	0.5	818	20	1232	31
10ZJS025-11	101	0.282619	0.000015	0.002030	0.000054	0.093725	0.001000	0.282615	-3.3	0.5	921	22	1371	33
10ZJS025-12	101	0.282715	0.000017	0.000754	0.000004	0.033992	0.000220	0.282714	0.1	0.6	756	24	1151	38
10ZJS025-13	101	0.282666	0.000017	0.000799	0.000033	0.035149	0.001700	0.282664	-1.6	0.6	826	24	1260	38
10ZJS025-14	101	0.282621	0.000020	0.001287	0.000026	0.058664	0.000690	0.282619	-3.2	0.7	900	28	1363	45
10ZJS025-15	101	0.282738	0.000016	0.001093	0.000053	0.050888	0.001200	0.282736	0.9	0.6	730	23	1100	36
10ZJS025-16	101	0.282693	0.000025	0.000661	0.000015	0.030676	0.000850	0.282692	-0.6	0.9	785	35	1199	56
10ZJS025-17	101	0.282706	0.000017	0.000838	0.000010	0.039419	0.001000	0.282704	-0.2	0.6	770	24	1171	38
10ZJS025-18	101	0.282667	0.000016	0.002018	0.000059	0.098700	0.003000	0.282663	-1.6	0.6	851	23	1263	36
10ZJS025-19	101	0.282770	0.000021	0.001351	0.000066	0.057421	0.002100	0.282767	2.1	0.7	689	30	1030	47
10ZJS025-20	101	0.282666	0.000016	0.000912	0.000020	0.040297	0.001200	0.282664	-1.6	0.6	828	23	1261	36

**10ZJS033 (Jiangzao granite)**

Spot No.	Age	$^{176}\text{Hf}/^{177}\text{Hf}$	1 SD	$^{176}\text{Lu}/^{177}\text{Hf}$	1 SD	$^{176}\text{Yb}/^{177}\text{Hf}$	$I_{\text{Hf}}$	$\epsilon_{\text{Hf(t)}}$	1 SD	$T_{\text{DM}}$	1 SD	$T_{\text{DM2}}$	1 SD
10ZJS033-01	144	0.282656	0.000013	0.001248	0.000017	0.036367	0.282653	-1.1	0.5	851	18	1261	29
10ZJS033-02	144	0.282617	0.000017	0.001311	0.000017	0.038564	0.282613	-2.4	0.6	907	24	1349	38
10ZJS033-03	144	0.282591	0.000018	0.002318	0.000056	0.064678	0.282585	-3.5	0.6	970	26	1413	40
10ZJS033-04	144	0.282690	0.000018	0.001479	0.000140	0.041972	0.282686	0.1	0.6	807	26	1187	40
10ZJS033-05	144	0.282612	0.000017	0.003808	0.000051	0.119514	0.282602	-2.9	0.6	980	26	1375	38
10ZJS033-06	144	0.282688	0.000020	0.004061	0.000199	0.123939	0.282677	-0.2	0.7	870	31	1207	45
10ZJS033-07	144	0.282659	0.000017	0.002631	0.000082	0.083941	0.282652	-1.1	0.6	879	25	1263	38
10ZJS033-08	144	0.282570	0.000017	0.002227	0.000061	0.067807	0.282564	-4.2	0.6	999	25	1459	38
10ZJS033-09	144	0.282622	0.000015	0.002059	0.000058	0.064242	0.282616	-2.3	0.5	919	22	1342	34
10ZJS033-10	144	0.282599	0.000016	0.001854	0.000049	0.056921	0.282594	-3.1	0.6	947	23	1392	36
10ZJS033-11	144	0.282631	0.000020	0.002243	0.000050	0.073110	0.282625	-2.0	0.7	910	29	1323	45

Appendices

10ZJS033-12	144	0.282601	0.000014	0.002759	0.000102	0.082821	0.282594	-3.2	0.5	968	21	1393	31
10ZJS033-13	144	0.282601	0.000015	0.001680	0.000023	0.052631	0.282596	-3.1	0.5	939	22	1387	33
10ZJS033-14	144	0.282588	0.000018	0.002590	0.000080	0.082764	0.282581	-3.6	0.6	982	27	1421	40

**10ZJS053 (Hecun dacitic-rhyolitic porphyry)**

Spot No.	Age	$^{176}\text{Hf}/^{177}\text{Hf}$	1 SD	$^{176}\text{Lu}/^{177}\text{Hf}$	1 SD	$^{176}\text{Yb}/^{177}\text{Hf}$	1 SD	$I_{\text{Hf}}$	$\varepsilon_{\text{Hf(t)}}$	1 SD	$T_{\text{DM}}$	1 SD	$T_{\text{DM2}}$	1 SD
10ZJS053-01	130	0.282660	0.000012	0.001392	0.000002	0.062532	0.000490	0.282657	-1.2	0.4	847	17	1260	27
10ZJS053-02	130	0.282563	0.000010	0.000976	0.000042	0.041611	0.000540	0.282561	-4.6	0.4	974	14	1474	22
10ZJS053-03	130	0.282635	0.000017	0.000705	0.000011	0.031798	0.000250	0.282633	-2.1	0.6	867	24	1312	38
10ZJS053-04	130	0.282621	0.000012	0.001002	0.000029	0.045406	0.000850	0.282619	-2.6	0.4	893	17	1345	27
10ZJS053-05	130	0.282592	0.000009	0.000579	0.000004	0.025570	0.000430	0.282591	-3.6	0.3	924	12	1407	20
10ZJS053-06	130	0.282672	0.000014	0.000980	0.000013	0.042087	0.000510	0.282670	-0.8	0.5	821	20	1231	31
10ZJS053-07	130	0.282628	0.000014	0.000793	0.000013	0.034821	0.001000	0.282626	-2.3	0.5	879	20	1328	31
10ZJS053-08	130	0.282601	0.000018	0.001053	0.000027	0.046992	0.001000	0.282598	-3.3	0.6	923	25	1390	40
10ZJS053-09	130	0.282624	0.000013	0.000599	0.000009	0.025671	0.000170	0.282623	-2.4	0.5	880	18	1336	29
10ZJS053-10	130	0.282510	0.000019	0.000768	0.000018	0.031807	0.000620	0.282508	-6.5	0.7	1043	27	1591	42
10ZJS053-11	130	0.282612	0.000014	0.001067	0.000043	0.046406	0.002300	0.282609	-2.9	0.5	908	20	1365	31
10ZJS053-12	130	0.282603	0.000022	0.001147	0.000018	0.046296	0.000230	0.282600	-3.2	0.8	922	31	1386	49
10ZJS053-13	130	0.282610	0.000015	0.001045	0.000020	0.042431	0.001300	0.282607	-3.0	0.5	910	21	1370	33
10ZJS053-14	130	0.282599	0.000021	0.001319	0.000031	0.054669	0.001500	0.282596	-3.4	0.7	932	30	1396	47
10ZJS053-15	130	0.282615	0.000012	0.000618	0.000011	0.026219	0.000680	0.282613	-2.8	0.4	893	17	1356	27
10ZJS053-16	130	0.282643	0.000017	0.001077	0.000020	0.043396	0.000840	0.282640	-1.8	0.6	864	24	1296	38
10ZJS053-17	130	0.282639	0.000012	0.000817	0.000011	0.034803	0.000790	0.282637	-1.9	0.4	864	17	1304	27
10ZJS053-18	130	0.282561	0.000016	0.001505	0.000023	0.063165	0.001600	0.282557	-4.7	0.6	991	23	1481	36
10ZJS053-19	130	0.282611	0.000018	0.001203	0.000011	0.047765	0.000770	0.282608	-2.9	0.6	912	25	1368	40

## Appendices

**10ZJS063 (Dashuang quartz monzonite)**

Spot No.	Age	$^{176}\text{Hf}/^{177}\text{Hf}$	1 SD	$^{176}\text{Lu}/^{177}\text{Hf}$	1 SD	$^{176}\text{Yb}/^{177}\text{Hf}$	$I_{\text{Hf}}$	$\varepsilon_{\text{Hf}(0)}$	1 SD	$T_{\text{DM}}$	1 SD	$T_{\text{DM2}}$	1 SD
10ZJS063-01	226	0.282303	0.000014	0.000403	0.000010	0.011463	0.282301	-11.7	0.5	1320	19	1991	31
10ZJS063-02	226	0.282306	0.000016	0.001253	0.000017	0.038873	0.282301	-11.7	0.6	1346	23	1992	35
10ZJS063-03	226	0.282293	0.000022	0.000934	0.000007	0.028346	0.282289	-12.1	0.8	1352	31	2018	49
10ZJS063-04	226	0.282446	0.000021	0.001772	0.000015	0.059653	0.282439	-6.8	0.7	1164	30	1687	47
10ZJS063-05	226	0.282210	0.000019	0.000833	0.000012	0.025672	0.282206	-15.0	0.7	1464	26	2200	42
10ZJS063-06	226	0.282307	0.000019	0.000703	0.000018	0.021078	0.282304	-11.6	0.7	1325	26	1985	42
10ZJS063-07	226	0.282301	0.000018	0.000637	0.000003	0.018915	0.282298	-11.8	0.6	1331	25	1998	40
10ZJS063-08	226	0.282292	0.000024	0.001702	0.000041	0.051946	0.282285	-12.3	0.8	1382	34	2027	53
10ZJS063-09	226	0.282299	0.000017	0.000686	0.000004	0.019822	0.282296	-11.9	0.6	1335	24	2003	38
10ZJS063-10	226	0.282306	0.000015	0.000784	0.000005	0.023393	0.282303	-11.6	0.5	1329	21	1988	33
10ZJS063-11	226	0.282277	0.000018	0.000913	0.000009	0.028517	0.282273	-12.7	0.6	1374	25	2053	40
10ZJS063-12	226	0.282314	0.000021	0.001565	0.000035	0.050873	0.282307	-11.5	0.7	1345	30	1978	46
10ZJS063-13	226	0.282257	0.000014	0.000637	0.000005	0.019574	0.282254	-13.3	0.5	1392	19	2095	31
10ZJS063-14	226	0.282450	0.000018	0.001532	0.000019	0.050529	0.282444	-6.7	0.6	1151	26	1676	40
10ZJS063-15	226	0.282430	0.000016	0.001196	0.000016	0.039315	0.282425	-7.3	0.6	1169	23	1717	36
10ZJS063-16	226	0.282307	0.000018	0.001098	0.000022	0.035388	0.282302	-11.6	0.6	1339	25	1989	40
10ZJS063-17	226	0.282286	0.000018	0.000693	0.000005	0.021916	0.282283	-12.3	0.6	1354	25	2031	40
10ZJS063-18	226	0.282226	0.000017	0.001126	0.000027	0.036359	0.282221	-14.5	0.6	1453	24	2168	37
10ZJS063-19	226	0.282225	0.000013	0.000477	0.000015	0.013050	0.282223	-14.5	0.5	1430	18	2164	29
10ZJS063-20	226	0.282271	0.000013	0.000480	0.000009	0.014032	0.282269	-12.8	0.5	1367	18	2062	29
10ZJS063-21	226	0.282235	0.000014	0.000478	0.000011	0.013914	0.282233	-14.1	0.5	1416	19	2142	31
10ZJS063-22	226	0.282245	0.000018	0.000866	0.000003	0.027489	0.282241	-13.8	0.6	1417	25	2123	40
10ZJS063-23	226	0.282346	0.000018	0.000940	0.000003	0.031364	0.282342	-10.2	0.6	1279	25	1901	40
10ZJS063-24	226	0.282312	0.000016	0.000708	0.000021	0.019857	0.282309	-11.4	0.6	1318	22	1974	35
10ZJS063-25	226	0.282264	0.000014	0.001066	0.000046	0.033148	0.282259	-13.2	0.5	1398	20	2083	31

Appendices

---

**10ZJS065 (Dashuang syenite)**

Spot No.	Age	$^{176}\text{Hf}/^{177}\text{Hf}$	1 SD	$^{176}\text{Lu}/^{177}\text{Hf}$	1 SD	$^{176}\text{Yb}/^{177}\text{Hf}$	1 SD	$I_{\text{Hf}}$	$\varepsilon_{\text{Hf(t)}}$	1 SD	$T_{\text{DM}}$	1 SD	$T_{\text{DM2}}$	1 SD
10ZJS065-01	223	0.282390	0.000017	0.001316	0.000130	0.058127	0.003800	0.282385	-8.8	0.6	1229	24	1809	38
10ZJS065-02	223	0.282431	0.000010	0.001130	0.000050	0.051442	0.001500	0.282426	-7.3	0.4	1166	14	1716	22
10ZJS065-03	223	0.282438	0.000017	0.000849	0.000040	0.039067	0.001700	0.282434	-7.0	0.6	1147	24	1698	38
10ZJS065-04	223	0.282401	0.000029	0.000941	0.000039	0.042174	0.001200	0.282397	-8.4	1.0	1202	41	1781	64
10ZJS065-05	223	0.282425	0.000017	0.001458	0.000022	0.069294	0.001100	0.282419	-7.6	0.6	1184	24	1733	38
10ZJS065-06	223	0.282377	0.000018	0.001184	0.000012	0.054702	0.000470	0.282372	-9.3	0.6	1243	25	1837	40
10ZJS065-07	223	0.282399	0.000013	0.001908	0.000048	0.088472	0.001900	0.282391	-8.6	0.5	1236	19	1794	29
10ZJS065-08	223	0.282358	0.000017	0.001530	0.000029	0.073578	0.002200	0.282352	-10.0	0.6	1282	24	1882	38
10ZJS065-09	223	0.282452	0.000012	0.000677	0.000009	0.031131	0.000530	0.282449	-6.5	0.4	1122	17	1666	27
10ZJS065-10	223	0.282413	0.000014	0.000489	0.000027	0.021165	0.001400	0.282411	-7.9	0.5	1171	19	1750	31
10ZJS065-11	223	0.282384	0.000017	0.001814	0.000035	0.090433	0.001900	0.282376	-9.1	0.6	1254	24	1827	38
10ZJS065-12	223	0.282414	0.000013	0.000841	0.000018	0.041049	0.001200	0.282410	-7.9	0.5	1180	18	1751	29
10ZJS065-13	223	0.282401	0.000016	0.001319	0.000048	0.059763	0.000870	0.282395	-8.4	0.6	1214	23	1785	35
10ZJS065-14	223	0.282422	0.000012	0.000786	0.000031	0.037150	0.002000	0.282419	-7.6	0.4	1168	17	1733	27
10ZJS065-15	223	0.282379	0.000016	0.001142	0.000030	0.049365	0.002000	0.282374	-9.2	0.6	1239	23	1832	35
10ZJS065-16	223	0.282414	0.000016	0.001788	0.000052	0.086608	0.002000	0.282407	-8.0	0.6	1211	23	1760	35
10ZJS065-17	223	0.282370	0.000020	0.000547	0.000022	0.023816	0.000750	0.282368	-9.4	0.7	1232	28	1846	44
10ZJS065-18	223	0.282447	0.000021	0.000948	0.000012	0.045530	0.001100	0.282443	-6.7	0.7	1137	29	1679	47
10ZJS065-19	223	0.282389	0.000024	0.001640	0.000140	0.081991	0.005400	0.282382	-8.9	0.8	1241	35	1814	53
10ZJS065-20	223	0.282398	0.000017	0.001437	0.000029	0.063316	0.001700	0.282392	-8.5	0.6	1222	24	1792	38
10ZJS065-21	223	0.282386	0.000014	0.001529	0.000011	0.073338	0.001600	0.282380	-9.0	0.5	1242	20	1820	31
10ZJS065-22	223	0.282350	0.000022	0.001310	0.000067	0.059733	0.003000	0.282345	-10.2	0.8	1286	31	1897	49

**10ZJS072 (Shuangcái andesitic-dacitic porphyry)**

Spot No.	Age	$^{176}\text{Hf}/^{177}\text{Hf}$	1 SD	$^{176}\text{Lu}/^{177}\text{Hf}$	1 SD	$^{176}\text{Yb}/^{177}\text{Hf}$	$I_{\text{Hf}}$	$\varepsilon_{\text{Hf(t)}}$	1 SD	$T_{\text{DM}}$	1 SD	$T_{\text{DM2}}$	1 SD
----------	-----	-----------------------------------	------	-----------------------------------	------	-----------------------------------	-----------------	------------------------------	------	-----------------	------	------------------	------

Appendices

10ZJS072-01	132	0.282656	0.000018	0.002150	0.000033	0.059637	0.282651	-1.4	0.6	871	26	1273	40
10ZJS072-02	132	0.282622	0.000022	0.001593	0.000060	0.042281	0.282618	-2.6	0.8	907	32	1346	49
10ZJS072-03	132	0.282606	0.000021	0.000726	0.000034	0.018976	0.282604	-3.0	0.7	909	29	1377	47
10ZJS072-04	132	0.282612	0.000022	0.001898	0.000012	0.047932	0.282607	-2.9	0.8	929	32	1370	49
10ZJS072-05	132	0.282598	0.000022	0.001459	0.000032	0.038944	0.282594	-3.4	0.8	938	31	1399	49
10ZJS072-06	132	0.282566	0.000024	0.004908	0.000084	0.129153	0.282554	-4.8	0.8	1084	38	1489	53
10ZJS072-07	132	0.282652	0.000029	0.003569	0.000179	0.107284	0.282643	-1.7	1.0	913	44	1290	65
10ZJS072-08	132	0.282695	0.000024	0.001494	0.000032	0.039540	0.282691	0.0	0.8	800	34	1182	54
10ZJS072-09	132	0.282624	0.000021	0.001112	0.000012	0.025928	0.282621	-2.4	0.7	893	30	1339	47
10ZJS072-10	132	0.282645	0.000023	0.001813	0.000187	0.048425	0.282641	-1.8	0.8	879	33	1296	51
10ZJS072-11	132	0.282631	0.000019	0.000843	0.000006	0.021382	0.282629	-2.2	0.7	877	27	1322	42
10ZJS072-12	132	0.282613	0.000021	0.001914	0.000050	0.051765	0.282608	-2.9	0.7	928	30	1368	47
10ZJS072-13	132	0.282654	0.000017	0.002564	0.000096	0.070575	0.282648	-1.5	0.6	884	25	1280	38
10ZJS072-14	132	0.282543	0.000021	0.001359	0.000034	0.036874	0.282540	-5.3	0.7	1014	30	1521	47
10ZJS072-15	132	0.282622	0.000020	0.000980	0.000006	0.025048	0.282620	-2.5	0.7	892	28	1343	45

**10ZJS081 (Hongling dacitic-rhyolitic porphyry)**

Spot No.	Age	$^{176}\text{Hf}/^{177}\text{Hf}$	1 SD	$^{176}\text{Lu}/^{177}\text{Hf}$	1 SD	$^{176}\text{Yb}/^{177}\text{Hf}$	1 SD	$I_{\text{Hf}}$	$\epsilon_{\text{Hf}(t)}$	1 SD	$T_{\text{DM}}$	1 SD	$T_{\text{DM2}}$	1 SD
10ZJS081-01	131	0.282621	0.000021	0.001195	0.000013	0.064283	0.001400	0.282618	-2.6	0.7	898	30	1345	47
10ZJS081-02	131	0.282652	0.000015	0.000875	0.000009	0.047800	0.000730	0.282650	-1.4	0.5	847	21	1274	34
10ZJS081-03	131	0.282626	0.000025	0.001279	0.000018	0.073513	0.000370	0.282623	-2.4	0.9	893	35	1335	56
10ZJS081-04	131	0.282650	0.000018	0.001379	0.000023	0.077626	0.000780	0.282647	-1.6	0.6	861	26	1282	40
10ZJS081-05	131	0.282637	0.000020	0.001124	0.000007	0.062532	0.000910	0.282634	-2.0	0.7	874	28	1309	45
10ZJS081-06	131	0.282725	0.000023	0.001602	0.000019	0.090669	0.001200	0.282721	1.1	0.8	759	33	1115	52
10ZJS081-07	131	0.282617	0.000017	0.001332	0.000028	0.071043	0.002100	0.282614	-2.7	0.6	907	24	1355	38
10ZJS081-08	131	0.282556	0.000017	0.000859	0.000023	0.046893	0.001000	0.282554	-4.8	0.6	981	24	1488	38
10ZJS081-09	131	0.282648	0.000016	0.000891	0.000006	0.047168	0.000700	0.282646	-1.6	0.6	853	22	1283	36
10ZJS081-10	131	0.282657	0.000016	0.001300	0.000021	0.069275	0.000990	0.282654	-1.3	0.6	849	23	1266	36

Appendices

10ZJS081-11	131	0.282614	0.000015	0.001053	0.000006	0.054385	0.000610	0.282611	-2.8	0.5	904	21	1360	33
10ZJS081-12	131	0.282598	0.000017	0.000838	0.000008	0.039859	0.000390	0.282596	-3.4	0.6	922	24	1395	38
10ZJS081-13	131	0.282677	0.000011	0.000890	0.000017	0.044005	0.000770	0.282675	-0.6	0.4	812	15	1219	25
10ZJS081-14	131	0.282618	0.000017	0.001162	0.000024	0.059758	0.001400	0.282615	-2.7	0.6	901	24	1352	38
10ZJS081-15	131	0.282664	0.000022	0.002044	0.000019	0.108409	0.000600	0.282659	-1.1	0.8	856	32	1254	49
10ZJS081-16	131	0.282637	0.000018	0.001040	0.000067	0.050639	0.001900	0.282634	-2.0	0.6	872	25	1309	40
10ZJS081-17	131	0.282600	0.000015	0.001880	0.000088	0.099100	0.004600	0.282595	-3.4	0.5	945	22	1396	33
10ZJS081-18	131	0.282649	0.000022	0.001147	0.000013	0.058837	0.001100	0.282646	-1.6	0.8	857	31	1283	49
10ZJS081-19	131	0.282716	0.000021	0.000827	0.000017	0.041713	0.000720	0.282714	0.8	0.7	756	30	1131	47
10ZJS081-20	131	0.282694	0.000026	0.001143	0.000035	0.060544	0.001600	0.282691	0.0	0.9	793	37	1182	58

**10ZJS096 (Zhujiaxiang andesitic porphyry)**

Spot No.	Age	$^{176}\text{Hf}/^{177}\text{Hf}$	1 SD	$^{176}\text{Lu}/^{177}\text{Hf}$	1 SD	$^{176}\text{Yb}/^{177}\text{Hf}$	1 SD	$I_{\text{Hf}}$	$\varepsilon_{\text{Hf(t)}}$	1 SD	$T_{\text{DM}}$	1 SD	$T_{\text{DM2}}$	1 SD
10ZJS096-01	131	0.282589	0.000024	0.001552	0.000066	0.083039	0.005400	0.282585	-3.7	0.8	952	34	1419	54
10ZJS096-02	131	0.282659	0.000020	0.000765	0.000026	0.041483	0.001700	0.282657	-1.2	0.7	835	28	1258	45
10ZJS096-03	131	0.282622	0.000017	0.000694	0.000009	0.036454	0.000190	0.282620	-2.5	0.6	885	24	1340	38
10ZJS096-04	131	0.282637	0.000023	0.003354	0.000310	0.174526	0.014000	0.282629	-2.2	0.8	929	35	1321	51
10ZJS096-05	131	0.282665	0.000016	0.001175	0.000016	0.063400	0.001500	0.282662	-1.0	0.6	835	23	1247	36
10ZJS096-06	131	0.282611	0.000019	0.003534	0.000170	0.178380	0.007300	0.282602	-3.1	0.7	973	29	1380	42
10ZJS096-07	131	0.282645	0.000024	0.002533	0.000110	0.119187	0.006100	0.282639	-1.8	0.8	896	35	1299	54
10ZJS096-08	131	0.282617	0.000018	0.001522	0.000077	0.083789	0.005000	0.282613	-2.7	0.6	912	26	1356	40
10ZJS096-09	131	0.282587	0.000015	0.001395	0.000028	0.077292	0.002300	0.282584	-3.8	0.5	951	21	1422	33
10ZJS096-10	131	0.282652	0.000015	0.001179	0.000082	0.063239	0.004100	0.282649	-1.5	0.5	854	21	1276	34
10ZJS096-11	131	0.282635	0.000023	0.000813	0.000011	0.044798	0.000610	0.282633	-2.0	0.8	869	32	1312	51
10ZJS096-12	131	0.282668	0.000025	0.001580	0.000094	0.084794	0.005200	0.282664	-0.9	0.9	840	36	1242	56
10ZJS096-13	131	0.282614	0.000013	0.001458	0.000016	0.082867	0.001200	0.282610	-2.8	0.5	914	19	1362	29
10ZJS096-14	131	0.282609	0.000022	0.001980	0.000130	0.111019	0.006200	0.282604	-3.1	0.8	935	32	1376	49
10ZJS096-15	131	0.282698	0.000022	0.001950	0.000088	0.102517	0.003200	0.282693	0.1	0.8	805	32	1177	49

Appendices

---

10ZJS096-16	131	0.282602	0.000017	0.003913	0.000290	0.215225	0.006700	0.282592	-3.5	0.6	997	27	1403	38
10ZJS096-17	131	0.282636	0.000017	0.001389	0.000053	0.074848	0.002500	0.282633	-2.1	0.6	881	24	1313	38
10ZJS096-18	131	0.282656	0.000012	0.000746	0.000019	0.041431	0.000890	0.282654	-1.3	0.4	838	17	1265	27

**10ZJS101 (Matou monzogranite)**

Spot No.	Age	$^{176}\text{Hf}/^{177}\text{Hf}$	1 SD	$^{176}\text{Lu}/^{177}\text{Hf}$	1 SD	$^{176}\text{Yb}/^{177}\text{Hf}$	$I_{\text{Hf}}$	$\epsilon_{\text{Hf}}(t)$	1 SD	$T_{\text{DM1}}$	1 SD	$T_{\text{DM2}}$	1 SD
10ZJS101-01	206	0.282535	0.000022	0.001385	0.000190	0.063302	0.282530	-4.0	0.8	1025	32	1495	49
10ZJS101-02	101	0.282622	0.000023	0.000913	0.000022	0.04911	0.282620	-3.2	0.8	890	32	1359	51
10ZJS101-03	101	0.282535	0.000031	0.000983	0.000012	0.056931	0.282533	-6.2	1.1	1014	44	1553	69
10ZJS101-04	205	0.282564	0.000024	0.000924	0.000043	0.044525	0.282560	-3.0	0.8	972	34	1427	53
10ZJS101-05	129	0.282302	0.000028	0.00138	0.000041	0.089188	0.282299	-13.9	1.0	1354	40	2055	62
10ZJS101-06	101	0.282544	0.000020	0.000834	0.000015	0.040715	0.282542	-5.9	0.7	997	28	1533	44
10ZJS101-07	101	0.282582	0.000021	0.000753	0.000016	0.037035	0.282581	-4.6	0.7	942	29	1448	47
10ZJS101-08	101	0.282624	0.000018	0.000849	0.000012	0.040139	0.282622	-3.1	0.6	886	25	1354	40
10ZJS101-09	101	0.282593	0.000020	0.001108	0.000056	0.054978	0.282591	-4.2	0.7	935	28	1425	45
10ZJS101-10	101	0.282617	0.000020	0.000782	0.000008	0.037891	0.282616	-3.3	0.7	894	28	1370	45
10ZJS101-11	101	0.282548	0.000016	0.001485	0.000031	0.071023	0.282545	-5.8	0.6	1009	23	1527	36
10ZJS101-12	101	0.282264	0.000018	0.000374	0.000007	0.019498	0.282263	-15.8	0.6	1371	25	2150	40
10ZJS101-13	101	0.282619	0.000026	0.002499	0.000065	0.123549	0.282614	-3.4	0.9	933	38	1373	58
10ZJS101-14	101	0.282539	0.000021	0.000684	0.000016	0.034526	0.282538	-6.1	0.7	1000	29	1543	47
10ZJS101-15	101	0.282576	0.000023	0.000665	0.000010	0.030945	0.282575	-4.8	0.8	948	32	1461	51
10ZJS101-16	101	0.282552	0.000024	0.001228	0.000068	0.052353	0.282550	-5.6	0.8	996	34	1517	53
10ZJS101-17	101	0.282659	0.000025	0.000826	0.000015	0.039387	0.282657	-1.8	0.9	836	35	1276	56
10ZJS101-18	101	0.282594	0.000024	0.000728	0.000003	0.035888	0.282593	-4.1	0.8	925	34	1421	53
10ZJS101-19	101	0.282412	0.000021	0.001561	0.000057	0.076688	0.282409	-10.6	0.7	1205	30	1829	46
10ZJS101-20	101	0.282628	0.000023	0.001013	0.000046	0.045916	0.282626	-2.9	0.8	884	32	1346	51

Appendices

---

**10ZJS104 (Shanghekou syenogranite)**

Spot No.	Age	$^{176}\text{Hf}/^{177}\text{Hf}$	1 SD	$^{176}\text{Lu}/^{177}\text{Hf}$	1 SD	$^{176}\text{Yb}/^{177}\text{Hf}$	$I_{\text{Hf}}$	$\varepsilon_{\text{Hf}}(t)$	1 SD	$T_{\text{DM1}}$	1 SD	$T_{\text{DM2}}$	1 SD
10ZJS104-01	130	0.282397	0.000020	0.000823	0.000086	0.038853	0.282395	-10.5	0.7	1202	28	1842	44
10ZJS104-02	130	0.282295	0.000018	0.011365	0.001100	0.505977	0.282267	-15.0	0.6	1859	82	2123	40
10ZJS104-03	130	0.282340	0.000017	0.005292	0.000200	0.240995	0.282327	-12.9	0.6	1452	28	1991	38
10ZJS104-04	130	0.282378	0.000024	0.003438	0.000092	0.186454	0.282370	-11.4	0.8	1320	36	1898	53
10ZJS104-05	130	0.282348	0.000025	0.004781	0.000071	0.229573	0.282336	-12.6	0.9	1418	39	1971	55
10ZJS104-06	130	0.282387	0.000028	0.002920	0.000150	0.131513	0.282380	-11.0	1.0	1287	42	1875	62
10ZJS104-07	130	0.282337	0.000021	0.005704	0.000340	0.260846	0.282323	-13.0	0.7	1475	37	2000	46
10ZJS104-08	130	0.282348	0.000020	0.003716	0.000120	0.195571	0.282339	-12.5	0.7	1375	30	1965	44
10ZJS104-09	148	0.282412	0.000019	0.003352	0.000078	0.144513	0.282403	-9.8	0.7	1266	28	1813	42
10ZJS104-10	130	0.282449	0.000019	0.001868	0.000110	0.101830	0.282444	-8.7	0.7	1162	27	1732	42
10ZJS104-11	151	0.282404	0.000013	0.002970	0.000190	0.163491	0.282396	-10.0	0.5	1264	20	1827	29
10ZJS104-12	130	0.282198	0.000051	0.014187	0.001000	0.629262	0.282164	-18.7	1.8	2278	142	2351	112
10ZJS104-13	130	0.282389	0.000024	0.005630	0.000220	0.290057	0.282375	-11.2	0.8	1389	39	1885	53
10ZJS104-14	156	0.282442	0.000014	0.003483	0.000230	0.166253	0.282432	-8.6	0.5	1225	22	1744	31
10ZJS104-15	130	0.282472	0.000015	0.007022	0.000280	0.344880	0.282455	-8.4	0.5	1312	28	1709	33
10ZJS104-16	130	0.282466	0.000014	0.000806	0.000007	0.044103	0.282464	-8.0	0.5	1105	20	1689	31
10ZJS104-17	130	0.282465	0.000022	0.003096	0.000160	0.142287	0.282457	-8.3	0.8	1178	33	1703	49
10ZJS104-18	130	0.282422	0.000023	0.005979	0.000400	0.289613	0.282407	-10.0	0.8	1351	41	1814	51
10ZJS104-19	130	0.282370	0.000027	0.007954	0.000140	0.369623	0.282351	-12.1	1.0	1526	47	1940	60
10ZJS104-20	130	0.282485	0.000016	0.001945	0.000012	0.110283	0.282480	-7.5	0.6	1112	23	1653	36

**10ZJS108 (Sucun syenogranite)**

Spot No.	Age	$^{176}\text{Hf}/^{177}\text{Hf}$	1 SD	$^{176}\text{Lu}/^{177}\text{Hf}$	1 SD	$^{176}\text{Yb}/^{177}\text{Hf}$	$I_{\text{Hf}}$	$\varepsilon_{\text{Hf}}(t)$	1 SD	$T_{\text{DM1}}$	1 SD	$T_{\text{DM2}}$	1 SD
10ZJS108-01	132	0.282435	0.000020	0.001527	0.000015	0.044332	0.282431	-9.2	0.7	1172	28	1762	44
10ZJS108-02	132	0.282399	0.000041	0.001074	0.000022	0.028495	0.282396	-10.4	1.5	1209	58	1839	91

Appendices

10ZJS108-03	132	0.282385	0.000021	0.001822	0.000018	0.051787	0.282381	-11.0	0.7	1253	30	1875	46
10ZJS108-04	132	0.282428	0.000020	0.001231	0.000011	0.034926	0.282425	-9.4	0.7	1173	28	1776	44
10ZJS108-05	132	0.282518	0.000022	0.001186	0.000015	0.032172	0.282515	-6.2	0.8	1044	31	1576	49
10ZJS108-06	132	0.282406	0.000024	0.001644	0.000052	0.045835	0.282402	-10.2	0.8	1217	34	1827	53
10ZJS108-07	132	0.282416	0.000025	0.001426	0.000011	0.038817	0.282412	-9.8	0.9	1196	35	1804	55
10ZJS108-08	132	0.282480	0.000030	0.003628	0.000024	0.103508	0.282471	-7.8	1.1	1174	45	1674	67
10ZJS108-09	132	0.282488	0.000024	0.001059	0.000005	0.029759	0.282485	-7.2	0.8	1083	34	1642	53
10ZJS108-10	132	0.282524	0.000033	0.002988	0.000039	0.084884	0.282517	-6.1	1.2	1088	49	1572	73
10ZJS108-11	132	0.282454	0.000028	0.001058	0.000021	0.029626	0.282451	-8.4	1.0	1131	39	1717	62
10ZJS108-12	132	0.282445	0.000027	0.001056	0.000009	0.028724	0.282442	-8.8	1.0	1144	38	1737	60
10ZJS108-13	132	0.282488	0.000024	0.001887	0.000043	0.050407	0.282483	-7.3	0.8	1107	35	1646	53
10ZJS108-14	132	0.282415	0.000026	0.001318	0.000022	0.036558	0.282412	-9.8	0.9	1194	37	1805	58
10ZJS108-15	132	0.282477	0.000030	0.000967	0.000010	0.027160	0.282475	-7.6	1.1	1096	42	1666	67

**10ZJS109 (Huangkang syenogranite)**

Spot No.	Age	$^{176}\text{Hf}/^{177}\text{Hf}$	1 SD	$^{176}\text{Lu}/^{177}\text{Hf}$	1 SD	$^{176}\text{Yb}/^{177}\text{Hf}$	$I_{\text{Hf}}$	$\epsilon_{\text{Hf}}(t)$	1 SD	$T_{\text{DM1}}$	1 SD	$T_{\text{DM2}}$	1 SD
10ZJS109-01	132	0.282492	0.000028	0.000873	0.000002	0.023632	0.282490	-7.1	1.0	1072	39	1632	62
10ZJS109-02	132	0.282503	0.000024	0.000911	0.000013	0.024523	0.282501	-6.7	0.8	1058	34	1608	53
10ZJS109-03	132	0.282459	0.000020	0.002460	0.000037	0.072804	0.282453	-8.4	0.7	1167	29	1714	44
10ZJS109-04	132	0.282520	0.000025	0.001081	0.000020	0.030404	0.282517	-6.1	0.9	1039	35	1571	56
10ZJS109-05	132	0.282493	0.000021	0.000797	0.000004	0.020886	0.282491	-7.0	0.7	1069	29	1629	47
10ZJS109-06	132	0.282445	0.000022	0.001282	0.000005	0.035174	0.282442	-8.8	0.8	1150	31	1739	49
10ZJS109-07	132	0.282497	0.000025	0.001966	0.000043	0.053689	0.282492	-7.0	0.9	1097	36	1627	56
10ZJS109-08	132	0.282521	0.000021	0.001186	0.000037	0.032951	0.282518	-6.1	0.7	1040	30	1569	47
10ZJS109-09	132	0.282513	0.000022	0.000934	0.000019	0.025431	0.282511	-6.3	0.8	1045	31	1586	49
10ZJS109-10	132	0.282512	0.000025	0.001479	0.000098	0.04034	0.282508	-6.4	0.9	1061	36	1591	56
10ZJS109-11	132	0.282491	0.000022	0.001002	0.000009	0.026806	0.282489	-7.1	0.8	1077	31	1635	49
10ZJS109-12	132	0.282493	0.000022	0.002543	0.000058	0.073720	0.282487	-7.2	0.8	1120	32	1639	49

Appendices

10ZJS109-13	221	0.282461	0.000018	0.001816	0.000021	0.051017	0.282453	-6.4	0.6	1144	26	1657	40
10ZJS109-14	213	0.282452	0.000022	0.000705	0.000007	0.018142	0.282449	-6.7	0.8	1123	31	1672	49
10ZJS109-15	201	0.282554	0.000022	0.002078	0.000075	0.058111	0.282546	-3.6	0.8	1018	32	1463	49

**10ZJS115 (Muchen diorite, MME)**

Spot No.	Age	$^{176}\text{Hf}/^{177}\text{Hf}$	1 SD	$^{176}\text{Lu}/^{177}\text{Hf}$	1 SD	$^{176}\text{Yb}/^{177}\text{Hf}$	$I_{\text{Hf}}$	$\epsilon_{\text{Hf}}(t)$	1 SD	$T_{\text{DM1}}$	1 SD	$T_{\text{DM2}}$	1 SD
10ZJS115-01	111	0.040317	0.000907	0.000003	0.282702	0.000008	0.282700	-0.1	0.3	777	11	1174	18
10ZJS115-02	111	0.064287	0.001429	0.000009	0.282689	0.000013	0.282686	-0.6	0.5	807	19	1206	29
10ZJS115-03	111	0.068090	0.001551	0.000018	0.282640	0.000013	0.282637	-2.3	0.5	879	19	1316	29
10ZJS115-04	111	0.048062	0.001124	0.000019	0.282653	0.000010	0.282651	-1.9	0.4	851	14	1285	22
10ZJS115-05	111	0.047518	0.001165	0.000003	0.282691	0.000013	0.282689	-0.5	0.5	798	18	1200	29
10ZJS115-06	111	0.044567	0.001067	0.000031	0.282657	0.000013	0.282655	-1.7	0.5	844	18	1276	29
10ZJS115-07	111	0.035495	0.00084	0.000003	0.282641	0.000013	0.282639	-2.3	0.5	861	18	1311	29
10ZJS115-08	111	0.038499	0.000895	0.000007	0.282650	0.000011	0.282648	-1.9	0.4	850	15	1291	25
10ZJS115-09	111	0.088170	0.001989	0.000032	0.282723	0.000013	0.282719	0.6	0.5	770	19	1132	29
10ZJS115-10	111	0.041578	0.000949	0.000011	0.282660	0.000011	0.282658	-1.6	0.4	837	15	1269	25
10ZJS115-11	111	0.031379	0.000720	0.000013	0.282680	0.000014	0.282679	-0.9	0.5	804	20	1223	31
10ZJS115-12	111	0.041334	0.000933	0.000004	0.282710	0.000014	0.282708	0.2	0.5	766	20	1157	31
10ZJS115-13	111	0.02532	0.000577	0.000005	0.282740	0.000010	0.282739	1.3	0.4	717	14	1088	22
10ZJS115-14	111	0.036094	0.000804	0.000003	0.282677	0.000012	0.282675	-1.0	0.4	810	17	1230	27
10ZJS115-15	111	0.042224	0.000958	0.000016	0.282743	0.000007	0.282741	1.3	0.2	720	10	1083	16
10ZJS115-16	111	0.048096	0.001082	0.000012	0.282701	0.000014	0.282699	-0.2	0.5	782	20	1178	31
10ZJS115-17	111	0.071291	0.001506	0.000029	0.282690	0.000010	0.282687	-0.6	0.4	807	14	1204	22
10ZJS115-18	111	0.048134	0.001071	0.000016	0.282684	0.000010	0.282682	-0.8	0.4	806	14	1216	22
10ZJS115-19	111	0.088957	0.00194	0.000049	0.282702	0.000014	0.282698	-0.2	0.5	799	20	1179	31
10ZJS115-20	111	0.039274	0.000871	0.000005	0.282772	0.000012	0.282770	2.4	0.4	678	17	1017	27

Appendices

---

**10ZJS116 (Muchen quartz monzonite)**

Spot No.	Age	$^{176}\text{Hf}/^{177}\text{Hf}$	1 SD	$^{176}\text{Lu}/^{177}\text{Hf}$	1 SD	$^{176}\text{Yb}/^{177}\text{Hf}$	$I_{\text{Hf}}$	$\varepsilon_{\text{Hf}}(t)$	1 SD	$T_{\text{DM1}}$	1 SD	$T_{\text{DM2}}$	1 SD
10ZJS116-01	112	0.061047	0.001341	0.000038	0.282687	0.000011	0.282684	-0.7	0.4	808	16	1211	25
10ZJS116-02	112	0.110504	0.002333	0.000027	0.282642	0.000011	0.282637	-2.3	0.4	896	16	1316	25
10ZJS116-03	112	0.078657	0.001939	0.000110	0.282698	0.000012	0.282694	-0.3	0.4	806	18	1189	27
10ZJS116-04	112	0.083604	0.001785	0.000082	0.282671	0.000018	0.282667	-1.2	0.6	841	26	1249	40
10ZJS116-05	112	0.070882	0.001434	0.000009	0.282685	0.000012	0.282682	-0.7	0.4	813	17	1216	27
10ZJS116-06	112	0.041896	0.000895	0.000006	0.282671	0.000010	0.282669	-1.2	0.4	821	14	1245	22
10ZJS116-07	112	0.042395	0.000935	0.000002	0.282718	0.000014	0.282716	0.5	0.5	756	20	1139	31
10ZJS116-08	112	0.049575	0.001072	0.000007	0.282705	0.000012	0.282703	0.0	0.4	777	17	1169	27
10ZJS116-09	112	0.109071	0.002252	0.000015	0.282706	0.000011	0.282701	0.0	0.4	801	16	1173	25
10ZJS116-10	112	0.056880	0.001157	0.000004	0.282659	0.000011	0.282657	-1.6	0.4	844	16	1273	25
10ZJS116-11	112	0.037168	0.000805	0.000005	0.282676	0.000013	0.282674	-1.0	0.5	812	18	1233	29
10ZJS116-12	112	0.049596	0.001076	0.000008	0.282670	0.000013	0.282668	-1.2	0.5	827	18	1248	29
10ZJS116-13	112	0.062718	0.001322	0.000012	0.282668	0.000011	0.282665	-1.3	0.4	835	16	1253	25
10ZJS116-14	112	0.050317	0.001092	0.000005	0.282699	0.000009	0.282697	-0.2	0.3	786	13	1183	20
10ZJS116-15	112	0.049013	0.001053	0.000005	0.282685	0.000013	0.282683	-0.7	0.5	805	18	1214	29
10ZJS116-16	112	0.049511	0.001082	0.000010	0.282677	0.000011	0.282675	-1.0	0.4	817	16	1232	25
10ZJS116-17	112	0.068932	0.001388	0.000010	0.282717	0.000010	0.282714	0.4	0.4	767	14	1144	22
10ZJS116-18	112	0.040602	0.000869	0.000006	0.282667	0.000014	0.282665	-1.3	0.5	827	20	1253	31
10ZJS116-19	112	0.086495	0.001747	0.000035	0.282663	0.000014	0.282659	-1.5	0.5	852	20	1266	31
10ZJS116-20	112	0.070948	0.001503	0.000032	0.282700	0.000015	0.282697	-0.2	0.5	793	21	1182	34

**10ZJS121 (Wangcun syenogranite)**

Spot No.	Age	$^{176}\text{Hf}/^{177}\text{Hf}$	1 SD	$^{176}\text{Lu}/^{177}\text{Hf}$	1 SD	$^{176}\text{Yb}/^{177}\text{Hf}$	$I_{\text{Hf}}$	$\varepsilon_{\text{Hf}}(t)$	1 SD	$T_{\text{DM1}}$	1 SD	$T_{\text{DM2}}$	1 SD
10ZJS121-01	133	0.282471	0.000023	0.000744	0.000005	0.020425	0.282469	-7.8	0.8	1098	32	1678	51
10ZJS121-02	133	0.282442	0.000021	0.000823	0.000024	0.022239	0.282440	-8.9	0.7	1141	29	1743	47

Appendices

10ZJS121-03	133	0.282497	0.000021	0.000856	0.000010	0.024402	0.282495	-6.9	0.7	1065	29	1621	47
10ZJS121-04	133	0.282457	0.000021	0.001371	0.000028	0.039437	0.282454	-8.4	0.7	1136	30	1713	47
10ZJS121-05	133	0.282487	0.000021	0.000886	0.000010	0.027227	0.282485	-7.3	0.7	1080	29	1643	47
10ZJS121-06	133	0.282439	0.000024	0.001159	0.000011	0.032946	0.282436	-9.0	0.8	1155	34	1751	53
10ZJS121-07	133	0.282479	0.000023	0.000923	0.000003	0.026361	0.282477	-7.6	0.8	1092	32	1661	51
10ZJS121-08	133	0.282458	0.000020	0.000803	0.000006	0.022363	0.282456	-8.3	0.7	1118	28	1707	44
10ZJS121-09	133	0.282529	0.000019	0.000657	0.000008	0.018830	0.282527	-5.8	0.7	1015	26	1549	42
10ZJS121-10	133	0.282479	0.000020	0.000818	0.000017	0.023998	0.282477	-7.5	0.7	1089	28	1661	44
10ZJS121-11	133	0.282473	0.000024	0.001068	0.000003	0.030326	0.282470	-7.8	0.8	1105	34	1675	53
10ZJS121-12	133	0.282463	0.000017	0.001164	0.000004	0.033175	0.282460	-8.1	0.6	1121	24	1698	38
10ZJS121-13	133	0.282484	0.000021	0.000747	0.000003	0.020936	0.282482	-7.4	0.7	1080	29	1649	47
10ZJS121-14	133	0.282556	0.000023	0.001932	0.000068	0.052248	0.282551	-4.9	0.8	1011	33	1496	51
10ZJS121-15	133	0.282456	0.000021	0.000905	0.000005	0.026008	0.282454	-8.4	0.7	1124	29	1712	47

**10ZJS125 (Muchen granitic porphyry)**

Spot No.	Age	$^{176}\text{Hf}/^{177}\text{Hf}$	1 SD	$^{176}\text{Lu}/^{177}\text{Hf}$	1 SD	$^{176}\text{Yb}/^{177}\text{Hf}$	$I_{\text{Hf}}$	$\epsilon_{\text{Hf}}(t)$	1 SD	$T_{\text{DM1}}$	1 SD	$T_{\text{DM2}}$	1 SD
10ZJS125-01	110	0.083477	0.001562	0.000006	0.282670	0.000013	0.282667	-1.3	0.5	837	19	1250	29
10ZJS125-02	110	0.092847	0.001798	0.000016	0.282698	0.000015	0.282694	-0.3	0.5	802	22	1188	34
10ZJS125-03	110	0.069253	0.001509	0.000015	0.282709	0.000014	0.282706	0.1	0.5	780	20	1162	31
10ZJS125-04	110	0.070522	0.001422	0.000037	0.282689	0.000010	0.282686	-0.6	0.4	806	14	1207	22
10ZJS125-05	110	0.092651	0.002006	0.00005	0.282642	0.000014	0.282638	-2.3	0.5	887	20	1314	31
10ZJS125-06	110	0.114822	0.002471	0.000034	0.282673	0.000013	0.282668	-1.3	0.5	853	19	1247	29
10ZJS125-07	110	0.083040	0.001774	0.000025	0.282702	0.000013	0.282698	-0.2	0.5	795	19	1179	29
10ZJS125-08	110	0.070575	0.001475	0.000017	0.282652	0.000011	0.282649	-1.9	0.4	860	16	1290	25
10ZJS125-09	110	0.037681	0.000815	0.000002	0.282682	0.000013	0.282680	-0.8	0.5	803	18	1219	29
10ZJS125-10	110	0.051846	0.001131	0.000019	0.282680	0.000013	0.282678	-0.9	0.5	813	18	1225	29
10ZJS125-11	110	0.061301	0.001326	0.000029	0.282681	0.000015	0.282678	-0.9	0.5	816	21	1224	34
10ZJS125-12	110	0.278263	0.004116	0.000560	0.282719	0.000015	0.282711	0.2	0.5	823	27	1152	34

Appendices

10ZJS125-13	110	0.118385	0.002535	0.000040	0.282667	0.000014	0.282662	-1.5	0.5	864	21	1261	31
10ZJS125-14	110	0.039136	0.000863	0.000120	0.282707	0.000011	0.282705	0.1	0.4	769	16	1164	25
10ZJS125-15	110	0.111635	0.002443	0.000071	0.282634	0.000011	0.282629	-2.6	0.4	910	16	1334	25
10ZJS125-16	110	0.061840	0.001267	0.000005	0.282689	0.000008	0.282686	-0.6	0.3	803	11	1206	18
10ZJS125-17	110	0.082584	0.001709	0.000008	0.282667	0.000013	0.282663	-1.4	0.5	844	19	1257	29
10ZJS125-18	110	0.077102	0.001631	0.000026	0.282679	0.000013	0.282676	-1.0	0.5	825	19	1230	29
10ZJS125-19	110	0.053903	0.001162	0.000013	0.282656	0.000013	0.282654	-1.8	0.5	848	18	1279	29
10ZJS125-20	110	0.141327	0.002916	0.000072	0.282674	0.000011	0.282668	-1.3	0.4	862	16	1247	25

**10ZJS129 (Yingcun granitic porphyry)**

Spot No.	Age	$^{176}\text{Hf}/^{177}\text{Hf}$	1 SD	$^{176}\text{Lu}/^{177}\text{Hf}$	1 SD	$^{176}\text{Yb}/^{177}\text{Hf}$	$I_{\text{Hf}}$	$\epsilon_{\text{Hf}}(t)$	1 SD	$T_{\text{DM1}}$	1 SD	$T_{\text{DM2}}$	1 SD
10ZJS129-02	134	0.282534	0.000026	0.001939	0.000067	0.051576	0.282529	-5.7	0.9	1043	38	1543	58
10ZJS129-03	134	0.282490	0.000029	0.000919	0.000001	0.023805	0.282488	-7.1	1.0	1076	41	1636	64
10ZJS129-04	134	0.282493	0.000025	0.001685	0.000004	0.047074	0.282489	-7.1	0.9	1094	36	1633	56
10ZJS129-05	134	0.282542	0.000026	0.001253	0.000025	0.033144	0.282539	-5.3	0.9	1012	37	1522	58
10ZJS129-07	134	0.282535	0.000024	0.000735	0.000002	0.018788	0.282533	-5.5	0.8	1008	34	1534	53
10ZJS129-08	134	0.282475	0.000026	0.001725	0.000003	0.046582	0.282471	-7.7	0.9	1121	37	1673	58
10ZJS129-09	134	0.282431	0.000024	0.000726	0.000005	0.019182	0.282429	-9.2	0.8	1153	33	1765	53
10ZJS129-10	134	0.282466	0.000029	0.001298	0.000047	0.034690	0.282463	-8.0	1.0	1121	41	1691	64
10ZJS129-11	134	0.282427	0.000028	0.000784	0.000007	0.020195	0.282425	-9.3	1.0	1160	39	1775	62
10ZJS129-12	134	0.282532	0.000029	0.001035	0.000023	0.026914	0.282529	-5.6	1.0	1021	41	1543	65
10ZJS129-13	134	0.282499	0.000024	0.000596	0.000002	0.015565	0.282498	-6.8	0.8	1055	33	1614	53
10ZJS129-14	134	0.282497	0.000024	0.001095	0.000029	0.029266	0.282494	-6.9	0.8	1072	34	1621	53
10ZJS129-15	134	0.282448	0.000026	0.000943	0.000002	0.024736	0.282446	-8.6	0.9	1136	36	1729	58
10ZJS129-16	134	0.282475	0.000026	0.000813	0.000007	0.021439	0.282473	-7.6	0.9	1094	36	1668	58

Appendices

---

**10ZJS131 (Muchen quartz monzonite)**

Spot No.	Age	$^{176}\text{Hf}/^{177}\text{Hf}$	1 SD	$^{176}\text{Lu}/^{177}\text{Hf}$	1 SD	$^{176}\text{Yb}/^{177}\text{Hf}$	$I_{\text{Hf}}$	$\varepsilon_{\text{Hf}}(t)$	1 SD	$T_{\text{DM1}}$	1 SD	$T_{\text{DM2}}$	1 SD
10ZJS131-01	110	0.282683	0.000022	0.001653	0.000070	0.044645	0.282680	-0.9	0.8	821	32	1223	49
10ZJS131-02	110	0.282793	0.000022	0.002489	0.000047	0.066101	0.282788	3.0	0.8	678	32	978	50
10ZJS131-03	110	0.282766	0.000021	0.000968	0.000008	0.025075	0.282764	2.2	0.7	689	30	1032	47
10ZJS131-04	110	0.282726	0.000024	0.001044	0.000004	0.027500	0.282724	0.8	0.8	747	34	1122	54
10ZJS131-05	110	0.282777	0.000020	0.001515	0.000020	0.042798	0.282774	2.5	0.7	683	29	1010	45
10ZJS131-06	110	0.282735	0.000023	0.001706	0.000048	0.047433	0.282731	1.0	0.8	747	33	1105	52
10ZJS131-07	110	0.282728	0.000020	0.001108	0.000030	0.029144	0.282726	0.8	0.7	745	28	1118	45
10ZJS131-08	110	0.282700	0.000019	0.001253	0.000053	0.034679	0.282697	-0.2	0.7	788	27	1181	43
10ZJS131-09	110	0.282744	0.000023	0.002490	0.000018	0.069681	0.282739	1.3	0.8	750	34	1088	52
10ZJS131-10	110	0.282735	0.000021	0.001458	0.000028	0.037909	0.282732	1.0	0.7	742	30	1104	47
10ZJS131-11	110	0.282772	0.000026	0.004158	0.000060	0.116420	0.282763	2.1	0.9	743	40	1033	58
10ZJS131-12	110	0.282712	0.000020	0.001395	0.000031	0.037908	0.282709	0.2	0.7	774	29	1155	45
10ZJS131-13	110	0.282773	0.000019	0.001383	0.000004	0.037801	0.282770	2.4	0.7	687	27	1018	43
10ZJS131-14	110	0.282738	0.000019	0.001161	0.000030	0.031511	0.282736	1.2	0.7	732	27	1096	43
10ZJS131-15	110	0.282771	0.000020	0.001289	0.000030	0.033892	0.282768	2.3	0.7	688	29	1022	45

**10ZJS132 (Muchen quartz monzonite)**

Spot No.	Age	$^{176}\text{Hf}/^{177}\text{Hf}$	1 SD	$^{176}\text{Lu}/^{177}\text{Hf}$	1 SD	$^{176}\text{Yb}/^{177}\text{Hf}$	$I_{\text{Hf}}$	$\varepsilon_{\text{Hf}}(t)$	1 SD	$T_{\text{DM1}}$	1 SD	$T_{\text{DM2}}$	1 SD
10ZJS132-01	112	0.282764	0.000019	0.001399	0.000010	0.040167	0.282761	2.1	0.7	700	27	1038	43
10ZJS132-02	112	0.282702	0.000024	0.001031	0.000003	0.028736	0.282700	-0.1	0.8	781	34	1176	54
10ZJS132-03	112	0.282686	0.000021	0.001455	0.000019	0.040362	0.282683	-0.7	0.7	812	30	1214	47
10ZJS132-04	112	0.282694	0.000019	0.001323	0.000006	0.037253	0.282691	-0.4	0.7	798	27	1195	43
10ZJS132-05	112	0.282716	0.000023	0.002243	0.000059	0.065923	0.282711	0.3	0.8	786	34	1150	52
10ZJS132-06	112	0.282728	0.000020	0.001326	0.000030	0.036208	0.282725	0.8	0.7	750	29	1119	45
10ZJS132-07	112	0.282701	0.000017	0.000883	0.000002	0.023982	0.282699	-0.1	0.6	779	24	1177	38
10ZJS132-08	112	0.282711	0.000018	0.001287	0.000068	0.036301	0.282708	0.2	0.6	773	26	1157	40

Appendices

10ZJS132-09	112	0.282676	0.00002	0.001013	0.000009	0.028521	0.282674	-1.0	0.7	817	28	1234	45
10ZJS132-10	112	0.282813	0.000017	0.000865	0.000003	0.024213	0.282811	3.8	0.6	621	24	926	38
10ZJS132-11	112	0.282735	0.000024	0.002341	0.000072	0.067951	0.282730	1.0	0.8	760	35	1108	54
10ZJS132-12	112	0.282714	0.000025	0.002827	0.000028	0.082295	0.282708	0.2	0.9	802	37	1157	56
10ZJS132-13	112	0.282699	0.000024	0.002007	0.000007	0.057848	0.282695	-0.3	0.8	806	35	1187	54
10ZJS132-14	112	0.282719	0.000019	0.000916	0.000007	0.025103	0.282717	0.5	0.7	754	27	1137	43
10ZJS132-15	112	0.282731	0.000025	0.002030	0.000019	0.055612	0.282727	0.9	0.9	760	36	1115	56
10ZJS132-16	112	0.282744	0.000021	0.001863	0.000016	0.054033	0.282740	1.3	0.7	737	30	1085	47

**10ZJS133 (Luojia granitic porphyry)**

Spot No.	Age	$^{176}\text{Hf}/^{177}\text{Hf}$	1 SD	$^{176}\text{Lu}/^{177}\text{Hf}$	1 SD	$^{176}\text{Yb}/^{177}\text{Hf}$	$I_{\text{Hf}}$	$\varepsilon_{\text{Hf}}(t)$	1 SD	$T_{\text{DM1}}$	1 SD	$T_{\text{DM2}}$	1 SD
10ZJS133-01	127	0.282627	0.000026	0.001217	0.000092	0.036987	0.282624	-2.4	0.9	891	37	1336	58
10ZJS133-02	127	0.282682	0.000025	0.000479	0.000005	0.013265	0.282681	-0.4	0.9	797	35	1209	56
10ZJS133-03	127	0.282723	0.000021	0.000945	0.000040	0.027920	0.282721	1.0	0.7	749	30	1119	47
10ZJS133-04	127	0.282636	0.000024	0.001211	0.000040	0.036896	0.282633	-2.1	0.8	878	34	1316	54
10ZJS133-05	127	0.282585	0.000023	0.000716	0.000003	0.021782	0.282583	-3.9	0.8	938	32	1427	51
10ZJS133-06	127	0.282580	0.000025	0.001001	0.000008	0.030643	0.282578	-4.1	0.9	952	35	1440	56
10ZJS133-07	127	0.282641	0.000023	0.000861	0.000011	0.025285	0.282639	-1.9	0.8	863	32	1303	51
10ZJS133-08	127	0.282630	0.000024	0.000617	0.000001	0.018409	0.282629	-2.3	0.8	873	34	1326	54
10ZJS133-09	127	0.282577	0.000025	0.000767	0.000002	0.022477	0.282575	-4.2	0.9	950	35	1445	56
10ZJS133-10	127	0.282607	0.000031	0.001525	0.000032	0.046566	0.282603	-3.2	1.1	927	44	1382	69
10ZJS133-11	127	0.282580	0.000024	0.000809	0.000004	0.024224	0.282578	-4.1	0.8	947	34	1439	54
10ZJS133-12	127	0.282683	0.000024	0.000712	0.000006	0.021182	0.282681	-0.4	0.8	801	34	1208	54
10ZJS133-13	127	0.282609	0.000020	0.000943	0.000040	0.029319	0.282607	-3.1	0.7	910	28	1375	45
10ZJS133-14	127	0.282682	0.000021	0.000882	0.000029	0.025308	0.28268	-0.5	0.7	806	30	1211	47
10ZJS133-15	127	0.282603	0.000022	0.000925	0.000054	0.027888	0.282601	-3.3	0.8	918	31	1388	49
10ZJS133-16	127	0.282635	0.000022	0.001358	0.000044	0.044389	0.282632	-2.2	0.8	883	31	1319	49
10ZJS133-17	127	0.282582	0.000021	0.001034	0.000026	0.030924	0.282580	-4.0	0.7	950	30	1435	47

Appendices

---

10ZJS133-18	127	0.282554	0.000020	0.001323	0.000015	0.039408	0.282551	-5.0	0.7	997	28	1499	45
10ZJS133-19	127	0.282590	0.000018	0.000611	0.000001	0.019088	0.282589	-3.7	0.6	928	25	1415	40
10ZJS133-20	127	0.282568	0.000022	0.000831	0.000035	0.025115	0.282566	-4.5	0.8	965	31	1466	49

---

**10ZJS135 (Sheyang syenogranite)**

Spot No.	Age	$^{176}\text{Hf}/^{177}\text{Hf}$	1 SD	$^{176}\text{Lu}/^{177}\text{Hf}$	1 SD	$^{176}\text{Yb}/^{177}\text{Hf}$	$I_{\text{Hf}}$	$\varepsilon_{\text{Hf}}(t)$	1 SD	$T_{\text{DM1}}$	1 SD	$T_{\text{DM2}}$	1 SD
10ZJS135-01	225	0.282483	0.000010	0.000537	0.000010	0.027509	0.282481	-5.4	0.3	1074	13	1592	21
10ZJS135-02	225	0.282494	0.000014	0.000606	0.000009	0.028931	0.282491	-5.0	0.5	1061	19	1569	31
10ZJS135-03	225	0.282374	0.000019	0.001406	0.000024	0.076240	0.282368	-9.3	0.7	1254	27	1842	42
10ZJS135-04	225	0.282538	0.000014	0.000714	0.000013	0.041280	0.282535	-3.4	0.5	1003	20	1472	31
10ZJS135-05	225	0.282447	0.000013	0.000725	0.000011	0.037372	0.282444	-6.7	0.5	1130	18	1674	29
10ZJS135-06	225	0.282512	0.000017	0.000555	0.000015	0.027928	0.282510	-4.3	0.6	1034	24	1528	38
10ZJS135-07	225	0.282500	0.000014	0.000656	0.000044	0.028888	0.282497	-4.8	0.5	1054	20	1556	31
10ZJS135-08	225	0.282529	0.000013	0.000530	0.000008	0.026135	0.282527	-3.7	0.5	1010	18	1490	29
10ZJS135-09	225	0.282491	0.000017	0.000471	0.000007	0.023347	0.282489	-5.1	0.6	1061	24	1574	38
10ZJS135-10	225	0.282448	0.000014	0.000411	0.000007	0.020864	0.282446	-6.6	0.5	1119	19	1669	31
10ZJS135-11	225	0.282335	0.000023	0.000714	0.000019	0.035127	0.282332	-10.6	0.8	1285	32	1922	51
10ZJS135-12	237	0.282437	0.000020	0.000915	0.000034	0.052961	0.282433	-6.8	0.7	1149	28	1691	44
10ZJS135-13	225	0.282457	0.000013	0.000555	0.000008	0.028055	0.282455	-6.3	0.5	1111	18	1650	29
10ZJS135-14	370	0.282071	0.000019	0.000519	0.000011	0.021110	0.282067	-16.8	0.7	1642	26	2414	42
10ZJS135-15	225	0.282401	0.000017	0.001073	0.000042	0.055889	0.282396	-8.3	0.6	1205	24	1779	38
10ZJS135-16	225	0.282432	0.000015	0.001152	0.000013	0.062147	0.282427	-7.3	0.5	1164	21	1711	33
10ZJS135-17	225	0.282443	0.000015	0.000968	0.00002	0.052970	0.282439	-6.8	0.5	1142	21	1685	33
10ZJS135-18	225	0.282455	0.000013	0.000921	0.000024	0.049042	0.282451	-6.4	0.5	1124	18	1658	29
10ZJS135-19	225	0.282451	0.000028	0.001032	0.000069	0.064103	0.282447	-6.6	1.0	1133	39	1668	62
10ZJS135-20	225	0.282431	0.000019	0.000761	0.000017	0.042914	0.282428	-7.2	0.7	1153	26	1710	42
10ZJS135-21	225	0.282420	0.000019	0.000757	0.000030	0.039235	0.282417	-7.6	0.7	1168	26	1734	42
10ZJS135-22	225	0.282390	0.000024	0.001347	0.000098	0.058393	0.282384	-8.8	0.8	1229	34	1806	53

---

**10ZJS136 (Lingkeng syenogranite)**

Spot No.	Age	$^{176}\text{Hf}/^{177}\text{Hf}$	1 SD	$^{176}\text{Lu}/^{177}\text{Hf}$	1 SD	$^{176}\text{Yb}/^{177}\text{Hf}$	$I_{\text{Hf}}$	$\varepsilon_{\text{Hf}}(t)$	1 SD	$T_{\text{DM1}}$	1 SD	$T_{\text{DM2}}$	1 SD
10ZJS136-01	134	0.282456	0.000019	0.002607	0.000014	0.079362	0.282450	-8.5	0.7	1176	28	1721	42
10ZJS136-02	134	0.282564	0.000020	0.00214	0.000131	0.063306	0.282559	-4.6	0.7	1005	29	1478	45
10ZJS136-03	134	0.282476	0.000023	0.001266	0.000031	0.037164	0.282473	-7.7	0.8	1106	33	1669	51
10ZJS136-04	134	0.282493	0.000020	0.000657	0.000001	0.018529	0.282491	-7.0	0.7	1065	28	1628	44
10ZJS136-05	134	0.282453	0.000017	0.000959	0.000005	0.027549	0.282451	-8.4	0.6	1129	24	1718	38
10ZJS136-06	134	0.282492	0.000021	0.001521	0.000023	0.044681	0.282488	-7.1	0.7	1091	30	1635	47
10ZJS136-07	134	0.282537	0.000023	0.001179	0.000007	0.034934	0.282534	-5.5	0.8	1017	33	1533	51
10ZJS136-08	134	0.282495	0.000020	0.000754	0.000012	0.020939	0.282493	-6.9	0.7	1065	28	1624	44
10ZJS136-09	134	0.282539	0.000017	0.004055	0.000015	0.123291	0.282529	-5.7	0.6	1099	26	1544	38
10ZJS136-10	134	0.282481	0.000021	0.001102	0.000018	0.032853	0.282478	-7.5	0.7	1094	30	1657	47
10ZJS136-11	134	0.282425	0.000016	0.002073	0.000036	0.062453	0.282420	-9.5	0.6	1204	23	1786	35
10ZJS136-12	134	0.282508	0.000024	0.000958	0.000022	0.028530	0.282506	-6.5	0.8	1052	34	1596	53
10ZJS136-13	134	0.282512	0.000022	0.001175	0.000012	0.033684	0.282509	-6.4	0.8	1053	31	1588	49
10ZJS136-14	134	0.282470	0.000018	0.000747	0.000013	0.021550	0.282468	-7.8	0.6	1099	25	1679	40
10ZJS136-15	134	0.282456	0.000016	0.002099	0.000128	0.062031	0.282451	-8.4	0.6	1160	23	1718	36
10ZJS136-16	134	0.282492	0.000020	0.002701	0.000196	0.080046	0.282485	-7.2	0.7	1127	30	1641	44
10ZJS136-17	134	0.282461	0.000019	0.002664	0.000064	0.082376	0.282454	-8.3	0.7	1171	28	1710	42
10ZJS136-18	134	0.282472	0.000018	0.00244	0.000111	0.076779	0.282466	-7.9	0.6	1148	27	1684	40
10ZJS136-19	134	0.282480	0.000018	0.001848	0.000036	0.055877	0.282475	-7.6	0.6	1118	26	1663	40
10ZJS136-20	134	0.282460	0.000020	0.001444	0.000027	0.044706	0.282456	-8.2	0.7	1134	28	1705	44

Appendices

---

**10ZJS143 (Jiuhua granitic porphyry)**

Spot No.	Age	$^{176}\text{Hf}/^{177}\text{Hf}$	1 SD	$^{176}\text{Lu}/^{177}\text{Hf}$	1 SD	$^{176}\text{Yb}/^{177}\text{Hf}$	$I_{\text{Hf}}$	$\varepsilon_{\text{Hf}}(t)$	1 SD	$T_{\text{DM1}}$	1 SD	$T_{\text{DM2}}$	1 SD
10ZJS143-01	133	0.282567	0.000025	0.000996	0.000023	0.057978	0.282565	-4.4	0.9	969	35	1463	56
10ZJS143-02	133	0.282577	0.000016	0.000671	0.000006	0.036591	0.282575	-4.0	0.6	947	22	1439	36
10ZJS143-03	133	0.282534	0.000017	0.000725	0.00001	0.040043	0.282532	-5.6	0.6	1008	24	1535	38
10ZJS143-04	133	0.282494	0.000013	0.000655	0.000006	0.036476	0.282492	-7.0	0.5	1062	18	1624	29
10ZJS143-05	133	0.282586	0.000017	0.000926	0.000013	0.051953	0.282584	-3.7	0.6	941	24	1421	38
10ZJS143-06	133	0.282564	0.000013	0.000712	0.000016	0.039272	0.282562	-4.5	0.5	966	18	1469	29
10ZJS143-07	133	0.282512	0.000014	0.001259	0.000048	0.070617	0.282509	-6.4	0.5	1054	20	1587	31
10ZJS143-08	133	0.282563	0.000019	0.000919	0.000010	0.048563	0.282561	-4.6	0.7	973	27	1472	42
10ZJS143-09	133	0.282558	0.000018	0.001572	0.000077	0.079099	0.282554	-4.8	0.6	997	26	1487	40
10ZJS143-10	133	0.282571	0.000013	0.000948	0.000014	0.049414	0.282569	-4.3	0.5	962	18	1454	29
10ZJS143-11	133	0.282595	0.000017	0.000508	0.000012	0.026308	0.282594	-3.4	0.6	918	24	1398	38
10ZJS143-12	133	0.282561	0.000018	0.001260	0.000028	0.065134	0.282558	-4.7	0.6	985	25	1478	40
10ZJS143-13	133	0.282607	0.000013	0.000905	0.000006	0.046777	0.282605	-3.0	0.5	911	18	1374	29
10ZJS143-14	133	0.282541	0.000013	0.001121	0.000075	0.047516	0.282538	-5.4	0.5	1009	18	1522	29
10ZJS143-15	133	0.282554	0.000014	0.001020	0.000040	0.052340	0.282551	-4.9	0.5	988	20	1493	31
10ZJS143-16	133	0.282575	0.000016	0.000529	0.000005	0.024942	0.282574	-4.1	0.6	946	22	1443	36
10ZJS143-17	133	0.282581	0.000026	0.000895	0.000016	0.047934	0.282579	-3.9	0.9	947	36	1432	58
10ZJS143-18	133	0.282519	0.000013	0.000689	0.000027	0.034780	0.282517	-6.1	0.5	1028	18	1569	29
10ZJS143-19	133	0.282554	0.000013	0.000854	0.000042	0.042192	0.282552	-4.9	0.5	984	18	1492	29
10ZJS143-20	133	0.282575	0.000015	0.000662	0.000011	0.035380	0.282573	-4.1	0.5	950	21	1444	33

**10ZJS149 (Shangsanzi granitic porphyry)**

Spot No.	Age	$^{176}\text{Hf}/^{177}\text{Hf}$	1 SD	$^{176}\text{Lu}/^{177}\text{Hf}$	1 SD	$^{176}\text{Yb}/^{177}\text{Hf}$	$I_{\text{Hf}}$	$\varepsilon_{\text{Hf}}(t)$	1 SD	$T_{\text{DM1}}$	1 SD	$T_{\text{DM2}}$	1 SD
10ZJS149-01	159	0.282687	0.000011	0.000582	0.000033	0.024173	0.282685	0.4	0.4	791	15	1178	25
10ZJS149-02	159	0.282641	0.000010	0.000631	0.000006	0.025075	0.282639	-1.2	0.3	857	13	1281	21

Appendices

10ZJS149-03	159	0.282733	0.000015	0.001688	0.000140	0.069991	0.282728	1.9	0.5	749	22	1082	34	
10ZJS149-04	869	0.282573	0.000014	0.001575	0.000030	0.065043	0.282547	11.3	0.5	976	20	1037	31	
10ZJS149-05	159	0.282598	0.000014	0.001241	0.000030	0.059514	0.282594	-2.8	0.5	932	20	1381	31	
10ZJS149-06	159	0.282548	0.000012	0.002066	0.000014	0.107681	0.282542	-4.6	0.4	1025	17	1498	27	
10ZJS149-07	159	0.282646	0.000013	0.000861	0.000021	0.039875	0.282643	-1.1	0.5	855	18	1271	29	
10ZJS149-08	159	0.282593	0.000014	0.000629	0.000019	0.025428	0.282591	-2.9	0.5	924	20	1388	31	
10ZJS149-09	159	0.282597	0.000015	0.000812	0.000006	0.038555	0.282595	-2.8	0.5	923	21	1380	33	
10ZJS149-10	159	0.282774	0.000016	0.000647	0.000008	0.027931	0.282772	3.5	0.6	671	22	983	36	
10ZJS149-11	159	0.282596	0.000015	0.000911	0.000042	0.032285	0.282593	-2.8	0.5	926	21	1383	33	
10ZJS149-12	159	0.282643	0.000008	0.000594	0.000005	0.023432	0.282641	-1.1	0.3	853	11	1276	18	
10ZJS149-13	159	0.282646	0.000015	0.001341	0.000120	0.053664	0.282642	-1.1	0.5	866	22	1274	34	
10ZJS149-14	836	0.282623	0.000014	0.000748	0.000005	0.027753	0.282611	12.8	0.5	885	20	914	32	
10ZJS149-15	823	0.282407	0.000014	0.001576	0.000023	0.073765	0.282383	4.4	0.5	1212	20	1434	31	
10ZJS149-16	159	0.282589	0.000016	0.000801	0.000038	0.025721	0.282587	-3.1	0.6	933	22	1399	36	
10ZJS149-17	159	0.282585	0.000015	0.000678	0.000058	0.024976	0.282583	-3.2	0.5	936	21	1407	33	
10ZJS149-18	159	0.282654	0.000013	0.000674	0.000021	0.025908	0.282652	-0.8	0.5	840	18	1253	29	
10ZJS149-19	159	0.282614	0.000011	0.000171	0.000007	0.009350	0.282613	-2.2	0.4	884	15	1339	25	
10ZJS149-20	159	0.282678	0.000013	0.000659	0.000013	0.027395	0.282676	0.1	0.5	806	18	1199	29	

**10ZJS154 (Lingshan syenogranite)**

Spot No.	Age	$^{176}\text{Hf}/^{177}\text{Hf}$	1 SD	$^{176}\text{Lu}/^{177}\text{Hf}$	1 SD	$^{176}\text{Yb}/^{177}\text{Hf}$	1 SD	$I_{\text{Hf}}$	$\varepsilon_{\text{Hf(t)}}$	1 SD	$T_{\text{DM}}$	1 SD	$T_{\text{DM2}}$	1 SD
10ZJS154-01	131	0.282621	0.000017	0.001764	0.000160	0.069713	0.003100	0.282617	-2.6	0.6	912	25	1348	38
10ZJS154-02	131	0.282651	0.000016	0.001473	0.000095	0.065524	0.003100	0.282647	-1.5	0.6	862	23	1280	36
10ZJS154-03	131	0.282655	0.000011	0.002227	0.000100	0.102792	0.003700	0.282650	-1.5	0.4	874	16	1275	25
10ZJS154-04	131	0.282650	0.000009	0.000851	0.000020	0.039639	0.001100	0.282648	-1.5	0.3	849	13	1279	21

Appendices

10ZJS154-05	131	0.282614	0.000012	0.000885	0.000025	0.039819	0.000570	0.282612	-2.8	0.4	900	17	1359	27
10ZJS154-06	131	0.282641	0.000019	0.002609	0.000200	0.100713	0.004000	0.282635	-2.0	0.7	904	28	1308	42
10ZJS154-07	131	0.282570	0.000013	0.001313	0.000084	0.058975	0.004100	0.282567	-4.4	0.5	973	19	1460	29
10ZJS154-08	131	0.282638	0.000012	0.001496	0.000190	0.060724	0.006200	0.282634	-2.0	0.4	881	18	1309	27
10ZJS154-09	131	0.282631	0.000011	0.001762	0.000160	0.066753	0.004300	0.282627	-2.3	0.4	897	16	1326	25
10ZJS154-10	131	0.282645	0.000013	0.001051	0.000021	0.048487	0.001300	0.282642	-1.7	0.5	861	18	1291	29
10ZJS154-11	131	0.282635	0.000012	0.000762	0.000014	0.036867	0.000590	0.282633	-2.0	0.4	868	17	1312	27
10ZJS154-12	131	0.282625	0.000014	0.001436	0.000140	0.052537	0.003200	0.282621	-2.4	0.5	898	20	1338	31
10ZJS154-13	131	0.282660	0.000016	0.001438	0.000070	0.061362	0.001000	0.282656	-1.2	0.6	848	23	1260	36
10ZJS154-14	131	0.282615	0.000016	0.001225	0.000046	0.051304	0.000690	0.282612	-2.8	0.6	907	23	1359	36
10ZJS154-15	131	0.282632	0.000120	0.004581	0.000210	0.156282	0.007300	0.282621	-2.5	4.2	970	187	1339	268
10ZJS154-16	131	0.282539	0.000023	0.001993	0.000093	0.106642	0.004300	0.282534	-5.5	0.8	1036	33	1532	51
10ZJS154-17	131	0.282639	0.000014	0.001262	0.000021	0.060119	0.000520	0.282636	-1.9	0.5	874	20	1306	31
10ZJS154-18	131	0.282624	0.000010	0.000946	0.000025	0.038184	0.000400	0.282622	-2.4	0.4	888	14	1337	22

**10ZJS155 (Lingshan syenogranite)**

Spot No.	Age	$^{176}\text{Hf}/^{177}\text{Hf}$	1 SD	$^{176}\text{Lu}/^{177}\text{Hf}$	1 SD	$^{176}\text{Yb}/^{177}\text{Hf}$	$I_{\text{Hf}}$	$\varepsilon_{\text{Hf(t)}}$	1 SD	$T_{\text{DM}}$	1 SD	$T_{\text{DM2}}$	1 SD
10ZJS155-01	129	0.282637	0.000023	0.001025	0.000025	0.025775	0.282635	-2.0	0.8	872	32	1311	51
10ZJS155-02	129	0.282680	0.000024	0.000860	0.000002	0.022228	0.282678	-0.5	0.8	808	34	1214	54
10ZJS155-03	129	0.282660	0.000024	0.000621	0.000008	0.016009	0.282659	-1.2	0.8	831	34	1258	54
10ZJS155-04	129	0.282650	0.000030	0.001121	0.000031	0.029608	0.282647	-1.6	1.1	856	42	1283	67
10ZJS155-06	129	0.282593	0.000024	0.000748	0.000004	0.019261	0.282591	-3.6	0.8	928	34	1408	54
10ZJS155-07	129	0.282664	0.000026	0.000929	0.000013	0.024493	0.282662	-1.1	0.9	832	37	1250	58
10ZJS155-08	129	0.282696	0.000026	0.000873	0.000003	0.022177	0.282694	0.1	0.9	786	37	1178	58
10ZJS155-09	129	0.282631	0.000025	0.001230	0.000014	0.032671	0.282628	-2.3	0.9	886	35	1326	56
10ZJS155-10	129	0.282650	0.000024	0.000793	0.000006	0.021424	0.282648	-1.6	0.8	849	34	1281	54
10ZJS155-11	129	0.282639	0.000027	0.001048	0.000024	0.026502	0.282636	-2.0	1.0	870	38	1307	60
10ZJS155-12	129	0.282695	0.000022	0.001112	0.000018	0.030753	0.282692	0.0	0.8	792	31	1182	49

Appendices

10ZJS155-13	129	0.282615	0.000020	0.000817	0.000003	0.021045	0.282613	-2.8	0.7	898	28	1359	45
10ZJS155-14	129	0.282674	0.000023	0.001085	0.000015	0.028777	0.282671	-0.7	0.8	821	33	1229	52
10ZJS155-15	129	0.282626	0.000019	0.001429	0.000002	0.037216	0.282623	-2.5	0.7	897	27	1338	42
10ZJS155-16	129	0.282728	0.000023	0.001651	0.000033	0.044904	0.282724	1.1	0.8	756	33	1111	52
10ZJS155-17	129	0.282656	0.000021	0.001011	0.000004	0.027315	0.282654	-1.4	0.7	845	30	1269	47
10ZJS155-18	129	0.282620	0.000021	0.000837	0.000001	0.021498	0.282618	-2.6	0.7	892	29	1348	47
10ZJS155-19	129	0.282656	0.000022	0.000804	0.000004	0.020414	0.282654	-1.3	0.8	841	31	1268	49
10ZJS155-20	129	0.282643	0.000021	0.001007	0.000001	0.025437	0.282641	-1.8	0.7	863	30	1298	47

**10ZJS156 (Lingshan MME)**

Spot No.	Age	$^{176}\text{Hf}/^{177}\text{Hf}$	1 SD	$^{176}\text{Lu}/^{177}\text{Hf}$	1 SD	$^{176}\text{Yb}/^{177}\text{Hf}$	$I_{\text{Hf}}$	$\epsilon_{\text{Hf(t)}}$	1 SD	$T_{\text{DM}}$	1 SD	$T_{\text{DM2}}$	1 SD
10ZJS156-01	133	0.282675	0.000024	0.001679	0.000017	0.049533	0.282671	-0.7	0.8	833	35	1228	54
10ZJS156-02	133	0.282718	0.000021	0.001206	0.000019	0.027641	0.282715	0.9	0.7	762	30	1129	47
10ZJS156-03	133	0.282674	0.000019	0.001357	0.000118	0.038924	0.282671	-0.7	0.7	827	27	1228	43
10ZJS156-04	133	0.282800	0.000031	0.007227	0.000044	0.220352	0.282782	3.3	1.1	768	53	978	70
10ZJS156-05	133	0.282624	0.000020	0.001862	0.000031	0.054937	0.282619	-2.5	0.7	911	29	1343	45
10ZJS156-06	133	0.282663	0.000019	0.001579	0.000068	0.045991	0.282659	-1.1	0.7	848	27	1254	43
10ZJS156-07	133	0.282634	0.000020	0.001997	0.000062	0.061186	0.282629	-2.1	0.7	900	29	1321	45
10ZJS156-08	133	0.282657	0.000018	0.000978	0.000020	0.030781	0.282655	-1.2	0.6	843	25	1264	40
10ZJS156-09	133	0.282623	0.000015	0.000877	0.000008	0.026138	0.282621	-2.4	0.5	889	21	1339	34
10ZJS156-10	133	0.282644	0.000014	0.000739	0.000004	0.020245	0.282642	-1.7	0.5	856	20	1292	31
10ZJS156-11	133	0.282660	0.000018	0.001151	0.000007	0.033092	0.282657	-1.1	0.6	843	26	1258	40
10ZJS156-12	133	0.282696	0.000014	0.000593	0.000011	0.016446	0.282695	0.2	0.5	780	20	1175	31
10ZJS156-13	133	0.282633	0.000020	0.000537	0.000006	0.014244	0.282632	-2.0	0.7	867	28	1315	45
10ZJS156-14	133	0.282625	0.000016	0.000520	0.000035	0.014717	0.282624	-2.3	0.6	877	22	1333	36
10ZJS156-15	133	0.282631	0.000021	0.001476	0.000014	0.044904	0.282627	-2.2	0.7	891	30	1325	47
10ZJS156-16	133	0.282653	0.000017	0.000935	0.000011	0.026913	0.282651	-1.4	0.6	848	24	1273	38
10ZJS156-17	133	0.282674	0.000023	0.001884	0.000026	0.054402	0.282669	-0.7	0.8	839	33	1231	52

Appendices

---

10ZJS156-18	133	0.282644	0.000022	0.000932	0.000050	0.027194	0.282642	-1.7	0.8	860	31	1293	49
10ZJS156-19	133	0.282666	0.000016	0.001032	0.000005	0.029389	0.282663	-0.9	0.6	832	23	1244	36
10ZJS156-20	133	0.282651	0.000013	0.000784	0.000005	0.022578	0.282649	-1.4	0.5	847	18	1276	29

**10ZJS170 (Wancunxiang syenogranite)**

Spot No.	Age	$^{176}\text{Hf}/^{177}\text{Hf}$	1 SD	$^{176}\text{Lu}/^{177}\text{Hf}$	1 SD	$^{176}\text{Yb}/^{177}\text{Hf}$	$I_{\text{Hf}}$	$\epsilon_{\text{Hf(t)}}$	1 SD	$T_{\text{DM}}$	1 SD	$T_{\text{DM2}}$	1 SD
10ZJS170-01	131	0.282687	0.000015	0.000615	0.000005	0.018170	0.282685	-0.2	0.5	793	21	1196	34
10ZJS170-02	131	0.282686	0.000019	0.001419	0.000028	0.045751	0.282683	-0.3	0.7	812	27	1203	43
10ZJS170-03	131	0.282671	0.000018	0.001152	0.000011	0.037320	0.282668	-0.8	0.6	827	26	1235	40
10ZJS170-04	131	0.282661	0.000019	0.001140	0.000013	0.035512	0.282658	-1.2	0.7	841	27	1257	43
10ZJS170-05	131	0.282663	0.000020	0.000987	0.000030	0.030304	0.282661	-1.1	0.7	835	28	1252	45
10ZJS170-06	131	0.282748	0.000027	0.001221	0.000066	0.038201	0.282745	1.9	1.0	719	38	1062	61
10ZJS170-07	131	0.282672	0.000015	0.001069	0.000024	0.032436	0.282669	-0.8	0.5	824	21	1232	34
10ZJS170-08	131	0.282668	0.000019	0.000908	0.000023	0.030296	0.282666	-0.9	0.7	826	27	1240	43
10ZJS170-09	870	0.281818	0.000014	0.000791	0.000009	0.020416	0.281805	-15.0	0.5	2004	19	2681	31
10ZJS170-10	131	0.282659	0.000020	0.001049	0.000050	0.032369	0.282656	-1.2	0.7	842	28	1261	45
10ZJS170-11	131	0.282666	0.000023	0.001011	0.000076	0.031502	0.282664	-1.0	0.8	831	33	1245	51
10ZJS170-12	131	0.282650	0.000017	0.000696	0.000011	0.021523	0.282648	-1.5	0.6	847	24	1279	38
10ZJS170-13	131	0.282638	0.000019	0.000845	0.000027	0.025841	0.282636	-1.9	0.7	867	27	1307	42
10ZJS170-14	131	0.282679	0.000015	0.001035	0.000010	0.032037	0.282676	-0.5	0.5	813	21	1216	34
10ZJS170-15	131	0.282645	0.000023	0.001104	0.000022	0.034499	0.282642	-1.7	0.8	863	33	1293	51
10ZJS170-16	131	0.282689	0.000020	0.001197	0.000064	0.038255	0.282686	-0.2	0.7	803	28	1195	45
10ZJS170-17	131	0.282698	0.000021	0.001428	0.000101	0.045790	0.282695	0.1	0.7	795	30	1176	47
10ZJS170-18	131	0.282690	0.000016	0.001115	0.000038	0.035864	0.282687	-0.1	0.6	799	23	1192	36

Appendices

---

**10ZJS171 (Wancunxiang syenogranite, endoskarn)**

Spot No.	Age	$^{176}\text{Hf}/^{177}\text{Hf}$	1 SD	$^{176}\text{Lu}/^{177}\text{Hf}$	1 SD	$^{176}\text{Yb}/^{177}\text{Hf}$	1 SD	$I_{\text{Hf}}$	$\varepsilon_{\text{Hf}(t)}$	1 SD	$T_{\text{DM}}$	1 SD	$T_{\text{DM2}}$	1 SD
10ZJS171-01	130	0.282634	0.000017	0.001164	0.000042	0.056425	0.001500	0.282631	-2.1	0.6	879	24	1317	38
10ZJS171-02	130	0.282594	0.000017	0.001341	0.000120	0.049120	0.001100	0.282591	-3.6	0.6	940	24	1407	38
10ZJS171-03	130	0.282537	0.000028	0.000994	0.000010	0.049100	0.001100	0.282535	-5.5	1.0	1011	39	1532	62
10ZJS171-04	212	0.282539	0.000022	0.000745	0.000009	0.029433	0.000710	0.282536	-3.7	0.8	1002	31	1477	49
10ZJS171-05	130	0.282649	0.000020	0.001578	0.000049	0.074585	0.002400	0.282645	-1.6	0.7	867	29	1285	45
10ZJS171-06	130	0.282625	0.000020	0.000633	0.000010	0.030604	0.000940	0.282623	-2.4	0.7	879	28	1334	45
10ZJS171-07	130	0.282663	0.000018	0.001292	0.000026	0.064734	0.001200	0.282660	-1.1	0.6	841	26	1253	40
10ZJS171-08	130	0.282676	0.000013	0.001025	0.000004	0.050718	0.000620	0.282674	-0.6	0.5	816	18	1222	29
10ZJS171-09	130	0.282663	0.000015	0.001351	0.000079	0.072509	0.005400	0.282660	-1.1	0.5	842	21	1253	34
10ZJS171-10	130	0.282651	0.000018	0.001148	0.000040	0.056453	0.002100	0.282648	-1.5	0.6	854	25	1279	40
10ZJS171-11	130	0.282637	0.000016	0.000753	0.000017	0.035956	0.000760	0.282635	-2.0	0.6	865	22	1308	36
10ZJS171-12	130	0.282650	0.000022	0.001062	0.000015	0.052814	0.001100	0.282647	-1.6	0.8	854	31	1280	49
10ZJS171-13	130	0.282629	0.000013	0.002000	0.000120	0.097474	0.007800	0.282624	-2.4	0.5	906	19	1332	29
10ZJS171-14	130	0.282631	0.000023	0.001018	0.000024	0.051187	0.001100	0.282629	-2.2	0.8	880	32	1323	51
10ZJS171-15	130	0.282619	0.000012	0.001277	0.000020	0.062398	0.000960	0.282616	-2.7	0.4	903	17	1351	27
10ZJS171-16	130	0.282630	0.000016	0.001041	0.000038	0.050909	0.002100	0.282627	-2.3	0.6	882	23	1325	36
10ZJS171-17	130	0.282635	0.000017	0.001115	0.000040	0.056832	0.001700	0.282632	-2.1	0.6	876	24	1314	38
10ZJS171-18	130	0.282670	0.000015	0.000574	0.000010	0.028488	0.000830	0.282669	-0.8	0.5	815	21	1233	34

**10ZJS172 (Damaoshan-Huaiyushan syenogranite-alkali feldspar granite)**

Spot No.	Age	$^{176}\text{Hf}/^{177}\text{Hf}$	1 SD	$^{176}\text{Lu}/^{177}\text{Hf}$	1 SD	$^{176}\text{Yb}/^{177}\text{Hf}$	1 SD	$I_{\text{Hf}}$	$\varepsilon_{\text{Hf}(t)}$	1 SD	$T_{\text{DM}}$	1 SD	$T_{\text{DM2}}$	1 SD
10ZJS172-01	130	0.282577	0.000013	0.001168	0.000007	0.056981	0.000540	0.282574	-4.1	0.5	960	18	1444	29
10ZJS172-03	130	0.282597	0.000015	0.000643	0.000008	0.033461	0.000900	0.282595	-3.4	0.5	918	21	1396	33
10ZJS172-04	130	0.282572	0.000014	0.000955	0.000033	0.052012	0.002100	0.282570	-4.3	0.5	961	20	1454	31
10ZJS172-05	130	0.282614	0.000015	0.000843	0.000028	0.038938	0.000810	0.282612	-2.8	0.5	899	21	1360	33

## Appendices

---

10ZJS172-06	130	0.282624	0.000016	0.000737	0.000004	0.037574	0.000220	0.282622	-2.4	0.6	883	22	1337	36
10ZJS172-07	130	0.282648	0.000016	0.000641	0.000040	0.035038	0.002300	0.282646	-1.6	0.6	847	22	1283	36
10ZJS172-08	130	0.282619	0.000012	0.001204	0.000065	0.058352	0.001500	0.282616	-2.7	0.4	901	17	1350	27
10ZJS172-09	130	0.282595	0.000017	0.001408	0.000099	0.071078	0.003900	0.282592	-3.5	0.6	940	24	1405	38
10ZJS172-10	130	0.282626	0.000021	0.001541	0.000130	0.068062	0.003300	0.282622	-2.4	0.7	899	30	1337	47
10ZJS172-11	130	0.282596	0.000018	0.002820	0.000320	0.114759	0.008700	0.282589	-3.6	0.6	976	28	1410	40
10ZJS172-12	130	0.282591	0.000015	0.000807	0.000004	0.041509	0.000410	0.282589	-3.6	0.5	931	21	1411	33
10ZJS172-13	130	0.282562	0.000017	0.001333	0.000031	0.071224	0.001900	0.282559	-4.7	0.6	985	24	1478	38
10ZJS172-14	130	0.282558	0.000026	0.003731	0.000680	0.214684	0.042000	0.282549	-5.0	0.9	1059	44	1500	58
10ZJS172-15	130	0.282548	0.000018	0.000845	0.000021	0.044693	0.001000	0.282546	-5.1	0.6	992	25	1507	40
10ZJS172-16	130	0.282606	0.000018	0.000515	0.000003	0.026108	0.000092	0.282605	-3.1	0.6	903	25	1376	40

---

**Appendix E. Table of whole-rock chemical compositions**

	Triassic						
	09ZJ01	10ZJS010	10ZJS011	10ZJS135	10ZJS062	10ZJS064	10ZJS065
				Qiuwang			
SiO <sub>2</sub>	73.98	65.50	73.41	67.64	63.62	65.08	65.21
TiO <sub>2</sub>	0.26	0.84	0.22	0.52	0.55	0.13	0.38
Al <sub>2</sub> O <sub>3</sub>	12.79	15.19	13.68	14.97	17.15	18.73	17.94
Fe <sub>2</sub> O <sub>3</sub> t	2.50	6.06	1.99	3.75	3.82	1.14	2.39
MnO	0.03	0.09	0.04	0.06	0.12	0.04	0.08
MgO	0.39	0.78	0.40	0.73	0.45	0.23	0.08
CaO	0.47	1.15	0.71	1.48	1.02	0.31	0.92
Na <sub>2</sub> O	2.62	3.17	0.85	2.90	4.04	5.12	4.71
K <sub>2</sub> O	5.21	4.71	6.05	6.03	7.13	7.95	7.27
P <sub>2</sub> O <sub>5</sub>	0.05	0.27	0.07	0.16	0.12	0.09	0.06
LOI	1.30	2.15	2.10	1.64	1.55	0.73	1.11
Total	99.60	99.90	99.52	99.88	99.56	99.55	100.16
Li	13.40	20.90	8.69	20.80	12.80	5.06	7.48
Be	4.55	4.37	4.90	2.45	1.39	1.32	1.42
Sc	5.0	7.2	3.8	6.7	11.3	1.1	6.7
V	3.4	25.1	3.4	20.8	4.3	6.6	2.0
Cr	0.99	2.92	0.78	3.52	3.02	3.80	0.65
Co	0.89	7.51	1.01	4.53	1.26	0.47	0.44
Cu	7.2	14.6	1343.0	6.0	2.1	1.7	2.6
Zn	82.4	115.0	175.0	70.4	93.7	31.7	59.4
Ga	27.9	29.8	33.4	22.3	22.2	17.4	22.1
Rb	303.0	275.0	479.0	193.0	112.0	171.0	106.0
Sr	48.3	126.0	44.8	302.0	137.0	81.4	48.4
Y	62.1	71.5	56.7	27.1	28.9	6.8	18.5
Zr	361	533	252	385	780	109	580
Nb	47.1	47.2	32.1	21.3	26.7	5.9	15.4
Cs	6.92	5.46	13.10	5.47	5.73	2.52	1.91
Ba	239	387	212	962	208	409	55
La	131.0	155.0	161.0	123.0	366.0	24.3	330.0
Ce	257.0	279.0	317.0	227.0	642.0	43.0	579.0
Pr	31.80	28.90	39.70	27.20	63.20	4.94	58.10
Nd	104.0	98.3	131.0	87.7	201.0	18.5	182.0
Sm	20.50	17.70	23.70	14.30	24.20	3.02	21.00
Eu	0.92	1.52	0.89	1.87	2.27	1.44	1.43
Gd	18.40	15.70	19.20	10.20	15.10	2.26	12.30
Tb	2.69	2.32	2.42	1.21	1.59	0.29	1.12
Dy	13.70	12.90	11.50	5.43	6.38	1.43	4.22
Ho	2.34	2.49	1.93	0.96	1.12	0.24	0.69
Er	6.04	6.75	5.07	2.67	2.98	0.67	1.94
Tm	0.72	0.99	0.62	0.33	0.39	0.09	0.26
Yb	4.53	5.88	3.97	2.29	2.34	0.57	1.69
Lu	0.62	0.83	0.53	0.32	0.37	0.10	0.28
Hf	10.60	14.90	8.63	9.88	16.40	2.63	13.00
Ta	2.97	4.23	3.50	1.03	0.98	0.27	0.64
Pb	35.6	33.0	67.5	32.7	47.3	30.4	37.6
Th	71.10	74.00	106.00	36.80	42.30	4.87	38.40
U	24.10	24.40	25.00	4.96	2.25	7.01	2.42

Units of major and trace elements are wt. % and ppm, respectively.

	Triassic				
	09ZJ09	10ZJS063	10ZJS066	10ZJS067	10ZJS067
	Dashuang (east)				
SiO <sub>2</sub>	59.92	61.46	59.26	60.50	
TiO <sub>2</sub>	0.83	0.78	1.01	0.93	
Al <sub>2</sub> O <sub>3</sub>	16.58	16.09	16.75	16.62	
Fe <sub>2</sub> O <sub>3</sub> t	5.49	4.57	6.01	5.65	
MnO	0.08	0.07	0.08	0.09	
MgO	2.66	2.03	2.63	2.45	
CaO	3.91	2.65	1.64	4.05	
Na <sub>2</sub> O	3.29	3.18	3.37	3.54	
K <sub>2</sub> O	5.16	6.41	4.86	4.46	
P <sub>2</sub> O <sub>5</sub>	0.46	0.38	0.46	0.43	
LOI	1.24	2.14	2.92	1.05	
Total	99.63	99.75	98.97	99.77	
Li	30.32	24.90	31.10	29.10	29.50
Be	3.25	3.02	2.35	3.23	3.10
Sc	10.4	11.2	11.6	11.7	10.8
V	94.0	69.7	84.7	79.8	77.2
Cr	68.65	26.10	45.60	40.30	38.30
Co	14.92	10.40	13.10	12.70	12.30
Cu	32.9	14.2	16.3	14.5	13.9
Zn	164.3	75.8	91.5	89.3	81.7
Ga	22.2	20.0	23.8	23.3	22.5
Rb	152.8	147.0	151.0	132.0	128.0
Sr	1049.4	1144.0	672.0	931.0	898.0
Y	24.0	33.4	31.8	30.3	29.7
Zr	338	345	382	347	290
Nb	19.9	26.2	24.4	23.8	23.4
Cs	2.30	2.01	2.92	2.82	2.68
Ba	1784	2486	1919	1526	1487
La	110.2	162.0	174.0	128.0	124.0
Ce	191.5	289.0	302.0	240.0	235.0
Pr	22.41	29.80	30.60	25.30	25.10
Nd	81.5	99.1	104.0	88.2	86.7
Sm	11.07	14.10	15.10	13.10	12.90
Eu	2.49	2.93	3.13	2.66	2.70
Gd	8.80	10.70	11.00	9.69	9.38
Tb	1.09	1.29	1.35	1.18	1.15
Dy	4.97	6.22	6.43	5.77	5.80
Ho	0.86	1.12	1.14	1.06	1.05
Er	2.39	3.20	2.94	2.91	2.88
Tm	0.33	0.44	0.43	0.40	0.40
Yb	2.02	2.75	2.30	2.51	2.44
Lu	0.31	0.39	0.33	0.36	0.35
Hf	9.20	7.99	8.76	8.07	6.52
Ta	1.60	1.93	1.47	1.50	1.47
Pb	31.8	38.2	29.2	28.3	27.4
Th	18.15	28.70	27.30	22.00	21.40
U	2.01	2.66	1.76	2.17	2.15

	09ZJ02	Jurassic			
		Xiepu		10ZJS012	10ZJS149
					Shangsanzhi
SiO <sub>2</sub>	75.38	78.49	75.09		68.43
TiO <sub>2</sub>	0.08	0.07	0.08		0.34
Al <sub>2</sub> O <sub>3</sub>	12.92	12.16	13		14.56
Fe <sub>2</sub> O <sub>3</sub> t	1.14	1.53	1.2		1.31
MnO	0.08	0.02	0.07		0.03
MgO	0.03	0.11	0.01		0.62
CaO	0.71	0.01	0.72		2.69
Na <sub>2</sub> O	3.93	0.07	3.82		2.65
K <sub>2</sub> O	4.78	5.24	4.85		4.98
P <sub>2</sub> O <sub>5</sub>	0.03	0.02	0.02		0.1
LOI	0.69	1.84	0.93		3.85
Total	99.77	99.56	99.79		99.56
Li	11.05	13.2	8.28	12	11.9
Be	6	2.70	6.59	1.64	1.72
Sc	2.5	2.16	2.4	4.2	4.4
V	3.1	0.35	0.9	28.8	29.5
Cr	22.24	0.68	0.65	6.78	6.65
Co	0.88	0.76	0.31	3.02	2.89
Cu	1.2		3.8	3.3	3.5
Zn	141.5	159	22.3	21.1	22
Ga	16.1	17.9	18.5	20.2	20.2
Rb	382.4	355	372	93.1	93.6
Sr	20	4.17	17.6	316	312
Y	38.3	67.6	41.6	7.3	7.3
Zr	74	88.9	79	143	146
Nb	16.5	43.0	20.4	6.4	6.6
Cs	5.87	8.36	4.53	4.88	4.76
Ba	40	72.8	18	819	828
La	13.6	7.33	16.2	27.3	27.7
Ce	29.2	8.77	39.4	50.2	50.6
Pr	3.74	2.80	4.78	5.57	5.65
Nd	14.7	11.7	17.6	20.3	20.1
Sm	4.11	4.47	4.78	3.36	3.26
Eu	0.12	0.069	0.13	0.88	0.91
Gd	4.72	5.64	4.86	2.3	2.44
Tb	0.96	1.24	0.91	0.3	0.3
Dy	6.01	9.02	5.93	1.38	1.43
Ho	1.28	2.06	1.26	0.24	0.26
Er	4.01	6.64	4.11	0.65	0.63
Tm	0.63	1.06	0.65	0.1	0.09
Yb	4.39	7.80	4.77	0.59	0.57
Lu	0.71	1.14	0.73	0.08	0.08
Hf	3.63	5.49	3.85	3.96	4.01
Ta	3.13	6.58	4.33	0.45	0.45
Pb	42.1	42.3	44.2	13.3	13.3
Th	28.7	21.9	42	9.63	9.47
U	13.31	8.58	15.5	2.47	2.45

	Jurassic						
	10ZJS033	10ZJS034	10ZJS035	10ZJS036	10ZJS039	10ZJS039-2	10ZJS044
	Jiangzao				Guangshan		
SiO <sub>2</sub>	75.20	72.94	74.73	75.23	75.11		70.40
TiO <sub>2</sub>	0.18	0.13	0.17	0.10	0.12		0.30
Al <sub>2</sub> O <sub>3</sub>	13.05	12.39	12.65	12.26	12.63		13.71
Fe <sub>2</sub> O <sub>3</sub> t	1.47	1.27	1.59	0.98	1.02		2.66
MnO	0.03	0.05	0.07	0.05	0.06		0.08
MgO	0.14	0.29	0.31	0.16	0.27		0.61
CaO	1.05	0.85	1.17	0.68	0.71		1.14
Na <sub>2</sub> O	3.74	3.57	3.73	3.52	3.26		3.56
K <sub>2</sub> O	4.25	4.33	4.01	4.83	4.82		4.11
P <sub>2</sub> O <sub>5</sub>	0.04	0.03	0.04	0.02	0.02		0.08
LOI	0.61	0.97	0.39	0.49	1.38		1.77
Total	99.75	96.80	98.86	98.31	99.40		98.41
Li	17.90	22.20	22.50	20.20	12.50	12.50	23.70
Be	3.15	3.26	3.72	3.86	3.60	3.75	2.38
Sc	4.5	4.5	5.0	3.6	4.5	4.5	5.0
V	13.0	9.2	12.9	4.2	5.3	5.3	29.9
Cr	0.61	3.98	3.22	2.40	8.28	8.81	5.72
Co	1.50	1.21	1.90	0.77	0.91	0.81	3.38
Cu	9.6	1.4	3.0	3.6	9.6	9.4	3.9
Zn	20.7	26.6	31.9	21.2	31.5	29.6	41.7
Ga	16.8	16.8	17.2	16.3	17.8	17.8	15.8
Rb	165.0	190.0	175.0	206.0	242.0	241.0	118.0
Sr	101.0	70.1	99.3	32.3	43.6	43.8	262.0
Y	58.1	58.6	58.4	64.6	68.2	71.8	32.3
Zr	114	99	117	86	106	106	126
Nb	28.9	21.9	25.2	29.8	35.1	35.7	14.3
Cs	1.84	4.54	3.21	4.41	5.28	5.17	6.37
Ba	286	307	340	79	237	239	545
La	27.6	19.6	25.0	18.5	23.0	23.7	29.3
Ce	56.9	42.9	51.6	42.1	51.4	53.1	57.7
Pr	6.75	5.58	6.40	5.41	6.59	6.95	6.63
Nd	25.3	22.1	24.6	21.4	25.9	27.5	24.5
Sm	6.47	6.38	6.09	6.08	7.43	7.46	5.06
Eu	0.51	0.51	0.56	0.27	0.38	0.40	0.89
Gd	6.70	7.24	6.46	6.72	8.29	8.42	4.90
Tb	1.25	1.33	1.22	1.32	1.56	1.57	0.81
Dy	8.18	9.22	8.08	9.04	10.20	10.40	5.03
Ho	1.76	1.94	1.80	2.03	2.16	2.27	1.03
Er	5.57	5.74	5.64	6.18	6.69	6.87	3.00
Tm	0.95	0.94	1.00	1.10	1.10	1.16	0.50
Yb	6.67	5.97	6.91	7.40	7.52	8.13	3.28
Lu	1.04	0.95	1.09	1.19	1.16	1.19	0.54
Hf	4.65	4.34	4.85	4.45	5.24	4.91	4.07
Ta	2.78	1.91	2.54	3.78	3.04	3.01	1.29
Pb	17.5	21.9	19.2	25.3	27.2	26.9	22.4
Th	26.30	24.50	21.50	28.30	25.20	25.40	15.40
U	11.60	5.43	5.95	6.99	7.38	7.45	3.67

	Cretaceous						
	10ZJS025	10ZJS026 Yujiashan	10ZJS030	09ZJ05	09ZJ06 Ru'ao	09ZJ07	10ZJS098 Zhujiaxiang
SiO <sub>2</sub>	58.79	57.66	58.65	66.49	55.29	63.54	61.82
TiO <sub>2</sub>	0.86	0.83	0.85	0.53	1.31	0.60	0.80
Al <sub>2</sub> O <sub>3</sub>	16.91	16.88	17.15	15.80	15.89	16.35	16.33
Fe <sub>2</sub> O <sub>3</sub> t	5.70	5.95	5.86	3.96	8.56	3.84	5.52
MnO	0.09	0.11	0.09	0.06	0.19	0.27	0.09
MgO	3.83	3.31	3.11	1.16	2.86	1.20	1.78
CaO	5.95	5.62	5.70	2.07	5.50	2.51	4.45
Na <sub>2</sub> O	4.02	4.16	4.42	4.20	3.48	4.19	3.01
K <sub>2</sub> O	2.33	2.32	2.07	3.96	2.84	4.54	3.89
P <sub>2</sub> O <sub>5</sub>	0.24	0.24	0.23	0.20	0.51	0.22	0.23
LOI	1.24	1.99	1.02	1.48	3.54	2.60	2.09
Total	99.97	99.09	99.15	99.91	99.96	99.87	100.01
Li	15.20	20.30	12.70	18.11	23.30	16.00	25.20
Be	1.40	1.52	1.47	2.35	1.69	2.17	1.99
Sc	13.5	12.2	12.0	6.0	19.0	8.1	14.4
V	129.0	124.0	114.0	49.3	152.0	50.3	80.1
Cr	63.50	32.60	35.90	9.67	1.11	3.97	20.60
Co	19.30	18.40	17.60	5.03	15.60	5.48	12.00
Cu	40.1	53.7	24.7	3.5	13.9	6.1	19.2
Zn	75.1	82.9	79.3	80.4	122.0	224.0	67.1
Ga	21.2	20.9	22.1	16.2	19.5	17.8	19.4
Rb	55.8	64.1	40.2	127.5	87.7	147.0	100.0
Sr	858.0	803.0	915.0	318.8	610.0	315.0	387.0
Y	14.1	15.7	13.5	20.0	30.0	22.9	33.0
Zr	130	100	116	212	204	199	271
Nb	5.9	6.7	6.0	11.1	11.3	11.8	13.3
Cs	2.40	2.82	1.51	3.32	3.11	5.69	2.16
Ba	698	659	771	876	804	931	686
La	23.2	24.2	23.4	37.5	34.1	39.2	39.1
Ce	47.4	50.1	46.7	68.5	68.9	67.1	77.5
Pr	5.95	6.15	5.82	7.94	8.52	8.10	9.15
Nd	23.7	24.3	23.3	29.0	34.1	30.0	35.4
Sm	4.45	4.68	4.36	4.62	6.94	5.44	7.03
Eu	1.34	1.25	1.34	1.22	1.85	1.59	1.65
Gd	3.79	3.87	3.71	4.45	6.38	4.90	6.67
Tb	0.49	0.53	0.49	0.66	0.92	0.69	0.99
Dy	2.72	2.90	2.62	3.53	5.37	3.89	5.66
Ho	0.49	0.55	0.48	0.72	1.05	0.80	1.12
Er	1.36	1.49	1.30	2.08	2.90	2.21	3.21
Tm	0.19	0.22	0.20	0.32	0.44	0.34	0.51
Yb	1.25	1.34	1.17	2.23	2.79	2.19	3.35
Lu	0.19	0.21	0.18	0.35	0.44	0.33	0.48
Hf	3.55	3.10	3.22	5.49	4.79	4.62	6.36
Ta	0.41	0.51	0.37	0.89	0.68	0.76	0.81
Pb	12.1	14.9	12.3	10.8	18.0	159.0	14.0
Th	6.55	7.29	3.71	11.17	5.82	9.85	8.76
U	1.48	2.06	0.94	2.09	1.27	1.84	1.98

Cretaceous								
	10ZJS052	10ZJS053	10ZJS054	10ZJS077	10ZJS081	10ZJS072	10ZJS073	10ZJS073-2
	Hecun		Hongling			Shuangcai		
SiO <sub>2</sub>	78.13	65.56	59.60	68.40	69.77	61.07	59.21	
TiO <sub>2</sub>	0.23	0.49	0.60	0.45	0.31	0.77	0.79	
Al <sub>2</sub> O <sub>3</sub>	11.20	14.87	15.80	15.08	13.66	15.83	15.84	
Fe <sub>2</sub> O <sub>3</sub> t	2.03	3.81	3.80	1.95	2.25	5.60	5.77	
MnO	0.04	0.09	0.12	0.05	0.05	0.11	0.10	
MgO	0.06	1.02	0.66	0.62	0.54	1.85	2.07	
CaO	0.02	2.43	4.52	1.77	1.43	3.50	3.81	
Na <sub>2</sub> O	0.07	3.29	0.75	5.30	3.11	4.03	3.66	
K <sub>2</sub> O	5.28	4.56	4.57	2.97	5.35	3.14	3.14	
P <sub>2</sub> O <sub>5</sub>	0.02	0.17	0.21	0.11	0.07	0.24	0.25	
LOI	2.87	3.55	7.60	3.47	3.07	4.01	5.42	
Total	99.95	99.83	98.22	100.17	99.62	100.14	100.07	
Li	115.00	23.50	54.90	9.90	8.08	41.00	43.10	43.60
Be	1.47	2.31	2.48	1.71	2.05	2.05	1.71	1.71
Sc	1.7	8.2	10.1	8.1	6.9	15.7	15.8	16.0
V	1.9	36.8	51.2	27.6	17.6	86.5	88.5	89.3
Cr	0.56	4.95	7.53	4.75	1.92	12.10	11.90	11.60
Co	0.47	5.56	5.53	3.09	3.11	11.70	12.40	12.40
Cu	4.1	5.6	10.3	5.7	5.5	14.4	11.9	14.0
Zn	87.3	65.5	49.7	35.0	40.8	112.0	82.3	82.0
Ga	25.3	17.4	18.6	19.1	17.7	20.2	20.1	19.7
Rb	167.0	140.0	149.0	80.1	154.0	92.9	95.6	96.0
Sr	6.2	278.0	181.0	169.0	101.0	393.0	232.0	233.0
Y	65.6	33.3	29.1	33.3	36.2	36.0	34.7	35.0
Zr	569	212	200	275	263	219	217	216
Nb	44.3	12.6	12.3	15.9	15.5	14.8	14.1	14.3
Cs	2.22	7.73	11.30	2.13	4.76	3.60	5.98	6.00
Ba	57	697	970	347	624	730	580	584
La	100.0	40.5	38.6	51.4	59.9	33.9	32.7	33.2
Ce	200.0	76.3	74.5	104.0	120.0	67.9	66.7	66.7
Pr	22.30	9.08	8.66	11.40	12.60	8.18	8.15	8.23
Nd	82.8	33.4	32.1	41.0	44.5	32.3	32.0	32.0
Sm	15.30	6.44	6.08	7.24	7.78	6.74	6.51	6.57
Eu	0.34	1.38	1.46	1.19	1.09	1.56	1.59	1.54
Gd	13.60	5.89	5.48	6.96	6.96	6.73	6.54	6.67
Tb	2.02	0.92	0.85	1.01	1.08	1.05	1.02	0.99
Dy	11.60	5.15	4.98	5.90	6.23	6.25	6.12	6.01
Ho	2.31	1.11	0.99	1.16	1.20	1.22	1.18	1.22
Er	6.70	3.10	2.89	3.42	3.55	3.57	3.47	3.53
Tm	1.06	0.48	0.44	0.55	0.56	0.56	0.55	0.51
Yb	6.62	3.19	2.83	3.58	3.60	3.50	3.48	3.45
Lu	1.04	0.50	0.43	0.54	0.54	0.52	0.52	0.52
Hf	13.40	5.55	5.14	7.24	7.09	5.73	5.69	5.73
Ta	2.48	0.89	0.82	1.07	1.08	0.94	0.89	0.89
Pb	9.5	12.6	15.6	4.6	16.1	14.7	11.3	11.4
Th	17.50	12.00	10.70	13.70	14.50	8.33	7.83	7.82
U	3.40	2.53	1.83	3.16	2.83	1.97	1.81	1.80

	Cretaceous						
	09ZJ13	09ZJ14	09ZJ15	10ZJS143	10ZJS145	10ZJS147	10ZJS148
	Tongshan			Jiuhua-Baijuhuajian			
SiO <sub>2</sub>	76.05	76.10	74.06	69.92	71.16	71.97	70.32
TiO <sub>2</sub>	0.11	0.16	0.18	0.33	0.26	0.25	0.39
Al <sub>2</sub> O <sub>3</sub>	12.38	12.67	12.60	13.99	13.33	12.78	13.64
Fe <sub>2</sub> O <sub>3</sub> t	1.13	1.43	1.65	2.99	2.54	2.44	3.22
MnO	0.02	0.02	0.05	0.05	0.05	0.04	0.05
MgO	0.08	0.23	0.09	0.30	0.24	0.17	0.42
CaO	0.50	0.13	0.70	1.22	1.52	1.46	1.10
Na <sub>2</sub> O	3.33	2.98	3.56	3.31	2.53	2.58	3.44
K <sub>2</sub> O	5.61	5.14	4.84	5.86	5.61	5.75	5.53
P <sub>2</sub> O <sub>5</sub>	0.02	0.03	0.04	0.08	0.07	0.05	0.10
LOI	0.58	0.91	1.98	1.43	2.18	2.01	1.32
Total	99.80	99.82	99.75	99.49	99.48	99.50	99.53
Li	14.40	7.28	102.79	11.60	22.00	20.80	25.30
Be	6.25	2.10	5.95	2.27	2.09	2.17	1.91
Sc	2.0	3.8	1.9	7.8	6.5	5.9	8.1
V	3.4	3.5	6.9	13.8	8.9	10.1	16.2
Cr	0.74	19.93	73.37	1.67	1.42	3.90	1.84
Co	0.68	4.04	1.77	2.78	1.33	2.05	2.99
Cu	2.2	62.9	6.4	4.1	4.0	1.9	5.4
Zn	14.5	58.9	300.1	48.5	26.5	50.6	56.3
Ga	18.6	18.6	17.9	19.6	20.0	18.2	19.0
Rb	352.0	211.8	294.9	131.0	185.0	151.0	129.0
Sr	23.2	82.5	33.2	119.0	87.7	93.2	116.0
Y	93.1	30.8	40.1	35.0	37.6	35.3	34.5
Zr	82	138	130	361	291	256	352
Nb	43.6	20.8	20.6	16.1	16.4	14.6	16.4
Cs	5.34	2.09	9.81	2.71	6.03	5.61	2.88
Ba	97	438	83	909	840	666	838
La	22.1	28.2	29.7	110.0	109.0	88.9	98.2
Ce	49.4	58.1	66.4	199.0	202.0	174.0	184.0
Pr	6.37	7.66	8.46	21.00	21.00	18.40	19.60
Nd	25.1	31.2	31.9	73.7	73.8	65.3	68.5
Sm	7.24	7.02	6.88	11.50	11.70	10.40	11.10
Eu	0.28	0.41	0.25	1.44	1.21	1.18	1.47
Gd	8.40	6.70	6.55	9.01	9.39	8.64	8.61
Tb	1.69	1.04	1.21	1.22	1.31	1.20	1.18
Dy	11.80	5.86	7.44	6.36	6.75	6.19	6.20
Ho	2.66	1.10	1.54	1.19	1.28	1.21	1.22
Er	8.60	3.01	4.87	3.56	3.68	3.52	3.48
Tm	1.52	0.41	0.80	0.52	0.56	0.55	0.52
Yb	10.30	2.67	5.54	3.48	3.59	3.47	3.40
Lu	1.67	0.40	0.88	0.50	0.52	0.52	0.50
Hf	4.05	5.56	5.81	8.68	7.42	6.76	8.56
Ta	4.89	1.72	2.57	0.95	1.03	0.97	0.98
Pb	30.1	42.2	25.7	16.8	11.7	24.7	16.9
Th	29.40	26.85	34.69	17.10	18.70	17.70	16.30
U	14.00	3.78	6.63	2.33	2.91	2.58	2.43

	Cretaceous						
	10ZJS115	10ZJS116	10ZJS124	10ZJS124-2	10ZJS125	10ZJS131	10ZJS132
	Muchen						
SiO <sub>2</sub>	52.22	65.63	60.75		72.18	62.10	68.45
TiO <sub>2</sub>	1.13	0.41	0.82		0.20	0.64	0.29
Al <sub>2</sub> O <sub>3</sub>	17.10	16.25	17.31		13.60	16.06	14.80
Fe <sub>2</sub> O <sub>3</sub> t	9.74	3.93	5.01		2.25	5.33	3.77
MnO	0.21	0.11	0.10		0.09	0.13	0.10
MgO	3.72	0.87	1.10		0.22	1.87	0.48
CaO	7.29	2.11	2.34		0.63	3.80	1.17
Na <sub>2</sub> O	3.82	4.17	4.73		3.85	3.59	4.15
K <sub>2</sub> O	3.41	5.71	5.67		5.58	5.08	5.93
P <sub>2</sub> O <sub>5</sub>	0.71	0.20	0.30		0.06	0.34	0.12
LOI	0.91	0.53	1.70		1.00	0.70	0.74
Total	100.25	99.92	99.85		99.66	99.64	100.00
Li	81.50	27.40	19.20	19.00	10.10	25.80	8.14
Be	3.21	5.11	2.37	2.38	9.16	5.04	5.34
Sc	15.7	4.3	8.0	8.1	2.2	9.1	2.9
V	202.0	41.9	34.1	38.5	8.8	95.6	21.4
Cr	1.54	0.89	1.99	1.46	0.58	6.33	1.49
Co	22.50	5.17	5.07	5.07	1.37	11.40	3.40
Cu	35.5	3.7	6.9	6.7	3.6	16.9	3.8
Zn	108.0	61.5	74.5	75.0	86.3	74.0	61.1
Ga	18.4	18.8	19.4	19.7	19.7	17.9	17.9
Rb	207.0	219.0	160.0	162.0	298.0	215.0	240.0
Sr	968.0	463.0	607.0	604.0	164.0	591.0	366.0
Y	27.4	35.0	24.5	27.3	54.6	29.9	33.0
Zr	283	239	249	258	261	230	271
Nb	11.8	25.1	22.2	22.7	53.4	24.1	20.5
Cs	11.90	3.44	2.17	2.20	2.02	4.49	3.45
Ba	635	572	1416	1433	222	514	518
La	37.3	69.6	46.9	48.1	82.3	47.9	54.6
Ce	69.9	120.0	82.3	83.1	155.0	86.8	94.7
Pr	8.73	13.30	9.56	9.89	17.80	9.86	10.80
Nd	36.7	46.4	37.4	37.6	61.3	37.0	38.9
Sm	7.81	8.44	7.29	7.53	11.30	7.03	7.04
Eu	2.38	1.31	2.54	2.49	0.50	1.51	1.01
Gd	7.11	7.18	6.11	6.24	9.52	6.12	6.30
Tb	1.00	1.05	0.87	0.89	1.49	0.91	0.94
Dy	5.30	5.92	4.68	4.73	8.55	4.92	5.30
Ho	0.93	1.12	0.88	0.94	1.73	0.94	1.08
Er	2.74	3.54	2.58	2.64	5.38	2.87	3.35
Tm	0.37	0.54	0.37	0.36	0.84	0.42	0.51
Yb	2.42	3.76	2.59	2.63	6.19	3.22	3.89
Lu	0.35	0.55	0.39	0.37	0.95	0.48	0.59
Hf	6.36	6.46	5.80	5.80	9.17	6.44	7.93
Ta	0.78	1.77	1.21	1.23	3.64	1.86	1.62
Pb	26.7	21.0	19.7	19.9	34.6	20.3	18.8
Th	8.42	19.50	8.53	8.78	43.60	19.90	26.70
U	2.46	4.15	1.45	1.41	6.93	3.83	5.10

	Cretaceous						
	10ZJS119	10ZJS121	10ZJS122	10ZJS099	10ZJS101	10ZJS104	10ZJS104-2
	Wangcun			Matou		Shanghekou	
SiO <sub>2</sub>	69.82	69.85	73.86	67.03	67.05	75.79	
TiO <sub>2</sub>	0.45	0.44	0.24	0.56	0.58	0.09	
Al <sub>2</sub> O <sub>3</sub>	14.44	14.37	12.88	15.50	15.71	12.75	
Fe <sub>2</sub> O <sub>3</sub> t	3.51	3.42	1.86	3.44	3.56	1.20	
MnO	0.05	0.04	0.05	0.10	0.09	0.05	
MgO	0.60	0.45	0.14	1.01	1.14	0.00	
CaO	0.34	0.32	0.45	2.39	2.70	0.49	
Na <sub>2</sub> O	3.61	3.61	2.38	4.15	3.96	4.22	
K <sub>2</sub> O	5.46	5.67	6.41	4.17	4.32	4.62	
P <sub>2</sub> O <sub>5</sub>	0.14	0.13	0.07	0.21	0.21	0.01	
LOI	1.35	1.44	1.26	1.38	0.57	0.61	
Total	99.75	99.73	99.61	99.93	99.88	99.83	
Li	25.50	25.70	12.70	20.40	16.00	70.40	69.70
Be	2.79	3.33	3.83	2.62	3.06	7.57	7.33
Sc	7.1	6.7	3.4	4.8	5.1	1.7	1.6
V	20.1	20.1	7.5	49.0	52.1	0.6	0.7
Cr	2.42	1.80	0.84	3.51	3.74	0.55	0.37
Co	3.71	2.97	1.62	4.62	5.65	0.10	0.09
Cu	7.2	4.4	3.9	8.7	5.7	1.1	0.9
Zn	67.2	65.1	62.5	58.7	48.7	31.1	31.0
Ga	18.9	18.5	17.5	18.5	19.8	23.1	23.2
Rb	203.0	207.0	299.0	144.0	147.0	484.0	485.0
Sr	177.0	202.0	86.8	538.0	618.0	4.9	4.9
Y	47.6	24.5	38.2	15.1	14.0	92.1	91.7
Zr	258	267	202	166	209	126	129
Nb	20.3	20.4	22.6	15.4	16.5	62.1	64.8
Cs	2.42	2.87	4.38	3.55	2.05	3.32	3.27
Ba	887	768	497	973	931	5	5
La	122.0	55.6	67.4	44.0	63.1	12.7	13.2
Ce	152.0	94.8	117.0	80.7	99.7	38.5	38.9
Pr	24.70	11.70	13.20	8.93	10.30	5.67	5.80
Nd	80.7	41.1	46.1	31.8	34.5	24.4	24.9
Sm	14.30	7.34	8.54	5.32	5.32	9.45	9.43
Eu	2.22	0.98	0.86	1.32	1.31	0.04	0.05
Gd	12.20	5.65	7.37	4.30	4.32	10.50	10.20
Tb	1.73	0.82	1.09	0.59	0.55	2.05	2.02
Dy	9.02	4.62	6.11	3.04	2.67	13.80	13.10
Ho	1.58	0.85	1.17	0.56	0.52	2.76	2.80
Er	4.56	2.71	3.61	1.71	1.55	8.83	8.75
Tm	0.61	0.40	0.53	0.24	0.22	1.39	1.37
Yb	4.03	2.75	3.77	1.73	1.68	10.00	9.85
Lu	0.56	0.40	0.54	0.24	0.27	1.47	1.46
Hf	6.97	7.29	6.22	4.45	5.72	8.18	8.17
Ta	1.25	1.38	1.80	1.10	1.17	4.88	4.91
Pb	29.0	23.9	35.7	23.8	21.8	45.3	45.2
Th	23.70	26.40	32.30	17.20	26.00	48.10	48.00
U	3.18	3.28	4.39	2.95	4.16	8.28	8.12

	Cretaceous				
	10ZJS109	10ZJS136	10ZJS133	10ZJS108	10ZJS129
	Huangkang	Lingkeng	Luojia	Sucun	Yingcun
SiO <sub>2</sub>	73.38	74.44	74.09	75.36	70.22
TiO <sub>2</sub>	0.22	0.21	0.28	0.14	0.36
Al <sub>2</sub> O <sub>3</sub>	12.60	12.84	12.10	12.25	14.16
Fe <sub>2</sub> O <sub>3</sub> t	1.90	1.76	2.65	1.55	2.95
MnO	0.05	0.04	0.07	0.04	0.06
MgO	0.27	0.21	0.13	0.01	0.55
CaO	0.92	0.74	0.35	0.63	1.60
Na <sub>2</sub> O	3.58	3.53	3.25	3.43	3.52
K <sub>2</sub> O	4.68	5.12	5.08	5.41	5.17
P <sub>2</sub> O <sub>5</sub>	0.06	0.06	0.04	0.01	0.11
LOI	2.04	0.76	1.56	0.90	0.82
Total	99.71	99.72	99.58	99.73	99.53
Li	9.69	27.10	32.30	3.78	17.50
Be	5.45	8.05	4.09	6.90	3.57
Sc	2.9	2.8	3.1	4.2	6.0
V	8.1	8.2	4.8	1.1	15.8
Cr	0.83	0.69	1.12	0.63	1.75
Co	1.51	1.37	1.20	0.22	3.09
Cu	1.8	1.2	3.0	2.1	4.0
Zn	25.7	20.5	103.0	25.8	54.1
Ga	18.8	18.8	25.4	21.0	19.0
Rb	322.0	342.0	248.0	347.0	204.0
Sr	132.0	134.0	54.3	20.9	255.0
Y	57.5	50.2	74.7	59.6	38.1
Zr	169	160	441	223	260
Nb	42.8	31.4	52.8	37.5	20.9
Cs	3.85	3.08	1.51	2.20	2.56
Ba	322	356	183	38	673
La	46.5	40.7	131.0	69.5	79.6
Ce	87.1	77.2	244.0	138.0	143.0
Pr	10.20	8.94	29.90	16.40	15.70
Nd	37.4	32.2	98.6	58.7	56.0
Sm	8.54	7.19	18.10	12.80	9.90
Eu	0.60	0.61	0.62	0.13	1.30
Gd	8.00	7.03	15.40	11.30	8.42
Tb	1.42	1.21	2.33	1.79	1.21
Dy	8.77	7.43	13.10	10.50	6.61
Ho	1.82	1.54	2.55	1.96	1.27
Er	5.82	4.64	7.48	5.90	3.70
Tm	0.95	0.76	1.07	0.86	0.53
Yb	6.59	5.48	7.38	6.09	3.68
Lu	0.96	0.79	1.05	0.84	0.54
Hf	6.20	5.64	12.70	8.31	7.34
Ta	4.22	3.12	3.29	2.83	1.45
Pb	24.3	21.3	29.2	37.9	27.0
Th	42.30	38.10	39.90	42.50	27.60
U	11.50	7.18	6.61	10.80	3.12

	Cretaceous							
	10ZJS162	10ZJS163	10ZJS163-2	10ZJS165	10ZJS172	10ZJS173	10ZJS175	10ZJS177
Damaoshan-Huaiyushan								
SiO <sub>2</sub>	76.11	74.93		76.39	74.16	75.71	77.10	76.34
TiO <sub>2</sub>	0.12	0.11		0.17	0.25	0.13	0.16	0.11
Al <sub>2</sub> O <sub>3</sub>	12.21	13.18		12.21	12.54	12.37	11.38	12.09
Fe <sub>2</sub> O <sub>3</sub> t	1.41	1.06		1.54	2.18	1.20	1.72	1.27
MnO	0.03	0.03		0.04	0.05	0.03	0.03	0.03
MgO	0.03	0.03		0.13	0.13	0.07	0.07	0.04
CaO	0.52	0.60		0.34	1.00	0.84	0.72	0.60
Na <sub>2</sub> O	3.27	3.91		3.14	3.35	3.51	3.07	3.55
K <sub>2</sub> O	5.41	5.33		5.05	5.31	5.15	4.84	5.15
P <sub>2</sub> O <sub>5</sub>	0.02	0.03		0.04	0.05	0.02	0.03	0.01
LOI	0.62	0.61		0.69	0.60	0.77	0.59	0.60
Total	99.75	99.82		99.74	99.62	99.78	99.70	99.79
Li	145.00	181.00	179.00	112.00	65.90	35.30	168.00	121.00
Be	5.02	7.55	7.43	6.90	7.24	10.60	5.89	7.22
Sc	2.7	2.1	2.2	2.8	5.0	3.0	2.9	3.4
V	1.0	1.4	1.5	4.9	7.4	1.6	2.9	0.6
Cr	0.95	0.63	1.07	0.91	1.53	0.51	0.68	0.45
Co	0.44	0.60	0.47	1.10	1.68	0.55	0.96	0.43
Cu	1.6	2.1	1.7	9.2	1.8	1.7	2.3	6.2
Zn	24.4	25.9	29.3	36.1	33.3	23.8	35.9	27.8
Ga	24.0	25.0	25.2	21.9	21.4	21.6	21.3	23.8
Rb	511.0	651.0	667.0	400.0	288.0	427.0	376.0	517.0
Sr	14.1	23.4	23.4	46.9	80.7	24.1	27.3	11.1
Y	166.0	100.0	99.9	48.8	62.6	91.6	93.6	187.0
Zr	206	140	118	164	225	172	222	170
Nb	54.4	52.1	52.9	33.6	29.4	52.5	51.2	92.7
Cs	12.20	16.80	16.70	15.30	9.52	6.89	18.30	11.90
Ba	36	69	69	146	268	76	92	13
La	90.4	53.5	52.3	47.5	99.2	60.3	81.6	46.2
Ce	141.0	103.0	100.0	93.6	184.0	117.0	152.0	99.8
Pr	20.40	11.70	11.60	10.60	20.20	13.80	16.80	12.80
Nd	72.3	40.1	39.1	36.1	69.1	48.9	55.9	48.8
Sm	16.60	9.47	9.42	7.02	12.50	11.00	10.90	14.20
Eu	0.24	0.27	0.26	0.31	0.78	0.25	0.31	0.08
Gd	16.50	9.23	8.89	6.29	10.70	10.60	10.20	15.70
Tb	3.32	1.86	1.88	1.11	1.69	2.04	1.86	3.37
Dy	22.80	13.00	12.80	7.15	9.86	13.70	12.00	23.60
Ho	4.98	2.90	2.90	1.53	1.95	2.91	2.60	5.27
Er	15.90	9.69	9.66	4.86	6.01	9.18	8.18	17.40
Tm	2.71	1.71	1.69	0.88	0.93	1.55	1.32	2.96
Yb	19.20	12.40	12.40	6.66	6.57	11.10	9.08	21.30
Lu	2.75	1.78	1.73	0.96	1.00	1.66	1.31	3.03
Hf	9.10	6.70	5.55	6.21	7.20	7.63	8.70	9.21
Ta	4.77	8.41	7.97	4.38	3.19	6.69	5.33	10.80
Pb	35.3	38.9	39.0	35.2	31.6	40.8	32.7	37.4
Th	65.10	51.90	52.90	57.40	32.40	55.00	81.50	75.80
U	15.70	21.60	20.60	16.20	8.01	16.50	26.00	32.50

	Cretaceous						
	10ZJS151	10ZJS153	10ZJS154	10ZJS155	10ZJS156	10ZJS170	10ZJS171
	Lingshan				Wancunxiang		
SiO <sub>2</sub>	76.35	76.27	74.16	69.57	56.53	73.02	56.92
TiO <sub>2</sub>	0.15	0.15	0.27	0.52	1.78	0.48	0.20
Al <sub>2</sub> O <sub>3</sub>	11.81	12.12	12.69	14.15	15.14	12.78	16.64
Fe <sub>2</sub> O <sub>3</sub> t	1.76	1.40	2.07	3.29	9.90	3.34	1.88
MnO	0.04	0.03	0.05	0.06	0.21	0.06	0.02
MgO	0.00	0.08	0.27	0.55	2.06	0.66	2.53
CaO	0.34	0.51	1.09	1.76	4.23	1.28	8.45
Na <sub>2</sub> O	4.06	3.24	3.30	3.77	3.37	2.99	8.36
K <sub>2</sub> O	4.86	5.55	5.15	5.23	5.83	4.36	0.49
P <sub>2</sub> O <sub>5</sub>	0.01	0.02	0.07	0.14	0.61	0.23	0.14
LOI	0.39	0.37	0.51	0.37	0.42	0.77	4.28
Total	99.77	99.75	99.64	99.41	100.08	99.98	99.91
Li	155.00	17.50	56.70	67.10	95.10	91.70	82.30
Be	3.70	12.30	6.80	9.12	5.53	2.98	8.75
Sc	1.0	1.3	3.1	6.5	14.6	9.3	6.4
V	1.3	2.9	12.8	29.9	109.0	30.4	15.5
Cr	0.46	0.49	0.73	1.23	0.53	7.96	3.14
Co	0.18	0.85	2.44	5.28	18.70	5.59	1.49
Cu	1.4	1.2	1.8	2.5	16.7	11.5	4.4
Zn	116.0	19.6	30.8	95.7	126.0	62.3	17.4
Ga	27.0	17.9	18.2	22.4	22.6	19.6	26.9
Rb	396.0	394.0	315.0	313.0	337.0	267.0	43.7
Sr	6.2	24.8	102.0	166.0	307.0	84.9	65.7
Y	117.0	34.7	32.4	46.2	43.1	58.0	45.2
Zr	523	139	185	302	323	240	123
Nb	71.2	31.7	30.1	39.4	59.0	23.8	24.6
Cs	10.30	8.75	13.00	14.50	17.90	21.50	7.89
Ba	30	26	301	520	707	214	12
La	97.0	80.8	75.9	86.4	73.0	59.7	33.6
Ce	201.0	145.0	135.0	160.0	149.0	129.0	71.3
Pr	21.10	13.60	12.70	16.20	16.60	14.40	8.39
Nd	70.6	39.5	39.1	52.1	60.8	53.9	30.6
Sm	13.80	6.02	6.15	8.71	10.60	11.20	6.93
Eu	0.29	0.30	0.83	1.35	2.55	0.95	0.41
Gd	13.50	4.78	5.22	7.78	9.65	10.50	6.13
Tb	2.39	0.79	0.82	1.26	1.39	1.65	1.15
Dy	14.80	4.81	4.77	7.23	7.57	10.00	7.24
Ho	3.17	1.08	1.00	1.46	1.48	1.91	1.52
Er	9.39	3.54	3.25	4.56	4.38	5.42	4.77
Tm	1.50	0.64	0.57	0.77	0.68	0.85	0.82
Yb	9.41	4.72	3.93	5.03	4.22	5.29	5.68
Lu	1.30	0.72	0.58	0.75	0.64	0.79	0.88
Hf	15.50	5.29	5.60	8.20	7.29	6.61	5.08
Ta	3.63	4.42	3.34	3.57	3.22	2.46	4.57
Pb	12.4	24.5	17.6	24.0	25.7	32.0	4.8
Th	36.50	87.00	60.50	51.60	14.20	30.50	31.30
U	11.90	13.20	12.20	12.90	3.23	7.81	18.30

## Appendix F. Permission to paper reproduction for Chapter 4

Zhu, K.-Y., Li, Z.-X., Xu, X.-S., Wilde, S.A., 2013. Late Triassic melting of a thickened crust in southeastern China: Evidence for flat-slab subduction of the Paleo-Pacific plate. Journal of Asian Earth Sciences 74, 265-279.



**Confirmation Number:** 11156229  
**Order Date:** 02/01/2014

### Customer Information

**Customer:** Kongyang Zhu  
**Account Number:** 3000745956  
**Organization:** Kongyang Zhu  
**Email:** zhukongyang@hotmail.com  
**Phone:** +61 (8)92663710  
**Payment Method:** Invoice

### This not an invoice

#### Order Details

##### Journal of Asian earth sciences

Billing Status:  
**N/A**

<b>Order detail ID:</b>	64412529	<b>Permission Status:</b>	Granted
<b>Article Title:</b>	Late Triassic melting of a thickened crust in southeastern China: Evidence for flat-slab subduction of the Paleo-Pacific plate	<b>Permission type:</b>	Republish or display content
<b>Author(s):</b>	Zhu, Kong-Yang ; et al	<b>Type of use:</b>	reuse in a thesis/dissertation
<b>DOI:</b>	10.1016/J.JSEAES.2013.01.010	<b>Order License Id:</b>	3320570100659
<b>Date:</b>	Jan 01, 2013	<b>Number of pages</b>	15
<b>ISSN:</b>	1367-9120	<b>Portion</b>	full article
<b>Publication Type:</b>	Journal	<b>Format</b>	both print and electronic
<b>Volume:</b>	74	<b>Are you the author of this Elsevier article?</b>	Yes
<b>Issue:</b>		<b>Will you be translating?</b>	No
<b>Start page:</b>	265	<b>Title of your thesis/dissertation</b>	Petrogenesis and Tectonic Setting of Mesozoic Granitic Rocks in Eastern South China
<b>Publisher:</b>	PERGAMON	<b>Expected completion date</b>	Mar 2014
		<b>Estimated size (number of pages)</b>	320
		<b>Elsevier VAT number</b>	GB 494 6272 12
		<b>Permissions price</b>	0.00 USD
		<b>VAT/Local Sales Tax</b>	0.00 USD / 0.00 GBP

**Note:** This item was invoiced separately through our **RightsLink service**. [More info](#)

\$ 0.00

Total order items: 1

Order Total: \$0.00

### Appendix G. Permission to paper reproduction for Chapter 5

Zhu, K.-Y., Li, Z.-X., Xu, X.-S., Wilde, S.A., 2014. A Mesozoic Andean-type orogenic cycle in southeastern China as recorded by granitoid evolution. American Journal of Science 314, 187-234.

### American Journal of Science

217 Kline Geology Laboratory  
Yale University  
P.O. Box 208109  
New Haven, Connecticut 06520-8109  
E.mail: [ajs@yale.edu](mailto:ajs@yale.edu)

**Campus address:**  
Kline Geology Laboratory  
210 Whitney Avenue  
**Telephones:**  
203 432-3131  
203 432-5668  
**FAX:**  
203 432-5668

January 6, 2014

Dr. Kong-Yang Zhu  
Department of Applied Geology  
Chinese Academy of Sciences  
Curtin University  
Kent Street  
Bentley, WA 6102 Australia

Dear Dr. Zhu,

We understand that you are publishing a doctoral thesis titled “Petrogenesis and Tectonic Setting of Mesozoic Granitic Rocks in Eastern South China.” You are requesting permission to publish the following paper in the thesis.

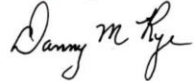
Zhu, K.Y., Li, Z. X., Xu, X. S., and Wilde, S. A., 2014, A Mesozoic Andean-type orogenic cycle in southeastern China as recorded by granitoid evolution: American Journal of Science, v. 314, n. 1-2, doi:10.2475/01.2014.06

Permission is granted for Kongyang Zhu to include the above-mentioned material in his higher degree thesis for the Curtin University, and to communicate this material via the Australasian Digital Thesis Program. This permission is granted on a non-exclusive basis and for an indefinite period.

We ask that you give credit to the American Journal of Science for the original work and permission for its use.

If material appears in our book with credit given to another source, authorization from that source is required.

Sincerely,



Danny M. Rye, Editor